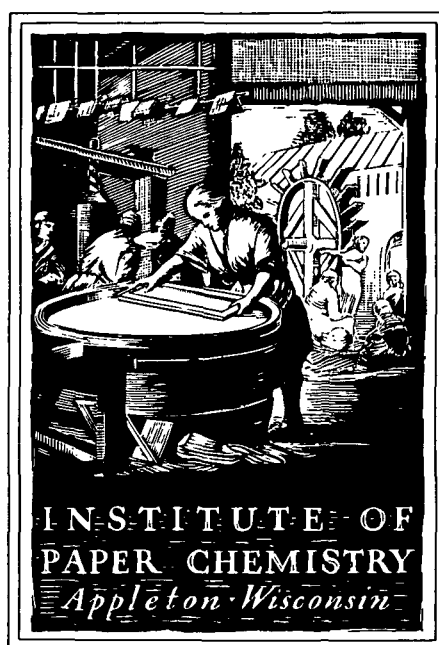# PROJECT ADVISORY COMMITTEE

Subcommittee on

Paper Properties and Uses

IPC STAFF STATUS REPORTS

This information represents a review of on-going research for use by the Project Advisory Subcommittees. The information is not intended to be a definitive progress report on any of the projects and should not be cited or referenced in any paper or correspondence external to your company.

Your advice and suggestions on any of the projects will be most welcome.

NOTICE & DISCLAIMER

September 30, 1988

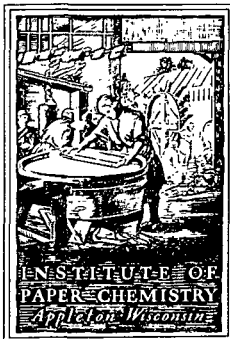TO: MEMBERS OF PAPER PROPERTIES AND USES PROJECT ADVISORY COMMITTEE

Attached for your review are the Status Reports for the projects to be
discussed at the Paper Properties and Uses PAC meeting scheduled for
October 19-20, 1988, in Appleton. A meeting agenda can be found inside the
booklet.

For those of you staying at the Continuing Education Center, the attached
pink card gives the combination to the front door so that you may gain
entrance if you arrive after the doors are locked. Room schedules are posted
in the lobby. If you have not indicated whether you will be attending the
meeting or have not yet reserved a room, please do so by notifying Sheila
Burton at 414/738-3259.

We look forward to seeing you on October 19-20. Best regards.

Sincerely yours,

Maclin S. Hall
Acting Director
Paper Materials Division

MSH/sb
Enclosure

TABLE OF CONTENTS

AGENDA

PAPER PROPERTIES AND USES
PROJECT ADVISORY COMMITTEE

October 19-20, 1988
The Institute of Paper Chemistry
Continuing Education Center (CEC)
Appleton, WI

Wednesday -- October 19

7:15 a.m.	BREAKFAST	
8:30	Welcome/Introductions	Betz/Hall
8:45	Status of IPC Move to Atlanta	Yeske
9:00	OVERVIEW OF PROJECTS	Hall
9:15	PROJECT REVIEWS	
	Strength Improvement and Failure Mechanisms	Waterhouse
	Internal Strength Enhancement	Stratton
	BREAK	
	Student Presentation	Goulet
	Fundamentals of Paper Surface Wettability	Etzler
12:00 noon	LUNCH (CEC Dining Room)	
1:00	TOUR OF PAPER MATERIALS DIVISION LABORATORIES	
2:00	PROJECT REVIEWS	
	Board Properties and Performance	Whitsitt/Halcomb/ Dees
	Process, Properties, Product Relationships	Habeger/Pan
	BREAK	
	Board Optical Transmission Meter	Hardacker
	On-Line Measurement of Paper Mechanical Properties	Hall/Habeger
5:15	SOCIAL TIME	
6:00	DINNER (CEC Dining Room)	

<u>Thursday -- October 20</u>

7:15 a.m.   BREAKFAST (CEC Dining Room)

8:00   COMMITTEE DISCUSSION OF PROJECTS (Krannert 108/109)

11:30   ADJOURNMENT/LUNCH (CEC Dining Room)

NEXT MEETING - March 22-23, 1989

PAPER PROPERTIES AND USES
PROJECT ADVISORY COMMITTEE

Mr. Dennis Betz, Chairman -- 6/89*
Assistant Research Director
P. H. Glatfelter Co.
228 S. Main Street
Spring Grove, PA 17362
(717) 225-4711

Dr. Keith A. Bennett -- 6/91
Senior Research Scientist
Weyerhaeuser Paper Company
WTC 2B42
Tacoma, WA 98477
(206) 924-6714

Dr. Robert L. Beran -- 6/89
Research Director
Westvaco Corporation
Covington Research Center
Washington Avenue
Covington, VA 24426
(703) 962-2111

Dr. Keith E. Bradway -- 6/91
Senior Research Scientist
Union Camp Corporation
P.O. Box 3301
Princeton, NJ 08543
(609) 896-1200

Dr. Von L. Byrd -- 6/91
Manager, End-Use Performance
Mead Corporation
Central Research Laboratories
8th & Hickory Streets
Chillicothe, OH 45601
(614) 772-3539

Mr. Richard P. Grant -- 6/89
Senior Engineer
Eastman Kodak Company
1669 Lake Avenue
Bldg. 36
Rochester, NY 14650
(716) 477-6537

Mr. Keith A. Kraft -- 6/91
Development Engineering Specialist
Minnesota Mining & Manufacturing Company
Carbonless Products Dept.
3M Center, Bldg 235 1E-33
St. Paul, MN 55144
(612) 736-4545

Dr. Leslie L. Martin -- 6/91
Senior Research Engineer
Potlatch Corporation
Fiber R & D, East End
Cloquet, MN 55720
(218) 879-2387

Dr. James J. Nault -- 6/90
Assistant Papermill Superintendent
Stone Container Corporation
P.O. Box 201
Hopewell, VA 23860
(804) 541-9754

Dr. Robert J. Niebauer -- 6/91
Project Manager, R&D
Crane & Co., Inc.
30 South St.
Dalton, MA 01226
(413) 684-2600

Dr. R. Heath Reeves -- 6/89
Sr. Research Associate
James River Corporation
Neenah Technical Center
1915 Marathon Avenue
Neenah, WI 54956
(414) 729-8148

Mr. Lowell Schleicher -- 6/89
Director of Basic Research
Appleton Papers Inc.
P.O. Box 359
Appleton, WI 54912
(414) 735-8857

*Date of retirement from committee.

PAC Project Advisory Committee continued.

Mr. Robert L. Smathers -- 6/89
Manager, Technical Services
MacMillan Bloedel Inc.
P.O. Box 336
Pine Hill, AL   36769
(205) 963-4391

Mr. David South -- 6/89
Director of Market Planning & Prod. Dev.
Chesapeake Corporation
P.O. Box 311
West Point, VA   23181
(804) 843-5252

Mr. Quinton W. Vancleave -- 6/90
Technical Manager
Kraft Paper and Paperboard Kraft
Georgia Pacific Corporation
133 Peachtree Street
Atlanta, GA   30303
(404) 521-5903

Mr. Dale C. Woodward -- 6/91
Mgr., Process Control Technology
Nekoosa Packaging
1660 Indian Wood Circle
P.O. Box 697
Toledo, OH   43694-0697
(419) 891-5990

9/88

THE INSTITUTE OF PAPER CHEMISTRY

Appleton, Wisconsin

Status Report

to the

PAPER PROPERTIES AND USES

PROJECT ADVISORY COMMITTEE

Project 3469

STRENGTH IMPROVEMENT AND FAILURE MECHANISMS

October 19-20, 1988

PROJECT SUMMARY

PROJECT NO. 3469: STRENGTH IMPROVEMENT AND FAILURE MECHANISMS

STAFF: J. Waterhouse   September 12, 1988

PROGRAM GOAL:

Identify critical parameters which describe converting and end-use performance
and promote improvements in cost/performance ratios.

PROJECT OBJECTIVE:

Establish practical methods for enhancing strength properties (especially
compressive strength) during paper manufacture and to evaluate deformation
behavior as it relates to sheet composition and structure.

PROJECT RATIONALE, PREVIOUS ACTIVITY and PLANNED ACTIVITY FOR FISCAL 1988-89 are
on the attached 1988-89 Project Form.

SUMMARY OF RESULTS LAST PERIOD: (October 1987 - March 1988)

(1) Fabrication of the formation tester is essentially complete.

(2) Software development for position and motion control of the formation
     tester is in progress.

(3) Formette handsheets containing different blends of NSSC and kevlar have
     been made.

(4) Student related work - "The effect of lignin and hemicellulose removal
     on the short span compressive strength potential of white spruce" Hilda
     Cedergren.

(5) Student related work - "Strength development through internal fibrillation
     and wet pressing" Thomas Bither.

SUMMARY OF RESULTS THIS PERIOD: (March 1988 - October 1988)

(1) Software development is in progress for the IPC Formation Tester: coef-
     ficient of variation, histograms, scan line, and image maps have been
     developed.

(2) The Promethium 147 beta source has been installed in the Formation Tester.

(3) The formation characteristics of a variety of paper samples have been
     measured including newsprint, tissue, fine paper, offset, and medium
     grades.

(4) Formette Handsheets containing different blends of NSSC pulp and synthetic
     fiber have been saturated with various binders and characterized.

(5) An out-of-plane biaxial device for measuring the deformation behavior of
     paper and board when subjected to combined stresses has been designed and
     fabricated.

(6) Student Related Work - Tom Bither has made fracture toughness and pore
     size distribution measurements as a function of wet pressing and refining.

(7) Student Related Work - Mikko Jokkio has completed a research study, "The
     Interaction of Base Paper and Coating on Coated Paper Properties".

PROJECT TITLE: Strength Improvement and Failure
                 Mechanisms

PROJECT STAFF: J. Waterhouse

PRIMARY AREA OF INDUSTRY NEED: Properties related to
                                 end use

Date: 2/3/88	
Budget: $100,000	
Period Ends: 6/30/89	
Project No.: 3469	

PROGRAM AREA: Improved converting processes and converted products

PROGRAM GOAL:

Identify critical parameters which describe converting and end-use performance
and promote improvements in cost/performance ratios.

PROJECT OBJECTIVE:

To evaluate deformation behavior and its relationship to sheet composition and
structure, and to establish practical methods for enhancing strength properties
(especially compressive strength).

PROJECT RATIONALE:

Deformation and strength properties are important in predicting end use perfor-
mance. An improved understanding of failure mechanisms and ways to improve cer-
tain strength properties are important to nearly all grades. The recognized
importance of compressive strength in linerboard and corrugating medium to box
performance provides impetus for research in this area. The approach is to meet
the objectives through new papermaking strategies.

RESULTS TO DATE:

We have shown that compressive strength of paper is highly related to a product
of in-plane and out-of-plane elastic stiffnesses. The relationship holds for
commercial and experimental sheets made under a variety of conditions. This
development suggests it will be possible to monitor compressive strength in the
mill using ultrasonic techniques.

Compressive strength is enhanced by high densification, which increases bonding,
and high fiber axial compressive stiffness. Thus compressive strength increases
with refining and wet pressing. Within a practical range, higher CD compressive
strength can be achieved by decreased fiber orientation, loose draws, and/or
increased CD restraint during drying. Where limitations to increased refining
and wet pressing exist, low levels of polymer addition could be used as a viable
means to improve compressive strength. The effect of pulp type and additives on
the stiffness-compressive strength correlation has been investigated. A tech-
nique involving small wood coupons and mini handsheets has been developed to
measure the compressive strength potential of wood fibers.

We have developed a torsion mode technique for measuring the out-of-plane shear
stress-strain behavior, and studied ZD shear straining on compressive strength.
Internal stress variations have been determined in the thickness direction

together with the variation of in-plane and out-of-plane properties. Measurements of the relative losses in elastic and strength properties due to super-calendering have been made. A procedure for determining the residual stress distribution in paperboard has been developed using a layer removal method.

A formation tester with the capability of making light transmission and reflectance, and mass density measurements has been designed and fabricated.

Commercial and laboratory formation samples of fine, tissue, newsprint and medium papers have been obtained and extensively characterized.

PLANNED ACTIVITY FOR FY 1988-89.

Formation - Continue development of IPC formation tester and evolve a menu of formation related parameters. Determine how the relationship between optical and mass density is affected by certain papermaking variables.

Compressive Strength - Develop fiber and polymer reinforcement strategies to improve compressive strength and also minimize losses due to forming and conditioning.

Internal Stresses - Determine how internal stress distribution is affected by refining and wet pressing and certain drying strategies.

Combined Stresses - Explore techniques for measuring the deformation behavior of paper and board when subjected to combined out-of-plane stresses.

STUDENT RELATED RESEARCH

T. W. Bither, Ph.D.-1988; H. R. Cedergren, M.S.-1988; M. H. Jokio, Special Student-1988

STRENGTH IMPROVEMENT AND FAILURE MECHANISMS

Project 3469

INTRODUCTION

Project 3469 "Strength Improvement and Failure Mechanisms" embraces the following areas: Compressive Strength Improvement, Formation Measurements, Combined Stress Measurements and Internal Stresses in Paper and Board. The Project Advisory Committee has expressed an interest in all of these areas, however they have recommended that Formation Measurements should receive first priority followed by Combined Stress Measurements if a choice has to be made because of manpower or funding limitations.

1. COMPRESSIVE STRENGTH IMPROVEMENT

In our last progress report we briefly discussed strategies for improving compressive strength in such a way as to minimize strength losses during corrugating. It was argued that losses in compressive strength are mainly due to the large bending strains which the medium is subjected to during corrugating resulting in machine direction losses as high as 40%.

One possibility of improving this situation is to make a medium which is more tolerant of the forming process. The basic idea is to incorporate a relatively low percentage of high modulus fibers into the outer layers of the medium and then activate them during the forming process. This might be accomplished by the addition of a synthetic polymer or bicomponent fiber binder system which will go through its softening temperature during flute formation.

To determine the feasibility of this approach several synthetic fiber/corrugating medium combinations and binder systems are currently being investigated as shown in the Tables 1 and 2 below:

Table 1. Fiber furnishes.

Fiber Series 1

1. NSSC pulp

2. NSSC/Kevlar "pulp" blends

Fiber Series 2

1. NSSC pulp

1. NSSC pulp/Kevlar staple blends

2. NSSC pulp/Kevlar "pulp" blends

3. NSSC pulp/1/4 in. glass fiber blends

4. NSSC pulp/1/8 in. glass fiber blends

Table 2. Binder series 1.

A. Carboxylated SBR $T_g = 42°C$

B. Carboxylated SBR* $T_g = 42°C$

C. Styrene latex

D. Styrene latex $T_g = 105°C$

E. SBR latex (99% styrene)

F. SBR latex (85% styrene) $T_g = 54°C$

---

*Plasticized version of 1., T_g Glass Transition Temperature as supplied by manufacturer.

Formette handsheets have been made using the various fiber com-
binations given in Table 1, i.e. series 1 and 2. The nondestructive charac-
terization of these base sheets are shown in the Tables 3 and 4 below:

Table 3. Summary of Formette handsheet properties - Series 1.

Sheet Structure and Furnish Series 1	Grammage g/m^2	Apparent Density, g/cm^3	In-Plane Anisotropy R	Mean In-plane Constant E/ρ (km/sec)^2	Out-of-plane Constant E$_z$/ρ (km/sec)^2
100 % NSSC	127	0.523	2.89	6.39	0.163
92% NSSC/ 8% Kevlar	132	0.467	2.77	5.36	0.127
20% (NSSC/Kev) 60% (NSSC) 20% (NSSC/Kev)	141	0.477	2.60	5.31	0.116
84% NSSC/ 16% Kevlar	133	0.439	2.55	4.89	0.100
20% (NSSC/Kev) 60% (NSSC) 20% (NSSC/Kev)	136	0.433	2.62	4.73	0.078

It will be noted that the apparent density of the Formette handsheets in Fiber Series 2 are higher than Fiber Series 1 because of increased wet pressing.

The effect of the various synthetic fiber additions, for the conditions given in Tables 3 and 4 above, on the in-plane and out-of-plane elastic constants without polymer addition are shown in Fig. 1 and 2. The greatest rate of loss in in-plane elastic constant is with Kevlar pulp addition, followed by the glass, while the Kevlar staple produces a rate of loss which is approximately equal to that produced by a reduction in wet pressing of the 100% NSSC sheet. Although the rate of reduction of in-plane elastic constants is

Table 4. Summary of Formette handsheet properties - Series 2.

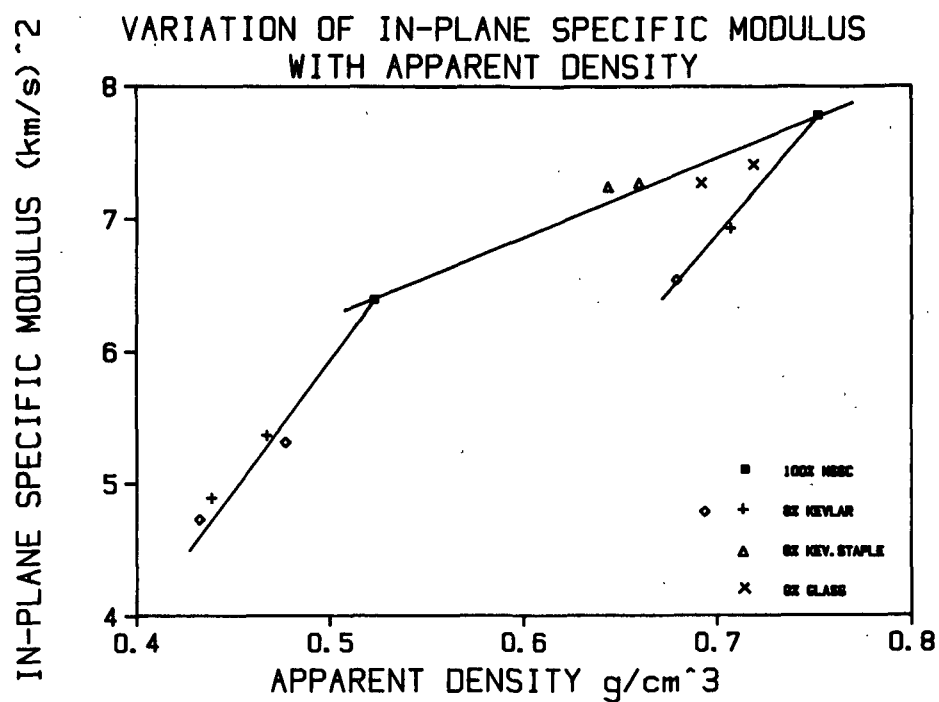| Sheet Structure and Furnish Series 1	Grammage g/m^2	Apparent Density, ρ g/cm^3	In-Plane Anisotropy R	Mean In-plane Constant E/ρ (km/sec)^2	Out-of-plane Constant E_z/ρ (km/sec)^2
100 % NSSC	118	0.752	2.42	7.78	0.217
92% NSSC/ 8% Kev. Stap.	115	0.660	1.83	7.27	0.165
20% (NSSC/Kev. Stap.) 60% (NSSC) 20% (NSSC/Kev. Stap.)	114	0.644	1.99	7.24	0.135
92% NSSC/ 8% Kevlar Pulp	114	0.707	2.58	6.93	0.167
20% (NSSC/Kev. Pulp) 60% (NSSC) 20% (NSSC/Kev. Pulp)	118	0.679	2.35	6.54	0.122
92% NSSC/ 8% 1/4" glass	118	0.719	2.90	7.41	0.187
20% (NSSC/1/4" glass) 60% (NSSC) 20% (NSSC/1/4" glass)	119	0.692	2.69	7.27	0.147
92% NSSC/ 8% 1/8" glass	123	0.721	3.19	7.44	0.194
20% (NSSC/1/8" glass) 60% (NSSC) 20% (NSSC/1/8" glass)	119	0.702	3.11	7.27	0.156

Figure 1. The effect of synthetic fiber addition on the variation
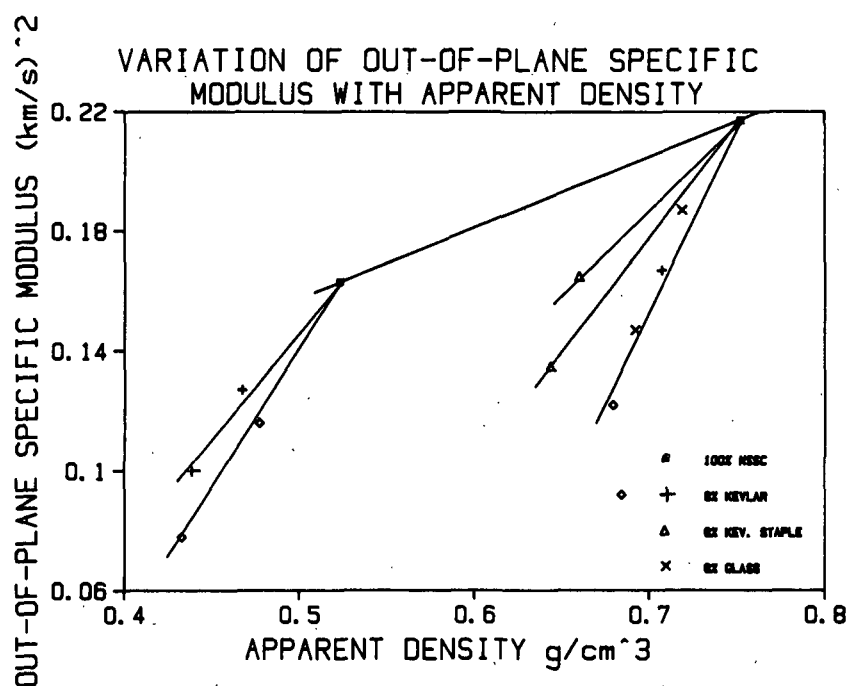of in-plane specific modulus with apparent density.

Figure 2. The effect of synthetic fiber addition on the variation
of out-of-plane specific modulus with apparent density.

independent of the location of the synthetic fiber, it is not the case for the out-of-plane elastic constants where we note that the triple layer sheets produce the highest rate of loss.

MD and CD samples cut from the above Formette handsheets were then saturated with the latex binders shown in Table 2 above. The conditions were such as to give a binder content around 10%. After saturation and removal of excess latex by blotters the samples were allowed to freely dry on screens in an environment of 50% RH 20°C. After nondestructive testing, the saturated samples were cut in half, and one half was heat treated at 125°C for 3 minutes using a nominal pressure of 7 kpa. The heat treated samples were also subjected to nondestructive testing. STFI short span compressive strength measurements were made on both the air dried and heat treated samples. Control samples were also saturated in distilled water only. These measurements are summarized in Table 5 below.

We note for all samples a large loss in in-plane elastic constant after saturation. This may be an undesirable effect which we will investigate in future work. In effect, we have by saturation and unrestrained drying, relaxed the internal stresses. The loss in in-plane elastic properties after saturation decreases with increasing Kevlar content, i.e. there is an average loss of 32.5%, 23.1% and 19.6% for 0%, 8% and 16% Kevlar contents respectively before heat treatment. The in-plane elastic constants generally increase with heat treatment, however it is only at the 16% Kevlar addition level, that a slight increase is found over that before polymer addition and heat treatment.

Heat treatment improves in-plane elastic constants, with the film forming latices (i.e. the SBR's) giving the greatest improvement. Heat treat-

Table 5. Elastic and compressive strength properties of latex saturated handsheets.

Sample	% Binder	$(C/\rho)_c$ $(k/s)^2$	$(C/\rho)_b$ $(k/s)^2$	$(C/\rho)_a$ $(k/s)^2$	$(C_z/\rho)_c$ $(k/s)^2$	$(C_z/\rho)_b$ $(k/s)^2$	$(C_z/\rho)_a$ $(k/s)^2$	$(\sigma/\rho)_c$ N/mg	$(\sigma/\rho)_b$ N/mg	$(\sigma/\rho)_a$ N/mg
100% NSSC Latex:										
A.	9.84	6.92	4.94	5.12	0.163	0.198	0.250	22.0	21.1	25.9
B.	9.98	6.92	4.62	5.21	0.163	0.183	0.230	22.0	20.1	23.8
C.	10.95	6.92	4.42	4.82	0.163	0.165	0.204	22.0	18.0	22.7
D.	11.92	6.92	4.48	4.54	0.163	0.159	0.191	22.0	19.4	22.2
E.	9.89	6.92	4.78	5.00	0.163	0.160	0.205	22.0	19.9	22.4
F.	10.42	6.92	4.78	5.54	0.163	0.170	0.237	22.0	19.6	25.7
H₂0 only			4.67			0.154		17.2		
8% Kevlar Latex:										
A.	11.22	5.36	4.39	4.77	0.127	0.158	0.195	17.4	17.5	21.7
B.	10.72	5.36	4.16	4.78	0.127	0.150	0.193	17.4	16.9	20.7
C.	11.31	5.36	3.93	4.33	0.127	0.131	0.174	17.4	14.9	19.7
D.	12.17	5.36	4.01	4.32	0.127	0.128	0.165	17.4	15.5	18.2
E.	9.70	5.36	4.01	–	0.127	0.136	0.168	17.4	–	–
F.	10.54	5.36	4.24	–	0.127	0.145	0.185	17.4	–	–
H₂0 only			3.75			0.113		13.6		
Kevlar-3 Ply 8% Latex:										
A.	9.28	5.62	4.46	5.31	0.116	0.152	0.178	19.6	17.5	20.8
B.	10.38	5.62	4.25	5.05	0.116	0.137	0.168	19.6	17.6	21.7
C.	11.20	5.62	3.90	4.52	0.116	0.119	0.142	19.6	15.5	19.3
D.	11.64	5.62	4.18	4.34	0.116	0.120	0.130	19.6	15.6	18.2
E.	10.33	5.62	4.25	4.71	0.116	0.122	0.149	19.6	16.6	19.9
F.	10.76	5.62	4.23	5.08	0.116	0.133	0.176	19.6	16.5	21.8
H₂0 only			3.71			0.116		14.7		
16% Kevlar Latex:										
A.	10.83	4.99	4.29	5.07	0.100	0.130	0.161	15.4	15.6	19.7
B.	10.78	4.99	4.32	5.05	0.100	0.123	0.158	15.4	15.5	19.6
C.	11.59	4.99	3.76	4.55	0.100	0.107	0.144	15.4	13.3	19.2
D.	12.98	4.99	3.85	4.16	0.100	0.108	0.115	15.4	14.1	16.1
E.	10.78	4.99	3.85	4.48	0.100	0.104	0.121	15.4	14.3	17.3
F.	11.15	4.99	3.99	5.11	0.100	0.113	0.148	15.4	15.1	19.5
H₂0 only			3.63			0.098		11.8		
Kevlar-3 Ply 16% Latex:										
A.	10.90	4.92	4.03	4.69	0.078	0.113	0.133	16.3	16.6	21.3
B.	10.91	4.92	4.25	4.77	0.078	0.117	0.131	16.3	18.0	20.5
C.	11.29	4.92	3.55	4.21	0.078	0.087	0.103	16.3	14.2	18.9
D.	12.99	4.92	3.84	4.29	0.078	0.092	0.105	16.3	14.9	18.9
E.	10.53	4.92	3.83	4.19	0.078	0.089	0.099	16.3	15.3	18.6
F.	11.22	4.92	3.99	4.80	0.078	0.097	0.124	16.3	15.9	20.7
H₂0 only			3.90			0.073		13.2		

---

[c]Control.

[b]Saturated only.

[a]Saturated and heat treated.

ment also appears to be more effective with increasing Kevlar content. Polymer addition and heat treatment have a greater effect on the longitudinal out-of-plane elastic constants. The improvement is again greatest with the film forming latices and increasing Kevlar content. Although heat treatment improves the performance of the non-film forming latices (i.e., styrenes C, D, & E) it does not equal that of the heat treated film forming latices (i.e., SBR's A, B, & F).

The improvement in elastic properties by polymer addition and heat treatment is also reflected in an improvement in compressive strength. Despite the improvement in elastic constants with increasing Kevlar content the absolute level of compressive strength is lower. This implies that the polymers evaluated to date are not effective in activating the Kevlar. Nevertheless, it will be interesting to see how the various fiber/polymer combinations perform in the fluting process (particularly their effect on forming losses) which we hope to evaluate soon.

2. FORMATION

The recent emphasis on improving paper quality has led to a renewed interest in formation. Formation is mainly concerned with small scale variations in optical properties, and mass density, but might also include related properties such as compressibility, roughness, porosity and deformation behavior.

Areas of focus for our research program include:
* Effect of papermaking variables on formation
* Effect of measurement variables
* Mass - optical density relationship

* Formation - optical properties

* Formation - mechanical properties

* Formation - end use performance

The recently fabricated IPC formation tester is shown in Fig. 3. It has the capability of making light transmission and reflectance measurements in the wavelength range of 400 - 700 nm, as well as beta particle absorption measurements. The tester can accept different size formation samples which are held in place with magnetic strips as shown in Fig. 4.

A close up view of the light source and beta collimator is shown in Fig. 5. The beta source, consisting of 50 mCi of Pm 147 on a 5 mm diameter aluminum disk with a 2μ silver window, has recently been installed in the tester. The circuit for making mass density measurements is shown schematically in Fig. 6. The aperture for light transmission and beta measurements is 1 mm x 1 mm.

In work to date we have been mainly concerned with making formation measurements using transmitted light. The circuit for this measurement is also shown in Fig. 6. The output from the photodiode circuit is fed to an AT type computer via a Metrobyte A-D converter board. This board has four software selectable gain settings of 10 volts, 1 volt, 100 mV, and 20 mV, which allow a wide range of light levels to be recorded. As the system is presently operated a thousand readings are averaged for each data point. With increasing grammage or absorption coefficient, e.g. unbleached board samples, the reduced level of transmittance requires an increase in the gain setting. In this situation noise can significantly contribute to the variance and thus be a limiting factor. We are currently investigating these limitations as well as the effects of table speed on formation measurements.
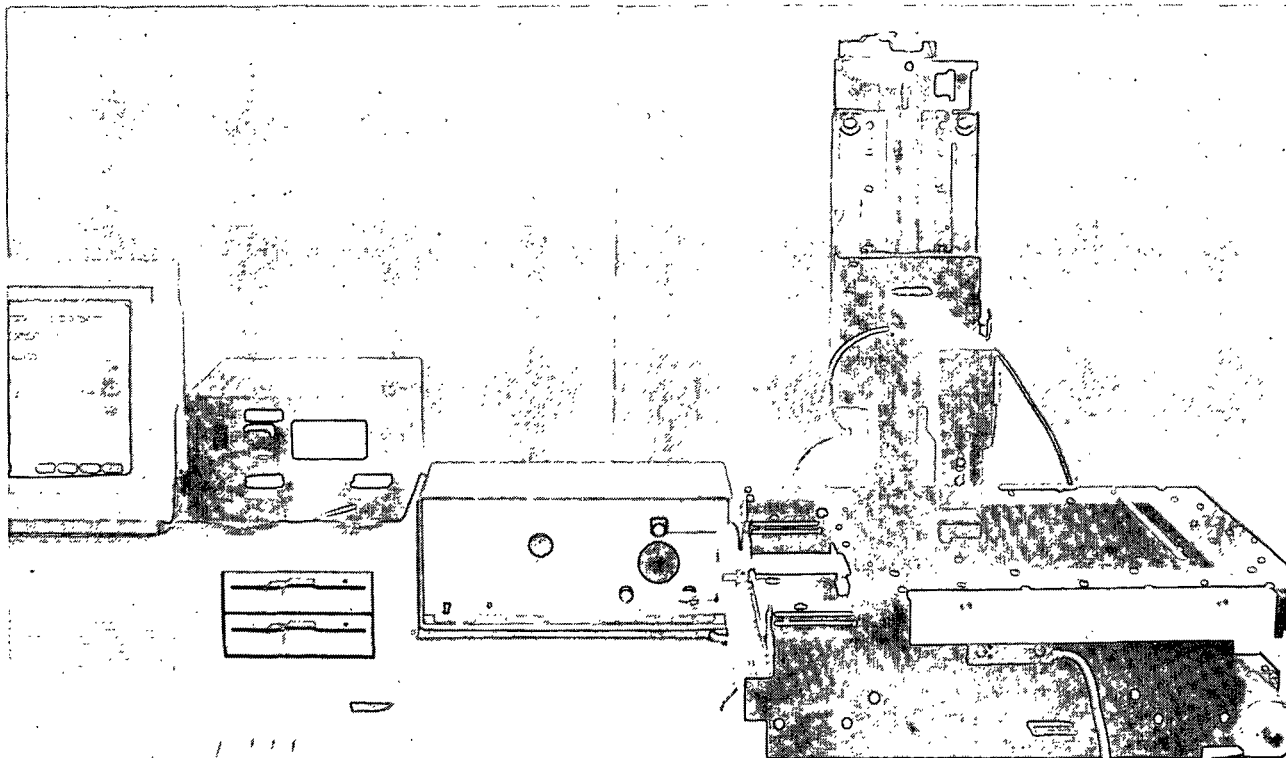
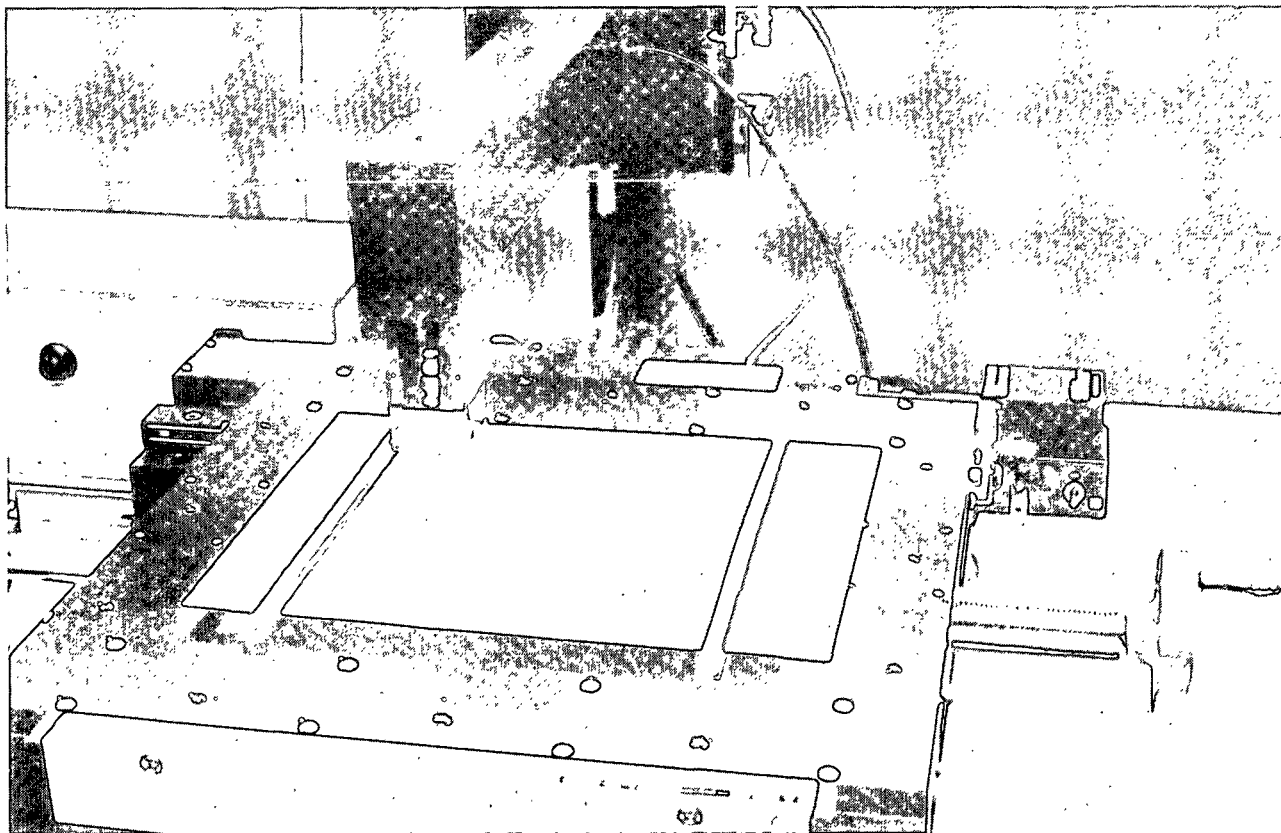Figure 3. General view of IPC formation tester.

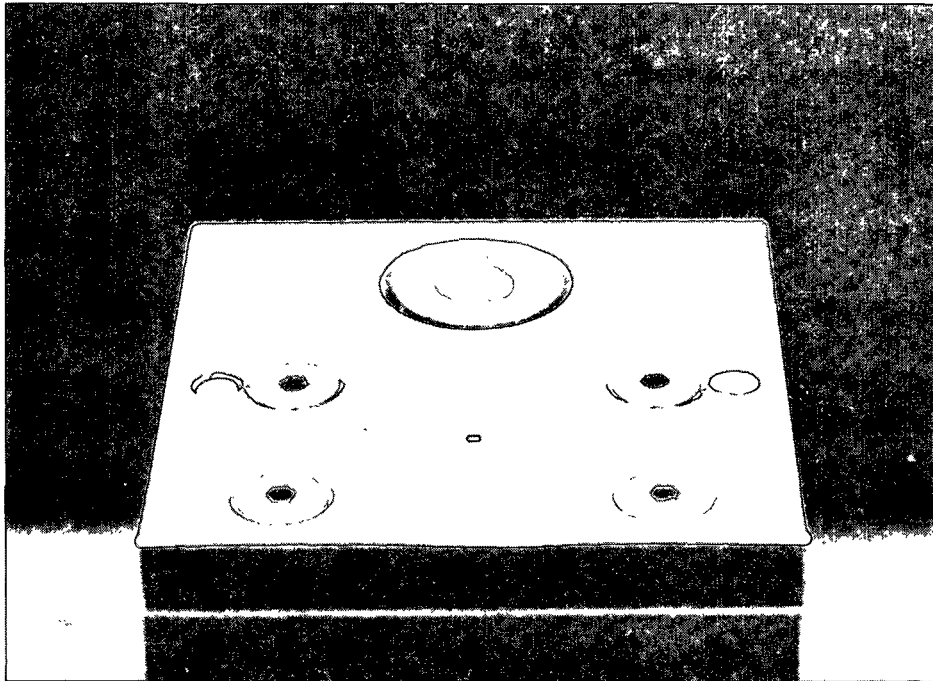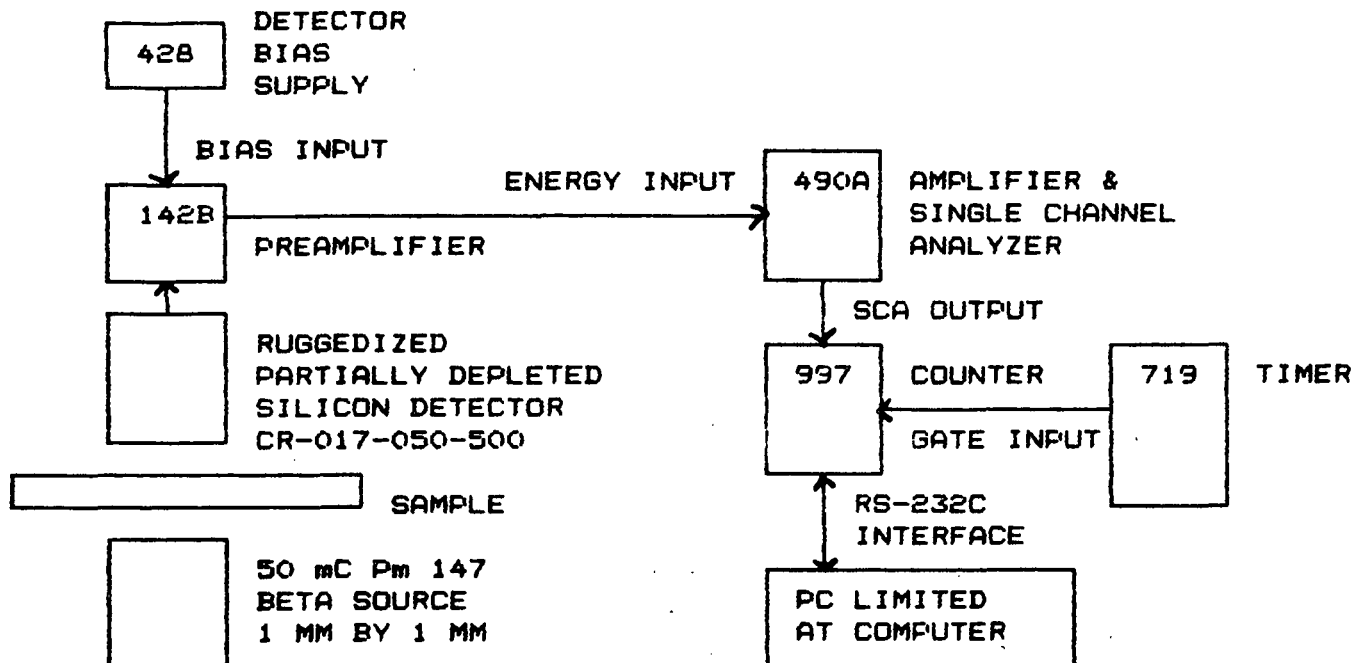Figure 4. IPC formation tester with formation sample in position.

Figure 5. View of light source and beta source collimator.

Formation measurements have been made on a variety of samples. Our basic measurement of formation is the coefficient of variation, or its recipro- cal if we require a number which correlates positively with visual assessment.

Histograms and our first attempt at making an image map are shown for samples having good formation (Figs. 7 and 9) and poor formation (Figs. 8 and 10) over an area of 80 mm x 80 mm. The histogram is divided into 1% increments above and below the mean, the total range is plus and minus 25%. Also shown is the average signal level, standard deviation, and coefficient of variation. The image map is based on three levels: the black areas represent values above 10% of the mean, white areas 10% below the mean, and grey areas within plus and minus 10% of the mean. Clearly the number of levels can be increased as required.

MASS DENSITY MEASUREMENT SYSTEM

```
┌──────┐    DETECTOR
│ 428  │    BIAS
└──────┘    SUPPLY
   │
   │ BIAS INPUT
   ↓
┌──────┐                ENERGY INPUT    ┌──────┐  AMPLIFIER &
│ 142B │───────────────────────────────→│ 490A │  SINGLE CHANNEL
└──────┘    PREAMPLIFIER                 └──────┘  ANALYZER
   ↑                                        │
┌──────┐    RUGGEDIZED                      │ SCA OUTPUT
│      │    PARTIALLY DEPLETED              ↓
│      │    SILICON DETECTOR    ┌──────┐  COUNTER  ┌──────┐  TIMER
│      │    CR-017-050-500      │ 997  │←──────────│ 719  │
└──────┘                        └──────┘           └──────┘
                                   │   GATE INPUT
┌────────────┐  SAMPLE             │
└────────────┘                     │ RS-232C
                                   │ INTERFACE
┌──────┐    50 mC Pm 147           ↕
│      │    BETA SOURCE         ┌──────────┐
│      │    1 MM BY 1 MM        │PC LIMITED│
└──────┘                        │AT COMPUTER│
                                └──────────┘
```

OPTICAL MEASURING SYSTEM

```
┌─┐    POWER SUPPLY                              ┐ TRANSMITTED
└─┘                                              ─ LIGHT
┌─┐    SILCON PHOTODIODE                           MEASURING
│ │    DETECTOR &                                ┘ SYSTEM
│ │    PREAMPLIFIER
└─┘
┌────────────┐ SAMPLE   ┌──────────────────┐    ┌──────────┐
└────────────┘          │METRABYTE DAS-1602│←──→│PC LIMITED│
┌─┐                     │A/D INTERFACE BOARD│   │AT COMPUTER│
└─┘    3.2 mm FIBER     └──────────────────┘    └──────────┘
│      OPTIC CABLE              ↑
│                        ┌─┐  POWER SUPPLY       ┐ REFLECTED
│                        └─┘                      ─ LIGHT
│                        ┌─┐  SILCON PHOTODIODE     MEASURING
└───────────────────────→│ │  DETECTOR &          ┘ SYSTEM
                         │ │  PREAMPLIFIER
                         └─┘
┌──────────┐  ORIEL VARIABLE WAVELENGTH
│          │  100 WATT QUARTZ HALOGEN
└──────────┘  LIGHT SOURCE
```
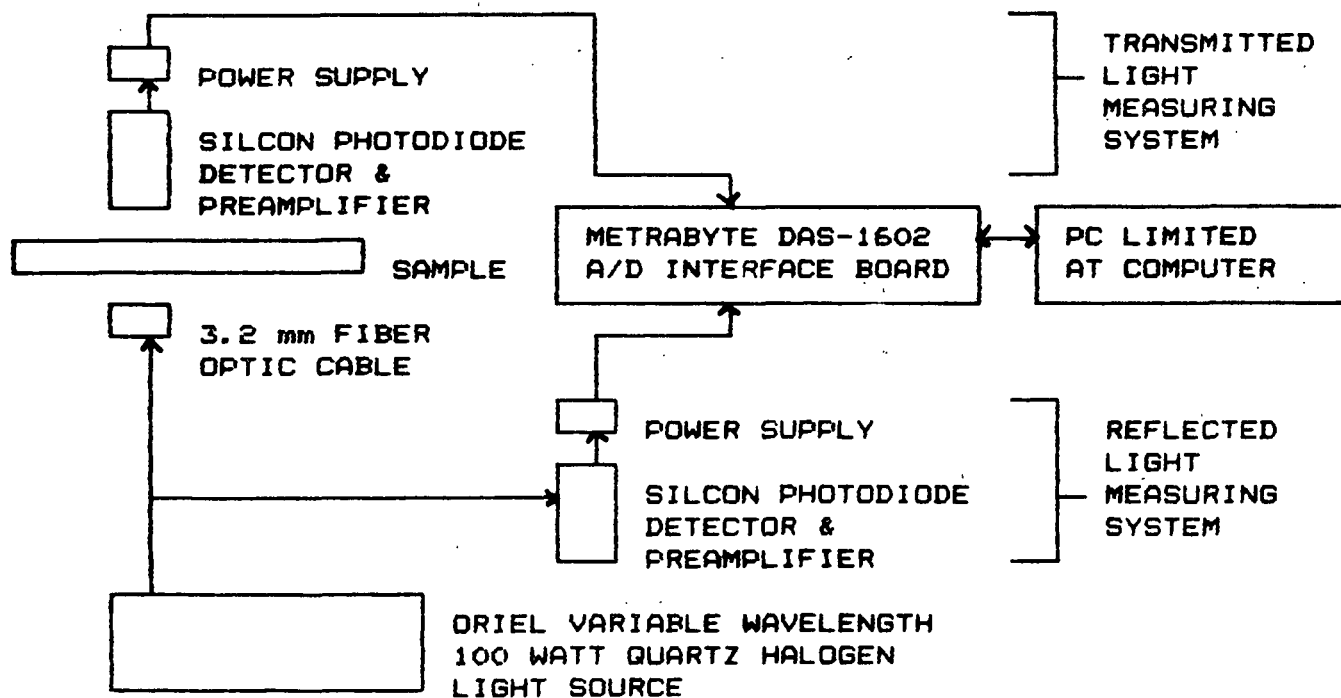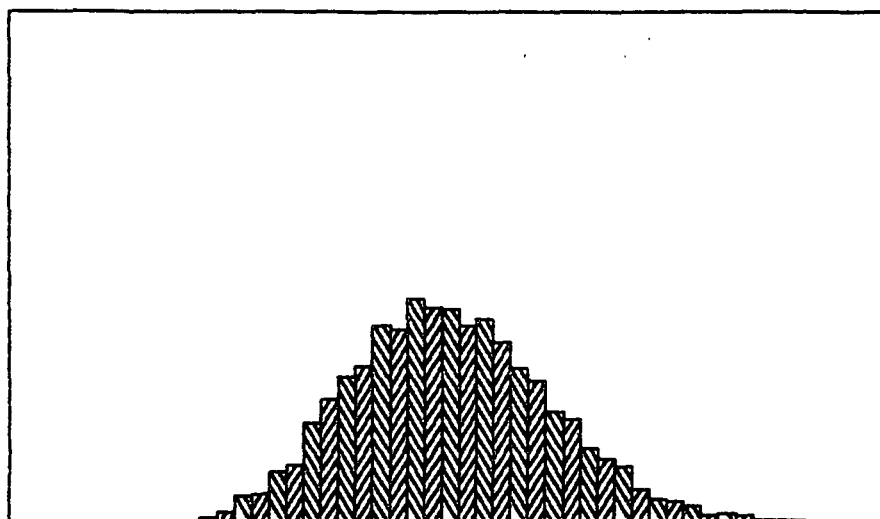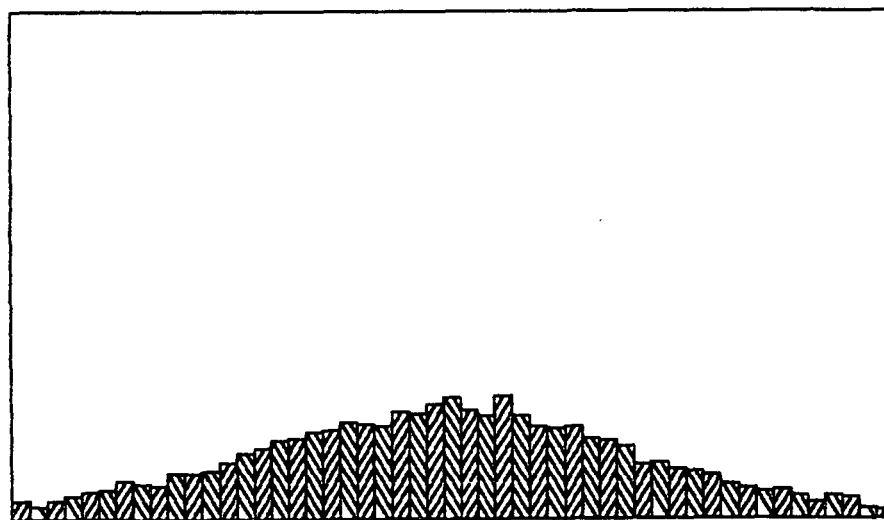
Figure 6.   Schematic layout of mass density and optical measuring
            system for IPC formation tester.

Sample Name   : 62-J-01
Total Number of Data Points: 6320
Average   : 0.3242
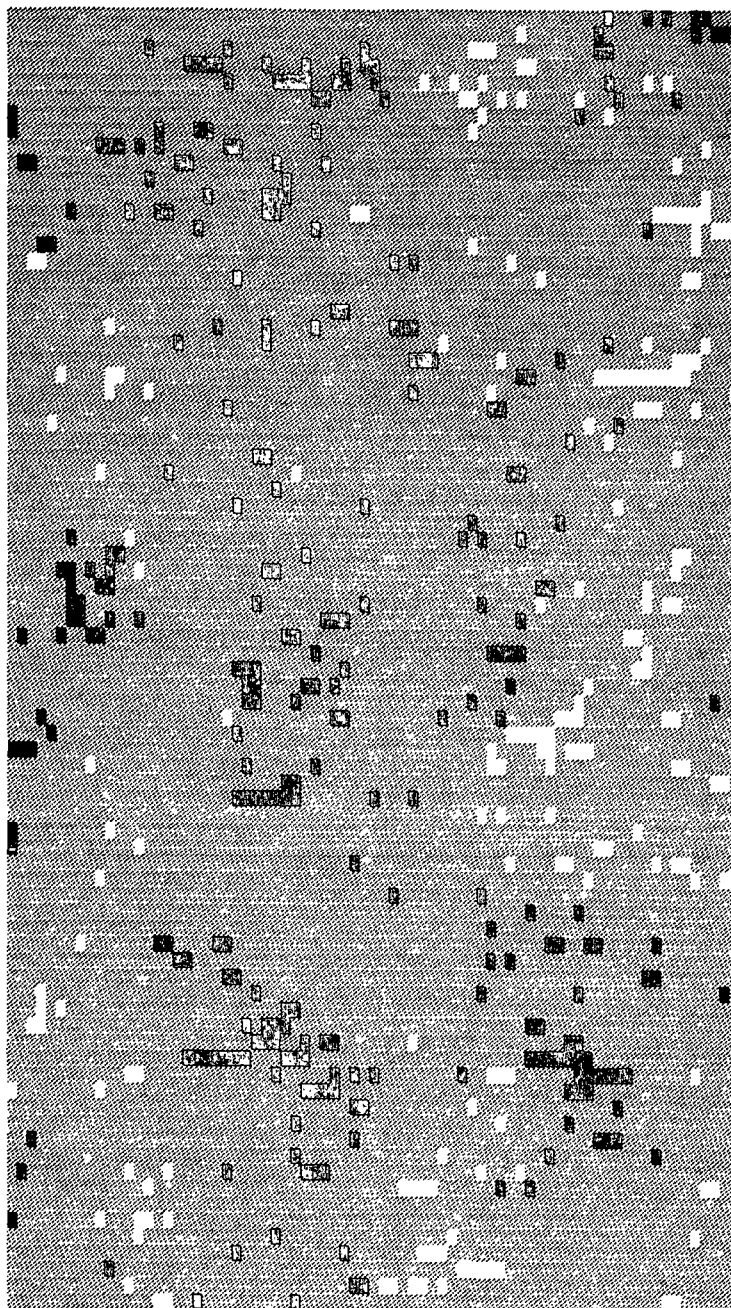Standard Deviation   : 0.0190
Percent of Variance   : 5.8474

Figure 7.   Histogram for commercial offset sample having good to
            fair formation.

Sample Name   : 114-I-01
Total Number of Data Points: 6340
Average   : 0.4990
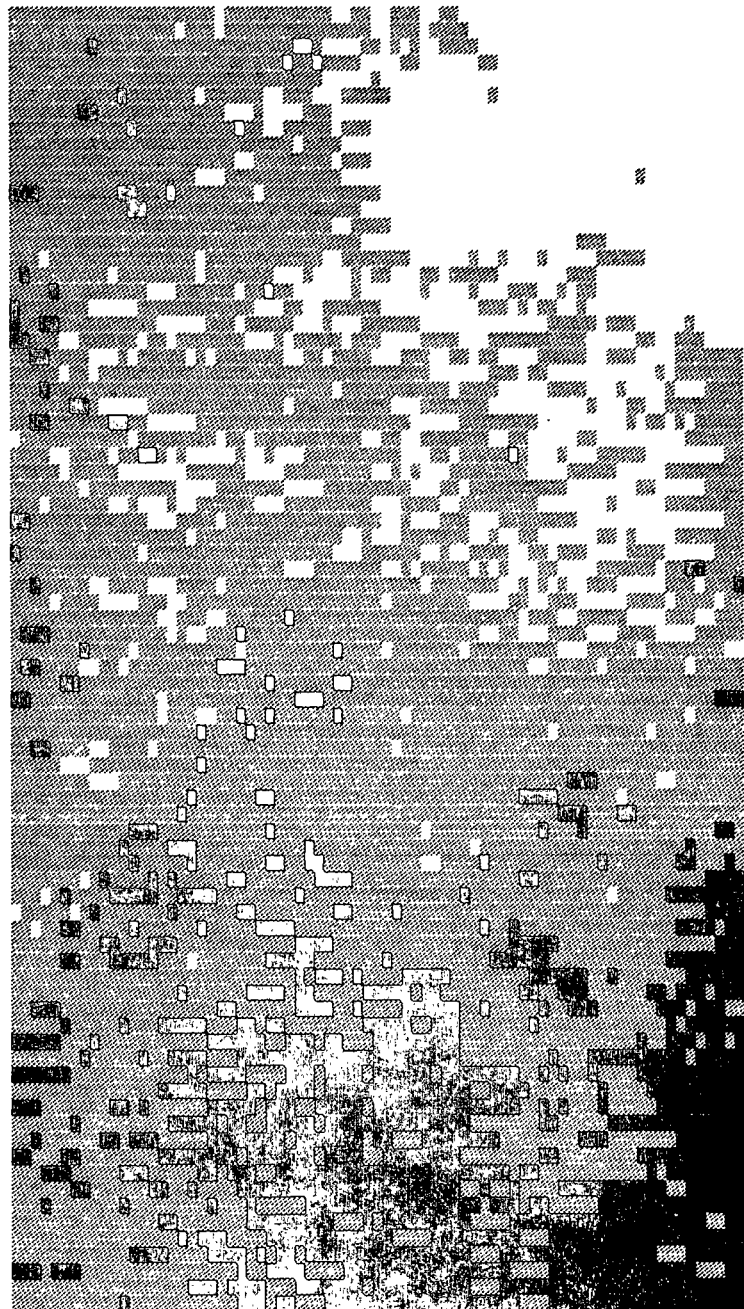Standard Deviation   : 0.0602
Percent of Variance   : 12.0692

Figure 8.   Histogram for a Noble and Wood handsheet made from a
            commercial offset furnish - poor formation.

```
Sample Name              :  62-j-01
Total Number of Data Points:  6320
Average                  :  0.3242
Standard Deviation       :  0.0190
Percent of Variance      :  5.8474
```



```
Image Map Key
Average transmitted light reading:  "  "
10% above average reading        :  "□"
10% below average reading        :  "  "
```

Figure 9. Image map for commercial offset sample having good to fair formation.

Sample Name   : 114-1-o1
Total Number of Data Points: 6340
Average   : 0.4990
Standard Deviation   : 0.0602
Percent of Variance   : 12.0692

Image Map Key
Average transmitted light reading: "░"
10% above average reading   :   "□"
10% below average reading   :   "▓"

Figure 10.   Image map for a Noble and Wood handsheet made from
              a commercial offset furnish - poor formation.

We are currently undertaking for API an evaluation of commercial formation measuring instruments. The IPC Formation Tester is to be used in this study to provide optical and mass density measurements for comparative purposes.

Commercial and handsheet formation samples for this evaluation consisting of newsprint, tissue, offset, bond and corrugating medium having recently been subjectively evaluated using a pair comparison technique. This provides a quantitative measurement of formation. In this comparison the judges consisting of ten "novices" and ten "experts" were asked to decide which of a pair was more uniform. No instructions were given as to what constituted uniformity. A light table was purchased for this purpose, and a plywood shield was constructed to mimimize the effects of stray illumination.

The ability of the IPC Formation Tester to assess the visual quality of newsprint (i.e. its uniformity) is shown in Fig. 11. The correlation is quite good having an $r^2 = 0.92$. The visual ranking in this instance is a pooled value of both the "novice" and "expert", and in this case there was little disagreement between them. In contrast, Fig. 12 shows no correlation between reciprocal coefficient of variance and visual ranking for newsprint formation samples made on the Formette Dynamique. As might be expected with this type of former, the formation range is much narrower. The newsprint formation samples in Fig. 12 include variations in grammage, fiber orientation, and color. Although there was now more disagreement between the "novice" and "expert" judges, they were still able to assess a definite range of formation values. If this kind of resolution is required of a formation measuring instrument it may be that other measures of formation may be more useful. We intend to study this point further in future work.
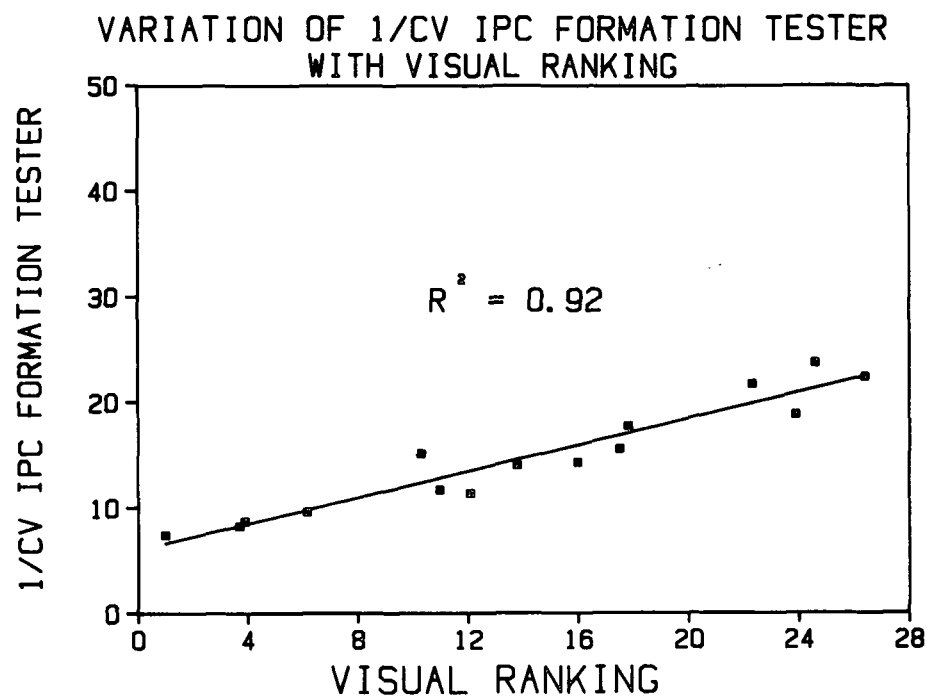
VARIATION OF 1/CV IPC FORMATION TESTER
WITH VISUAL RANKING

$R^2 = 0.92$

Figure 11. IPC formation index vs. visual ranking index for
commercial and handsheet newsprint samples.

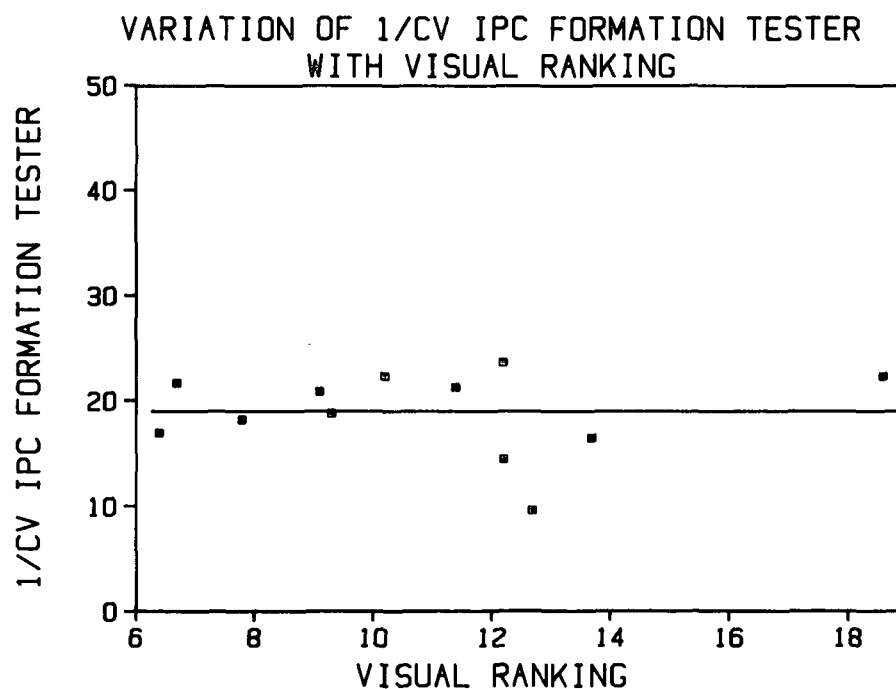VARIATION OF 1/CV IPC FORMATION TESTER
WITH VISUAL RANKING

Figure 12. IPC formation index versus visual ranking index for
Formette handsheets from a commercial newsprint
furnish.

There are perhaps only one or two commercial instruments which are capable of measuring the formation of unbleached board. Our early version of the MK microformation formation tester is one such instrument. We find a large difference in M.K. Formation Index (F.I.) between commercial and Formette handsheet samples made from the same furnish e.g. commercial F.I.= 5, Formette F.I.= 60. In preliminary tests using the IPC Formation Tester we also found a large difference in coefficient of variation between the 26-lb commercial and Formette handsheet samples, e.g. commercial 53.2% and Formette 21.6%. The coefficient of variation is surprisingly high for the Formette sheet! Using this and other commercial corrugating medium furnishes, 50 g/m^2 Formette handsheet were made, and formation measurements were performed on them using the IPC Formation Tester. These sheets were also evaluated subjectively as in the pair comparison tests referred to above. The correlation between reciprocal coefficient of variance and visual ranking, is again poor; in addition the variance values are considered to be high for Formette handsheets. There is a considerable variation in color between these various furnishes which is evidenced by large differences in absorption coefficient, as well as dirt being present. Mass density measurements should help in resolving this problem and variance measurments at other wavelengths may be more meaningful with this type of furnish.

"The Interaction of Base Paper and Coating on Coated Paper Properties" is the title of Mikko Jokkio's (a special student from Finland) A290 Research Project. The focus of his study was the effects of base paper formation on coating structure, and coated paper properties including the formation of the coated paper. His results were obtained on handsheets having a nominal grammage of 55 g/m^2 and a furnish containing 50% kraft and 50% mechanical pulp. Coated sheet formation was best for the sheet which had the best base sheet formation
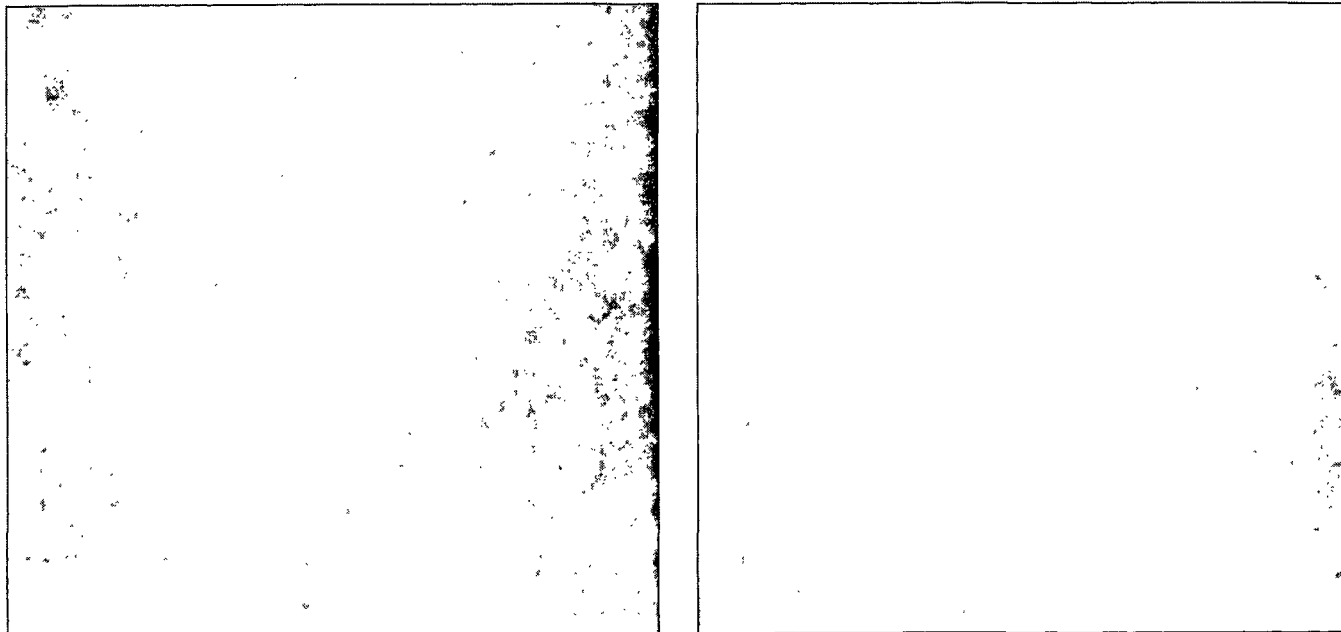
Figure 13.   Handsheet formation before and after coating - #11
             good base sheet formation - before c.v. = 6.5%,
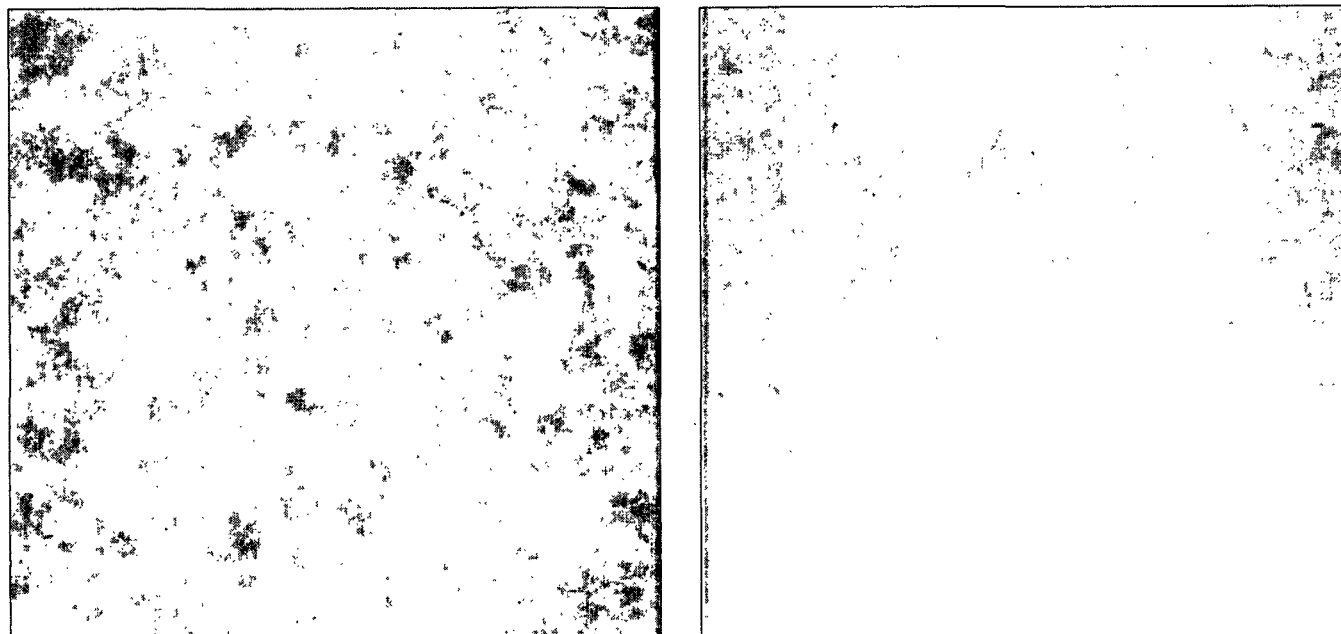   after c.v. = 6.0%.

Figure 14.   Handsheet formation before and after coating -   #46
             poor base sheet formation before - before c.v. = 10.2%,
             after c.v. = 6.9%.

despite the heavy coating layer of 20 g/m^2. The effect of coating on a base sheet with good and bad formation is shown in Figs. 13 and 14. The effectiveness of the coating in improving the formation of the base sheet is shown in Fig. 15 and 16 which show line scans of light transmission before and after coating for samples #11 and #46 shown in Fig. 13 and 14 respectively.

3. COMBINED STRESS MEASUREMENTS

Combined stresses, particularly combinations of out-of-plane stresses, occur in a number of converting processes such as corrugating and calendering. In past work we have investigated out-of-plane shear deformation behavior and in student-related work supercalendering.

An out-of-plane biaxial device for measuring the deformation behavior of paper and board when subjected to combined out-of-plane stresses has recently been designed and fabricated. It is based on a device originally developed by Arcan, Hashin, and Voloshin[1], for measuring the in-plane shear deformation behavior of composites.

The out-of-plane biaxial fixture without the sample holder in place is shown in Fig. 17. The paper sample size is nominally 1 in. x 3/4 in. and is bonded to the sample holder using photographic mounting tissue following a similar procedure adopted for making out-of-plane shear deformation measurements (Waterhouse J. F., Tappi 67 (6) June 1984). The sample holder with a 42-lb linerboard sample in place is shown in Fig. 18. The biaxial fixture with the sample and sample holder in place is shown in Fig. 19. This assembly is then loaded into the Instron and depending on the hole settings selected, the sample

---

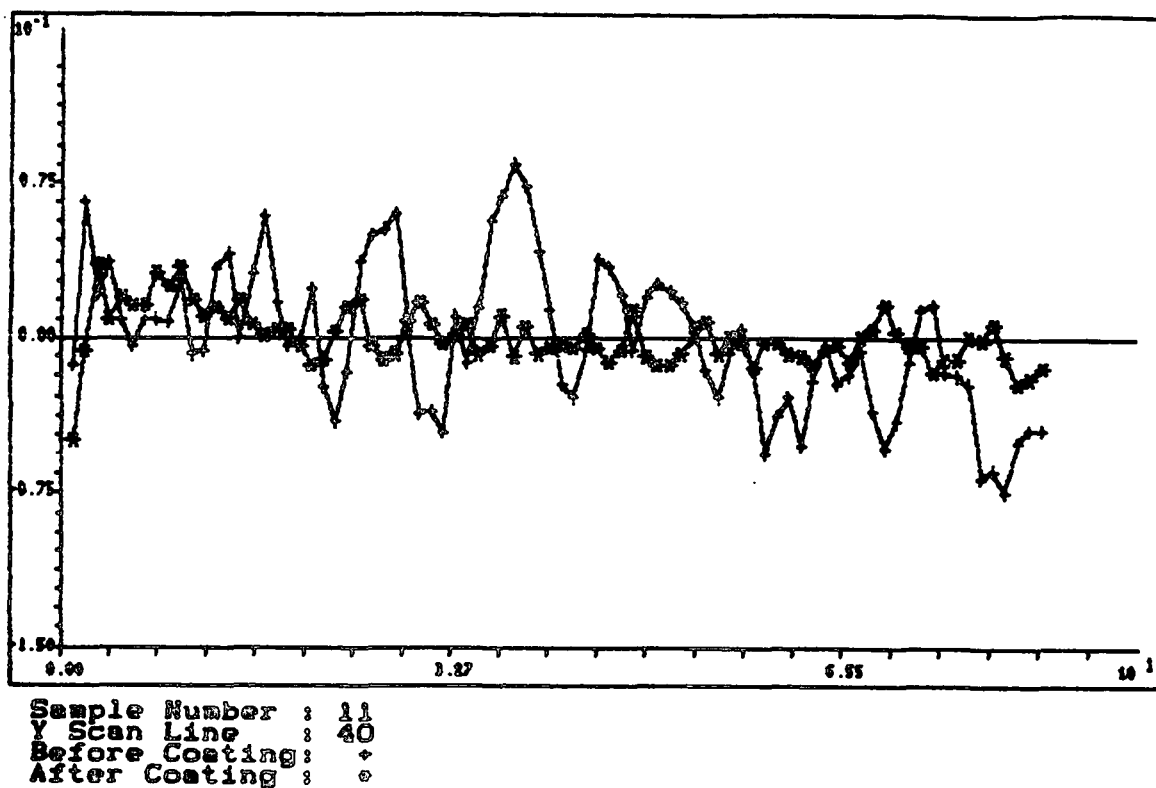[1]Arcan. M., Z. Hashin, and A. Voloshin. Experimental Mechanics 18 (April, 1978) pg. 141-146.

Sample Number : 11
Y Scan Line : 40
Before Coating: ◇
After Coating : ⊙

Figure 15.   The variation of transmitted light as a function of
             position - #11 single scan line 40 before and after
             coating.

Sample Number : 46
Y Scan Line : 40
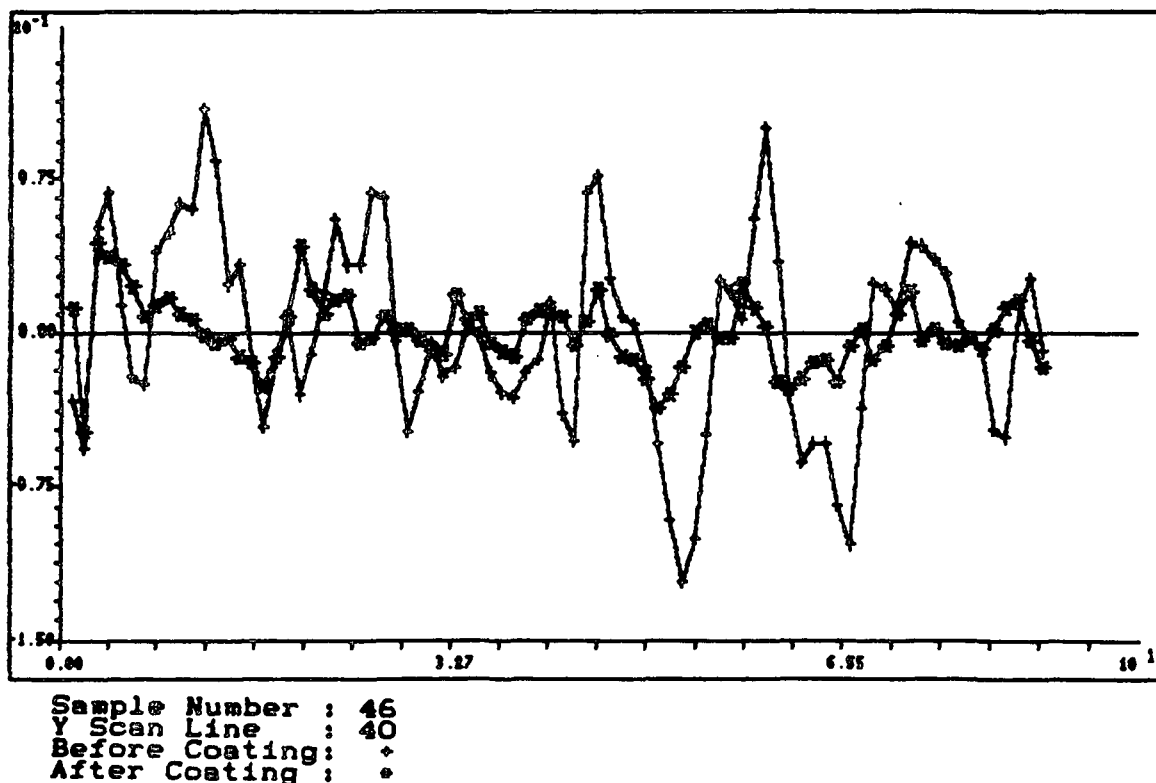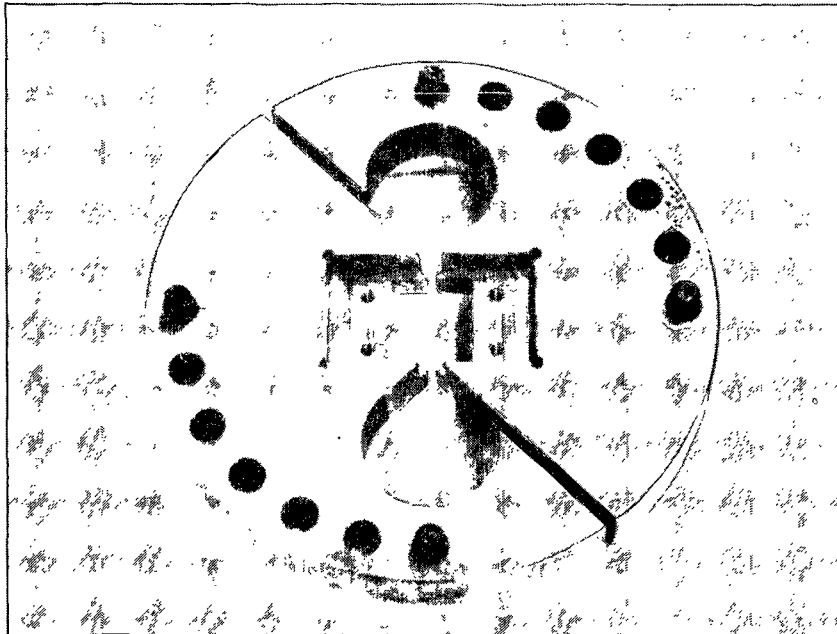Before Coating: ◇
After Coating : ●

Figure 16.   The variation of transmitted light as a function of
             position - #46 single scan line 40 before and after coating.

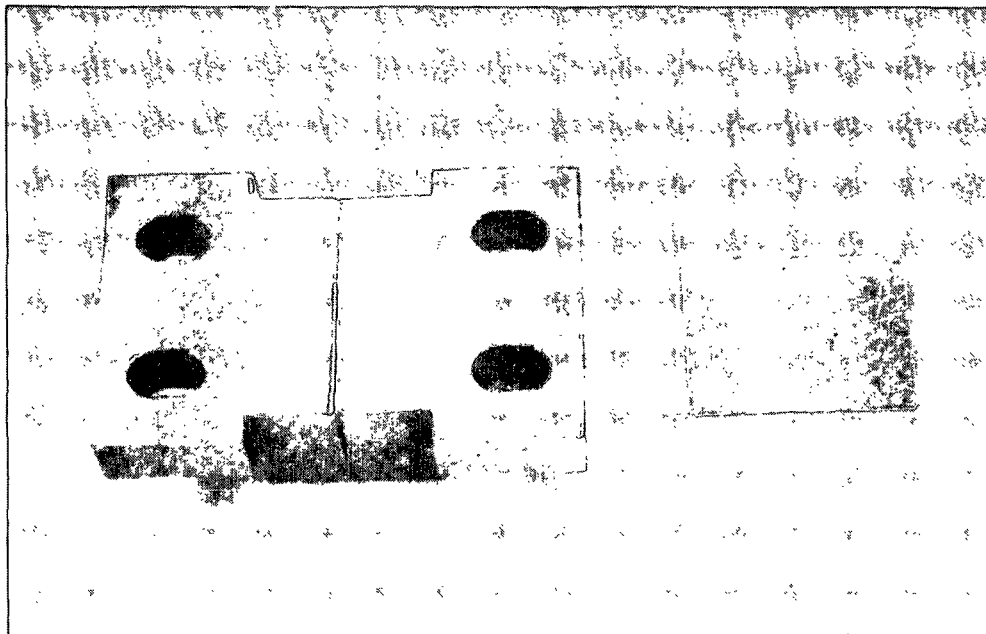Figure 17. Out-of-plane biaxial fixture without sample holder.
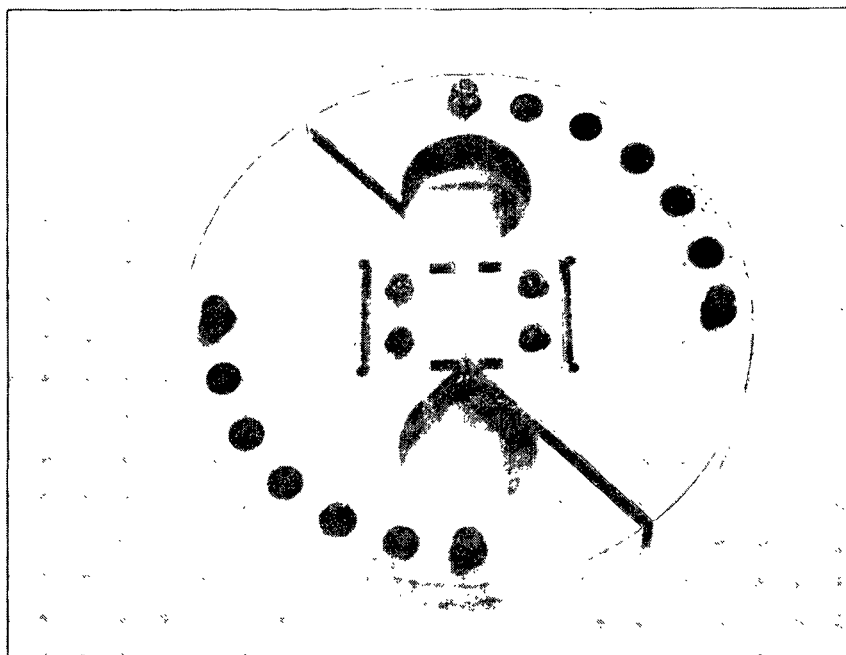

Figure 18. Sample holder.

Figure 19.   Out-of-plane biaxial fixture with sample and holder
             in place.

4. INTERNAL STRESSES IN PAPER AND BOARD

Internal stresses in paper and board are an important factor in converting and end use behavior. These stresses which are generated during the papermaking process may be modified during converting, and can play an important role in dimensional stability related problems such as curl, and some elastic and failure properties.

A presentation entitled "The Layer Removal Technique for Determining Residual Stresses in Paper" was made at the 1988 International Symposium held at Miami University, Oxford, Ohio May 16-19 1988. The theme of this meeting was "Paper, a Physically Engineered Product".

With regard to the importance of residual stresses in curl problems we have begun to examine the problem of off-axis curl, i.e. its likely causes and prediction. The recent development of the Robotic in-plane tester is an important new tool for analyzing and understanding this problem.

OTHER WORK

A paper "Monitoring the Effects of Aging" has been prepared for presentation at the 1988 Tappi Paper Preservation Symposium, Washington D.C. October 20, 1988 and is included in Appendix 1. This paper is based on a presentation made to the Committee on Preservation of Historical Records in 1985 and organized by the National Academy of Sciences.

STUDENT RELATED WORK

1. "Strength Development through Internal Fibrillation and Wet Pressing" is the title of Tom Bither's doctoral research. In recent work Tom has made some interesting measurements of fracture toughness and pore size distribution on handsheets which have varying levels of refining and wet pressing. He basically finds that at a given level of apparent density refining produces smaller pores and a higher level of fracture toughness than does wet pressing.

2. "The Interaction of Base Paper and Coating on Coated Paper Properties", is the title of Mikko Jokkio's A290 Research Project which has been mentioned previously.

Appendix 1

MONITORING THE AGING OF PAPER

John F. Waterhouse
Research Associate
The Institute of Paper Chemistry
Appleton, WI 54912

ABSTRACT

This paper briefly reviews the degradation mechanisms and environmental factors affecting the aging of paper, as well as methods for measuring its progress. Prospects for employing nondestructive procedures such as ultrasonic wave propagation techniques for monitoring the extent of aging are also discussed.

INTRODUCTION

Most materials will undergo some form of breakdown or degradation during their lifetime. The extent of degradation will depend on the material, its environment, and the mechanisms involved. This is an important, and often neglected area of research, particularly so in the case of paper. The magnitude and seriousness of this problem was the subject of recent hearings on information storage at the National Archives by the Committee on Preservation of Historical Records (1) in which this author participated. Paper as an archival material and its deterioration was a major concern of this committee. Presently 3 billion pieces of paper are resident in the National Archives, 530 million of which are considered to be at a high risk of loss.

We certainly need to learn more about deterioration, its amelioration and simulation. There is also a concomitant need to be able to effectively monitor the process of deterioration, which is the main subject of this paper.

A number of terms have been used to describe the deterioration of paper including aging, loss of permanence, and durability. Browning (2) defines permanence and durability as follows:

  "Permanence refers to the retention of properties such as strength and color over extended periods. It is influenced by both internal factors (e.g., chemical composition) and external conditions (the effect of light, atmospheric contaminants, etc.)."

  "Durability refers primarily to the ability of the paper to fulfill its intended function during intensive usage without reference to long periods of storage."

Browning also states, "A paper may be permanent (in retaining its original characteristics) but nondurable (e.g., because of low initial strength), or durable (in resisting intensive usage over a short period) but nonpermanent (e.g., because of the presence of acids).

Although the emphasis would probably be on permanence for archival usage, a minimum level of

durability would be required to access stored information. In library usage circulating books will require an even higher level of durability but nowhere near as high as might be demanded by currency. It is also interesting to note that one of the main measurements of permanence is the fold test - also a measurement of durability! The general term aging is used in what follows to embrace both permanence and durability.

The degradation of paper is complicated by the mechanisms involved and their dependence on raw materials and the papermaking process. In what follows we will briefly consider how some of the mechanisms and environmental factors affect aging and its measurement and the prospects for monitoring it nondestructively.

DEGRADATION MECHANISMS AND ENVIRONMENTAL FACTORS AFFECTING THE AGING OF PAPER

The mechanisms which may occur under natural and simulated aging conditions listed below have been investigated and reviewed by a number of researchers (3-7):

* HYDROLYSIS
* OXIDATION
* CROSSLINKING
* THERMAL DEGRADATION
* PHOTOCHEMICAL

These reactions can also be affected by the following environmental factors:

* Temperature and Moisture
* Radiation
* Pollutants
* Biological and Chemical
* Mechanical

The above mechanisms and environmental factors will usually result in changes at the molecular level: however, they may be more conveniently monitored at other levels of organization, i.e., changes in fiber or bond strength, optical properties, or viscoelastic behavior.

Wilson and Parks (6) specifically discuss these mechanisms in relation to their effect on measurable changes in the physical, chemical, and mechanical properties of paper. Table 1 of their paper, reproduced below, summarizes these effects and their direction.

Table 1 illustrates the complexity of the relationship between measurable properties and possible reactions. Clearly no single measurement would be a satisfactory indicator of the type of reaction which had taken place during aging. Furthermore the monitoring of properties which are enhanced by certain reactions, e.g., modulus and wet strength, might be misleading indicators of the actual state of degradation.

Not included in Table 1, although discussed by Wilson and Parks (6), are changes in crystallinity. Atalla (8) has also discussed changes in crystallinity and polymorphic form in cellulose as a result of pulping and environmental variables, and their implications for paper conservation.

Table 1. Reactions, or changes that might occur during natural and accelerated aging of paper and their effects on various tests. [Taken from Wilson and Parks (6) courtesy of the Restaurator.]

Reaction or Change: P = Primary, S = Secondary

Test	Hydrolysis P	Hydrolysis S	Oxidation P	Oxidation S	Crosslinking P	Crosslinking S	Bonding "Order"[a] Decrease P	Bonding "Order"[a] Decrease S	Thermal[b] Decomposition P	Thermal[b] Decomposition S
DP[c]	↓		↓	↑	↑		--	--	↓	
Acid, H+		↑	↑		--		--	--	↑	
Carboxyl		↑	↑			↓	--	--		
Aldehyde	↑		↑↓			↓	--	--	↑	
Ketone	--	--	↑			↓	--	--	↑	
Peroxide	--	--	↑		--	--	--	--	↓	
Moisture regain	--	--	↑↓		↓		↑		--	--
Alkali solubility	↑		↑		↑		--	--	↑	
Fold	↓		↓		↓			↓	↓	
Tear	↓		↓		↓			↑	↓	
Burst	↓		↓		↓		↓		↓	
Tensile	↓		↓		--	--		↓	↓	
Elongation	↓		↓		↓		↓		↓	
Modulus	↓		↓		↑		↓		↓	
TEA[d]	↓		↓		↓		↓		↓	
Zero span	↓		↓			↓	--	--	↓	
Wet tensile	↓		↑	↑			--	--	--	--
Blue reflectance	↓	↓	↓		--	--	--	--	↓	

[a]Includes degradation of bonds formed by sizing agents.
[b]Probably occurs only during accelerated aging.
[c]Degree of polymerization.
[d]Tensile energy absorption.

METHODS FOR MONITORING THE PROGRESS OF AGING

The properties listed in Table 1 for monitoring the progress of aging might be updated to include other endurance tests such as fatigue, creep failure, and flex testing. In the area of nondestructive testing, ultrasonic, electrical, and even subjective testing might be added. Next we will briefly discuss endurance and tensile testing before considering nondestructive testing using ultrasonic techniques as a possible means of monitoring the state and progress of aging.

Destructive Testing

Fold endurance is one of the most sensitive indicators of both permanence and durability, although it is not particularly well understood. The test is highly variable, and only a small area of the sample is tested. Special precautions are necessary to ensure constant temperature and moisture in the fold area. The sample is subjected to a complex stress situation as shown in Fig. 1.
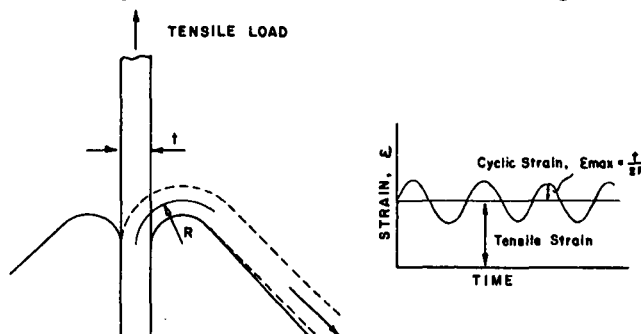

Fig. 1 Schematic of MIT fold tester and sample strain history.

Superimposed on a constant tensile stress is a cyclic bending stress, and in some cases a significant shear component is developed. The magnitude of these stresses will depend on the deformation behavior of the paper.

Cardwell, Lyon, and Luner (9) have suggested that it is more meaningful to compare fold results at the same ratio of applied load to failure load. The present author (10) also used a similar idea and calculated the ratio of applied stress to failure stress to account for differences in sample grammage and polymer content when measuring the fold endurance of polymer impregnated paper as shown in Fig. 2.
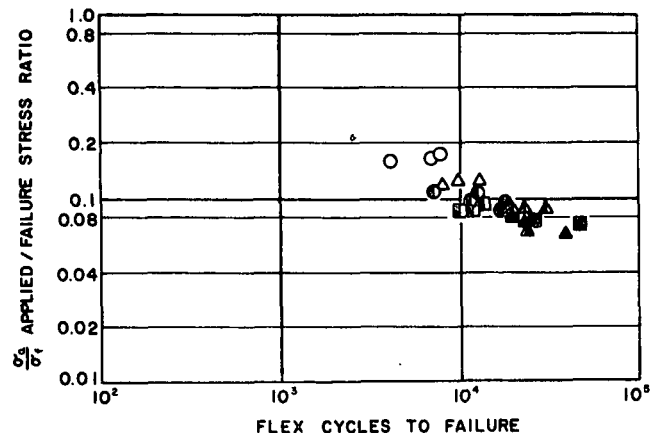

Fig. 2 Flex cycles to failure as a function of applied stress for neoprene impregnated handsheets of varying grammage.

Creep failure (duration of load) is another form of endurance test which involves measuring the times to failure at various levels of applied load. It has been suggested by Coleman (11), Fulmer and Guthrie (12), and Caulfield (13), that creep failure and fold can be modeled by applying the theory of absolute reaction rates. This modeling suggests that there is no essential difference in the mechanism leading to failure in a creep or fatigue test of certain materials.

In comparing the creep and fatigue behavior of polymethylmethacrylate, Penn and McKenna (14) reported that fatigue measurements fell between two boundaries comprising creep and fatigue predictions. In metal fatigue, fracture mechanics is the main approach, where failure is controlled by the rate of crack growth per cycle.

The flex tester developed by Graminski (15) is probably closer to simulating end use performance where durability is important, i.e., the handling of currency. One important difference in the flex test is that a larger area of the sample is tested. The applied stresses are similar to those of the fold tester, although the bend radius is larger. Graminski investigated how the tensile load elongation curve is affected by flexing. For a high grade rag paper there appears to be a loss in modulus with flexing, and after about ten thousand flexes there is a reduction in both tensile and elongation. It would be interesting to determine how aged samples perform on the flex test.

The tensile load/elongation curve may be modified in a number of ways by aging. In an accelerated aging test (Fig. 3) Graminski (16) has shown that modulus increases, whereas maximum load and elongation both decrease. TEA is also significantly reduced.
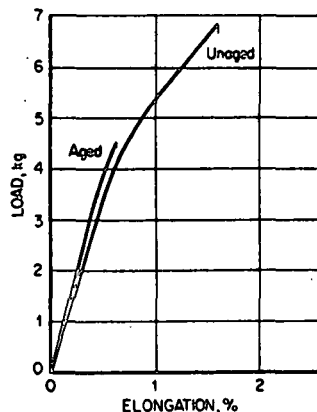

Fig. 1. Load-elongation curves of paper unaged and aged 15 days at 90°C and 50% RH.

Fig. 3 Effect of aging on the load elongation behavior of paper [taken from Graminski (16) courtesy TAPPI.]

Graminski suggested that the increase in initial modulus may be due to an increase in crosslinking or crystallinity. Page (17) found, using accelerated heat aging, a slight increase in normal span tensile strength before it decreased at the highest level of beating. This is explained by a loss in fiber strength being offset by an increase in bond strength.

It would seem reasonable, in view of Graminski's results, that fold endurance should correlate with TEA. Using the data of Wilson and Hebert (18), Fig. 4 illustrates that there is indeed a reasonable correlation.

Nondestructive Testing

Although a number of nondestructive test methods are possible for determining the aging of paper, we will limit our consideration to ultrasonic techniques. There has been a significant development in these techniques as applied to paper over the last ten years. Procedures have been developed by Baum, Habeger, and Wink for determining both in-plane and out-of-plane elastic constants of paper (19-20), as well as relating these measurements to the end use performance of paper (21). Ultrasonic techniques have also been developed by Baum and Habeger (22) for the on-line measurement of mechanical properties; and in more recent work Pankonin and Habeger (23) have developed techniques for measuring the ultrasonic viscoelastic parameters of paper.

Ultrasonic measurements were one of a number of techniques employed by Smith (24) to monitor changes in sonic modulus with years since publication of identical books kept in libraries in Appleton, Chicago, and New York. Smith's results are shown in Fig. 5. Although the sonic modulus

differences are not statistically significant, other measurements he made support the trend shown in Fig. 5 that the books in the New York library became embrittled with age due to air pollution.
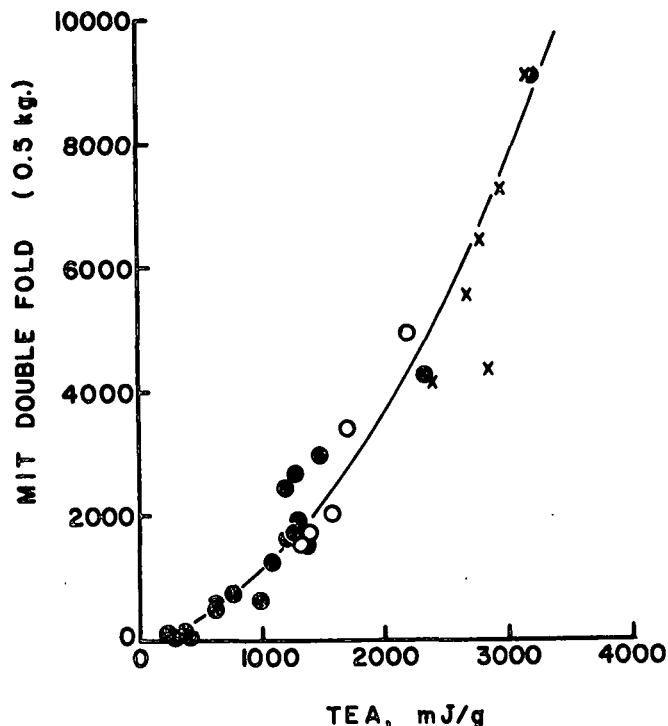

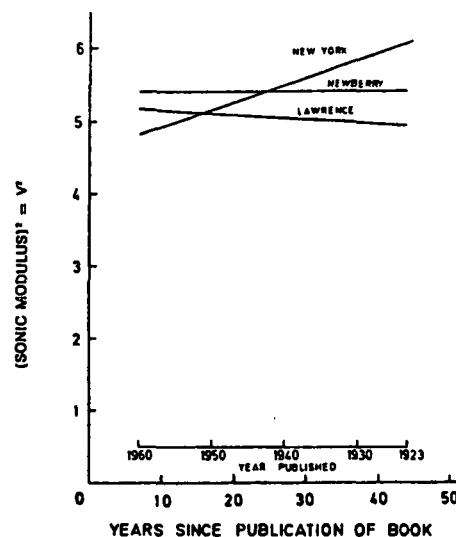**Fig. 4** Variation of MIT double fold with TEA using data of Wilson and Hebert (18).

Fig. 5 Sonic modulus measurements of aging. [Taken from Smith (24) courtesy of the Restaurator.]

Some in-plane and out-of-plane ultrasonic measurements of heat aged samples made by Waterhouse and Brennan (25) are shown in Table 2.

Table 2. Ultrasonic testing of heat-aged paper samples.

Sample Scratch Pad Paper	Basis Wt., g/m²	Density, g/cm³	$\overline{E}/\rho$, (km/sec)²	E_z/ρ, (km/sec)²
Control	59.3	0.791	7.23	0.102
Heat aged[a] 30 min	58.5	0.797	7.85	0.102
Heat aged[a] 60 min	57.5	0.783	7.64	0.102
Heat aged[a] 120 min	58.0	0.802	7.73	0.0995
Heat aged[a] 180 min	56.2	0.776	7.59	0.0989

[a]Air circulating oven 400°F.

These results were somewhat disappointing in view of the fact that the 120 and 180 min heat aged samples were extremely delicate.

Further work is therefore required to determine if more meaningful measurements of the aging process can be made. In addition to exploring other frequencies we would also like to determine the extent of changes in viscoelastic behavior.

An interesting study has recently been conducted by Barrett (26) to determine why certain European handmade papers have such excellent permanence and durability compared with papers made in the same time period (1400-1800) which are in very poor condition. As part of this investigation ultrasonic and other measurements were made at IPC on good and poor samples supplied by Barrett and are summarized in Table 3.

Table 3. Characterization of handmade papers made between 1400 and 1800. [Taken from Barrett (24)].

Sample #/year	Grammage g/m²	IPC Density g/m³	E_z/ρ (km/sec)²	E/ρ (km/sec)²	G/ρ (km/sec)²	Grain Ratio	Zero Span km/g	% Gelatin Predicted	pH
GOOD CONDITION									
G12/1483	91.8	0.869	0.419	6.07	2.47	1.13	84	10.8	7.3
	96.4	0.742	0.455	5.83	2.27	1.41	--	--	--
G17/1400	85.4	0.638	0.389	6.16	1.84	1.56	74	--	7.5
G1/1685	78.7	0.819	0.275	6.07	2.19	1.23	111	9.7	--
G2/1701	74.6	0.823	0.334	6.13	2.23	1.39	108	12.1	7.9
G3/1704	84.6	0.793	0.317	6.43	2.51	1.27	107	--	8.4
POOR CONDITION									
P39/1590	61.5	0.797	0.042	3.16	1.07	1.36	87	7.12	4.4
P32/1685	89.1	0.907	0.064	2.86	1.12	1.34	74	--	6.4
P35/1695	62.5	0.769	0.068	2.84	1.12	1.47	66	2.71	5.0
P46/1710	75.8	0.780	0.137	3.60	1.33	1.21	77	--	6.4
P44/1711	70.6	0.847	0.058	2.99	1.39	1.32	81	6.07	6.5
	71.6	0.840	0.062	3.20	1.39	1.65			

It is interesting to note that the in-plane and out-of-plane elastic constants of the good papers are much higher than those of the poor papers. In fact the out-of-plane constants of the good papers are considered to be very high compared with present day printing and writing papers. It later became clear that gelatin was the main factor responsible for the high elastic constants. The poor samples contained a lower percentage of gelatin, and FTIR measurements indicated that it was in a degraded state and that pH values were on the acid side. There were also strong indications that fiber strength (zero-span strength) of the poor papers was also reduced.

In Barrett's study ultrasonic measurements served two main purposes: first they provided data on the magnitude of elastic constants to be expected for European papers made in this time period, and secondly they identified which were the poor papers. Further work will be required to determine

if these and other nondestructive measurements can identify the reason for the difference in performance between the the good and poor papers, i.e., were the good papers stored in a more favorable environment or were there vital composition and manufacturing differences?

PROSPECTS FOR NONDESTRUCTIVE TESTING

The complexities of the aging process, both chemical and mechanical, make it difficult at the moment to envisage a single test which might be used to predict unambiguously the overall mechanical condition of an aged sample of paper. There is obviously a need to investigate the effects of raw materials, papermaking process variables and different aging mechanisms on the viscoelastic properties of paper using ultrasonic and other nondestructive techniques. There is also an associated need of increasing our understanding of how aging mechanisms affect property measurements at different structural levels of organization within paper.

REFERENCES

1. Preservation of Historical Records. National Research Council, National Academy Press, Washington, D.C., 1986.

2. Browning, B. L. Permanence. IPC Bibliographic Series No. 213, Editors Byrne, J. and Weiner, J., 1964.

3. Luner, P., Tappi 52(5):796-805(May, 1969).

4. Roberson, D. D., Tappi 59(12):63-9(Dec., 1976).

5. Browning, B. L. and Wink, W. A., Tappi 51(4): 156-62(April, 1968).

6. Wilson W. K. and Parks E. J., Restaurator 3: 37-61(1979).

7. Luner, P., Wood Sci. Technol. 22:81-97(1988).

8. Atalla, R. H. Preservation of Paper and Textiles of Historic and Artistic Value. Editor Williams, J. C., Vol. 2, 1979, Advances in Chemistry Series 193, American Chemical Society, 1981.

9. Cardwell R., Lyon, L., and Luner, P., Tappi 55 (2):228-33 (Feb., 1972).

10. Waterhouse J. F., unpublished work.

11. Coleman, B. D., J. Polymer Sci. 20:447-55(1956).

12. Fulmer, G. E. and Guthrie, J. L., J. Appl. Polymer Sci. 13:445-58(1969).

13. Caulfield, D. F., Wood Fiber Sci. 17(4):504-21 (1985).

14. Penn, R. W. and McKenna G. B. Durability of Macromolecular Materials. Editor Eby, R. K., ACS Symposium Series 95, American Chemical Society, 1979.

15. Graminski, E. L. 5th International Fundamental Research Symposium, Cambridge, Sept., 1973.

Tech. Sect. B.P.B.M.A.

16. Graminski, E. L., Tappi 53(3):406-10(March, 1970).

17. Page, D. H., Tappi 52(4):674-81(April, 1969).

18. Wilson, W. K. and Hebert R. L., Tappi 52(8): 1523-9(Aug., 1969).

19. Baum, G. A., IPC Technical Paper Series No. 119, Dec., 1981.

20. Habeger, C. C. and Wink, W. A., J. Appl. Polymer Sci. 32:4503-40(1986).

21. Baum, G. A., Appita 40(4):288-94(July, 1987).

22. Habeger, C. C. and Baum, G. A., Tappi J. 69 (6):106-10(June, 1986).

23. Pankonin, B. and Habeger, C. C. J. Polymer Sci. Part B, Polymer Physics 26:339-52(1988).

24. Smith, R. D., Restaurator Suppl. 2, 1972.

25. Waterhouse, J. F. and Brennan, D. B., unpublished work.

26. Barrett, T. J. Early European Papers/ Contemporary Conservation Papers., Research Report, School of Art and Art History, University of Iowa, Iowa City, Iowa, 1987.

THE INSTITUTE OF PAPER CHEMISTRY

Appleton, Wisconsin

Status Report

to the

PAPER PROPERTIES AND USES

PROJECT ADVISORY COMMITTEE

Project 3526

INTERNAL STRENGTH ENHANCEMENT

October 19-20, 1988

PROJECT SUMMARY

PROJECT NO. 3526: INTERNAL STRENGTH ENHANCEMENT

PROJECT STAFF: R. Stratton, K. Hardacker   September 12, 1988

PROGRAM GOAL: Bring new attributes to fiber based products

PROJECT OBJECTIVE:

To improve internal strength and moisture tolerance in paper and paperboard.
The short term goals are to establish those parameters fundamental to inter-
fiber and intra-fiber bonding in conventional and ultra high yield pulps and to
control these parameters, if possible, by chemical or mechanical treatments.

PROJECT RATIONALE, PREVIOUS ACTIVITY, AND PLANNED ACTIVITY FOR FISCAL 1988-89
are on the attached 1988-89 Project Form.

SUMMARY OF RESULTS LAST PERIOD: (October 1987 - March 1988)

(1) Internal addition of rigid SBR latex produces substantial enhancement of
    properties. At equal composition external addition of latex provides better
    tensile strength but internal addition provides better compressive strength.

(2) Sheets externally treated with latex can be readily repulped with good
    dispersion of the fibers.

(3) Treatment with either the SBR latex or PAE leads to reduced sheet wet-
    tability as measured by the water drop test. This may result in glueability
    problems with water-based adhesives.

(4) Treatment with PAE results in large increases in tensile strength but much
    lower increases in compressive strength. Conversely, subsequent treatment
    with CMC adds a small and a large increment to these two strength values,
    respectively.

(5) Internal addition of PAE or PAE/CMC produces stronger sheets than does
    external addition. The presence of the strength aid(s) within the bond area
    is more effective than when it is relegated to the periphery of the bond.

(6) The combination PAE/CMC produces greater strength enhancement than PAE
    alone.

(7) External treatment of corrugating medium with PAE alone or combinations of
    PAE/pearl starch or PAE/CMPS enhance MD and CD tensile and compressive
    strengths.

(8) The statistical analysis of the fiber/fiber single bond studies has been
    completed and a report covering this work is being written.

SUMMARY OF RESULTS THIS PERIOD: (March 1988 - October 1988)

(1) The instrument to measure bond strength using sheets has been constructed.
    Improvements over previously used models include a frictionless air bearing
    in place of high precision ball bearings.

(2) Techniques have been developed to prepare sheets for use with this instru-
    ment, to operate the instrument, and to measure the scattering of the sheets
    before and after delamination.

(3) The effects of crosshead speed and basis weight on the bond strength deter-
    mination have been characterized.

(4) A series of pulps with yields from 47 to 80% were produced by kraft cooking
    southern pine. These were beaten to several levels of freeness. A portion
    of each of the beaten pulps was then classified on the IPC Web Former. Some
    fines from each of the four yields were retained for later addition back to
    the pulp. This series of pulps will be used to study the effects of yield,
    refining, and fines on bond strength using the standard tests and the new
    instrument described above.

(5) Measurements on the whole pulps at the two lowest yields have been
    completed. The results are being analyzed.

(6) Adsorption experiments showed virtually all PAE is adsorbed on whole pulps
    at the usual dosages.

(7) Photomicrographs of ruptured tensile specimens treated at various levels
    with PAE/CMC revealed a shift in mode of failure from bond strength-
    controlled to fiber strength-controlled with increasing dosage.

(8) In preparation for joint experiments with Bill Whitsitt on the effect of
    strength additives on corrugated containers, several additive systems were
    screened for their effect on the wettability of the linerboard and medium.
    Two systems were found which should enhance the strength of the components,
    have little effect on glueability, and permit facile recycling of the corru-
    gated board.

(9) A paper covering some of the work on this project presented at recent PAC
    meetings has been written and will be presented at the Paper Chemistry
    Symposium 1988 in Stockholm, September 27-29. A copy of the paper is
    appended to this report.

PROJECT TITLE: Internal Strength Enhancement

PROJECT STAFF: R. Stratton/K. Hardacker

PRIMARY AREA OF INDUSTRY NEED: Properties related to end
                                 use

| Date: 2/3/88 |
| Budget: $200,000 |
| Period Ends: 6/30/89 |
| Project No.: 3526 |

PROGRAM AREA: Moisture tolerant, superior strength paper
                and board

PROGRAM GOAL: Bring new attributes to fiber based products

PROJECT OBJECTIVE:

To improve internal strength and moisture tolerance in paper and paperboard.
The short term goals are to establish those fundamental parameters affecting
inter-fiber and intra-fiber bonding in conventional and ultra high yield pulps
and to control these parameters, if possible, by chemical or mechanical treat-
ments.

PROJECT RATIONALE:

Major limitations of paper and board for many uses are low internal bond
strength and poor moisture tolerance. Improved internal strength and enhanced
moisture resistance would allow a number of present grades to be produced using
less fiber and would also allow new end uses to be developed.

At present, commercial papers do not attain strength levels that realize the
full potential of the wood fibers. Most paper mechanical properties are
markedly degraded with increasing moisture content. We need to better
understand the nature of fiber properties and fiber-to-fiber bonding and changes
in them with increasing moisture content, if we are eventually to improve the
moisture tolerance of paper.

RESULTS TO DATE:

The major areas of activity and results can be separated into two areas:
handsheet studies of strength enhancement by chemicals; and bonding studies at
the level of individual fibers. A number of polymers have been shown to be
effective strength aids for a variety of chemical and mechanical pulps. In par-
ticular, combinations of a cationic polymer followed by an anionic polymer have
provided substantial improvements in dry (50% RH), moist (92% RH), and wet ten-
sile strength. Although fines contribute to strength, polymer adsorbed on long
fiber is much more effective in improving strength than that adsorbed on fines.
Use of a rigid SBR latex provided marked improvement in compressive strength
measured at high humidity. Techniques have been developed to prepare, handle,
and measure individual fiber/fiber bonds. Significant improvements in bond
strength were achieved when strength aids were used. For unrefined fibers the
location of bond failure (as observed in the scanning electron microscope) was
shifted from between the fibers to within the fiber wall by the addition of a
strength aid. Unrefined latewood fibers were found to produce stronger bonds
than earlywood fibers. Comparison of lightly refined to heavily refined fibers

showed that the strength of individual bonds did not change with refining. When wet strength is not required, the use of strength aids acting by ionic interactions only allows the preparation of sheets that can be readily repulped.

Individual fiber bonds prepared using such additives were as strong as those made with covalently-bonding strength aids. Measurements of the loss of individual bond strength with increasing moisture content paralleled the similar losses in sheet strength and individual fiber axial strength.

PLANNED ACTIVITY FOR FY 1988-89:

An instrument will be constructed which will allow the measurement of bond strength using sheets.

This instrument will be used along with conventional tests to assess the effects of pulp yield, refining, type and level of addition of strength aid, and fines content on bonding. Correlations with in-plane and out-of-plane ultrasonic measurements will be sought to clarify the influence of bonding on these potentially on-line tests.

Methods will be developed to determine the relative contributions of fiber strength and bond strength when strength additives are employed.

Other additive systems will be explored as either internal or external treatments to enhance tensile and compressive strength under normal and high relative humidity conditions.

STUDENT RELATED RESEARCH:

J. E. Biasca, Ph.D.-1988; P. R. Proxmire, Ph.D.-1988; M. T. Goulet, Ph.D.-1988, C. O. Luettgen, Ph.D.-1990; C. E. Miller, Ph.D-1989; S. L. Molinarolo, Ph.D.-1988; D. L. Horstmann, M.S.-1989; M. W. Sachs, M.S.-1989; J. H. Breining, M.S.-1988; M. A. Friese, M.S.-1988.

Status Report

INTERNAL STRENGTH ENHANCEMENT

Project 3526

BOND STRENGTH MEASUREMENTS

In previous work on this project we have measured bond strength using individual fiber/fiber pairs. We have explored the effects of refining, type of pulp, strength aid treatment, and moisture content on the bond strength and have reported these results in previous Status Reports. We have a number of other parameters that need to be investigated but the time required to obtain the data renders the single-fiber technique infeasible. In addition, some objections can be raised concerning the validity of the technique itself.

To avoid these objections and to facilitate the collection of the needed data in a timely manner, we have chosen to use a different technique which uses a sheet of paper instead of a single fiber/fiber bond. This inherently measures a large number of individual fiber/fiber bonds simultaneously and precludes the need for a large number of tests to obtain a statistically significant average value for the strength. The technique has been recently described by Skowronski and Bichard (1) and was used much earlier to test the peeling strength of laminated metals (2). Essentially the force required to split a piece of paper at a constant rate is measured in an Instron tensile tester. The strip of paper is attached to a freely turning wheel which maintains the angle of splitting (peeling) at a constant value near 90°. The results are normalized on a bonded area basis using the concept of Nordman et al. (3) of the relationship between optical scattering and unbonded area. Measurements of the scattering are made on the sheet before and after splitting and the increase is proportional to the new surface area created. This area is assumed to be equal to the area of the bonds that were broken in the test.

Apparatus

The attachment for the Instron is similar to that described previously (1). A major difference is that, instead of precision ball bearings, an air bearing is used to eliminate friction contributions to the measured force. The wheel is 4.78 cm in width and 14.27 cm in diameter.

Diffuse reflectance of the sheet (R_0 and R_∞) was measured with a TB-1C Technidyne reflectance meter.

Exploratory Measurements

Because paper is a viscoelastic material, it was necessary to determine the dependence of the peeling force on the rate of peeling. Samples were tested in the Instron at different crosshead speeds, and the results are shown in Table 1.

Table 1.   Effect of crosshead speed on bond
energy.

Speed, in./min	Bond Energy, J/m^2
0.5	58.6
1.0	60.5
2.0	63.6
5.0	63.8
10.0	64.8

Although there is a definite trend of increasing bond energy with increasing rate of peeling, it is only about 10% over a 20-fold range in speed. For future work an intermediate value of 1.0 in./min was chosen. This is also comparable with the rate used by previous workers: 2 cm/min (1).

The results depend upon measurements of both the delamination force and the optical scattering. The accuracy of the latter may be a function of the

sheet basis weight. A series of sheets prepared under identical conditions but with different basis weights were tested. The results are given in Table 2.

Table 2. Effect of basis weight on bond energy.

Basis Weight, g/m^2	Bond Energy, J/m^2
30	84.2
60	52.4
90	60.6
120	66.2

Except for the value at 30 g/m^2, there appears to be a trend for bond energy to increase with basis weight. For the 30 g/m^2 case the thinness of the sheet caused the split to occur very near the adhesive tape with an uneven amount of fiber being found on the tape. It is suspected that the bond energy for this sample is not valid. For the heavier basis weights the values for R_0 and R_∞ were only slightly different from one another. Since the scattering coefficient (Kubelka-Munk equation) depends on $R_0 - R_\infty$, poor accuracy resulted. Apparently, sheets in the intermediate range of basis weights should be most reliable.

The dependence on basis weight was further examined with the following results.

Table 3. Effect of basis weight on bond energy.

Basis Weight, g/m^2	Bond Energy, J/m^2
40	62.2
50	63.1 (0.4)
60	61.6 (1.4)

The values in parenthesis are the standard deviations for four repli-
cates. The variation among the three basis weights is approximately within the
reproducibility of the measurements. It is concluded that there is negligible
dependence on basis weight in the range examined.

It was noted that the sheets rarely split down the center. Usually
there was more fiber remaining on the wire side (which was the side facing away
from the wheel during the test.) Whether this reflects an uneven distribution
of properties in the z-direction caused by uneven distribution of density or
fines, or whether it is a result of the geometry of the peeling test is not known
at present. Local formation of the sheet seems to play a part, also. At any
rate, the reflectance factor R_0 measured through the sheet after the split is
dependent upon the side exposed to the diffuse illumination. To account for the
uneven split, scattering measurements were taken on both the wire and felt sides
of the sheet and averaged. This was performed on the sheet both before and after
the split and helps to reduce some of the experimental error in the measurement.

Pulps

The intent of this work is to determine the effects of pulp yield,
refining, fines content, and strength aid and their interactions on the bond
strength of paper. To accomplish this a series of pulps were produced by kraft
pulping from a single loblolly pine log. A broad range of yields were covered
as listed in Table 4.

Table 4. Pulp properties.

Pulp	Yield	Kappa No.
11	47.5	34.7
12	51.2	42.2
13	60.4	116.0
14	80.7	167.0

The cooked chips were passed once or twice (depending on yield) through a Sprout-Waldren disc refiner with 10 to 35 mil plate separation for defiberization. Subsequently, the pulps were beaten to various levels in a Valley Beater. The resulting freenesses of the eleven pulps are listed in Table 5.

Table 5. Pulp freeness.

Pulp	Freeness Levels, mL CSF
11	685 (unrefined), 600, 350, 200
12	740 (unrefined), 340
13	750 (unrefined), 600, 350
14	780 (unrefined), 340

The levels were chosen to provide a range of degrees of refining that might be similar to commercial practice for various grades and to allow comparison among the four pulps. The influence of yield on fiber stiffness is reflected in the unrefined freeness level.

To separate the effects of fines from those of fiber flexibility (yield and refining), portions of the seven beaten pulps were classified. This was achieved by twice passing the whole pulp at very dilute consistency (0.01%) over the IPC Web Former using a 72 x 56 mesh wire. Fines from the first pass of each of the four whole pulps with nominal 350 mL CSF freeness were retained. These were allowed to settle, and the supernatant liquid was decanted. Formaldehyde was added to the whole (dewatered), classified (dewatered), and fines to prevent biological growth. The materials were stored in a cold room at 40°F until used. We thus have a set of four unrefined, seven refined whole, and seven refined classified pulps, as well as the fines from four beaten pulps of different yields.

In addition to the bond strength tests, the usual physical properties will be measured. These will include tensile properties, STFI compression strength, zero span tensile strength, density, and the in-plane and out-of-plane shear and longitudinal stiffnesses as measured ultrasonically.

Handsheets will be prepared as usual on the Noble & Wood sheet mold except that the wet pressing will be done at one of five pressures. These pressures (0, 20, 50, 100, and 200 psi) will produce sheets with a range of densities and strengths and will permit estimations of relative bonded area according to the procedures of Ingmanson and Thode (4).

To date measurements have been completed on the unrefined and three beaten pulps from the material of 47.5% yield (pulp 11). Analysis of these results is in progress.

External Treatment of Liner and Medium

In the last Status Report we discussed work done in cooperation with Bill Whitsitt (Project 3571). We treated strips of corrugating medium by immersion in a bath containing either PAE, PAE/starch, or PAE/carboxymethylated potato starch. The treated strips were then used in the IPC corrugator to produce board. Difficulty in glueing was found in this last step and was traced to the presence of PAE in the sheet. Apparently, this material lowers the surface energy of the treated medium sufficiently to interfere with the wetting (penetration) of the adhesive during corrugated board production.

To overcome this problem, we have been examining other strength aid combinations. We have found two which, in addition to minimizing the wetting problem, also produce strength through ionic rather than covalent bonds. This

should lead to a product which is readily repulpable but will, of course, have no wet strength.

We plan to treat (externally) both liner and medium with these strength aids and to produce corrugated board from various combinations of the treated and untreated components. These studies should show the relative effects of improving the strength of the medium and/or liners on the corrugated board properties.

Adsorption of PAE

We have been using PAE as a strength aid for some time and have assumed that it is completely adsorbed. Recent work (5) has suggested that this may not be so. We, therefore, carried out an adsorption study of PAE on a beaten whole softwood, unbleached kraft pulp. The pulp at 0.5% consistency was treated with a given dosage of PAE, allowed to mix for 5 minutes, and then was filtered under vacuum on a 2.0 μm Nuclepore membrane. The filtrate containing any unadsorbed PAE was tested for its presence using a colloid titration technique. Here a cationic dye (orthotoluidine blue) and a fixed amount of an anionic polymer (potassium polyvinyl sulfate, PVSK) are mixed with an aliquot of the filtrate. The dye and the PVSK form a complex which alters the absorption spectrum of the dye. Cationic polymer binds to the PVSK more strongly than does the dye and if present will displace the latter. The absorption from the resulting "free" dye can be determined by spectrophotometer and the concentration of cationic polymer (here PAE) can be calculated from a calibration curve.

The results showed that at the usual level of addition, 1% PAE on fiber, approximately 96% of the PAE was adsorbed within five minutes. Thus, we can be confident that virtually complete adsorption of the PAE takes place.

Literature Cited

1. Skowronski, J. and Bichard, W., J. Pulp Paper Science 13(5), J 165(1987).

2. Aero Research Ltd., Duxford, Cambridge (England), Technical Notes, No. 59(1947), quoted by N. A. DeBruyne in "Adhesion and Adhesives", N. A. DeBruyne and R. Houwink, eds., Elsevier, New York, 1951, p. 463.

3. Nordman, L., Gustafsson, Ch., and Olofsson, G., Paperi ja Puu, 35(8), 315(1954).

4. Ingmanson, W. L. and Thode, E. F., Tappi, 42(1), 83(1959).

5. Neal, C. W., Notes 1988 TAPPI Wet and Dry Strength Short Courses, Chicago, April 13-15, p.1.

APPENDIX

Dependence of Sheet Properties on the Location of Adsorbed Polymer

Robert A. Stratton
The Institute of Paper Chemistry
Appleton, Wisconsin U.S.A.

SUMMARY

By choosing the point of addition of the strength aid, the papermaker
can control its location in the sheet. This study explored the effect of
various points of addition on dry (50% RH) and moist (92% RH) tensile and
compressive strength and on wet tensile strength. A combination of polyamide
polyamine epichlorophydrin (PAE) and carboxymethylcellulose (CMC) was used with
a southern pine unbleached kraft pulp.

Strength aids added separately to the classified pulp components (long
fiber and fines) produced the highest strengths when adsorbed on the long fiber
only. Attempts to achieve this effect (without classifying the pulp) by adding
the strength aid before beating were unsuccessful.

The much larger percentage enhancement of strength for classified com-
pared with whole pulps was shown to be due to a shift in the mechanism of
failure. Untreated sheets have a strength that is governed by the bond strength
between the fibers. With the addition of a strength aid, the bond strength is
increased and the individual fiber properties (fiber axial and wall strengths)
become the limiting factor.

Wet-end addition of strength aids was shown to be much more effective
than external additions. It is important to have the polymer within the
crossover region between two fibers (i.e., the bonded area) and not just around
the periphery of the bond. The combination of PAE and CMC produced greater

strength than PAE alone. Both tensile and compressive strengths could be improved by the combination, but the relative effect of the two polymers on the two strengths was different.

INTRODUCTION

The recent trend in papermaking is toward weaker sheets. This is a result of several factors: (1) lower basis weights, and increasing percentages of (2) hardwood, (3) secondary (recycled) fiber, and (4) mineral fillers. Despite these changes papermakers would like to maintain or even enhance the strength of the paper. To accomplish this, they have turned increasingly to the use of chemical strength aids. Although effective, these usually polymeric materials are rather expensive. It is essential to use them efficiently.

Strength aids may be added at a variety of points in the wet end or at the size press. The particular point of addition gives the papermaker some control over the ultimate location of the strength aid within the sheet. The work presented below was undertaken to clarify whether this "location" had a strong influence on the resulting sheet properties.

In the following discussion the "location" of the strength aid will be used in either of two senses. First, it will be concerned with whether the polymer is adsorbed on the long fiber fraction or the fines fraction of the pulp. In the second case it will refer to whether the polymer(s) is within the fiber/fiber bonded area or whether it is only external to this area. Both of these "locations" can be influenced by the point of addition.

EXPERIMENTAL

Materials

Southern pine unbleached kraft pulps were used. Because this work extended over a period of several years, a number of similar but distinct pulps were employed. All were in the 47-49% yield range. The pulps were beaten in a Valley beater to a level of about 350 mL CSF unless stated otherwise. In some cases the beaten pulps were classified by two passes at very dilute consistency (0.01%) over the IPC Web Former. The separated fines were saved for later readdition to the long fiber fraction.

A wet-strength aid, polyamide polyamine epichlorohydrin (PAE), which has also been shown to improve dry strength (1), was used in conjunction with carboxymethylcellulose (CMC). Espy (1) has shown that the latter provides a synergistic effect with PAE on the strength properties. The CMC was a low viscosity material with a 0.7 degree of substitution. Our exploratory studies showed that an addition ratio of 0.4:1.0 (CMC:PAE) was optimum in agreement with previous work (1). Unless otherwise indicated the addition rate was 1% PAE and 0.4% CMC based on o.d. pulp.

Tap water was used throughout and was adjusted to a pH of 4.5 unless otherwise indicated.

Procedures

Handsheets

The required amount of PAE solution, (1% w/v) was added to a vigorously stirred batch of pulp at 0.5% consistency. Moderate stirring was

then continued for five minutes. The CMC solution (1%w/v) was then added under
similar conditions. A series of handsheets was then formed from this treated
batch of pulp. An aliquot of the pulp sufficient to form a 62 g/m^2 sheet was
diluted to 0.04% consistency in a Noble & Wood sheet mold. After formation,
the sheet was couched from the 100 mesh monel wire onto blotters. The
sheet/blotter sandwiches were pressed at 50 psi for five minutes and then dried
on a steam drum at 105°C for seven minutes.

Tub Sizing

For some experiments sheets were formed as above but without one or
both of the additives. These (dried) sheets were then immersed in a tray con-
taining a solution of the additive at a concentration necessary to give the
desired pickup. After immersion for 30 sec, the sheet was passed through a
squeeze roll and dried on the steam drum at 105°C for seven minutes. Pickup
(dosage) was based on the wet weight of the squeezed sheet and the air dry
weight of the sheet before immersion. This assumes pickup is by imbibition of
the polymer solution only and neglects polymer adsorption effects. These should
be small at the short time and stagnant (no mixing) conditions of the immersion.
Sheets dipped in water-only trays served as controls to ascertain the effects of
rewetting the sheets and of additional drying (curing) time on the physical
properties.

Beating

For some experiments the strength aids were added before refining in
the following manner. A batch of pulp at 1.8% consistency was circulated in the
Valley beater with no load on the bedplate. The pulp was treated with 1% PAE
(based on o.d. pulp) and circulation was continued for two minutes. Treatment

with 0.4% CMC followed with further circulation for three minutes. (The shorter

times used here, compared with the handsheet studies, reflect the higher pulp

consistency and thus collision frequency.) After the polymers were added and

adsorbed, weight was added to the bedplate and beating for the desired time

was carried out. The beaten pulp was diluted to 0.5% consistency and handsheets

were formed as described above.

Testing

The dried handsheets were preconditioned at 20% RH, 73°F for 24 hours

and then conditioned at 50% RH, 73°F for 24 hours before testing. Dry and wet

tensile tests were performed according to the TAPPI Standard Methods T494 and

T456, respectively. Samples to be tested "moist" were conditioned at 92% RH,

73°F for 24 hours and then tested at those conditions.

Polymer Adsorption

The amount of PAE adsorbed on the pulp under the standard conditions

(0.5% pulp consistency, 5 minute contact time, moderate agitation) was deter-

mined by difference by measuring the amount of unadsorbed PAE. Samples of a

beaten pulp (350 mL CSF) were treated with various dosages of PAE (0.9-4.5% based

on o.d. pulp) according to the standard conditions listed above. At the end of

the contact time, the pulp slurry was quickly filtered on a Nuclepore 2.0 μm

membrane under vacuum. The filtrate was analyzed for PAE using a colloid titra-

tion method (2) with spectrophotometric detection.

RESULTS AND DISCUSSION

Polymer Adsorption

Because arguments in the following sections depend upon an assumed location of the strength aids, it is important to determine what fraction of the polymers are adsorbed under the standard conditions. The unadsorbed fraction may, of course, adsorb on the pulp's surface at a later time or form a complex in solution with an oppositely charged polymer. This latter event would defeat the effectiveness of both polymers.

When determining the adsorption of a polymer on a pulp containing fines, it is essential to separate the pulp from the supernatant solution by using a very small pore filter. Otherwise polymer adsorbed on colloidal-sized fines will be present in the supernatant and may be measured as unadsorbed polymer. The choice of a 2.0 μm pore size filter was a compromise between the conflicting goals of eliminating fines in the filtrate and of achieving a reasonable flow rate through the filter.

The adsorption at pH 4.5 of PAE on a beaten whole pulp was measured as described in the Procedures section. The results in Fig. 1 show that, at the dosage used in most of the experiments to be discussed (1% based on o.d. pulp or equivalently here 50 mg/L), approximately 96% of the PAE is adsorbed. A negligible amount remains unadsorbed, and hence the location of the PAE in the system can be assigned unambiguously.

(Figure 1 here)

The zeta potential of the fines of the PAE adsorption samples (and of other samples at lower dosages) was determined by microelectrophoresis. The isoelectric point is at a dosage of about 0.15%. The zeta potential at a PAE

dosage of 1% is + 14 mV. At higher dosages it appears to reach a plateau of + 18 mV. It is interesting that almost 100% adsorption is still possible at 1% dosage when the surface is strongly cationically charged.

It should be mentioned that the curve in Fig. 1 is not an equilibrium adsorption isotherm. Adsorption was measured after a contact time of five minutes. At low dosages equilibrium may have been reached, but certainly at the higher dosages with the concomitant highly charged pulp surfaces, more adsorption will occur with time.

Having proved the virtually complete adsorption of the PAE under our experimental conditions, we turn our attention to the subsequent adsorption of the CMC. Here Neal (3) has shown, over a similar range of dosages of PAE and CMC, that the CMC is completely adsorbed. Thus, we can be confident in the following studies that the PAE and CMC added to the pulp are essentially 100% adsorbed.

Location on Fibers and Fines

It is well-known that the presence of fines in a pulp enhances the strength properties. The exact mechanism is not clear. Likewise, how strength aids interact with fibers and fines to improve strength is not known. To distinguish the effects of strength aid adsorption on fibers and fines, we used a classified pulp and its associated fines. The whole pulp before classification had 12% fines determined by a Bauer-McNett classification through a 200 mesh screen. The several pulps and components were each treated with 1.5% PAE (based on o.d. pulp) and the four samples are denoted as follows:

a) Classified - Only the long fiber is treated and used to prepare
    handsheets.

b) Whole - The unclassified pulp is treated and used. This is equivalent
    to the typical addition method in the mill.

c) Separately - The classified pulp and the separated fines are each
    treated with PAE. The treated components are then blended in an 88/12
    fiber to fines ratio, and handsheets are formed.

d) Fiber only - The classified pulp is treated and is then mixed in an
    88/12 ratio with untreated fines.

The results are listed in Table I.

Table I. Effect of Polymer Location on Strength (1.5% PAE)

Treatment	Breaking Length, km		
	Dry	Moist	Wet
Classified	5.4	3.7	1.7
Whole	6.3	4.5	2.1
Separately	6.8	4.8	2.3
Fiber only	7.1	4.9	2.4

The effect of including the fines in the furnish can be seen by com-
paring the results for the "classified" and "whole samples". Fines increase all
three strength properties. It is well-known that fines adsorb a disproportion-
ate share of additives because of their large surface area (4-6). This is
reflected in the results here on the "whole" and "separately" samples. Carrying
out the PAE adsorption so that the fiber and fines receive equivalent dosages

based on their weight ("separately") rather than on their surface area ("whole") leads to increased strength. It is perhaps surprising that treatment of just the long fiber ("fiber only") produces greater strength than the treatment of both fines and fiber ("separately"). It is possible that not treating the fines reduces their tendency to attach to the long fiber prior to formation. This in turn would decrease the interference of the attached fines with fiber/fiber bonding. This hypothesis assumes that the fines contribute their positive effect (cf. "classified" vs. "fiber only" samples) by attachment to the fibers along the periphery of the fiber/fiber bond. Such a location of the fines would occur naturally due to surface tension forces during drying and would help to bolster the bond strength at the periphery where stress concentrations are highest. Further work is required to verify this hypothesis.

The above results suggest that treatment of just the long fiber with a strength aid is one method to maximize strength. Since classifying refined stock in the mill is probably not economically feasible, an alternate scheme was sought. One possible method would be to treat the pulp before refining. The strength aid could then only adsorb on long fiber. So long as most of the fibers' outer walls (containing the adsorbed polymer) remained intact during subsequent refining, the method should be successful. Obviously, the more outer wall removed during refining to form fines, the lower the fraction of the polymer that will be associated with the long fiber.

To test the proposed method, we added the strength aids to the beater before refining as described in the Procedures section. The treated pulp was then beaten for one of several intervals, and handsheets were then prepared as usual. For comparison untreated pulp was beaten for the same periods of time

after which strength aid addition and sheet formation proceeded as usual. Treated and untreated pulps had similar freenesses after a given interval of refining.

The results for moist tensile and compressive strengths are presented in Fig. 2 and Fig. 3, respectively. Evidently, either method of strength aid addition enhances the properties, but addition after refining is the more effective. The data point at 50 minutes for "after refining" in Fig. 3 is believed to be in error, because all other physical properties (including dry STFI compressive strength) showed an increase from 25 to 50 minutes. Both dry (50% RH) and wet tensile strengths showed similar behavior to that in Fig. 2 and Fig. 3. In the case of "before refining" addition, apparently sufficient wall material is removed via fines production during the beating process that the advantage of adsorbing the polymers just on the long fibers is lost.

(Figure 2 and 3 here)

The results in Fig. 2 are replotted as the tensile factor (i.e., the ratio of the tensile strength with additives to that without the additives) in Fig. 4. Here the decreased effectiveness of the strength aids with refining is clear. The strength enhancement is cut almost in half at 50 minutes beating time (450 mL CSF) compared with the unbeaten pulp.

(Figure 4 here)

To clarify this behavior, we added the strength aids (1% PAE, 0.4% CMC) to a whole pulp beaten to 350 mL CSF and to the same pulp after the fines had been removed. The results for the (dry) tensile strength are presented in Table II.

Table II.   Influence of Fines on Strength Aid Effectiveness

| | Breaking Length, km | | |
	No strength aid	With strength aid	Enhancement, %
Whole Pulp	6.1	8.3	36
Classified Pulp	3.9	7.8	100

The greater effectiveness with the classified pulp is striking. Two hypotheses can be suggested.

1. Because of the much greater surface area of the whole pulp, the strength aid dosage used may lead to the polymers being spread too thinly to achieve the maximum potential enhancement. For the classified pulp the used dosage may be much nearer the optimum.

2. Sheet strength is a function of both fiber/fiber bond strength and individual fiber tensile strength (7). Upon incorporation of the strength aids into the sheet, we may have so strengthened the bonds that the fiber strength is now the "weak link".

To test the first hypothesis we treated a whole pulp with a range of dosages of PAE and CMC keeping the CMC/PAE ratio at 0.4 as shown to be optimum (1). The results are plotted in Fig. 5 where the dosage is the sum of the PAE and CMC percentages. A similar pattern is exhibited by the tensile strength for each moisture level. There is a rapid initial rise in strength enhancement followed by a plateau. The dosage used in the work described above (Fig. 2-4 and Table II) was equivalent to 1.4% on the abscissa of Fig. 5. This is near the beginning of the plateau or maximum strength possible with this pulp and strength aid. Apparently this dosage is adequate to provide sufficient polymer

adsorption to both fines and fiber to produce strong bonding. Further incre-
ments of strength aid add nothing more to the strength.

(Figure 5 here)

Such behavior suggests that the second hypothesis may be viable.
Fiber strength is now the weak link; it is generally believed that polymeric
strength aids such as those used here do not improve fiber strength. Evidence
for this hypothesis was sought by examining the fibers in the region of failure
of tensile test specimens. Typical results are shown in Fig. 6 and Fig. 7 at 9x
and 50x magnification, respectively. Evidence for bond failure is a predomi-
nance of fiber pull-out with little fiber rupture. Predominantly fiber failure
should result in little fiber pull-out. The progression from left to right in
Fig. 6 and Fig. 7 corresponds to dosages of 0, 0.7, and 2.8%. In Fig. 5 the
latter two are seen to lie in the steeply rising and plateau portions, respec-
tively. From 0 to 2.8% there is a steady progression of decreasing fiber pull-
out and increasing fiber rupture. We conclude that the strength aid has shifted
the mode of failure. This result agrees with the findings of previous workers
(8, 9). They compared pulps which were untreated or treated with 10% locust
bean gum. Using dyed fibers, they were able to quantify the fraction of fibers
broken as a function of treatment. By increasing the bond strength either by
refining or by chemical additive, they observed more fiber breakage.

(Figure 6 and 7 here)

This finding also helps to explain the behavior seen in Fig. 4. At
zero beating time the strength aids contribute a large enhancement to the
stiff, poorly-bonded fibers. With increasing beating the fibers are rendered
more flexible and conformable, and fines are produced. Both of these factors
lead to improved bond strength, and the potential for further sheet strength
enhancement with additives is concomitantly reduced.

Strength aids can also affect the locus of bond failure. For single fiber/fiber bonds, we have shown (10) that for untreated fibers the failure occurs between the two fibers with little or no disruption of the walls (top of Fig. 8). When the fibers are treated with PAE and CMC as above, the failure now occurs within the wall of one or both fibers (bottom of Fig. 8). The location of the failure has been changed and the bond strength has been increased (10).

(Figure 8 here)

Location in the Vicinity of the Bond

It is generally believed that polymeric additives improve strength by one or more of the following factors:

a) by increasing the total number of (hydrogen) bonds per unit fiber to fiber crossover area because of the ability to bridge across the gap between the rough surfaces of the fibers,

b) by increasing the bonded area because of the ability to bridge the larger gap between the fibers around the periphery of the fiber/fiber bond,

c) by increasing the toughness of the bond because of the long chain nature of the polymer and its ability to permit deformation in the bonded area without bond failure, and

d) as a result of b) and c) above the polymer-treated fibers can better withstand the stress concentrations that naturally arise around the periphery of the bond.

In addition, for some materials including those used here (1), covalent bonds formed between the additive and the fiber surface replace or supplement the much

weaker hydrogen bonds between the untreated fibers. Such materials are also wet
strength aids. For this use they are believed (11) to function by either: 1)
forming a covalent, water-insensitive bond between the fibers ("reinforcement")
or, 2) forming a crosslinked network around the fibers ("protection"), thereby
preventing water penetration to the traditional hydrogen bonds between the
fibers and also minimizing fiber swelling.

These hypothesized mechanisms for wet and dry strength additives
suggest that the detailed location of the polymer in and/or around the
fiber/fiber bonds will influence the sheet strength. To determine whether the
location is indeed important, we used a series of internal and/or external
methods of treating the fibers. These would correspond, respectively, to wet-
end addition and tub sizing-type processes in the mill. Sheets were formed from
untreated (U), treated with 1% PAE (TP), or treated with 1% PAE followed by 0.4%
CMC (TPC) classified unbleached softwood kraft pulp. The fines had been removed
from the beaten pulp (before treatment) to heighten the differences among the
several internal and external treatments and to eliminate the strength-enhancing
effect of the fines. Because the polymer additives also act as fines retention
aids, comparison of the effect of the several strength aid treatments could be
obscured by concomitant variations in fines retention if unclassified pulp were
used.

Some of the dried sheets (U, TP, TPC) were subsequently immersed in
trays containing water, PAE solution, or CMC solution as described in the Proce-
dures section. The various sequences of treatment were chosen to apply the
strength aids to particular surfaces. An example of a sheet whose fibers had
been treated by wet-end addition of PAE (coded TP) followed by subsequent sheet

immersion in CMC solution is shown schematically in Fig. 9. It is assumed here that fiber/fiber bonding is not disturbed by immersion in CMC solution and that the latter cannot enter the bonded regions. This is a reasonable assumption when PAE (or PAE/CMC) is the bonding agent because of the covalent bonds formed with the fibers (1). It is less clear whether this also holds for untreated (U) sheets. However, the relatively short immersion time (30 sec) and the substantial wet web strength of the sheets reflected in their ease of handling through the steps of removal from the immersion bath and passage through the squeeze rolls imply that extensive fiber/fiber bonding was maintained in this case, also.

(Figure 9 here)

The results from these experiments are displayed in Fig. 10-13. For dry tensile strength (Fig. 10), moist compressive strength (Fig. 11) and wet tensile strength (Fig. 12) several trends are evident. a) Introducing a strength aid, either PAE or CMC, at the wet end, produces greater strength than if the polymer is added externally. This implies that supplementing the bonding in the crossover area between the fibers is an important mechanism for these agents. For wet tensile strength this suggests that the "reinforcement" mechanism predominates over that of "protection". b) Increases in strength of PAE-containing sheets produced by subsequent immersion in water and redrying reflect additional crosslinking of the PAE with itself and/or additional reaction of PAE's azetidinium groups with carboxylate groups on the fibers (or CMC, if present). c) When the untreated sheet (U) is immersed once or twice in water, the dry and moist compressive and tensile strengths (and also the values not reported here for tensile energy absorption, extensional stiffness, and strain at failure) suffer severe losses. This suggests loss of bonding during the immersion and incomplete recovery of the bonding during the subsequent squeezing

and drying processes. The absence of a corresponding significant loss in density and the high level of solids (40%) out of the squeeze roll (cf. 37% solids after pressing for 5 min at 50 psi), however, do not support this explanation. It is difficult to rationalize the losses in strength due to water immersion because the drying conditions (time, temperature, and amount of restraint) were the same for all sheets.

(Figure 10-13 here)

The combination PAE/CMC has rather different effects on the compressive and tensile strengths as shown in Fig. 13. Adding PAE externally to an untreated sheet or internally (wet-end addition) produces a large increase in tensile strength. Subsequent external treatment with CMC provides only a small additional increment. A somewhat larger effect is seen when the CMC is added internally (cf. TP and TPC) showing the importance of the latter within the bonded (crossover) area. For compressive strength the opposite is found. Adding PAE only, whether internally or externally produces little or no improvement. However, when CMC is incorporated either internally (cf. TP and TPC) or externally, substantial increases result. Apparently, tensile strength and compressive strength are dependent in different ways on the bonding produced by the strength aid(s). This suggests that a more detailed study of the interactions between the polymers and the cellulose surfaces and between the polymers themselves could produce the understanding needed to design still more effective strength aids.

CONCLUSIONS

The optimum location of the strength aid is on the long fiber, not the fines. Strength aids can improve the bond strength to the point where fiber failure in the axial direction or within the cell wall becomes the limiting factor (weak link). Because wet-end addition is much more effective than external addition, the function of the strength aids is to increase the bond strength within the bonded area.

ACKNOWLEDGMENTS

LITERATURE

1. Espy, H. H., Proc. 1983 TAPPI Papermakers Conf., Portland, OR, April 25-27, p.191.

2. Proxmire, P. R. and Stratton, R. A., Proc. 1988 TAPPI Papermakers Conf., Chicago, IL, April 11-13, p.131.

3. Neal, C. W., Notes 1988 TAPPI Wet and Dry Strength Short Course, Chicago, IL, April 13-15, p.1.

4. Marton, J., Ind. Eng. Chem. Prod. Res. Dev. 21(2):146(1982).

5. Marton, J. and Marton T., Tappi J. 65(11):105(Nov., 1982).

6. Sandstrom, E. R., Paper Trade J. 163(2):47(1979).

7. Page, D. H., Tappi 54(4):673(April, 1969).

8. Van den Akker, J. A., Lathrop, A. L., Voelker, M. H. and Dearth, L. R., Tappi 41(8):416(Aug., 1958).

9. Helle, T., Svensk-Papperstidn. 66(24):1015(1963).

10. Stratton, R. A., Proc. NSF Workshop on Solid Mechanics Related to Paper, Minnowbrook, NY, Aug. 13-15, 1986, in press.

11. Stannett, V. T., in "Wet Strength in Paper and Paperboard", TAPPI Monograph Series No. 29, 1965, p.85.

LIST OF CAPTIONS

Fig. 1.   Adsorption isotherm for PAE on a whole beaten softwood unbleached kraft
          pulp. Contact time is five minutes.

Fig. 2.   Evolution of moist (92% RH) tensile strength with beating as influenced
          by mode of strength aid addition.

Fig. 3.   Evolution of moist (92% RH) STFI compressive strength with beating as
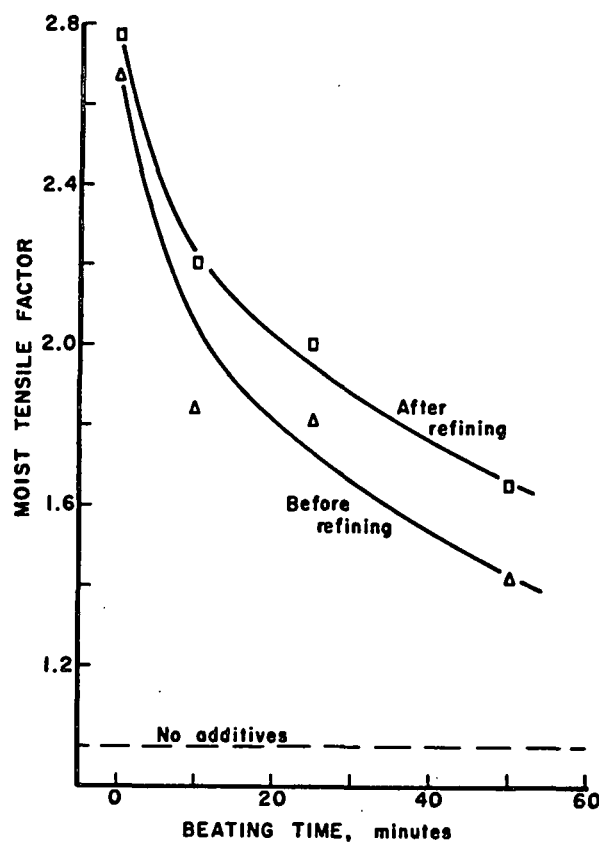   influenced by mode of strength aid addition.

Fig. 4.   Variation with beating of the ability of the strength aid (PAE/CMC) to
          enhance the moist tensile strength.

Fig. 5.   Influence of strength aid dosage (% PAE + % CMC) on the tensile
          strength of sheets made from a whole beaten softwood unbleached kraft
          pulp. CMC:PAE is 0.4.

Fig. 6.   Photomicrographs of the failure region of tensile test specimens at the
          indicated strength aid dosages. Magnification 9X.

Fig. 7.   Photomicrographs at 50X magnification of the same regions as in Fig. 6.

Fig. 8.   SEM photomicrographs of the formerly bonded region of a fiber/fiber
          pair after bond breakage. Top: no strength aid. Bottom: treated with
          1% PAE/0.4% CMC.

Fig. 9.   Schematic of a portion of a fiber/fiber bond showing location of PAE
          and CMC when the PAE has been added at the wet end and the CMC has been
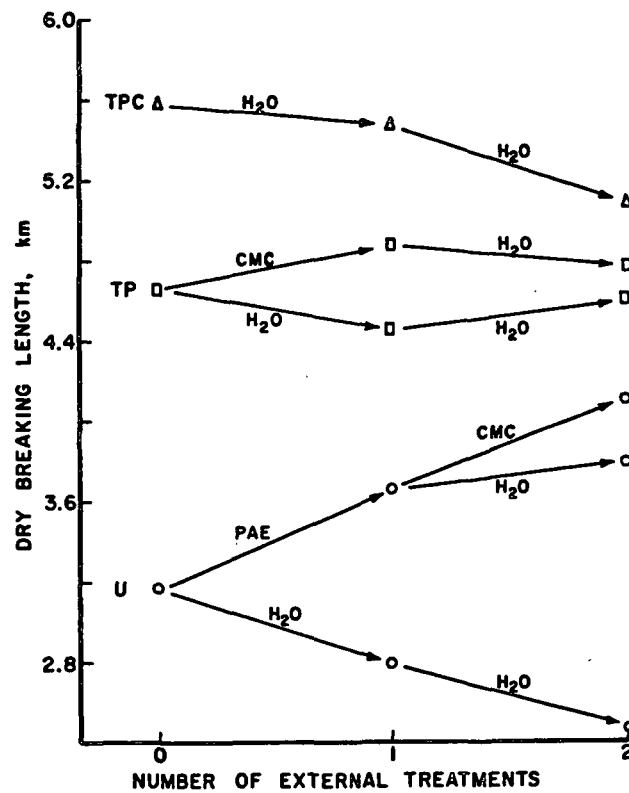   added after sheet formation.

Fig. 10. Effect of a sequence of internal and external treatments on the dry
          (50% RH) tensile strength. U = untreated, TP = PAE added internally,
          TPC = PAE followed by CMC added internally. Codes above the arrows
          refer to immersion of dried sheets into baths of aqueous solutions of
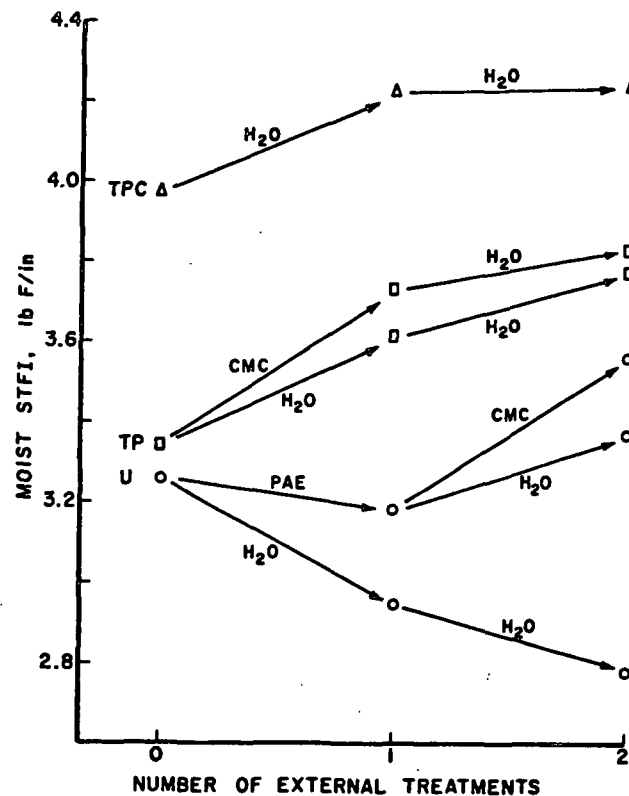   the indicated components.

Fig. 11. Effect of a sequence of internal and external treatments on the moist
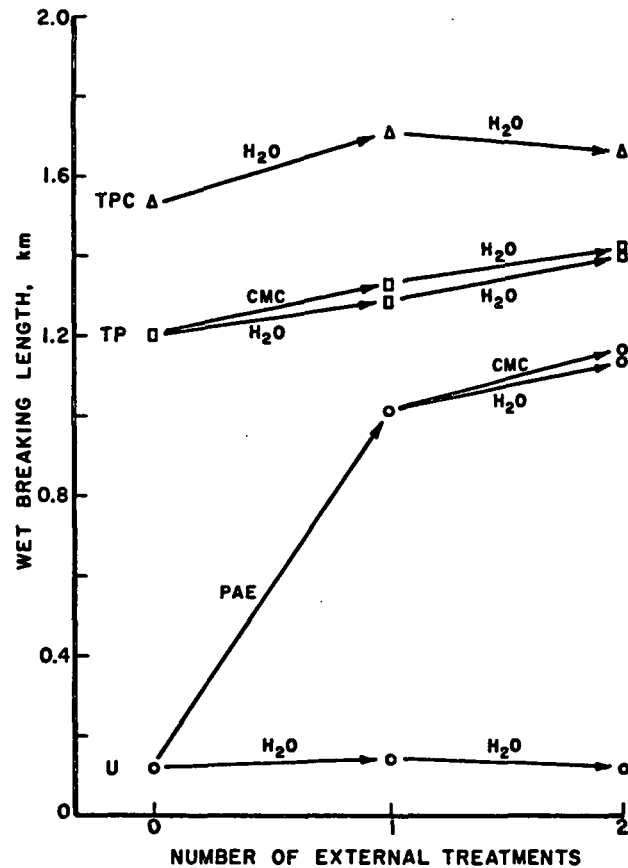   (92% RH) STFI compressive strength. Codes same as Fig. 10.

Fig. 12. Effect of a sequence of internal and external treatments on the wet
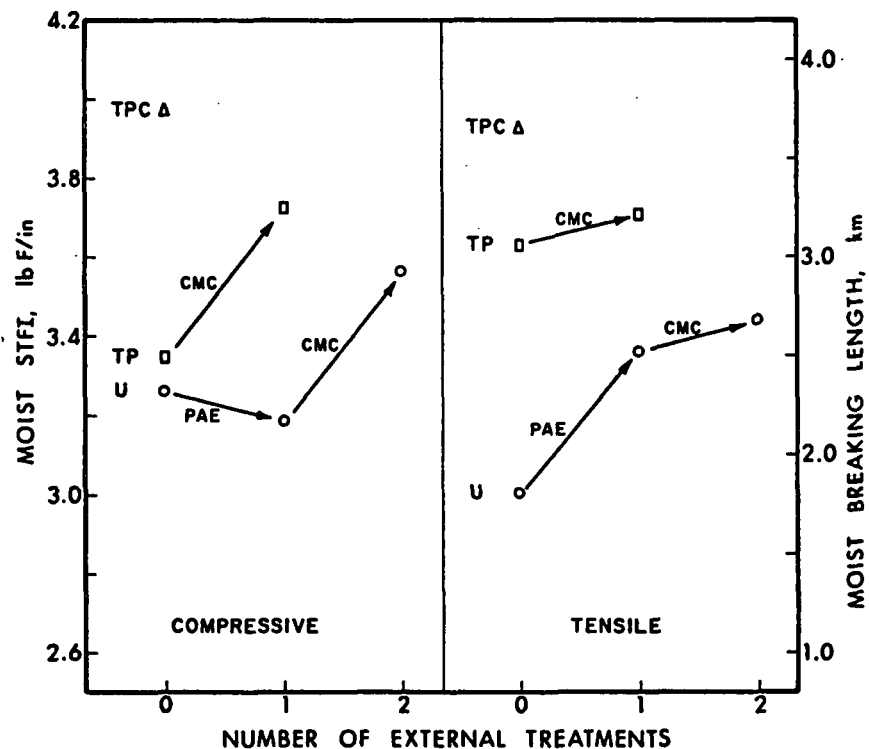   tensile strength. Codes same as Fig. 10.

Fig. 13. Comparison of the relative effects of PAE and CMC on the compressive
          and tensile strength. Codes same as Fig. 10.
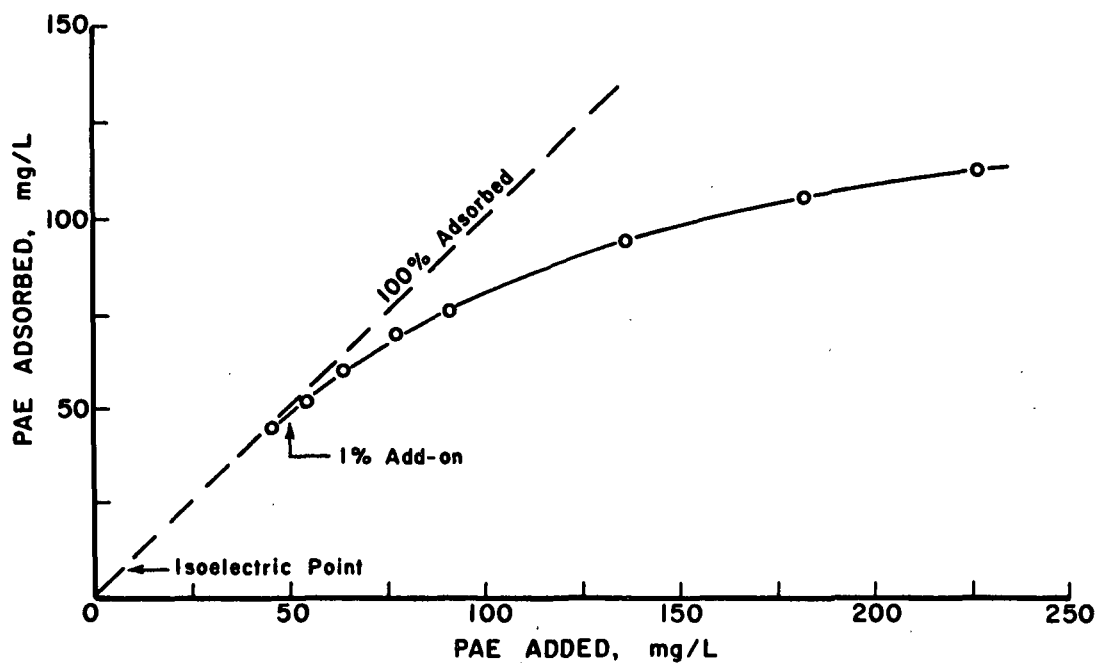
Figure 1. Adsorption isotherm for PAE on a whole beaten softwood unbleached
kraft pulp. Contact time is five minutes.
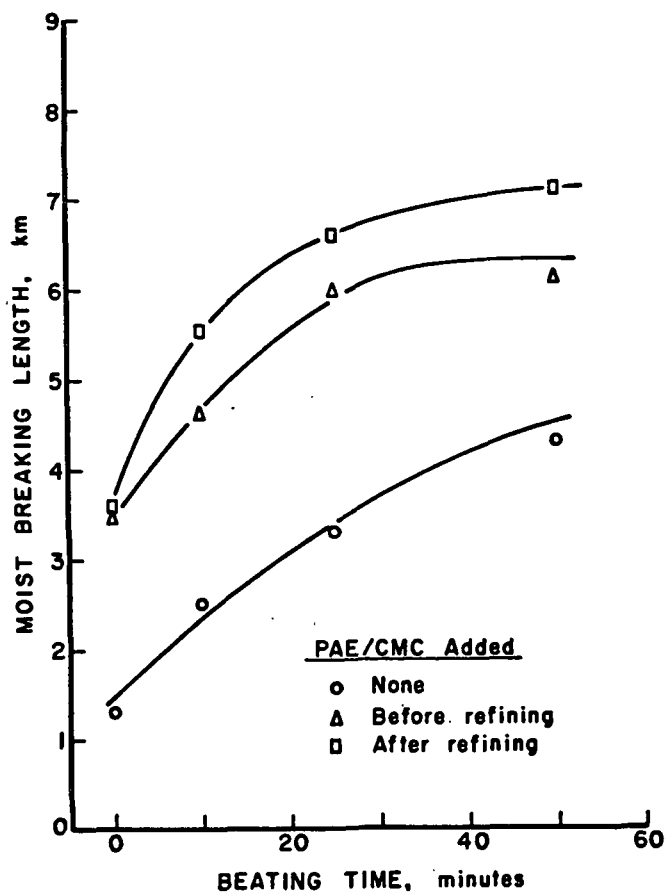
Figure 2. Evolution of moist (92% RH) tensile strength with beating as
influenced by mode of strength aid addition.
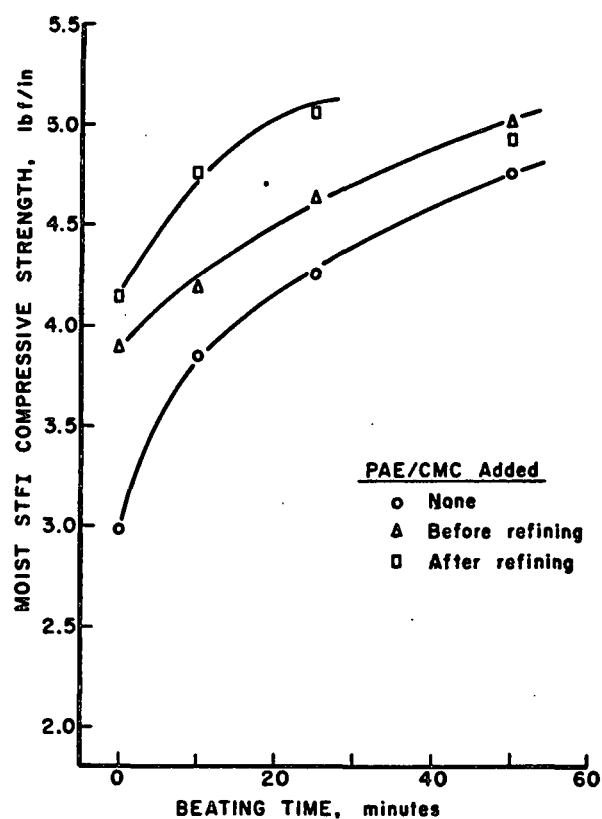
Figure 3. Evolution of moist (92% RH) STFI compressive strength with beating as influenced by mode of strength aid addition.

Figure 4. Variation with beating of the ability of the strength aid (PAE/CMC) to enhance the moist tensile strength.
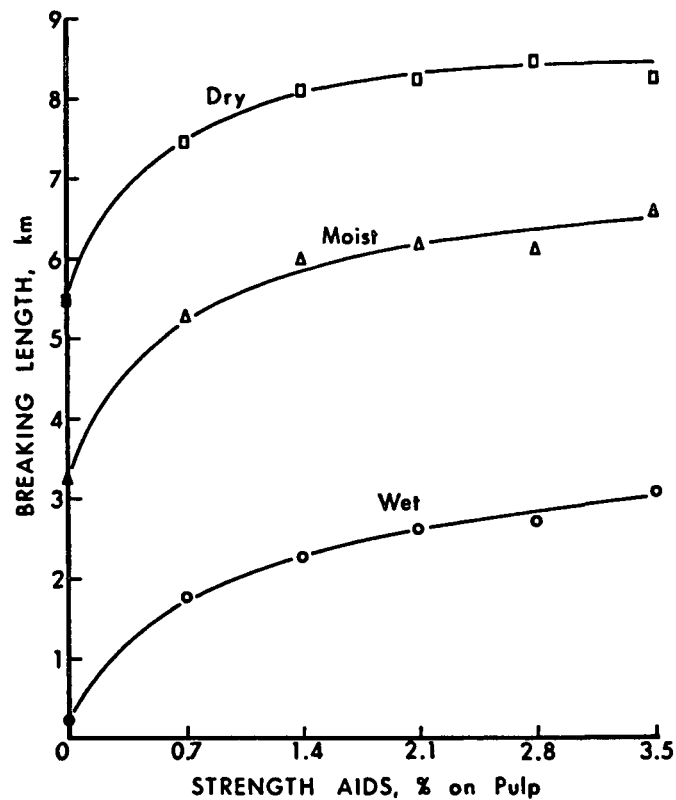
Figure 5.   Influence of strength aid dosage (% PAE + % CMC) on the tensile
            strength of sheets made from a whole beaten softwood unbleached kraft
            pulp. CMC:PAE is 0.4.
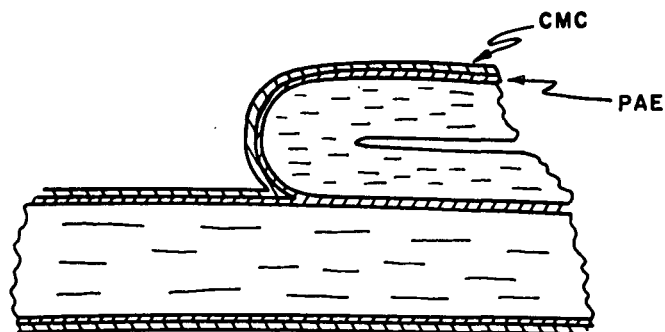
Figure 9.   Schematic of a portion of a fiber/fiber bond showing location of PAE
            and CMC when the PAE has been added at the wet end and the CMC has
            been added after sheet formation.

Figure 10. Effect of a sequence of internal and external treatments on the dry
(50% RH) tensile strength. U= untreated, TP = PAE added internally,
TPC = PAE followed by CMC added internally. Codes above the arrows
refer to immersion of dried sheets into baths of aqueous solutions of
the indicated components.

Figure 11. Effect of a sequence of internal and external treatments on the moist
(92% RH) STFI compressive strength. Codes same as Fig. 10.

Figure 12. Effect of a sequence of internal and external treatments on the wet tensile strength. Codes same as Fig. 10.

Figure 13. Comparison of the relative effects of PAE and CMC on the compressive and tensile strength. Codes same as Fig. 10.

THE INSTITUTE OF PAPER CHEMISTRY

Appleton, Wisconsin

Status Report

to the

PAPER PROPERTIES AND USES

PROJECT ADVISORY COMMITTEE

Project 3646

FUNDAMENTALS OF PAPER SURFACE WETTABILITY

October 19-20, 1988

PROJECT SUMMARY

PROJECT NO. 3646:   FUNDAMENTALS OF PAPER SURFACE WETTABILITY

PROJECT STAFF: F. Etzler/R. Stratton   September 12, 1988

PROGRAM GOAL:

Develop an understanding of the interactions between liquids and the paper
surface and their dependence on sheet properties.

PROJECT OBJECTIVE:

To improve our understanding of the influence of the structure and properties
of paper and board on liquid absorption and penetration.

PROJECT RATIONALE, PREVIOUS ACTIVITY AND PLANNED ACTIVITY FOR FISCAL 1988-89 are
on the project form that follows.

SUMMARY OF RESULTS TO DATE: (March 1988 - October 1988)

A survey of the literature concerning the state of water in cellulosic materials
has been performed. It was found the many of the conclusions regarding the
state of water adjacent to cellulosic surfaces reported in the paper, textile
and forest products journals are probably in error as they conflict with the
experimental observations made in model systems. The data can, however, be suc-
cessfully reinterpreted so as to remove the apparent conflict. It is expected
that these results will be published.

Programs to be used for calculation of the the properties of Vornoi polyhedra
have been written and tested on elementary systems. Calculations on simulated
bulk water are presently in progress. These calculations will shed light on the
structure of water near interfaces.

Drop penetration times on kraft linerboard samples have been measured. The
results indicate that the Washburn equation is useful in interpreting the drop
penetration results. The Washburn equation suggests the the surface chemistry
of the paper plays an important role in the printability of linerboards.

PROJECT TITLE: Fundamentals of Paper Surface
                Wettability

PROJECT STAFF: F. Etzler/R. Stratton

PRIMARY AREA OF INDUSTRY NEED: Properties related
                                to end uses

Date: 2/5/88
Budget: $75,000
Period Ends: 6/30/88
Project No.: 3646

PROGRAM AREA: Performance and Properties of Paper and Board

PROGRAM GOAL:

Develop an understanding of the interactions between liquids and the paper
surface and their dependence on sheet properties.

PROJECT OBJECTIVE:

To improve our understanding of the influence of the structure and properties
of paper and board on liquid absorption and penetration.

PROJECT RATIONALE:

Many converting and end uses of paper and board are associated with the appli-
cation of a liquid to the surface. These include the processes of printing,
coating, production of combined corrugated board, surface sizing, and exposure
of the product in use to a variety of liquids. In many cases (printing,
coating, etc.), the phenomena of interest occur at very short time scales, far
removed from equilibrium. To improve these processes and to point the way for
new products, it is important to understand the influence of the sheet structure
and surface properties on the interactions with liquids.

RESULTS TO DATE:

New project.

PLANNED ACTIVITY FOR FY 1988-89:

Dr. Frank Etzler has recently joined the faculty and staff of IPC and will
direct this project. A literature review will be conducted to ascertain the
state of knowledge in the subject area. Based on the results of the review, a
research program will be designed and implemented by Dr. Etzler to extend our
knowledge in specific areas of liquid-sheet interactions.

Status Report

FUNDAMENTALS OF PAPER SURFACE WETTABILITY

Project 3646

The objective of this project is to understand the interaction of liquids with paper materials in a fundamental way. It appears important to assess the current state-of-the-art and suggest future research paths. The long-term objective of the project is to achieve a fundamental understanding of the role of liquid-paper interactions in paper making and in determining paper properties. The current work has been directed to: 1) reviewing the literature regarding the present understanding of water-cellulose interactions; 2) comparing results from model systems with that known for water-cellulose systems; 3) refinements to Etzler's statistical thermodynamic model for vicinal water; and 4) the effect of paper surface chemistry on liquid penetration (particularly as related to flexographic printing).

The Structure of Water Near Surfaces

The nature of the liquid state at the molecular level continues to be a forefront topic of research in physics and chemistry. Despite the efforts of a considerable number of able researchers, much regarding the nature of the liquid state remains to be learned. Fortunately, much progress has been made in the last decade; this progress suggests that considerable advances will be made in the coming years. The nature of liquids near surfaces is, at present, receiving considerable attention by both experimentalists and theoreticians. A fundamental understanding of the processes important in determining the nature interfacial (vicinal) liquids has not been achieved. Indeed, considerable ignorance of the state of vicinal liquids exists. Many fundamental experiments are necessary in order for progress to be made.

As the state of water near cellulosic surfaces is of considerable importance to paper manufacture, it is important to discuss the current understanding of water near solid surfaces. A comparison of vicinal water in model substrates and in cellulosic substrates is also of importance.

It is known that the properties of water near surfaces are modified by propinquity to solid surfaces. To date the most comprehensive studies of interfacial water properties have been performed on water in silica and clays. Silicas and clays are nearly ideal substrates as water may be placed in pores of known size and geometry. It has been shown, for instance, that water in pores with a radii of 1-20 nm, exhibits a larger heat capacity, lower density and higher viscosity. [See for instance, Etzler, F.M., Langmuir, 4, 878 (1988).]

From studies of water in clays and from density measurements of water in silica gel, it appears that water is structurally modified to distances of 3-6 nm. It also appears that the structural modification decays in an approximately exponential manner with distance from the liquid-solid interface.

From work on a number of systems, it appears that the properties of vicinal water to a good first approximation are independent of the physico-chemical details of the surface. For example, it has been shown that heat capacity of water near a wide variety of surfaces in larger than the bulk. This aspect, however, deserves further attention.

The heat capacity of vicinal water appears to be a particularly useful quantity for understanding the nature of water in cellulosic systems; thus, this quantity is considered further. Stey (Ph.D. Thesis, University of Pittsburgh, 1967) has calculated the model independent distribution of single particle enthalpies for water and a number of other liquids. It was found that the

distribution for water is unusual in that the distribution is bimodal. This

type of distribution contrasts with the nearly Maxwell-Boltzmann type distribu-

tions found for more simple liquids. Some of Stey's results are seen in Fig. 1.
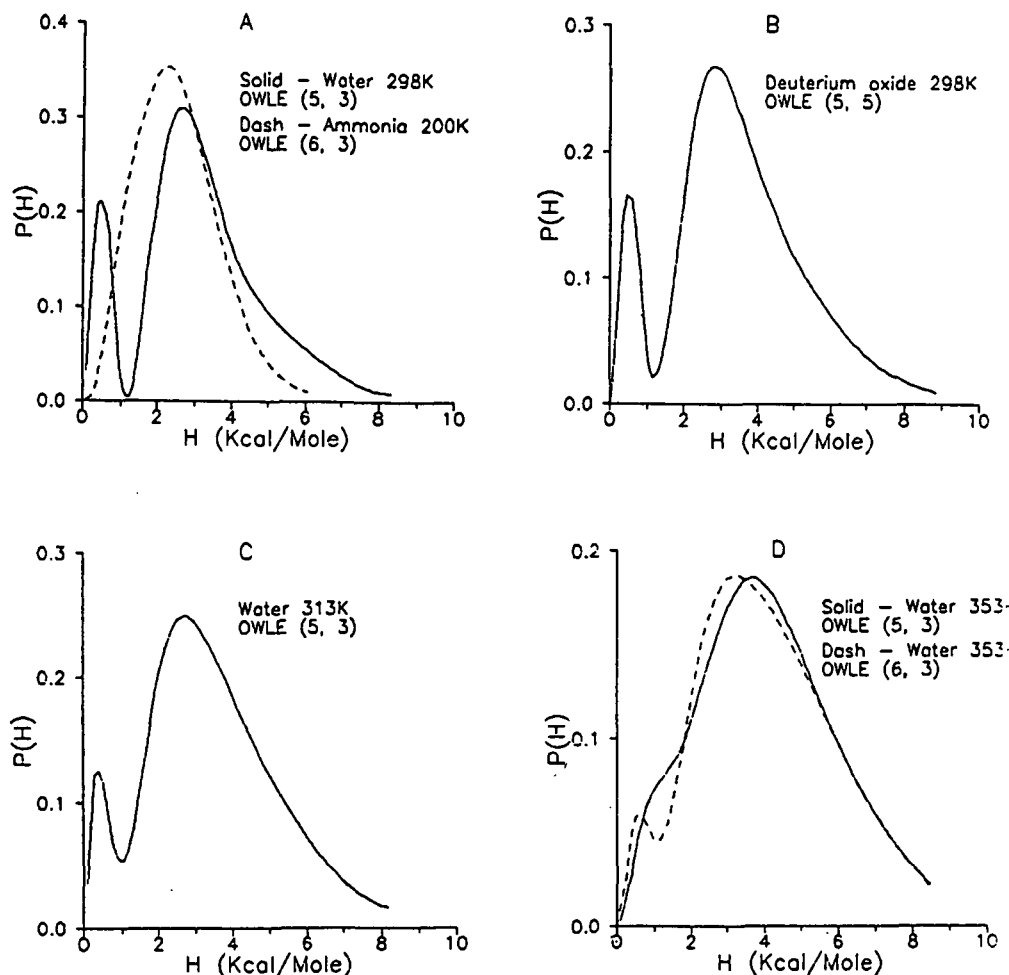
Figure 1.   Stey's distribution functions. Probability, P(H), vs.
            enthalpy, H. (A) Water at 298 K and NH_3 at 200 K.
            (B) D_2O at 298 K. (C) H_2O at 313 K. (D) H_2O at 353 K.

It appears that the molecules represented by the low enthalpy peak in

Stey's distribution are 4-hydrogen bonded water molecules while the high

enthalpy peak represents molecules with 0,1,2 or 3 hydrogen bonds. The number

of peaks in the distribution cannot be predicted from the number of hydrogen

bonding states. It is generally presumed that liquid state distributions would be

nearly of the Maxwell-Boltzmann type.

The heat capacity, C_p, is related to the variance, Δh^2, of single particle enthalpies, through the well-known statistical thermodynamic relation:

$$C_p = \sigma_h^2 / RT^2 \tag{1}$$

For a bimodally distributed liquid the heat capacity may be considered as follows:

$$C_p = x(1)C_p(1) + x(2)C_p(2) + x(1)x(2) \frac{\Delta H^2}{RT^2} \tag{2}$$

Here $x(1)$ refers to the fraction of 4-hydrogen bonded water molecules. If it is assumed that hydrogen bonding is non-cooperative then $x(1)$ equals the fourth power of the hydrogen bond probability between adjacent water molecules. $C_p(1)$ it taken to be the heat capacity of ice and $C_p(2)$ is estimated using a variety of experimental data, including, for instance, the activation energy of the rotational correlation time. At 298K $C_p(2)$ = 16 cal/K mole. ΔH is the mean enthalpy of transfer between the two peaks in Stey's distribution or 2.55 kcal/mole. $C_p(1)$, $C_p(2)$ and ΔH for deuterium oxide may also be estimated. At 298 K approximately 6-10% of the water molecules in bulk water are 4 hydrogen bonded.

The heat capacity of water and deuterium oxide in silica pores of various diameters has been measured. The results are shown in Fig. 2. A significant feature of the graph is the presence of the maxima near 7 nm pore radius. Figure 3 shows C_p as a function of $x(1)$ as calculated from Eqn. 2. Significantly, Fig. 3 suggests that vicinal water differs from the bulk in that hydrogen bond probability between adjacent molecules is enhanced by propinquity to solid surfaces and that the magnitude of the experimentally observed maxima may be calculated on the basis of Stey's earlier calculations. Density measurements

HEAT CAPACITY
Water / Deuterium oxide
in Silica Pores
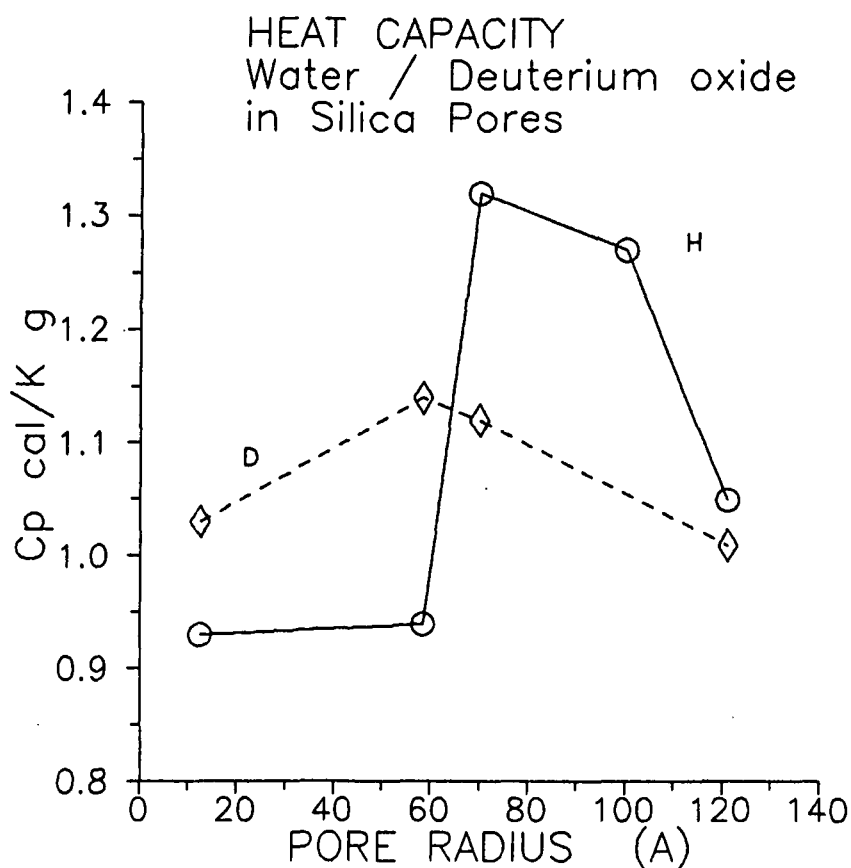
Figure 2. Heat capacities of water in silica pores as a function
of pore radius at 298 K: squares H_2O; diamonds, D_2O.
Radius in Angstroms (10 Å = 1 nm).

on water in silica pores are in agreement with the heat capacity measurements
and suggest that hydrogen bond probability between adjacent water molecules
decays to the bulk value in an approximately exponential manner. Significant
structuring extends 3-6 nm. The density of water in 7 nm radius silica pores is
2-3% lower than the bulk at 298 K.

Water in Cellulosic Materials

Measurement of the properties of water associated with polymeric
substances is difficult as it is often impossible to separate polymer properties
from water properties. Nonetheless several attempts have been made to measure
the properties of water associated with cellulosic and other polymers. Early
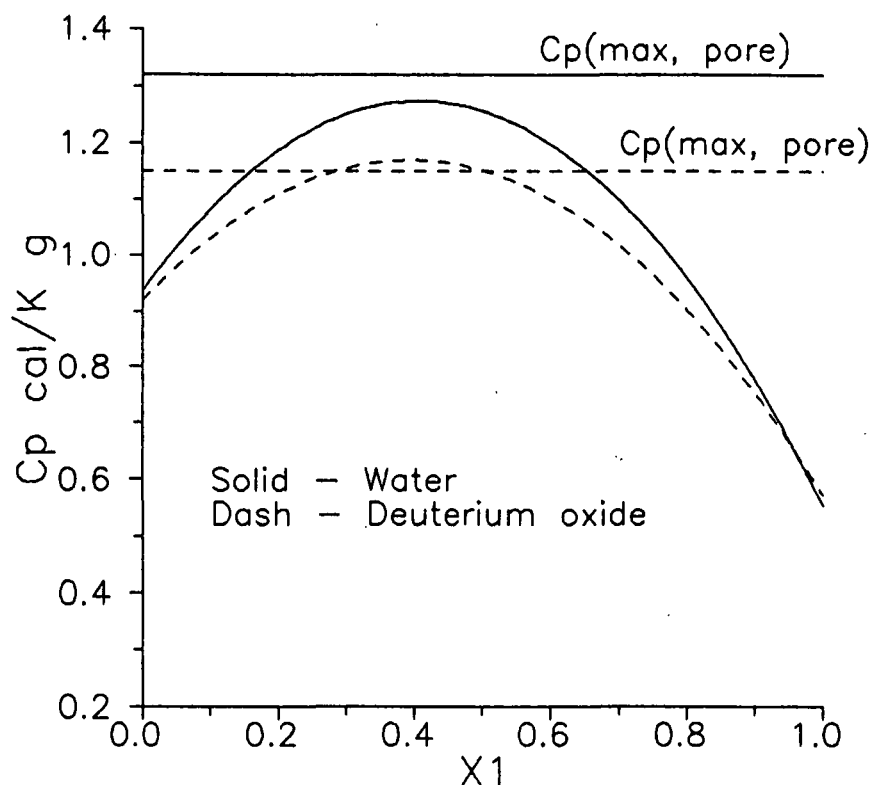
Figure 3. Hypothetical heat capacity of water and deuterium
           oxide as a function of x(1) at 298 K.

attempts to measure the density of water in wood suggested that the water had a

density much larger than bulk water (Indeed much greater than the density of Ice

VIII at 25 kbar!). Other measurements suggested that the expansivity of water

was larger than the bulk. These results have been used to suggest that water

associated with cellulosic materials is less structured than the bulk. This

conclusion is in conflict with experimental evidence collected for water in clay

and silica pores.

The use of thermal expansion as an indicator of vicinal water struc-

ture appears to be premature. It is not yet clear from statistical thermo-

dynamics what the effect of enhanced hydrogen bonding between water molecules in

pores would have on the magnitude of the thermal expansion coefficient.
Reexamination of the apparent specific volume data for liquids associated with
wood collected earlier by Weatherwax and Tarkow suggests that the high apparent
density of water is due primarily to the opening of new pores (This is also an
earlier conclusion of Weatherwax and Tarkow.) and that the density of water in
the pores is 0.98 or 2% lower than the bulk if ethanol is treated as an unmodi-
fied pore liquid (Pore density equal to bulk density). This assumption is con-
sistent with density measurements of water and alcohols in silica pores.

Figure 4 shows the apparent heat capacity of water in two kinds of
wood. Figure 5 shows the apparent heat capacity of water in gelatin and starch
suspensions. Both results are consistent with heat capacity measurements made
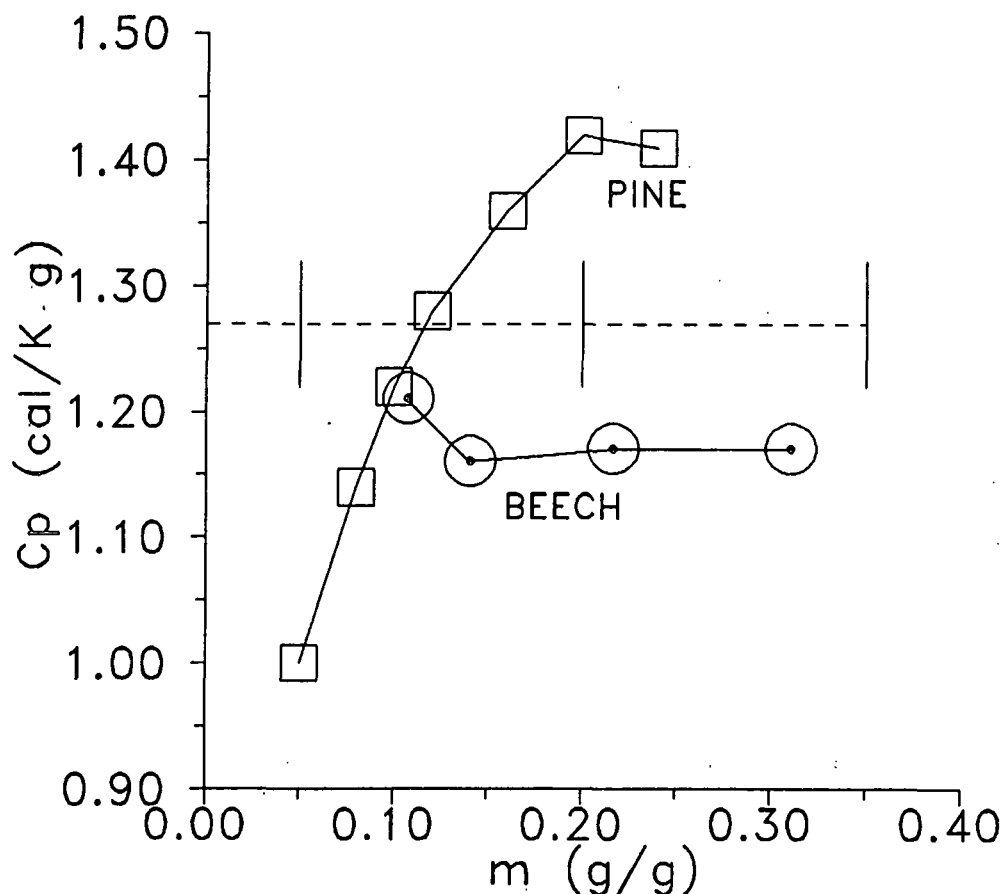
Figure 4.   Apparent heat capacity of water in woods. Squares - pine;
            circles - beech; dashed line - maximum heat capacity as
            calculated from author's model
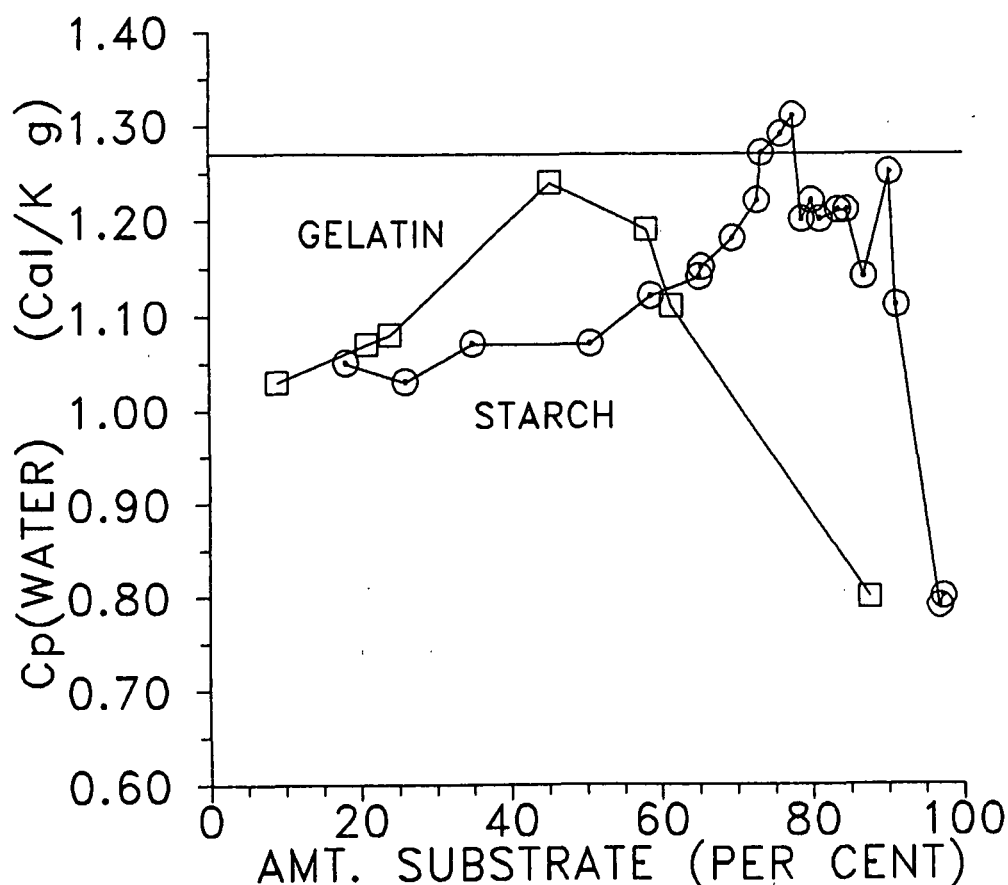
Figure 5.   Apparent heat capacity of water versus per cent of
            substrate material in mixture. Squares - gelatin;
            circles - starch. Horizontal line - maximum heat
            capacity calculated from author's model.

in silica gel. In short, it appears that the properties of water associated

with cellulosic materials and in silica gel are nearly identical and that water

adjacent to either surface is more structured than the bulk.

VORONOI POLYHEDRA AND THE STRUCTURE OF VICINAL WATER

The results of Stey's calculations have been used successfully to

correlate a number of thermodynamic properties of water near surfaces. Thus, it

appears that Stey's calculated distribution can be used to make correct predic-

tions of and correlations between macroscopic properties. Stey's calculation

also makes predictions regarding the microscopic or molecular behavior of water. From thermodynamics Enthalpy, $H = E + PV$, where P is pressure, V is volume and E is energy. The single particle enthalpies discussed by Stey can thus be broken into two parts - a volume part (N.B. $P = $ Constant) and an energy part. At present it is not clear whether energy or volume is the major factor in determining the form of Stey's enthalpy distribution.

It is not possible to calculate the distribution of molecular volumes in liquid via Stey's arguments without detailed knowledge of the intermolecular potential energy function. Knowledge of this function is not necessary, however, for the calculation of single particle enthalpies. It is possible, however, to estimate the distribution of molecular volumes from molecular dynamics calculations. The distribution of molecular volumes for liquid water is presently being calculated for simulated water.

The volume of a molecule in a system can be regarded as the volume of the Voroni polyhedra whose center is the molecular center of mass. The Voroni polyhehra represents all points in space which are closer to the a given molecular center of mass (or other reference point) than to any other molecular center of mass. The temperature dependence of the isothermal compressibility for liquid water suggests that this distribution may not be nearly normal.

It is hoped that this activity which is being cooperatively conducted between scientists at the University of North Carolina - Chapel Hill and IPC will attract some federal support.

Penetration of Liquids into Kraft Linerboard

The penetration of liquids into kraft linerboards has been measured. The penetration of liquids into a porous substrate is governed by the Washburn equation:

$$\frac{dh}{dt} = [r/4\eta h]\gamma_{LV}\cos \tag{3}$$

Here η is the liquid viscosity, θ is the contact angle and γ_{LV} is the liquid-vapor surface tension and (dh/dt) is rate of penetration. According to the Washburn equation if a surface is not wet (contact angle > 90°) then the rate of penetration is negative which in turn implies that the liquid will not penetrate. If surface is completely wet (contact angle = 0) then the Washburn equation becomes:

$$\frac{dh}{dt} = [r/4\eta h]\gamma_{LV} \tag{4}$$

thus penetration is governed primarily by viscosity and not surface energetics when θ = 0. Drop penetration time measurements made on a large number of kraft linerboard samples suggest that paper surface energy may play a significant role in flexographic printing. Linerboard samples which are not wet by typical inks have been found to exhibit poor print quality.

This work has also been supported by FKBG.

FUTURE WORK

It is planned to:

1. Begin calorimetric measurements of heat capacities of water in model substrates and in cellulosic materials in order to understand better the nature of pore water.

2. Continue to explore the distribution of Voronoi volumes in bulk water and to acquire and study data for simulations of water near solid surfaces.

3. Investigate possible experiments which may lead to an understanding of how the physico-chemical details of a surface may influence the structure of vicinal water.

4. Investigate the feasibility of making direct force measurements between cellulosic particles. It is hoped that such measurements would yield information regarding the effects of vicinal water on interparticle forces. (This may relate to paper strength etc.)

5. Investigate the suitability of thermoporometry for use on cellulosic materials. Thermoporometry is a technique for determining pore sizes for materials immersed in a liquid such as water. This technique will be important for detailed investigations of water in cellulosic materials. The analysis is performed on a differential scanning calorimeter.

THE INSTITUTE OF PAPER CHEMISTRY

Appleton, Wisconsin

Status Report

to the

PAPER PROPERTIES AND USES

PROJECT ADVISORY COMMITTEE

Project 3571

BOARD PROPERTIES AND PERFORMANCE

October 19-20, 1988

PROJECT SUMMARY

PROJECT NO. 3571: BOARD PROPERTIES AND PERFORMANCE   September 12, 1988

PROJECT STAFF: W. J. Whitsitt, R. A. Halcomb, J. Dees

PROGRAM GOAL:

Develop relationships between critical paper and board property parameters and
how they are achieved in terms of raw material selection, principles of sheet
design, and processing conditions.

PROJECT OBJECTIVE:

•To develop relationships between container performance, combined board and
 component properties.

•To improve the performance/cost ratios of combined board (including medium).

•The short term goals are directed to (1) using structural models to assess
 the impact of papermaking factors on combined board and box performance and
 (2) improving liner and medium end-use and converting performance properties.

PROJECT RATIONALE, PREVIOUS ACTIVITY AND PLANNED ACTIVITY FOR FISCAL 1988-89 are
on the Project Form that follows.

SUMMARY OF RESULTS LAST PERIOD: (October 1987 - March 1988)

Section 1 - Liner and Medium Improvement

(1) To supplement the wet end additive work under Project 3526 the effects of
    chemical surface treatments on board properties and convertability is in
    process. As an initial step a commercial medium was surface treated with
    the following agents: starch, carboxymethylated potato starch (CMPS), PAE,
    PAE/starch and PAE/CMPS.

(2) The PAE and PAE/starch/CMPS treatments increased MD tensile at 50%, high
    humidity and under wet conditions as expected. The improved strength
    achieved with the PAE type treatments should help runnability on the corru-
    gator.

(3) The greatest increases in MD and CD STFI short span compressive strength and
    Concora were achieved with the PAE and PAE/starch/CMPS treatments. This
    held true at both 50% RH and 92% RH. Thus increases in ECT at 50% RH due to
    treatment of the medium should be retained at high RH.

(4) The PAE type treatments had little effect on medium porosity but greatly
    increased the water drop. Thus the PAE type treatments greatly reduced the
    wettability of the sheet and this would be expected to affect bonding on the
    corrugator.

(5) As expected the PAE type treatments increased flat crush. The increases ranged up to 55%.

(6) Modest improvements in ECT were obtained with the PAE treatments of the medium.

(7) The pin adhesion results indicated that it is more difficult to bond the PAE treated sheets, presumably because of the reduced wettability. Some modification of the starch formulation may be desirable.

(8) Additional work is being planned to extend the trials to linerboard and investigate a wider range of additives.

Section 2 - Runnability Modeling and Strength Losses

(1) Our model indicates that the medium is exposed to higher stresses as speeds increase during forming. The higher stresses increase high-lows, strength losses and ultimately, cause flute fracture.

(2) Current work shows that 26, 33 and 40-lb mediums exhibit losses in tensile strength. At low speeds the tensile strengths of the formed mediums are about 75-85% of the strength of the unformed medium.

(3) On the average 40-lb mediums exhibit greater losses in strength than 26- or 33-lb mediums as expected.

(4) As speed increases and approaches the point where fractures can be seen the tensile strength decreases and approaches zero. Fiber-to-fiber bond damage must occur before the fractures can be visually detected.

(5) The losses in strength are being analyzed using the runnability model to show the relation between the corrugating stresses and strength losses.

(6) Work is being planned to show how high temperatures similar to those in corrugating affect the tensile load-elongation properties of the medium.

Section 3 - ECT and Box Compression Relationships

(1) A study has been carried out to check our ECT and flexural stiffness models. For this purpose experimental linerboard were made under different conditions and fabricated into corrugated board. Small size tubular structures were made and compression tested.

(2) Excellent agreement between predicted and observed ECT results were obtained with models based on the STFI strengths of the components as well as models based on the elastic stiffnesses of the components. The latter lends credence to the use of elastic stiffnesses to characterize component quality.

SUMMARY OF RESULTS THIS PERIOD: (March 1988 - October 1988)

Section 1 - Combined Board Warp -- Liner Orientation Effects

(1) Past Institute research shows that the shape, elastic stiffness vs. orientation diagrams (termed polar plots) can vary greatly across paper machines

depending on wet-end conditions. These variations of shape, area, and angle of lean are known to correlate with converting or end-use performance of some papers. For example, variations in the polar angle of lean could affect the development of twist warp in the manufacture of combined board.

(2) Therefore, a study is being carried out to determine the effects of combining single- and double-face (SF and DF) liners with polar angles ranging up to 15 degrees from the MD of the corrugated board on warp development.

(3) When SF and DF liners with polar angles deviating in opposite directions were combined into corrugated board, major twist warp occurred as moisture content changed. The degree of twist warp increased steadily as the polar angle increased from 0 to 15 degrees. Thus such combined boards will be dimensionally unstable as they pick-up or lose moisture.

(4) When the liners had polar angles deviating in the same direction from the MD, little twist warp developed as moisture content changed.

(5) These results indicate that information on ways to reduce stiffness variations on the paper machine can help the box plants reduce warp and hence, productivity.

(6) Further tests at other RH levels are in progress and additional work on other moisture effects is planned.

Section 2 - Liner and Medium Improvement -- Chemical Additives

(1) Past work showed that surface treatments with PAE type materials enhanced compressive strength and other corrugating runnability properties. However, such treatments greatly reduced wettability, and hence, reduced bonding strength on the corrugator.

(2) The Surface Science Group is now screening other additives for surface application which will increase strength without making major reductions in wettability. These trials will be completed for the March meeting.

Section 3 - Runnability Modeling -- Strength Losses

(1) Application of our runnability model shows that the losses in tensile strength of the medium during fluting are well related to the applied stresses predicted from the model. When the stress ratio approaches unity, flute fracture should occur.

(2) When the applied stress ratio was below about 0.75 the tensile strengths of the fluted mediums ranged from about 75 to 85% of their original strength for 33-lb mediums. At higher stress ratios above 0.90 the tensile strengths rapidly declined and fractures were observed. We believe this is an excellent confirmation of the theory used in developing the model.

(3) Similar results were observed with 40-lb mediums but more extreme losses and fracturing were observed.

(4) This completes the planned work on tensile strength losses during fluting.

Section 4 - Runnability Modeling -- High Temperature Furnish Effects.

(1) A study to determine the effects of varying medium chemical composition on high temperature tensile property behavior and runnability is in process.

(2) For this purpose experimental sheets are being prepared from furnishes with varying degrees of delignification and, in some cases, with synthetic fiber/polymer blends incorporated in the outer layers. The sheets will be tested to determine how the furnish chemical and fiber composition affect the high temperature tensile properties and, hence runnability.

Section 5 - Runnability Modeling -- Speed and Strain-Rate Effects

(1) A simple viscoelastic model to represent the medium tensile properties is being developed to be used with our runnability model to (a) study ways to optimize tensile characteristics for high speed runnability and (b) explain speed and strain rate effects on runnability and strength retention. It should also help explain moisture and temperature effects during corrugating.

(2) An initial summary of the model concept is summarized in this report.

Section 6 - Flat Crush and Flute Formation Modeling

(1) Examination of medium specimens, which had been subjected to bending around a radius similar in size to that of a flute tip, showed that damage occurred to the fibers on the compression side of the bend at regular intervals. The damage appeared to be primarily fiber buckling, however some shear delamination of the sheet was observed. In general, the fibers in the tension zone of the bend and the fibers between the buckled areas appeared to be undamaged.

(2) A laboratory study to determine the factors which affect the location and extent of damage to the medium during bending is being conducted.

(3) The results of the testing program are being used to refine the finite element model of flat crush loads on a flute. Nonlinear finite element methods are being used in a parameter study of flat crush load resistance.

Section 7 - Commercial Box Abuse Study

(1) A testing program has been started which will study the effects of simulated service abuse on box performance. The abuse conditions include precrush of the combined board and elevated relative humidity conditions.

PROJECT TITLE: Board Properties and Performance

PROJECT STAFF: W. Whitsitt/R. Halcomb/J. Dees

PRIMARY AREA OF INDUSTRY NEED: Properties related to
                                end uses.

PROGRAM AREA: Performance and Properties of Paper
               and Board

| Date: 2/3/88 |
| Budget: $180,000 |
| Period Ends: 6/30/89 |
| Project No: 3571 |

PROGRAM GOAL:

Develop relationships between critical paper and board property parameters and
determine how they are achieved in terms of raw materials, sheet structure and
processing conditions.

PROJECT OBJECTIVE:

* To develop relationships between container performance, combined board proper-
  ties, and component properties.

* To improve the performance/cost ratios of combined board, linerboard, and
  medium.

* The short term goals are to (1) use structural models to assess the impact of
  papermaking factors on combined board and box performance and (2) improve
  medium end-use and converting performance properties.

PROJECT RATIONALE:

There are many aspects of container and component performance which have not
been adequately related to board properties through sound structural models.
Such models would identify the critical board properties needed for end use
performance. They would be used to select papermaking approaches to maintain
or improve box performance at less cost. An important step is to incorporate
the elastic stiffnesses of the board into such models, if possible. This will
enable us to use our knowledge on how papermaking factors affect the elastic
stiffnesses to make board improvements.

RESULTS TO DATE:

Our Rayleigh-Ritz analyses of box failure under several types of load indicated
that compressive strength (ECT) is the limiting property governing performance.
Further analyses of the ECT behavior of corrugated board showed that present
local buckling models fail to properly predict ECT strength when the strength of
the liners or medium is changed by certain papermaking operations, e.g. wet
pressing. Therefore new models have been developed which show that ECT is pri-
marily dependent on the compressive strength and/or elastic stiffnesses of the
liners and medium. The bending stiffness of the liners appears to have only a
minor effect on ECT. The importance of linerboard bending stiffness has been a
point of concern to our industry and these results indicate that it is much less
important than compressive strength. We are extending this work to combined
board flexural stiffness and box compression.

In the case of medium we have shown that the compressive strength is lowered by high bending and shear stresses imposed during forming. These losses in strength lower flat crush and ECT. The losses are inversely related to the density and Z-direction elastic stiffness of the medium. Densification via wet pressing is one way to improve end-use performance of medium.

Our current forming models indicate that satisfactory high speed runnability on the corrugator is dependent on at least four medium properties as well as nip geometry and medium web tension. Better runnability is obtained as MD tensile strength and stretch are increased and the coefficient of friction of the medium and medium thickness are decreased.

PLANNED ACTIVITY FOR FY 1987-88:

As noted above, our short term objectives are directed to (1) using structural models to assess the impact of papermaking factors on combined board and box performance and (2) improving medium end-use and converting performance properties. The structural models we are developing show how the elastic stiffnesses and compressive strengths of the components will affect combined board compressive strength (ECT) and box compressive strength.

During 1987 we will expand these analyses to optimize strength-to-weight ratios. This will include consideration of the impact of papermaking changes on ECT, combined board flexural stiffness and box compression in relation to combined board basis weight. Both commercial and experimental boards will be used to validate the work. Another part of our structural research is directed to identifying the main medium properties affecting the flat crush load-deflection properties of combined board. For this purpose finite element techniques are being used to determine the stresses involved in forming the flute arch and their subsequent effects on converting and end-use performance.

In the converting area we have developed a model which reveals that critical speeds for flute fracture and high-lows depend on four properties of the medium, the nip geometry of the fluting rolls, and the medium web tension. During FY 1987-88 we plan to expand our model to consider other flute geometries and to study the potential effects of papermaking changes on both runnability and compressive strength. Currently data is being collected to determine how strength losses during fluting are related to the model stress predictions.

In another part of our fluting work power spectral techniques are being used to determine why high-lows tend to occur at periodic intervals and to relate the frequencies involved to machine elements. While a part of this work will be shifted over to FKBG, basic research on vibration phenomena as related to high-low generation will continue under this project.

BOARD PROPERTIES AND PERFORMANCE

Project 3571

The objectives of this project are to: (1) develop relationships between container performance, combined board and component properties, and (2) determine ways to improve the cost/performance ratios of medium and liner-board. To fulfill these objectives both end-use performance and processing runnability on the corrugator are being considered. Our current work is divided into several parts, namely; (1) combined board warp vs. liner directionality effects, (2) liner and medium improvement, (3) runnability modeling, (4) ECT and box compression performance and (5) finite element analysis of flat crush and fluting stresses.

We have written two papers for presentation at the fall TAPPI Corrugated Container Conference. They are:

Whitsitt, W. J., "Papermaking Factors Affecting Box Properties", IPC Technical Paper No. 288 (May, 1988)

Schrampfer, K. E. and Whitsitt, W. J., "Faster, Alternative ECT Test Procedure", IPC Technical Paper No. 289 (May, 1988)

The first paper summarizes a portion of past work on this project. The second paper discusses work sponsored by the Fourdrinier Kraft Board Group (FKBG) on ECT test technology. Both papers will be published in TAPPI this fall and are appended to this report.

COMBINED BOARD WARP -- LINER ORIENTATION EFFECTS

Institute research allows us to rapidly measure specific elastic stiffness as a function of angle from the machine direction[1]. The results,

---

[1]Baum, G. A. Polar Diagrams of Elastic Stiffness: Effect of Machine Variables. IPC Technical Paper Number 242, June 1987.

plotted as polar diagrams, give information concerning headbox flows, jet-to-wire differentials, conditions in open draws and drying constraints. Variations in these factors affect quality uniformity and, hence board performance.

A typical in-plane polar plot is shown in Fig. 1[1]. The area and major axis of the shape can be computed and the angle (called polar angle) the axis makes with the MD can be determined. The shape, area and angle of lean of the polar plots vary across the width of the paper machine.
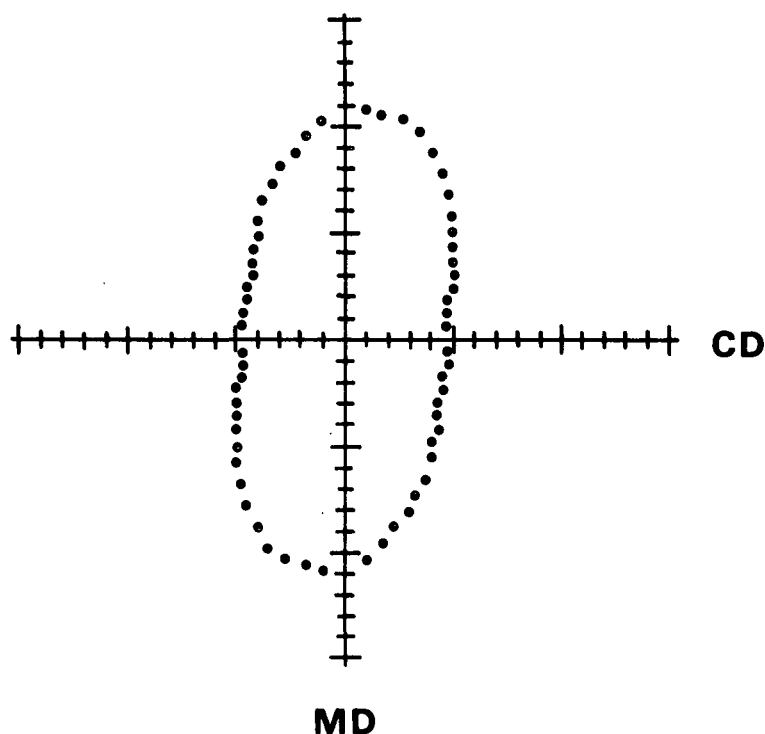
Figure 1. Typical in-plane polar plot.

For example, Fig. 2, taken from Baum's work, shows that the polar angles can vary greatly across the width of a paper machine. The differences in polar angle were attributed to stock flows from the headbox which have a flow component at right angles to the MD. The changes in polar angle across one linerboard machine are shown in Fig. 3. On this machine, about 300 inches wide,
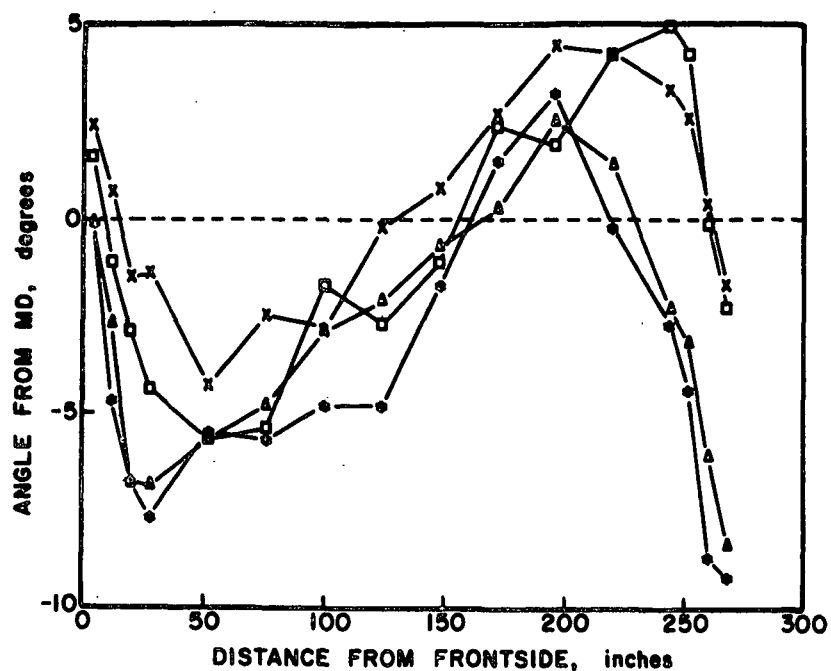
Figure 2. Angle of lean (polar angle) vs. position across the
           machine for four separate reel turn-ups.
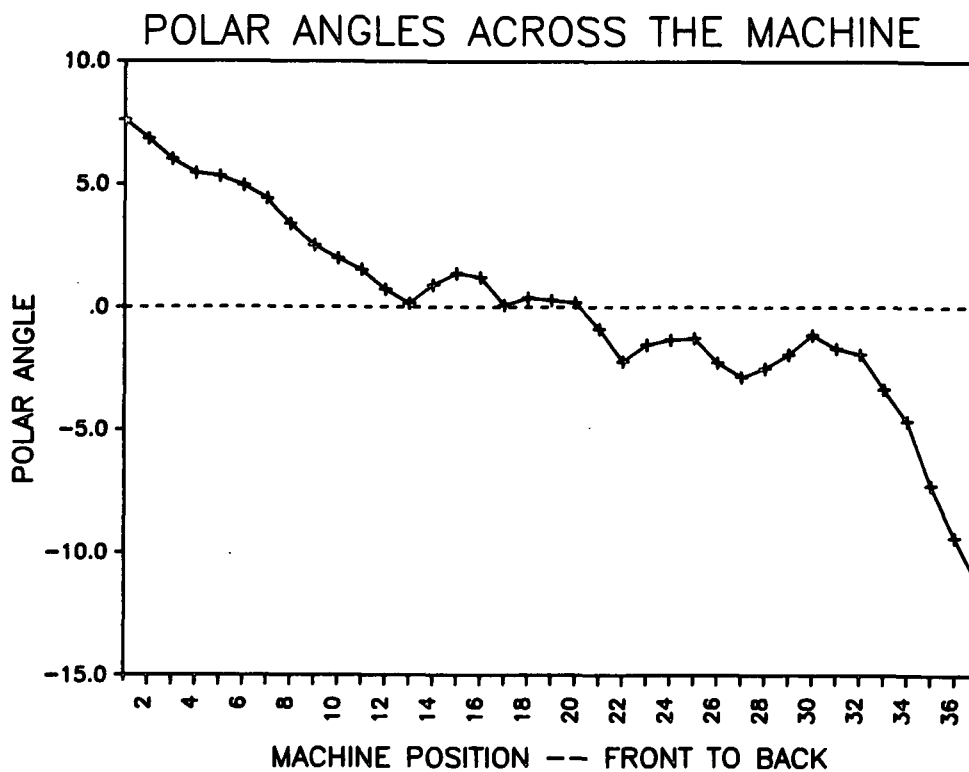
Figure 3. Large changes in polar angle can occur across a
           linerboard machine and, hence affect quality.

the polar angles were highest at the front, near zero over the middle region and sharply declined to about -10 degrees near the back of the machine. When the angular deviations become large, Baum noted that difficulties can be encountered in converting and end-use applications.

The shape, area, and MD/CD ratios also can vary greatly across machines although the profile for a given machine is often quite constant[1]. Factors influencing such profiles have been discussed in detail in past status reports on Project 3467 by Baum and co-workers.

Combined board warp must be avoided in the production of corrugated board. Excessive warp causes problems in feeding sheets to down-stream equipment such as flexo-folder-gluers. If too badly warped, jam-ups occur and the board may have to be scrapped.

Commonly combined board may warp in the MD, or CD, or various combinations of MD/CD warp, called twist warp. While warp is very dependent on the moisture conditions of the single-face and double-face liners at time of bonding, it is basically a manifestation of the hygroexpansivity of the liners. Therefore, papermachine factors which introduce differences in the hygroexpansivity characteristics of the liners can be expected to affect the proclivity to warp and the type of warp. The changes in elastic stiffness and polar orientation across a machine should also affect the hygroexpansivity of the sheet and hence, affect the warp proclivity.

In the case of corrugating, two linerboard webs are glued to medium to make single-wall board. If their moisture contents and dimensional stability properties are too dissimilar, excessive warp is likely to occur. For example, combining edge-cut linerboard rolls from one side of the machine profile shown in Fig. 3 could be expected to cause twist warp because the liner polar angles

deviate from the MD of the corrugated board. As the moisture content of the combined board changes with RH, the contraction or expansion characteristics of the two liners would tend to twist the combined board because of the misalignment of the liner properties with regard to the flute direction of the medium.

Two extreme cases can occur. In one case the polar angles of the two liners deviate in the same direction from the machine direction of the corrugated board (Fig. 4a). Less tendency for twist warp to occur would be expected with this configuration because the polar angle misorientations of the liners match each other. In the other case the polar angles of the single- and double-face liners deviate in opposite directions from the machine direction of the corrugated board (see Fig. 4b). Major twist warp should be obtained in this case because the dimensional changes of the liners will tend to twist the flutes as moisture content is varied.

a) Liner polar angles in
same direction

b) Liner polar angles in
opposite direction
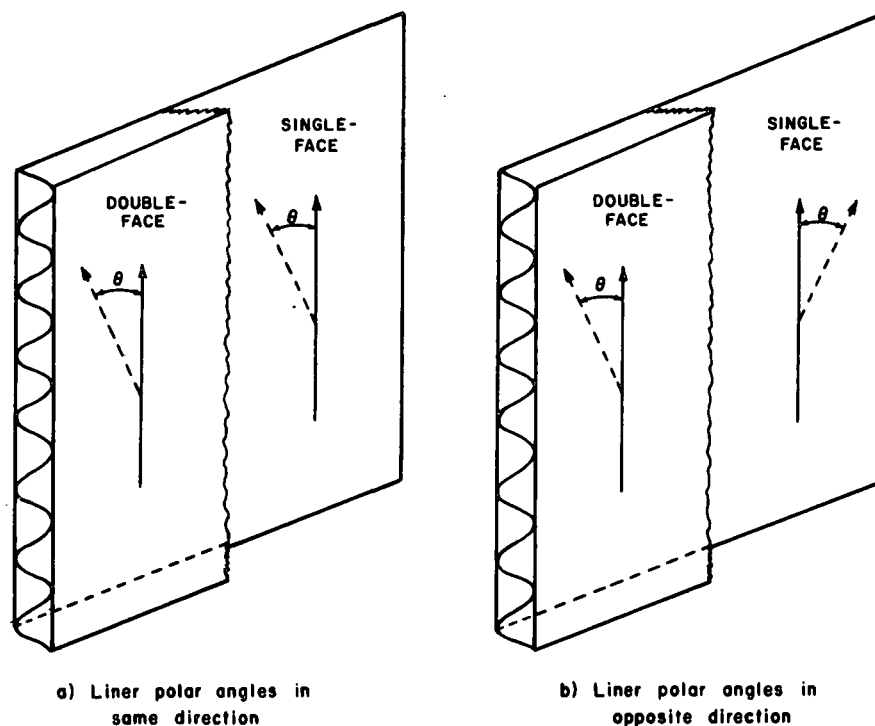
Figure 4.   Two opposite cases of liner polar angle misalignment.
Case (b) promotes twist warp.

To study the potential effects of liner polar angles on warp, combined boards were made up using 42-lb single- and double-face liners cut at 0, 5, 10 and 15 degrees to the average polar angle for the sample. For this purpose a 72-inch wide roll of linerboard on hand at the Institute was selected. Ultrasonic stiffness polar diagrams were performed every 12 inches across the roll width to determine the base stiffness characteristics across the width. This was done at start and end of the 100-foot strip taken for corrugating. The polar angles were essentially constant across the width (Fig. 5) and averaged 1.7 degrees from the machine direction.
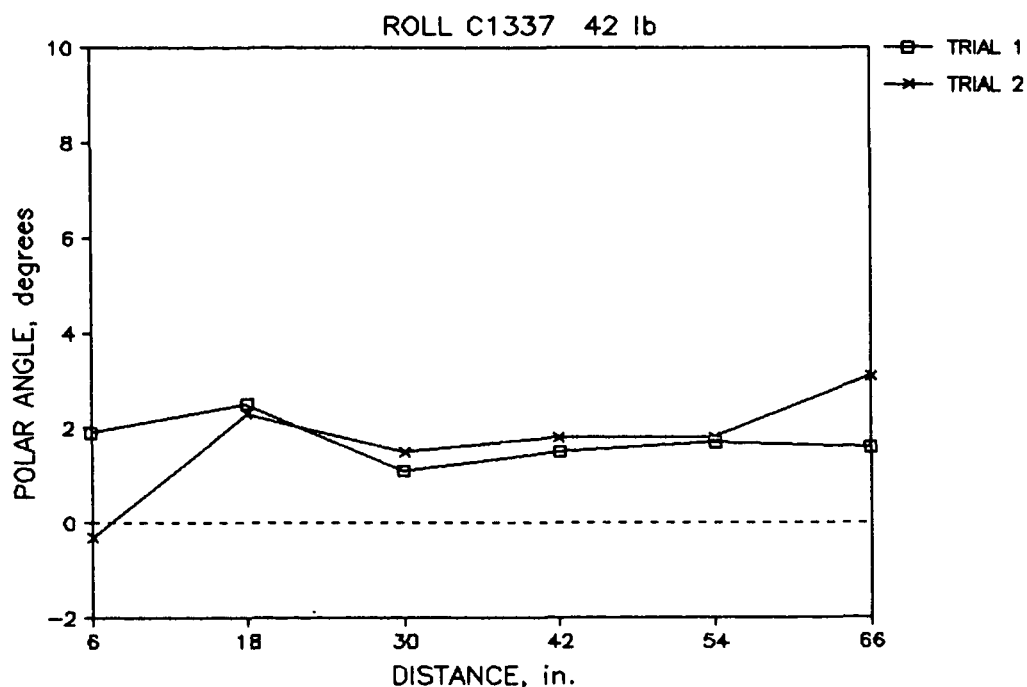
Figure 5. Polar angle deviations from machine direction for the
           42-lb liner used in fabricating combined board.

Linerboard sheets were then cut to have polar angles of -15, -10, -5, 0, +5, +10, and +15 degrees referenced to the polar angle of the base liner. The liners were fabricated into single-faced board on the Institute's pilot corrugator using a 26-lb medium. Double-faced boards were then prepared to have the following orientations:

1. Polar angles of SF and DF liners in same direction (case a) in the combined board: 0, 5, 10, and 15 degrees.

2. Polar angles of SF and DF liners in opposite direction (case b) in the combined board: 0, 5, 10 and 15 degrees.

After double-backing the sheets were allowed to dry at 50% RH and then placed in other RH atmospheres to determine the effect of moisture changes on warp. This simulates temporary storage of sheets off the corrugator in various plant atmospheres. The test RH levels being employed are 25, 70 and 90%.

The warp of the double-faced boards was measured relative to the centerpoint of the 12 by 40-inch sheets. The sheet was rested on a 4 inch high center support for this purpose. Warp measurements were taken at each corner and at the center of each edge. Table 1 shows the data obtained after exposing the boards to 90% RH. The warp measurements at 50% RH were subtracted from the 90% RH results to show how the warp changed due to humidity.

Combined boards made with liner polar angles deviating in opposite directions (Case b) from the MD of the combined board exhibited large twist warps when exposed to higher RH atmospheres. A three-dimensional view of the warped surface of the 10 degree samples (in comparison to the zero degree samples) shows that very large amounts of twist are induced with 10 degree liner polar angle deviations in the 90% RH atmosphere (see Fig. 6). The amount of twist warp increased steadily as the polar angle deviations increased from 0 to 15 degrees (Fig. 7). These results indicate that such combined boards will be dimensionally unstable as they pick-up or lose moisture. This can occur even if the moisture contents of the two liners are equal just before bonding. The combined board may appear relatively flat off the corrugator but further changes in moisture will tend to cause warp to develop.

Table 1. Combined board warp results at 90% RH for polar angles ranging from 0 to 15 degrees.

D.F.	S.F.	Board Orientation Angle, degrees[a]	Test RH, %		Warp, in., at various board locations[b]							
					A	B	C	D	E	F	G	H
left	right	15	50		3.51	3.92	3.03	3.35	3.44	3.87	3.02	3.38
			90		0.40	3.62	4.00	2.24	0.05	3.57	3.86	2.28
				DIF	3.11	0.30	-0.97	1.11	3.39	0.30	-0.84	1.10
left	right	15	50		3.40	3.90	3.10	3.47	3.44	3.90	3.01	3.30
			90		0.12	3.56	4.00	2.53	0.00	3.57	3.84	2.14
				DIF	3.28	0.34	-0.90	0.94	3.44	0.33	-0.83	1.16
				AV	3.20	0.32	-0.94	1.03	3.42	0.32	-0.84	1.13
left	left	15	50		3.16	3.90	3.09	3.34	3.10	3.95	3.50	3.36
			90		3.18	3.85	2.88	3.10	2.94	3.86	3.21	3.32
				DIF	-0.02	0.05	0.21	0.24	0.16	0.09	0.29	0.04
left	left	15	50		3.25	3.90	3.45	3.34	3.29	3.91	3.38	3.28
			90		3.16	3.85	3.18	3.23	3.10	3.90	3.08	3.23
				DIF	0.09	0.05	0.27	0.11	0.19	0.01	0.30	0.05
				AV	0.04	0.05	0.24	0.18	0.18	0.05	0.30	0.05
left	right	10	50		3.57	3.90	3.02	3.30	3.42	3.89	3.14	3.48
			90		1.12	3.54	3.68	2.65	0.70	3.70	3.96	2.83
				DIF	2.45	0.36	-0.66	0.65	2.72	0.19	-0.82	0.65
left	right	10	50		3.52	3.89	3.12	3.38	3.47	3.87	3.09	3.39
			90		1.30	3.65	3.73	2.81	1.00	3.72	3.83	2.72
				DIF	2.22	0.24	-0.61	0.57	2.47	0.15	-0.74	0.67
				AV	2.34	0.30	-0.64	0.61	2.60	0.17	-0.78	0.66
left	left	10	50		3.04	3.88	3.64	3.60	3.40	3.82	3.18	3.18
			90		3.32	3.87	2.86	3.11	2.87	3.82	3.08	3.38
				DIF	-0.28	0.01	0.78	0.49	0.53	0.00	0.10	-0.20
left	left	10	50		3.18	3.86	3.40	3.42	3.16	3.87	3.39	3.37
			90		3.55	3.88	3.13	3.45	3.56	3.85	3.00	3.38
				DIF	-0.37	0.02	0.27	-0.03	-0.40	0.02	0.39	-0.01
				AV	-0.33	-0.01	0.53	0.23	0.07	0.01	0.25	-0.11

Note: [a]Liner polar angle.
      [b]Corner measuring points: A, C, E, G
         Side center points: B, F
         End center points: D, H

Table 1 continued. Combined board warp results at 90% RH for polar angles
                    ranging from 0 to 15 degrees.

D.F.	S.F.	Board Orientation Angle, degrees[a]	Test RH, %		Warp, in., at various board locations[b]							
					A	B	C	D	E	F	G	H
left	right	5	50		3.38	3.87	3.40	3.58	3.58	3.87	3.18	3.39
			90		2.40	3.77	3.82	3.24	1.92	3.75	3.83	3.17
				DIF	0.98	0.10	-0.42	0.34	1.66	0.12	-0.65	0.22
left	right	5	50		3.53	3.91	3.30	3.45	3.38	3.87	3.34	3.54
			90		2.20	3.75	3.59	2.85	1.70	3.80	3.90	3.21
				DIF	1.33	0.16	-0.29	0.60	1.68	0.07	-0.56	0.33
				AV	1.16	0.13	-0.36	0.47	1.67	0.10	-0.61	0.28
left	left	5	50		3.30	3.90	3.47	3.48	3.33	3.90	3.42	3.40
			90		3.14	3.80	2.80	3.18	3.26	3.90	2.87	3.19
				DIF	0.16	0.10	0.67	0.30	0.07	0.00	0.55	0.21
left	left	5	50		3.19	3.88	3.48	3.52	3.40	3.92	3.40	3.43
			90		3.18	3.86	2.92	3.14	3.08	3.87	2.97	3.26
				DIF	0.01	0.02	0.56	0.38	0.32	0.05	0.43	0.17
--	--	0	50		3.52	3.93	3.48	3.59	3.52	3.91	3.48	3.59
			90		3.48	3.81	3.06	3.30	3.01	3.82	3.37	3.56
				DIF	0.04	0.12	0.42	0.29	0.51	0.09	0.11	0.03
--	--	0	50		3.52	3.92	3.50	3.60	3.60	3.91	3.49	3.57
			90		3.19	3.68	3.05	3.38	3.20	3.74	3.26	3.49
				DIF	0.33	0.24	0.45	0.22	0.40	0.17	0.23	0.08
				AV	0.19	0.18	0.44	0.26	0.46	0.13	0.17	0.06

Note: [a]Liner polar angle.
       [b]Corner measuring points: A, C, E, G
        Side center points: B, F
        End center points: D, H

COMBINED BOARD WARP PROFILE
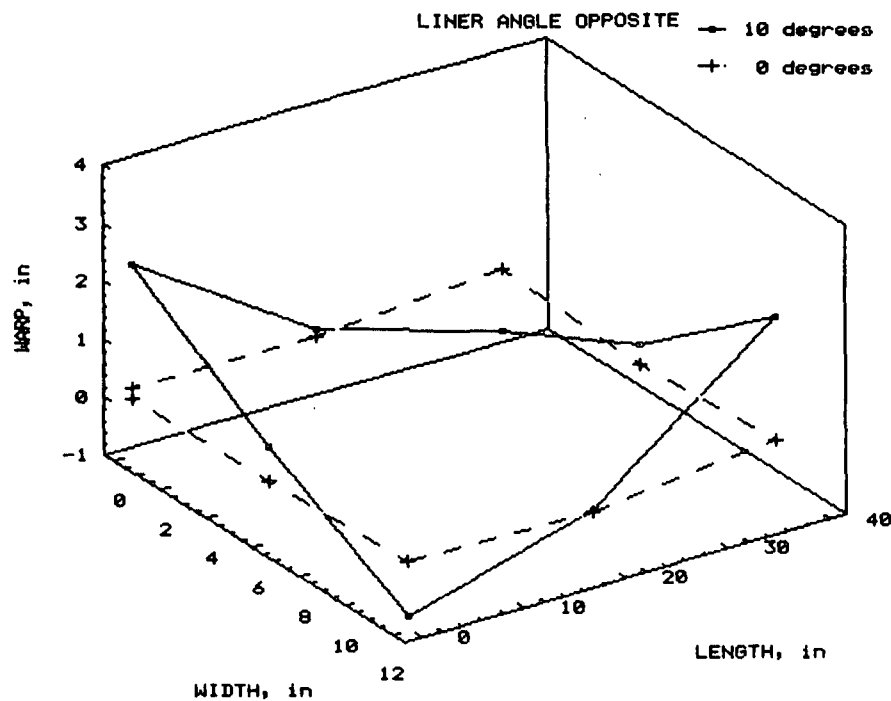
Figure 6. Comparison of warp obtained with 0 and 10 degrees of liner polar angle deviation in opposite directions from the MD of the combined board.

COMBINED BOARD WARP PROFILE
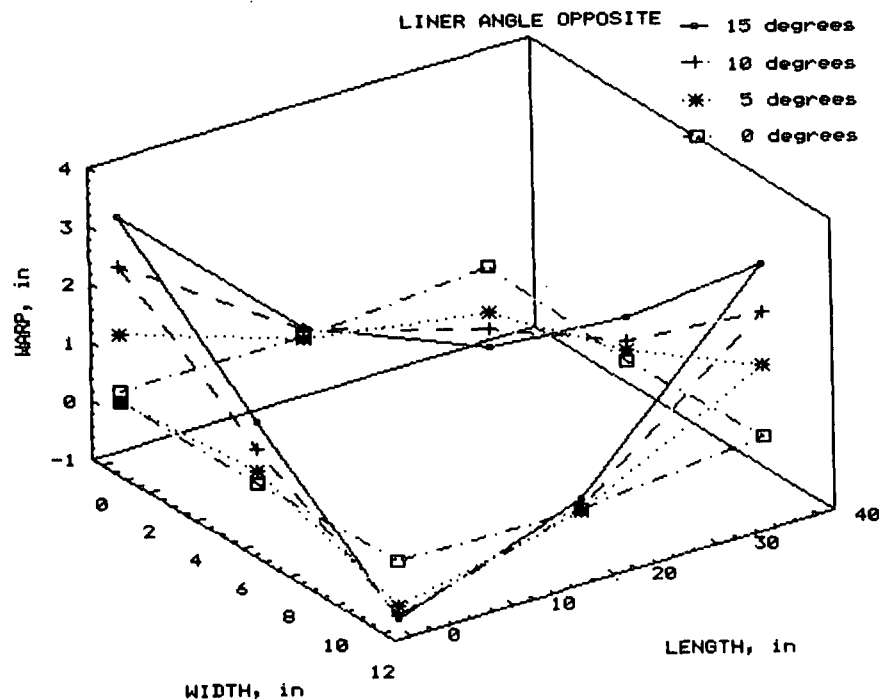
Figure 7. The amount of twist warp at 90% RH increased steadily with increasing polar angle deviation in opposite directions from MD of combined board.

Figures 8 and 9 show that the combined boards made with liner polar angles deviating in the same direction from the MD of the combined board tended to exhibit small changes in warp when exposed to 90% RH. This was true for the whole range of angular deviations studied (Fig. 9).

Hygroexpansivity measurements at various angular orientations to the MD of the liners are planned. These data will supplement the elastic stiffness results discussed above.

In general, box plant personnel have no information on the angular characteristics of linerboard rolls being combined and it is not clear that they could entirely compensate for such deviations on the corrugator. However, as information is developed on the effect of various paper machine factors on linerboard uniformity, it should be possible to reduce the magnitude of polar angle deviations and hence, promote less warp in the box plant from this cause. An FKBG study of liner and medium paper machine stiffness profiles is planned for next year which will provide baseline information in this area. In our funded work we plan to extend this work to show how moisture at time of bonding and polar angle deviations affect the degree of warp.

LINER AND MEDIUM IMPROVEMENT -- CHEMICAL ADDITIVES

In Project 3526 various wet end additives are under study as a means to increase fiber-to-fiber bonding strength under normal and humid conditions. Duopolymer systems comprised of CMC/PAE and PAA/PAE have been found to be effective strength agents for a variety of bleached and unbleached, conventional kraft and high yield pulps. However, these treatments may reduce wettability and, hence, affect converting operations.

COMBINED BOARD WARP PROFILE
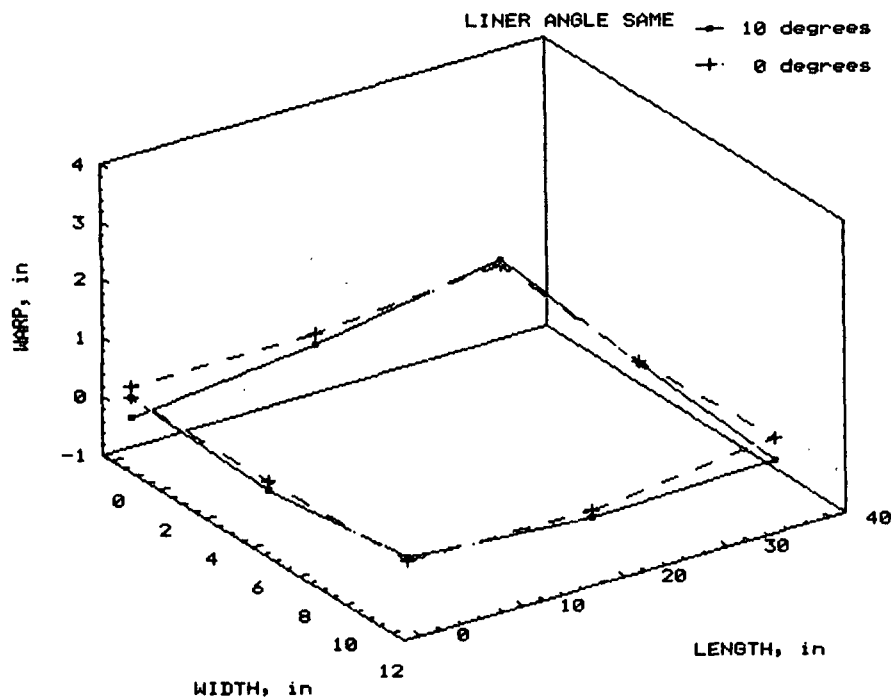
Figure 8.   Combined board warp profiles for boards made with
            SF and DF liner polar angles of 0 and 10°, in same
            direction.

COMBINED BOARD WARP PROFILE
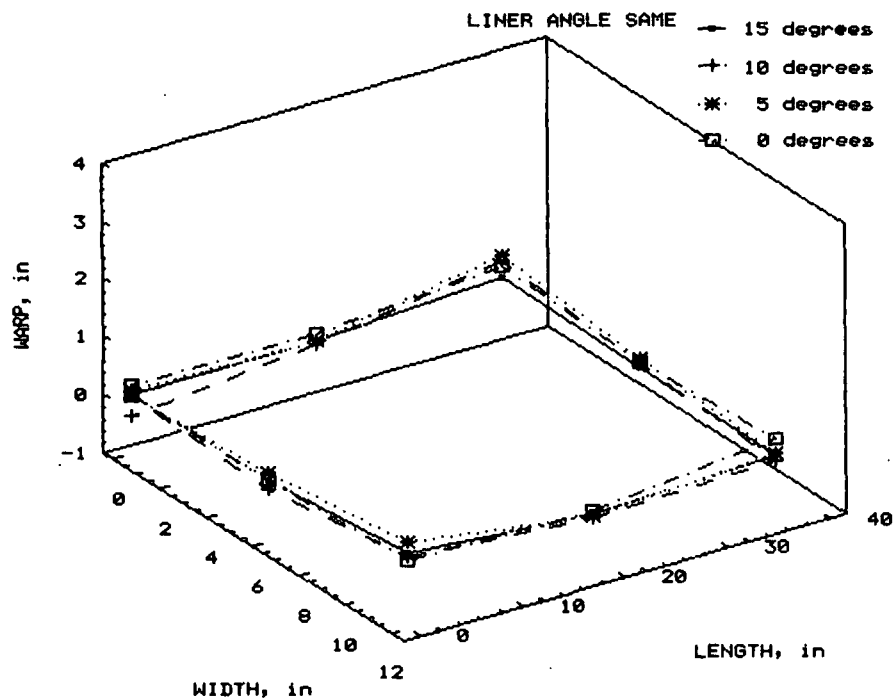
Figure 9.   Combined board warp profiles for boards made with SF
            and DF liner polar angles in same direction.

As an alternative to wet-end treatments we are studying the merits of using chemical surface treatments of linerboard and medium to improve converting and end-use corrugated board performance. This approach is being pursued jointly under this project and Project 3526. Our Surface Science Group selects and applies the selected agents; the converting behavior and end-use tests are being carried out by the Container Group.

Initial trials with various surface treatments were summarized in the March status report. For this purpose a commercial medium was surface treated with the following agents: starch, carboxymethylated potato starch (CMPS), PAE, PAE/starch and PAE/CMPS. Relatively large increases in compressive strength, tensile strength, and Concora were achieved with the PAE and PAE/starch/CMPS treatments. This held true at both 50 and 92% RH. These medium treatments increased combined board flat crush as expected. The ECT increases obtained with these agents were about as expected considering the liner/medium basis weight ratio in combined board.

However, the PAE type treatments greatly increased the water drop of the medium, making it much less receptive to the aqueous starch adhesive used in corrugating. As a result the pin adhesion results indicated that it was more difficult to bond the PAE treated sheets at high corrugating speeds because of the reduced wettability of the medium. With such treatments some modification of the starch formulation could be necessary. The reduced wettability resulting from PAE type treatments could also affect other high speed glueing or printing operations.

Currently, the Surface Science Group is screening other additives with regard to their ability to enhance strength under normal and high humidities but with less effect on the wettability of the linerboard or medium. These

screening trials are in process. The agents which show promise will be used
to tub size treat both linerboard and medium. This work is discussed under
Project 3526.

The treated boards will then be corrugated to determine their run-
nability on the corrugator and the effects of the selected agents on strength.
Most of this work should be completed for the March report.

RUNNABILITY MODELING -- STRENGTH LOSSES

Our runnability model shows that flute fracture, high-lows and medium
strength retention during fluting are dependent on medium properties, nip
geometry, and operational factors. Higher MD tensile strength and stretch and
lower medium friction and thickness promote forming medium with fewer high-lows
and less chance of flute fracture (see Fig. 10).
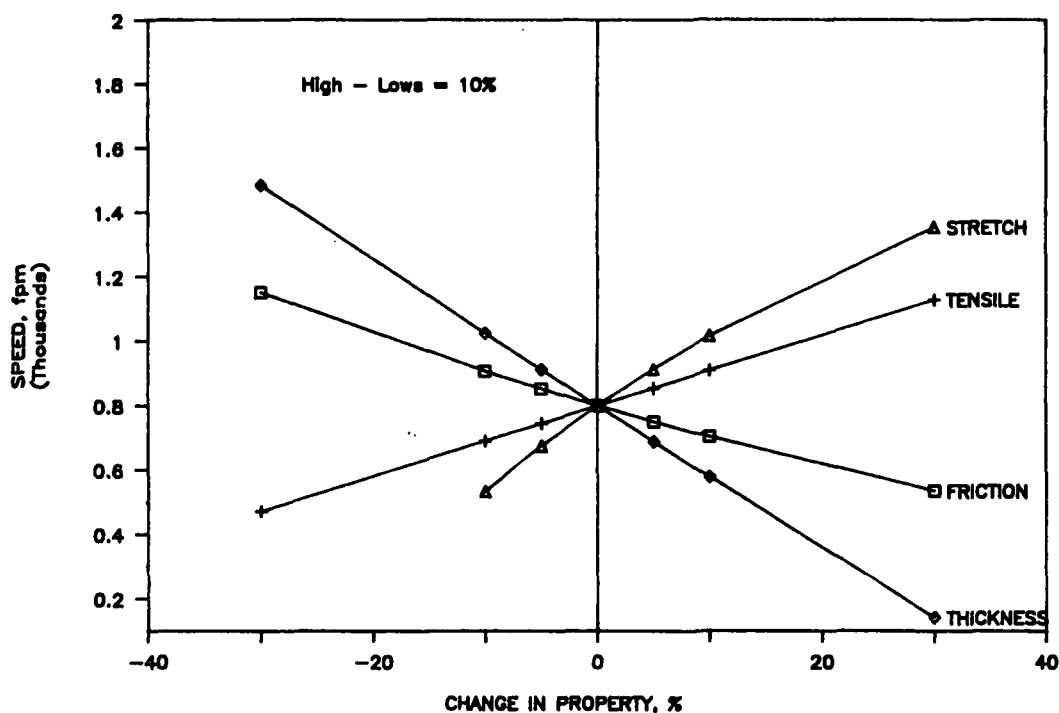
Figure 10. Effects of changes in medium properties on the speed
at which high-lows equal 10%.

We are also using the runnability model to study the effects of the fluting stresses on the strength properties of medium after fluting. This information is needed for our finite element analyses of the structural performance of corrugated board after fluting. For example, our past work has shown that flat crush and ECT will be affected by how much compressive strength loss occurs in the fluting process. The strength loss information is also another way to validate the uses of the runnability model.

As discussed in the last report, work is being carried out to determine how the tensile strength of the formed medium is affected by corrugating speed. As speed increases the medium is exposed to higher stresses during forming. It is these stresses which promote strength losses, high-low flute formation and flute fracture. For the purpose of this work several 26-, 33-, and 40-lb mediums were evaluated using long span tensile tests on the formed but unbonded medium.

As speed increases and approaches the point where fractures can be seen the tensile strength decreases. For example, Fig. 11 shows that the tensile strength for a 33-lb medium decreased from about 85% at 200 fpm to 34% at 1000 fpm. Occasional minor fractures could be seen in the 1000 fpm sample which accounts for the low strength values. Even if not visually evident the lower strengths at 600 and 800 fpm suggest that fiber-to-fiber bond damage is occurring. A more extreme example for another medium was shown in the last status report where the tensile strength was near zero after fluting at 800 fpm.

The stresses applied during fluting of a given medium are estimated as follows:

$$\text{Stress Ratio} = T/T_f = S_r \tag{1}$$

where:

T_f = ultimate MD tensile strength

$$\text{and } T = (T_0 + S/k_1)e^{\mu\theta} + [50k_2 \, T_f \, t/(R + t/2)\varepsilon] \tag{2}$$

where:

T_0 = brake tension, lb/in.

S = speed, fpm

μ = hot coefficient of medium friction

θ = effective total wrap angle in nip, radians

t = medium thickness, in.

R = radius of curvature of flute tip, in.

ε = MD stretch, %

k_1 and k_2 = empirical constants

PERCENT TENSILE RETENTION vs. SPEED
ROLL NO. 6518, 33 lb MEDIUM
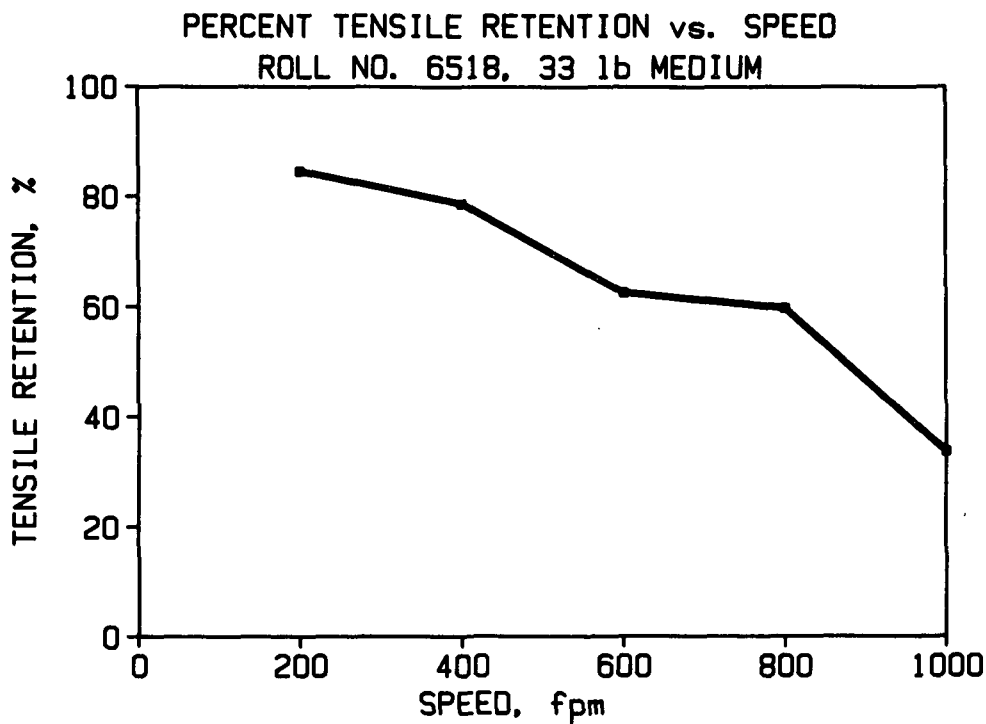
Figure 11. Tensile stresses of the fluted medium decline as
corrugator speed increases and the medium is
more highly stressed.

The stress ratios were calculated using the appropriate medium properties using Equations (1) and (2) for all the mediums tested. For the three 33-lb mediums evaluated, the tensile strength losses decreased as the stresses applied to the medium increased (Fig. 12). When the applied stress ratio was below about 0.75 the tensile strengths of the fluted mediums ranged from about 75 to 85% of their original strength. At higher stress ratios near 0.90 the fluted tensile strengths rapidly declined. Visible flute fractures are expected to occur as the stress ratios approach unity. In fact, some minor fractures were observed in medium 6518 with a stress ratio of 0.92. We believe this is an excellent confirmation of the theory used in developing the runnability model.

TENSILE RETENTION VS. STRESS RATIO
33 lb MEDIUMS
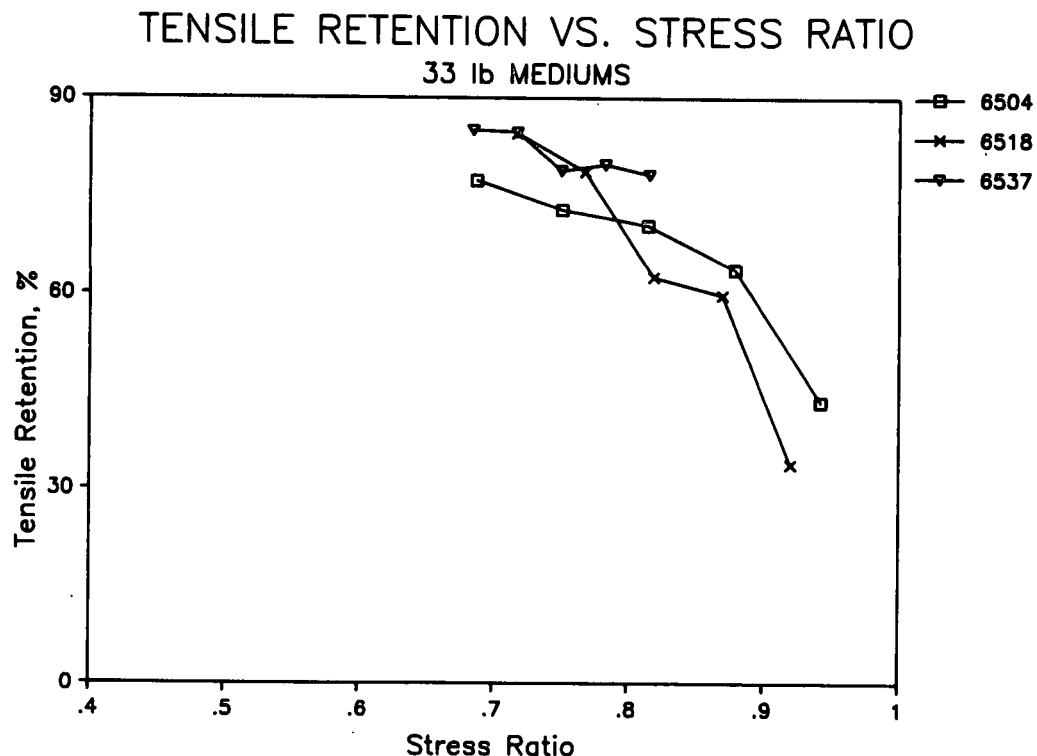
Figure 12.   Tensile strengths of fluted 33-lb mediums decrease at high levels of applied stress during fluting.

A study to determine the effects of varying medium chemical composition on high temperature tensile property behavior and runnability is in process. A schematic plan for material selection is shown in Fig. 16. This work is being carried out cooperatively under Projects 3571 and 3469. We are making 26-lb mediums from four furnishes and blends of the four furnishes. They are NSSC high yield semichemical hardwood, unbleached softwood kraft, bleached softwood kraft representing a highly delignified furnish and a blended NSSC furnish with synthetic fiber/polymer additive.
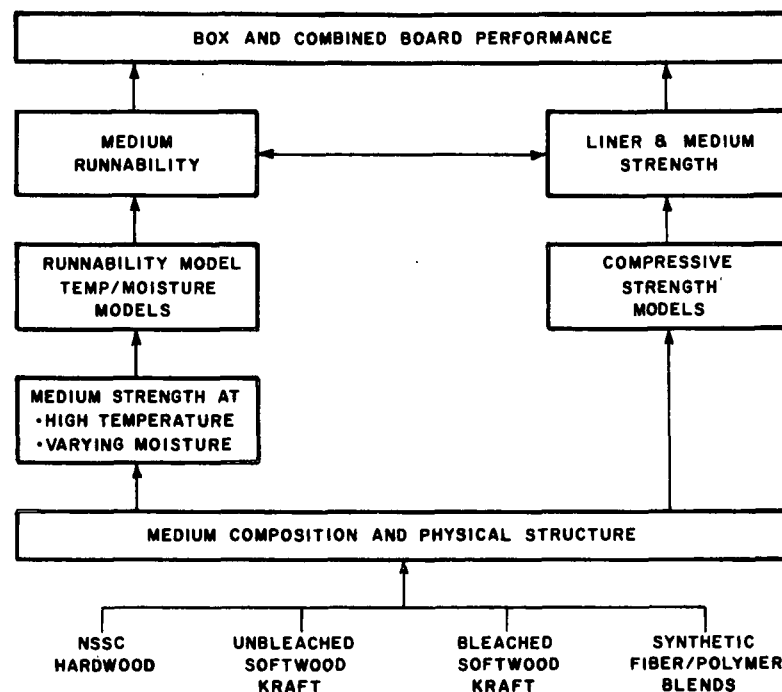
Figure 16.   Schematic plan for high temperature medium furnish study.

Experimental mediums are being made on the Formette and wet pressed at two levels from these furnishes as follows:

1. NSSC/unbleached softwood: 100/0%, 50/50%, 0/100%

2. NSSC/bleached softwood: 50/50%, 0/100%

3. NSSC with synthetic fiber-polymer blends in outer layers.

The NSSC and unbleached kraft sheets have been prepared and are being tested to determine their base properties. The bleached kraft and synthetic fiber/polymer blended sheets will be made in the near future. Table 2 summarizes the ultrasonic stiffness tests on the NSSC and unbleached kraft furnishes. Figure 17 shows that the base furnishes exhibit significant differences in geometric mean stiffness and, hence, should exhibit large differences in their strength and runnability properties. The chemical composition of the furnishes is also being determined.
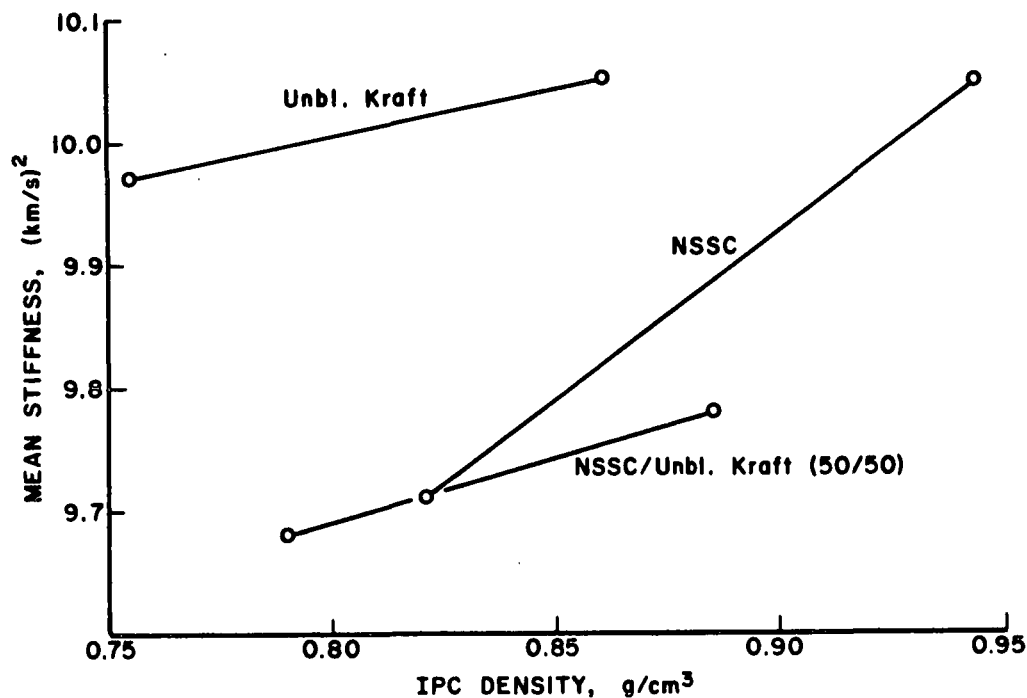
Figure 17. Elastic in-plane stiffness of base furnishes.

High temperature tensile tests will be carried out at temperatures of 225°F and 350°F using a heating time of 1 second. To check the effects of initial moisture content the specimens will be tested after conditioning to 50 and 80-85% RH.

Table 2. Base furnish properties.

	100% Unbl NSSC		100% Unbl SW Kr.		50/50 NSSC/Unbl Kr.	
Sample No.:	77-1	79-1	86-1	84-1	88-1	90-1
Wet Pressing:	Low	High	Low	High	Low	High
In-Plane Sonic Tests						
MD-CD Geom. Mean V^2, (km/sec)^2	9.71	10.05	9.97	10.05	9.68	9.78
Stiffness Ratio	2.37	2.26	2.08	1.96	2.22	2.22
NUXY	0.18	0.15	0.21	0.21	0.19	0.18
NUYX	0.43	0.34	0.44	0.4	0.41	0.41
Geom. Mean Nu	0.28	0.23	0.3	0.29	0.28	0.27
E_x/ρ, (km/sec)^2	13.77	14.31	12.8	12.87	13.29	13.43
E_y/ρ, (km/sec)^2	5.81	6.32	6.16	6.58	6	6.06
G/ρ, (km/sec)^2	3.16	3.36	3.26	3.38	3.23	3.48
MD-CD G. Mean E/ρ, (km/sec)^2	8.94	9.51	8.88	9.2	8.93	9.02
E_x, TAPPI, Gpa	6.21	6.95	7.01	7.59	6.35	6.92
E_y, TAPPI, Gpa	2.62	3.07	3.38	3.88	2.87	3.12
G, TAPPI, Gpa	1.43	1.63	1.79	2	1.55	1.79
E_x, IPC, Gpa	11.3	13.51	9.66	11.08	10.5	11.89
E_y, IPC, Gpa	4.77	5.97	4.65	5.67	4.74	5.37
G, Gpa	2.6	3.17	2.46	2.91	2.56	3.08
Phys. Test Results						
Basis wt., g/m^2	119.2	124.9	126.7	125.6	125.8	127.9
Caliper, (TAPPI), μm	264.4	257	231.1	212.9	263.1	248.2
st. dev.	18.29	20.31	6.11	5.84	25.38	16.2
Caliper, (soft pl.), μm	145.2	132.3	167.9	145.9	159.2	144.5
st. dev.	3.94	2.75	2.81	2.13	3.05	2.46
Density (TAPPI), g/cm^3	0.451	0.486	0.548	0.59	0.478	0.515
Density (soft pl.), g/cm^3	0.821	0.944	0.755	0.861	0.79	0.885

Note: Other furnishes being prepared: bleached kraft and synthetic fiber blends.

Corrugating trials will be carried out under controlled but normal conditions at 600 fpm. The resulting board samples will be tested for flute height, high-lows, flat crush and ECT. We plan to analyze the results to compare the effects of the following factors on high temperature tensile behavior and runnability: pulp chemical composition and type, density and non-cellulosic fiber amount and location.

RUNNABILITY MODELING -- SPEED EFFECTS

Several simple viscoelastic models were examined for their abilities to qualitatively describe dynamic properties of mediums. Specifically this preliminary work focused on the decrease in fracture speed with increase in brake tension.

The linear viscoelastic models considered included the standard linear model with two springs and one dashpot and the Berger model with two springs and two dashpots. The three element model shown in Fig. 18 was chosen for this discussion and will be referred to as the viscoelastic model. A computer optimization program was used to help determine values for the spring stiffness parameters and the dashpot dampening coefficient. Parameter values of λ_1 = 1700 lb/in., λ_2 = 2100 lb/in. and μ_3 = 3 lb-sec/in. were selected to give the viscoelastic model characteristics similar to those observed for the MD direction of medium 6811. Medium 6811 exhibited an ET of about 1700 lb/in. and a tensile load of 19 lb/in. at a strain of 0.02 in./in. at high temperature.

Using results from previous computer simulations of the labyrinth it was possible to model the MD tension history of the medium as it leaves the supply roll and is drawn towards the centerline of the nip. This modeled tension history is a function of the medium friction coefficient, roll geometry,
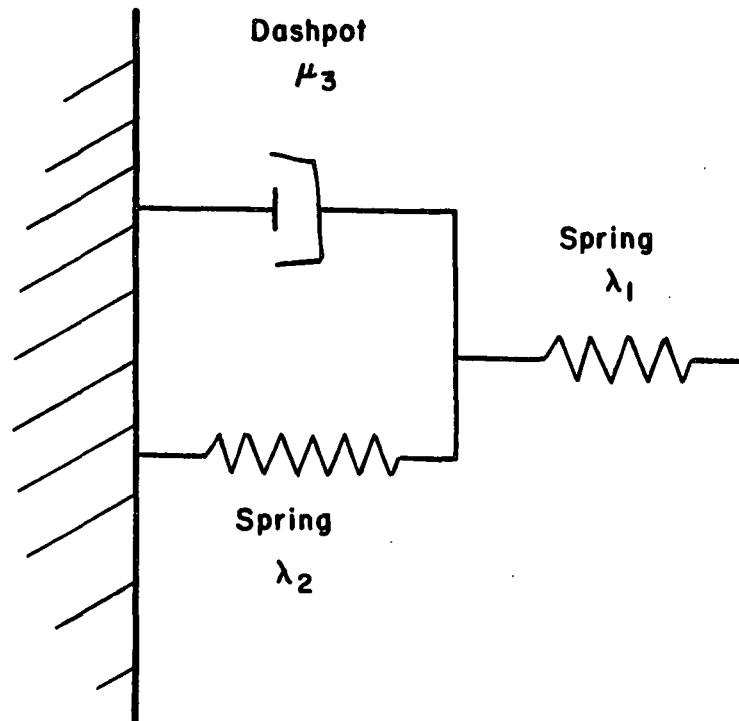
Figure 18. Simple viscoelastic model for describing
the dynamic behavior of medium.

initial brake tension and corrugating speed. For this study the roll geometry
and friction coefficient were held constant. Then the initial brake tension
determines the maximum web tension and the corrugating speed determines the
interval of time required for that maximum to be reached. A faster speed
requires the maximum tension to be reached in a shorter time.

This tension history model for the medium in the labyrinth was applied
to the viscoelastic model described above. The stresses and strains in each of
the three individual components, the two springs and the dashpot, were then ana-
lyzed. It was hypothesized that a critical stress for one of the three com-
ponents was responsible for the connection between initial brake tension and
fracture speed. This hypothesis of a critical component load gave good results
when applied to the dashpot, the component giving the viscoelastic model its

dynamic behavior. A critical dashpot load of 1.83 lb/in. was chosen by trial and error.

A computer program was written to use (1) the differential equation for the three element viscoelastic model, (2) the tension history model for the medium in the labyrinth, and (3) the critical dash pot load. The program computed the fracture speed corresponding to any specified initial brake tension. The results for brake tensions from 1.75 to 4.5 lb/in. are shown in Fig. 19. Note that the model correctly predicts that increasing medium brake tension decreases flute fracture speed.
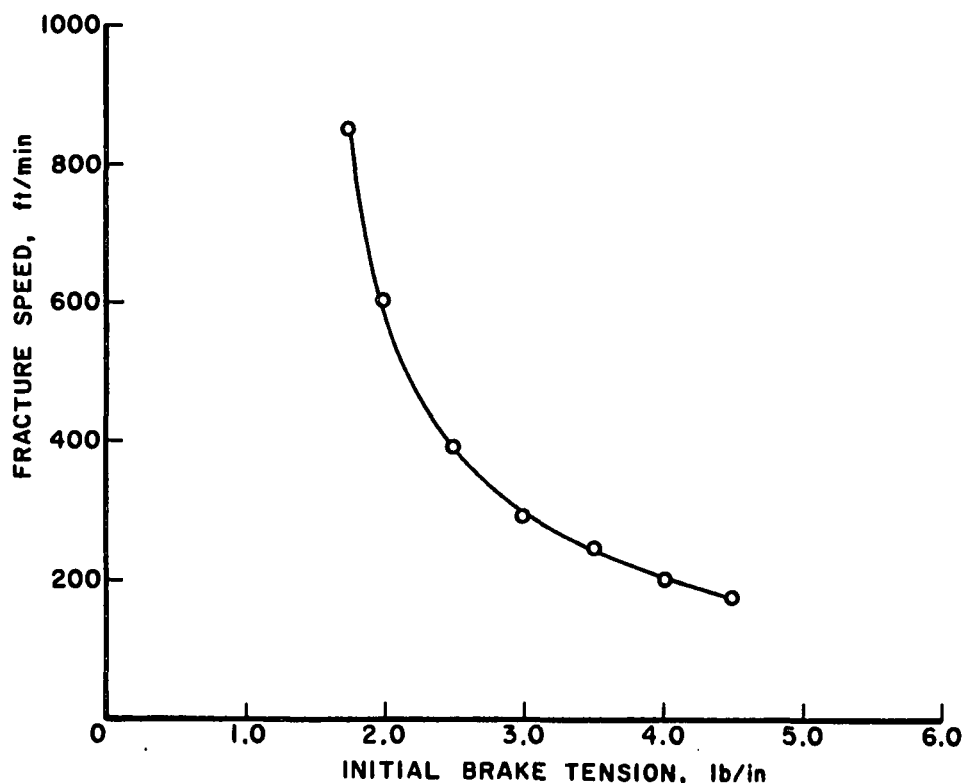
Figure 19. Linear viscoelastic model relationship between corrugating speed and brake tension.

This heuristic work suggests that a simple viscoelastic model may provide a useful tool for conceptualizing and studying the dynamic properties of

mediums. In particular it may provide a mechanism for relating how furnish and papermaking factors affecting the stress-strain curve influence such runnability properties as fracture speed, high lows and strength retention.

FLAT CRUSH AND FLUTE FORMATION MODELING

This portion of the project is directed toward studying ways to reduce the compressive strength loss that occurs in the medium during the corrugating process. Past research has shown that the medium experiences considerable damage to the MD compression strength during flute formation. Damage to the compression strength of the medium decreases the combined board's flat crush strength, edgewise compression strength, flexural stiffness and box compression strength. Determining the factors that would minimize the compression strength losses requires an understanding of the type and extent of the damage to the fibers. The research in this portion of the project has focused on building a greater understanding of the physical damage to the medium during flute formation. If the damage mechanism is understood, effective ways of reducing the damage may be developed.

During the flute forming process, the medium is subjected to a variety of stresses which include tension, bending, shear and thickness direction compression. It has been shown, in past research, that a significant portion of the strength reduction in the medium was due to bending. Also, our recent study of the geometry and stresses occurring during flute formation demonstrated that all portions of the medium making up a flute have been subjected to a significant level of bending during the forming process. The stresses due to bending during flute formation are apparently of sufficient magnitude to exceed the elastic range of the medium on the compression side (concave side) of the bend.

A previous progress report presented some of the results of a study which attempted to identify the extent of damage to the medium through its thickness. That study involved grinding thin layers off the surface of the medium, after bending, in an attempt to determine the contribution of each fiber layer to the total compression strength. While the grinding technique showed some promise, the testing was temporarily discontinued due to questions concerning the effect of grinding on the compression strength test results. However, observations of the way in which the medium performs when it bends around a radius may prove to be significant in explaining the damage mechanism in the medium during flute formation.

Presently, a testing program is being conducted to study the effects of bending on damage to the medium. In the testing, a length of medium (in the machine direction) was pulled 180 degrees around a rod, with a radius similar to that of a flute tip. A 1.0 lb/in. tension force was maintained on the specimen during the bending. It was observed, as the medium specimen was pulled around the radius, that it did not completely conform to the circular shape of the rod. Rather, it initially flexed elastically as it entered the bending area. This was due to the fact that the medium had a measurable amount of flexural stiffness (if the medium had zero flexural stiffness, it would conform completely to the circular shape). Thus, the medium initially acted like an overhanging or cantilever beam as it entered the bending area. The medium did not contact the rod until it was pulled to a length such that the elastic limit was exceeded in the medium at the point of entry to bending (this was also the point of maximum bending stress). The damage that occurred appeared to be limited to a localized section at the start of the bend, while the remainder of the cantilevered section of medium was undamaged. It also appeared, at the location of the damage,

that the fibers on the compression side of the medium buckled while the fibers on the tension side of the bend were undamaged. This damage pattern formed a partial hinge condition at the cantilevered support and resulted in the medium deflecting further, contacting the rod and conforming more closely to the circular shape. That process continued as more of the medium was pulled around the radius. Another section of the medium was then cantilevered out as it entered the bending area until the stresses at the start of the bend exceeded the elastic limit and again formed a damage point or partial hinge in the medium. The lines of damage, which ran across the width of the specimen, were located at approximately a 0.030 inch spacing. The result was that the medium, after bending, was made up of a series of apparently undamaged lengths linked by areas which were locally damaged. This is in contrast to previous assumptions that the damage would be uniformly distributed along the length of the medium.

After the medium specimens had been bent around the rod, the failure lines could be observed, on what had been the compression side of the bend. The failure lines appeared as small tubular shaped eruptions of the surface. The lines were very difficult to see on relatively thin medium specimens or specimens with a rough surface. To demonstrate the formation of the failure lines in a way that could be photographed, a length of liner board (11 mil caliper) with a relatively smooth surface was bent around the radius. The surface disruptions were photographed at a magnification of 10 and are shown in Fig. 20. The surface checking shown on Fig. 20 is normally an indication of compression damage, but the extent or depth of the damage to the fibers is not revealed from this view.

A side view of the specimen in Fig. 20 was prepared for observation under the microscope. The prepared specimen was carefully reformed around a

0.125 inch diameter rod. Three localized failure regions can be observed in Fig. 21. Two of the damaged areas are outlined. The area in the box on the right, in Fig. 21, has been magnified by a factor of 100 and is shown in Fig. 22. Figure 22 shows that the fibers on the compression side have buckled outward and the fiber buckling extends through more than 75% of the thickness. The buckled fibers would be ineffective in resisting compression forces. Only the fibers at the top surface (tension side) at the damage location appear to be capable of resisting further loading. The damaged area outlined on the left side of Fig. 21 has also been magnified by a factor of 100 and is shown on Fig. 23. In this area, the fibers on the compression side, comprising about 50% of the thickness, appear to have buckled inward and do not look like they would to be capable of resisting further loading. As with the area shown in Fig. 22, the fibers on the tension side of the bend in the damaged zone appear to be unaffected.

The next series of figures illustrates some of the difficulties in observing the damaged areas and in determining the extent of damage to the medium after bending. Figure 24 shows a specimen after bending and after it was forced to return to a nearly flat condition. The box on the right of Fig. 24 outlines a tubular surface disruption that was magnified by a factor of 100 and shown in Fig. 25. Only a small amount of surface disruption of the fibers are evident on what had been the compression side of the bend. The remainder of the fibers through the thickness appear to be undamaged.

Figure 26 shows the specimen, previously shown in its flat configuration in Fig. 24, after it was reformed around a 0.125 in diameter rod. Two areas of interest are outlined in the boxes on Fig. 26. The outlined area on the right in Fig. 26 has been magnified by a factor of 100 and is shown in
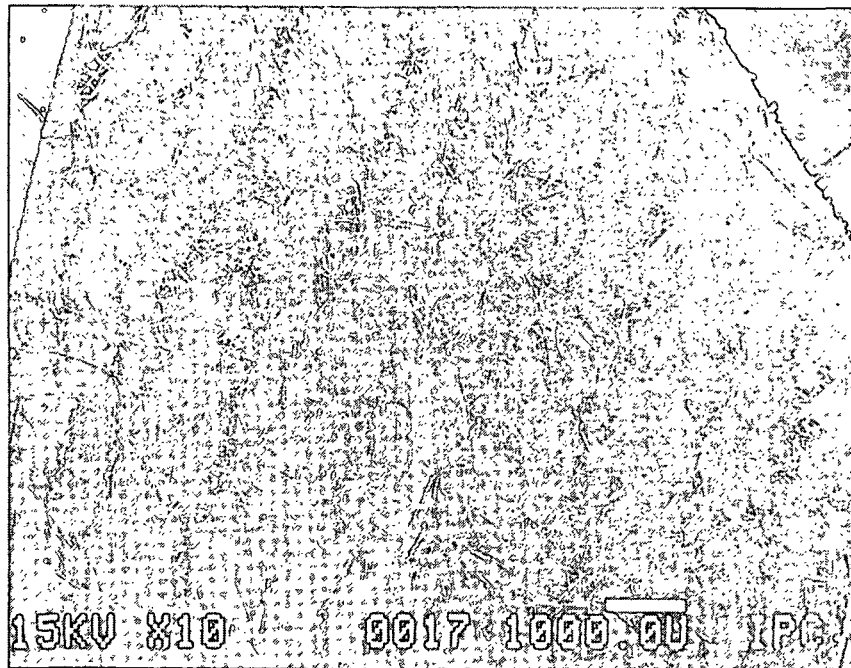
Figure 20. Surface checking was observed on the compression side of the medium after bending (view magnification = 10).
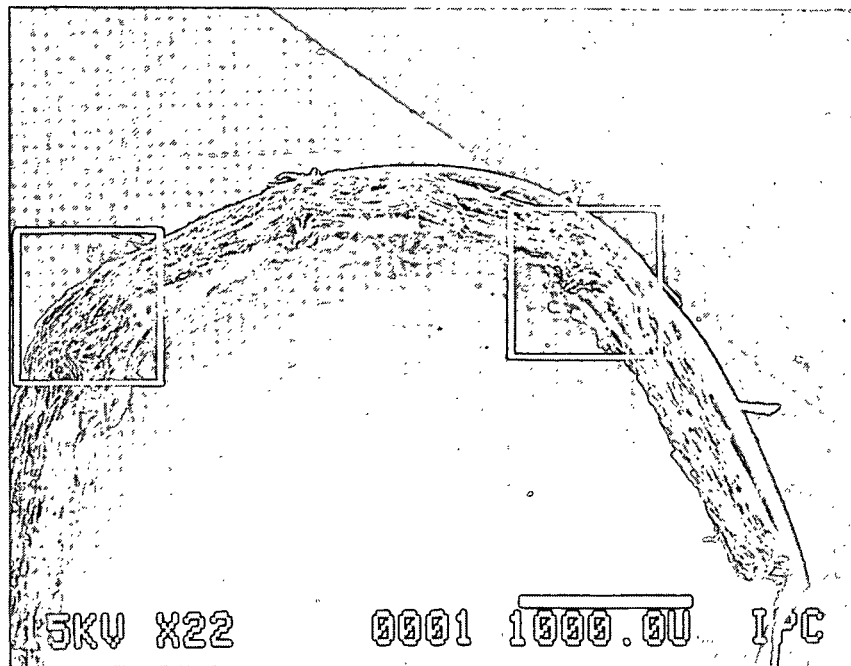
Figure 21. A side view of the specimen after bending shows three damage locations (view magnification = 22). The damaged area in the box at the right has been magnified and is shown in Fig. 22. The damaged area in the box on the right has also been magnified and is shown on Fig. 23.
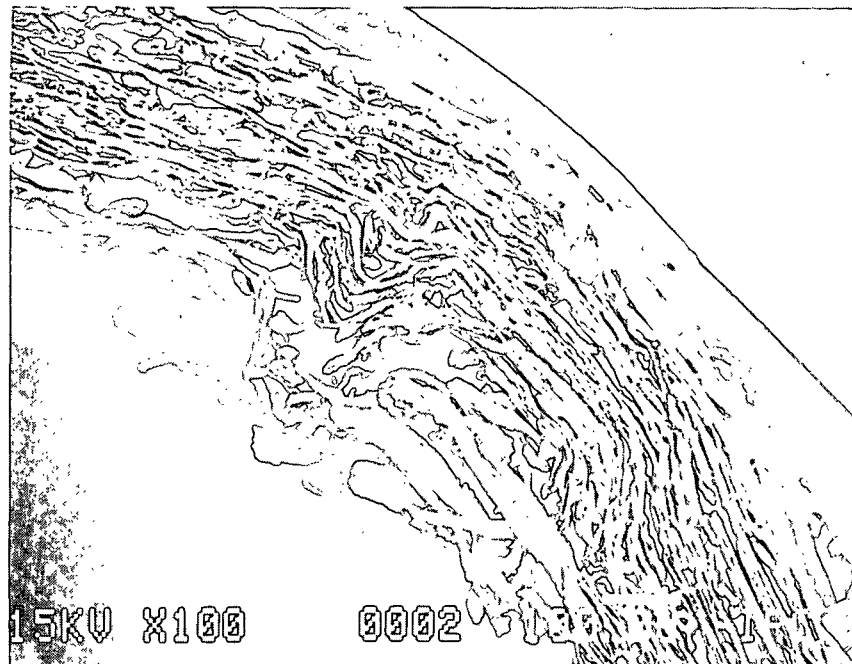
Figure 22. Fiber buckling in the damaged area occurred through about
            75% of the thickness (view magnification = 100).
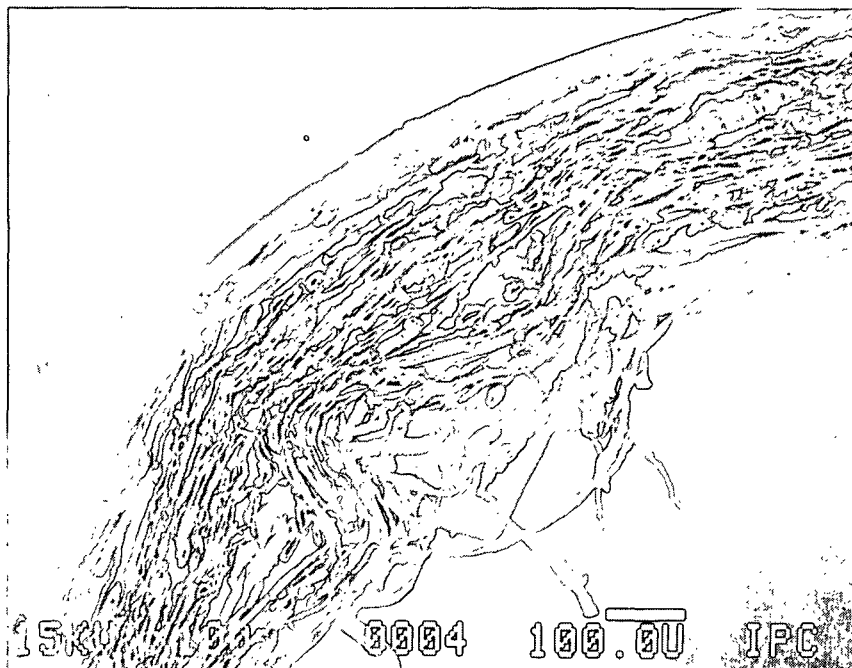
Figure 23. An inward buckling of the fibers appears to have occurred
            in this damaged area, through about 50% of the thickness
            (view magnification = 100).
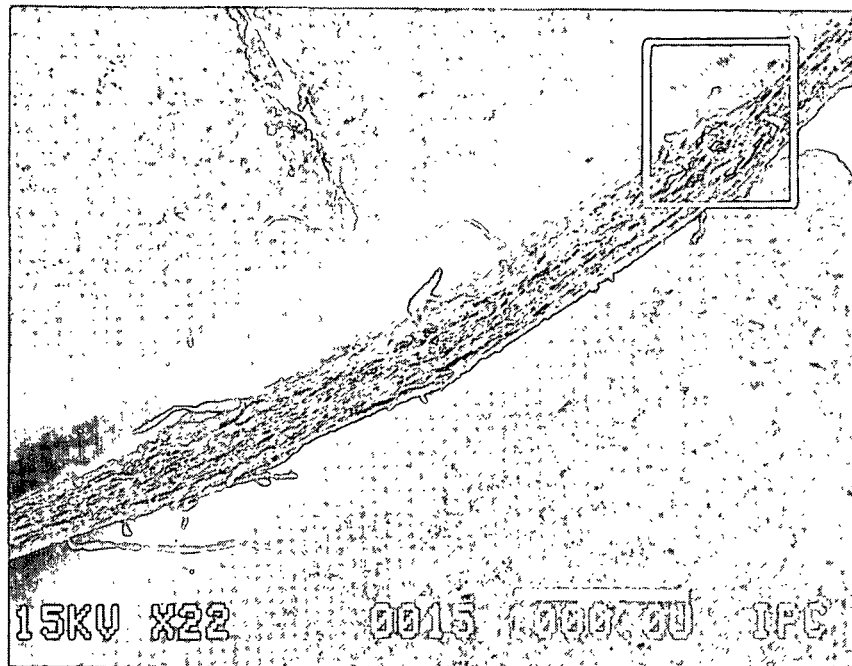
Figure 24. Side view of a specimen after bending and straightening back to a nearly flat configuration (view magnification = 22). The only detectable damage is a surface disturbance shown in the box on the right (this area has been magnified and is shown in Fig. 25).
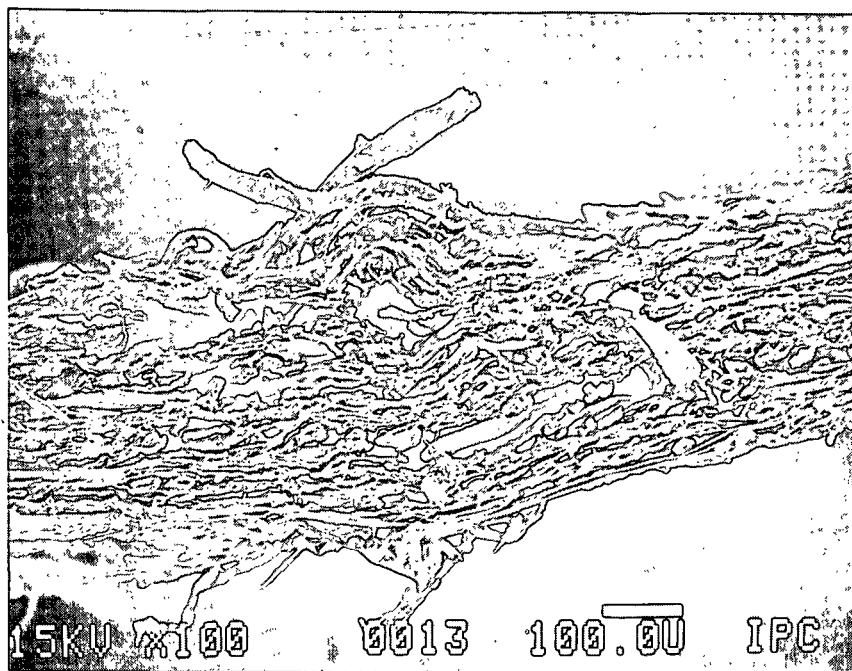
Figure 25. Side view of surface checking (view magnification = 100).
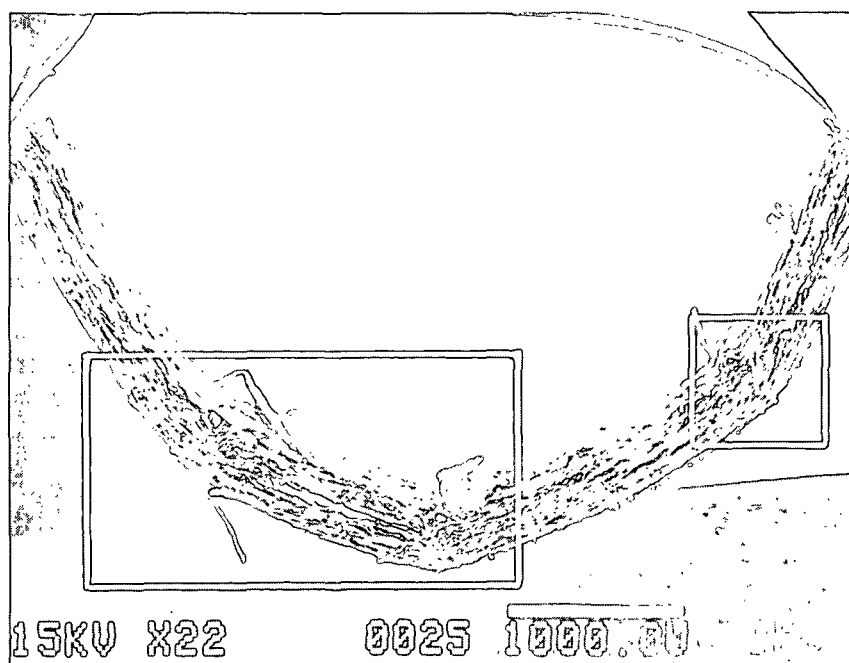
Figure 26. Side view of the specimen in Fig. 24, after it was reformed
            around a 0.125 in. dia. rod (view magnification = 22).
            The boxed area on the right shows the rebuckling of the
            fibers at what looked like a surface disturbance in Fig. 24
            (this area has been magnified further and is shown in Fig 27).
            The damaged area outlined at the right was undetectable in
            Fig. 24 (this area has also been magnified and is shown in
            Fig. 28).
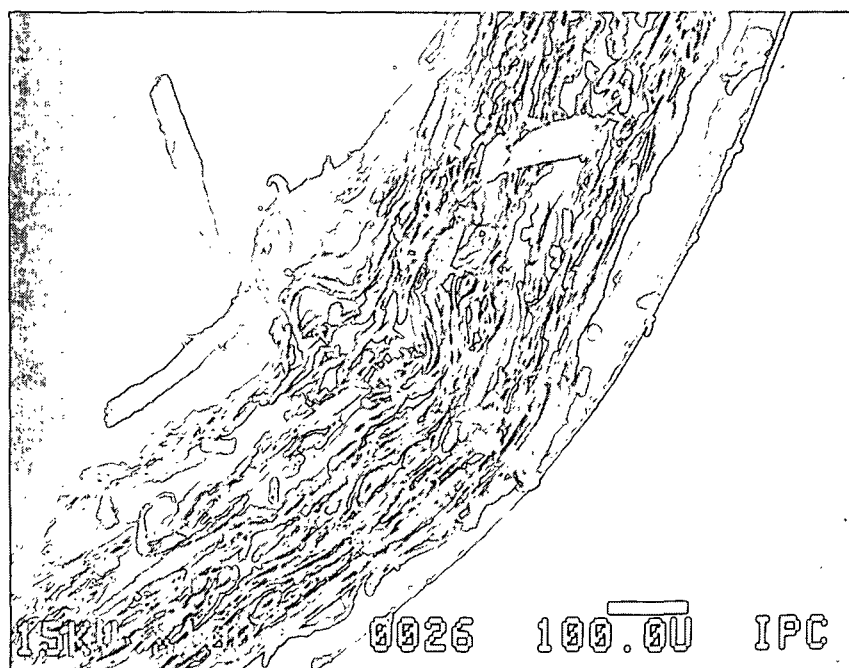
Figure 27. The fibers, in compression, buckle at a surface disturbance of
            the fibers when the specimen was reformed around the radius
            (view magnification = 100).

Fig. 27 (this is the same area shown in Fig. 25 of the failure zone in the flat configuration). Figure 27 shows how the fibers rebuckle when loaded with compression forces from the bending process. This was a relatively shallow damage zone with fiber buckling traveling through about 50% of the specimen thickness.

The box on the left side of Fig. 26 reveals another type of damage pattern to the fibers occurring during bending. This damage was not detectable when the specimen was in its flat configuration (Fig. 24). The area is shown in slightly higher magnification on Fig. 28. It shows two sets of buckled fibers on each end of a delaminated section of the specimen. This failure zone indicates that, in some areas, the damage may be a combination of fiber buckling and shear delamination. Figure 29 is a close-up view of the outlined area on Fig. 28 at one end of the delaminated section.

The surface eruptions of fibers were relatively easy to compress back into the sheet in the z direction. However, it is unlikely that the fibers would recover their compressive strength effectiveness after buckling in the bending process. The z-direction compression, that occurs in the medium during the corrugating process, may press the buckled fibers back into the sheet and mask the location of the compressive failure lines in the finished flute.

Presently, a testing apparatus has been designed and is being constructed for the purpose of studying the bending process more closely. The apparatus will allow the study of medium bending under different tensions, wrap angles, radius of bend, and speed. The effect of forcing the medium to conform to the radius will also be examined.
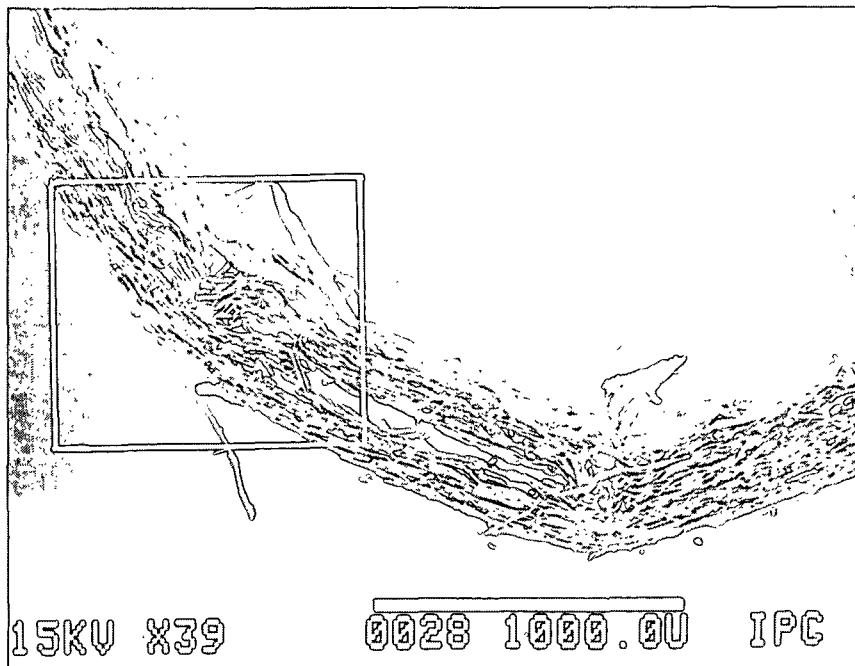
Figure 28. This damaged area appears to be fiber buckling at each end of a delamination in the sheet (view magnification = 39). The boxed area on the left side of the delamination has been magnified further and is shown on Fig. 29.

Figure 29. Side view of a damaged zone showing fiber buckling and sheet delamination (view magnification = 100).

A finite element analysis of flat crush loads on a flute is presently being conducted. This analysis was previously attempted assuming uniform medium properties. A new analysis will look at the effect of damaged zones of the medium at intervals around the flute. A nonlinear finite element analysis program is being used for this large deflection problem.

COMMERCIAL BOX ABUSE STUDY

During the manufacture and working life of a corrugated container, the combined board is many times subjected to conditions which are less than ideal for optimum performance of the box. Feeder rolls on the manufacturing line may compress the board in the thickness direction past the elastic limit. Excessive thickness direction compression (precrush) may adversely affect the flat crush load resistance, flexural stiffness, ECT, and box compression strength. After manufacture, the container may be subjected to elevated relative humidities in a warehouse. Therefore, this portion of the project is directed toward determining the effects of simulated service abuse conditions on commercial board and boxes. The simulated service abuse conditions that will be examined include the following:

1. Thickness direction compression (precrush) of the board.
2. Exposure to elevated relative humidity conditions.
3. Combined effects of precrush and elevated relative humidities.

Past research has shown that, in general, the above abuse conditions reduce box performance. However, a quantitative assessment of the performance of commercially produced combined board when subjected to the abuse conditions is necessary to judge the relative importance of the conditions. The testing program would also develop baseline results for ECT, flexural stiffness and box compression strength with commercial board.

Corrugated board blanks have been obtained for use in the testing program. The boards are C flute with 69-lb liners. Boards with 26-lb and 33-lb mediums will be tested.

The simulated service abuse conditions which will be used in this testing are as follows:

1. The boards will be subjected to two levels of precrush. The precrush levels are presently being determined in a pilot study. In addition, a set of control samples with no precrush will be tested. All precrushing will be conducted at 50% RH and 73°F. Precrushing of the corrugated board blanks will be done with a roll press.

2. The boards will be subjected to relative humidity conditions of 50% and 85-90% at a temperature of 73°F.

Combining the two service abuse conditions (3 precrush levels and 2 relative humidity conditions) will result in a total of six different conditions to assess.

The following tests will be conducted on the board specimens: caliper, basis weight, flat crush load deformation curves, ECT, MD and CD flexural stiffness, and top load box compression. Tests on the component materials will be conducted where possible.

APPENDIX

PAPERMAKING FACTORS AFFECTING BOX PROPERTIES

W. J. Whitsitt
Container Group Leader
The Institute of Paper Chemistry
P.O. Box 1039
Appleton, WI 54912

ABSTRACT

This study was directed to determining the effects
of selected papermaking changes in the manufacture
of linerboard and medium on combined board and box
compression properties. The effects of the follow-
ing factors were considered: increased wet press-
ing, reduced directionality, and strength additives.
Our results show that linerboards made with
increased wet pressing exhibit higher compressive
strengths due to increased fiber bonding. Combined
boards made with more highly wet pressed liners
exhibit increased ECT and flexural stiffness. This
indicates that the increases in liner compressive
strength are more important to box compression
properties than the reductions in thickness accom-
panying wet pressing. Reducing the MD/CD stiffness
ratio of the liners increases ECT and has little
effect on the geometric mean flexural stiffness of
the combined board. Based on the McKee box formula,
higher box compressive strength should be achieved
with more highly wet pressed liners and liners with
lower MD/CD ratios.

INTRODUCTION

During their service life, corrugated containers
are often subjected to high compressive loads.
Therefore, compressive strength is the single most
important end-use requirement for corrugated boxes.
McKee, et al. (1) showed that the top load compres-
sive strength of a box is dependent on two proper-
ties of the combined board. They are edgewise com-
pressive strength (ECT) and flexural stiffness.
Their work reveals that ECT is about three times
more important than flexural stiffness.

ECT is mainly dependent on the compressive
properties of the components; combined board·
flexural stiffness depends primarily on the elastic
moduli of the liners and to a limited extent on the
medium. Both are also dependent on corrugating
quality.

Recently, we have shown that the compressive
strength of paperboard is related to the elastic
moduli of the board because the fibrous elements
within the board become unstable and buckle (2).
(Note: the terms elastic moduli or stiffness refer
to the Young's moduli of the paperboard.) These
moduli can be conveniently measured using non-
destructive ultrasonic techniques (3). Our work
has shown that the elastic moduli are well related
to the compressive strength of containerboard and
to ECT (4). Because of their nondestructive nature,
ultrasonic techniques can be used in the laboratory
and on the paper machine to monitor and control
product quality (5).

Various relationships between the combined
board properties and containerboard properties have
been developed. For example, ECT is commonly pre-
dicted from the compressive strengths of the com-
ponents. However, there has been concern that such
relations would not hold when containerboard is wet
pressed more and becomes thinner. These concerns
have intensified as our industry has begun to
improve compressive strength via improved pressing
and lower MD/CD ratios. Some of these same con-
cerns arise when efforts are made to select liner
and medium components to optimize box compression
strength for a given combined board weight (6,7).

To show how selected papermaking changes
affect ECT and combined board flexural stiffness,
linerboards were made having different ratios of CD
compressive strength to the bending stiffness.
(Note: to avoid confusion between the bending
properties of the components and combined board,
the term "bending stiffness" will refer to the com-
ponent property; "flexural stiffness" will refer to
the combined board property.) Special mediums were
also made to determine the effects of increased wet
pressing on runnability and combined board strength.
The tests on the combined boards made from these
materials were analyzed to show the effects of the
following papermaking factors: increased wet
pressing, reduced MD/CD ratio and selected strength
additives.

As part of our current work, various relation-
ships between combined board and component proper-
ties are being examined to determine their accuracy
when papermaking and other conditions are varied.
Another goal of our work is to incorporate the
elastic moduli of the components in such relation-
ships. This will allow use of the expanding tech-
nology of ultrasonic testing to characterize board
and box performance. The results of these analyses
will be summarized in a future paper.

LITERATURE REVIEW

The relationship between ECT and component charac-
teristics has been analyzed in two main ways. The
first and simplest approach is to sum the compres-
sive strengths of the components allowing for the
draw of the medium. This approach gives good pre-
dictive accuracies if based on appropriate sta-
tistical weighting factors.

In the second approach, combined board is
treated as a structure comprised of narrow flat
plate elements of liner between flute tops and flat
or curved plates of medium (Fig. 1). These
miniature plate elements could become unstable and
buckle in the same way that a box panel buckles in
top load compression. When such local buckling
occurs, the combined board ECT could be dependent
on the edgewise compression and bending properties
of the liners and medium. Various papermaking fac-
tors can affect the compressive and bending prop-
erties of containerboard in different ways, e.g.,
wet pressing or refining. It has been speculated
that if local buckling is of importance, then fac-
tors such as improved wet pressing of the liners
and medium might not increase ECT and box compres-
sion in the expected way because of the decreases
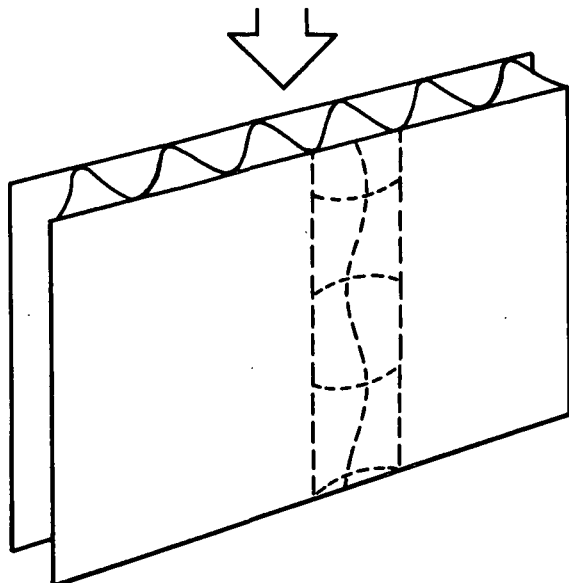in component thickness.

Fig. 1. Corrugated board showing component plate elements.

The second approach has been pursued by workers at the Institute, the Forest Products Laboratory, and other locations (8-10). The more recent model by Johnson treats the combined board component elements as a case of inelastic buckling and assumes the components are isotropic rather than orthotropic. The solutions are nonlinear and require empirically fitted CD compressive stress-strain curves. This approach requires specialized testing (11) and a sophisticated computer analysis. As one alternative, ECT may be analyzed using the same approach as used in developing the McKee box formula (10). In this approach the compressive failure of each miniature plate element will depend on the edgewise compressive strength and bending stiffness of the liner or medium element; then the ECT strength equals the sum of the liner and medium miniature plate element compressive strengths. In past work good agreement with observed ECT strengths was obtained (10) using this approach.

The combined board flexural stiffness in each direction is estimated by summing the products of the elastic modulus of each component times its moment of inertia relative to the neutral axis of the combined board (12-14). As a good approximation combined board stiffness is equal to $EtH^2/2$ for a balanced constructed where E is the elastic modulus of the liners, t is liner thickness, and H is the combined board caliper. Thus, papermaking factors which increase E in the appropriate direction and t will increase the combined board stiffness in that direction. Combined board flexural stiffness is sensitive to the caliper of the combined board; thus, it is necessary to avoid crushing the board during conversion.

EXPERIMENTAL PROCEDURES

To determine how selected papermaking factors affect board and box properties, experimental linerboards and mediums were made. The linerboards were fabricated into combined board on the Institute's

pilot corrugator using a 26-lb commercial medium. The experimental mediums were combined with commercial 42-lb liners.

The experimental linerboards and mediums were made using a Formette Dynamique sheet former and dried on a belted drum press to simulate machine pressing and drying. Two sets of sheets were prepared for this study under varying conditions as follows:

Set 1. Experimental Linerboards. The sheet making conditions were varied to give linerboards with varying ratios of compressive strength to flexural stiffness in order to check the effects of liner bending stiffness on combined board and box properties. For this purpose 33-, 42-, and 69-lb liners were made at three wet pressing levels with a MD/CD elastic modulus ratio of about 2.5. At the intermediate wet pressing level, liners were made having MD/CD elastic modulus ratios of about 3, 2.5, and 1.0. Some additional sheets were made with a starch additive using application rates of 2 and 4%. The furnish was a 100% softwood kraft pulp.

Set 2. Experimental Mediums. The 26-lb oriented mediums were made using three wet pressing levels. A furnish comprised of 75% semichemical fiber and 25% softwood kraft was used. The liner-boards and mediums were tested for compressive strength following the TAPPI procedures for ring crush and STFI short span compression. The in-plane and thickness direction elastic moduli were determined using the procedures developed by Baum and co-workers (5). The combined board tests were carried out using TAPPI procedures.

DISCUSSION OF RESULTS

Papermaking Effects - Linerboard

As wet pressing is increased, fiber-to-fiber bonding and sheet density increase; hence, most sheet properties increase. For example, the CD short span compression results for linerboard in Fig. 2 increase as density increases. Thus, from a compression standpoint the denser liners would be expected to increase ECT and hence, box compressive strength.

In contrast the geometric mean bending stiffnesses of the liners decrease with increasing density as shown in Fig. 3. This would be expected because the bending stiffness of the liners is dependent on the cube of the thickness and Young's modulus. The increases in density due to increased wet pressing decrease thickness sufficiently to counterbalance the increases in elastic moduli obtained by densification. Figure 3 shows that large changes in the bending stiffnesses of the liners were obtained in this study. If the bending stiffnesses of the liners have an important effect on combined board ECT, then large decreases in the bending stiffnesses of the liners due to increased densification would be expected to lower ECT and hence, box compressive strength. One of the objects of the present work is to test this hypothesis.

As the MD/CD ratio of the sheet is decreased (Fig. 4), the CD STFI short span compressive

2

2

strengths of linerboard increase. Thus, making a squarer linerboard sheet would be expected to increase ECT and box compressive strength. On the other hand changing the MD/CD ratio has little effect on the geometric mean bending stiffness of the liners (Fig. 5). Therefore, the bending stiffness changes for the linerboard will not affect the geometric mean flexural stiffness of the combined board and hence, box compression (from the McKee formula). These changes in the MD/CD ratios of the liners provided another way to determine if the bending stiffnesses of the liners have a major effect on box compressive strength.

Fig. 4. CD STFI short span compressive strengths of linerboard increase as the MD/CD stiffness ratios are decreased.

Fig. 2. CD STFI short span compressive strength increases as wet pressing and hence, density increases.
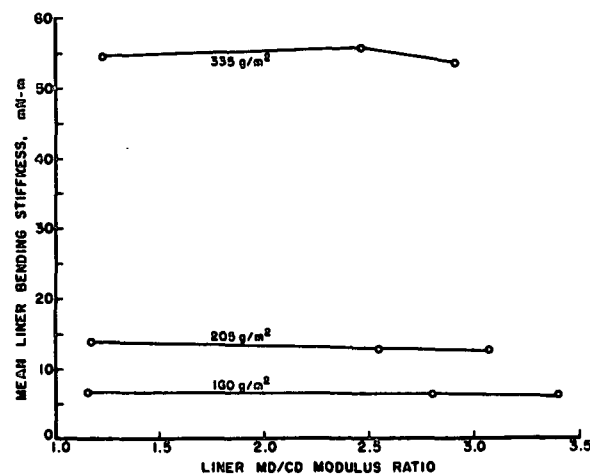
Fig. 5. Geometric mean bending stiffnesses of the linerboards are not greatly affected by MD/CD ratios.

Some of the experimental linerboard sheets were made with a starch additive to increase fiber-to-fiber bonding. Two levels of addition, 2 and 4% were used. The starch treatments tended to increase compressive strength and the bending stiffnesses of the liners. However, the effects of the treatments were smaller than obtained with the wet pressing and MD/CD ratio changes discussed previously.

Figure 6 compares the short span compression and bending stiffness results on the 205 g/m² liners for the papermaking changes discussed above. The changes in MD/CD ratio increased the STFI strength by about 50% but made only a small change in the bending stiffness of the liners. Increased wet pressing decreased the flexural stiffness by a factor of three but increased STFI compressive strength by 40%. The results for the 160 and 335 g sheets show similar trends (not illustrated).

Fig. 3. Geometric mean bending stiffnesses of linerboard decrease as density increases.

3
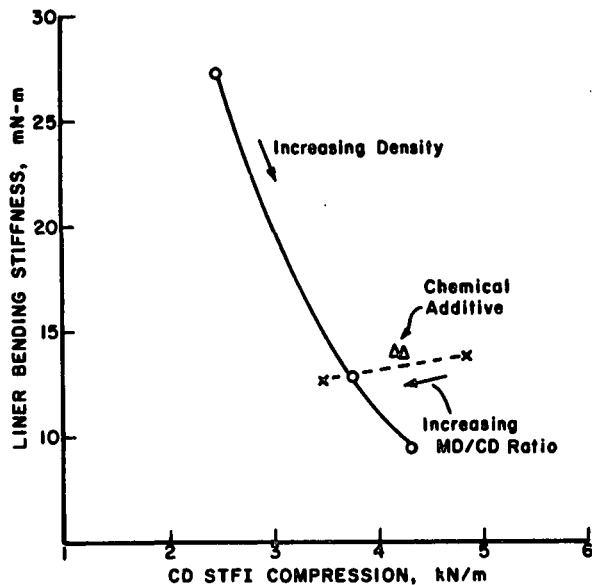
Fig. 6. Effects of papermaking factors on the short
span compression and bending stiffness of
205 g/m² linerboard.

As mentioned previously the CD compressive
strength of paperboard is related to the elastic
moduli in the CD and thickness directions, E_x and
E_z, respectively. Figure 7 shows that CD STFI
short span compressive strengths are highly related
to the elastic stiffness function derived by
Habeger and Whitsitt (2). The predicted relation-
ship holds for all of the papermaking conditions
used in making these linerboard sheets. In general
the elastic moduli of paperboard are affected by
wet pressing (Fig. 8) and MD/CD ratio in the same
way as compressive strength. Thus, these results
show that the ultrasonic moduli can be used to pre-
dict compressive strength.

Papermaking Effects - Combined Board

The linerboards made under the conditions described
above were combined with a 26-lb commercial medium
on the Institute's pilot corrugator. The single-
faced board was then double-backed and the combined
board was tested for ECT and flexural stiffness.

Increasing the density of linerboard by wet
pressing increased combined board ECT (Fig. 9).
This held true for combinations made with 33-, 42-,
and 69-lb liners. Thus, densification of the
liners is an effective way to increase the compres-
sive strength of the combined board and should
contribute to increased top load box compressive
strength.

Figure 10 shows that combined board flexural
stiffness is increased by using the stronger liners
obtained by increased wet pressing. The increases
in combined board flexural stiffness were achieved
at all three liner basis weight levels. Even
though wet pressing decreased the thickness of the
liners, the combined board flexural stiffness
increases because the increase in elastic moduli of
the liners more than counterbalances the decreases
in liner thickness.
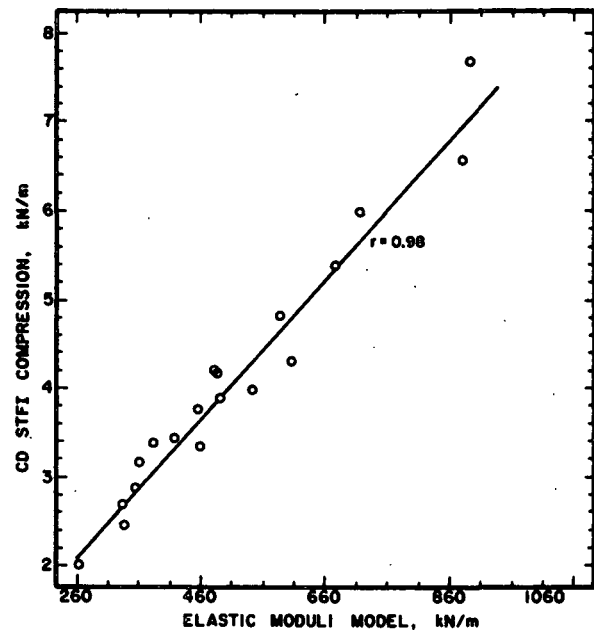
Fig. 7. CD STFI compression results are highly re-
lated to the product of the elastic moduli
in the CD and thickness directions as pre-
dicted by theory.
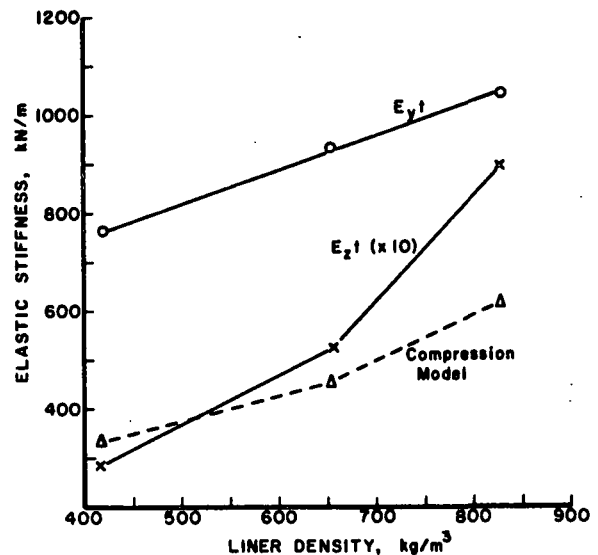
Fig. 8. The elastic moduli used to predict CD com-
pressive strength increase with density in
the same way as compressive strength.

Thus, using the thinner but stronger and
stiffer liners increased both material properties
in the McKee box formula, namely ECT and flexural
stiffness.

Therefore, box compressive strength should
increase as liner density is increased by improve-
ment in wet pressing during manufacture.

4
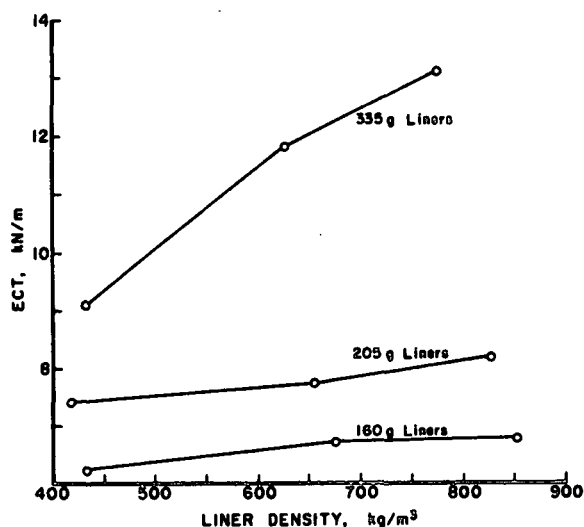
Fig. 9. Increasing liner density via wet pressing increases combined board ECT.
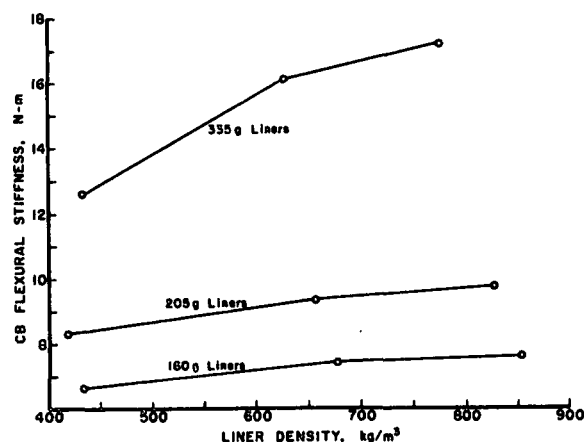
Fig. 10. Increasing liner density vis wet pressing increases combined board flexural stiffness.
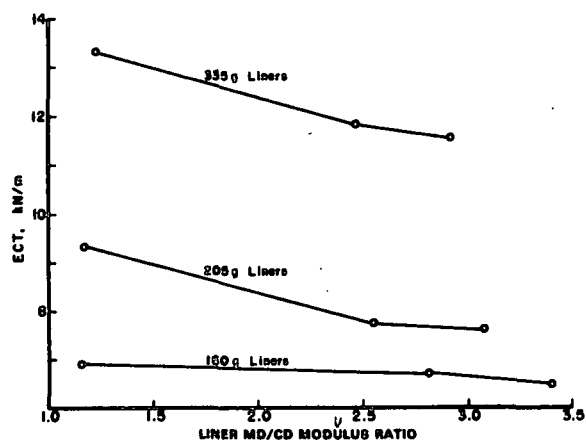

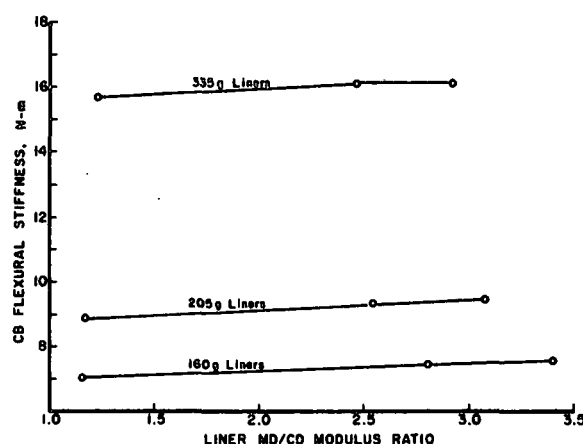**Fig. 11.** Decreasing the MD/CD modulus ratio of linerboard increases combined board ECT.

Fig. 12. The geometric mean combined board flexural stiffness is not affected by changes in the MD/CD modulus ratio of linerboard.

Despite the fact that densification reduces the bending stiffness of the liners, ECT increases. Thus, it appears that ECT strength is primarily dependent on the compressive strength of the components; the thickness and bending characteristics of the liners have only a limited effect at a given basis weight. Local buckling models which place too much emphasis on the latter factors could underestimate the potential improvements in ECT performance from papermaking factors such as wet pressing.

Making a squarer linerboard increases ECT strength as shown in Fig. 11. This would be expected because CD compressive strength increases as fewer fiber elements are aligned in the machine direction, drying restraints held constant. On the other hand the geometric mean combined board flexural stiffness is not affected by changing the MD/CD ratio of the liners (Fig. 12). In this case the increases in CD flexural stiffness are counterbalanced by the decreases in MD stiffness.

Therefore, box compressive strength should be increased by papermaking changes which reduce liner MD/CD ratios because of the increases in ECT. Work is in progress to validate these box predictions and compare the various ECT models which have been proposed.

Papermaking Effects - Medium

In past work we have made and tested mediums which were wet pressed to increase their density, compressive strength and hence, their strength retention during fluting (15). Densification improved most strength properties including the STFI short span compressive strength. However, CD ring crush passed through a maximum at a density of 750-800 kg/m^3 (Fig. 13). Compression tests on the combined board showed that increasing the corrugating medium density markedly increased ECT strength (Fig. 14). Thus, the STFI short span compressive strength test results on the medium were more indicative of combined board performance.
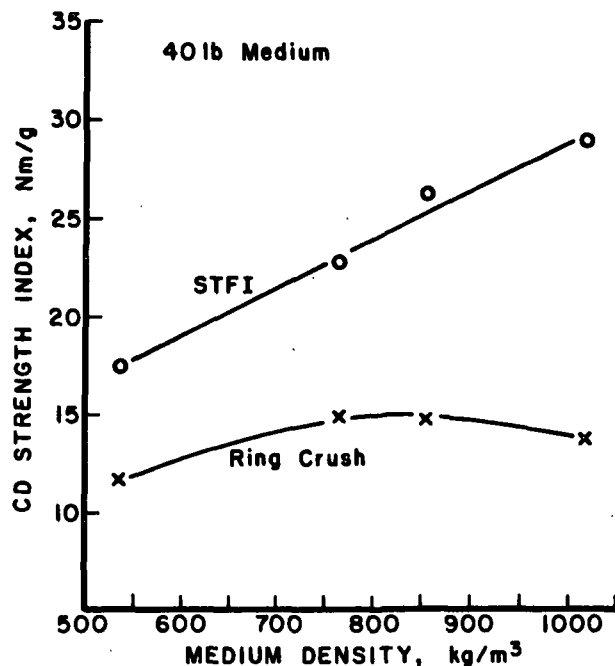
Fig. 13. Increasing medium density increases CS short span compressive strength, but ring crush results exhibit a maximum at intermediate densities.
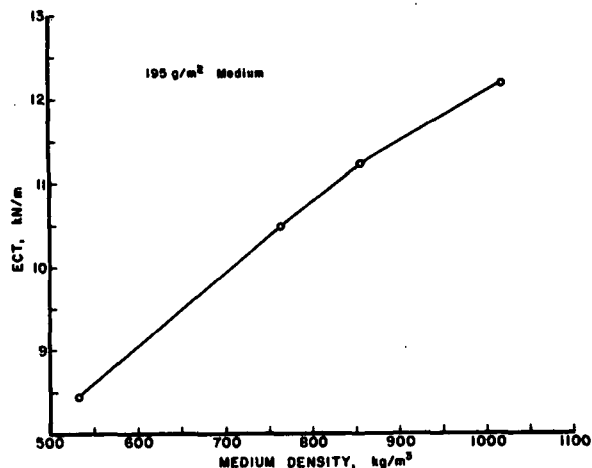

Fig. 14. Increasing medium density increases ECT.

The increases in ECT strength due to the use of denser, stronger medium result in higher box compression results. In addition the stronger medium increases flat crush strength and hence, reduces crushing during conversion and end-use.

CONCLUSIONS

In this work we have determined the effects of making papermaking changes in the manufacture of linerboard on combined board and box properties. The results show:

1. Increased wet pressing improves the compressive strength of linerboard but reduces its bending stiffness.

2. Combined boards made with linerboards which are more highly pressed exhibit improved ECT. This indicates that ECT is primarily dependent on the compressive strength of the liners; the thickness and bending stiffness characteristics of the liners apparently have a much smaller effect.

3. Combined boards made with densified liners by wet pressing exhibit higher flexural stiffnesses despite the fact that wet pressing reduced liner thickness.

4. Reducing the MD/CD ratio of linerboard increases the CD compressive strength of the liners and hence, ECT, but has little or no effect on the geometric mean flexural stiffness of the combined board.

5. Based on the McKee box formula higher box compressive strength should be achieved with more highly pressed liners or liners with lower MD/CD ratios.

LITERATURE CITED

1. McKee, R. C., Gander, J. W., and Wachuta, J. W., Pbd. Pkg. 48(8):149-159(Aug., 1963).

2. Habeger, C. C. and Whitsitt, W. J., Fibre Sci. Technol. 19:215-239(1983).

3. Mann, R. W., Baum, G. A., and Habeger, C. C., Tappi 63(2):163(1980).

4. Whitsitt, W. J. Compressive strength relationships and factors. Compression Symposium (Forest Products Laboratory, Madison, WI) Oct. 1-3, 1985.

5. Baum, G. A. and Habeger, C. C., The Institute of Paper Chemistry Technical Paper Series No. 187, June, 1986.

6. Jonson, G. and Ponton, E., TAPPI Corrugated Conference Proc., 1984. p. 39.

7. Augustin, H., TAPPI Corrugated Conference Proc., 1985. p. 35.

8. Koning, J. W., Jr., Tappi 61(8):69-71(April, 1978).

9. Johnson, M. W., Urbanik, J. J., and Denniston, W. E., U.S. Forest Products Laboratory Report No. 348, 1979.

10. The Institute of Paper Chemistry. Relation-

ship between the edgewise compression strength of combined board and component properties. Project 1108-4, Preliminary Report to the Fourdrinier Kraft Board Institute, Inc., June 18, 1963.

11. Gunderson, D., Appita 37(2):127(1983); 37(4): 307(1984).

12. Koning, J. W., Jr. and Moody, R. C., Tappi 54

(11):1879(1971).

13. Kellicutt, K. Q., Tappi 44(1):201A(1961).

14. The Institute of Paper Chemistry, Stiffness Report One to the FKBI, Oct. 10, 1955.

15. Whitsitt, W. J. and Baum, G. A., Tappi 70(4): 107(1987).

Faster, alternative ECT test procedure

K. E. Schrampfer, W. J. Whitsitt
The Institute of Paper Chemistry
Appleton, Wisconsin 54912

ABSTRACT This study was directed toward improving Edge Crush Test (ECT)
measurement technology by developing a simpler, more efficient method of sample
preparation and testing. The specific objective was to compare ECT results
obtained with specimens prepared using newer ECT sample cutting and supporting
procedures with results obtained using the current TAPPI Test Method (T 811).
An alternative ECT test procedure using unwaxed 2 x 2-inch specimens has been
developed which compares favorably with the TAPPI procedure specifying waxed-end
specimens. The test averages are about equal to those obtained with the TAPPI
procedure, and within sample test variability is much lower.

The 2 x 2-inch specimen is cut using a two-bladed automatic ECT cutter.
The specimens are tested in a test fixture which supports the ends of the speci-
men with clamps at a controlled pressure. The fixture fits between the platens
of flexible and rigid platen compression testers. No waxing of the ends is
required.

Introduction

Edgewise compressive strength (ECT) is an important structural property of corrugated board because it is directly related to top-load box compressive strength. The TAPPI ECT Test Method (T 811)(1) requires specimens to be cut on a circular saw, with specimen height depending on flute type. The specimen's loaded edges are reinforced with wax to prevent edge failure. While this procedure is accurate, it is also time consuming and requires operator care. For these reasons a quicker and safer method of cutting and supporting test specimens was sought.

Several alternate cutting methods which use industrial knife blades were examined. These included a hand-operated Weyerhaeuser cutter, a hand-operated cutter marketed by the Sumitomo Corporation of Japan, and an automatic, dual-blade Billerud cutter sold by AB Lorentzen & Wettre, all used to make rectangular specimens. Other specimens' shapes, such as the necked-down shape (2-4), were not pursued because the cutting procedures are more involved. For simplicity, the feasibility of using a single specimen height was explored.

Several alternate methods of supporting specimens during testing were investigated to eliminate the need for waxing. These included the SCAN-P33:71 support blocks (5), the Morris holder (6), and a test fixture marketed by Sumitomo. ECT values obtained using these specimen cutting and supporting techniques were compared to those obtained using the TAPPI method.

ECT results obtained on new rigid-platen compression testing machines were also compared to those obtained on a conventional flexible-platen machine. The original TAPPI Test Method (T 811) mandates the use of a flexible-platen compression testing machine. Newer compression testers utilize rigid platens

equipped with a load cell. TAPPI has revised method T 811 to permit use of
these machines (See TAPPI Test Method T 823) (7).

ECT test equipment

The Weyerhaeuser cutter has a plastic block into which an industrial
blade is clamped. The operator cuts the board by pushing the block along a
guide on the base. Both machine- and cross-machine-direction cuts can be made,
but only in two-inch widths. The blade is beveled on both sides and is 15.5
mils thick.

Similar to the Weyerhaeuser cutter, Sumitomo's cutter uses an
industrial blade mounted on a hand-operated carriage. The board is held in
place by two guides mounted at right angles. One of the guides is adjustable,
allowing any specimen size to be cut. The blades are 24 mils thick and also
beveled on both sides.

The Billerud cutter, made by AB Lorentzen & Wettre, is an automatic
device which uses air pressure to drive the cutting blades (Fig. 1). Two
18-mil-thick blades are mounted on a moving carriage one or two inches apart,
depending on the cutter. The cutting edge of each blade is beveled on one side
only and mounted with the beveled edge facing outward. The specimen is cut
cleanly by the inside, unbeveled edge of each blade. For our tests the speci-
mens were cut to 2-inch heights, except where otherwise noted. The board was
precut into two-inch cross-machine direction widths using a different method.
Care must be taken to make sure the blades are mounted squarely to produce a cut
edge perpendicular to the plane of the board; shims are sometimes necessary.
The blades must be replaced after approximately 150 cuts because of dulling.

[Figure 1 here]

The Morris holder, developed by the Weyerhaeuser Co., uses two plates, each of which contains a 6-mm deep groove to support the specimen's loaded edges. Groove width is adjustable to accommodate normal board calipers. The grooves are beveled at a 5-degree angle, becoming narrower at the specimen's unwaxed edges.

Sumitomo's test fixture (Model D-105) provides direct support to the loaded edges of an unwaxed specimen (Fig. 2). Two clamps support the top and bottom 2 cm of the specimen. While the fixture is designed for specimens with a height of 60 mm, a specimen height of 2 inches works well. This results in an unsupported column height of approximately 10 mm. In the original design each clamp was operated by hand tightening a bolt. To eliminate this source of operator error, the fixture was redesigned using springs to achieve a constant clamping pressure as discussed in a later section.

[Figure 2 here]

Both flexible- and rigid-platen testers were used in this work.

Compression testing machines

Sixty-six combined board lots, made by members of the Fourdrinier Kraft Board Group (FKBG), were tested on a flexible-platen and a rigid-platen tester using the TAPPI ECT method. These lots ranged from 150-lb single-wall (SW) to 350-lb double-wall (DW). Figure 3 illustrates the good agreement between the average ECT value for each combined board series using each tester. The results confirmed that a rigid-platen compression testing machine is an acceptable alternative to the flexible-platen type.

[Figure 3 here]

Alternate ECT testing methods

A short series of tests was performed comparing three alternate cutting methods. The Weyerhaeuser and Billerud cutters both appeared to perform satisfactorily, while the Sumitomo cutter did not. The most probable explanation for this is the geometry of the cutting blade. The Sumitomo cutter uses a thick blade beveled on both sides. This will tend to deform the liner as it is being cut, causing premature edge failure during the ECT test. A thinner, single-beveled blade would be preferred, although this was not tried. The Weyerhaeuser cutter avoids this problem by using a thinner double-beveled blade, while the Billerud cutter uses two thin single-beveled blades mounted such that the specimen edges are cut with the straight, unbeveled edges of each blade. Any cutting method which follows these guidelines should be satisfactory.

Based on initial trials, the sixty-six combined board lots mentioned above were tested on a rigid-platen tester using the following test methods: (1) TAPPI Test Method T 811: grooved blocks, saw-cut, height depending on board type, waxed; (2) Clamped Specimen (CS): Sumitomo's test fixture, Billerud-cut, 2-inch height, unwaxed; (3) SCAN-P33:71, Billerud-cut, 1-inch height, unwaxed; (4) TAPPI Useful Method UM 814: Morris holder, Weyerhaeuser-cut, 2-inch height, unwaxed. Two-inch specimen widths were used in all cases.

As seen in Fig. 4-5, the CS ECT values are in very good agreement with TAPPI ECT values, averaging about one percent high. All correlations with the TAPPI method are good: within-grade correlations range from 0.67 to 0.80, while the correlation over all board grades is 0.955. The coefficient of variation for the CS method averages 4.0%, compared to 8.6% using the TAPPI method (Fig.

6). Excellent agreement with TAPPI ECT values, good correlations, and lower variability all suggest that the CS method is a successful ECT test method.

[Figures 4, 5, and 6 here]

Edge failures often occur when testing with the CS fixture; however, this did not result in low test values (see Fig. 4). ECT values from methods 3 and 4 averaged approximately fifteen percent lower than TAPPI ECT values, and were not pursued further.

These results indicated that the CS method showed the most promise as a faster, simpler alternative to the TAPPI method. To further verify the accuracy of this method, an additional 150 lots were tested after improving the support fixture. These lots, also provided by FKBG members, ranged from 150-1b SW to 500-1b DW.

Modified Sumitomo test fixture

The clamps on the original Sumitomo test fixture are hand-tightened until "snug". Because this is a possible source of operator error, a new clamping system which uses springs to exert a constant pressure was designed by Sumitomo. The clamps lock open for removal and insertion of the specimen, then slide closed when released to exert a stable, repeatable clamping pressure. The redesigned fixture came with springs which had a spring constant of K = 10.1 1b/in and produced a clamping pressure of 5.3 psi for all board calipers. This fixture was used to test the additional 150 lots mentioned above, the results of which are shown in Fig. 7-8. Within-grade correlations with the TAPPI ECT values were good, ranging from 0.81 to 0.93. The overall correlation coefficients is an excellent 0.991. Thus, controlling the clamping pressure improved the correlations between the CS and the TAPPI methods.

[Figures 7 & 8 here]

Within-lot variability of the CS method again averaged lower than that of the TAPPI method, measuring 3.9% as opposed to 5.5% (Fig. 9).

[Figure 9 here]

The overall average ECT is 2.7% lower than the corresponding TAPPI value, which is not as good as with the original fixture. Close examination of the average percent difference by series reveals that the values are about 0.5% low up to and including 200-lb SW series, about 3.0% low for the 275-lb SW to 350-lb DW series, and about 6.6% low for the 500-lb DW series. This is evident by the way the regression line drops away from the 1-1 line as board series increases (see Fig. 8). This indicated that a stronger clamping pressure was required.

To test this hypothesis, a group of 29 lots was retested using a series of stronger springs. It was found that the difference between the two methods decreased with increasing clamping pressure. Shown in Fig. 10 are the results using a higher, more optimal clamping pressure. Using springs with a spring constant of $K = 20.4$ lb/in. obtained from Sumitomo, the fixture exerts clamping pressures of approximately 7.1 and 11.6 psi on boards with calipers of 150 and 300 mils, respectively. The average CS ECT value is only 0.7% lower than the average TAPPI value. Within-lot variabilities are relatively constant with increasing clamping pressure, always remaining lower than TAPPI values.

[Figure 10 here]

While the agreement between the TAPPI and the CS ECT test methods using the $K = 20.4$ lb/in. springs is good, one problem was encountered with these

strong springs: opening the clamps repeatedly was difficult for the operator. The clamp design was then modified to make them easy to operate, even with the stiffer springs. As a final test, the 29 lots were rechecked with this arrangement. The results were in good agreement over the entire range of combined boards tested. This arrangement has been recommended to Sumitomo as the final working design.

Box compression study

Because of the importance of ECT in the end-use performance of the box, box compression predictions were made using each ECT method and compared to actual box compression values. Predictions were made using the McKee box compression formulas (8):

Long Formula:

$$P = 2.028 \ (ECT)^{0.746} \ [(D_x D_y)^{0.5}]^{0.254} \ Z^{0.492}$$

Short Formula:

$$P = 5.874 \ (ECT) \ H^{0.508} \ Z^{0.492}$$

$$\text{where} \quad D_{x,y} = \text{Flexural Stiffness}$$

$$H = \text{Combined Board Caliper}$$

$$Z = \text{Box Perimeter}$$

These equations were used to predict the top-load box compression strength of the initial SW lots. Predictions made with the TAPPI and the CS ECT values were high (7.2-8.9%) using the long formula and slightly low (1.7-3.7%) using the short formula. Box predictions made with the other ECT methods were much lower because of the low ECT values. To better compare results from the various ECT methods, the constants in the McKee equations were rederived using the TAPPI single-wall ECT data.

Long Formula:

$$P = 2.180 \, (ECT)^{0.727} \, [(D_x D_y)^{0.5}]^{0.273} \, z^{0.454}$$

Short Formula:

$$P = 7.178 \, (ECT) \, H^{0.546} \, z^{0.454}$$

New box predictions, made with the TAPPI and the CS ECT values, averaged 0.7% and 2.2% high, respectively, using the long formula and 5.8% and 3.9% low, respectively, using the short formula. The average prediction accuracies achieved with the other ECT methods were again much lower. Thus the best prediction accuracy was obtained with the proposed new method using the clamped square specimen.

Conclusions

The Clamped-Specimen ECT test procedure developed here agrees very well with the TAPPI ECT procedure and is much faster and simpler to use. Specimens are cut quickly and safely using industrial knife-blades. Proper maintenance is required to ensure the blades are sharp and mounted squarely. The dual-blade Billerud cutter was found to work exceptionally well if the blades are replaced as they become dull. A single specimen size of 2 x 2 inches was shown to be satisfactory.

To further simplify the ECT method, a test fixture was used which eliminates the need for waxing. The fixture is made by the Sumitomo Corporation of Japan. Spring-operated clamps support the top and bottom 20 mm of the specimen during testing. The optimal clamping pressure was determined to be approximately 7.1 psi for 150-mil board and approximately 11.6 psi for 300-mil board. Springs with a spring constant of 20.4 lb/in. mounted in the Sumitomo test fixture produce the desired clamping pressures. The fixture fits between the

platens of the compression testing machine. Flexible- and rigid-platen testers
were shown to produce equivalent results.

Acknowledgments

The authors wish to thank the members of the Fourdrinier Kraft Board Group of
the American Paper Institute for its funding and support of this project (9),
and The Institute of Paper Chemistry personnel for their help in various phases
of the testing.

The support provided by the Sumitomo Corporation of America, AB
Lorentzen and Wettre (through Scanpro Instruments) and Testing Machines, Inc.,
is gratefully acknowledged. The Sumitomo Corporation provided the Model D-105
fixture and made design changes to give a controlled clamping pressure. AB
Lorentzen and Wettre modified their cutter to give a 2-inch wide cut. One rigid
platen tester was obtained on loan from Testing Machines, Inc.; a second rigid
platen tester was obtained under special arrangements from AB Lorentzen and
Wettre.

Literature cited

1. TAPPI Test Method T 811 om-83, Edgewise Compressive Strength of Corrugated
   Fiber-board (Short Column Test).

2. McKee, R. C., Gander, J. W., and Wachuta, J. R., Pbd. Pkg. 46, no. 11:
   70-76 (Nov., 1961).

3. The Institute of Paper Chemistry Compression Report 7 to the Fourdrinier
   Kraft Institute, May 17, 1960.

4. Koning, J. W., Jr., Tappi 69(1): 74(1986).

5. Scandinavian Pulp, Paper, and Board Testing Committee; Edgewise Crush
   Resistance of Corrugated Board, SCAN-P33:71

6. TAPPI Useful Method UM 814, Corrugated board edge compression test (Morris
   specimen holder procedure).

7. TAPPI Test Method T 823 pm-84, Edgewise compressive strength of corrugated
    fiber board (rigid support method).

8. McKee, R. C., Gander, J. W., and Wachuta, J. R., Pbd. Pkg. 48, no. 8:
    149-159 (Aug., 1963).

9. Schrampfer, K. E., Whitsitt, W. J., and Baum, G. A.   Report One to the
    Fourdrinier Kraft Board Group of API, Feb. 1, 1987.
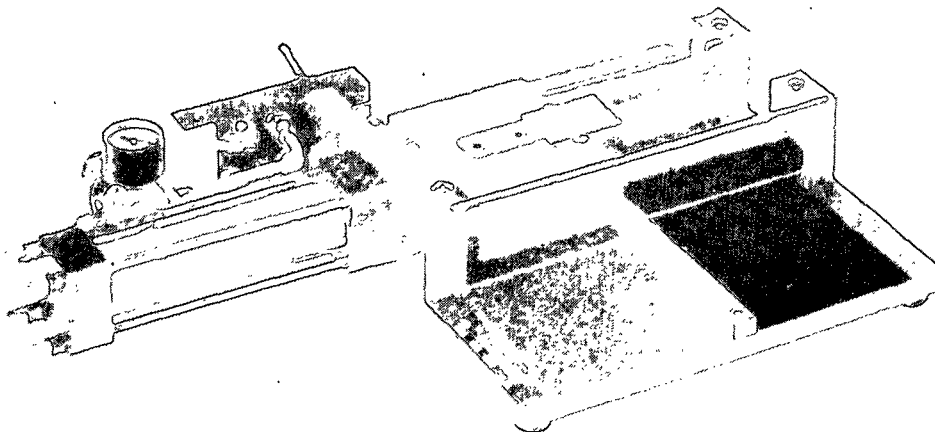
Figure 1. Billerud automatic cutter.
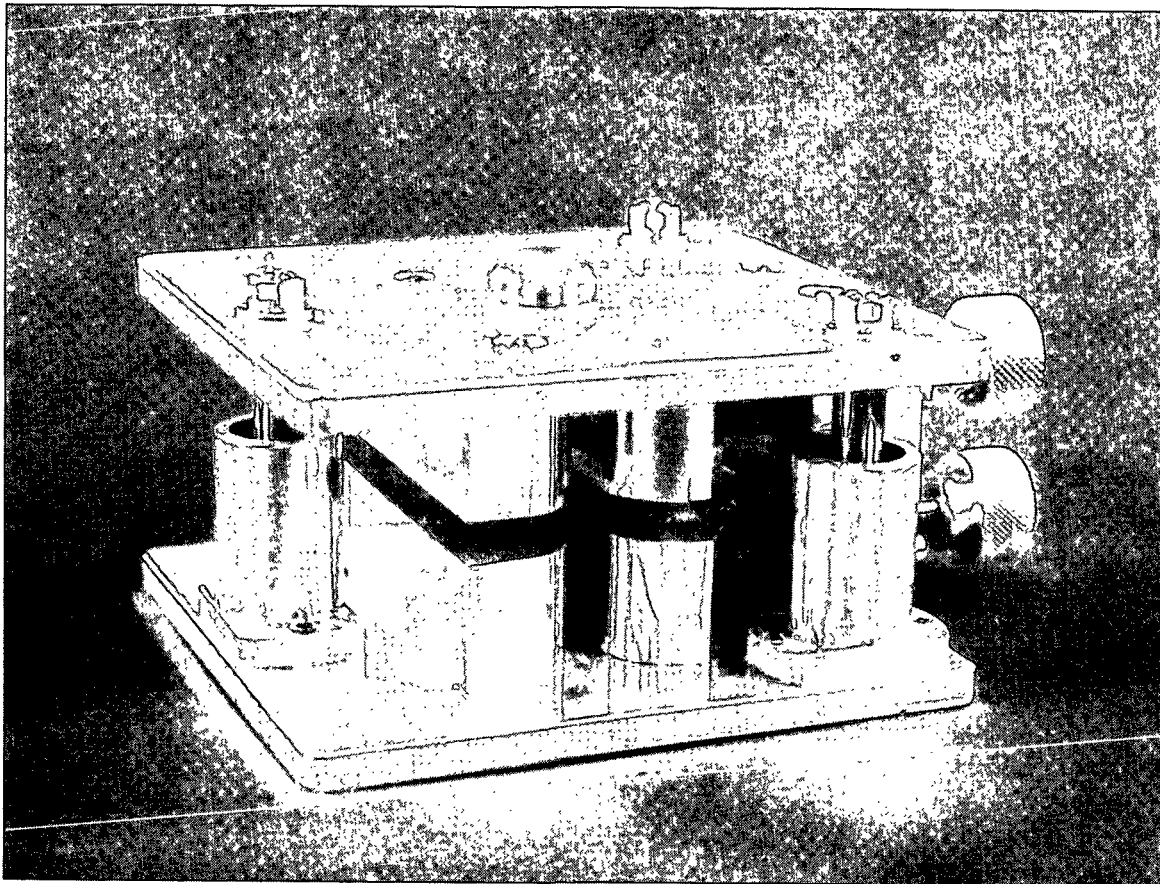
2.   Sumitomo's test fixture, Model D-105.

BOARD SERIES

AVERAGE ECT, lb/in

Flexible-Platen Tester
Rigid-Platen Tester
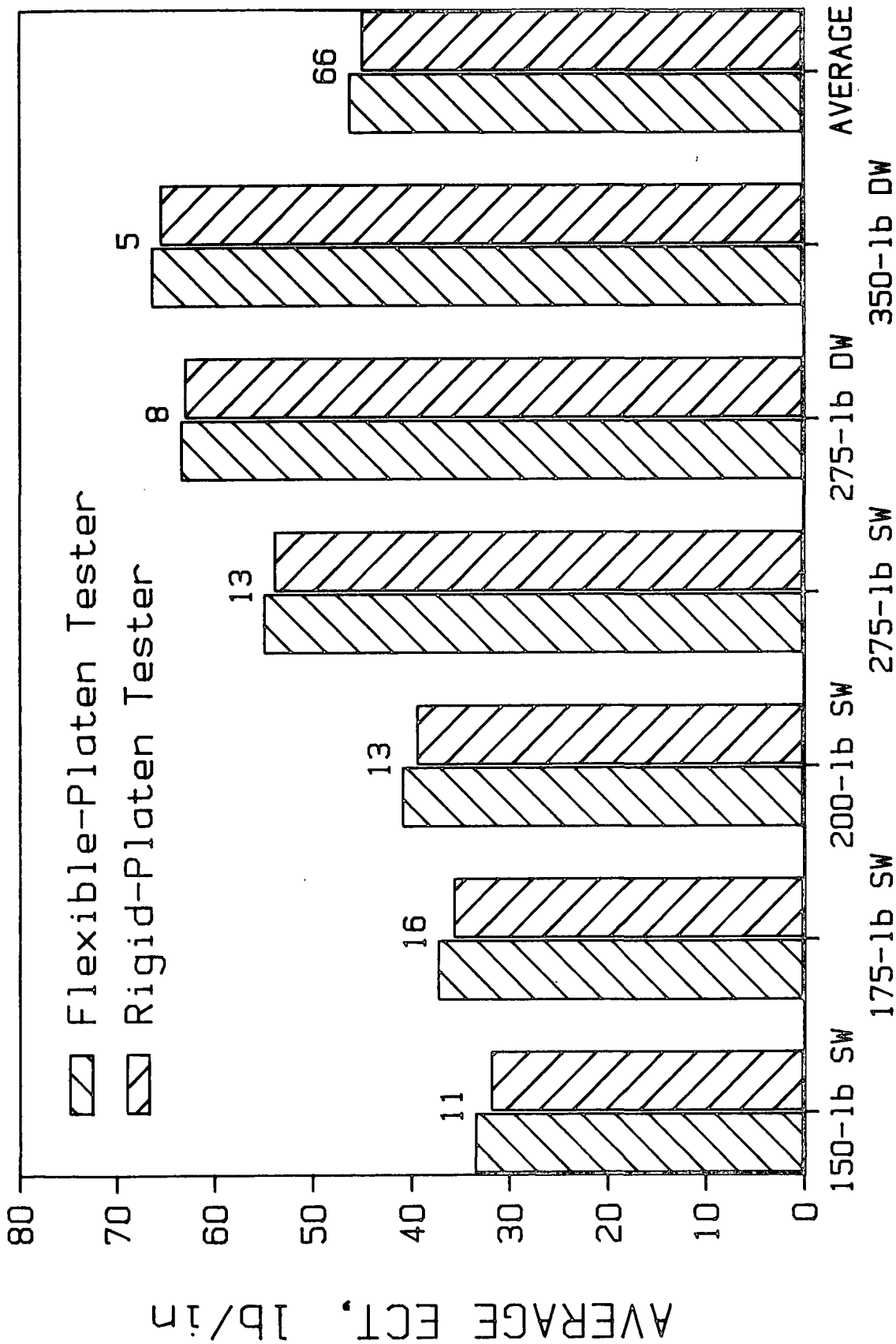
3. Flexible- and rigid-platen compression testing machines give equivalent ECT test results.

BOARD SERIES

AVERAGE ECT, lb/in
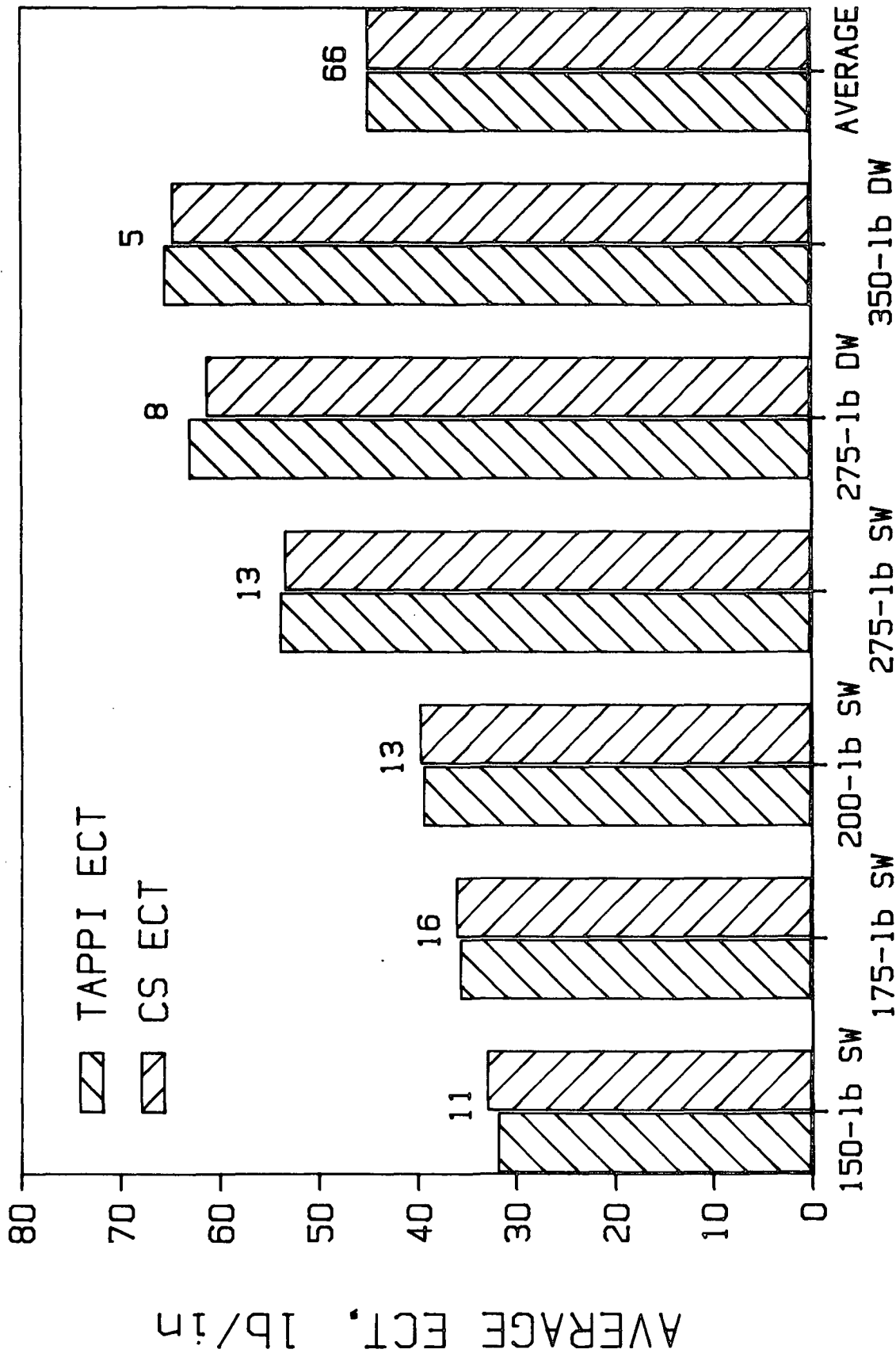
4. Clamped Specimen ECT test results, unwaxed, are in close agreement with TAPPI unwaxed ECT results (66 combined board lots).

CS ECT, lb/in

TAPPI ECT, lb/in

r=0.955
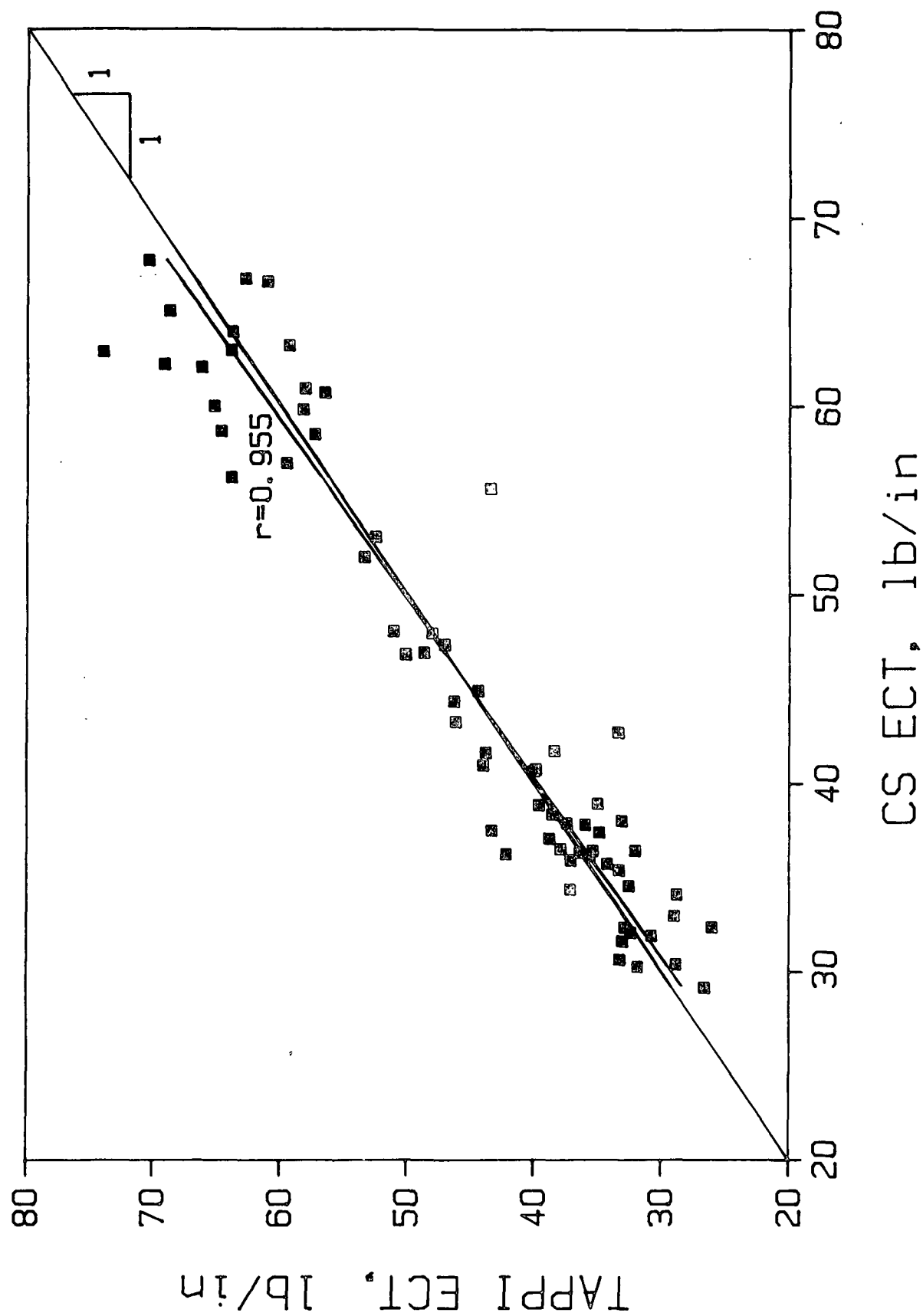
5. Clamped Specimen ECT tests are also well correlated with TAPPI ECT test results (66 combined board lots).

BOARD SERIES

AVERAGE WITHIN-LOT VARIABILITY, %

TAPPI ECT

CS ECT

150-lb SW   11
175-lb SW   16
200-lb SW   13
275-lb SW   13
275-lb DW   8
350-lb DW   5
AVERAGE   66
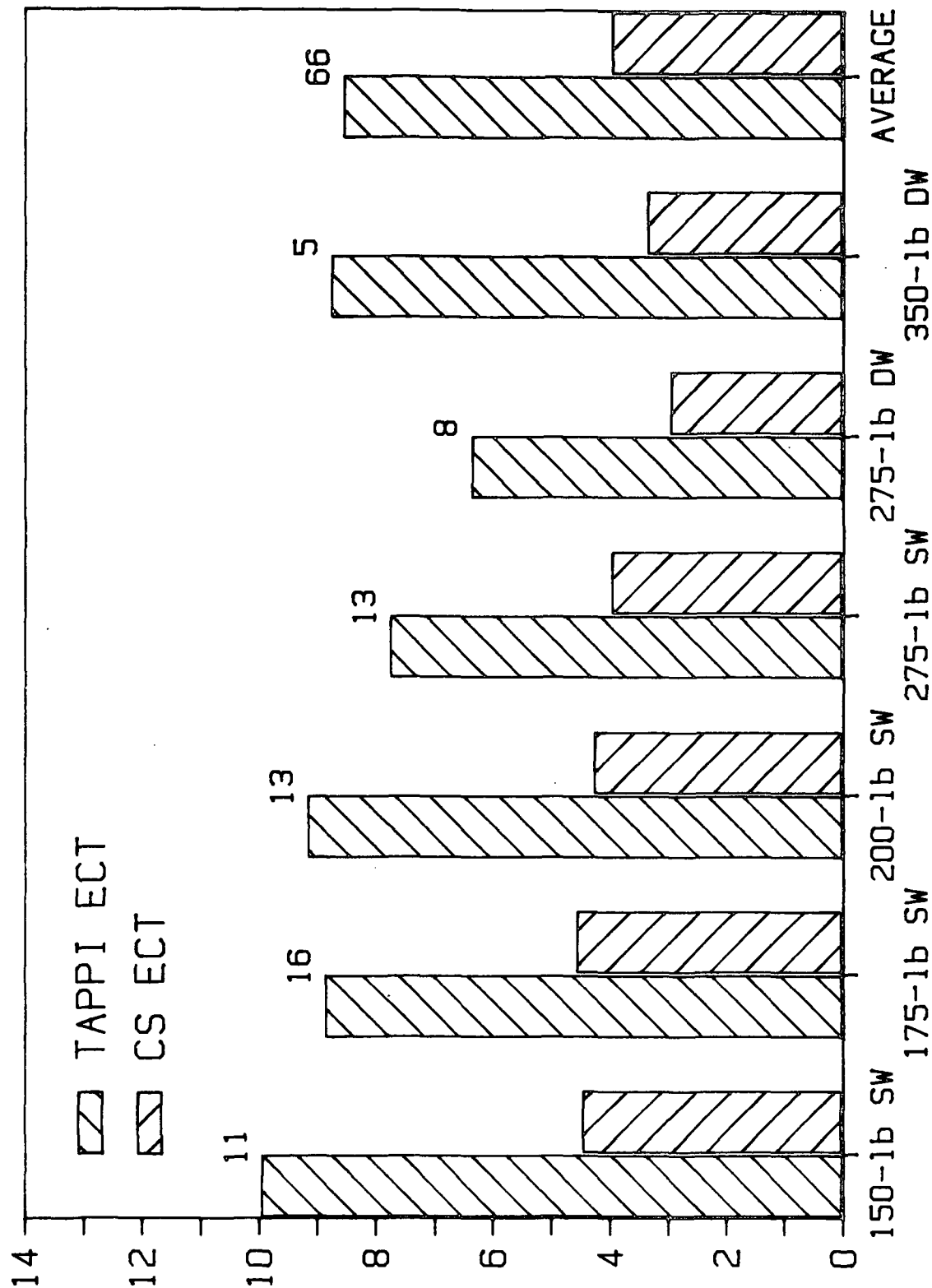
6. Clamped Specimen ECT test results exhibit much less variability than TAPPI ECT test results (66 combined board lots.)
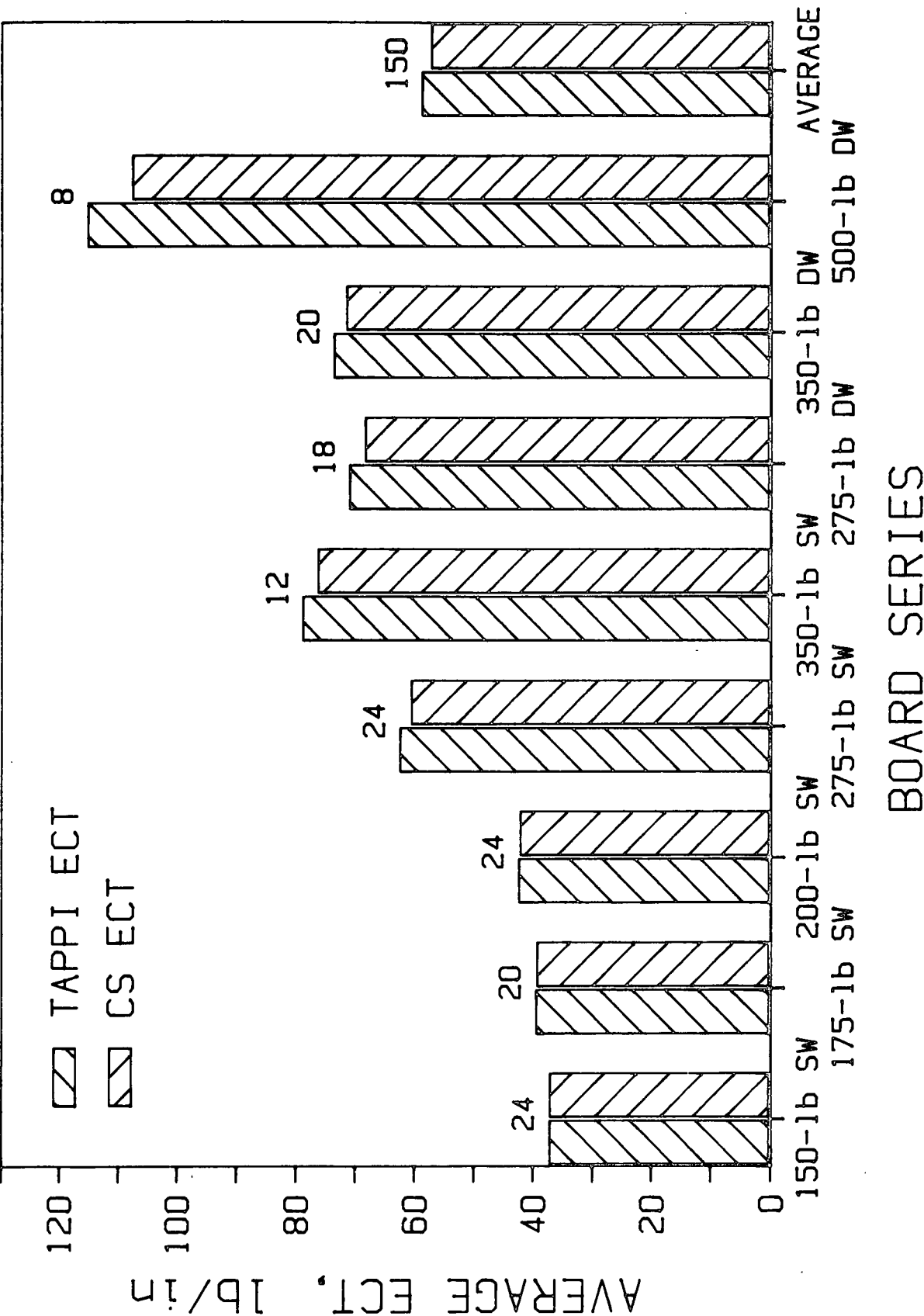
7. With insufficient clamping pressure, Clamped Specimen ECT results tend to be slightly lower than TAPPI results for high-series combined boards (150 combined board lots).

CS ECT, lb/in

TAPPI ECT, lb/in

r=0.991
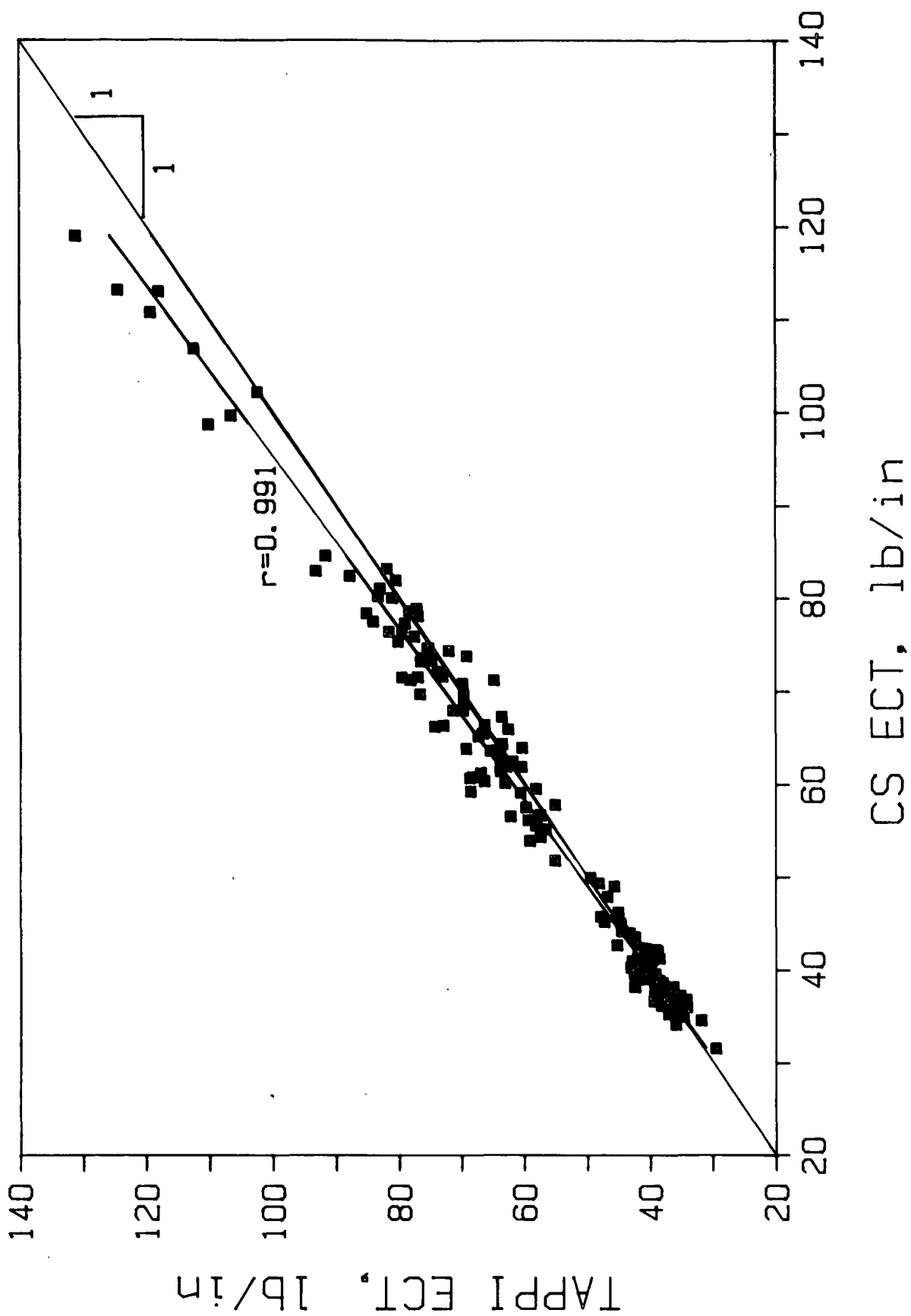
8. Even with insufficient clamping pressure, Clamped Specimen ECT results
    still correlate well with TAPPI results (150 combined board lots).

9. Clamped Specimen ECT variability is still lower than that of TAPPI, in spite of low clamping pressure (150 combined board lots).
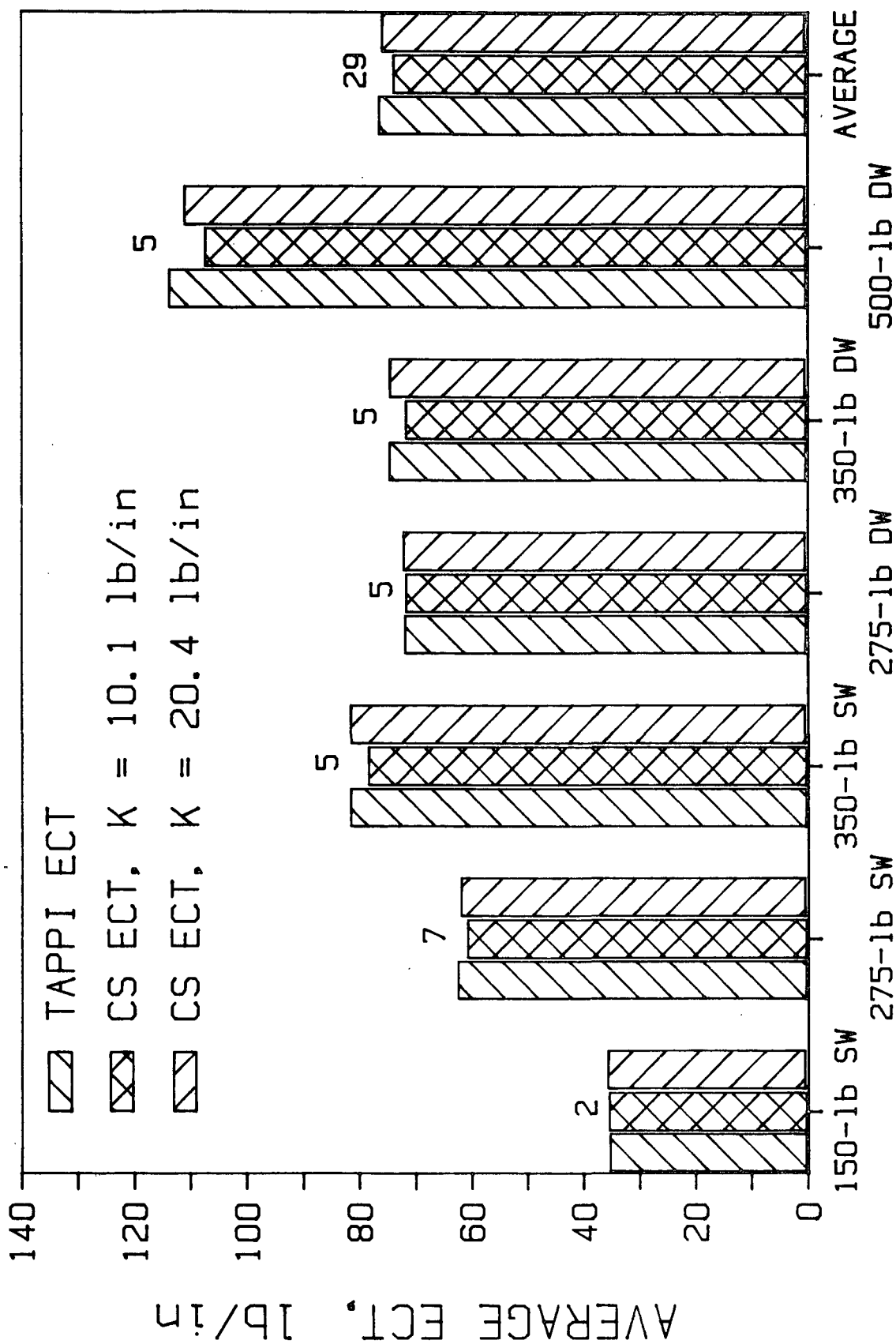
BOARD SERIES

10. With the K = 20.4-lb/in springs, the Clamped Specimen ECT test results are again in close agreement with the TAPPI test results for SW and DW boards (150 combined board lots).

THE INSTITUTE OF PAPER CHEMISTRY

Appleton, Wisconsin

Status Report

to the

PAPER PROPERTIES AND USES

PROJECT ADVISORY COMMITTEE

Project 3467

PROCESS, PROPERTIES, PRODUCT RELATIONSHIPS

October 19-20, 1988

PROJECT SUMMARY

PROJECT NO. 3467:   PROCESS, PROPERTIES, PRODUCT RELATIONSHIPS

PROJECT STAFF: C. Habeger, K. Hardacker, Y. Pan   September 12, 1988

PROGRAM GOAL:

Develop relationships between the critical paper and board property parameters
and how they are achieved in terms of raw material selection, principles of
sheet design, and processing conditions.

PROJECT OBJECTIVE:

(1) To improve our capability of characterizing paper and board materials,
(2) to relate measured parameters to end-use performance (especially in the case
    of Z-direction measurements), and
(3) to relate measured parameters to machine and process variables.

PROJECT RATIONALE, PREVIOUS ACTIVITY, AND PLANNED ACTIVITY FOR FISCAL 1988-89
are on the attached 1988-89 Project Form.

SUMMARY OF RESULTS LAST PERIOD: (October 1987 - March 1988)

(1) The mechanical and electronic portions of the in-plane robotic tester are
    complete.

(2) Software development is continuing and a demonstration of the robot is
    scheduled for the PAC meeting.

(3) A paper entitled "Using Neoprene-Faced, PVDF Transducers to Couple
    Ultrasound into Solids" has been prepared for the Journal of the American
    Acoustical Society.

(4) Out-of-plane loss work has been extended to a study of medium damage from
    corrugation.

(5) Preliminary tests on two new possible directions for future research were
    conducted.

(6) Bernie Berger (Transient Moisture Effects in Paper) and Jim Biasca (Bending
    Refining) are nearing completion of the Ph.D.'s.

SUMMARY OF RESULTS THIS PERIOD: (March 1988 - October 1988)

(1) The robotic in-plane tester has been refined and tested, and it is ready for
    routine operation. Commercialization by RoboTest appears to be on schedule.

(2) Using the additional computing capabilities available with the IBM PC AT on
    the robotic tester, an improved technique was developed to measure in-plane
    elastic constants. This provides better estimates for in-plane Poisson
    ratios and the first ever measurement of C_{16} and C_{26}.

(3) New out-of-plane longitudinal ultrasonic transducers, which are capable of pulse-echo measurements, were constructed. These give a much improved method for determining out-of-plane acoustic losses in paper. Also, they allowed the development of a new technique that provides an ultrasonic measure of surface properties.

(4) An investigation of the ability of out-of-plane ultrasonic measurements to predict softness in tissue was promising.

(5) Papers for publication concerning the in-plane robot and the effect of environment on in-plane velocities were prepared.

(6) A suitable flash lamp was obtained and installed on the Board Optical Transmission Meter (BOTM), the instrument being developed for determining the optical scattering coefficient of heavy-weight papers.

(7) The optical and electronic systems for measuring the peak intensities of the source and transmitted light have been completed and put in working order.

(8) Good agreement has been observed between values of the transmittance of light-weight papers determined from R_0 and R_∞ measured on the TB-1 Brightness Tester and from R_0 and the transmittance determined with the BOTM.

PROCESS, PROPERTIES, PRODUCT RELATIONSHIPS

Project 3467

I. PROGRESS ON THE ROBOTIC IN-PLANE TESTER

During the last period, we have introduced a number of small software and hardware changes which have improved the accuracy and reliability of this instrument. The system is now used routinely and operates with very few problems. A paper, describing the operation of the robotic tester, is included in the appendix of this report. These changes, along with suggested improvements that can be incorporated into new instruments, have been documented and communicated to RoboTest. They are busily developing a commercial instrument, and they hope to ship their first unit by year's end. We think that commercialization is an important step, since it provides a practical means for paper laboratories to perform a complete, reliable, and rapid characterizations of paper elastic properties. In addition, it will give the paper manufacturer the means to intelligently assess the utility of on-line ultrasonic measurements for his (or her) product and the means to check the performance of on-line ultrasonic instruments.

After considering about a dozen different plastic materials, we have chosen 0.005-inch thick polyester sheets to be the IPC standards for comparing in-plane velocity measurements on different machines at different times. These samples suffered only slight velocity variations after being immersed in water overnight and after being subjected to two weeks of Wisconsin summer weather. To stabilize their mechanical properties, we have conditioned each sample in a 70°C oven for two days; they are insensitive to thermal cycling below this limit. These samples yielded relatively strong ultrasonic signals when tested with our standard bender transducers, and have velocities not far below those

observed on common paper samples. They have a velocity squared orientation ratio of about 1.25 to 1. This is large enough to use the samples for comparison of polar plot angle determinations. Samples, with the complete results of IPC testing, will be furnished to interested parties. Users are made aware that the velocities decrease somewhat with temperature and that exact comparisons must be made at the stated temperature.

A significant advantage of the robotic instrument (over our original Apple IIe based automated tester) is that it is driven by a PC AT class computer and is capable of complex data analyses. Now that the instrument is functioning, the major effort this period has been to implement a more complete determination of elastic properties. As will be discussed below, this leads to a better estimation of Poisson's ratio on highly anisotropic samples, and, most interestingly, to a means for assessing whether or not paper is orthotropic.

We have discussed the longitudinal in-plane polar plots extensively in previous reports; they are graphic displays of the velocities squared of ultrasound measured at 5° increments. Figure 1 is an example of such a plot for a chipboard specimen. Since these velocities were measured with bender transducers which contact the paper over dimensions much smaller than the transducer separations, they are essentially the velocities determined between point contact transducers. Musgrave [Musgrave M. J. P., Proc. Royal Soc. A266(1166): 339-355 and 356-366 (1954)] calls these the velocities of information propagation, and he demonstrates that, for off-axis measurements in anisotropic materials, they differ from the phase velocities. Phase velocities are those measured from the plane waves generated by transducers of infinite extent. Note well that the two are the same in the principal directions of orthotropic materials, and large differences occur only off-axis on very anisotropic

THE INSTITUTE OF PAPER CHEMISTRY
ROBOTIC IN-PLANE ULTRASONIC VELOCITIES

POLAR PLOT OF LONGITUDINAL INFORMATION PROPAGATION VELOCITY SQUARED

OPERATOR: C. C. Habeger
PROJECT : 3467
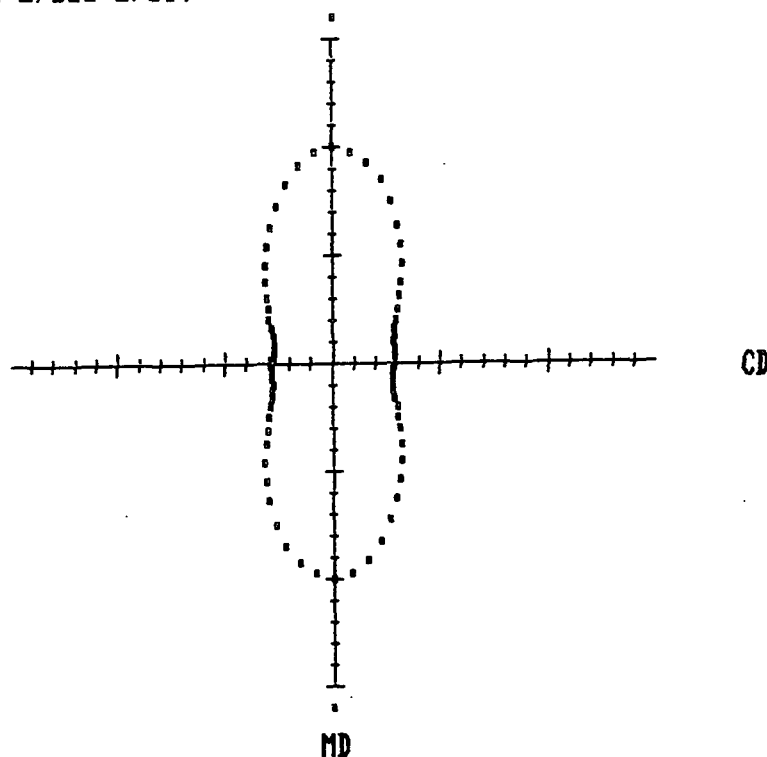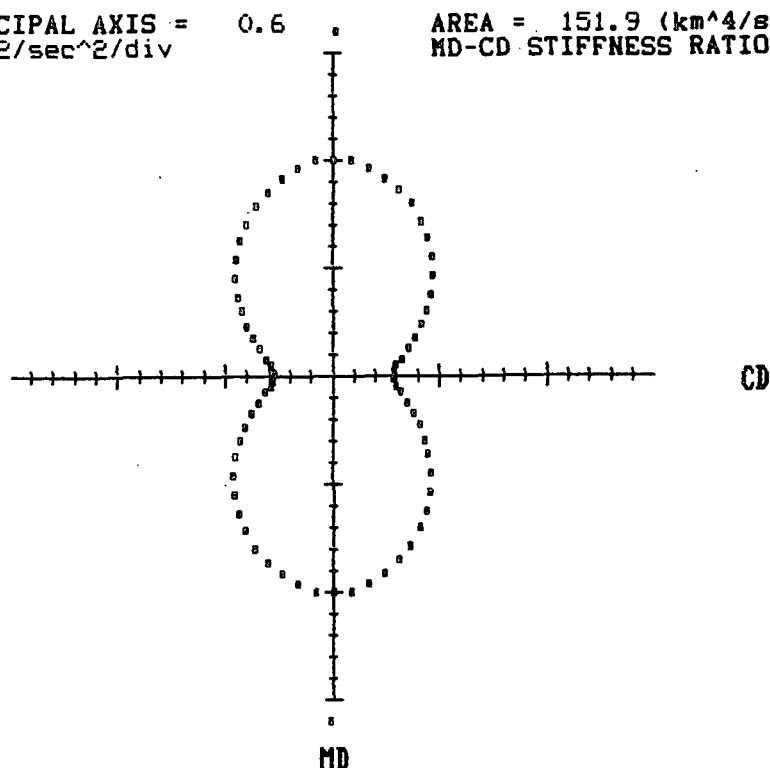SAMPLE : Chipboard top

DATE: SEPTEMBER 12, 1988
TIME: 17:32:45

SIGNALS AVERAGED PER MEASUREMENT = 4
NUMBER OF TESTS PER ANGLE   = 16
SIGNAL DISTANCE   = 50.0 mm
SAMPLE HOLDER NUMBER   = 2

ANGLE DEGREES	VEL SQR KM2/SEC2	COEF OF VARIATION	ANGLE DEGREES	VEL SQR KM2/SEC2	COEF OF VARIATION
0	10.12	0.019	90	2.86	0.016
5	9.86	0.026	95	2.85	0.017
10	9.47	0.031	100	2.86	0.023
15	8.83	0.036	105	2.89	0.018
20	8.02	0.025	110	2.98	0.014
25	7.17	0.042	115	3.13	0.019
30	6.39	0.030	120	3.35	0.018
35	5.67	0.024	125	3.68	0.021
40	5.00	0.023	130	4.00	0.019
45	4.45	0.025	135	4.40	0.017
50	4.01	0.019	140	4.93	0.013
55	3.62	0.021	145	5.55	0.016
60	3.38	0.020	150	6.25	0.016
65	3.17	0.026	155	6.98	0.023
70	3.02	0.029	160	7.76	0.015
75	2.95	0.025	165	8.64	0.020
80	2.90	0.017	170	9.32	0.034
85	2.88	0.013	175	9.79	0.028

ANGLE TO MAJOR PRINCIPAL AXIS =   0.5
GRAPH SCALE = 1 km^2/sec^2/div

AREA =   109.3 (km^4/sec^4)
MD-CD STIFFNESS RATIO = 3.54

CD

MD

PLOT OF VEL SQR VS ANGLE AS SEEN FROM FELT SIDE

Figure 1. Longitudinal polar plot of information propagation
velocity squared for a chipboard sample.

samples. Musgrave demonstrated a graphical relationship between polar plots of information propagation velocity and phase velocity. This is: a line drawn at a point on the phase velocity (not velocity squared) polar plot perpendicular to the radial direction will be tangent to the information propagation velocity polar plot. From this prescription, we have programmed the computer to construct the phase velocity plot from the information propagation velocity plot. Figure 2 presents the phase velocity squared plot for the chipboard sample. Notice the large differences in the two plots. Chipboard was chosen for this demonstration since is one of the most anisotropic (in this case 3.5 to 1.0) papers commonly encountered. This exaggerates the contrast in shapes and allows the reader to readily perceive the effects of transforming between plots.

There is a well known mathematical relationship between the phase velocity squared polar plot and the mass specific planar stiffnesses of an orthotropic planar material. This is:

$$V_p(\theta)^2 = 0.5[A(\theta) + (A(\theta)^2 - 4B(\theta))^{1/2}], \tag{1}$$

where

$$A(\theta) = (C_{11}/\rho)\cos^2\theta + (C_{22}/\rho)\sin^2\theta + C_{66}/\rho, \tag{2}$$

and

$$B(\theta) = [(C_{11}/\rho)\cos^2\theta + (C_{66}/\rho)\sin^2\theta][(C_{66}/\rho)\cos^2\theta$$
$$+(C_{22}/\rho)\sin^2\theta] - [(C_{12}/\rho)+(C_{66}/\rho)]^2\sin^2\theta\cos^2\theta. \tag{3}$$

The C_{ij}/ρ terms in the above equations represent the mass specific planar elastic stiffnesses. Equation (1) allows the phase velocity polar plot to be constructed from the elastic properties. This relationship could be inverted to determine the elastic constants from the polar plot. However the four C_{ij}/ρ terms are over determined by the 18 listed velocities squared. In

THE INSTITUTE OF PAPER CHEMISTRY
ROBOTIC IN-PLANE ULTRASONIC VELOCITIES

POLAR PLOT OF LONGITUDINAL PHASE VELOCITY SQUARED

OPERATOR: C. C. Habeger   DATE: SEPTEMBER 12, 1988
PROJECT : 3467   TIME: 17:33:56
SAMPLE : Chipboard top

SIGNALS AVERAGED PER MEASUREMENT =   4
NUMBER OF TESTS PER ANGLE   =   16
SIGNAL DISTANCE   = 50.0 mm
SAMPLE HOLDER NUMBER   =   2

ANGLE DEGREES	VEL SQR KM2/SEC2	ANGLE DEGREES	VEL SQR KM2/SEC2
0	10.12	90	2.86
5	10.04	95	2.85
10	9.81	100	3.02
15	9.56	105	3.31
20	9.20	110	3.72
25	8.84	115	4.20
30	8.36	120	4.69
35	7.80	125	5.24
40	7.25	130	5.82
45	6.62	135	6.48
50	6.02	140	7.09
55	5.38	145	7.65
60	4.81	150	8.22
65	4.29	155	8.69
70	3.81	160	9.13
75	3.36	165	9.49
80	3.01	170	9.81
85	2.88	175	10.04

ANGLE TO MAJOR PRINCIPAL AXIS =   0.6   AREA =   151.9 (km^4/sec^4)
GRAPH SCALE = 1 km^2/sec^2/div   MD-CD STIFFNESS RATIO = 3.54

MD
PLOT OF VEL SQR VS ANGLE AS SEEN FROM FELT SIDE

Figure 2. Longitudinal polar plot of phase velocity squared for
a chipboard sample.

this case the proper approach is to optimize the elastic constants to give the best least square fit to the phase velocity squared polar plot.

Before proceeding, remember that we are talking about determining all of the in-plane elastic constants from a longitudinal polar plot. The C_{11}/ρ and C_{22}/ρ terms strongly influence these velocities, while C_{66}/ρ and C_{12}/ρ have smaller effects on the shape of this polar plot. A better way to determine C_{66}/ρ is to take it directly from shear velocity measurements. The Poisson term (C_{12}/ρ) was previously determined from shear measurements at 45°, but, as argued in earlier PAC reports, shear at 45° is tainted by longitudinal interferences in very anisotropic samples. The off-axis longitudinal measurements are less affected by shear impurities since the longitudinal disturbances propagate faster. In either case, the determination of the Poisson term comes from its second order effect on velocities; however, the longitudinal is a cleaner signal, and, with polar plots, velocities at many angles can reduce variability. Therefore, an improved estimate of C_{12}/ρ will be obtained by optimizing C_{11}/ρ, C_{22}/ρ, and C_{12}/ρ to fit the phase velocity squared polar plot.

The optimal elastic parameters are determined as follows: (1) a longitudinal phase velocity squared polar plot is obtained; (2) 16 shear velocities are measured in the cross direction, and C_{66}/ρ is set equal to the average of the square; (3) initial guesses for C_{11}/ρ, C_{22}/ρ, and C_{12}/ρ are made by taking the maximum and minimum velocities squared from the polar plot and by using Campbell's relation; (4) the computer uses a straightforward optimization procedure to find the values of C_{11}/ρ, C_{22}/ρ, and C_{12}/ρ that minimizes the sum of the squares of difference between the experimental and theoretical values of the phase velocities squared in the polar plot; and (5) the values of the best fit

parameters and the "average relative error" (the square root of the least square sum divided by the sum of the experimental velocities squared) are reported. See the upper right hand portion of Fig. 3 for results on the chipboard sample. As is typical of the paper samples tested so far, the relative error is running around 0.1%. We consider this to be a fine fit, and we feel it indicates that the orthotropic model of paper elastic properties does a good job of predicting the shape of the phase velocity polar plot. The Poisson ratios are calculated from the C_{ij}/ρ terms and printed below the average error. These generally run lower than those calculated by the shear 45° technique. For normal machine-made papers, with a MD/CD modulus ratio of about 2 to 1, the difference is about 10%; for squarer sheets the difference is less; and it can be up to 20% on highly oriented samples. We feel that this validates the ultrasonic method for determining Poisson's ratios on reasonably square paper samples by giving an independent confirmation of the shear 45° method.

This optimization approach can be pushed one step further. Equation 1 assumes that the paper has orthotropic symmetry. General (nonorthotropic) planar materials have two additional elastic parameters, C_{16}/ρ and C_{26}/ρ. These are zero when measured relative to the principal axes of orthotropic materials. These parameters quantify the coupling between shear and normal stresses and strains along the principal axes. For example, C_{16} equals the ratio of normal stress in the x direction resulting solely from a shear strain in the x-y plane. In terms of the left-handed rotations in which we express our polar plots, dropping the orthotropic assumption means the $A(\theta)$ and $B(\theta)$ in Equations 2 and 3 change to $A(\theta)'$ and $B(\theta)'$, where

$$A(\theta)' = A(\theta) - 2\cos\theta\sin\theta((C_{16}/\rho)+(C_{26}/\rho)) \tag{4}$$

and

THE INSTITUTE OF PAPER CHEMISTRY
ROBOTIC IN-PLANE ULTRASONIC VELOCITIES

OPTIMUM MASS SPECIFIC STIFFNESSES FROM LEAST SQUARED
FIT TO LONGITUDINAL PHASE VELOCITY

OPERATOR: C. C. Habeger
PROJECT : 3467
SAMPLE : Chipboard top

DATE: SEPTEMBER 12, 1988
TIME: 17:34:58

ORTHOTROPIC STIFFNESSES
C11 / rho = 10.038 KM2/SEC2
C22 / rho =   2.787 KM2/SEC2
C66 / rho =   1.889 KM2/SEC2
C12 / rho =   1.194 KM2/SEC2

GENERAL STIFFNESSES
C11 / rho = 10.039 KM2/SEC2
C22 / rho =   2.788 KM2/SEC2
C66 / rho =   1.889 KM2/SEC2
C12 / rho =   1.193 KM2/SEC2
C16 / rho = -0.007 KM2/SEC2
C26 / rho =   0.014 KM2/SEC2

C66 / rho (Campbell) =   1.746 KM2/SEC2

Average relative error = 0.000952
Stiffness ratio = 3.60

Average relative error = 0.000931
Stiffness ratio = 3.60

Poisson's Ratios
Vxy =   0.119
Vyx =   0.429
Geometric Mean = 0.226

Poisson's Ratios
Vxy =   0.119
Vyx =   0.428
Geometric Mean = 0.225

ANGLE TO MAJOR PRINCIPAL AXIS = 0.6
GRAPH SCALE = 1 km^2/sec^2/div

AREA = 135.4 (km^4/sec^4)

POLAR PLOT OF LONGITUDINAL MASS SPECIFIC STIFFNESS
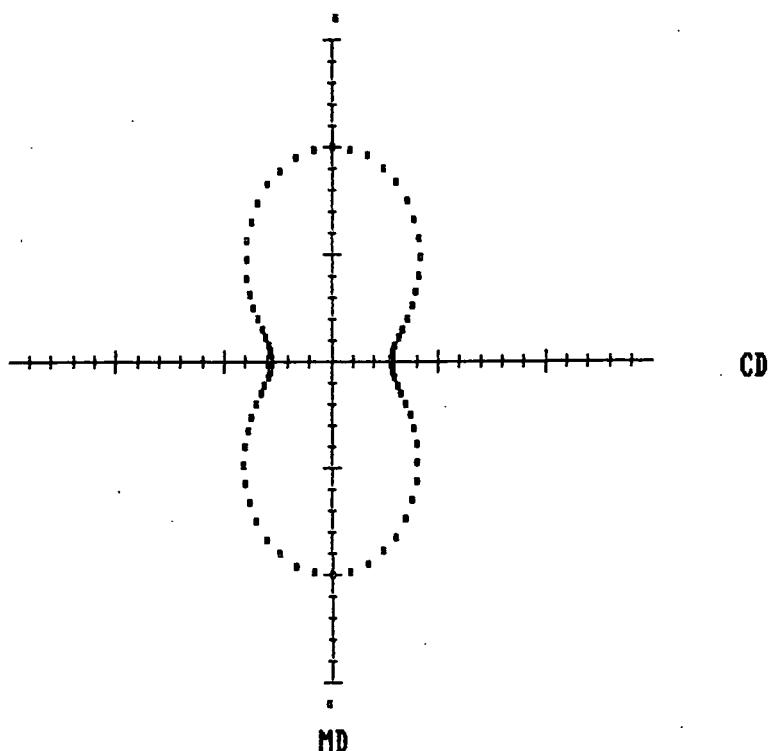
PLOT OF SPECIFIC STIFFNESS AS SEEN FROM FELT SIDE

Figure 3. In-plane elastic stiffnesses from polar plot optimization
for a chipboard sample.

$$B(\theta)' = [(C_{11}/\rho)\cos\theta^2+(C_{66}/\rho)\sin\theta^2-2\cos\theta\sin\theta(C_{16}/\rho)]$$

$$[(C_{66}/\rho)\cos\theta^2+(C_{22}/\rho)\sin\theta^2-2\cos\theta\sin\theta(C_{26}/\rho)] \qquad (5)$$

$$-[(C_{16}/\rho)\cos\theta^2+(C_{26}/\rho)\sin\theta^2-\cos\theta\sin\theta((C_{12}/\rho)$$

$$+(C_{66}/\rho))]^2.$$

Now, the optimization routine is readministered, allowing C_{16}/ρ and C_{26}/ρ to adjust. The results for chipboard are in the upper left hand portion of Fig. 3. Notice (as is typical of other paper samples tested) that the major elastic parameters change only slightly, the nonorthotropic constants are very small, and the average relative error shows little improvement. It is typical (as seen in Fig. 3) for the signs of C_{16} and C_{26} to be opposite and for the absolute value of C_{26} to be about twice as great as C_{16}.

A complete set of elastic parameters is now available, and a third polar plot can be constructed. This is the value of normal mass specific stiffness as a function of angle to the x axes. It is obtained by rotating the stiffness tensor. The plot for the chipboard sample is at the bottom of Fig. 3. This is the plot that is, perhaps, of the most interest; it is the actual stiffness (not some ultrasonic velocity squared) as a function of angle. The reader is reminded that the differences in the polar plots for chipboard is extreme due to its high anisotropy.

Now we will discuss the significance of the C_{16} and C_{26} measurements. Since they are quite small, they may arise from variations in the measurements or from a lack of homogeneity in the paper samples. They are not completely due to instrumental variations as repeating polar plots and calculating new nonorthotropic constants (without moving the sample) gives averages that are nonzero with high confidence. The standard deviations are usually about equal

to the magnitude of the parameters. Rotating the sample, or turning it over, or translating it bit does, however, result in big changes. When averaged over such sampling variations, the parameters for a variety of papers (linerboard, medium, fine paper, and chipboard) were not significantly different from zero. This seems to be telling us that, within the capabilities of our ultrasonic techniques, we are unable to detect lack of orthotropic behavior in paper.

One situation in which we expected to find lack of orthotropic behavior was with machine-made papers having average fiber alignment not along the MD. These papers have one axis of symmetry for wet straining and drying stresses and another for fiber orientation. The orthotropic assumption cannot be rigorously applied to these sheets, and we hoped to have a measure of the coupling between shear stress and strains and normal stresses and strains resulting from this misalignment. However, (when determined along the principal axes of the polar plots) the nonorthotropic parameters were no more significant on misaligned sheets than on aligned sheets taken from the same CD profile. The CD strip tested was a computer form paper in which the angle of the principal axis to the MD varied from plus to minus ten degrees. None of the tested samples had parameters conclusively different from zero. In fact, if we average all the parameters from the 90 different polar plots ran on samples from the profile, we get $C_{16}/\rho = -0.001 \mp 0.019$ km^2/sec^2 and $C_{26}/\rho = 0.003 \mp 0.033$ km^2/sec^2. It required over 30,000 velocity measurements to get this result, and we can say only with a confidence level of 73% that the average of C_{16} is below zero and with an 82% confidence that C_{26} is above zero for this CD strip.

Before we can declare that the in-plane elastic parameters of paper conform extremely well to the orthotropic symmetry assumption, we must

demonstrate independently that we have a valid technique for measuring C_{16} and C_{26}. That is, we must measure the correct values in samples known to be nonorthotropic. We are pursuing this by bonding together orthotropic plastic sheets with their principal axes misaligned. In this case C_{16} and C_{26} of the laminate can be calculated from a parallel average of the elastic parameters of the components. The measured and calculate values should match. At present we are having difficulties bonding the sheets sufficiently well with a thin couplant; however, we have some new ideas and hope to check the technique by this method soon.

Another interesting exercise with this approach is to inspect other anisotropic planar samples and see if they are orthotropic. We looked at three samples: a polypropylene sheet with an aspect ratio of 2 to 1; a cellophane sheet with an aspect ratio of 1.5 to 1; and a polyester sheet (our standard) with an aspect ratio of 1.25 to 1. These samples are more homogeneous than paper, and we hoped to improve our resolution. The polypropylene sample yielded very small nonorthotropic parameters. Figure 4 is the third page print out (similar to Fig. 3) for a typical polypropylene run. This test was replicated six times; C_{16}/ρ was 0.0007 $\mp$ 0.003 km^2/sec^2 and C_{26} was -0.0015 $\mp$ 0.005 km^2/sec^2. As with paper the magnitude of C_{26} is generally twice that of C_{16}, and the two are of opposite signs. The polypropylene sample is also remarkably orthotropic, and, being more uniform, it exhibits much less variability in C_{16} and C_{26}. The cellophane results were similar to those from paper: average values were near zero with a standard deviation of about 0.010. The polyester sheet is the really interesting one. Figure 5 is a typical first page result and Figure 6 is a typical third page report. (The difference between polar plots is much smaller here than for chipboard as the polyester is less

THE INSTITUTE OF PAPER CHEMISTRY
ROBOTIC IN-PLANE ULTRASONIC VELOCITIES

OPTIMUM MASS SPECIFIC STIFFNESSES FROM LEAST SQUARED
FIT TO LONGITUDINAL PHASE VELOCITY

OPERATOR: C. C. Habeger   DATE: AUGUST 12, 1988
PROJECT : 3467   TIME: 15:12:58
SAMPLE : Polypropylene 9 72 F

ORTHOTROPIC STIFFNESSES   GENERAL STIFFNESSES
C11 / rho = 10.010 KM2/SEC2   C11 / rho = 10.012 KM2/SEC2
C22 / rho =   5.028 KM2/SEC2   C22 / rho =   5.029 KM2/SEC2
C66 / rho =   2.195 KM2/SEC2   C66 / rho =   2.195 KM2/SEC2
C12 / rho =   2.026 KM2/SEC2   C12 / rho =   2.024 KM2/SEC2
                                         C16 / rho =   0.003 KM2/SEC2
                                         C26 / rho = -0.006 KM2/SEC2

                                         C66 / rho (Campbell) =   2.423 KM2/SEC2

Average relative error = 0.000884   Average relative error = 0.000880
Stiffness ratio = 1.99   Stiffness ratio = 1.99

Poisson's Ratios   Poisson's Ratios
Vxy =   0.202   Vxy =   0.202
Vyx =   0.403   Vyx =   0.403
Geometric Mean =   0.286   Geometric Mean =   0.285

ANGLE TO MAJOR PRINCIPAL AXIS = -6.2   AREA =   174.3 (km^4/sec^4)
GRAPH SCALE = 1 km^2/sec^2/div

POLAR PLOT OF LONGITUDINAL MASS SPECIFIC STIFFNESS

PLOT OF SPECIFIC STIFFNESS AS SEEN FROM FELT SIDE

Figure 4.   Longitudinal polar plot of information propagation velocity
            squared for a polypropylene sheet.

THE INSTITUTE OF PAPER CHEMISTRY
ROBOTIC IN-PLANE ULTRASONIC VELOCITIES

POLAR PLOT OF LONGITUDINAL INFORMATION PROPAGATION VELOCITY SQUARED

OPERATOR: C. C. Habeger   DATE: AUGUST 30, 1988
PROJECT : 3467   TIME: 17:59:28
SAMPLE : Polyester 101 top 72 F

SIGNALS AVERAGED PER MEASUREMENT =   4
NUMBER OF TESTS PER ANGLE   =   8
SIGNAL DISTANCE   = 50.0 mm
SAMPLE HOLDER NUMBER   =   2

ANGLE DEGREES	VEL SQR KM2/SEC2	COEF OF VARIATION	ANGLE DEGREES	VEL SQR KM2/SEC2	COEF OF VARIATION
0	5.93	0.025	90	4.76	0.009
5	5.95	0.011	95	4.84	0.012
10	5.77	0.027	100	4.89	0.010
15	5.63	0.019	105	4.93	0.016
20	5.48	0.024	110	5.03	0.011
25	5.32	0.026	115	5.08	0.014
30	5.17	0.019	120	5.19	0.003
35	5.11	0.021	125	5.23	0.010
40	4.98	0.017	130	5.36	0.010
45	4.90	0.027	135	5.48	0.009
50	4.86	0.027	140	5.58	0.007
55	4.77	0.016	145	5.68	0.011
60	4.71	0.011	150	5.79	0.014
65	4.67	0.011	155	5.84	0.013
70	4.70	0.008	160	5.97	0.009
75	4.70	0.012	165	5.97	0.011
80	4.67	0.019	170	5.98	0.016
85	4.74	0.010	175	5.97	0.012

ANGLE TO MAJOR PRINCIPAL AXIS = -13.4   AREA =   87.7 (km^4/sec^4)
GRAPH SCALE = 1 km^2/sec^2/div   MD-CD STIFFNESS RATIO = 1.25

PLOT OF VEL SQR VS ANGLE AS SEEN FROM FELT SIDE

Figure 5. Longitudinal polar plot of information propagation velocity
squared for a polyester sheet.

THE INSTITUTE OF PAPER CHEMISTRY
ROBOTIC IN-PLANE ULTRASONIC VELOCITIES

OPTIMUM MASS SPECIFIC STIFFNESSES FROM LEAST SQUARED
FIT TO LONGITUDINAL PHASE VELOCITY

OPERATOR: C. C. Habeger   DATE: AUGUST 30, 1988
PROJECT : 3467   TIME: 18:1:36
SAMPLE : Polyester 101 top 72 F

ORTHOTROPIC STIFFNESSES   GENERAL STIFFNESSES
C11 / rho =   6.007 KM2/SEC2   C11 / rho =   6.008 KM2/SEC2
C22 / rho =   4.701 KM2/SEC2   C22 / rho =   4.701 KM2/SEC2
C66 / rho =   1.685 KM2/SEC2   C66 / rho =   1.685 KM2/SEC2
C12 / rho =   1.758 KM2/SEC2   C12 / rho =   1.756 KM2/SEC2
                                            C16 / rho =   -0.051 KM2/SEC2
                                            C26 / rho =   0.060 KM2/SEC2

                                            C66 / rho (Campbell) =   1.769 KM2/SEC2

Average relative error =   0.001481   Average relative error =   0.000811
Stiffness ratio = 1.28   Stiffness ratio = 1.28

Poisson's Ratios   Poisson's Ratios
Vxy =   0.293   Vxy =   0.292
Vyx =   0.374   Vyx =   0.373
Geometric Mean   =   0.331   Geometric Mean   =   0.330

ANGLE TO MAJOR PRINCIPAL AXIS = -12.6   AREA =   88.7 (km^4/sec^4)
GRAPH SCALE = 1 km^2/sec^2/div

POLAR PLOT OF LONGITUDINAL MASS SPECIFIC STIFFNESS

MD

PLOT OF SPECIFIC STIFFNESS AS SEEN FROM FELT SIDE

Figure 6.   In-plane elastic stiffnesses from polar plot optimization
            for a polyester sheet.

anisotropic.) Notice in Fig. 6 the significant improvement in relative error when nonorthotropic constants are added. When four runs were made on this sample, C_{16}/ρ was -0.048 ∓ 0.006 km^2/sec^2 and C_{26}/ρ was 0.056 ∓ 0.007. These numbers are significantly different from zero! Also note that the absolute value of C_{26} is only slightly larger than C_{16}. The principal axes of this sample is aligned over 10° off the MD, and presumably changes in the direction of the drawing tension during extrusion produced a nonorthotropic sheet. A necessary (but not sufficient) condition that the sample is orthotropic is that the raw data (Fig. 5) have reflectional symmetry about the principal axes. A careful inspection of Fig. 5 shows that this symmetry is violated, as the polar plot bugs out a little just clockwise of the main axis. As shown in Fig. 6 this phenomenon can be reproduced by an appropriate choice of C_{16} and C_{26}.

As far as we know, this is the first time measurements of C_{16} and C_{26} have been attempted in planar materials. We think that the upshot of this for paper will be that it is more orthotropic than we ever dreamed possible. However, we shall investigate further. For plastic sheets, this technique may be of real diagnostic interest, since preliminary results indicate that the extrusion process can generate relatively large nonorthotropic behavior.

II. PROGRESS WITH LABORATORY OUT-OF-PLANE INSTRUMENTATION

During the last period, we have designed, built, and checked out new ZD longitudinal transducers. These differ from the previous design in that the transducers contain two active electrodes and can be used to simultaneously send and receive ultrasonic signals. The purpose of this is allow investigation of the signals reflected from the paper-transducer interface as well as those transmitted through the sample to a second transducer. The ability to quantify

the reflected component of the signal provides two important advantages. First
of all, in our previous attempts to determine the attenuation of ultrasound in
transmission through paper samples, we were forced to assume that the trans-
ducers and sample were acoustically well coupled. We had established that this
was not the case, but we had no means to correct for the greater than assumed
energy reflection at the interfaces. Therefore, our attenuation results con-
tained a term that depended on the interface, and we were unable to confidently
discuss acoustic losses within the bulk of the sample. Now we can look at the
signal coming back from the first transducer-sample interface, actually measure
the reflection coefficient, and correct the transmitted signal for interfacial
losses. The second advantage is that examining directly the reflection coef-
ficient gives a method for acoustically assessing the surface characteristics of
the sample. The quality of coupling is a function of sample surface charac-
teristics that could be rapidly and nondestructively determined with ultrasonic
techniques.

The construction of the new transducers is depicted in Fig. 7. Notice
that these are similar to the original ZD longitudinal transducers, in that: (1)
Kynar film, with solid Kynar backings, are used as active piezoelectric ele-
ments; (2) a soft neoprene layer couples energy into the paper; and a low-loss
polystyrene disk is used for impedance matching between the Kynar and the
neoprene. The difference is that a second layer of active film, separated from
the first by a Kynar layer, has been added, and electrical connection to the
transducer casing is provided for both signals. Figures 8 and 9 are pictures of
a transducer before application of the neoprene front-face, and after final
assembly.
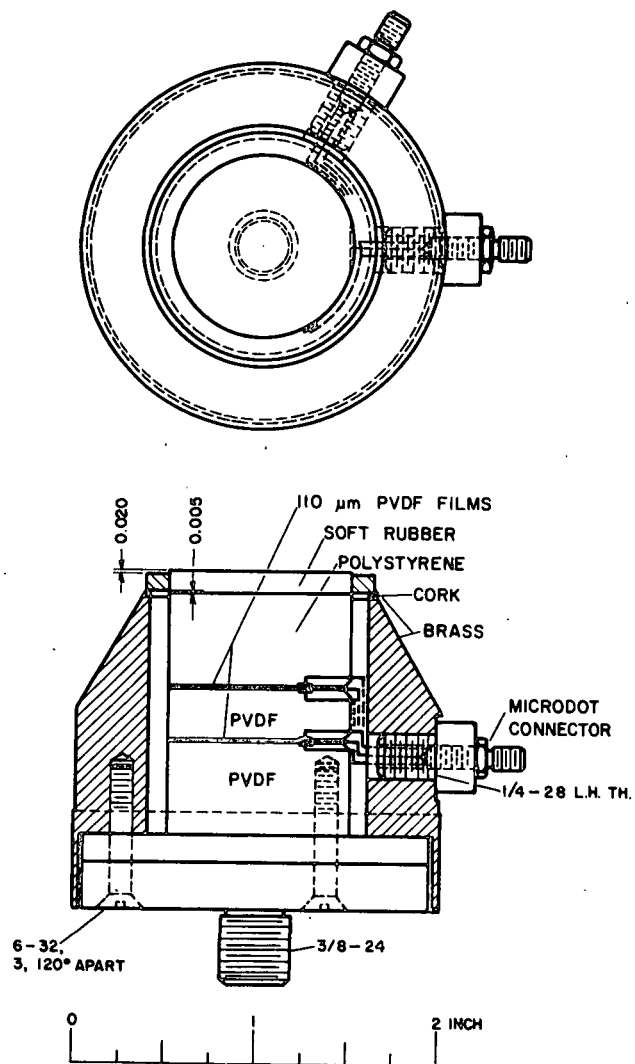
Figure 7. Schematic diagram of the pulse-echo PVDF transducer.

Figure 8. Photograph of the pulse-echo PVDF transducer during assembly, before addition of the neoprene-face.
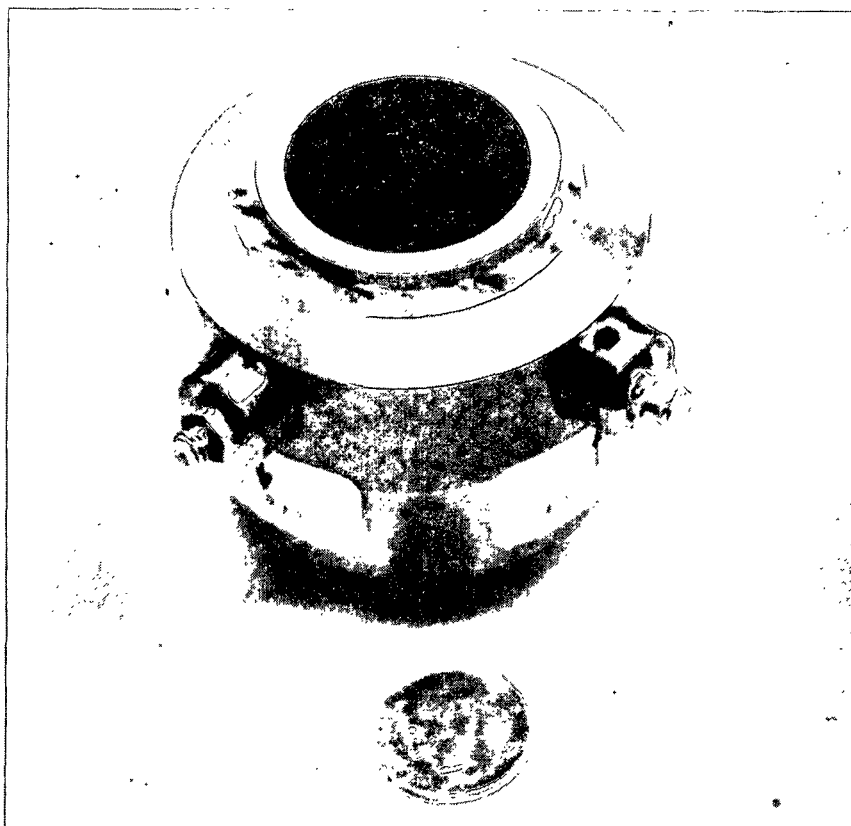
Figure 9.   Photograph of the assembled pulse-echo PVDF transducer.

. These transducers can be used in a pulse-echo mode: one electrode is excited and the signals reverberating off the interfaces are detected in the other. Figure 10 is a picture of the resulting oscilloscope trace when this experiment was preformed before addition of the neoprene layer (as in Fig. 8). The first small pulse comes directly form the electromagnetic radio frequency coupling between the two films. The first large pulse is the ultrasonic signal communicated directly between the two film layers. The large inverted signal is the first reflection from the polystyrene-air interface. Signal inversion occurs when a signal is reflected in going from a high to a low impedance material, as is the case here. Notice that the amplitude of this signal is about 3/4 that of the first ultrasonic signal. The ratio is less than one since the second signal has additional transmission losses at two Kynar-polystyrene

interfaces, small viscous and diffraction losses though the polystyrene, and small reflectional losses at the polystyrene-air interface. The small trailing signal is a polystyrene reflection with an addition multiple reflection in the interconnecting Kynar disk. Fortunately the Kynar is quite lossy, and this signal is severely attenuated.

Figure 11 is the oscilloscope trace of the reflected signal from an assembled transducer with air contact to the front-face. The first three signals have the same origin as in Fig. 10. The time between the second and third signal is less due to the shortening of the polystyrene layer. Notice that third signal amplitude is decreased, as much better energy transfer is achieved between polystyrene and neoprene than polystyrene and air. The fourth signal, which was not present before neoprene addition, is the first reflection off the neoprene-air interface. As can be seen by comparing Figs. 10 and 11, this signal contains a small amount of interference from the weak trailing signal, seen distinctly in Fig. 10. Figure 12 is the same trace with a linerboard sample applied to the front-face with a 50 kPa loading pressure. The reflection at the neoprene-sample interface is decreased, since some energy is not reflected, but is transferred into the sample.

Assuming that the reflection at the neoprene-air interface is complete, the reflection coefficient at the neoprene-sample interface is equal to the ratio of the fourth signal amplitude in Fig. 12 to that in Fig. 11. The computer controlling the ZD longitudinal instrument has been programmed to do a Fourier analysis of these two signals, calculate a frequency dependent reflection coefficient, and an average reflection coefficient.
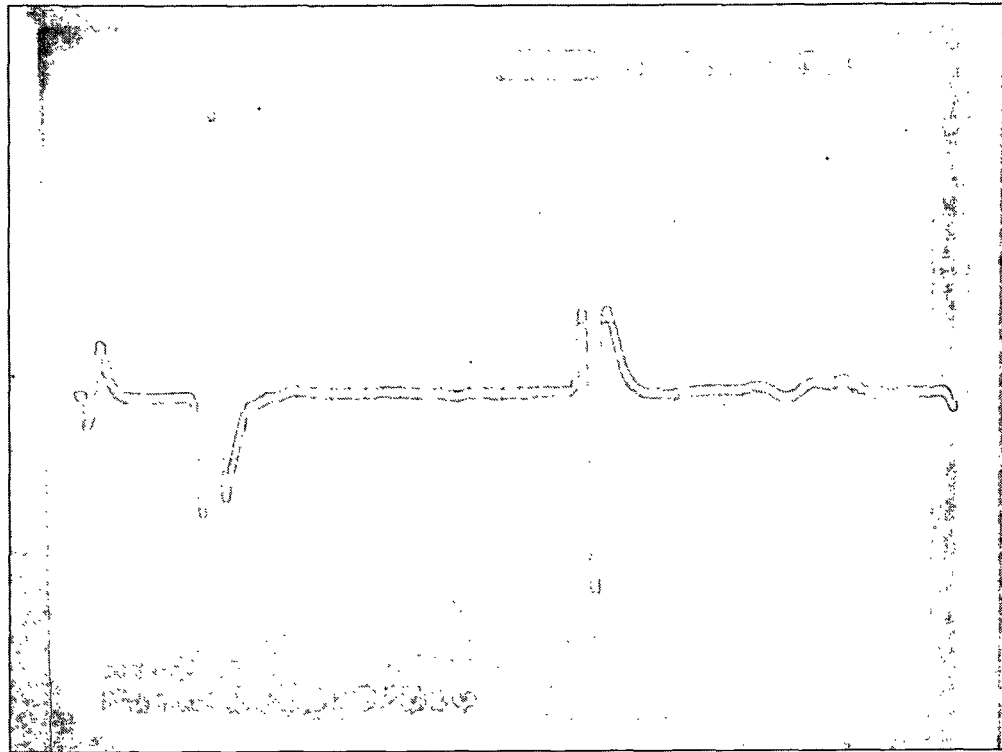
Figure 10. Before application of neoprene front-face, oscilloscope trace of the receiver signal of the pulse-echo transducer resulting from a single pulse at the transmitter.
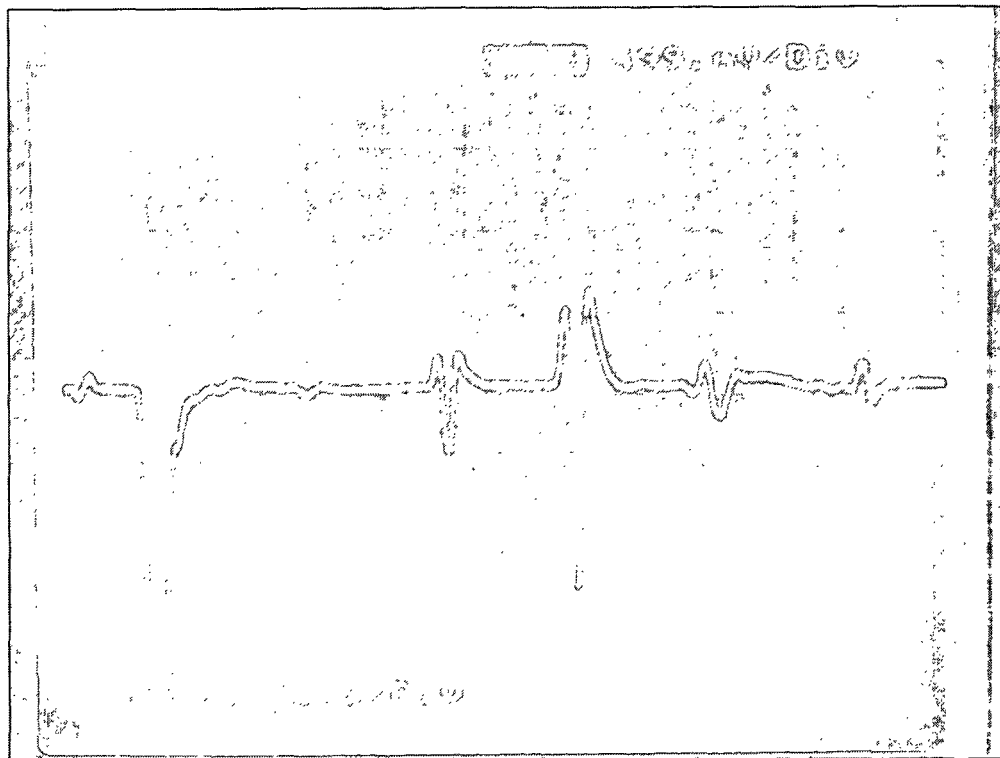
Figure 11. After application of neoprene front-face, oscilloscope trace of the receiver signal of the pulse-echo transducer resulting from a single pulse at the transmitter.
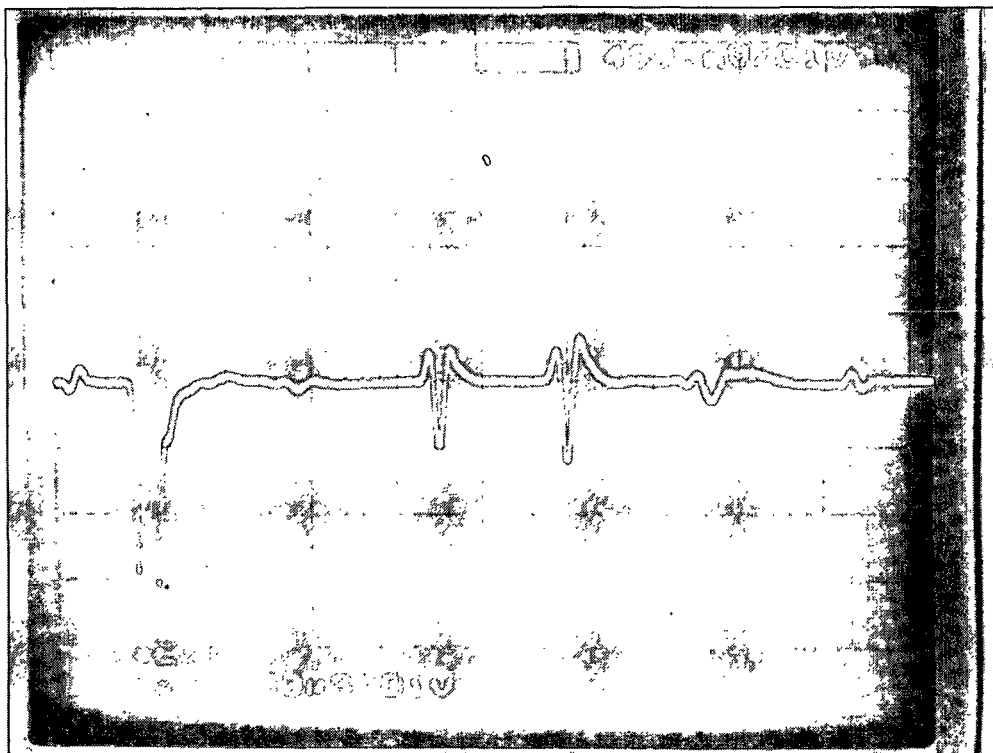
Figure 12.   After loading of a linerboard sample to the neoprene
             front face, oscilloscope trace of the receiver signal
             of the pulse-echo transducer resulting from a single
             pulse at the transmitter.

If the coupling were "perfect", as we were forced to assume earlier,
the sample-paper reflection coefficient, R_T, would equal $(Z_P-Z_N)/(Z_P+Z_N)$. The
symbols Z_P and Z_N are used to designate the ultrasonic impedance of the paper
and neoprene. The impedance of a material is its ultrasonic velocity times its
density. The neoprene impedance was previously determined to be about 1.61 X
10^6 kg/m^{2}sec, and the impedance of the paper can be determined from our normal
ZD longitudinal measurement procedure. Therefore by comparing R_T with the
measured reflection coefficient, R_E, we can gauge the effect of surface irregu-
larity on the coupling of ultrasound between neoprene and paper. There are a
number of ways to do this. We decided to take the ratio of the perfect to the
experimental transmission coefficients as an indicator of poor coupling. Since
the transmission coefficient is one minus the reflection coefficient, this can
be expressed as $C = (1-R_T)/(1-R_E)$.

We have just started playing with this technique, and, as yet, there are not many results. However, we will present a few preliminary numbers. Figure 13 is a plot of reflection coefficient, R_E, vs. density for a subset of the sheets prepared by Brian Berger for his thesis. These are all are formed from unbleached kraft loblolly pine furnishes, but they vary widely in wet pressing, refining, and lignin content. The trends observed in Fig. 13 are in accord with our naive expectations. That is, the portion of energy reflected decreases as density rises, reducing the impedance mismatch between the neoprene and the sample. Also, R_E is greater on wire side, presumably due to the greater roughness there. Using the measured ZD velocities and densities to convert the R_E values into poor coupling coefficients, produces Fig. 14. This is not quite what we expected. The relative loss in transmission due to poor coupling generally increases with density, even though we expect surfaces irregularity to be decreasing. However, at the highest densities (the most refined samples) C does appear to drop off. We also examined three commercial samples: a liner-board (ρ = 791 kg/m^3, C = 1.43); a corrugating medium (ρ = 649 kg/m^3, C = 2.61); and a heavily coated bleached board (ρ = 694 kg/m^3, C = 0.76). As might be expected, the linerboard showed considerably better, and the medium considerably poorer, coupling when compared with Fig. 14 samples at the same density. The shocker is that C for the coated board is less than 1.0; the coupling is actually better than could possibly be obtained from a uniform sheet with velocity and density equal to the average in the board. The coating is probably concentrated at the surface, causing transmission to be better than in a comparable uniform board.

It is clear that we are yet to fully appreciate the meaning of the ultrasonic reflection coefficients. In time, we hope to know: what are the
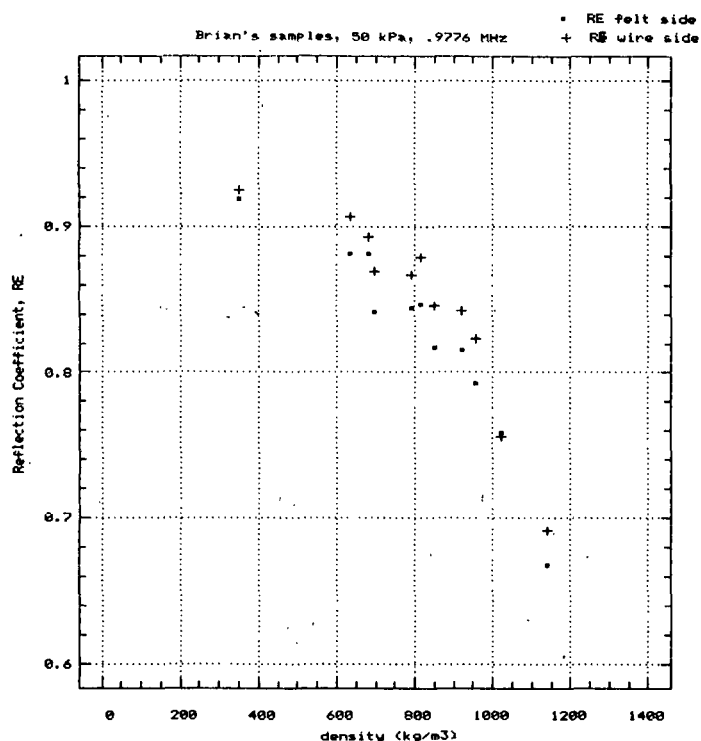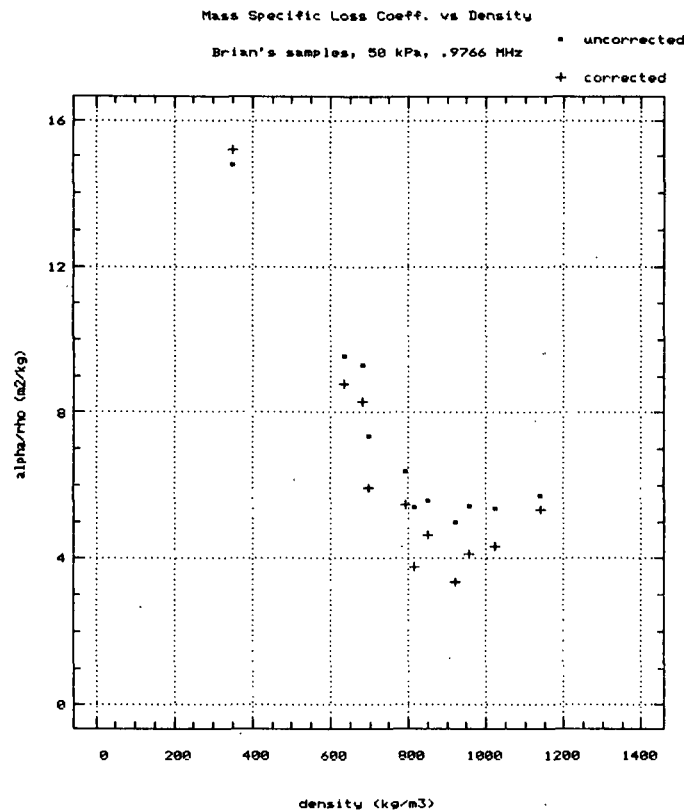
Figure 13. Ultrasonic reflection coefficient as a function of density for a series of samples varying in wet pressing, refining, and yield.
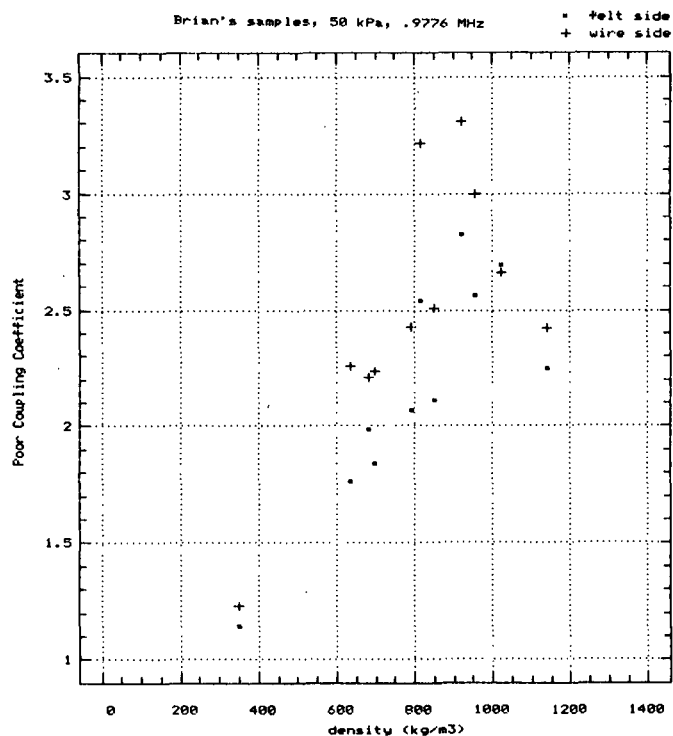

Figure 14. Ultrasonic poor coupling coefficient as a function of density for a series of samples varying in wet pressing, refining, and yield.

scale of surface irregularities that R_E is sensitive to?; how does it relate to established smoothness tests?; what are the effects of loading pressure?; and are there any real-life concerns that this test can be applied to?

Regardless of the meaning of R_E, its measurement provides a way to compensate for imperfect coupling in ZD loss calculations. In the past, we have registered very large ZD attenuation coefficients; however, we hesitated to discuss them, as we worried that they arose from poor interfacial coupling. Now, we can directly measure this effect and present loss numbers with more confidence. Loss calculations are done in light of the following equations, which gives the ratio, SR, of the signal transmitted through the sample to that through a thin aluminum foil reference in terms of the paper loss coefficient, α, the caliper, t, and the measured reflection coefficients between the neoprene and the wire side of the sample, R_EW, the neoprene and the felt side, R_EF, and the neoprene and the foil, R_EA:

$$SR = (1-R_EF^2)^{1/2}(1-R_EW^2)^{1/2}\exp(-\alpha t)/(1-R_EA). \tag{6}$$

Therefore, if the reflection ratios from the reference foil and the two sample surfaces are measured in addition to the caliper and SR, α can be determined from Equation 6.

The values of α were calculated for the samples introduced above. In order to display the results on a specific mass basis, α was divided by density and plotted against density (see Fig. 15). The value of α/ρ equals the natural logarithm of the ratio of the signal in to the signal out in passing through 1.0 kg/m^2 of material. Notice that the attenuation, expressed in this manner, decreases with density, but perhaps shows a slight increase for the highly refined samples. The main point in Fig. 15 is that the correction for imperfect

Mass Specific Loss Coeff. vs Density

Brian's samples, 50 kPa, .9766 MHz

• uncorrected

+ corrected

Figure 15. Mass specific ultrasonic attenuation coefficient as a
function of density for a series of samples varying in
wet pressing, refining, and yield.

reflection only slightly decreased the calculated loss. The reason for this is
that not only did we account for imperfect coupling at the neoprene-sample
interface, but also we corrected for the energy reflected at the interface bet-
ween the neoprene and the reference foil. Originally we had to assume that no
reflection occurred at the foil interface. As seen in Equation 6, the two
corrections compensate for each other, and, as it turns out for these samples,
they in fact almost cancel.

Compared to losses experienced during in-plane ultrasound propagation,
these are very large loss coefficients. One way to demonstrate this is to
express the loss in terms of the loss tangent. In-plane loss tangents (at about
100 kHz) rarely exceed 0.1. However, as is demonstrated in Fig. 16, they are

many times larger in the out-of-plane direction at about 1.0 MHz. This, perhaps, is because the fibers are very lossy in their radial direction, or maybe it is due to scattering from fiber level structure. At this point, it seems unlikely that scattering is the complete answer, since α does not increase as rapidly with frequency as expected for Rayleigh scattering. At any rate, we are now more confident in reporting large ZD losses, and we are better equipped to investigate the causes.

Quite a bit of software development is necessary before this test becomes routine. We need to automatically excite transmitters from both sides of the sample and program the computer to calculate R_EF and R_EW. The program that analyses the reference foil must also determine R_EA. Reports of corrected loss coefficients and coupling coefficients must be generated.
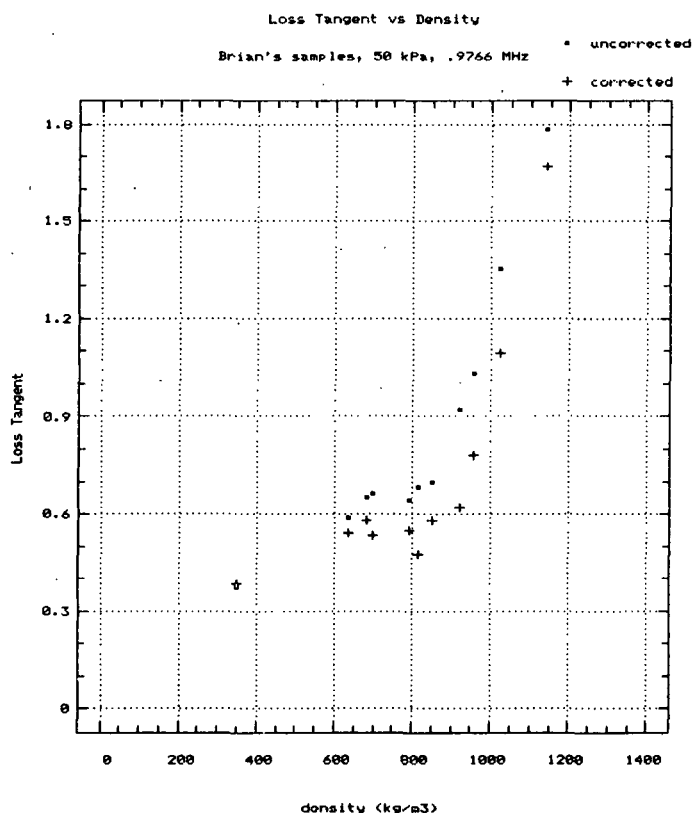
Figure 16. Ultrasonic loss tangent as a function of density for a series of samples varying in wet pressing, refining, and yield.

III. EMPIRICAL RELATIONSHIPS BETWEEN TISSUE SOFTNESSES AND
OUT-OF-PLANE ULTRASONIC MEASUREMENTS

SUMMARY

This report is an analysis of possible relations between subjective softness rankings of tissue and using Z-direction (ZD) ultrasonic measurements developed at The Institute of Paper Chemistry [1]. Results of ultrasonic velocity, energy loss, and strength properties are reported for fourteen kinds of commercially available tissue samples. It was found that the acoustic impedance of tissue in the Z-direction and the ultrasonic attenuation during the transmission correlate significantly with the panel softness ranking. A multiple regression analysis selected statistically the acoustic impedance, ultrasound attenuation level per unit basis weight, and basis weight and yielded a coefficient of multiple correlation (r^2) of 0.884 for bulk softness ranking (crumpling), and 0.785 for surface softness ranking (tactile sensation).

When the tissue samples were divided into facial tissue and toilet tissue, the same regression analysis showed extremely high coefficients in both the bulk (over 0.97) and surface softness rankings (over 0.90), but with different partial regression coefficients of each factors. In the case of facial tissue, acoustic impedance showed the highest significance level in the model; but in the case of toilet tissue, the specific attenuation level was most important.

The results showed that there is a potential for adopting ultrasonic techniques to make instrumental evaluations of the properties which contribute to the subjective softness sensation.

INTRODUCTION

Softness of tissue paper is an important quality to the consumer, and it is also important to the paper makers because the level of tissue softness is closely related to the marketing share of the product [2]. Softness here means a subjective impression which is perceived through the interaction of the material with the tactile sensory system of the human being. It is a very complex function of a multitude of physical and psychological interactions [3,4]. Softness can be divided into bulk softness and surface softness [3,5]. The former is intimately related to the flexural property of paper, and the latter is connected with the magnitude and the distribution of surface irregularities [3,5]. Much research has been done on the evaluation of softness of tissue papers both subjectively and instrumentally [3-21].

i. Instrumental Study of Softness

Panel assessment of the softness of tissue is the most popular method used in the quality control. It directly reflects the sensation performance of the product in its end-use. However, the assessment is time- and labor-consuming. Because of these shortcomings, much pioneering work has been done in the last 60 years, attempting to evaluate the softness of paper instrumentally. Below, several instruments which are commonly used are briefly described.

In the early 1930's, Clark studied the softness of paper and developed the Clark stiffness tester which is suitable for measuring the softness of tissue [12]. This method recently was adopted as a TAPPI Standard Method T451 hm-84. The test consists of clamping one end of a strip of paper between rotating jaws. The jaws are aligned vertically with sample above the jaws. The sample is bent toward one side by its own weight, and the jaws are turned in the opposite direction of the bending. The sample length is adjusted until there is

a difference of 90 degrees between the two positions of the jaws which just
cause the strip to bend to the other side. The longer the length, the stiffer
the paper. The Clark stiffness tester proved to be very sensitive to the flexi-
bility of paper. However, it has the shortcomings of being time-consuming,
being operator dependent, and difficult to run on the tissue.

The Handle-O-Meter was originally designed to measure the softness of
textiles [16,19]. It can also be used to evaluate the softness of tissue pro-
ducts (see TAPPI Standard Method T498 cm-85). The principle is to push a sheet
of paper through a narrow slot by means of a bar. The resistance to the bar is
measured electrically through a arm connected to the bar. The stiffer the
paper, the larger the resistance. The Handle-O-Meter is easy to operate, repro-
ducible and sensitive to softness, but the results are affected by basis weight
and by the level of surface roughness of the samples.

Brown developed a very simple method for measuring softness [13]. The
apparatus consisted of a 250 ml beaker and a 100 ml graduate cylinder. Two
tissue samples to be tested are separately crumpled loosely and stuffed into the
beaker. The graduate cylinder is then put on the top of the paper. The weight
was adjusted to make the paper volume equal to 25 to 35 ml. The product of the
weight exerted and the height in the beaker are taken as the index of softness.
This method seems to simulate the subjective crumpling test of tissues, but it
is sensitive to variations in the initial crumpling operation. It is not popu-
lar, probably because it is not very scientific.

The Peirce tester is a cantilever type flexibility tester which can
measure the "stiffness length" required to drop the free end of the sample strip

1 in. from the horizontal position. It showed good correlation with the results obtained using the Clark stiffness tester [14].

Recently in Japan, a new surface friction tester has been commercialized [22]. 0.5-mm diameter piano wire was used as a friction detecting element. By drawing the wire on the paper surface under a certain pressure and speed, the coefficient of surface friction can be recorded. It was shown that the surface tactile sensation of tissue or diaper materials can be evaluated even with varying moisture content [22].

ii. Factors Affecting the Softness of Tissue

Since the perception of softness is a subjective impression of the tactile sensory system of a human being, it is not surprising that different people give a different panel softness index to the samples. In addition to the physical properties of paper, panel assessment conditions, such as the color, smell, and the sound of crumpling the paper also affect the results [2,4].

The softness of paper is also affected by the physical properties. According to Lyne [15], the apparent density, flexure rigidity, compressibility or resilience, and surface smoothness of paper are the main factors. These intensive parameters are closely related to the fundamental structure of paper, the properties of fibers, and the bonding level between fibers. Simply, the more rigid the fiber and more bondings between fibers, the harsher is the paper. In addition to intensive parameters, extensive properties such as thickness, basis weight, and sample size, and ply numbers affect softness [6-8].

Many previous works demonstrated that the softness of paper correlates significantly with the flexural rigidity (EI) of the paper [3,7-9]. Flexural rigidity can be measured directly by means of the Clark stiffness tester [12],

the Torsion pendulum method [6] and other methods [14,16]. Sometimes flexural rigidity is calculated from Young's modulus (E) obtained by tensile measurement and the thickness (flexural rigidity $\propto Et^3$, where t is thickness). Because the thickness of the tissue is hard to measure rigorously, tensile stiffness (Et) measurements are preferred to flexural rigidity measurements [3,7-9].

Surface smoothness is also considered to be an important factor in the evaluation of the softness. It was observed that when two papers are almost of the same flexibility, the one with the smoother surface feels softer. It was also reported that the drum side of a creped tissue usually has a smoother surface and feels softer than the felt side [3,24]. Hollmark has studied surface smoothness and developed an instrument for evaluating surface softness which is related to surface smoothness [5]. He found correlation coefficients as high as 0.98 could be obtained between panel softness index and a combination of the tensile stiffness with his surface softness index [3].

In most cases, single parameters measured instrumentally do not correlate with the subjective softness very well. The research work carried out at The Institute of Paper Chemistry developed a simple multiple regression model for predicting the subjective softness from a proper combination of several physical properties measured instrumentally [6-9]. Similar to the work done by Hollmark [3], it was shown again that flexural rigidity is the main component of the softness of tissue, but instead of surface softness suggested by Hollmark, compressibility of paper in the Z-direction, the thickness and basic thickness (thickness measured under non-creped state) were used in the model [6,7]. In Progress Report Six of Project 2220, a coefficient of multiple regression of 0.988 is obtained. However, in Report 3 of Project 2817, they could not confirm

the reasonable relationship between the compressibility and softness when the samples were aged for years [11].

iii. Ultrasonic Measurement of Softness

Although there are many test methods that evaluate certain physical properties that are more or less correlated with the softness of tissue, to the author's knowledge, none has become widely recognized or accepted. There still is an unresolved problem of evaluating the softness of tissues instrumentally. Therefore, new studies and ideas are welcome.

In this study, both in-plane and out-of-plane ultrasonic velocity measuring instruments developed at The Institute of Paper Chemistry were used to test the tissue samples. It was found that an in-plane technique was incapable of coupling a sufficient signal into the specimen. However, using the out-of-plane longitudinal instrument, the measurement succeeded due to the much shorter transmit times and better coupling achieved with the low-impedance, neoprene-surfaced IPC transducers [1].

It is well known that denser paper sheets, having higher ZD stiff-nesses, will transmit ultrasound faster than less stiff ones. Therefore, changes in ZD velocity might correlate with changes in softness. In addition to the velocity, the ultrasonic attenuation level during transmission can also be taken as an index of sheet structures and surface conditions.

SAMPLE DESCRIPTION

The tissue samples in this study were commercially available. There were seven kinds of facial tissues and seven kinds of toilet tissues. These were comprised of 1- and 2-ply tissues (Table 1).

Table . Description of the tissue samples

Sample No.	Origin (Co.)	Plies No.	Basis weight* g/m^2	Type
1	A	1E	24.78	Toilet tissue
2	B	1P	29.19	Toilet tissue
3	C	2	15.73	Toilet tissue
4	D	2	16.45	Facial tissue
5	E	2	15.50	Facial tissue
6	F	1	41.90	Toilet tissue
7	G	2P	16.69	Toilet tissue
8	B	2	14.74	Facial tissue
9	B	2L	19.75	Facial tissue
10	C	2	14.34	Facial tissue
11	C	2	21.80	Toilet tissue
12	F	2	15.50	Toilet tissue
13	A	2	16.86	Facial tissue
14	H	2	14.50	Facial tissue

E — highly embossed; L — lotion treated;
P — pattern printed.
* — Basis weight are all measured by a single piece.

From each of the 14 kinds of samples, eight specimens were selected (2-ply ones were gently divided into single plies) and coded for test. To eliminate the size difference between facial tissue and toilet tissues, all the samples were prepared in a size of 4.5 in. x 8 in. for the panel ranking of the softness by six panelists. All the samples were conditioned and all the tests were carried out in a room controlled at 50% RH and 73°F.

To put the tissue results in prespective, tests were also performed on non-tissue papers. There were four grades of linerboards, one coated board, one writing paper, and a non-woven rayon paper.

TEST PROCEDURES

i. Basis Weight

Basis weight was determined on eight single pieces of each sample. Material from these weighed samples was subsequently used for the other tests described in this section.

ii. Thickness

The soft platen thickness was determined by means of the caliper-measuring system built into the ZD longitudinal ultrasonic equipment [1,23]. Before the measurement, the reading was calibrated using 8 micrometer aluminum foil and 1575 micrometer steel plates [1]. Eight measurements were made on each of four sheets, and the overall average was recorded.

iii. Ultrasonic Measurement

The longitudinal velocity and the attenuation level of ultrasound in the ZD of paper depend a great deal on the load applied to the top transducer. At high pressure, the caliper is lower, delay time is shorter, and the level of ultrasonic attenuation is lower. A suitable pressure was selected by comparing results at pressures between 8.95 kPa and 135 kPa. If the delay time is less than 0.2 μsec, multiple reflections interfere with the transmitted pulse, and velocity and loss measurements lose validity. Delay times are longer at low pressure; however, ultrasonic coupling is decreased and signal-to-noise ratio falls off. Therefore, there are trade-offs between high and low pressures and a reasonable compromise must be established. After considerable tests, a pressure of 20 kPa was chosen for all of the ultrasonic measurements and thickness determination reported below. The technique is described in a previous report [1].

iv. <u>Tensile Stiffness</u>

In order to investigate the relationship between the softness and in-plane flexibility and compare that with the parameters measured in the Z-direction, in-plane tensile tests were performed on the tissue samples. Extensional stiffness, E_t, the product of the modulus of elasticity, E, and the thickness, t, is used here. It was determined from the slope of the initial straight-line portion of the load-elongation curve. The tensile test was carried out using an Instron by following TAPPI Standard Method T404 om-87 with cross head speed of 1 in./min.

v. <u>Z-direction Compressibility</u>

Static compressibility of tissue samples was calculated from thickness measurements at 8.95 and 20 kPa.

vi. <u>Panel Ranking of the Softness</u>

Two men and four women in the Paper Testing Laboratory at The Institute of Paper Chemistry were asked to do the panel ranking of softness on fourteen samples of tissue. Two rankings were conducted: (1) hand crumpling; (2) fingertip feel. The crumpling softness was considered to represent the bulk softness and the tactile sensation by fingertips for the so-called surface softness. Panel tests were carried out using a paired-comparison technique. By this method, rankings were obtained from the subjective evaluation of pairs of specimens. A pair of specimens was presented and the subject was asked to judge which was the softer. Specimen pairs drawn from a set of samples were presented in a random fashion until each sample had been compared to all the others. Recording the panel results was done as follows: +1 for the softer one, -1 for the harsher one, and 0 denoting no difference between the two samples. The results were tabulated into the recording sheets shown in Appendix I, and the

ranking was determined by adding the results. To express the softness ranking
more conveniently, all rankings were made positive by adding the constant which
shifted the lowest ranking to 1.

RESULTS AND DISCUSSION

i. Panel Ranking

The results obtained in the panel ranking of softness are given in
Table 2, where the samples are referred to by arbitrary code numbers. Table 3
shows the correlation coefficients between individual panelists (referred by
arbitrary letter) and those between each panelist and the average values.
Clearly, there is a general consistent agreement between different panelists.
However, a little higher correlation coefficient was obtained in the case of
crumpling than in the tactile sensation, which indicates better reproducibility
in subjective ranking of bulk softness using palms than surface softness using
fingertips.

In Fig. 17, both crumpling and tactile softness rankings are presented
to show the correlation between bulk softness and surface softness encountered
with these samples. It is obvious that there is good agreement between the
softness ranked by bulk and by surface tactile sensation. It was observed that
highly embossed tissue samples tend to give relatively lower tactile softness,
while the lotion-treated tissue gave lower bulk softnesses. Embossing or lotion
do not seem to affect the bulk softness as much as they do the surface softness.

ii. Ultrasonic Properties of Tissue

A. Parameters related to sheet flexural rigidity

The ultrasonic velocities of various kinds of papers are shown in
Fig. 18. As generally expected, softer papers gave smaller velocities than

Table 2. Results of bulk and surface softness ranking.

Sample No.	Crumpling ranking	Standard deviation	Tactile ranking	Standard deviation
1	7.7	1.80	6.5	2.36
2	21.7	2.43	18.8	4.02
3	22.0	2.83	18.3	3.30
4	11.0	2.16	10.8	2.11
5	21.8	0.69	20.8	1.77
6	1.0	0.00	1.0	0.00
7	15.0	2.24	16.8	3.02
8	23.7	1.80	22.5	2.22
9	24.0	1.00	26.3	0.75
10	15.5	2.87	16.2	2.73
11	3.0	0.00	3.3	0.75
12	12.0	2.83	14.2	2.27
13	9.7	1.37	11.7	2.62
14	9.5	1.71	9.5	3.69

Table 3. Correlation between softness ranking
by an individual panelist and the
average of a panelists.

Panelist Code	Correlation coefficients	
	Crumpling	Tactile
A	0.98	0.87
B	0.97	0.96
C	0.98	0.94
D	0.93	0.96
E	0.98	0.98
F	0.97	0.95
Average	0.97	0.94
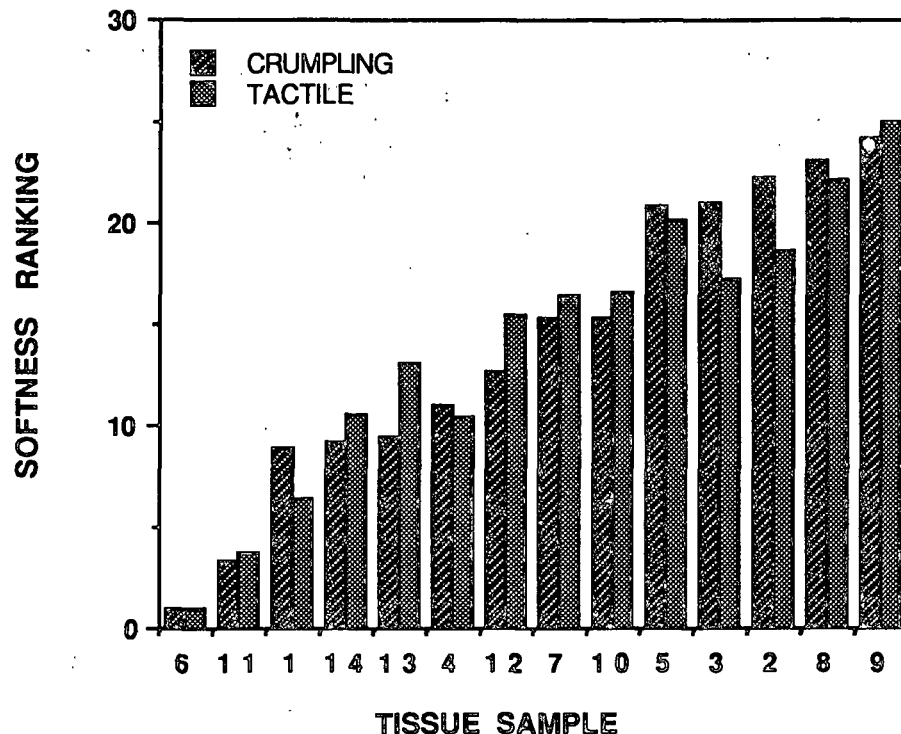
Figure 17. Softness ranking of commercially available tissue samples.

harder ones. However, some kinds of paper boards showed lower velocity values than some kinds of tissue samples. This indicated that the magnitude of V_{ZD} is not informative enough to tell the difference in the softness of papers.

On the other hand, the out-of-plane stiffness, C_{33}, can be calculated from V_{ZD} and density as shown by Eqn. 7. Because of a positive correlation between in-plane and out-of-plane elasticity of paper, it can be said that higher C_{33} means less flexural properties of paper, or more crumpling resistance.

$$V_{ZD}^2 = C_{33}/density. \tag{7}$$

Figure 19 presents the C_{33} of various kinds of papers. Clearly, softer papers showed lower C_{33} values as expected. However, the calculation of C_{33}
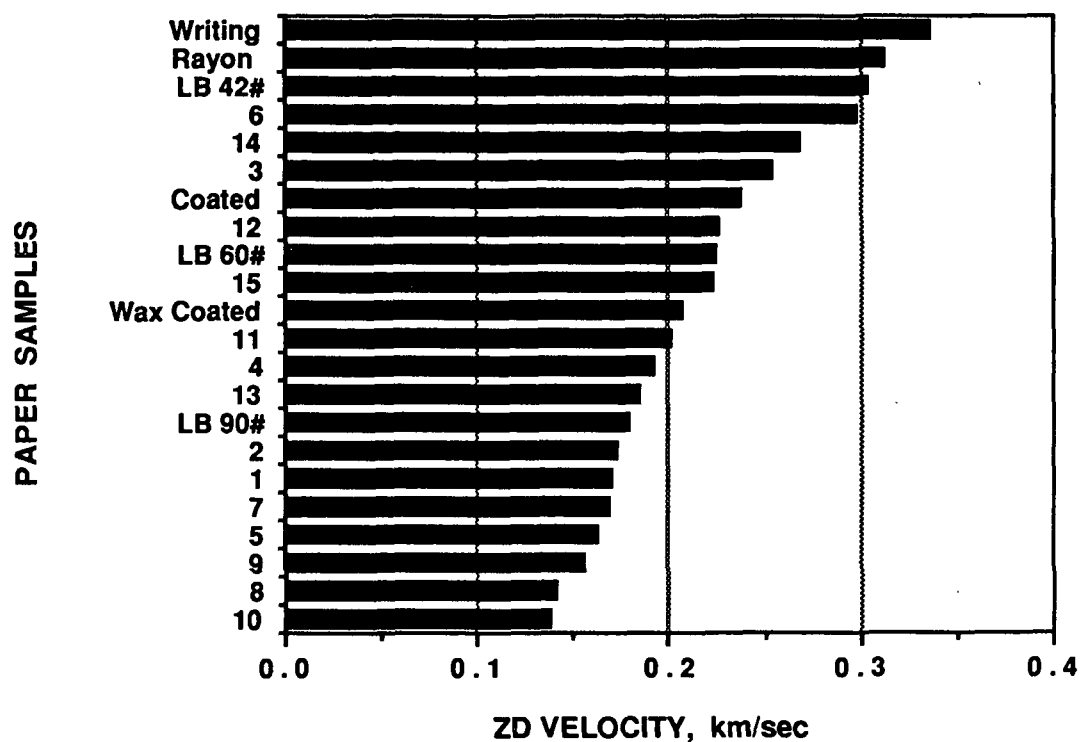
Figure 18.   Z-direction ultrasonic velocity of regular papers
and tissue samples.
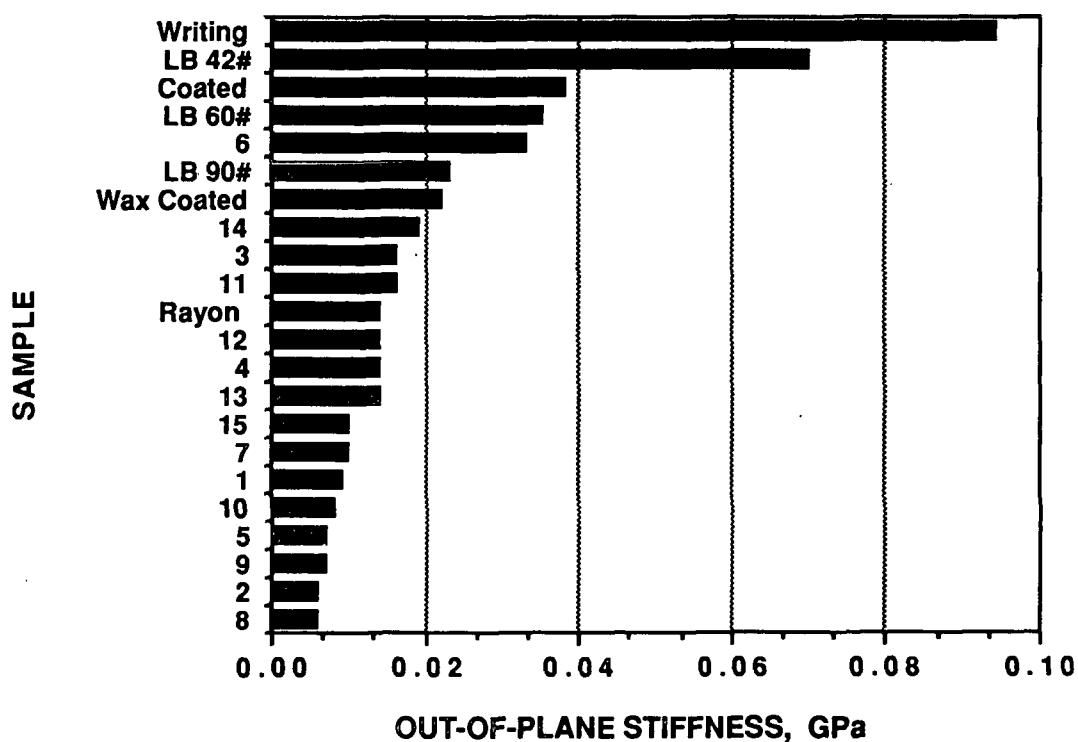
Figure 19.   Out-of-plane stiffness of regular papers and tissue
samples.

needs the value of sheet thickness or density, which is usually hard to measure in the case of tissue samples. Consequently, some new factors similar with C_{33} but without knowing of thickness are desirable.

Upon many experimental results, the acoustic impedance, Z, was found to be an excellent parameter to deal with the softness of paper. In acoustics, Z is defined as driving force divided by velocity of the sound. Z of paper in ZD can be measured and calculated using the following equation:

$$Z = \text{density} * V_{ZD}$$
$$= BW/t, \tag{8}$$

where, BW is basis weight of the paper and t is delay time. Note that calculating Z does not need the thickness value of papers. Figure 20 shows the difference in the acoustic impedances of various kinds of papers, including liner boards, writing paper, and 15 grades of tissues. Obviously, harder papers showed distinctly higher Z values than all kinds of tissue samples tested.

B. Loss Measurement

The amplitude of ultrasonic energy transfer through a specimen is influenced by reflections at the transducer-paper interfaces, by viscoelastic dissipation in the sample, and by scattering by the fibrous structure. Assuming the coupling between two surfaces is perfect, the ratio of the transmission to the incident acoustic pressure amplitude is $2Z_2/(Z_1+Z_2)$, where Z_1 is the acoustic impedance of rubber, and Z_2 is the acoustic impedance of paper in ZD. If coupling is less than perfect, the ratio can be much smaller.

First, the magnitude of the acoustic impedance of paper affects the loss. Since Z_2 is much smaller than that of rubber in ZD, an increase in Z_2
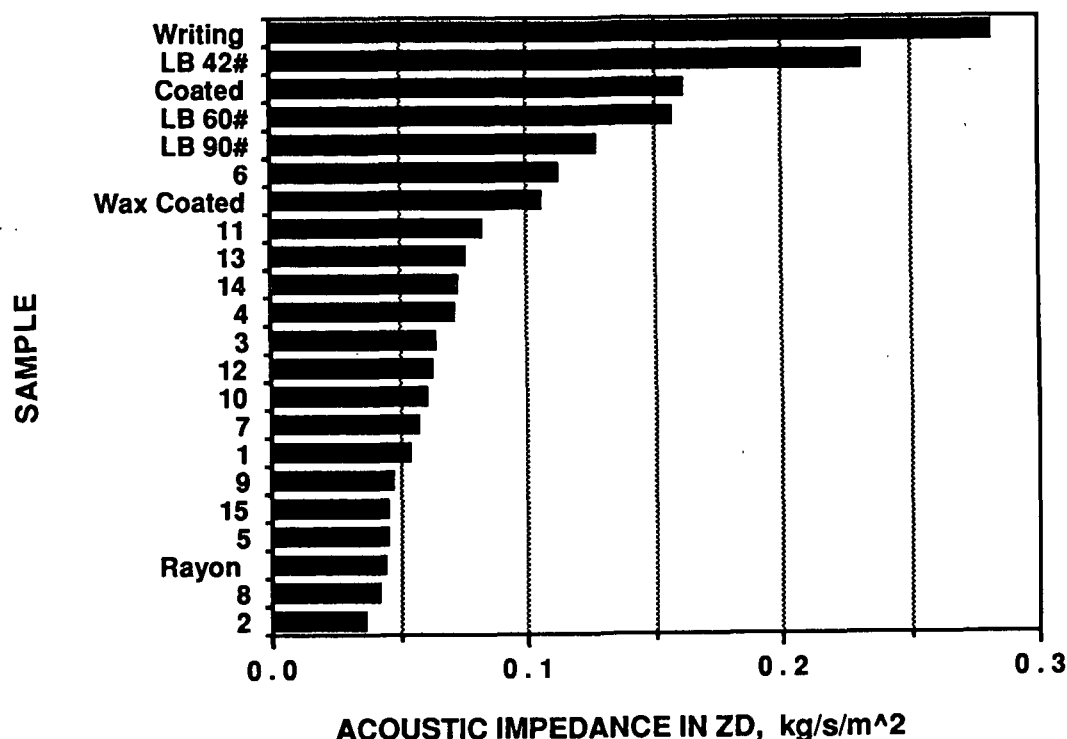
Figure 20. Acoustic impedance of regular papers and tissue
            samples.

will lead to increasing the transmission. The surface contour is another fac-
tor, because it governs a large part of the contact area between the transducer
and paper surface, especially in the case of low loads. The higher the surface
roughness or the dirtier the surface of the transducers (contaminated by cellu-
losic powders or dust on the sticky rubber-surfaced transducer's surface), the
smaller the transmission energy of ultrasound.

The interfacial loss, namely the loss due to mismatch in acoustic
impedances and the surface roughness of paper sheets, is not a function of the
thickness of the sample. On the other hand, the attenuation inside the sheet
due to the absorption and scattering is proportional to the thickness. So the
loss measurement here is the total loss at the interfaces and in bulk of a paper

sample. By introducing a coupling coefficient to represent the coupling loss, the ratio of ultrasonic energy through a paper to that through a standard foil sample can be expressed as follows:

$$R_{mean} = Amplitude_{paper}/Amplitude_{foil}$$
$$= 4Z_1Z_2/(Z_1+Z_2)^2 (Coupling\ Coefficient)e^{-\alpha x} \qquad (9)$$

To investigate the factors which govern sound attenuation in the Z-direction, a liner board specimen was tested as the basis weight was reduced progressively by surface grinding. The ratio was measured on these ground samples. Figure 21 shows the results. In the case of 50 kPa load used, the ratio decreased with the increase in thickness. However, in the case of 20 kPa load, the ratio was unexpectedly almost independent of the changes in thickness within a testing range of 0.11 mm to 0.55 mm. This indicates that when a low load is used in the loss measurement, the interfacial loss seems to dominate almost the whole loss and the transmission through sheet structures does not cause a significant level of attenuation compared with that at the interface. Since the surface condition is an important aspect of the softness of the tissue paper, a low load (20 kPa) was selected to accentuate the surface effect.

Surface roughness affects both surface softness and ultrasonic attenuation. There should exist a certain correlation between surface softness and the loss measurement. Figure 22 shows the value of R_{mean} for a range of papers and tissues. As expected, tissues showed much lower R_{mean} values of ultrasonic energy transmission than did the papers.

iii. Multiple Regression Analysis

Using the physical properties measured instrumentally and the average panel ranking of softness, a multiple regression analysis was conducted. First,
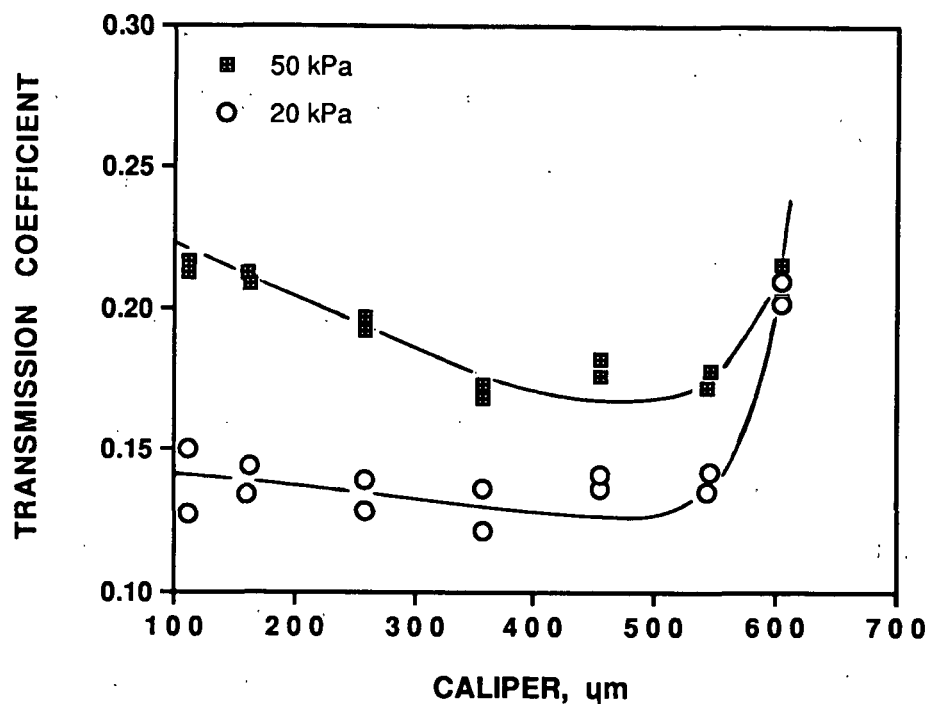
Figure 21. Transmission coefficient as a function of caliper and the load pressure.
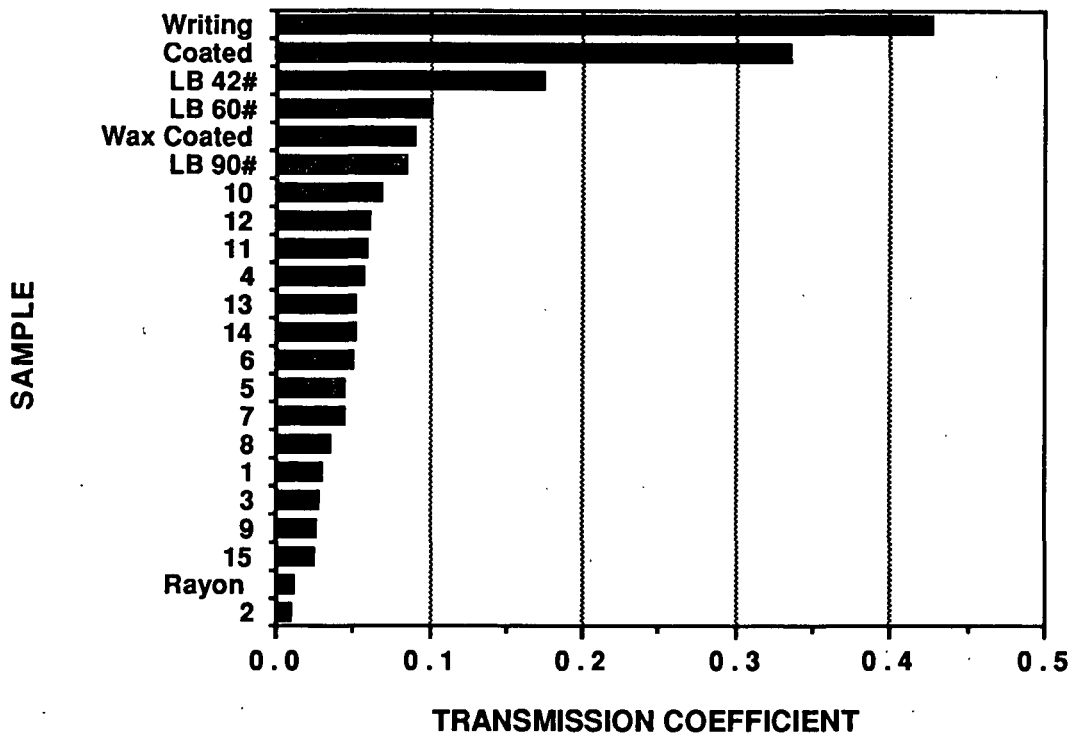
Figure 22. Transmission coefficient of regular papers and tissue samples.

the properties which significantly correlate with the subjective softnesses were described, and then a mathematical relationship between the physical properties and the following softnesses were presented. For the first trial, we used the simple mathematical model.

$$y = a_1x_1 + a_2x_2 + \ldots + a_nx_n + C \tag{10}$$

Where y = panel softness rank;

a = partial regression coefficient of factor x;

x = measured physical properties, and

C = a constant.

Using equation (1), regression analysis was conducted on the tissue samples. The dependent variables were crumpling and tactile softness ranking. The independent variables employed in the regression are (1) the acoustic impedance; (2) attenuation ($A = -20\log R_{mean}$); (3) mass specific attenuation (A/BW); (4) basis weight (BW); (5) thickness; (6) tensile stiffness; (7) Young's modulus geometrically averaged in MD and CD; (8) density; (9) out-of-plane stiffness; (10) delay time; and (11) Z-direction compressibility.

First, the simple regression was done to find the correlation coefficient between panel softness and single physical properties. Tables 4 lists in order of significance the variance ratios (F-ratio) and correlation coefficients for each variable. The highest correlation coefficient is $r^2 = 0.698$ in the case of crumpling softness ranking and the acoustic impedance, and $r^2 = 0.664$ between the tactile softness ranking and the mass specific attenuation. These two values suggest the significance of ultrasonic measurement of the softness and the necessity of using multiple regression analysis.

Table 4. Correlations between measured physical properties and both bulk
          and surface softness ranking.

Sample No.	Variables	Variance ratio (F-ratio)		Correlation coefficient	
		Crumpling ranking	Tactile ranking	Crumpling ranking	Tactile ranking
1	Acoustic impedance, Z, [kg/s/m^2]	27.83	23.75	-0.836	-0.815
2	Mass specific attenuation, A/BW, [dBm^2/g]	16.71	15.95	0.763	0.755
3	Basis weight, BW, [g/m^2]	2.94	4.11	-0.444	-0.505
4	Tensile stiffness, Et, [kN/m]	5.54	5.92	-0.562	-0.575
5	Young's modulus, E, [MPa]	8.41	8.25	-0.635	-0.638
	Emd, [MPa]	8.09	7.86	-0.635	-0.629
	Ecd, [MPa]	8.78	8.82	-0.650	-0.651
6	Out-of-Plane stiffness, C_{33}, [GPa]	13.06	14.45	-0.722	-0.739
7	Attenuation level, A, [dB]	4.75	2.52	0.532	0.417
8	Thickness t, [μm]	0.03	0.26	0.051	-0.144
9	Density, ρ, [kg/m^3]	2.74	1.38	0.431	-0.322
10	Delay, [μsec]	11.31	0.64	0.314	0.225
11	ZD compressibility, % $(1-t_{20kPa}/t_{8.95kPa})$	0.21	0.05	0.131	0.066

The multiple regression analysis was used on an examination of various
combinations of ten independent variables. The Statgraphics (multiple
regression analysis software) calculates coefficients of multiple correlation,
r^2; the variance ratio, F; degrees of freedom; and other statistical values.
Generally, the variables involved in the mathematical model were selected based
on the F value because its magnitude gives an indication of the significance of
the regression. Table 5 shows an example of a multiple regression analysis.

The variables at the left side are selected for the model because they have the largest F values. Note that introducing only Z, basis weight and mass specific attenuation into the regression model yielded a correlation coefficient (r^2) of 0.884 for the crumpling softness ranking! That is, 88.4% of the overall variation in the subjective softness ranking (crumpling) of those 14 tissue samples can be associated with the variation in these 3 parameters which are easily measured.

Table 5.   An example of multiple regression analysis.
           (Stepwise selection of variables into the model.)

Selection Formard   Maximum steps: 500   F-to-enter: 4.00
Control: Manual   F-to-remove: 4.00

R-squared: 0.88386   Adjusted: 0.84902   MSE: 8.85884   d.f.: 10

Variables in Model	Coeff.	F-Remove	Variables Not in Model	P.Corr.	F-Enter
1. Z	-187.989	10.0602	4. meanE	0.4803	2.6990
2. A/BW	22.2496	15.6484	5. Et	0.4325	2.0713
3. BW	0.6662	9.0702	6. Emd	0.5344	3.5974
			7. Ecd	0.3595	1.3362
			8. thickness	0.3778	1.4985
			9. compressibility	0.0534	0.0257
			10. C_{33}	0.3611	1.3492
			11. delay	0.2438	0.5686

When doing multiple regression analysis, Z or A/BW showed the highest variance ratio, followed by basis weight or tensile stiffness in most of the cases. Generally, the more parameters introduced into the model, the higher the correlation coefficient. However, it is better to select only those parameters which can be measured easily. Fortunately, Z and A/BW enter the model with the highest F-ratios. Basis weight and tensile stiffness were the next most significant parameters. We decided to choose basis weight for the third parameter as it is convenient to measure.

Figures 23 and 24 give the results of the three parameters regression analysis of crumpling and tactile sensation softness ranking separately with respect to the predicted values. For 14 kinds of commercial tissue samples, the bulk softness by crumpling showed a higher correlation coefficient than the surface softness by tactile sensation by fingertips. This indicates that parameters measured by ultrasonic measurements are related a little more closely to the bulk softness than to the surface softness. In the case of tactile panel ranking, two points especially tend to scatter from the main population. One is a facial tissue treated with lotion, the surface of which had a higher than predicted smoothness sensation. It may be that the lotion increased subjective softness. Softness was over-predicted on a highly embossed toilet tissue. Possibly, it is the embossing that reduced the surface softness ranking. This would be consistent with the observations of Hollmark [3].

Facial tissues are somewhat different from toilet tissues in their manufacture. For instance, toilet tissues sometimes are highly embossed, while facial tissues may contain lotion or de-bonding agents to soften the tissue. These may affect the evaluation of softness instrumentally. Table 6 shows the results of regression analysis carried out on facial tissue and toilet tissue separately using the same regression analysis. In both the cases, extremely high correlation coefficients were obtained.

By comparing the corresponding coefficient of each independent variable, it is obvious that the contribution of Z, A/BW, and basis weight to softness is different with facial tissue and toilet tissue. In the case of facial tissue, Z is the most significant variable followed by basis weight and A/BW. For toilet tissue, A/BW is most important one followed by basis weight and Z. The reason for this is not clear. But it seems that A/BW plays a
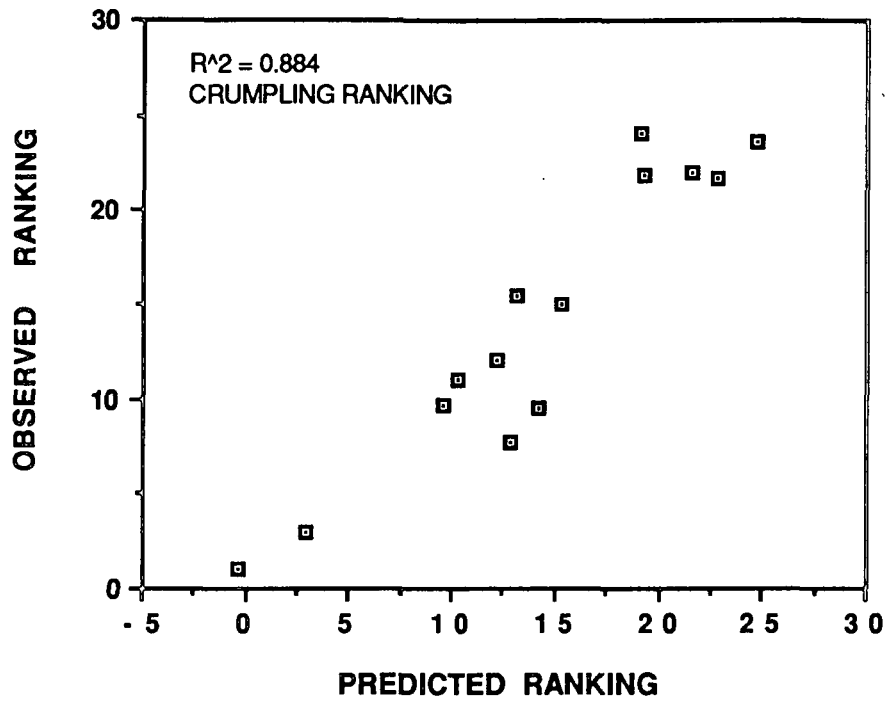
Figure 23.   Correlation between ultrasonically predicted
             softness ranking and crumpling ranking.
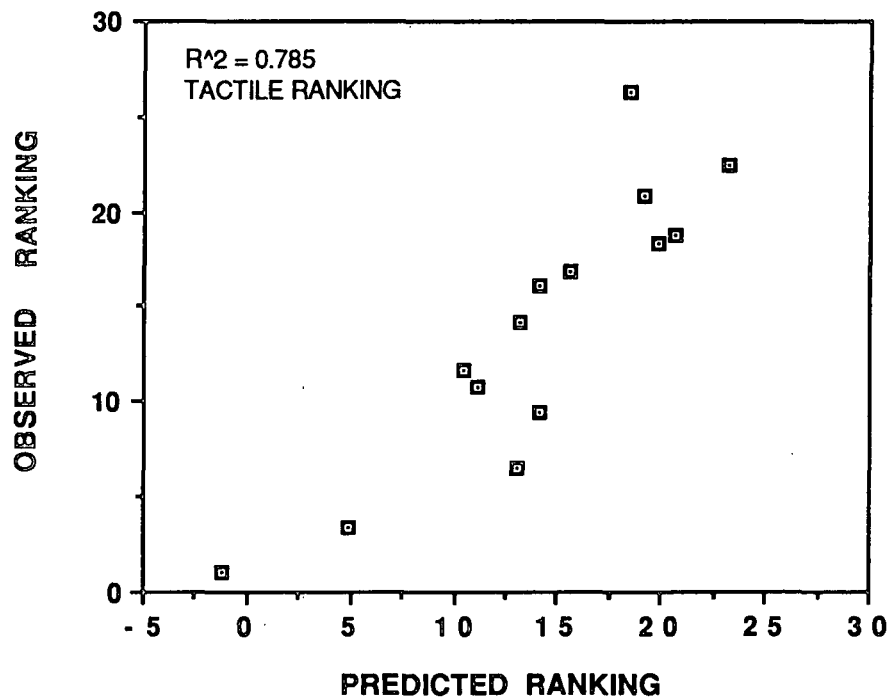
Figure 24.   Correlation between ultrasonically predicted
             softness ranking and tactile ranking.

Table 6. Results of multiple regression analysis.

		Corresponding coefficient				Correlation coeff. of multiple regression (r^2)
		Z [MPa/s]	A/BW [dBm^2/g]	BW [g/m^2]	Constant	
Overall	Crumpling	-187.99	22.25	0.67	-21.48	0.884
	Tactile	-188.04	15.95	0.37	-6.13	0.785
Facial	Crumpling	-441.86	1.21	0.59	30.54	0.997
	Tactile	-412.18	-0.05	1.08	22.51	0.971
Toilet	Crumpling	-103.31	26.90	0.77	-36.46	0.970
	Tactile	- 95.18	19.71	0.437	-19.83	0.896

stronger role in embossed samples because of the greater surface effects, while
Z is most important for creped facial tissues in predicting softness instrumen-
tally.

CONCLUSION

Z-direction ultrasonic measurements were made on 14 samples of commer-
cially available tissue. A multiple regression analysis yielded a three-factor
correlation coefficient squared of multiple correlation of 0.884 for bulk soft-
ness ranking, and 0.785 for surface softness ranking. This indicates that a
significant level of the variance in both the average bulk and surface softness
rankings of six panelists can be accounted for by the three independent physical
properties. These are acoustic impedance, mass specific attenuation and basis
weight.

Effects of embossing and lotion on tissue softness were observed. Lotion tends to increase, and embossing tends to reduce subjective surface softness. Both have smaller effects on the bulk softness than on the surface softness with respect to instrumentally predicted softness. Facial tissue was somewhat different from toilet tissue in the instrumental softness measurement. By dividing the samples into facial and toilet tissue groups, 3-factor analysis yielded an extremely high coefficient of multiple correlation (Table 6).

Though good correlations have been achieved for the evaluation of softness of tissue by means of the out-of-plane ultrasonic technique, we are aware that these correlations need not imply causal relationships. We cannot say that Z and A/BW are the main factors affecting the softness of tissue. They may happen to be correlated with some factor(s) which govern the softness for the samples of tissue available here. Consequently, studies and testing on more extensive tissue samples with knowledge of the paper-making conditions affecting the evaluation are necessary to understand the relation between Z, A/BW and the subjective tissue softness.

IV. SCATTERING COEFFICIENTS OF BOARD

INTRODUCTION

The degree of bonding of paper is commonly estimated from the light scattering coefficient determined from the reflectance of a single sheet on a black background (R_0) and the reflectance of a stack of sheets thick enough that addition of another sheet does not change the reflectance value (R_∞). For high basis weight papers, however, there is little difference between R_0 and R_∞; consequently, the calculation is imprecise.

A way around the dilemma is provided by the Kubelka-Monk theory, which shows that the scattering coefficient can also be determined from one reflectance and one transmittance (T) value. IPC student B. J. Conor was assigned the design and construction of an instrument based on reflection and transmission values as a second-year research problem [25]. The instrument was later refined and evaluated by Knox and Wahren [26], who demonstrated that transmittance of heavy boards (to 699 g/m^2) could be measured, and that very good correlation was obtained for values of scattering coefficient of lighter weight papers calculated from measurements of R_0 and R_∞ and from measurement of R_0 and T.

In this instrument, the light source is a continuously-operated incandescent lamp. Photomultiplier tubes detect incident and transmitted light levels. The specimen is sandwiched between two Teflon diffusers, which become the top and bottom sheets of the "specimen stack". Specimen transmittance is calculated from the measured light transmission of the stack and the previously determined reflectances of the top and bottom "sheets" [26]. The reflectance of the sample is determined on a separate instrument, such as the TB-1 brightness tester.

The results obtained with the instrument are satisfactory, but getting valid measurements is a rather demanding operation. In view of an anticipated routine use for the measurements, it was decided to construct a new instrument, much easier to operate, and which measures both transmission and reflectance values.

NEW INSTRUMENT

As a basic concept for the new instrument, the specimen is placed between two integrating cavities. With the specimen to be viewed over a 15-mm diameter area, minimum integrating sphere size [27] is about 20 cm diameter. For easy, rigid attachment of source, detectors, and mounting means to the spheres, they have been made as spherical cavities inside cubic blocks. Figure 25 shows the arrangement.

The upper cube is fixed in place and has attached to it the flash lamp source, the source intensity detector, and the reflected intensity detector. An air actuator moves the lower cube up and down on linear bearings to permit insertion and closing on a specimen. This lower cube supports the transmitted intensity detector. The sphere surfaces are lined with barium sulfate.

Illumination is provided by a xenon flash lamp discharging approximately 150 Joules. This gives the very high intensity level needed for sufficient light to pass through heavy specimens for detection. The very short duration (about 100 μsec) minimizes heating effects on the specimen. An infrared-removing filter in the port through which the illumination enters the sphere further reduces heating of the specimen. An additional filter is also placed here to remove ultraviolet radiation, which might otherwise induce fluorescence in the specimen.
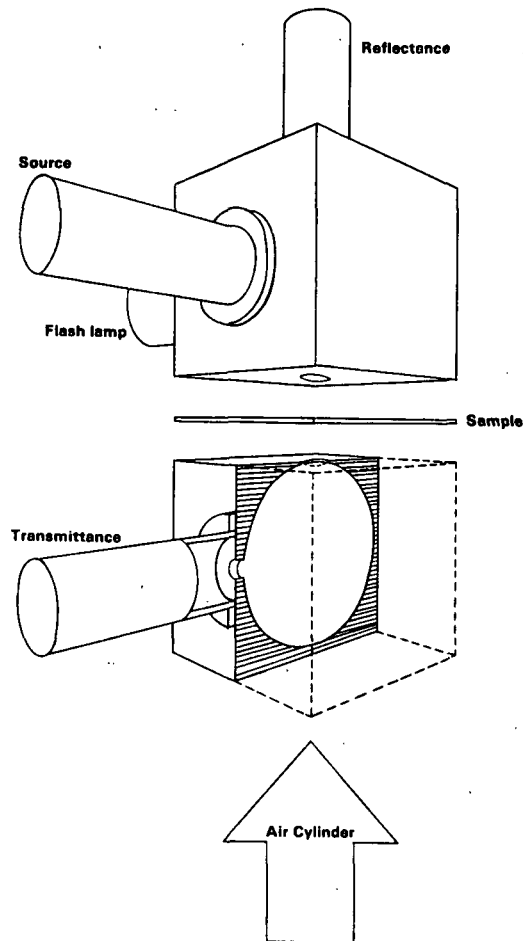
Figure 25. Schematic of the Optical Transmission Meter.

Three photodetectors are used. Those sensing the light level in the upper sphere (reference) and that reflected from the specimen are silicon photodetectors, chosen for stability and ruggedness. This type was also tried for detection of the transmitted light, but it was found necessary to use a photomultiplier tube (PMT) in order to get the combined sensitivity and frequency response required. Optical filters are placed just ahead of the photosensors to give spectral responses approximating the CIE Y-function for illuminant A.

The output of each photodetector goes to a peak-detector circuit. This peak value is then displayed on a digital panel meter in arbitrary units.

The arrangement is shown schematically in Fig. 26. Analog and digital outputs
are also provided for future direct input to a computer.

Flash Lamp   Photocells/Amplifiers
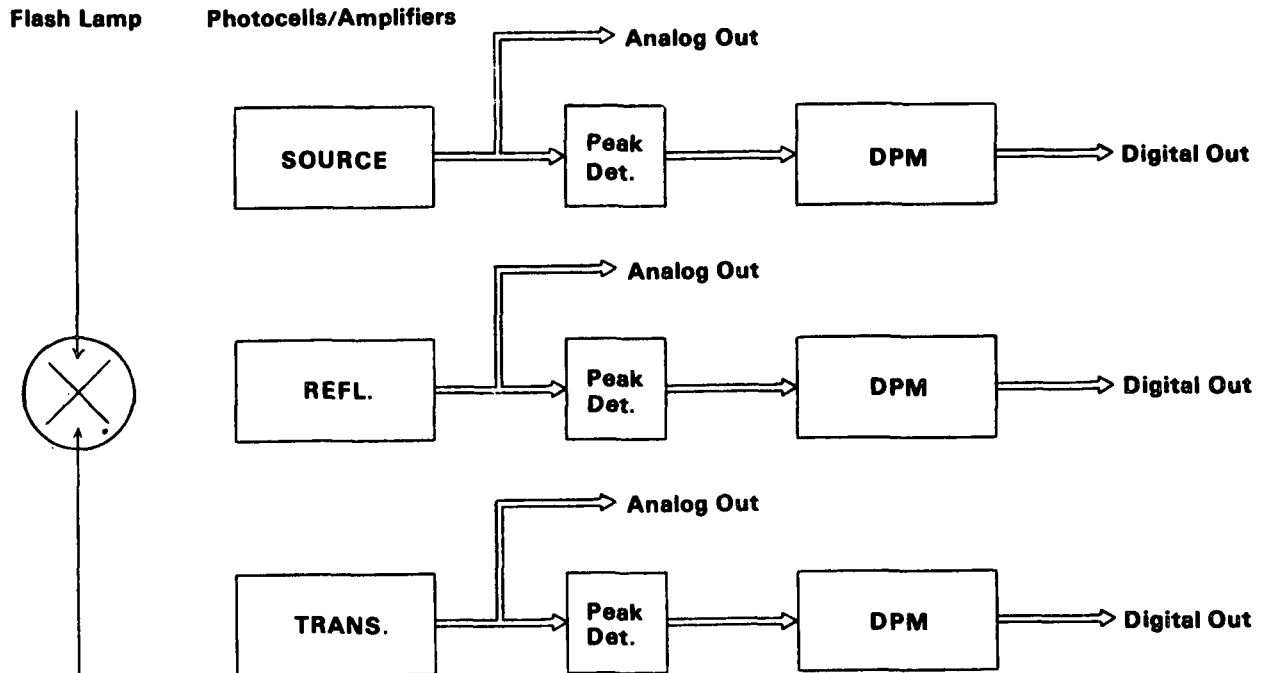
Figure 26. Block diagram of the detector circuits.

A check was made of the instrument response by calculating transmit-
tance values of six lightweight papers from measurements of R_0 and R_∞ on the
TB-1 brightness tester and from the TB-1 measurement of R_0 and the new instru-
ment's measurement of T. The high transmission level necessitated greatly
reducing the amount of light which could reach the PMT, which was accomplished
by placing a diaphragm in the PMT port and by moving the PMT farther out from
the port. Calibration of transmission was performed by noting the transmission
meter readings for brass shim stock specimens, each having a round hole of
accurately known diameter in it, then plotting these readings against the ratios
of the areas of the holes to the area of the specimen port.

The results of the test are listed in Table 7, where it can be seen that the agreement in transmittance values calculated by the two methods is reasonably good. The validity of measurements of much heavier weight specimens remains to be determined.

Table 7. Transmittance values of light-weight sheets calculated from Kubelka-Monk theory.

| Sample | TB-1 (Y-function) | | | BOTM | |
	R_0	R_∞	T, calc	T_A	T, calc
White bond	0.728	0.799	0.192	0.453	0.193
White bond	0.721	0.780	0.205	0.490	0.210
Pink memo	0.584	0.633	0.221	0.308	0.204
Deinked	0.708	0.750	0.162	0.366	0.171
Yellow memo	0.721	0.823	0.225	0.500	0.214
Cream tab card stock	0.767	0.815	0.148	0.378	0.147

Readings are the average of one reading on each of five specimens.

T_A is the apparent transmittance of the specimen sandwiched between the Teflon sheets.

Thought was given to use of a logarithmic amplifier with the PMT to eliminate the need to adjust the amount of light reaching the PMT as the specimen transmission changes over several decades, but the frequency response of available logarithmic amplifiers falls below that needed at the lower light levels. Consequently, the linear response circuitry will be retained and future work directed at providing a more convenient means of making the adjustment. Some possibilities include an iris diaphragm, a sliding strip with a series of

hole sizes, change of distance from PMT to port, PMT supply voltage level, and amplifier gain. When this is accomplished, attention will be directed to reflectance measurement.

LITERATURE CITED

1. Habeger, C. C., Wink, W. A., and Van Zummeren, M. L., IPC Technical Paper Series No. 269 (Jan., 1988).

2. Bates, J. D., Tappi 48(4):63A-64A (1965).

3. Hollmark, B. H., Tappi 66(2):97-99 (1983).

4. Leporte, L. E., Project 2817, Report 2, The Institute of Paper Chemistry, (March, 1970).

5. Hollmark, B. H., The Fundamental Properties of Paper Related to Its Use (Ed., F. M. Bolam), Technical Sec., BPBIF, p.696 (1976).

6. Van Eperen, R. H., Hardacker, K. W., Wink, W. A., and Van den Akker, J. A., Project 2220, Report 5, The Institute of Paper Chemistry, (Aug., 1962).

7. Van Eperen, R. H. and Wink, W. A., Project 2220, Report 6, The Institute of Paper Chemistry, (June, 1965).

8. Van Eperen, R. H., Gander, J. W., and Wink, W. A., Project 2220, Report 7, The Institute of Paper Chemistry, (Feb., 1967).

9. Van Eperen, R. H., Gander, J. W., and Wink, W. A., Project 2220, Report 8, The Institute of Paper Chemistry, (Jan., 1968).

10. Leporte, L. E., Project 2817, Report 1, The Institute of Paper Chemistry, (Jan., 1970).

11. Leporte, L. E., Project 2817, Report 3, The Institute of Paper Chemistry, (Jan., 1971).

12. Clark, J. d'A., Paper Trade J., TAPPI Sec., P 169-172 (March, 1935).

13. Brown, T. M., Paper Mill, P 19-21 (June, 1939).

14. Yang, C., Tappi 39(8):146A-149A (1956).

15. Lyne, L. M., Pulp & Paper Canada, P 79-82 (July, 1950).

16. Wardwell, F. B., Tappi 48(4):60A-61A (1965).

17. Ray, J. E., Tappi 48(4):57A-58A (1965).

18. Lyne, M. B., Whiteman, A. and Donderi, D. C., Pulp & Paper Canada 85(10):43-50 (1984).

19. Lashof, T. W., Tappi 43(5):175A-178A (1960).

20. Lyne, L. M., Pulp & Paper Canada 51(7):80-82 (1950).

21. Yang, C., Tappi 39(8):146A-149A (1956).

22. Kato Tech Co., Kyoto, Japan (July, 1988).

23. Wink, W. A. and Baum, G. A., Tappi 66(9):131-133 (1983).

24. Oliver, J. F., Tappi 63(12):91-95 (1980).

25. Conor, B. J. Development of a prototype instrument for measurement of dif-
    fuse light transmission properties of paper and board. A291 Research
    Problem. 30 p. The Institute of Paper Chemistry, Appleton, WI (June 21,
    1982).

26. Knox, J. M., and Wahren, D. Determination of light scattering coefficient
    of light and heavy sheets. Tappi J. 67. no. 8:82-85 (Aug., 1984).

27. McNicholas, H. J. Absolute methods in reflectometry. J. Res. NBS 1, no.
    1:29-74 (July 1928).

APPENDIX I

PANEL RANKING OF SOFTNESS OF TISSUE SAMPLES

NAME: **DATE:**

EXPERIENCED: YES/NO

SAMPLE   A

	1	2	3	4	5	6	7	8	9	10	11	12	13	14	TOTAL +	TOTAL −	o
1	■																
2		■															
3			■														
4				■													
5					■												
6						■											
7							■										
8								■									
9									■								
10										■							
11											■						
12												■					
13													■				
14														■			
TOTAL																	

S A M P L E   B (row label on left side)

+ denotes softer than;
− denotes harsher than;
o denotes no difference.

APPENDIX II

Using a robot based instrument to measure the in-plane
   ultrasonic velocities of paper

C. C. Habeger, M. L. Van Zummeren, W. A. Wink
The Institute of Paper Chemistry
Appleton, WI 54912

and

B. M. Pankonin and R. Goodlin
Mead Corporation
Chillicothe, Ohio

ABSTRACT

This paper is a discussion of the development of an instrument that automati-
cally determines with ultrasound the in-plane mass specific elastic stiffnesses
of planer materials. It uses a standard laboratory robot to incorporate many of
the features on an earlier apparatus (1). The result is more versatile, more
reliable, and easier to manufacture instrument. Special broadband transducers
were also built and they are discussed.

Introduction

In a previous publication (1), some of us described an instrument which automa-
tically measures the in-plane velocities of ultrasound in paper samples. This
was a custom designed, pneumatically-driven apparatus with specially developed
electronic circuitry, all controlled by an Apple computer. Two ultrasonic
transducers were suspended from a carriage above the sample. Air cylinders
applied the transducers to the sample, at which time one was electrically pulsed
and the resulting signal from the other was digitized and stored in the com-
puter. The transducers then were lifted from the sample, their separation was
increased, and a second signal was taken and stored. The time-of-flight velo-
city of ultrasound was found using a cross-correlation calculation to determine
the difference in arrival times of the two pulses. The carriage was translated,

and velocities at other positions on the sample were determined. The sample holder was mounted on a platter, which was rotated by a computer controlled stepping motor. This allowed the velocity of ultrasound to be found at different angles to the machine direction. Also, by rotating the transducers 90° about their axes, the computer could effect velocity measurements of both shear and longitudinal waves. The standard testing routine was to calculate the longitudinal velocities in the MD (the machine direction) and in the CD (perpendicular to the machine direction), the shear velocity at 45° to the MD, and the average of the shear velocities along the MD and the CD. Assuming the sample is orthotropic, this allowed the determination of the four independent mass specific elastic stiffnesses. Another test routine was the measurement of the longitudinal (or shear) velocities in 5° increments from the MD.

The purpose of this paper is to describe an improved, second generation instrument. A major drawback of the first instrument is that it consisted of custom designed mechanical and electronic components, making it difficult for others to build a comparable system. The new instrument is centered around a commercial, laboratory robot and uses almost entirely off-the-shelf electronics. The robot "end effecter" is a special item; however, a third party is willing to manufacture it. In addition to ease of reproduction, the new system provides higher quality measurements and is more versatile. As described below, new transducers, with higher bandwidth and greater modal purity, were designed and constructed for this instrument. These provide increased sensitivity and reduce the ultrasonic signal interferences encountered on problem samples. Repeatability in the coupling between the transducers and the sample is improved by deadweight loading the transducers instead of applying them to the sample with air pressure. Since the loading pressure was greatly decreased, the possibility of damage to low density paper samples is reduced. The new

system is more convenient, as four samples (rather than one) can be tested
without operator intervention. In fact, since the sample is not moved during
testing, it would be straightforward to add a sheet manipulating mechanism and
test a large number of samples in a single run. A final improvement is the
replacement of the original Apple IIe computer with a PC AT compatible machine.
This increases the speed of operation and provides the opportunity for per-
forming more complex calculations.

General Description

The overall operation of the instrument is summarized by the schematic diagrams
in Fig. 1 and 2. The manipulation of the probes, necessary to scan the sample
and to orient the transducers for measurements in different directions relative
to the MD, is achieved with a standard laboratory robotic arm, the Mitsubishi RM
501. The arm has five axes of rotation: (1) a "waist" rotation which determines
a radial axis for the arm motion; (2) a "shoulder" rotation; (3) an "elbow"
rotation which, in combination with the shoulder, defines the radial and ver-
tical positions of the end of the arm; (4) a "wrist pitch" rotation which
fixes the angle of the end of the arm to the vertical; and (5) a "wrist roll"
rotation which turns the end of the arm about its axis. Attached to the end of
the arm is a custom-built "end effecter". This is a carriage which holds the
ultrasonic transducers. Computer-controlled air cylinders, mounted on the end
effecter, can rotate each transducer 90° about its axis to allow both shear and
longitudinal testing, while a third air cylinder can separate the transducers,
so that ultrasonic waves with two different path lengths through the sample can
be compared. Figure 3 is a photograph of a robot arm with an end effecter
attached.

Figures 1-3 here

A typical velocity measurement proceeds as follows. The robot positions the end effecter at the proper position above the sample. With the carriage in the closed position, the transducers are lowered to the sample. Through a digital I/O port the computer triggers a Wavetek model 143 Function Generator to emit one cycle of an 80 kHz sine wave. This signal is applied to one of the ultrasonic transducers on the end effecter. A sound wave is generated in the sample and picked up by the other transducer. The received signal is amplified by a Panametrics model 5050AE Ultrasonic Preamplifier and sent to a Hewlett Packard 54200 Digital Oscilloscope. The oscilloscope, which was triggered at the same time as the function generator, digitizes the signal at a rate of 10 MHz and stores the signal. An adjustable number of additional ultrasonic signals are collected. By digital averaging, the oscilloscope produces a low-noise, composite signal and transfers it to the computer over a GPIB bus. The robot lifts the transducer from the sample and activates the air cylinder which separates the transducers. The transducers are returned to the sample, and another composite signal is produced. As described previously (1), the computer uses a cross correlation technique to calculate a time-of-flight velocity. The probes are again lifted, the robot moves the end effecter to a new position above the sample, and another velocity is determined.

There are two standard tests that can be performed. One is a determination of the orthotropic, in-plane, mass specific elastic stiffness of the sample. This is done by measuring longitudinal velocities in the MD and CD and shear velocities in the CD and at 45° to the MD. The only significant difference in the approach for the new instrument is that only CD shear is used rather than an average of CD and MD shear. For an orthotropic sample the shear velocities are the same in the two principal directions; however, shear measurements are to

some extent contaminated by longitudinal impurities. Since bimorph transducers

generate stronger CD shear waves than MD shear waves and stronger MD longitudi-

nal than CD longitudinal waves, the CD shear is the much purer signal, and it

gives a better measure of mass specific shear stiffness of the sample. The

other standard test is to calculate the longitudinal or the shear velocities at

5° increments and to graph a "polar plot" of the results. A complete descrip-

tion of both tests, along with typical reports, is presented in the earlier

publication (1). There are four stations, two of which can be seen in Fig. 3,

that hold samples, and up to four samples can be tested per run.

End Effecter

Since it is a custom-designed apparatus, the end effecter deserves some addi-

tional description. Its function is to house the transducers and mount to the

end of the robot arm. It also must provide a means to rotate each transducer

about its axis and translate one transducer with respect to the other. The

transducers are easily seen in Fig. 4, which is a photograph of the end effecter

from the bottom side. They are attached to hardened splined shafts which are

manufactured to fit into splined linear ball bushings mounted on the end

effecter. When the dust seals are removed, a shaft will slide easily in its

bushing, while the spline prevents rotation of the shaft in the bushing. When

the end effecter is lowered to bring the transducers in contact with the sample,

the shafts slide freely in their bushings, and the transducers are applied to

the sample in a repeatable fashion with a force equal to the weight of a shaft

and a transducer (about 20 grams).

The splined bushings fit snugly into custom-machined Teflon sleeves, which

are pressed into aluminum blocks on the end effecter. The sleeves allow the

bushings to rotate between shear and longitudinal orientations, but at the same time, they prevent lateral play in the transducers. Rotation of the bushings, along with the spline shaft and transducers, is accomplished through double-action air cylinders. The air cylinder pistons connect to levers attached to the top of the splined bushings. The air cylinders are pivot-mounted so that they can swivel as the bushing rotates in the Teflon sleeve. A small magnet is epoxied to each lever, and Hall effect detectors are positioned to sense the presence of the magnets at the extremes of the 90° rotation. This allows the computer to verify that directed rotations have been completed.

As can be seen in Fig. 4, the end effecter frame is a light-weight aluminum yoke with two parallel steel shafts clamped across the gap. Aluminum blocks house the splined bushings and rest on the shafts. One block is rigidly clamped, whereas the other is mounted to ball bushings that ride on the shafts. A double-action air cylinder is attached to the fixed block, and its piston bolts to the other block. When prompted by the computer, the blocks can be pulled together or the mobile block can be pushed against an end stop. Switches attached to the mobile block feed back the location of the mobile block to the computer.

Figure 4 here

Transducers

The transducers designed for the robotic tester are modified versions of those used on the first instrument ($\underline{1}$); therefore, a brief description of antecedent transducers is in order. They were constructed from standard 0.533 mm thick sheets of a lead titanate zirconate piezoelectric ceramic (PZT 5H). These sheets are parallel bimorphs. That is, they are composed of two layers of

ceramic that are polarized in the same direction. There are conductive layers on the outer surfaces of a sheet and in the middle. The outer surfaces were grounded, and the inner layer became an electrically shielded active electrode. Mechanical motion could be generated by applying a voltage to the middle electrode. This caused one ceramic layer to contract, the other layer to expand, and the sheet to bend. Conversely, bending could be sensed electrically by monitoring the voltage at the center electrode. Construction of a transducer began by cutting a 6.35 mm wide by 10.30 mm long rectangle out of the bimorph sheet. One end was rounded to a radius of 4.0 mm. The other end was rigidly clamped into a transducer housing, so that the free length of the bimorph was 7.9 mm.

When two transducers as described above were applied to a paper sample, ultrasonic energy could be effectively transferred. Relatively pure longitudinal waves were generated if the transducers were facing each other, while transverse (or shear) waves were detected when the transducers were rotated 90° about their long axes. These transducers did operate satisfactorily, but they also had shortcomings.

First of all, the modal purity could be improved. In order to separately determine transverse and longitudinal velocities, it is important that only motion perpendicular to the transducer face is generated and received. If modes of oscillation (other than pure bending) are excited, the transducers can become sensitive to motion along the face. This creates less of a problem for the longitudinal measurement, since the longitudinal wave is faster, and the analyzed portion of the signal in the far spacing is usually complete before the shear wave arrives. However, the shear signal is invariably tainted by the

(predominantly rotation about the out-of-plane axis) and fundamental, first
order, and second order "twists" (predominantly rotations about an axis parallel
with the length). The twists probably would not efficiently transfer ultrasonic
energy into the sample; however, the wobble could conceivably produce longitudi-
nal waves when the transducers were aligned for shear and vice versa.

An experimental spectrum of the transducer response was obtained by placing
the transducers on a paper sample. A continuous wave from a frequency synthe-
sizer was applied to one transducer, and the other was input to a lock-in
amplifier. The source frequency was swept, and the output of the lock-in was
plotted. A strong peak was noted at 56 kHz. This is undoubtedly the second
order bend. Its lower than predicted frequency is likely due to the less
than perfect clamping afforded by the transducer housing. The next strongest
peak was at 36 kHz. This presumably is the fundamental wobble which was pre-
dicted to be at 35 kHz. The experimental and calculated values are closer for
the wobble, since perfect clamping is not as important in establishing the
assumed boundary conditions.

From this analysis, it is clear that the transducers are being unwisely
operated in a region with too many resonances. Secondary motions are being
excited, and the transducers are not broadband. The straightforward solution
is to simply shorten the transducers and rely on the fundamental bending motion.
The wobble would be jacked out of the operating frequency range, and bandwidth
would be increased by running below the lowest frequency resonances. Although
the twists may not represent a problem, a concern is that the fundamental twist
could be excited. This is avoided by decreasing the width, but not so much that
the fundamental wobble comes into play. Another solution would be to reinforce

the beam in some creative way. This was explored, but no promising scheme was uncovered.

All of these considerations led, of course, to the construction of miniature transducers. As demonstrated in Fig. 5, they are much shorter than the original ones. The transmitter has a bending length of 1.5 mm, and the receiver has a free length of only 1.3 mm. Mathematically and experimentally, these transducers have no resonances below 200 kHz. The receiver is cut smaller than the transmitter to increase its sensitivity and to avoid any coincidence of resonant frequencies. The bimorphs are epoxied into grooves in a Delrin housing in an effort to improve the clamping.

Figure 5 here

The miniature transducers do provide superior performance. It is now possible to generate pulses as short as 10 μsec. Minimum pulse widths previously were over 100 μsec. Sensitivity, as measured at the initial peak, was approximately tripled. The contamination of shear measurements by longitudinal impurities was reduced. This was verified by comparing the ratios of MD to CD shear velocities made on highly anisotropic sheets with the two types of transducers. For a set of ten sheets, with stiffness anisotropy ratios of over four, the miniature transducers gave an average shear anisotropy ratio of 1.04, while the original transducers produced a ratio of 1.08.

Conclusions

The robotic in-plane tester is a clear improvement over the previous automatic instrument. It is faster. The results are more reproducible. It can test more samples. It is much less likely to damage a specimen. It uses improved

transducers. It is capable of performing complex mathematical analyses (to be discussed in another publication) on the results. These are all important advances, but perhaps the most significant feature is that the robotic system is suitable for commercialization. In fact, during 1989, RoboTest Corp. plans to manufacture and market a version of the robotic tester.

Acknowledgment

Reference

1. Van Zummeren, M., Young, D., Habeger, C., Baum, G., and Treleven, R., Ultrasonics 25:288(1987).

Elbow

Shoulder

Wrist

End Effector
with Transducers

RM5OI
ROBOT

Waist

4

FILTER

I

2   R   T

3

FOUR STATION
SAMPLING TABLE

PREAMP

In   DIGITAL
OSCILLOSCOPE   Trig

GPIB

HP54200

FUNCTION
GENERATOR

Trig   Out

DIGITAL
I/O

MOTOR POWER

MOTOR CONTROL

I/O RAIL

PC AT   COMPUTER

RS-232

ROBOT
CONTROLLER

DC
POWER SUPPLY
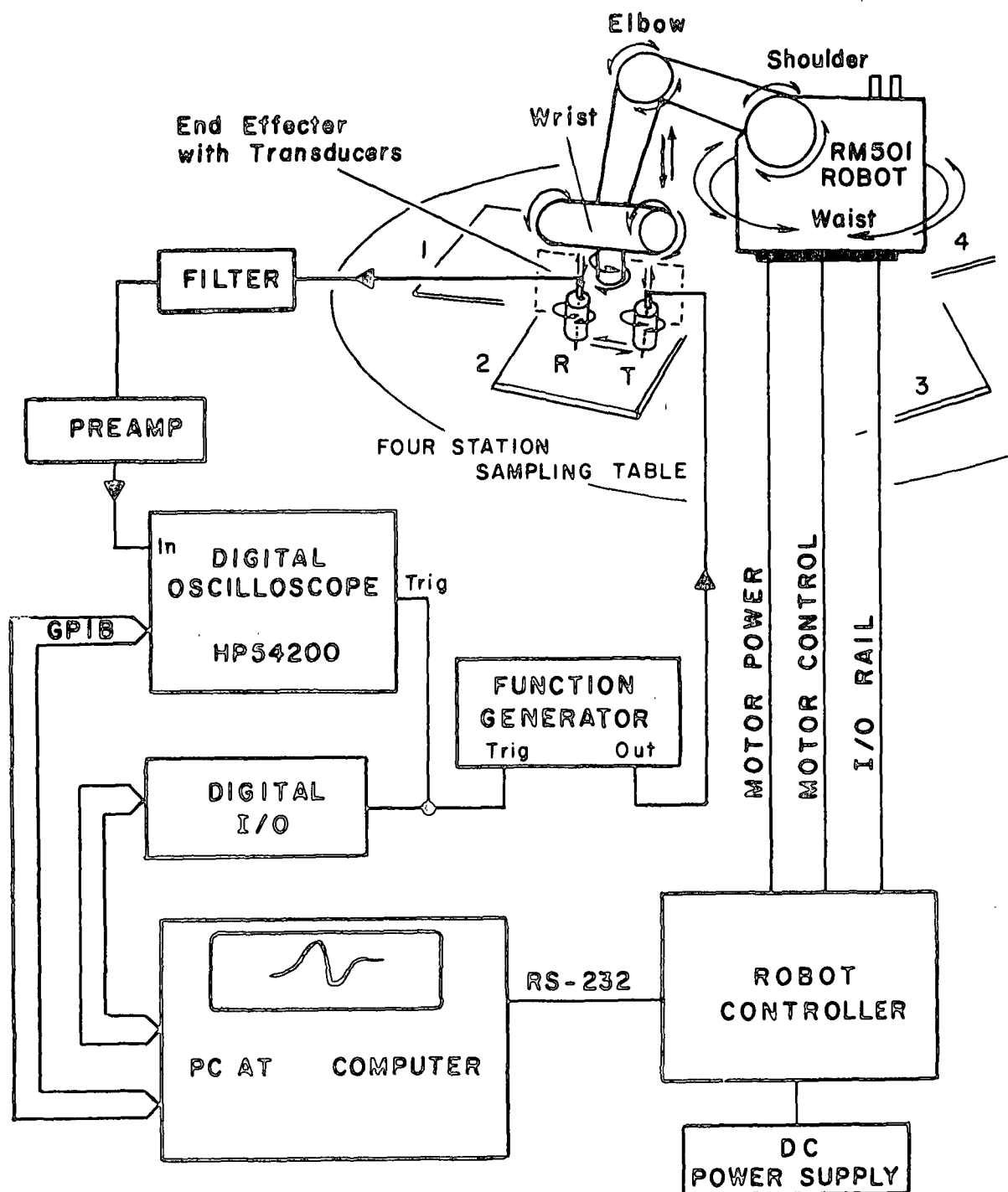
Fig. 1.   Overall schematic of the robotic tester.
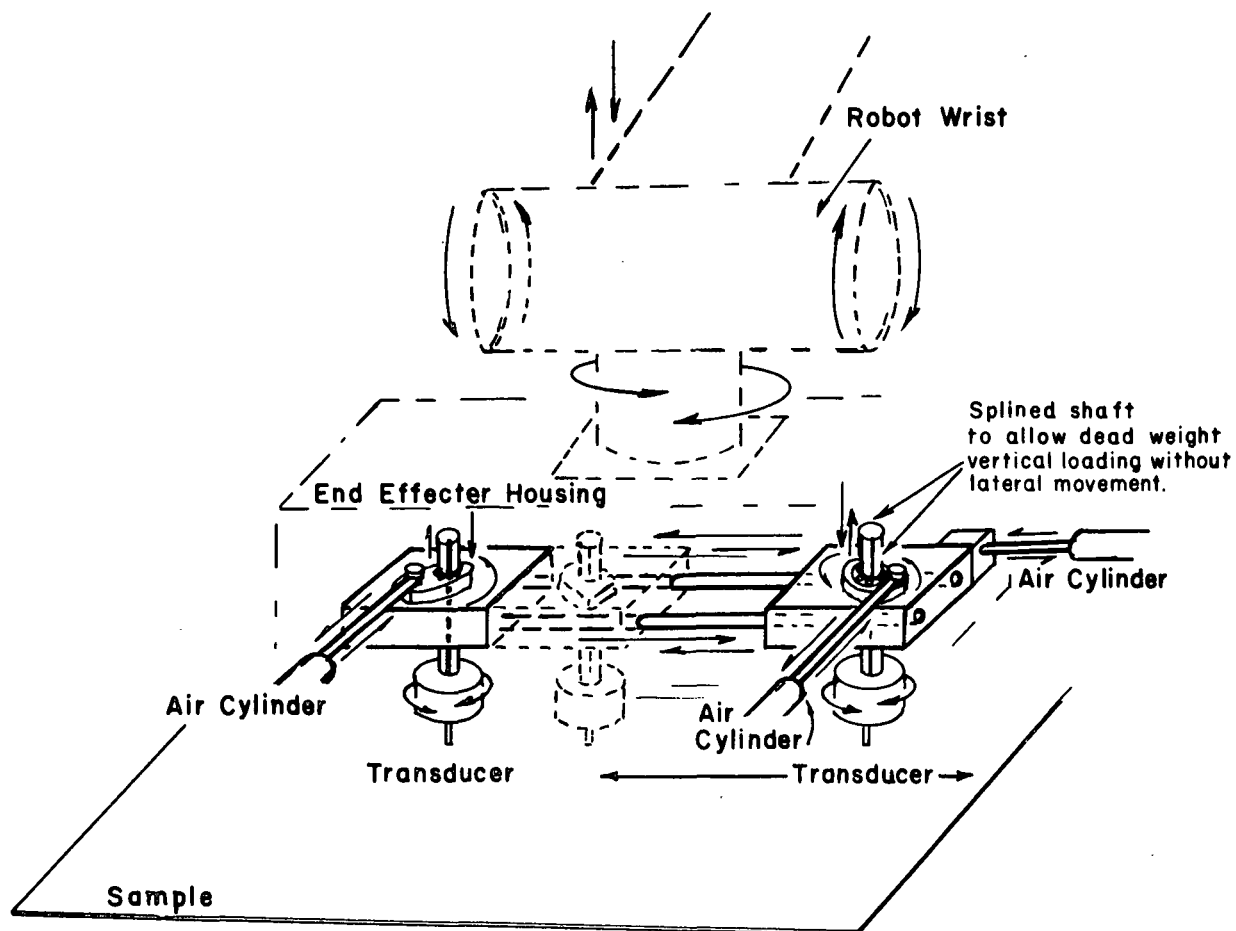
DETAIL OF ROBOTIC END EFFECTER WITH TRANSDUCERS

Fig. 2.   Schematic of the end effecter.
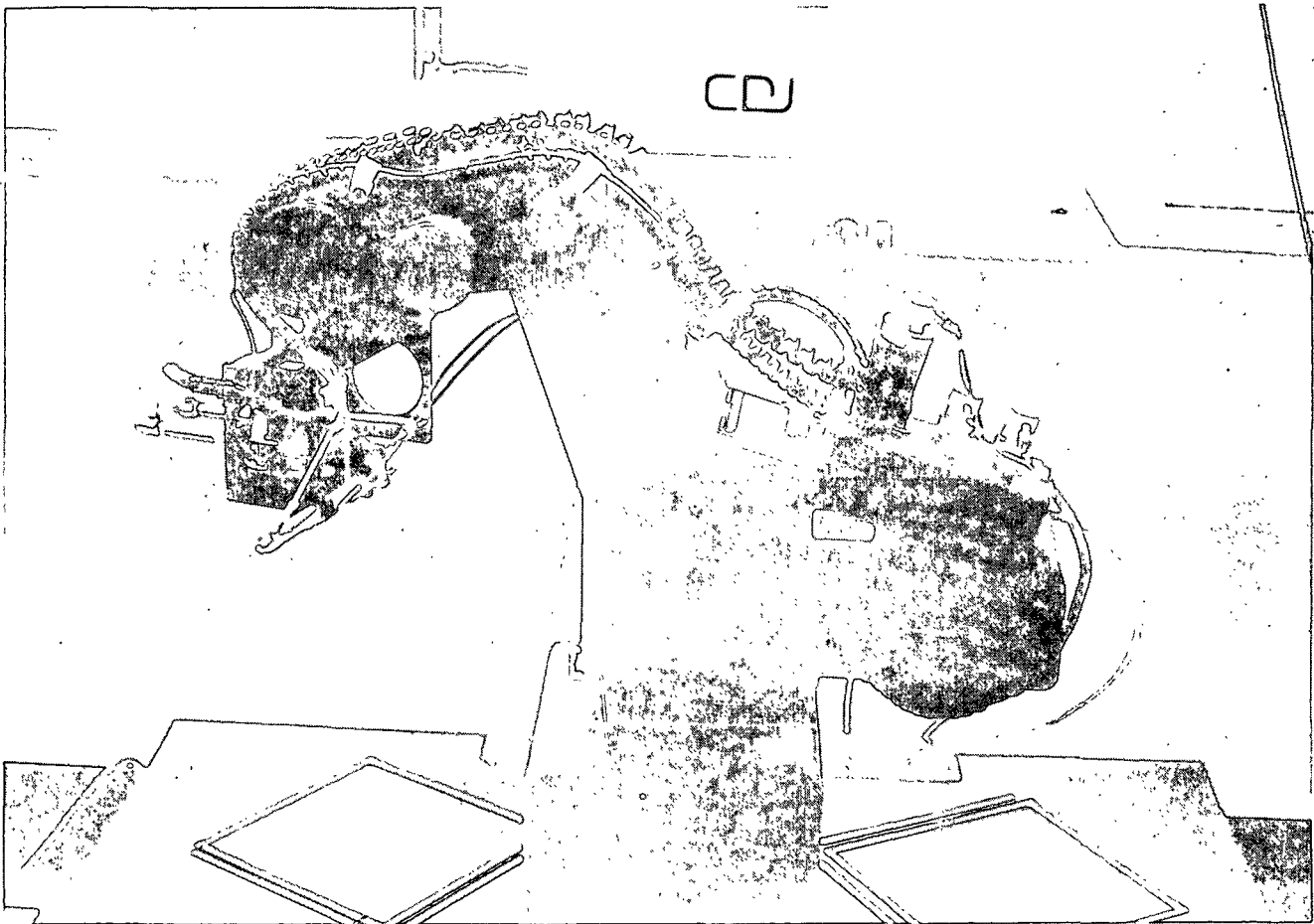
Fig. 3. Photograph of the robotic tester.
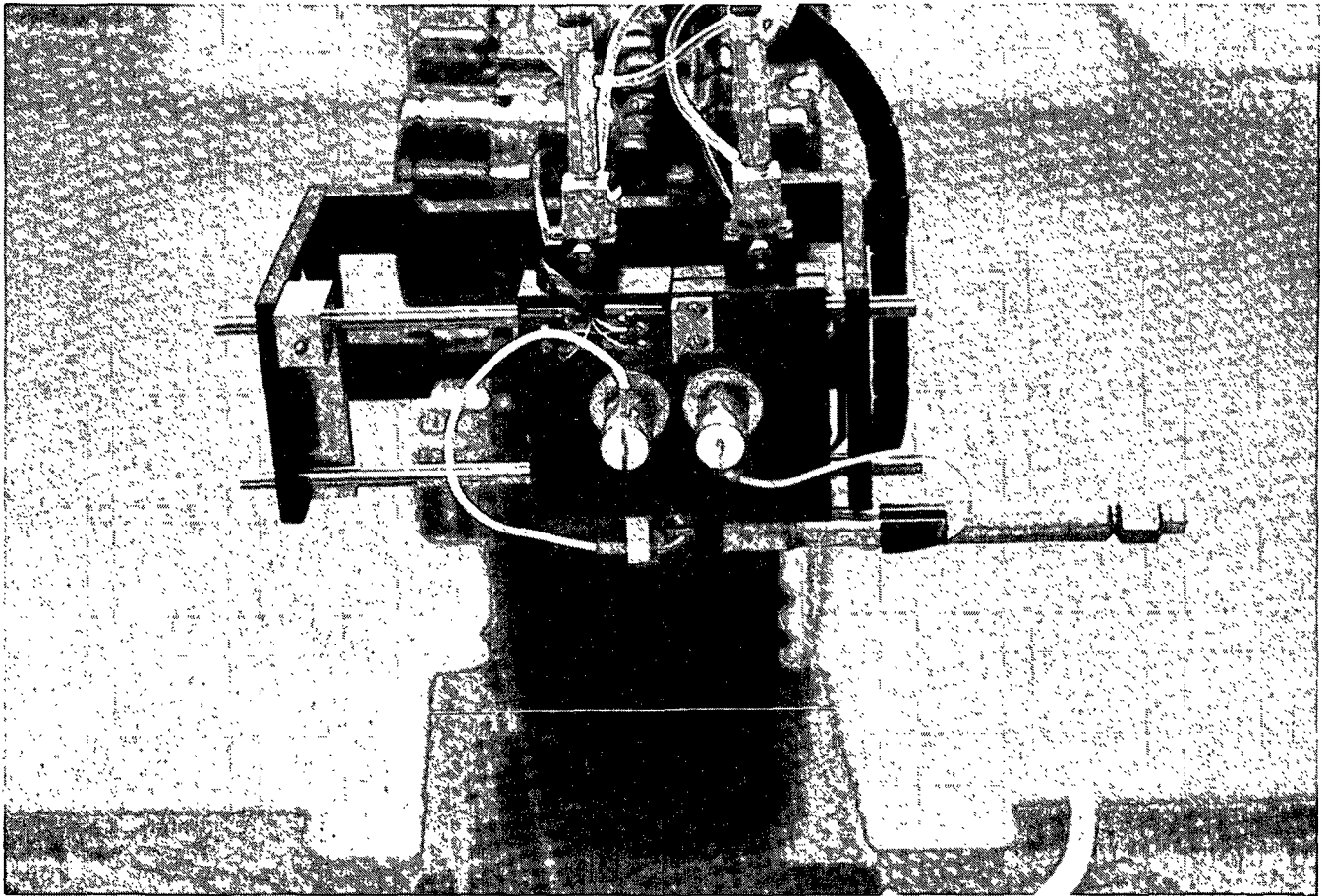
Fig. 4. Photograph of the end effecter.

MINIATURE   IN-PLANE   BENDER   TRANSDUCER

CERAMIC
BIMORPH

COAXIAL CABLE

TRANSMITTER: A = 1.5mm., B = 2.5mm.
RECEIVER: A = 1.3mm., B = 1.3mm.

SET SCREW

BRASS

DELRIN

A

B

0   0.5   1 inch
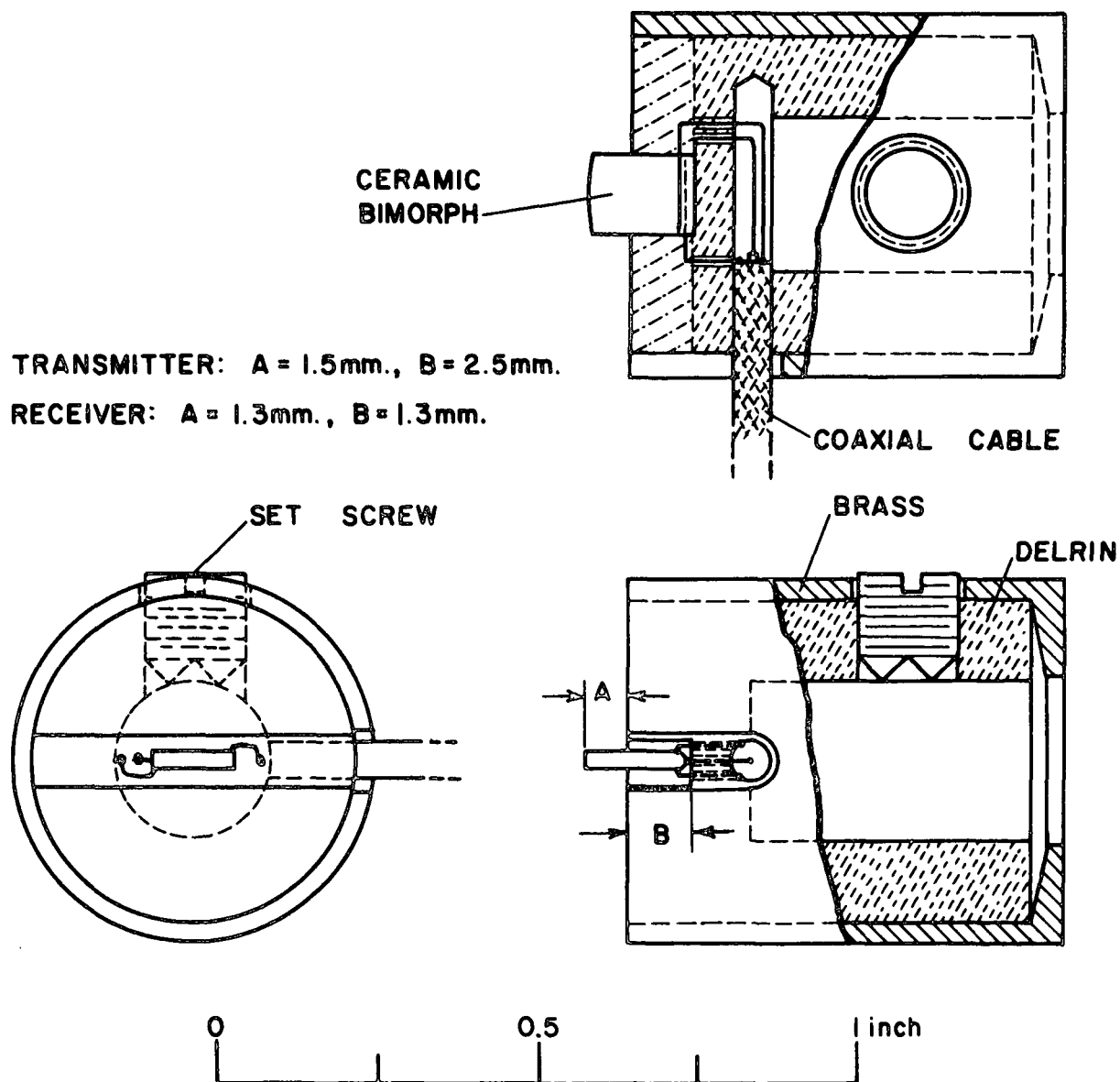
Fig. 5. Mechanical drawing of the transducers used in the robotic tester.

THE INSTITUTE OF PAPER CHEMISTRY

Appleton, Wisconsin

Status Report

to the

PAPER PROPERTIES AND USES

PROJECT ADVISORY COMMITTEE

Project 3332/3613

ON-LINE MEASUREMENT OF PAPER MECHANICAL PROPERTIES

October 19-20, 1988

PROJECT SUMMARY

PROJECT NO. 3332: ON-LINE MEASUREMENT OF PAPER MECHANICAL PROPERTIES

PROJECT STAFF: C. C. Habeger, M. S. Hall   September 12, 1988

PROGRAM GOAL: Develop ways to measure and control manufacturing processes.

PROJECT OBJECTIVE:

To develop the capability to measure elastic parameters on a moving paper web.
Current emphasis is on out-of-plane measurements.

PROJECT RATIONALE, PREVIOUS ACTIVITY, AND PLANNED ACTIVITY FOR FISCAL 1988-89
are on the attached 1988-89 Project Form.

SUMMARY OF RESULTS LAST PERIOD: (October 1987 - March 1988)

(1) Evaluation of the out-of-plane rotary instrument was very satisfactory and
    it is being used for routine caliper and velocity testing.

(2) Experimentation with commercial fluid-filled wheels for out-of-plane
    velocity measurement shows some promise.

(3) In-plane on-line velocity measurement is being attempted with surface coated
    bender transducers.

SUMMARY OF RESULTS THIS PERIOD: (March 1988 - October 1988)

(1) On-line operation of the IPC neoprene-faced wheel transducers has been
    simulated. The results are encouraging.

(2) A technique for molding neoprene to transducer front-faces is being
    developed.

(3) New out-of-plane wheel transducers, which we hope can withstand the tem-
    perature and wear experienced on-line, are under construction.

(4) Preliminary investigations of the fluid-filled wheels in an on-line measure-
    ment of out-of-plane properties have begun. These wheels should provide
    rugged, easily manufactured ZD velocity gage, once adequate temperature com-
    pensation is achieved.

(5) New, hopefully broader banded, immersion transducers have been designed for
    the fluid-filled wheels.

(6) The surface-hardened bimorph transducer have been tested for on-line, in-
    plane operation. With a better surface hardening procedure (now in
    development), they should provide significant advantages over the presently
    used extended, resonant transducers.

PROJECT TITLE: On-Line Measurement of Paper
                 Mechanical Properties

PROJECT STAFF: M. Hall/C. Habeger

PRIMARY AREA OF INDUSTRY NEED: Properties related
                                 to end uses

| DATE: 2/3/88 |
| PERIOD ENDS: 6/30/89 |

BUDGET: $50,000

PROJECT NO.:   3332

PROGRAM AREA: On-Machine Uniformity -- Sensors and Control

PROGRAM GOAL:

Develop ways to make on-line measurement of product properties and process
parameters in order to control manufacturing processes.

PROJECT OBJECTIVE:

To develop the capability to measure mechanical properties on a moving paper
web. Current emphasis is on out-of-plane measurements. This project is con-
cerned with the development of a laboratory instrument using wheel-type ultra-
sonic transducers. A related DOE-sponsored project is concerned with the
development of sensors suitable for making measurements on the paper machine
and subsequent control of the paper making process.

PROJECT RATIONALE:

The ability to measure mechanical properties on the paper machine will provide
a means to continuously monitor product quality related to end-use performance.
It also provides data needed to relate product characteristics to process
variables for paper machine control.

RESULTS TO DATE:

A theory for the propagation of ultrasound in paper was developed. Devices
were constructed to make on-machine measurement of the in-plane elastic
parameters of paper and board. These devices were successfully tested in mill
environments. Another version of the equipment for in-plane measurement was
constructed and tested. This design used two receivers located at different
distances from a transmitter, all mounted in a drum. Thus, this version was
self-calibrating and could be used for on-machine measurement of light weight
paper grades.

A cross correlation technique was implemented to improve the accuracy in
measuring the transit time of an ultrasonic pulse for in-plane velocity
measurements. Equipment was developed for measuring the effects of moisture
and temperature on paper elastic properties. The feasibility of ZD signal
transfer between rubber-faced, ceramic transducers at high paper speeds was
demonstrated.

A high-frequency, low impedance, ultrasonic transducer was developed for
out-of-plane measurements using a plastic (PVDF) piezoelectric material. This
type of transducer is superior to commercial ceramic transducers for our
applications.

The background information and experience provided by this project was the basis for obtaining a Department of Energy contract to develop "On-Machine Sensors to Measure Paper Mechanical Properties".

Wheel-type transducers for ZD measurement have been constructed with a continuous PVDF piezoelectric film around the circumference. Mechanical hardware and electronics have been assembled to provide a practical laboratory instrument for profiling caliper and ZD velocity by feeding a paper sample through the nip between two wheel-type transducers.

PLANNED ACTIVITY FOR FY 1988-89:

The laboratory instrument using wheel-type transducers to make ZD velocity and caliper measurements will be completed. Its performance and advantages relative to the present ZD laboratory instrument will be determined.

Most of the research activity in this program area will be performed under the closely related DOE project. The DOE project will be concerned primarily with transducer design selection and hardware design and construction to integrate in-plane and thickness-direction ultrasonic measurements into an assembly that can be used on a moving web and pilot paper machine.

STUDENT RELATED RESEARCH:

D. B. Macdonald, M.S.-1988.

Status Report

ON-LINE MEASUREMENT OF PAPER MECHANICAL PROPERTIES

Project 3332/3613

We are working on three new approaches for making on-line ultrasonic measurements. Two of these are attempts to determine calipers and out-of-plane longitudinal velocities. The first will use neoprene-coated wheel transducers, which will be similar to those used in our rotary, ZD laboratory instrument. (A paper describing the rotary gauge is included in the appendix.) The second out-of-plane technique employs commercial fluid-filled wheels. For in-plane measurements, we are experimenting with surface-hardened, bimorph transducers. These are similar to the transducers used in our laboratory instruments.

The progress that we have made on each endeavor is discussed individually below.

NEOPRENE FRONT-FACE, PVDF WHEEL TRANSDUCERS

One of the purposes for building the ZD rotary laboratory unit (See the appendix for details.) was to assess the possibilities for doing on-line caliper and ZD velocity measurements with soft platens. We have modified the instrument, so that, continuous belts can be run through the nip between the transducer wheels at speeds of up to 190 m/min. A description of the results of velocity and caliper measurements as a function of speed for three different board samples follows.

Calibration of the wheel transducers is normally done by stepping, under computer control, one thick and one thin (8 μm aluminum foil) shim through the nip. The readings of the LVDT at each step for both shims is recorded. Ultrasonic pulses at the receiver wheel are digitized and stored for each position on the thin shim. When a sample is stepped through the nip, its caliper at

each step is determined by interpolation of the LVDT readings for the calibration shims at that step. The time-of-flight through the sample is defined as the time of the peak in the cross correlation function of the foil ultrasonic signal, at that step, and the ultrasonic signal through the sample.

Individual calibration at discrete positions of the wheels is not feasible for continuous operation, and the calibration procedure was altered for on-line operation. As before, two shims are stepped through the nip. Measurements are made at 30 locations uniformly spaced around the circumferences of the wheels. This time, the LVDT readings for the thick and thin shims are averaged, as are the digital ultrasonic signals through the foil. In order to test a belt sample, the wheels are operated at constant speed (not under computer control); a number (20 for the tests below) of LVDT and ultrasonic signal are stored and averaged; caliper and velocity are calculated using calibration averages and sample averages; the results are printed; and the cycles repeats until the operator interrupts. Since the calibration is done at zero speed while the sample readings are taken during rotation, the influence of dynamic factors can be quantized by analyzing the results as a function of speed.

Three different commercial board samples were tested: a 42-lb/1000 ft^2 liner board; a 26 lb/1000 ft^2 corrugating medium; and a 600 µm thick coated board. The samples were cut into strips; a section at the ends of each strip was surface ground half way through; and a belt was formed by bonding the two ground ends together. A belt of aluminum foil about 50 µm thick was also formed. A series of measurements were made at speeds up to 190 m/min for all four belts and a special series of runs was made on bare neoprene without a belt. Preliminary testing revealed that the system was vibration prone. There were large variations in the caliper measurements, especially at speeds where

resonant vibrations were excited in the instrument. This problem was addressed by adding a dashpot, made from a plunger immersed in a viscous fluid. With the dashpot in place, variance in the average caliper readings, printed by computer, were less than 1.0 µm at all speeds.

The raw caliper readings as a function of belt speed are plotted in Fig. 1 for the five runs. As one would expect, the wheel separation increased with speed in each case. Possible reasons for this are that: centrifugal forces act on the neoprene; there is less time for the neoprene to conform; the wheels are expanding due to an increase in temperature; and air is entrained between the wheels. Notice that a jump in caliper is experienced at the lowest speed, followed by a gradual increase with speed. The total rise in reported caliper is about 70 µm in each case.

As is clear from Fig. 1, the observed changes in paper caliper can be partially compensated using the reported foil calipers. This is demonstrated in Fig. 2, where the change in caliper of the foil is subtracted from the reported paper calipers. In a real on-line situation, it would be impractical to make corrections with a foil belt; however, the wheels could be transported past the edge of the web and the neoprene-to-neoprene displacements could be recorded as a function of speed. Caliper compensation, using neoprene separations, is presented in Fig. 3. Notice that the compensated calipers are stable, and that, for the two thinner boards, the neoprene correction is actually better than the foil correction. At the higher speeds, both corrected calipers are independent of speed, and we have every indication that the results could easily be extended to higher speeds.
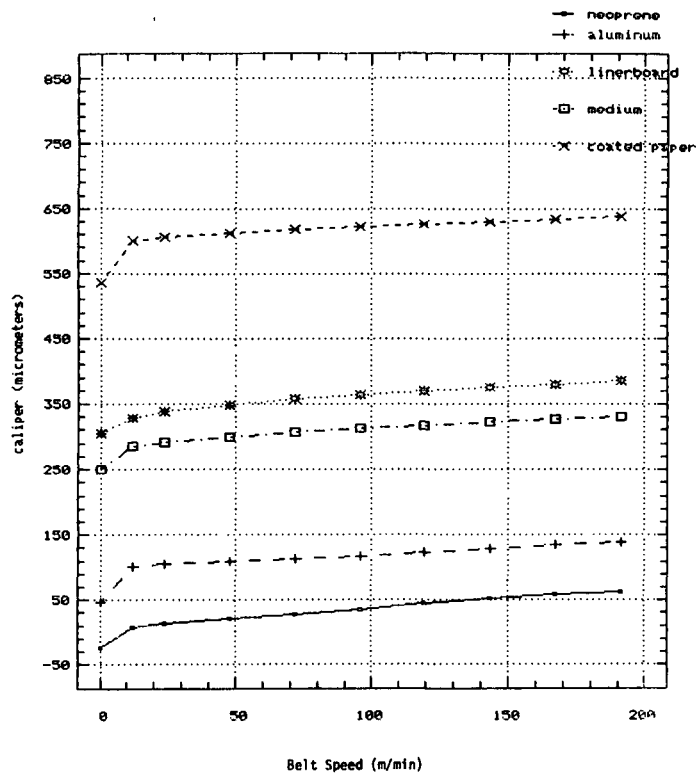
Fig. 1.   IPC wheel raw caliper
          readings versus belt speed
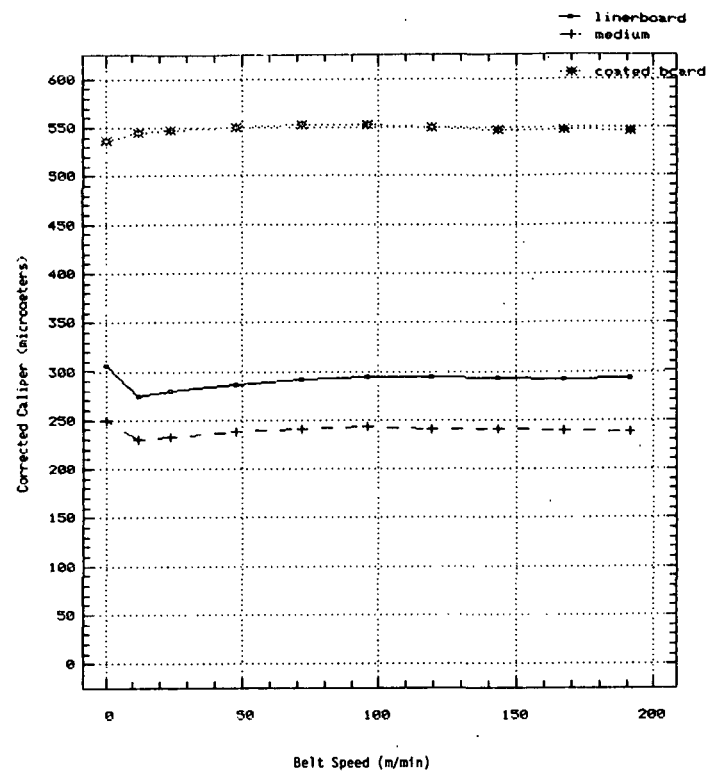
Fig. 2.   IPC wheel caliper corrected for
          changes in foil caliper versus
          belt speed.
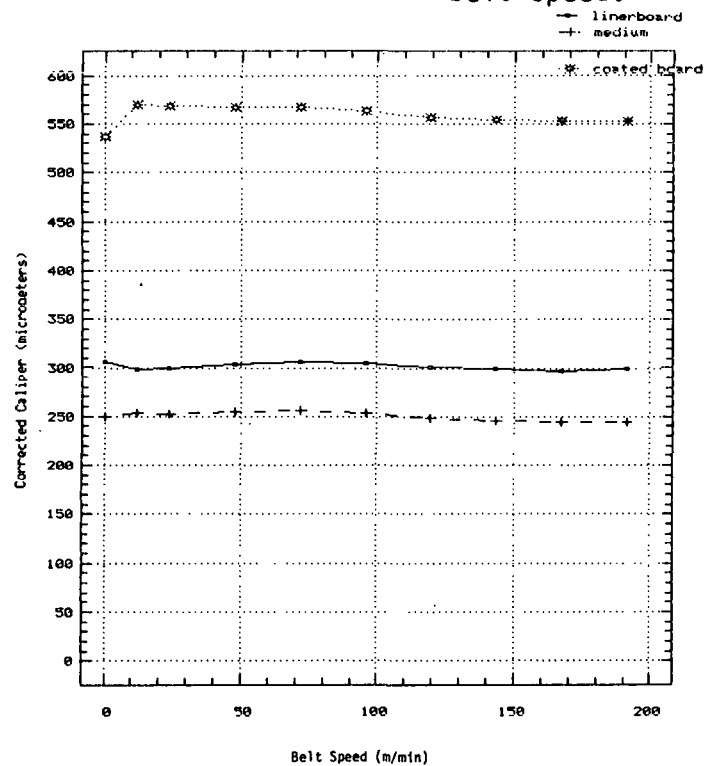
Figure 3.   IPC wheel caliper corrected for changes in
            neoprene-neoprene separation versus belt
            speed.

The factors that caused the caliper to appear to increase with speed have a similar effect on the time-of-flight delays. The raw time-of-flight delays for the four belts and for the neoprene-to-neoprene contact are plotted in Fig. 4. The time delays experience a step increase followed by a gradual rise. The raw velocity is simply the reported caliper divided by the raw delay time (Fig. 1 values divided by Fig. 4 values). These are presented in Fig. 5 for the three paper belts. The neoprene (or for that matter the aluminum) delays can be used to correct the paper time-of-flights in velocity calculations. This is done in Fig. 6, where corrected velocity (defined as caliper minus change in neoprene caliper divided by delay minus change in neoprene delay) is graphed versus belt speed. Since delay and reported caliper both increase with speed, the increases cancel, to some extent, in the velocity calculations, and raw velocities are more stable than the delays or calipers. In fact, it is difficult to argue that the corrected velocities in Fig. 6 are a better indicator of the static values than are the raw numbers in Fig. 5.

We consider the preliminary results, presented above, to be encouraging. We were able to roughly reproduce soft platen calipers at speed, when we used the apparent neoprene-to-neoprene separations for compensation. The dynamic velocity measurements looked good with and without correction.

We don't consider the wheels in the rotary ZD instrument to be suitable for on-line operation, and we are presently constructing a new version. The major concern is, of course, wear to the soft neoprene front-faces. The new wheels will be coated with a harder neoprene, which we hope can withstand the rigors of on-machine operation. If these wheels are applied to the web while rotating at web speed, we think they have a chance of lasting. Another significant change will be the use of Penwalt's improved high-temperature, high-
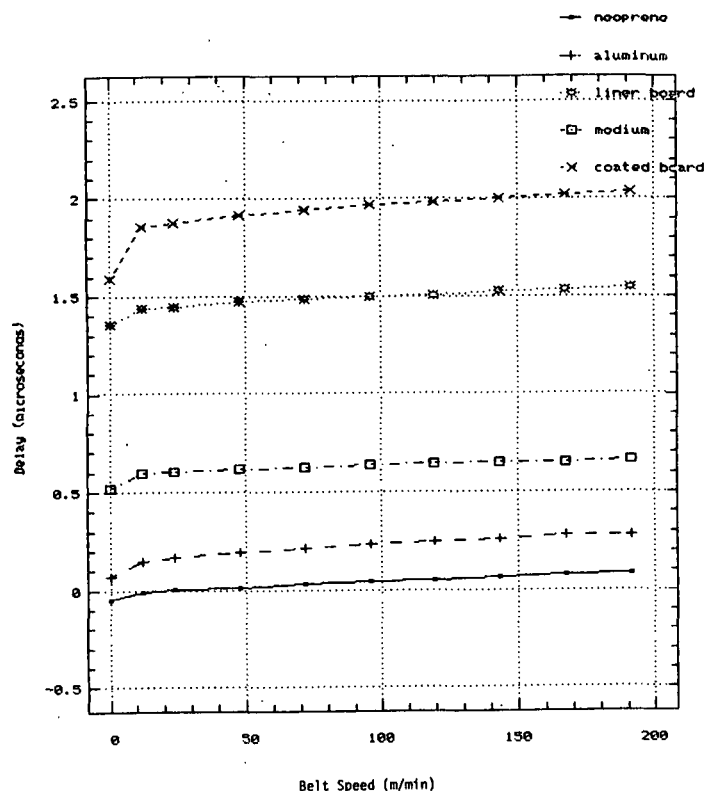
Fig. 4.   IPC wheel raw time-of-flights
          versus belt speed.
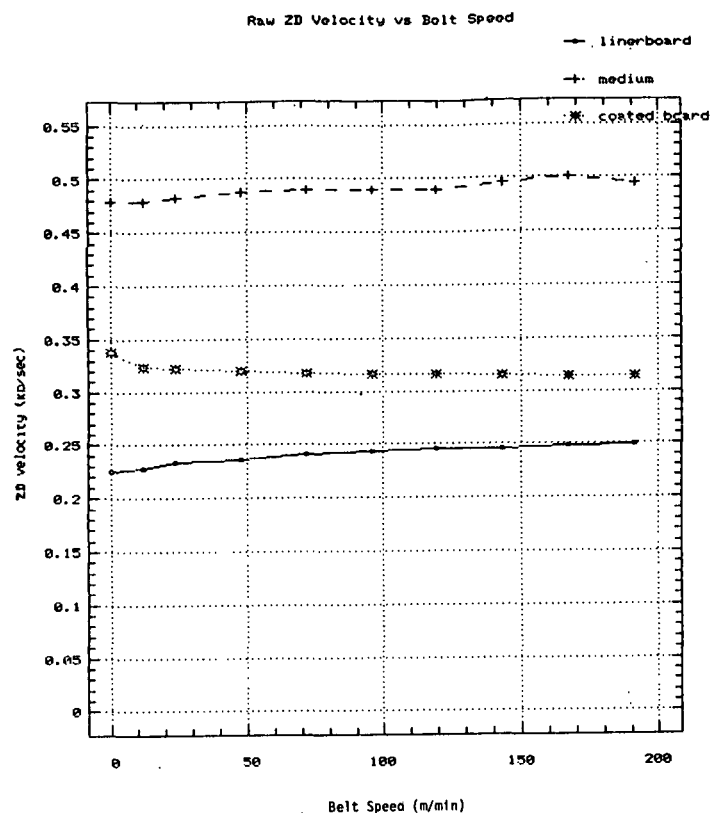
Fig. 5.   IPC wheel raw ZD velocities
          versus belt speed.
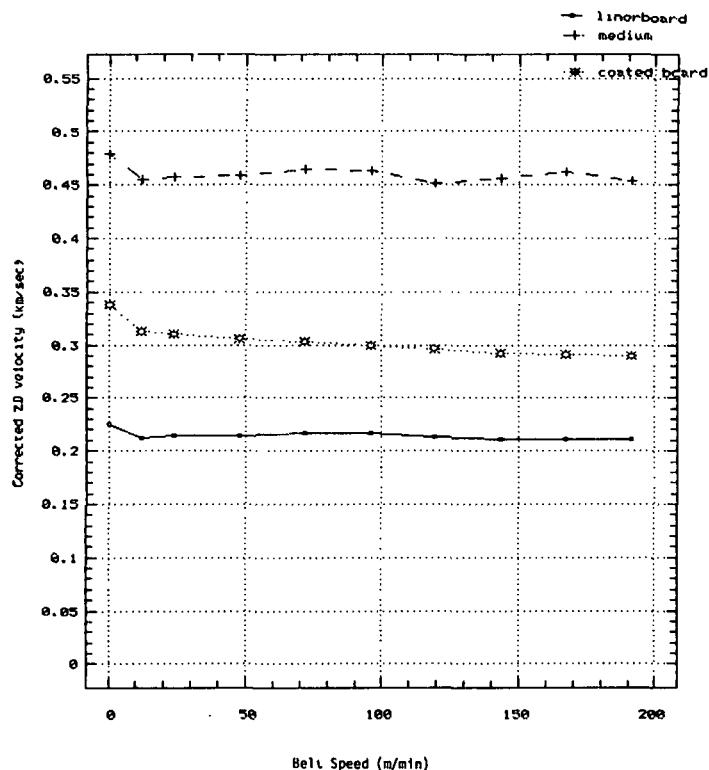
Figure 6.   IPC wheel ZD velocities corrected for neoprene-
            neoprene separation and time-of-flight changes
            versus belt speed.

sensitivity, PVDF film. This product is still in the experiment stage, and samples are hard to come by. However, after a frustrating six month wait, we have obtained a sufficient amount of the film to produce two wheels. Construction is under way, and we expect to have wheels that can operate on the web strainer within a couple months.

There is one other innovation that we are incorporating into the construction of the new wheels. This is the molding of a neoprene front-face to the Kynar rim. Previously, we used a special fixture (see appendix) to bond a spliced, neoprene belt to the Kynar. We now are experimenting with molding our own neoprene. Early results show that, with proper pretreatment of the Kynar, we can establish excellent bonds between the neoprene and the Kynar. These bonds appear to be more uniform than the epoxied interfaces. It is no longer necessary to load the neoprene (and thereby leave the finished front-face in a nonuniform stress state) while epoxy is setting. In addition, the splice is eliminated. By varying the recipe, we can produce neoprenes over a wide durometer range (including the durometer used in the soft platen caliper measurement). If this technique is successful, it would obviously, also, be used in the construction of future flat laboratory transducers.

FLUID-FILLED WHEEL TRANSDUCERS

As discussed in the last PAC report, we are also experimenting with commercially available fluid-filled wheels for on-line measurement. Here, a rubber-rim wheel, filled with liquid, is mounted, through bearings, to a stationary shaft. An immersion-style ultrasonic transducer is fixed to the shaft. For ZD measurements on paper, a sample is passed in the nip between two such wheels, and ultrasonic signals are communicated between the wheels. As depicted

in Fig. 7, when the spacings between the transducers and the wheel rim are unequal, there are three distinct pulses resulting in one wheel when a single pulse is induced in the other wheel. The first signal, coming at t_1, goes directly from the transmitter (through fluid, rubber, sample, rubber, and fluid) to the receiver. At t_2, a second signal, which results from a multiple reflection between the transducer, closer to the rim, and the rim, arrives. The final signal of interest, coming at t_3, contains a multiple reflection between the rim and the other transducer. The differences in t_1, t_2, and t_3 with and without sample (Dt_1, Dt_2, and Dt_3, respectively) are related to the velocity of ultrasound in the sample, V_S, the velocity of ultrasound in the fluid, V_F, and the caliper of the sample, cal, as shown in Equations 1, 2, and 3.

$$Dt_1 = cal(1/V_S - 1/V_F) \tag{1}$$

$$Dt_2 = Dt_1 - 2d_1/V_F \tag{2}$$

$$Dt_3 = Dt_1 - 2d_2/V_F \tag{3}$$

In the above Equations, d_1 and d_2 represent the change in fluid length in the two wheels resulting from sample insertion. Their sum must equal the caliper. Therefore, these equations can be solved for V_S and the caliper, cal, as in Equations 4 and 5.

$$cal = 0.5(2Dt_1 - Dt_2 - Dt_3)V_F \tag{4}$$

$$V_S = V_F/(1 + Dt_1V_F/cal) \tag{5}$$

So, by analyzing all three pulses, the caliper as well are the ZD longitudinal velocity of ultrasound can be calculated.

In measuring the time-of-flight of pulses, it is important to produce narrow pulses. This reduces the possibility of pulse overlap, and improves the resolution. Originally ceramic piezoelectric transducers were used. In the
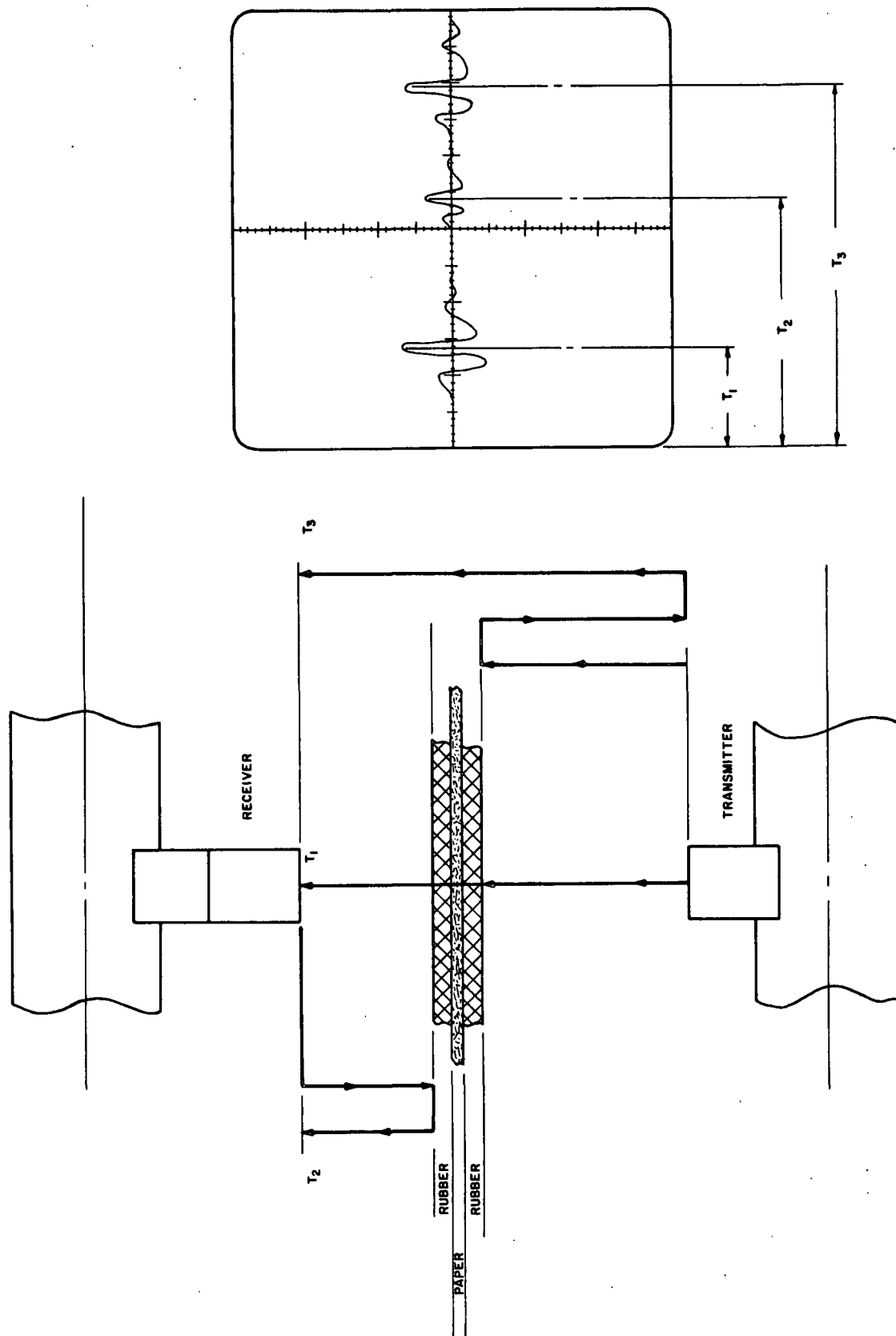
Figure 7.   Schematic diagram of the definition of T_1, T_2, and T_3.

last period, we have changed to commercial PVDF transducers, and we have thereby

achieved a significant improvement in bandwidth.

However, minimum pulse widths are still about twice those realized in

our PVDF wheel transducers. We see no reason for this, and we feel that we are

capable of making better PVDF immersion transducers. In the near future, we

plan to construct our own versions. These will simply be Kynar backings with

PVDF films directly applied to one end. The front-face will be sealed, and the

PVDF films will come in direct contact with the fluid.

As can be seen from Equations 4 and 5, in order to calculate caliper

and ZD velocity, it is important to know the velocity of ultrasound in the

fluid. We have developed a method to determine V_F. The time of arrival of t_1

is plotted as a function of the spacing between the shafts of the wheels. The

Velocity of ultrasound in the fluid is merely the inverse of the slope of this

line. The result, at room temperature, is V_F = 1644 m/sec.

In this last period, we have just began making simulated on-line

measurements using the IPC web strainer. We discovered early on that to get

stable and reproducible results, it was necessary to use the signal averaging

and cross correlation software designed for the rotary wheel transducers. The

software was modified to handled the signals encountered in the fluid-filled

wheels, and the transducer leads from the rotary ZD instrument were connected to

the fluid-filled wheels (instead of the IPC wheels).

A preliminary on-line test of the fluid-filled wheels was conducted as

follows. The wheels are rigidly mounted on the web strainer, so that the

distance between axles is fixed. The paper belt, to be tested, is threaded

through the nip. The belt is run at speed (for at least 15 minutes) until the

temperature of wheels stabilizes. The rotary instrument is set to function in the calibration mode, with the signal preset delay adjusted to capture one of the three fluid-filled wheel signals. The web is stopped and quickly removed from the nip of the wheels. While gently turning the wheels by hand, the computer takes and averages thirty references. The web is inserted back into the nip, and the web strainer is returned to its original speed. The rotary instrument is set to operate in the on-line mode (as used with the rotary belt tests described above). The computer averages thirty receiver wheel signals and calculates the time of the peak in the cross correlation function between the reference and the sample signal. The results are printed out, and the process repeats until the operator interrupts. The printed results are averaged to get one of the Dt's. This process is repeated two more times with different preset delays, and the other two Dt's are recorded. Results of the calipers and velocities of a 33 lb/1000 ft^2 corrugated medium obtained in this way are presented in Fig. 8 and 9. The "static cal." line in Fig. 8 and the "static vel." line in Fig. 9 represent the values measured with our standard laboratory ZD instrument. To get the "static cal." line in Fig. 9, the laboratory caliper was inserted into Equation 5 to calculate the ZD velocity in the sample.

The reason that we brought the wheels up to speed right before taking the reference signal was that we noticed significant shifts in the Dt's with web speed. We attributed this to temperature increases. Since there is a relatively long length of fluid between the transducers, changing fluid velocity can cause big changes in transit times. The proper way to handle this difficulty is to: (1) measure the velocity of ultrasound in the fluid as a function of temperature; (2) measure the effects of temperature on t_1, t_2, and t_3; (3) implant a thermocouple, which is interfaced to the computer, in one of the wheels; (4)

Ultrasonic Caliper Measured by
Fluid-Filled Wheels vs Web Speed
— Wheel cal.
-+- Static cal.

Fluid-Filled Wheel ZD velocities
vs Web Speed
— Wheel Cal.
-+- Static Cal.
-*- Static Vel.
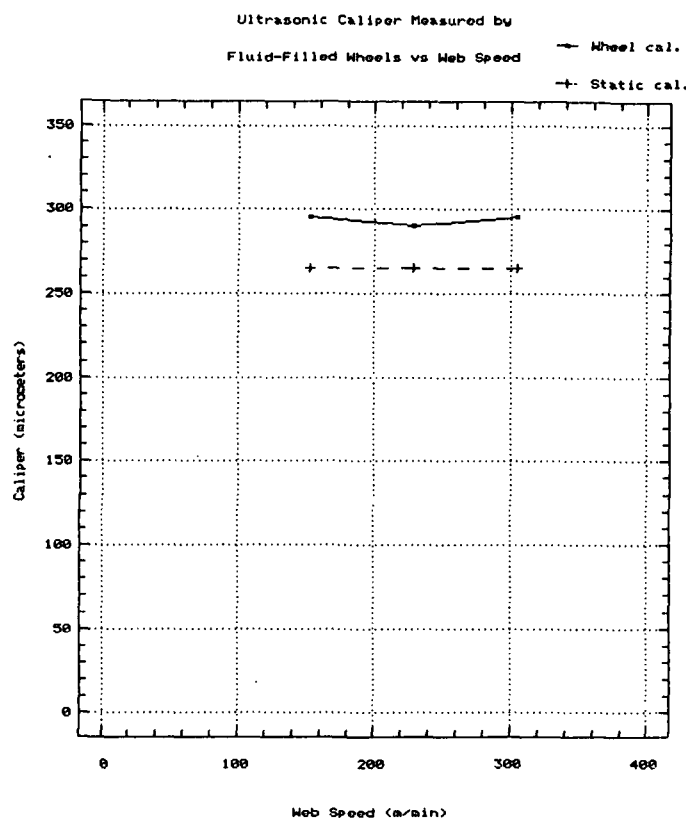
Fig. 8.   Fluid-filled wheel calipers versus belt speed.
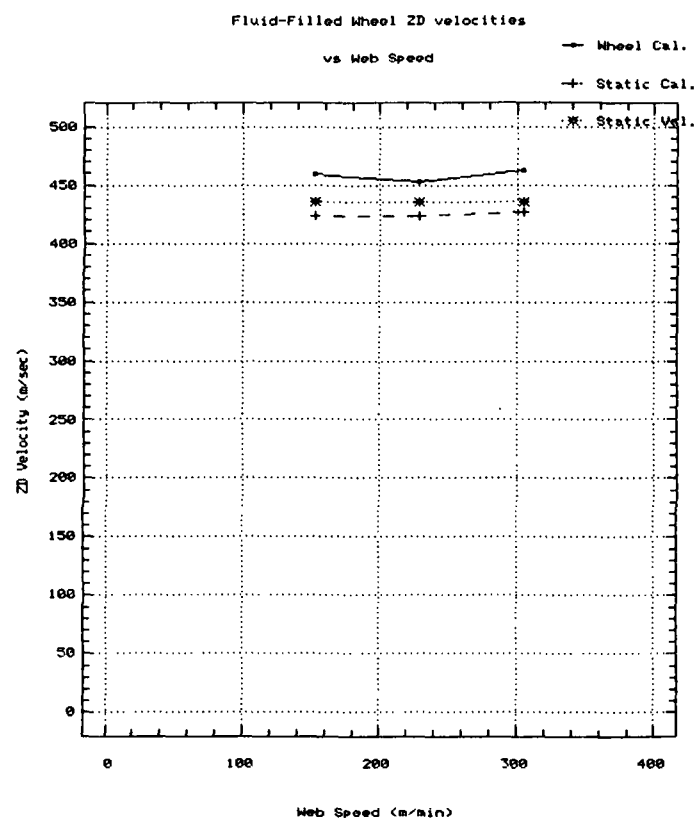
Fig. 9.   Fluid-filled wheel ZD velocities versus belt speed.

use the results of steps 1 and 2 to calculate Dt_1, Dt_2, and Dt_3; and (5) input the value of V_F from step 1 into Equations 4 and 5 to get sample ZD velocity and caliper. We have, on order, a digital thermometer which will monitor a thermocouple, mounted in a wheel, and report the results to the computer. With this in place, we intend to perform steps 1 and 2 and to make further preliminary tests of the fluid-filled wheel system.

ON-LINE BIMORPH TRANSDUCERS

As discussed in the last PAC report, we are making on-line measurements with bimorph transducers. Their major advantages are that they are broadbanded and they have a much smaller contact area to the web. In addition, on an extended web, it could be possible to produce time-separated longitudinal and shear pulses, allowing us to measure two velocities at a time. The major concern is that they will not stand up to on-line use. Last period we developed a surface hardening technique, which we hoped would solve this problem. However, tests, conducted this period, demonstrated that wear could occur in some extreme conditions. We have subsequently altered the recipe for our surface coating, and we are confident that this will lead to more durable units. Testing will follow directly.

One of the concerns of the three-transducer techniques is that the results can be sensitive to loading conditions on the transducers. The bimorphs should reduce this problem, as they have very small contact areas. A typical example of the effects of tension, during on-line operation, on an in-plane velocity calculation with the bimorph transducers is shown in Fig. 10. Here, a 45 lb/1000 ft^2 linerboard belt was run at 30 m/min on the web strainer. The belt drove a drum containing three bimorph transducers, which measured CD longitudinal velocity as the transducers contacted the belt. The computer averaged 25 pulses from near and far transducer separations and printed out the cross correlation velocities for the averaged signals. Tension was increased by incrementing the position of a idler roll. In Fig. 10, the average of 3 reported velocities is plotted versus the location of the idler roll. The range of tensions is extreme; at the lowest level there is barely sufficient sample transducer contact to produce a signal, while at the highest tension the web
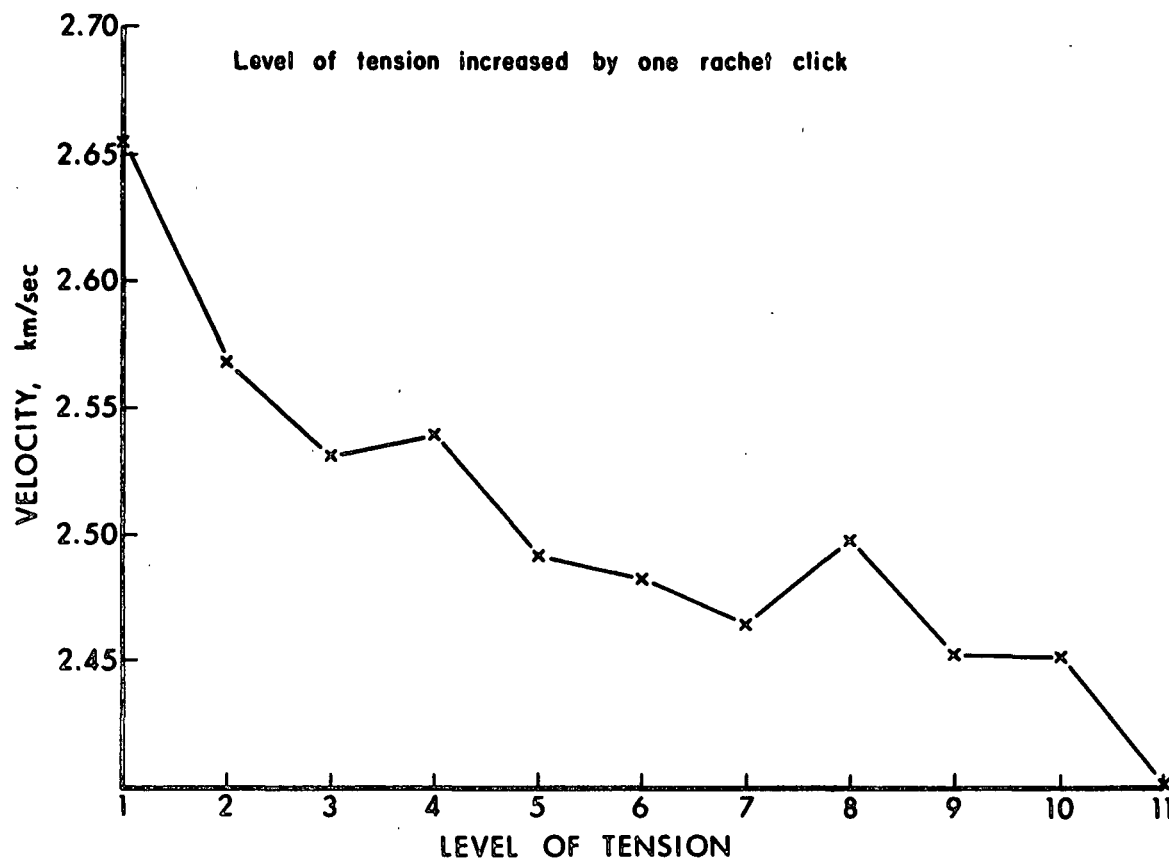
Figure 10.   On-line bimorph CD longitudinal velocities versus
              wet tension.

soon broke. In the intermediate tension range, a regime of fairly constant

reported velocity appears. However, we would like to improve this performance,

and we shall experiment with different groove geometries and transducer

loadings.

We also tested commercial boards and plotted the velocities as a func-

tion of web speed. The transducers were spaced in the cross direction, so that

by rotating the transducers we could alternately make CD longitudinal and shear

velocity measurements. Four different samples were tested: a 26 lb/1000 ft^2

corrugating medium; a 33 lb/1000 ft^2 corrugating medium, a 69 lb/1000 ft^2 liner-

board; and a 45 lb/1000 ft^2 linerboard. The web tension was set in the inter-
mediate region of Fig. 10. The computer did signal averaging on thirty "near"
and "far" signals, calculated a cross correlation velocity, and printed the
results. The average of about twenty reported velocities are plotted versus
speed in Figs. 11 and 12 for the CD longitudinal and shear velocities. The
results plotted at zero web speed actually are the average of single sheet
measurements made on the robotic in-plane tester. A comparison of the zero
speed velocities with the dynamic ones is an indication of how well the on-line
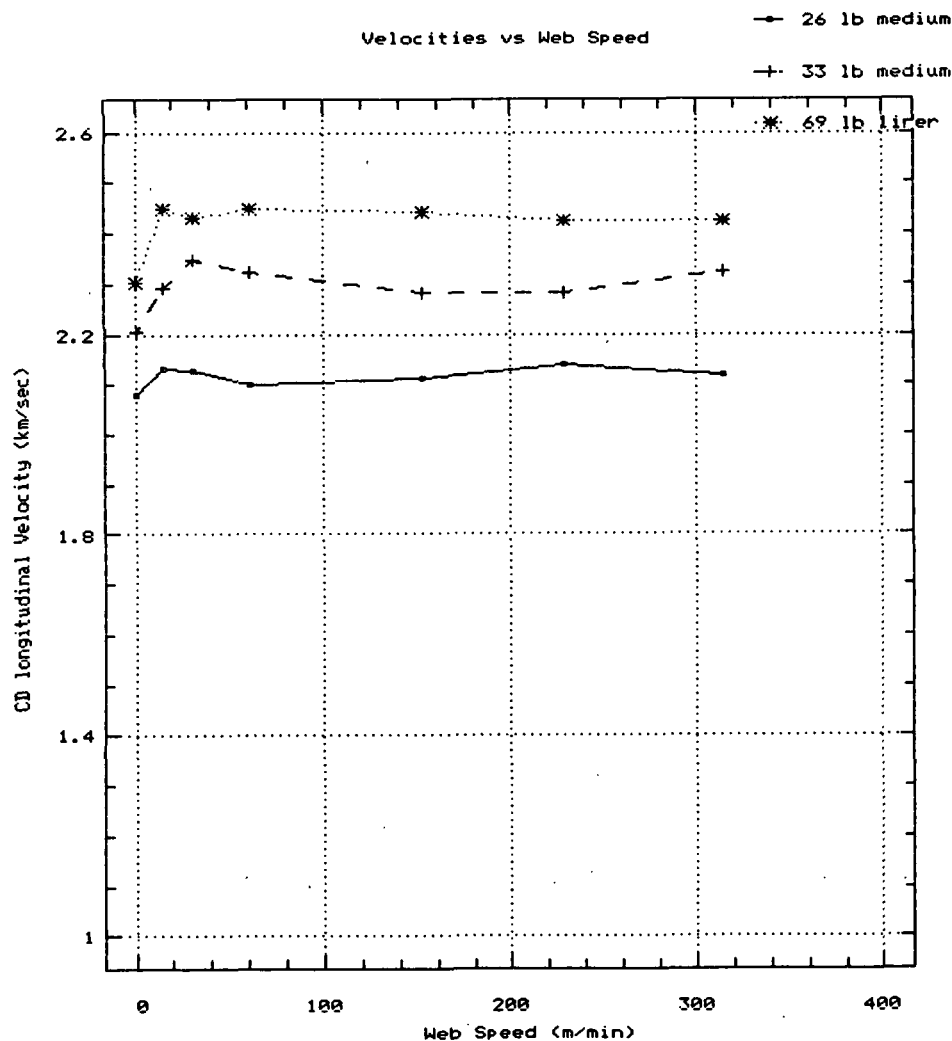
Figure 11. On-line bimorph CD longitudinal velocities versus
             web speed.

system reproduces the two-transducer results. The on-line results are a little higher (probably due to transducer mismatchings), but the rankings are maintained and the results are remarkably independent of web speed.
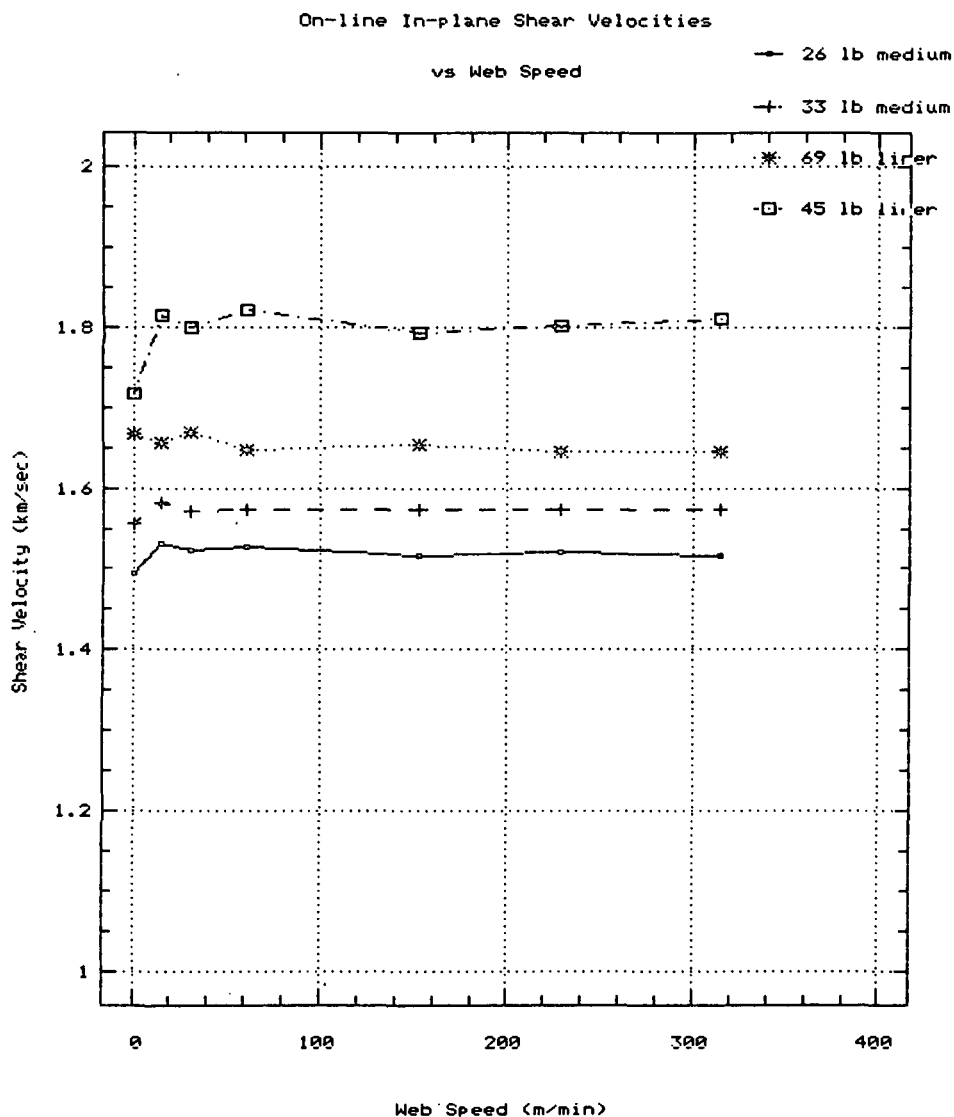
Figure 12. On-line bimorph shear velocities versus web speed.

APPENDIX

AUTOMATED MEASUREMENTS OF OUT-OF-PLANE, ULTRASONIC ELASTIC
  STIFFNESSES IN PAPER*

C. C. Habeger, W. A. Wink, and M. L. Van Zummeren
The Institute of Paper Chemistry
Appleton, WI 54912

ABSTRACT

The main purpose of this article is to introduce a new instrument which pro-
files the caliper and out-of-plane, longitudinal velocity of ultrasound in
paper. The instrument employs wheel transducers that are uniformly active over
their circumference. They use PVDF piezoelectric films for transduction and
have soft neoprene front-faces for effective coupling to paper. Instruments
that use flat disk transducers for measuring out-of-plane shear and longitudinal
velocities are also discussed. All three instruments are automated and
computer-controlled. The results from the rotary instrument are shown to com-
pare well with the system using longitudinal flat transducers when equivalent
loads are chosen.

BACKGROUND

In this article we will discuss three different elastic stiffnesses of
paper which involve the out-of-plane direction (or ZD). They are the ZD longi-
tudinal stiffness (C_{33}), the shear stiffness (C_{55}) in the plane determined by
the machine direction (or MD) and the ZD, and the shear stiffness (C_{44}) in the
plane of the cross-machine direction (or CD) and the ZD. The ZD longitudinal
stiffness is the ratio of ZD stress to ZD strain when no strain is permitted in
the MD or the CD. This is a few percent greater than the ZD Young's modulus,
which is the ratio of stress to strain in the absence of in-plane stresses. The
shear ZD stiffnesses are identical to the ZD shear moduli. These three ZD

elastic parameters will be calculated from measurements of the velocities of a bulk longitudinal and two shear waves (one polarized in the MD and one in the CD) traveling in the ZD. The square of an ultrasound bulk velocity is equal to the corresponding elastic stiffness divided by the apparent density. Therefore, the quantities actually measured are the square roots of the "mass specific elastic stiffnesses". These measurements are made at frequencies of about 1 MHz. Since paper is a viscoelastic material, its mechanical properties depend on test frequency, and the ultrasonic stiffnesses are greater than would be determined in other experiments having longer time constants. The difference is on the order of 20-40% when compared with a 1 Hz (or approximately one second duration) test at standard conditions.

The degree of fiber to fiber bonding and the amount of ZD fiber orientation are the most important factors influencing the ZD stiffnesses. Since the preponderance of fibers in a sheet of paper are nearly oriented in the MD-CD plane, the ZD stiffnesses are roughly two orders of magnitude lower than the in-plane stiffnesses. In machine made papers, C_{55} is significantly larger than C_{44}, and the ZD anisotropy ratio, C_{55}/C_{44}, is roughly equal to the square root of the in-plane stiffness ratio, C_{11}/C_{22}. As compared to in-plane properties, the ZD stiffnesses exhibit greater dependence on manufacturing process variations and are more sensitive to the moisture and temperature at test. It has been observed that the ZD stiffnesses increase upon refining and wet pressing[1,2] and fall when wet straining[1], calendering[3], or supercalendering[4] are performed. In addition, furnish[5] and yield[2] are known to affect ZD stiffnesses. It has also been demonstrated that ZD stiffnesses can be useful as nondestructive indicators of strength properties. For example, the ZD longitudinal stiffness of single ply sheets correlates with ZD tensile strength[1], ZD stiffnesses are important in

modeling the in-plane compressive strength[5] of paperboard, and ZD longitudinal
stiffness correlates with the retention of medium compressive strength during
corrugation[6].

INTRODUCTION

Time-of-flight, ZD, ultrasound velocity calculations in paper are made by
measuring the caliper and dividing by the transit time of an ultrasonic pulse
through a sample, which is placed between a transmitter and receiver. There are
published reports of the basic approach[7,8,9,10] for making ZD measurements in
paper. The purpose of this paper is to discuss the advantages of three newly-
developed instruments. These instruments incorporate computer control to
improve measurement accuracy and repeatability, to reduce testing time, and to
provide automatic reporting of results. For the longitudinal measurement, they
also employ specially developed ultrasonic transducers which are made with a
plastic piezoelectric film. These transducers provide greater bandwidth and are
more efficient at coupling acoustic energy into paper. The fundamental dif-
ference between the instruments is that two use flat longitudinal or flat shear
transducers and require an operator to manually present the paper to the trans-
ducers, while the third has motor-driven, longitudinal, wheel transducers that
automatically sample the specimen. The method of construction of the flat,
longitudinal transducers has been reported elsewhere[11]. Nevertheless, we
briefly describe it as an aid to understanding the rotary transducers, which
are discussed for the first time.

The paper begins with a discussion of what we feel are the important con-
siderations in the design of ultrasonic transducers for ZD coupling to paper.
The three types of transducers are then described: the flat longitudinal trans-
ducers are reviewed; the proprietary, flat shear transducers are very briefly

discussed; and the rotary longitudinal transducers are presented in detail. The mechanics of the ZD instruments are described. This is followed with an explanation of the electronics and the operations of the instruments. All through the presentation, the features of the rotary instrument are stressed, while the other two are mentioned only when they are significantly different. The final topic is a comparison of the results obtained from the flat and rotary longitudinal instruments.

DESIGN CONSIDERATIONS

The transducers are the critical components of the ZD velocity instruments. For optimum transfer of mechanical energy into paper, they should conform perfectly to the paper surface and have the same mechanical impedance as the appropriate ZD wave in the sample. The impedance is equal to the density of the material times the sound velocity, or, since the velocity is the square root of stiffness divided by density, the impedance can be expressed as the square root of the stiffness times the density. For smooth, perfectly bonded surfaces, the ratio of transmitted to incident energy is

$$TE = 4Z_1Z_2/(Z_1+Z_2)^2, \tag{1}$$

where Z_1 and Z_2 are the impedances of the two materials. The value of TE is maximum if $Z_1 = Z_2$. Paper has very low ZD stiffnesses and ZD impedances, and it is not feasible to build broadband transducers that have impedances as low as those found in paper. Therefore, the transducers should be designed to have the smallest possible impedances. In the limit that one material has the much larger impedance, TE from Equation 1 becomes proportional to the impedance ratio, and the coupling efficiency varies as the inverse of the impedance of the higher impedance material.

Equation 1 gives the optimum energy transfer for perfectly bonded materials. Poorly coupled surfaces can result in greatly degraded transmission. Good acoustic bonding is normally achieved through epoxy or viscous fluid interfaces. These procedures, however, are unacceptable for paper applications since they grossly alter the mechanical properties of paper and since they render a potentially nondestructive measurement destructive. Ultrasonic transducers for ZD testing in paper should have the lowest feasible impedance and should couple to rough paper surfaces without altering the sample properties.

Another important consideration in transducer design is the duration of the ultrasonic pulse. In time-of-flight velocity determinations, the measured transit time of a pulse is used to calculate the velocity. The time resolution of the pulse improves as it narrows. Ideally, the pulse width would be much shorter than the transit time through the sample. However, the fibrous structure of paper places a lower limit on the pulse width. In a heterogeneous material, scattering severely attenuates and disperses the signal when the pulse width approaches the transit time through the structural elements. This means that the effective wave length of the pulse in paper must be greater than the scale of heterogeneity (roughly the fiber width). The ratio of transit time to pulse width therefore must be considerably less than the caliper divided by fiber width. In addition, the pulse width is limited on the high end by the transit time through the sample. If the pulse width is greater than twice the transit time, a secondary pulse, resulting from reflections at the transducer-sample interfaces, will interfere with the main pulse. This will make it difficult to resolve the main pulse, and it will result in an arbitrarily low calculated velocity. So, there are conflicting requirements on the pulse width; it must fall between the transit times through the fiber width and through the sample.

Another way of reaching the same conclusion is to realize that ultrasonic stiffness determinations assume a homogeneous material and, if the approach is to be valid, there must be some wavelength, intermediate between the fiber width and sample caliper, at which the material appears homogeneous. This, of course, means that there are fundamental reasons that measurements become suspect on thin papers, and care must be taken in interpreting the results.

For most paper samples, scattering of ZD ultrasonic energy becomes prohibitive at frequencies above 2 MHz. Therefore, we have chosen to make our measurements with a pulse width of about 1.0 μsec as a compromise between good resolution and good signal to noise ratio. In order to produce and receive discrete pulses of this duration, the transducers should be broadband as well as sensitive in the megahertz frequency regime. Broadband transducers have flat frequency responses, and they can faithfully convert between mechanical and electrical energies without signal distortion. They do not have resonances which lead to oscillations that increase the pulse width. In summary, the objectives in designing ultrasonic transducers for ZD operation in paper is that they are low impedance, are broadband and sensitive in the megahertz frequency range, and can couple ultrasonic energy efficiently without altering the properties of the paper. As will be demonstrated below, we accomplished this by (1) using a high loss, low impedance plastic piezoelectric rather than a standard ceramic piezoelectric, (2) carefully designing the transducers to avoid any resonances near 1 MHz, and (3) coupling longitudinal waves into the paper through soft neoprene.

FLAT, LONGITUDINAL TRANSDUCERS

The construction of the flat longitudinal transducers is diagrammed in Figure 1. The piezoelectric elements are 110 μm thick polyvinylidene fluoride

(PVDF or Kynar) films. They are bonded together in stacks either two or four layers deep. The active electrode of the transducer is connected to the stack center, while the outer surfaces are grounded. Films on either side of the center electrode are stacked with opposite polarity so that all films act in unison. The stack is bonded to a cylinder of unpolarized Kynar. This aids in the production of broadband transducers by providing a good impedance match, which reduces reflections off the back-side of the stack. The Kynar is also a good absorber of ultrasonic energy and helps to mechanically isolate the films from the transducer housings. The other side of the stack is bonded to a layer of polystyrene. Polystyrene is a plastic with low ultrasonic attenuation and of intermediate impedance between the Kynar and the neoprene front-face, which is attached to the top face of the polystyrene. Lateral expansion of the neoprene disk is restrained by a tightly fitting brass ring that is acoustically isolated from the transducer body by a thin layer of cork. A comprehensive description of the transducer construction is provided elsewhere[11].

Figure 1 here

The transit time of ultrasound waves through the polystyrene and neoprene layers is considerably greater than 1 μsec. This ensures that multiple reflections through these materials do not interfere with the main pulse. The impedances of the Kynar film, polystyrene, and neoprene are, respectively, about 3.8, 2.5, and 1.6 kg/m^2s. The ZD impedances of paper are about an order of magnitude lower than these values; however, these PVDF transducers provide a significantly better impedance match than do standard ceramic piezoelectric elements which have impedances of about 25 kg/m^2s. The purpose of the soft neoprene is to conform to the rough paper surfaces so that reasonable caliper

values[12] and good ultrasonic coupling are obtained. The benefits and limitations of neoprene coupling and the effects of loading pressure are discussed extensively in the previous publication[11]. At a loading pressure of 50 kPa, energy is efficiently coupled into paper, and the errors in velocity calculations resulting from imperfect coupling are very small.

The performance of the transducers can be judged by examining the C.R.T. traces depicted in Figure 2. These represent signals from receiver transducers that are coupled at 50 kPa loading pressure through a thin aluminum foil sample to identical transmitters that are pulsed with a 1.5 MHz single-cycle sine wave. In order to get an expanded view of the main pulses, the oscilloscope is operated in a delayed mode with the traces starting about 12 μsec after the transmitters are pulsed. The time base of the expanded traces is 182 nanoseconds per division. The two traces are generated by using two different transducer pairs. The bottom trace was obtained from transducers built with four layer stacks of 110 μm thick standard PVDF piezoelectric film from Pennwalt corporation, while two layer stacks of an experimental PVDF copolymer film (also from Pennwalt) were used for the top trace. The oscilloscope gain is twice as great for the bottom trace. Notice that in both cases narrow, well-defined pulses of about a microsecond duration were achieved. The copolymer stack gives significantly improved performance in that a higher amplitude, shorter duration signal is realized.

Figure 2 here

SHEAR TRANSDUCERS

The transducers used for ZD shear velocity measurements were custom-made by Ultran Laboratories, and the method of their construction is proprietary.

Instead of coupling longitudinal waves into the sample, motion is polarized per-
pendicular to the direction of propagation. Two different ZD shear modes can be
produced by orienting the direction of polarization in the MD or CD. These
transducers are low-impedance and broadband. The received pulse, observed under
the conditions described for Figure 2, are similar to those shown in Figure 2.
Since elastomers do not propagate shear waves, neoprene front-faces are not
helpful. Polystyrene front-faces are used here, and coupling to paper samples
is less effective. Signal to noise ratios are lower in heavier samples, and
more care must be taken to avoid measurement anomalies arising from surface
roughness[10,11].

ROTARY, LONGITUDINAL TRANSDUCERS

The wheel transducers are intended to replicate in a rotary instrument,
which drives the sample through the nip between the wheels and tests at discrete
intervals, the performance of the flat, longitudinal transducers. Fabrication
of these wheels introduced some new challenges. For proper ultrasonic coupling,
it is mandatory that all transducer interfaces are uniformly bonded with thin
layers of epoxy or fluid couplants. We found this difficult to accomplish at
the film interfaces and at the Kynar-neoprene boundary in the cylindrical
geometry needed for the wheels. As one might expect, we were unsuccessful in
developing a straightforward technique of uniformly bonding PVDF film strips
between plastic cores and rings to produce transducer wheels. We were success-
ful, however, at coupling the films with small amounts of silicone grease and
fitting an undersized plastic ring over a plastic core wrapped with the film
layers. Adhering a neoprene belt uniformly to the circumference of a wheel pre-
sented another set of special difficulties. We overcame these by constructing a
fixture that, by the application of negative or positive gage air pressure,

could expand or contract the diameter of the neoprene belt. During assembly, adhesive is applied to the rim of the wheel; the neoprene belt is expanded and placed around the rim; the belt is contracted; and the adhesive is allowed to set.

Fabrication of a transducer wheel begins with the construction of the plastic core and ring between which the PVDF films will be secured. The core, which provides the transducer back-face, is a 2.54 cm thick, 7.145 cm diameter Kynar disk. In order to accomplish later steps in the assembly, a mandrel is pressed into a hole in the center of the core. The 2.54 cm thick ring has a 7.188 cm inside diameter and a roughly 8.25 cm outside diameter. It is also made of Kynar. Better sensitivity would be realized with a polystyrene ring. However, since polystyrene is brittle and its thermal expansion coefficient is well below that of Kynar, transducers made of Kynar and polystyrene have an annoying tendency to fracture. A Kynar ring does not provide as good an impedance match to the neoprene, and it dissipates some ultrasonic energy. Nonetheless, the assembled structure is tough and tight, and it is not destroyed when thermally cycled.

The 110 μm thick PVDF films must be carefully cut to ensure that when each film is wrapped on the core its ends will touch but not overlap. The first of the four films is cut so that its ends are butted when wrapped inside the Kynar ring. The second film is slightly shorter; its ends meet when wrapped inside the ring and the first film. The third and fourth films are likewise each slightly shorter. Electrical contact to the film interfaces is accomplished with number 36 copper wires. The ends of these wires are flattened to a thickness of 12 μm by placing them between smooth, hardened steel surfaces under load in a press and striking the loaded assembly once with a heavy hammer.

Assembly begins by metering a thin, uniform layer of silicone grease to one side of each PVDF film. The first and second films are greased on the positive polarity side, while the third and fourth films are greased on the negative side. A small amount of silicone grease is also applied to the core at three locations, 120 degrees apart on the periphery. At each location, a flat end of a copper wire is fixed. The fourth strip is wrapped around the core with the greased side facing inward, and the third strip is wrapped around the fourth, greased side also in. The flat ends of three copper wires are placed on deposits of grease applied at 120 degree intervals around the third film. The second and first films are then wrapped around the core with greased side facing inward. The film butt joints and the electrode wires present small defects in the structure. During assembly, care was taken to maintain even spacing between these imperfections. A specially designed "compression fixture" is used to expel excess grease from the interfaces. The core and compression fixture are placed in a sealed polyethylene bag and stored in a freezer for twelve hours. The Kynar ring is greased uniformly, and the flat ends of copper wires are applied at 120 degree separations. The ring with wires is heated in an 80°C oven for two hours. The cold core must be inserted inside the hot ring as rapidly as possible. First, the ring is placed on a flat surface. The core is removed from the compression fixture and placed over the ring. A Teflon plate is set upon the core, and the core is pressed into the ring. A 20 pound weight is rested on the plate and left for 24 hours.

The wheel is then mounted in a lathe and machined to an outer diameter of 8.09 cm. The front-face is a 25.09 cm taper-cut strip from a 0.318 cm thick, 4.13 cm wide section of 5-10 durometer soft neoprene, manufactured by Crane Packing Co. The ends of the strip are cleaned with a Freon TA solvent and

bonded together with a thin layer of Armstrong 520 adhesive that has been
diluted with xylene. The outer edges of the neoprene belt are glued to the fix-
ture which was designed to uniformly apply the belt to the core. The fixture is
centered and held by a plate mounted in the tail stock of the lathe. Vacuum is
applied to the fixture, and the diameter of the belt expands. The transducer
assembly is turned in the lathe, and a doctor blade meters a 0.02 cm layer of
Loctite Black Max adhesive to its circumference. The doctor blade is quickly
removed, and the rotation of the transducer assembly is halted. The wheel on
the tail stock is turned, and the neoprene belt is centered over the transducer
assembly. Vacuum is released from the fixture. Pressure is applied and held
for three hours. The edges of the neoprene are cut to remove the wheel from the
fixture. A surgical blade is cemented to a blank lathe cutting tool supported
by the tool holder of the lathe. With the wheel rotating, the blade is slowly
turned into the neoprene, and a 2.54 cm wide neoprene front-face with smooth,
right angle cuts is produced. The three wires from the stack center are
soldered to a single lead wire, as are the six exterior ground wires.
Construction of the wheel is completed by replacing the mandrel with a shaft and
by attaching aluminum sidewalls that house the wheel and restrain the lateral
expansion of the neoprene. The two lead wires are threaded through a hole in
the shaft and connected to terminals on a mercury slip ring attached to the end
of the shaft. Precision deep-groove radial ball bearings are press fit on each
side of the shaft so that the wheel can be securely supported in stationary
yokes. Due to the irregularity of the neoprene, the diameters of these wheels
vary about 40 µm around their circumferences. When coupled together and
rotated, there is less than a 10% variation in signal strength.

MECHANICAL APPARATUS

The mechanical mounting apparatus, electronic instrumentation, and measurement procedures are similar for the three instruments. However, the rotary instrument is necessarily more complicated. Therefore, we will describe its operation in detail and point out differences in the other systems when appropriate.

A drawing of the mechanics of the rotary instrument is presented in Figure 3. The mounting for the wheels is similar to the paper caliper instrument developed by Hardacker[13]. The yoke for one wheel transducer is attached to the anvil of the caliper gage, while the other is bolted to the pressure foot. A Daedal (model 4801) linear motion ball-slide allows the pressure foot low-friction vertical motion, while at the same time providing rigid horizontal restraint. In the original caliper gage[13] and in the two flat transducer instruments, the same functions are achieved with graphite pistons that slide in a precision-bore glass tube. The ball-slide was used in the rotary device since we felt it could better deal with the extra stresses encountered in rotation. The core of a linear variable differential transformer, attached to the slide, moves vertically in a fixed L.V.D.T. coil as the pressure foot rises and falls. This generates an electrical signal that is proportional to the displacement of the upper wheel. The shaft of the bottom wheel is driven by a computer-controlled stepping motor. There is a mechanism that, when manually engaged, rotates the wheels until the splices in the neoprene front-faces are aligned. The two flat transducer gages do not have stepping motors or alignment mechanisms, but they instead are equipped with a computer-controlled motor that raises and lowers the pressure foot.

Figure 3 here

ELECTRONIC INSTRUMENTS

Figure 4 is a representation of the electronics used in the rotary instrument. A Superior Electric model MO63 stepping motor drives the lower wheel. It is regulated by a Superior Electric 230 PTO motor controller, which receives instructions over digital I/O lines from the PC class AT computer. The L.V.D.T. and amplifier are identical to the one described by Hardacker[13]. The signal from the L.V.D.T. amplifier goes to an H.P. 3487A Multimeter. This is used as a high speed (up to 50 samples/second) digital voltmeter. It communicates the elevation of the upper wheel to the computer over a GPIB bus.

Figure 4 here

The upper wheel performs the function of ultrasonic transmitter. The drive signal (a 1.5 MHz, single-cycle, sine wave) originates from a Wavetek model 143 function generator. This signal is amplified to 100 volts by a E.N.I. model 2401 R.F. power amplifier and applied to the wheel through mercury slip rings. An ultrasonic wave then propagates through the specimen, and an electric signal is created in the lower wheel. This signal passes through mercury slip rings to a Panametrics 5050AE ultrasonic preamplifier, which is set to a gain of 60 dB. The output of the preamplifier goes to a LeCroy 6103 variable gain amplifier which is the front end of the LeCroy 8013A transient recorder. The gain of the 6103 amplifier is adjusted by the computer in order to take full advantage of the 8 bit resolution of the transient recorder. Under computer direction, the transient recorder performs 8192 eight bit analog to digital conversions at a 100 MHz sampling rate. Upon request, it transmits the results over a GPIB bus to the computer.

Capture of an ultrasonic signal begins when the computer instructs the transient recorder to digitize a receiver signal. As the acquisition starts, a trigger output from the transient recorder activates the emission of a pulse by the function generator. The transmitter is then fired and the resulting ultrasonic signal is received, amplified, and digitized. The signal is then transferred to the computer over the GPIB bus. This process is repeated an adjustable number of times with the computer digitally averaging the results. The other two systems use a different digitizer (an H.P. 1980A digital oscilloscope) and do not signal average, but the data gathering strategy is the same.

Figure 5 is a photograph of the rotary instrument and a C.R.T. display of an averaged signal produced when the wheels are directly coupled. Notice that there is a longer positive overshoot at the end of signal than observed in the Figure 2 traces with flat transducers. As a result, the pulse width is about 50% greater. There are two reasons for this: (1) the pressure is not uniform in the nip between the wheels, and there is a range of transit times; and (2) the wheels have a large capacitance (about 5000 pf) making it difficult for the power amplifier to supply the high frequency components of the pulse. The pulse is sufficiently short to produce a discrete pulse through most paperboard samples, but the rotary system cannot be used on some lower basis weight samples that are acceptable in the other instruments.

<div align="center">Figure 5 here</div>

TESTING PROCEDURE

Before samples can be tested a calibration is performed. After positioning the wheel with the alignment mechanism, the first step in the calibration

procedure is to place an 8 μm strip of aluminum foil in the nip and notify the computer. The computer feeds the foil though the nip in increments. The number of steps (usually about 10) and separation between steps (usually about 1 cm) are selected by the operator. Upon completion of each step, the computer allows the neoprene to settle for an operator chosen length of time (usually about 1 sec) and then reads the digital multimeter. Next, it fires the appropriate number of ultrasonic pulses and stores the average signal in memory. If the signal level is outside the optimum range for the transient recorder, the gain to the 6103 amplifier is adjusted, the wheels back off, and the test is repeated. The computer reads the multimeter again and stores the average of this value and the first reading. After the multimeter readings and ultrasonic signals are stored for all steps, the computer returns the wheels to the aligned position, backing the foil out of the nip in the process. Now, a thicker calibration sheet is presented to the wheels. It has a known caliper, somewhat greater than the thickest sample to be tested. This is stepped between the wheels and analyzed as before, but only the multimeter readings are recorded. The wheels again return to the aligned position and the calibration shim is retrieved.

Paper samples can now be profiled. A specimen is placed in the nip and analyzed in the same manner as the aluminum foil. The caliper at each position is determined by linear interpolation of the multimeter readings on the calibration standards at the same location. Using an optimization routine, the computer then determines the time which gives a maximum in the cross correlation function of the sample ultrasonic signal and the aluminum foil signal at the same position. The time-of-flight is this time minus a 10 nsec correction for the transit through the aluminum foil. The time-of-flight velocity is the caliper divided by the time-of-flight. The calipers, times-of-flight, and velocities, along

with their averages and standard deviations, are reported. A typical printout
for a linerboard sample is presented in Figure 6.

Figure 6 here

For operation of the flat transducer instruments, the computer controls a
motor that raises and lowers a pressure foot (rather than a stepping motor that
turns the wheels). Calibration is simplified since it is required only at one
position. In order to conduct a measurement, the computer lowers the pressure
foot and, after the prescribed time, takes multimeter readings and an ultrasonic
signal. The jaws part; the operator moves the sample; and the next position is
tested. Velocities are calculated in the same way, and a report, similar to
Figure 6, is generated.

COMPARISON OF ROTARY AND FLAT LONGITUDINAL INSTRUMENTS

The caliper and ZD ultrasound velocity of paper depend on the loading
pressure. Therefore, a standard measurement pressure must be chosen in order to
make valid comparisons between samples. We selected 50 kPa as the normal
pressure for the flat transducers, partly because it is the TAPPI standard value
for hard-platen caliper. The wheels, however, apply a distribution of loading
pressures across the nip, and results from the two instruments are not comple-
tely equivalent. Therefore, we tested a variety of paper samples at 50 kPa in
the flat longitudinal instrument and at different loads in the rotary instru-
ment. The load at which the comparison was best was taken as the standard for
the rotary instrument.

The results of this comparison are presented for neoprene-platen caliper in
Table 1 and for longitudinal ZD velocity in Table 2. The samples tested were a
42 lb/1000 ft^2 linerboard (A), a 69-lb linerboard (B), a 90-lb linerboard (C), a

26 lb/1000 ft^2 corrugating medium (D), a 40-lb medium (E), a 60-lb bleached
posterboard (F), a two-ply coated chipboard (G), a heavy wax-coated chipboard
(H), a 90-lb chipboard (I), and a 74 gm/m^2 bleached writing paper (J).
Disregarding sample (J) for the moment, notice that the comparisons for both
caliper and velocity are optimum at about 600 to 800 grams. At 600 grams, the
ratio of rotary to flat caliper is 0.999 ± 0.010, and the ratio of rotary to
flat velocity is 0.992 ± 0.022. The values at 800 grams are 0.995 ± 0.012 and
1.008 ± 0.024. The two loads give equally good comparisons; however, 800 grams
was chosen as the standard since it provided a stronger ultrasonic signal.

Tables 1 and 2 here

As mentioned earlier, in order to make valid time-of-flight measurements,
the pulse width must be short enough that a discrete signal, which has no inter-
ference from multiple reflections, is generated. This means that the pulse
width must be less than twice the caliper divided by the velocity. Since the
pulse width in the rotary instrument is larger, there are samples that can be
tested with the flat transducer, but not with the rotary ones. Sample J is such
a paper. It is barely in the valid regime for the flat transducers. Notice
that the rotary velocities are significantly lower for this sample. This is
because the interference from the first multiple reflection makes the pulse
appear to arrive later and causes the peak in the cross correlation function to
occur at a larger time.

CONCLUSIONS

The computer-controlled instruments described above provide a repeatable
measurement of paper caliper and, on sufficiently heavy sheets, of ZD ultrasound
velocity. When operated at the appropriate load, the flat and rotary instruments

agree well on caliper and longitudinal velocity. Because of improved
instrumentation and the elimination of the need for operator scanning, the
rotary device samples about twice as fast as the flat transducer model. Out-of-
plane elastic properties, which are important indicators of mechanical
integrity, can now be rapidly measured without damaging the sample.

In addition to being a valuable laboratory instrument, the rotary system
provides an opportunity to investigate, in a controlled manner, the influence of
dynamic phenomena on measurements of soft-platen caliper and ZD velocity. Belts
can be stepped through the nip at a constant rate, and measurements can be made
as a function of web speed. This will give guidance into the design of possible
on-line ZD ultrasonic velocity gages. Developments in this area will be
discussed in a later article.

REFERENCES

1. Fleischman, E. H., Baum, G. A., and Habeger, C. C., Tappi 65(10):115(1982).

2. Berger, B. F., and Baum, G. A., in The Eighth Fundamental Research
   Symposium held at Oxford, edited by V. Punton Mechanical Engineering
   Publications Limited: 339(1985).

3. Berger, B. J., Master's Thesis from The Institute of Paper Chemistry, 1985.

4. Charles, L. A., and Waterhouse, J. F., J. Pulp Paper Sci. (1988).

5. Habeger, C. C., and Whitsitt, W. J., Fibre Sci. Technol. 19(3):215(1983).

6. Whitsitt, W. J., and Baum, G. A., Tappi 70(4):107(1987).

7. Habeger, C. C., Mann, R. W., and Baum, G. A., Ultrasonics 17(2):57(1979).

8. Mann, R. W., Baum, G. A., and Habeger, C. C., Tappi 62(8):115(1979).

9. Mann, R. W., Baum, G. A., and Habeger, C. C., Tappi 63(2):163(1980).

10. Habeger, C. C., and Wink, W. A., J. Appl. Polymer Sci. 32:4503(1986).

11. Habeger, C. C., Wink, W. A., and Van Zummeren, M. L., J. Acoust. Soc. Am.
    Sept., 1988.

12. Wink, W. A., and Baum, G. A., Tappi 66(9):131(1983).

13. Hardacker, K. W., The Institute of Paper Chemistry, Technical Paper Series No. 138:(1984).

Table 1. A comparison between the calipers in microns of paper samples as measured with the flat transducer at 50 kPa and at different loads in the rotary instrument.

Sample	50 kPa	400 g	600 g	800 g	1000 g	1200 g
A	260.0	271.0	266.0	264.7	264.0	263.5
B	461.6	463.7	458.5	457.9	458.2	457.2
C	624.6	638.0	627.9	624.2	622.9	622.3
D	188.6	188.8	185.6	183.0	183.9	184.9
E	315.1	319.6	313.5	311.8	311.0	310.3
F	513.3	512.0	510.7	508.8	509.5	508.8
G	710.8	716.7	711.7	710.4	711.1	709.9
H	1109.6	1115.6	1113.2	1112.2	1114.7	1112.6
I	679.8	680.1	678.2	677.1	678.7	678.1
J	97.4	94.2	91.9	91.5	92.4	92.3

Table 2. A comparison between the ZD longitudinal velocities in km/s of paper samples measured with the flat transducers at 50 kPa and at different loads in the rotary instrument.

Sample	50 kPa	400 g	600 g	800 g	1000 g	1200 g
A	0.315	0.308	0.317	0.325	0.330	0.338
B	0.243	0.233	0.235	0.239	0.241	0.242
C	0.194	0.188	0.191	0.194	0.196	0.198
D	0.449	0.437	0.448	0.457	0.459	0.473
E	0.465	0.453	0.453	0.460	0.462	0.470
F	0.258	0.249	0.255	0.259	0.262	0.264
G	0.189	0.181	0.184	0.187	0.189	0.191
H	0.221	0.217	0.219	0.221	0.222	0.222
I	0.278	0.267	0.272	0.275	0.278	0.280
J	0.404	0.375	0.382	0.382	0.377	0.375
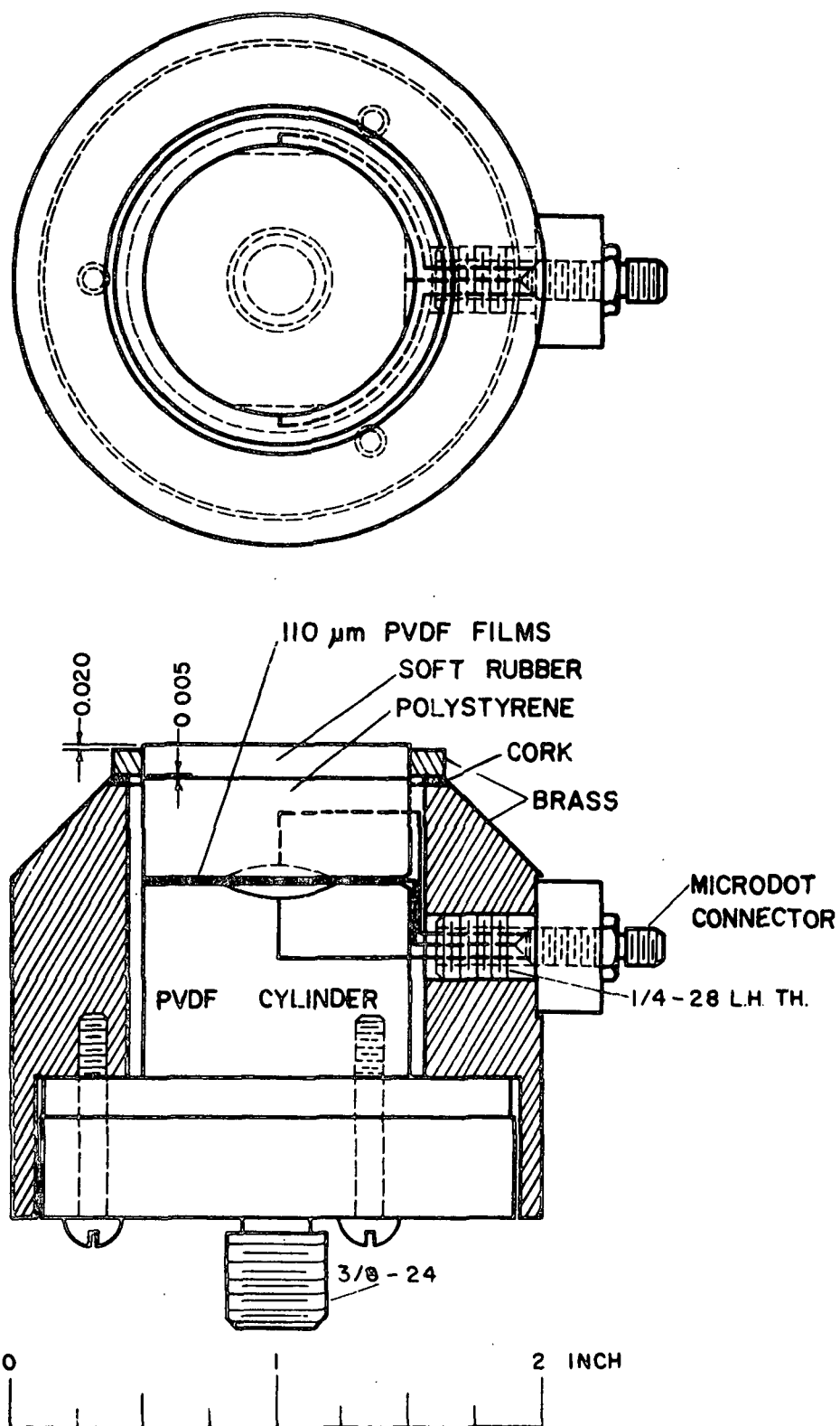
Figure 1.   A mechanical drawing of the flat longitudinal
            transsducers.
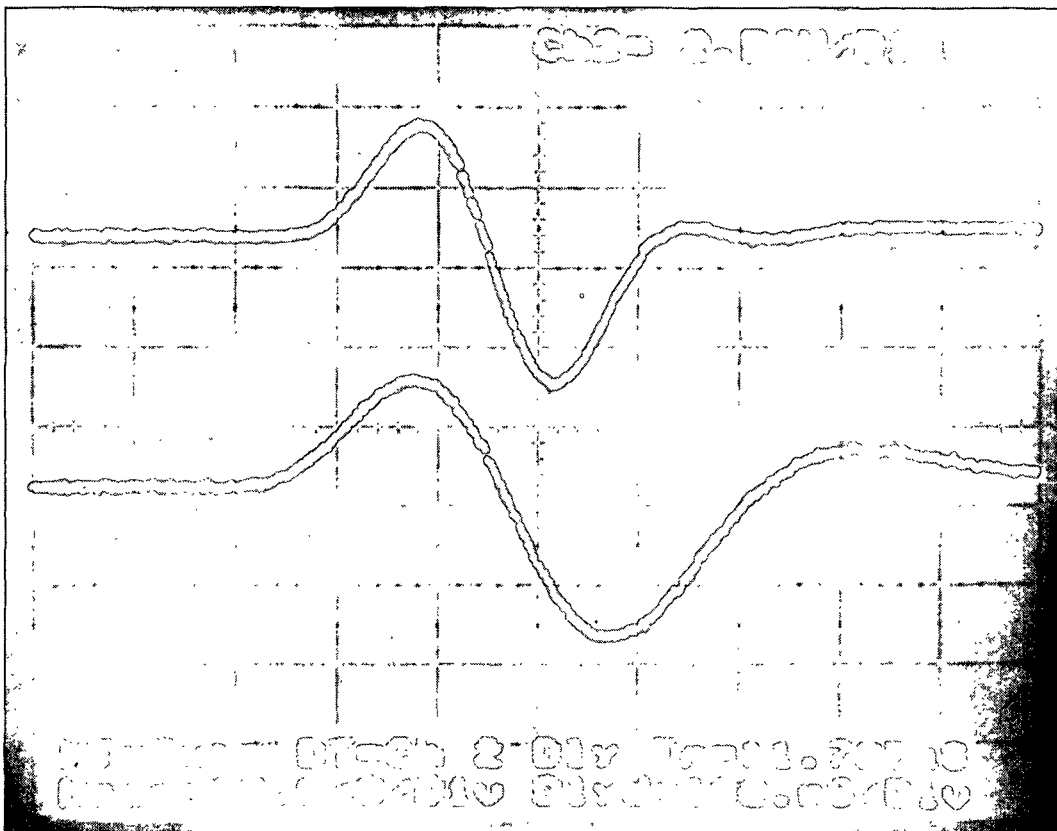
Figure 2. Oscilloscope traces of the signals resulting from
direct coupling between the copolymer PVDF and the
standard PVDF longitudinal transducers.

THICKNESS & 2D ULTRASONIC VELOCITY PROFILER

FRAME

BALL SLIDE

STEPPING MOTOR

TRANSMITTER

RECEIVER

DEAD WEIGHT

LVDT

COUNTER WEIGHT

ALIGNMENT MECHANISM
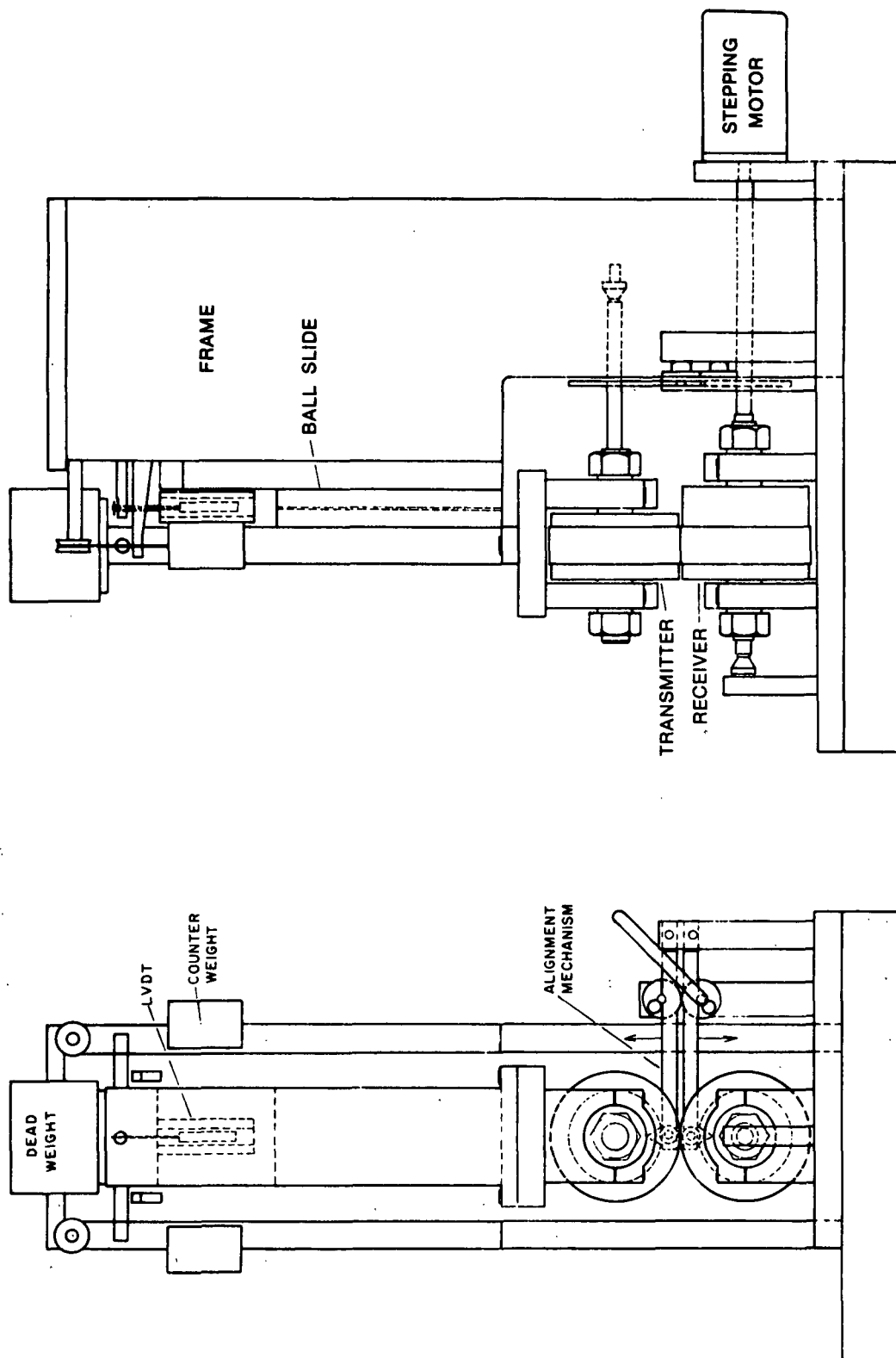
Figure 3.   A mechanical drawing of the rotary 2D ultrasound instrument.
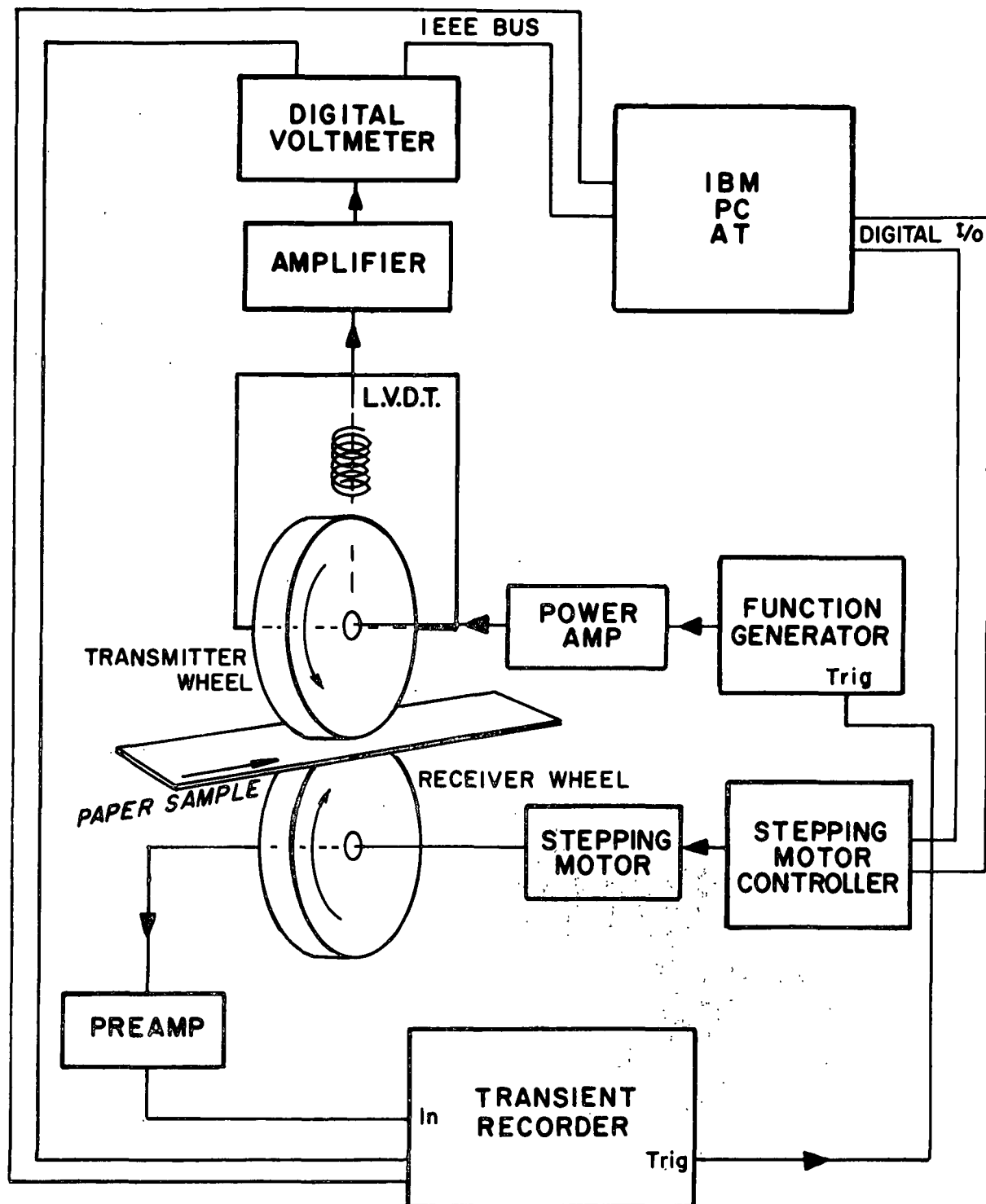
Figure 4. An operational schematic of the rotary ZD ultrasound instrument.
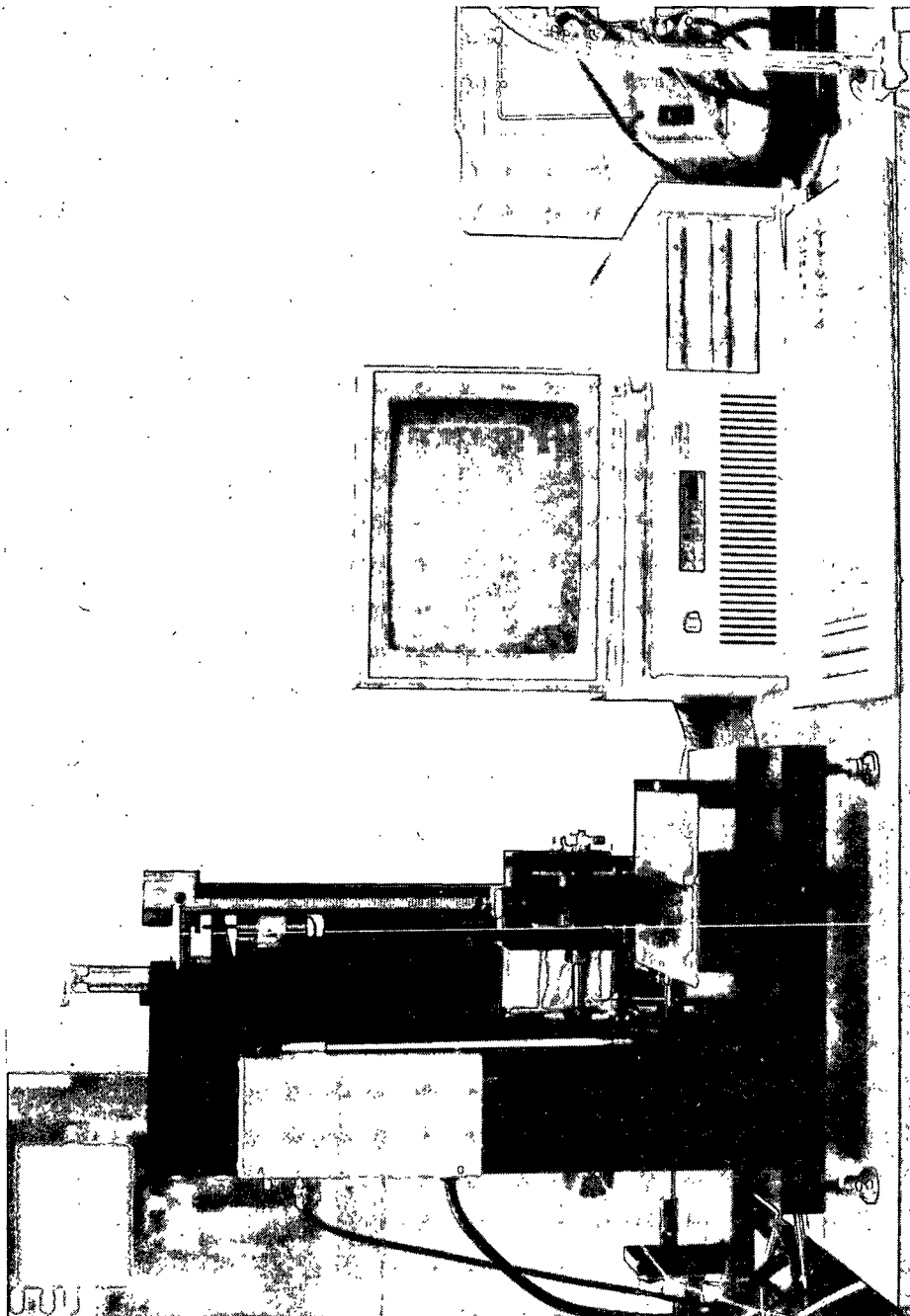
Figure 5. A photograph of the rotary ZD ultrasound instrument with a C.R.T. display of a direct coupled signal.

THE INSTITUTE OF PAPER CHEMISTRY
ROTARY ZD VELOCITY MEASUREMENT

OPERATOR: CCH
DATE: JUNE 28, 1988
TIME: 13:30:4

PROJECT: 3467
SAMPLE: liner board

TEST NUMBER	CALIPER (microns)	DELAY (micro sec)	VELOCITY (km/sec)	V SQR (km^2/sec^2)
1	309.1	1.2559	0.246	0.061
2	307.0	1.2965	0.237	0.056
3	305.3	1.2696	0.240	0.058
4	313.3	1.3180	0.238	0.056
5	311.2	1.3403	0.232	0.054
6	307.8	1.2925	0.238	0.057
7	307.1	1.3032	0.236	0.056
8	307.1	1.3224	0.232	0.054
9	304.7	1.3060	0.233	0.054
10	309.0	1.3132	0.235	0.055
AVERAGE	308.1	1.3018	0.237	0.056
STD DEV	2.6	0.0249	0.004	0.002

GRAMMAGE (g/m^2) =   209.00
DENSITY (g/cm^3) =   0.678
C33 (GPa)   =   0.038

V*RHO (E+6 kg/(sec*m^2)) =   0.161

STABILIZATION DELAY (secs)   =   1
THIN SHIM THICKNESS (microns)   =   8.0
THICK SHIM THICKNESS (microns)   =   793.0

REFERENCE CALIPER (microns)   =   8.00
INTEGRATION WINDOW   =   507
TEST INTERVAL   =   0.39
TEST INTERVALS CALIBRATED   =   10

TRANSMITTER - IPC#1; RECEIVER - IPC#2

Figure 6. A report generated by the rotary ZD ultrasound instrument
           for a linerboard sample.

S L I D E   M A T E R I A L

for the

PAPER PROPERTIES AND USES

PROJECT ADVISORY COMMITTEE

MEETING

October 19-20, 1988

The Institute of Paper Chemistry
Continuing Education Center
Appleton, Wisconsin

NOTICE & DISCLAIMER

SLIDE MATERIAL

PROJECT ADVISORY COMMITTEE
PAPER PROPERTIES AND USES

October 19-20, 1988

TABLE OF CONTENTS

SECTION 1

INTRODUCTION

PAPER PROPERTIES AND USES

PAPER MATERIALS DIVISION

COOPERATIVE RESEARCH

FUNDED RESEARCH

ACADEMIC/CONTINUING EDUCATION

TESTS AND ANALYSIS

CONSULTING

BRIGHTNESS STANDARDS

Acad/CE (14%)   T/A/C (18%)

Bright (7%)

Coop/Doe (29%)

Funded (32%)
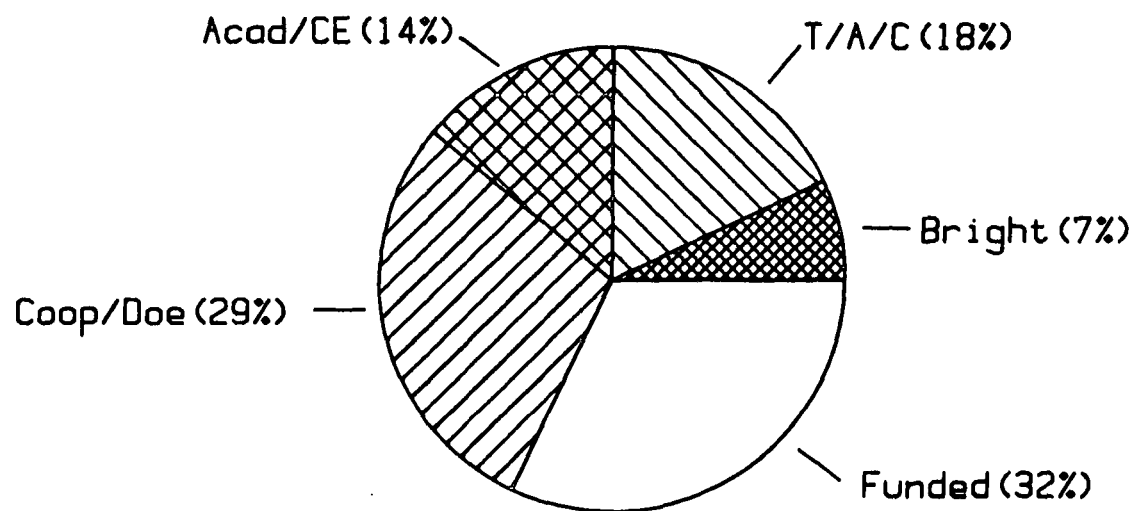
Div 10 Budget FY1988-89

1988

CONTINUING EDUCATION COURSES

COMPRESSION AND CONVERTING PROPERTIES OF BOARD

Bill Whitsitt -- May 24-26

PAPER PROPERTIES AND THEIR MEASUREMENT

John Waterhouse -- August 22-26

API

FOURDRINIER KRAFT BOARD GROUP

- LINER/MEDIUM BASELINE STUDIES

- HIGH-LOW MONITOR

- FRICTION TEST INSTRUMENTATION

- HIGH-SPEED SINGLE-FACE RUNNABILITY

- SINGLE-FACE BONDING

- DOUBLE-BACKER BONDING

- FLUTING OF HEAVYWEIGHT MEDIUMS

- PRINTABILITY OF LINERBOARD

AMERICAN PAPER INSTITUTE

MEASUREMENT TECHNOLOGY COMMITTEE

- FREENESS/DRAINAGE MEASUREMENTS

- FORMATION MEASUREMENTS

- NEW WORK

FUNDED RESEARCH

PAPER MATERIALS DIVISION

- BOARD PROPERTIES AND PERFORMANCE

- STRENGTH IMPROVEMENT AND FAILURE
  MECHANISMS

- PROCESS, PROPERTIES, PRODUCT
  RELATIONSHIPS

- INTERNAL STRENGTH ENHANCEMENT

- ON-MACHINE MEASUREMENTS

- FUNDAMENTALS OF SURFACE WETTABILITY

SECTION 2

Project 3469

STRENGTH IMPROVEMENT AND FAILURE MECHANISMS

STRENGTH IMPROVEMENT AND FAILURE MECHANISMS

COMPRESSIVE STRENGTH IMPROVEMENT

• FORMING LOSS REDUCTION BY SYNTHETIC FIBER
  AND POLYMER ADDITION

FIBER FURNISHES

FIBER SERIES 1

1. NSSC PULP

2. NSSC/KEVLAR "PULP" BLENDS

FIBER SERIES 2

1. NSSC PULP

1. NSSC PULP/KEVLAR STAPLE BLENDS

2. NSSC PULP/KEVLAR "PULP" BLENDS

3. NSSC PULP/1/4" GLASS FIBER BLENDS

4. NSSC PULP/1/8" GLASS FIBER BLENDS

BINDER SERIES 1

TYPE	T_g
A. CARBOXYLATED SBR	42°C
B. CARBOXYLATED SBR*	42°C
C. STYRENE LATEX	
D. STYRENE LATEX	105°C
E. SBR LATEX (99% STYRENE)	
F. SBR LATEX (85% STYRENE)	54°C

*Plasticized version of 1.

SUMMARY OF FORMETTE HANDSHEET PROPERTIES - SERIES 1

SHEET STRUCTURE AND FURNISH SERIES 1	GRAMMAGE g/m^2	APPARENT DENSITY, g/cm^3	IN-PLANE ANISOTROPY R	MEAN IN-PLANE CONSTANT E/ρ (km/sec)^2	OUT-OF-PLANE CONSTANT E_z/ρ (km/sec)^2
100 % NSSC	127	0.523	2.89	6.39	0.163
92% NSSC/ 8% Kevlar	132	0.467	2.77	5.36	0.127
20% (NSSC/Kev) 60% (NSSC) 20% (NSSC/Kev)	141	0.477	2.60	5.31	0.116
84% NSSC/ 16% Kevlar	133	0.439	2.55	4.89	0.100
20% (NSSC/Kev) 60% (NSSC) 20% (NSSC/Kev)	136	0.433	2.62	4.73	0.078

SUMMARY OF FORMETTE HANDSHEET PROPERTIES - SERIES 2

SHEET STRUCTURE AND FURNISH SERIES 1	GRAMMAGE g/m^2	APPARENT DENSITY, g/cm^3	IN-PLANE ANISOTROPY R	MEAN IN-PLANE CONSTANT E/ρ $(km/sec)^2$	OUT-OF-PLANE CONSTANT E_z/ρ $(km/sec)^2$
100 % NSSC	118	0.752	2.42	7.78	0.217
92% NSSC/ 8% Kev. Stap.	115	0.660	1.83	7.27	0.165
20% (NSSC/Kev. Stap.) 60% (NSSC) 20% (NSSC/Kev. Stap.)	114	0.644	1.99	7.24	0.135
92% NSSC/ 8% Kevlar Pulp	114	0.707	2.58	6.93	0.167
20% (NSSC/Kev. Pulp) 60% (NSSC) 20% (NSSC/Kev. Pulp)	118	0.679	2.35	6.54	0.122
92% NSSC/ 8% 1/4" glass	118	0.719	2.90	7.41	0.187
20% (NSSC/1/4" glass) 60% (NSSC) 20% (NSSC/1/4" glass)	119	0.692	2.69	7.27	0.147
92% NSSC/ 8% 1/8" glass	123	0.721	3.19	7.44	0.194
20% (NSSC/1/8" glass) 60% (NSSC) 20% (NSSC/1/8" glass)	119	0.702	3.11	7.27	0.156

The effect of synthetic fiber addition on the variation
of in-plane specific modulus with apparent density.
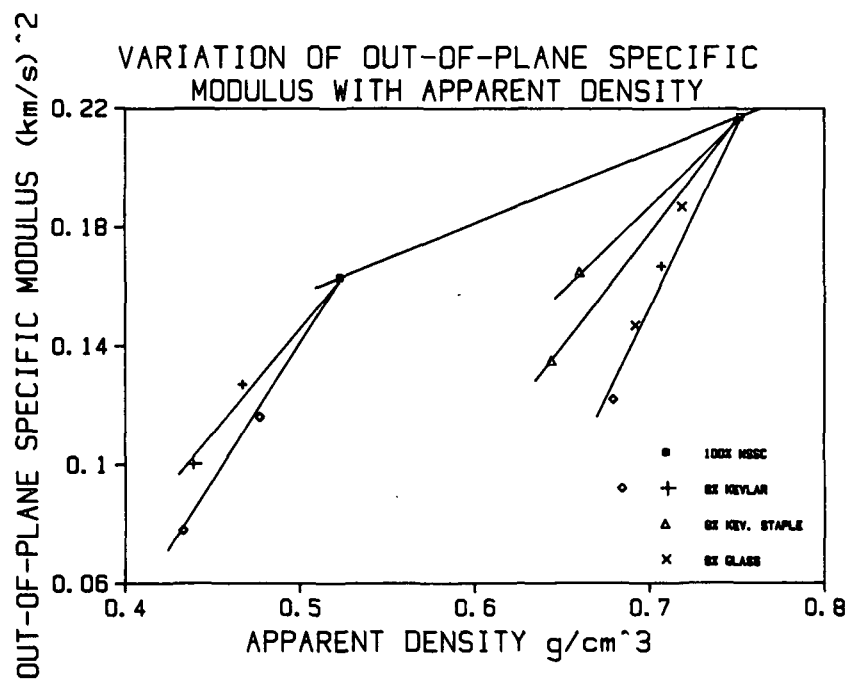
The effect of synthetic fiber addition on the variation
of out-of-plane specific modulus with apparent density.

EFFECT OF SATURATION AND DRYING RESTRAINT
ON SPECIFIC COMPRESSIVE STRENGTH

SAMPLE	COMP. STR. CONTROL Nm/g	COMP. STR. FREE DR. Nm/g	COMP. STR. REST. DR. Nm/g
100% NSSC	22.0	17.2	22.0
8% KEVLAR	17.4	13.6	-
KEVLAR-3 PLY 8%	19.6	14.7	18.4
16% KEVLAR	15.4	11.8	14.6
KEVLAR-3 PLY 16%	16.3	13.2	16.8

FIBER SERIES 1
SPECIFIC COMPRESSIVE STRENGTH Nm/g

FURNISH:	100% NSSC	8% KEV.P	3-PLY 8% KEV.P	16% KEV.P	3-PLY 16% KEV.P
Latex:					
A	25.9	21.7	20.8	19.7	21.3
B	23.8	20.7	21.7	19.6	20.5
C	22.7	19.7	19.3	19.2	18.9
D	22.2	18.2	18.2	16.1	18.9
E	22.4	-	19.9	17.3	18.6
F	25.7	-	21.8	19.5	20.7
H_2O	17.2	13.6	14.7	11.8	13.2

FORMING LOSS AS A FUNCTION OF POLYMER
TYPE FOR 100% NSSC PULP

FLAT CRUSH AS A FUNCTION OF POLYMER
TYPE FOR 100% NSSC PULP
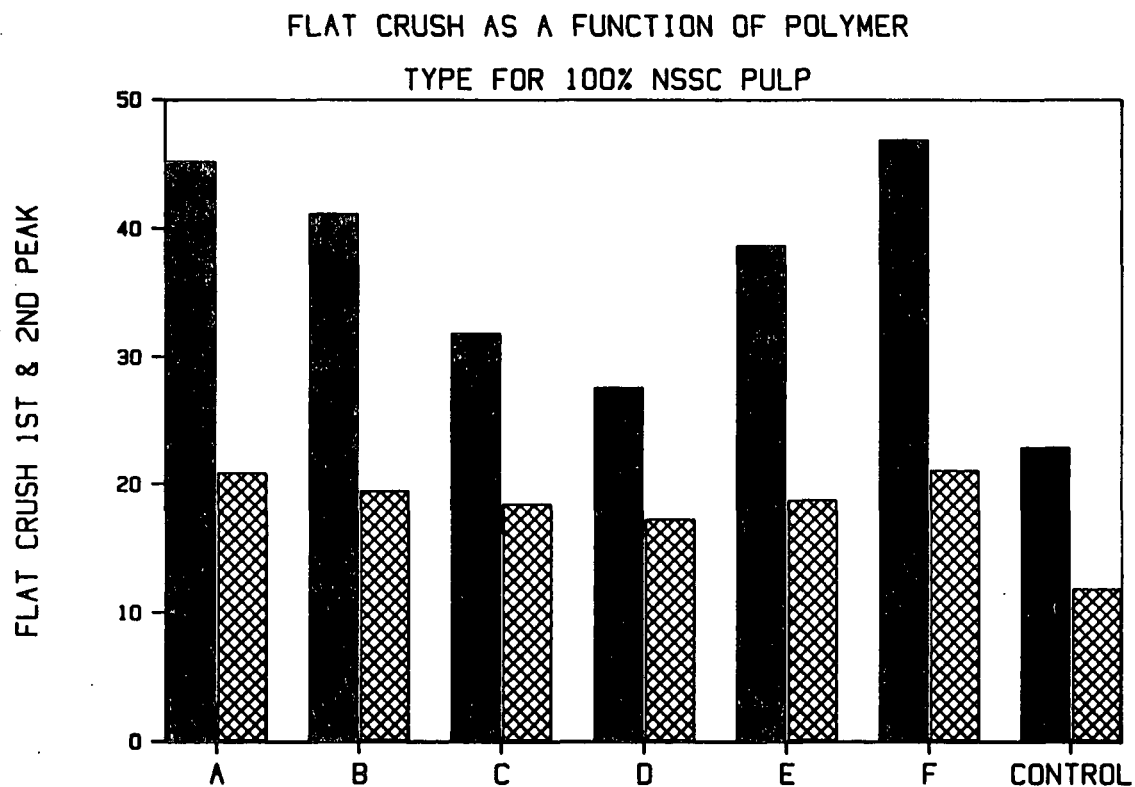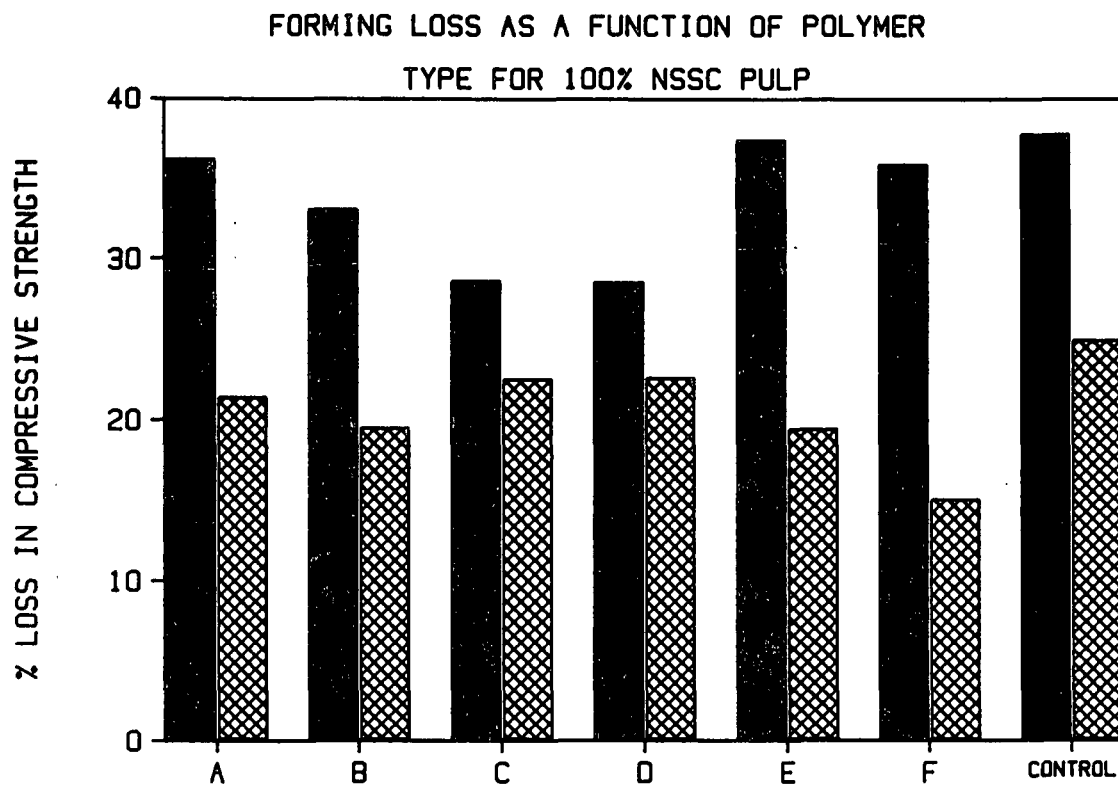
VARIATION OF FLAT CRUSH WITH
FLANK COMPRESSIVE ST. - 100% NSSC
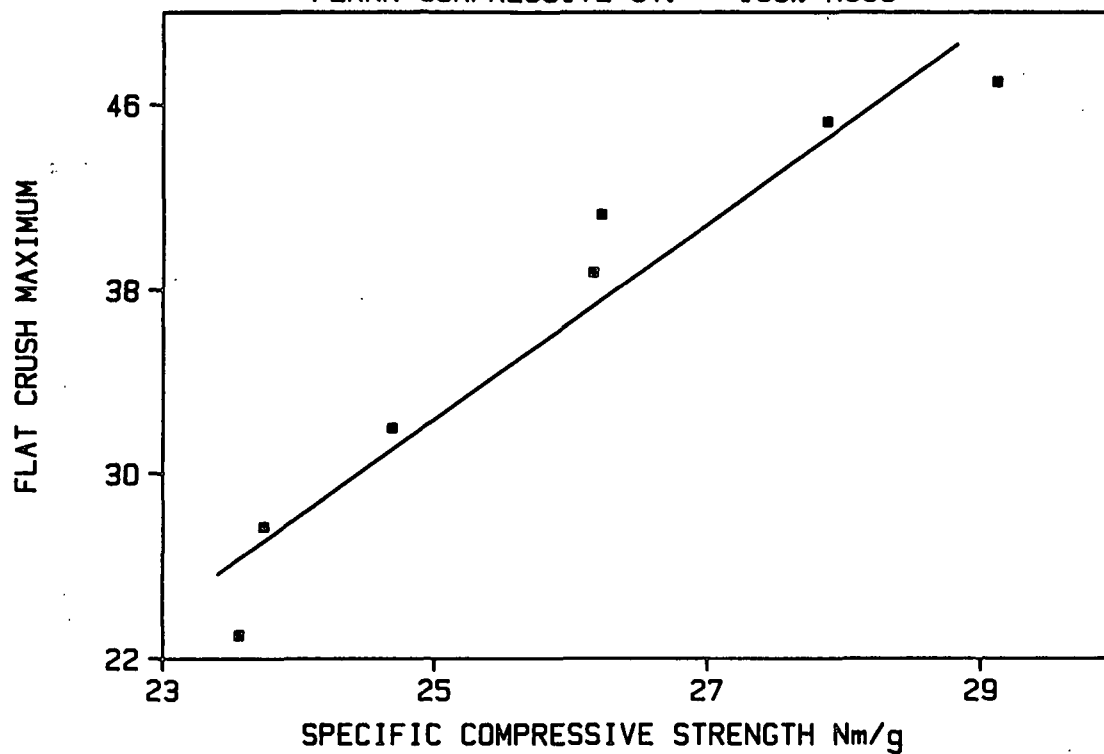
FIBER SERIES 2

SPECIFIC COMPRESSIVE STRENGTH Nm/g

FURNISH:	100% NSSC	8% KEV.S	3-PLY 8% KEV.S	8% KEV.P	3-PLY 8% KEV.P	8% 1/4" GLASS	3-PLY 8% 1/4" GLASS	8% 1/8" GLASS	3-PLY 8% 1/8" GLASS
Latex:									
A	30.3	27.1	27.4	27.5	27.5	30.1	28.3	29.8	29.4
B	32.0	27.3	27.3	29.5	27.4	29.8	28.0	29.6	29.1
C	26.2	23.8	23.3	23.4	23.9	25.2	25.3	25.6	25.2
D	29.3	24.8	23.7	25.0	24.8	26.6	25.1	26.3	24.3
E	29.3	25.7	25.4	25.8	25.6	26.7	26.2	26.4	26.7
F	32.2	27.1	27.1	29.0	28.0	32.2	27.9	30.0	30.2
H_2O	24.8*	20.7*	19.3	21.2*	20.8*	21.9	21.2	21.1	20.6

*Estimated

FIBER SERIES 2

ELASTIC ANISOTROPY R

FURNISH:	100% NSSC	8% KEV.S	3-PLY 8% KEV.S	8% KEV.P	3-PLY 8% KEV.P	8% 1/4" GLASS	3-PLY 8% 1/4" GLASS	8% 1/8" GLASS	3-PLY 8% 1/8" GLASS
Latex:									
A	2.97	1.95	2.01	3.00	2.66	3.63	3.41	3.67	3.71
B	3.21	1.88	2.10	2.91	2.65	3.51	3.59	3.96	3.43
C	3.18	2.04	2.09	3.11	2.89	3.39	3.27	3.91	3.16
D	3.19	2.13	2.19	3.16	2.87	3.43	3.59	4.20	3.42
E	2.63	1.94	1.98	2.99	2.74	3.32	3.16	3.74	3.51
F	3.08	1.96	2.03	2.77	2.69	3.38	3.18	3.40	3.35
H_2O	-	-	2.37	-	-	3.37	2.99	3.82	3.22
Control	2.42	1.83	1.99	2.58	2.35	8.90	2.69	3.19	3.11

FORMATION

AREAS OF FOCUS

* EFFECT OF PAPERMAKING VARIABLES ON FORMATION

* EFFECT OF MEASUREMENT VARIABLES

* MASS - OPTICAL DENSITY RELATIONSHIP

* FORMATION - OPTICAL PROPERTIES

* FORMATION - MECHANICAL PROPERTIES

* FORMATION - END USE PERFORMANCE
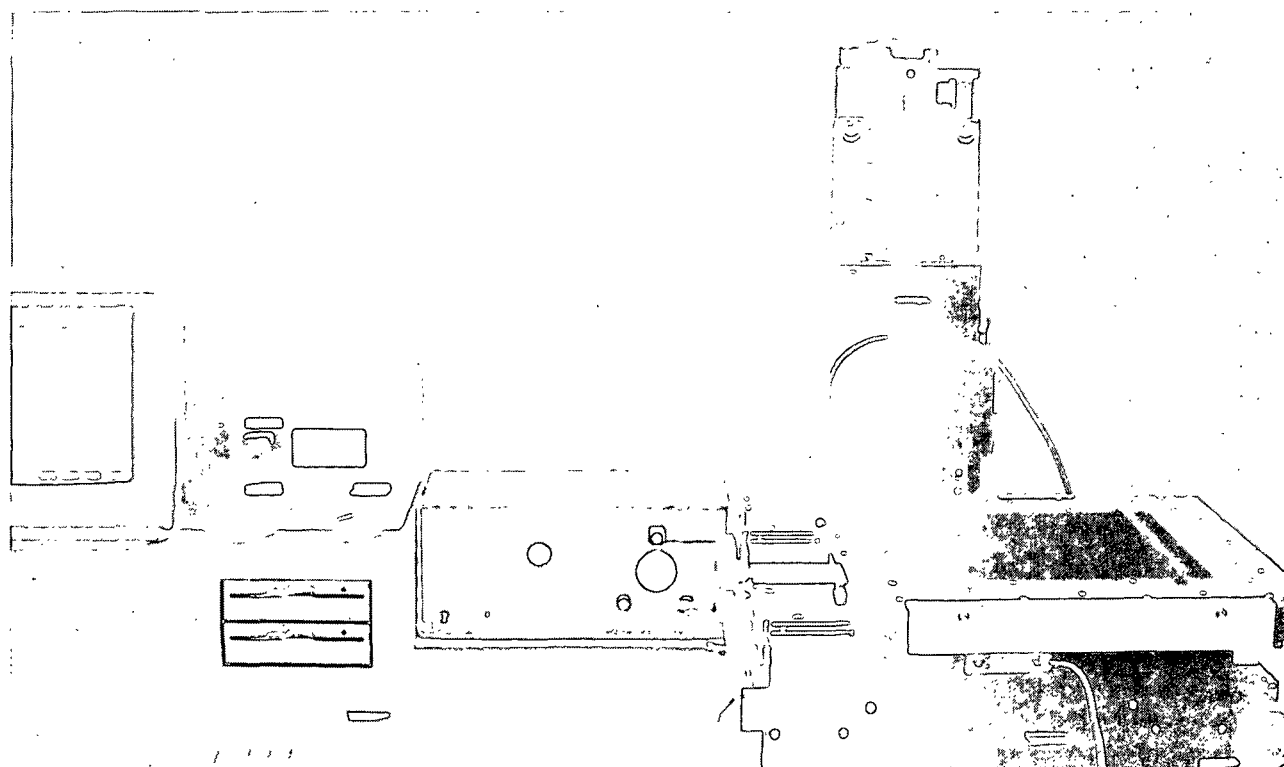
General view of IPC formation tester.
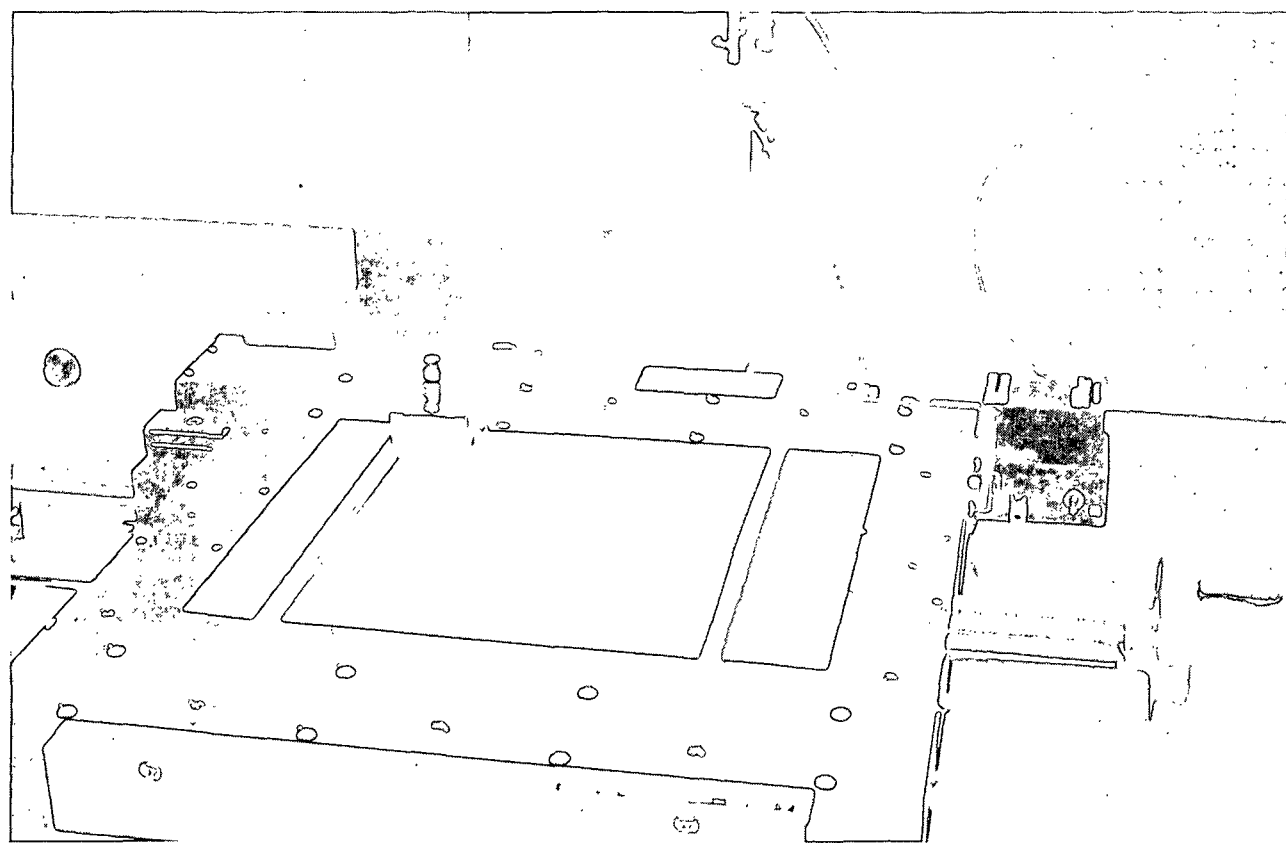
IPC formation tester with formation sample in position.
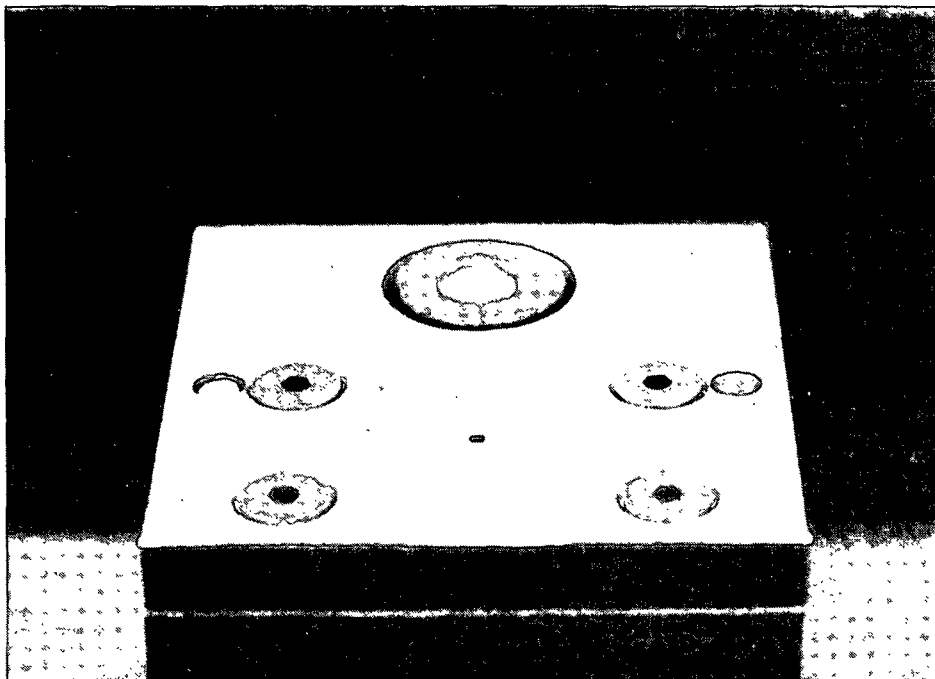
View of light source and beta source collimator.

MASS DENSITY MEASUREMENT SYSTEM

428 — DETECTOR BIAS SUPPLY

BIAS INPUT

142B — PREAMPLIFIER

ENERGY INPUT

490A — AMPLIFIER & SINGLE CHANNEL ANALYZER

RUGGEDIZED PARTIALLY DEPLETED SILICON DETECTOR CR-017-050-500

SCA OUTPUT

997 — COUNTER   719 — TIMER

GATE INPUT

SAMPLE

RS-232C INTERFACE

50 mC Pm 147 BETA SOURCE 1 MM BY 1 MM

PC LIMITED AT COMPUTER

OPTICAL MEASURING SYSTEM

POWER SUPPLY

SILCON PHOTODIODE DETECTOR & PREAMPLIFIER

TRANSMITTED LIGHT MEASURING SYSTEM

SAMPLE

METRABYTE DAS-1602 A/D INTERFACE BOARD

PC LIMITED AT COMPUTER

3.2 mm FIBER OPTIC CABLE

POWER SUPPLY

SILCON PHOTODIODE DETECTOR & PREAMPLIFIER

REFLECTED LIGHT MEASURING SYSTEM

ORIEL VARIABLE WAVELENGTH 100 WATT QUARTZ HALOGEN LIGHT SOURCE

Schematic layout of mass density and optical measuring system for IPC formation tester.

```
Sample Name                   :   62-J-O1
Total Number of Data Points:   6320
Average                       :   0.3242
Standard Deviation            :   0.0190
Percent of Variance           :   5.8474
```

Histogram for commercial offset sample having good to
fair formation.


```
Sample Name                   :   114-I-O1
Total Number of Data Points:   6340
Average                       :   0.4990
Standard Deviation            :   0.0602
Percent of Variance           :   12.0692
```

Histogram for a Noble and Wood handsheet made from a
commercial offset furnish - poor formation.

```
Sample Name              :  62-j-o1
Total Number of Data Points:  6320
Average                  :  0.3242
Standard Deviation       :  0.0190
Percent of Variance      :  5.8474
```



```
Image Map Key
Average transmitted light reading:  "░"
10% above average reading        :  "█"
10% below average reading        :  "░"
```

Image map for commercial offset sample having good to
fair formation.

Sample Name   : 114-i-o1
Total Number of Data Points: 6340
Average   : 0.4990
Standard Deviation   : 0.0602
Percent of Variance   : 12.0692

Image Map Key
Average transmitted light reading: "%"
10% above average reading   :   "▐"
10% below average reading   :   "▌"

Image map for a Noble and Wood handsheet made from
a commercial offset furnish - poor formation.

VARIATION OF 1/CV IPC FORMATION TESTER
WITH VISUAL RANKING

IPC formation index vs. visual ranking index for commercial and handsheet newsprint samples.

VARIATION OF 1/CV IPC FORMATION TESTER
WITH VISUAL RANKING

IPC formation index versus visual ranking index for Formette handsheets from a commercial newsprint furnish.

Handsheet formation before and after coating - #11 good base sheet
formation - before c.v. = 6.5%, after c.v. = 6.0%.
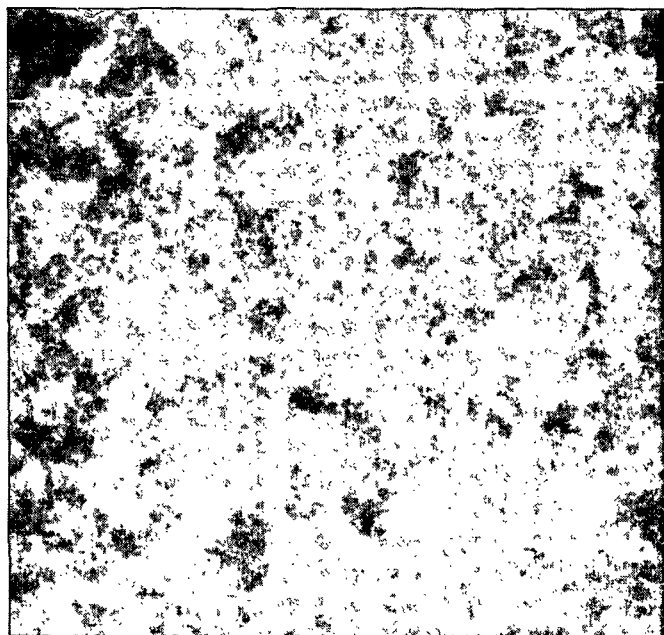
Handsheet formation before and after coating - #46 poor base
sheet formation before - before c.v. = 10.2%, after c.v. = 6.9%.

```
Sample Number : 11
Y Scan Line   : 40
Before Coating:  +
After Coating :  •
```

The variation of transmitted light as a function of position -
#11 single scan line 40 before and after coating.


```
Sample Number : 46
Y Scan Line   : 40
Before Coating:  +
After Coating :  •
```
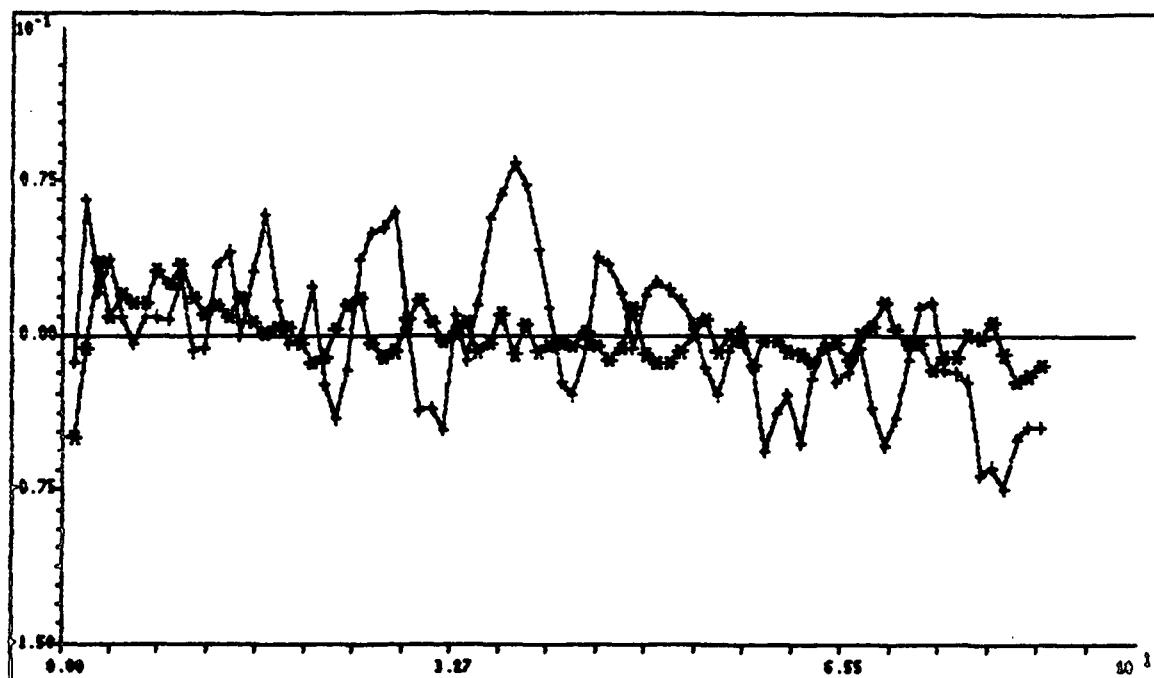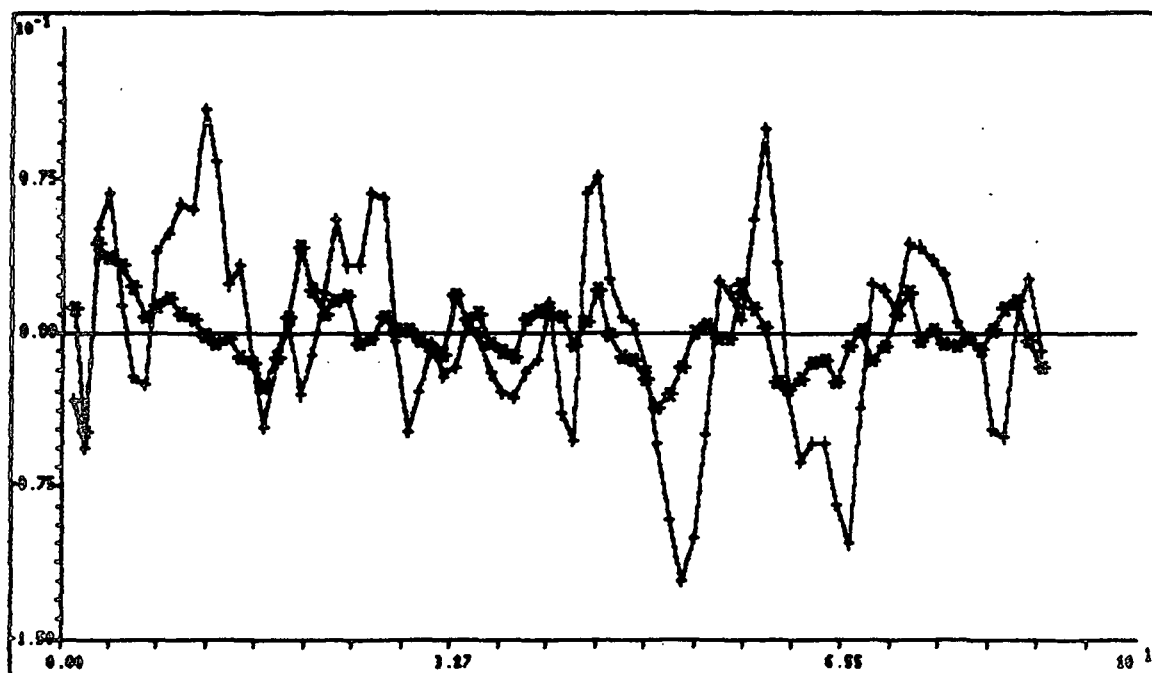
The variation of transmitted light as a function of position -
#46 single scan line 40 before and after coating.

COMBINED STRESS MEASUREMENTS

- SUPERCALENDERING

- CORRUGATING
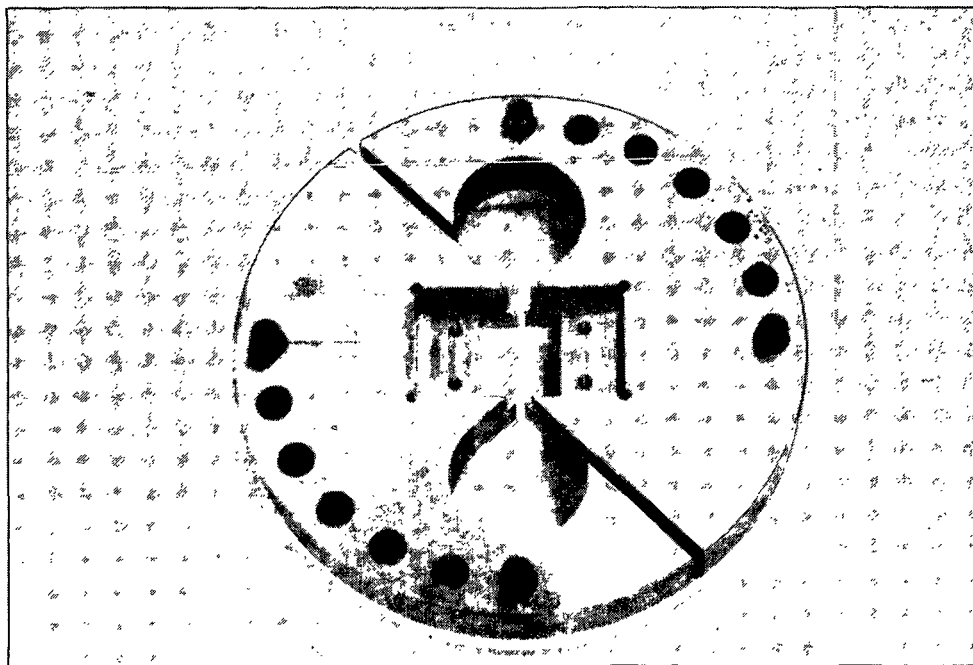
Out-of-plane biaxial fixture without sample holder.
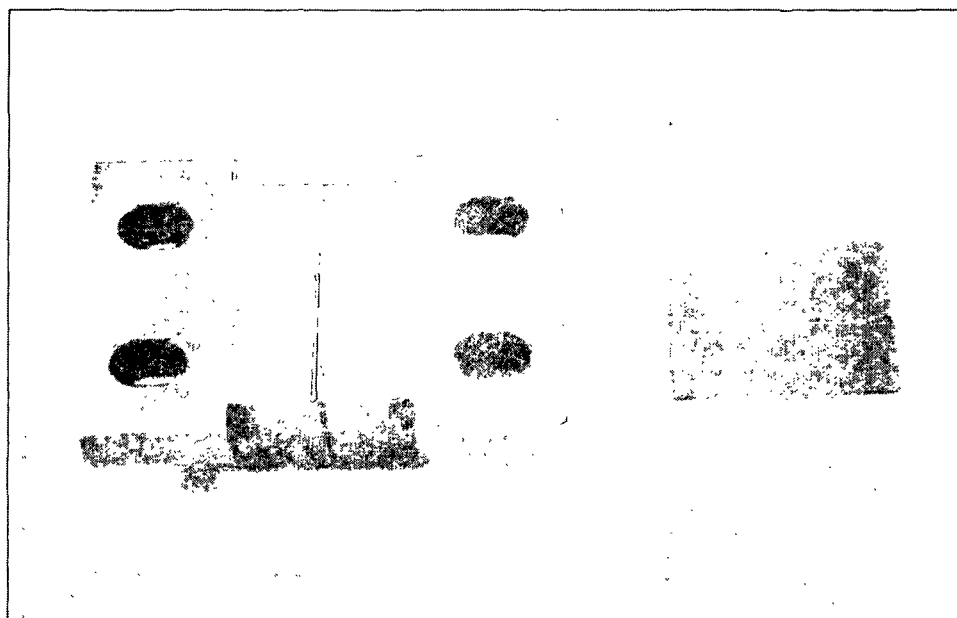
Sample holder.
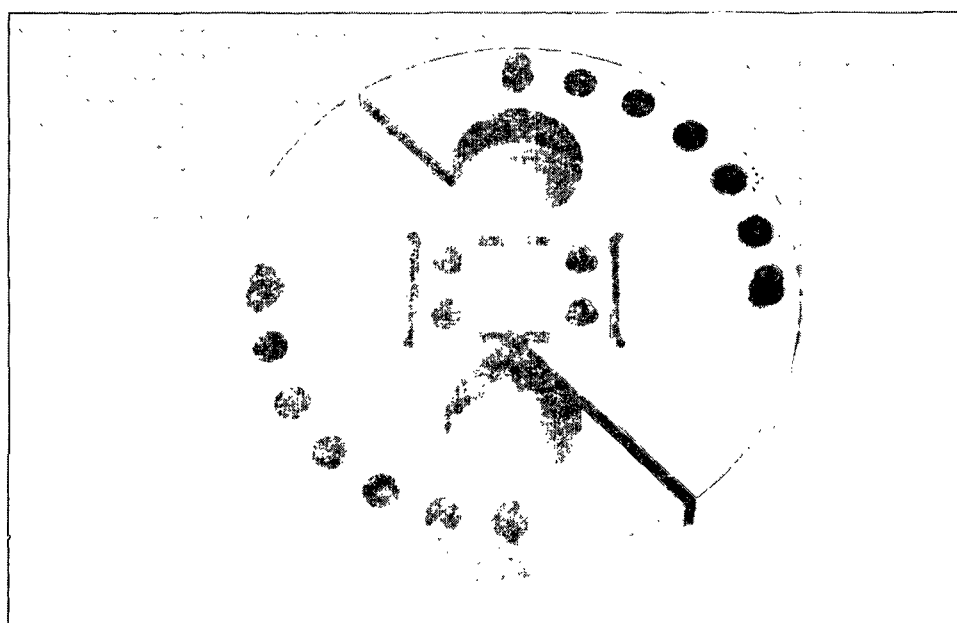
Out-of-plane biaxial fixture with sample and holder in place.

STUDENT RELATED WORK

- Ph.D. Candidate
  Thomas Bither

"STRENGTH DEVELOPMENT THROUGH INTERNAL
FIBRILLATION AND WET PRESSING"

- M.S. Candidate
  ROBERT ALOISI

- Special Student
  Mikko Jokio

"THE INTERACTION OF BASE PAPER AND COATING ON
COATED PAPER PROPERTIES"

- Ero Palokangas

SECTION 3

Project 3526

INTERNAL STRENGTH ENHANCEMENT

INTERNAL STRENGTH ENHANCEMENT

Tape

Sample
with
Tape

120

|← 48 →|

FRONT VIEW

Tape

Sample

SIDE VIEW
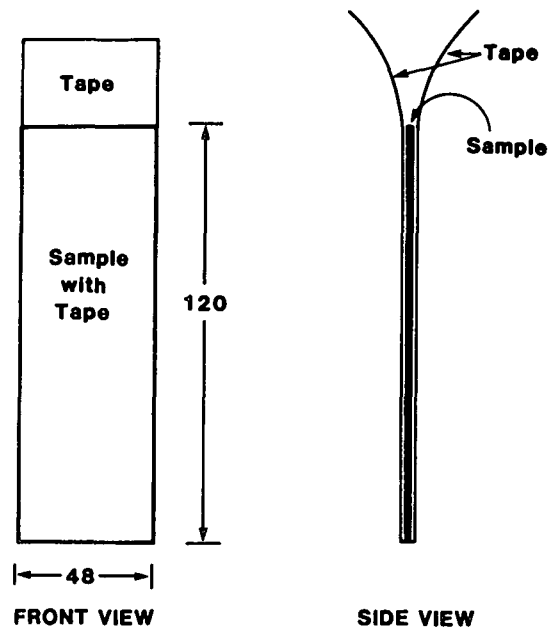
Application of adhesive tape to sample.

Test
Area

20

60

|← 40 →|
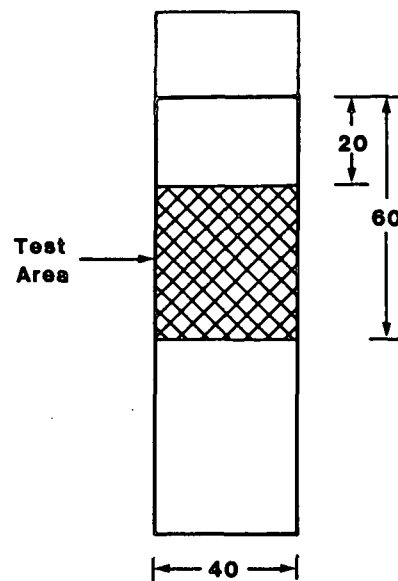
Outlining test area.
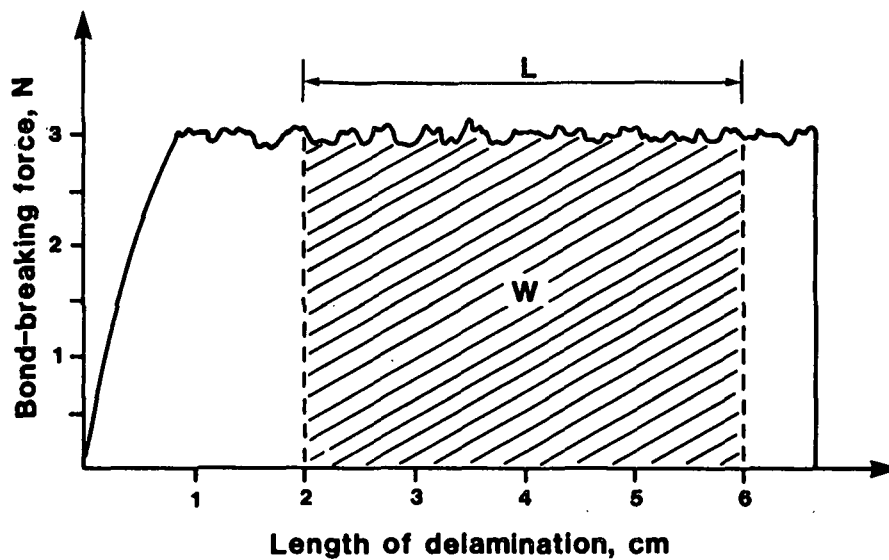
Graph of the force required for sample delamination.

EFFECT OF CROSSHEAD SPEED ON BOND ENERGY

SPEED, in./min	BOND ENERGY, J/m^2
0.5	58.6
1.0	60.5
2.0	63.6
5.0	63.8
10.0	64.8

EFFECT OF BASIS WEIGHT ON BOND ENERGY

BASIS WEIGHT, g/m^2	BOND ENERGY, J/m^2
40	62.2
50	63.1 (0.4)
60	61.6 (1.4)

PULP PROPERTIES

PULP	YIELD	KAPPA NO.
11	47.5	34.7
12	51.2	42.2
13	60.4	116.0
14	80.7	167.0

PULP FREENESS

PULP	FREENESS LEVELS, ml CSF
11	685 (unrefined), 600, 350, 200
12	740 (unrefined), 340
13	750 (unrefined), 600, 350
14	780 (unrefined), 340

PRETEST SCATTERING vs TENSILE INDEX

PRETEST SCATTER vs E

$y = 31.663 - 3.5945e\text{-}3x \quad R^2 = 0.917$
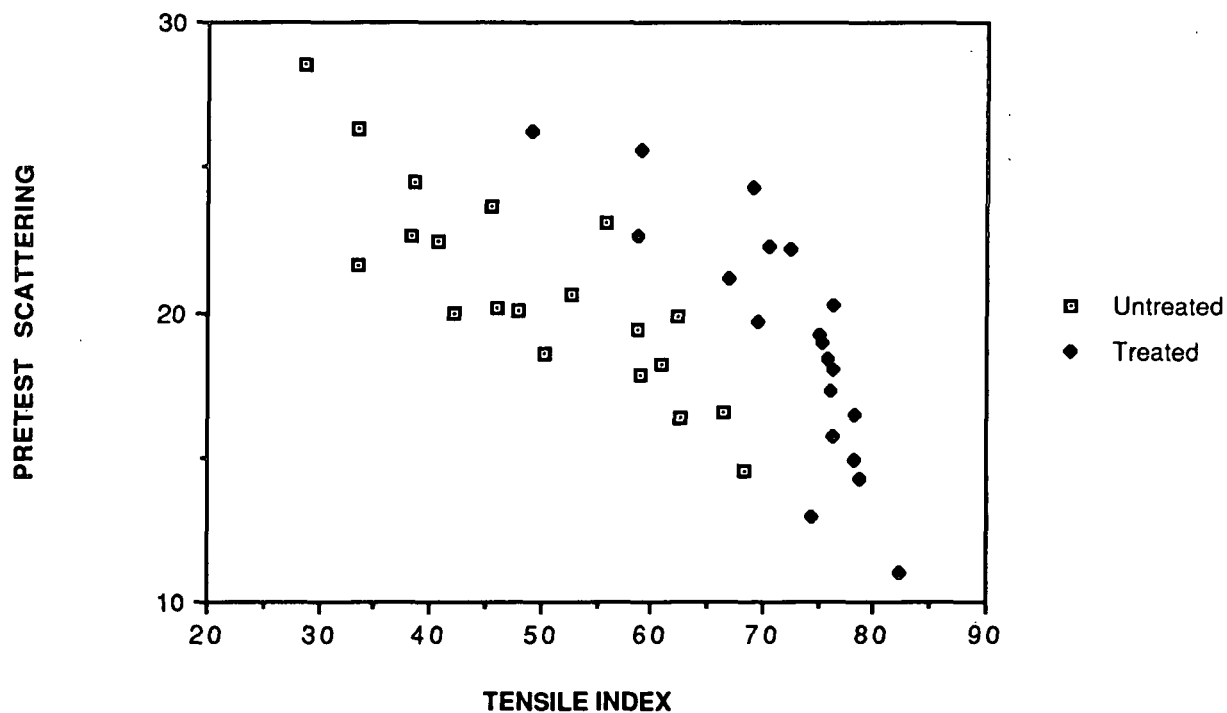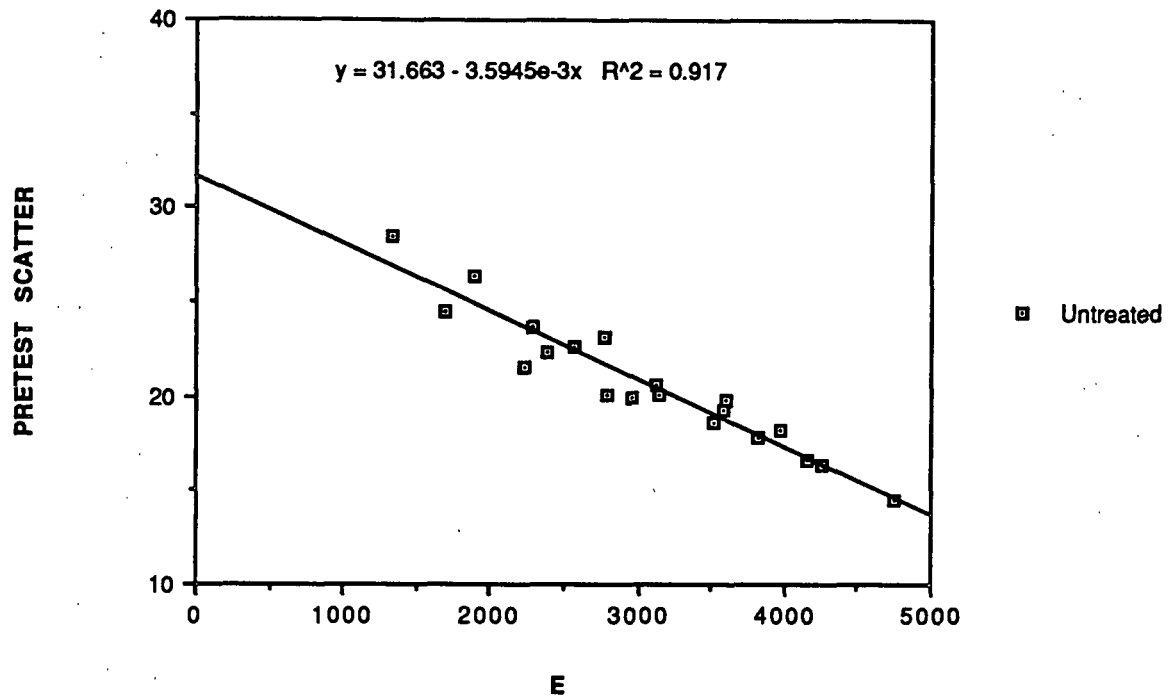
□ Untreated

PRETEST SCATTER vs E, (Treated)

$y = 33.467 - 4.5396e\text{-}3x \quad R^2 = 0.937$

● Treated
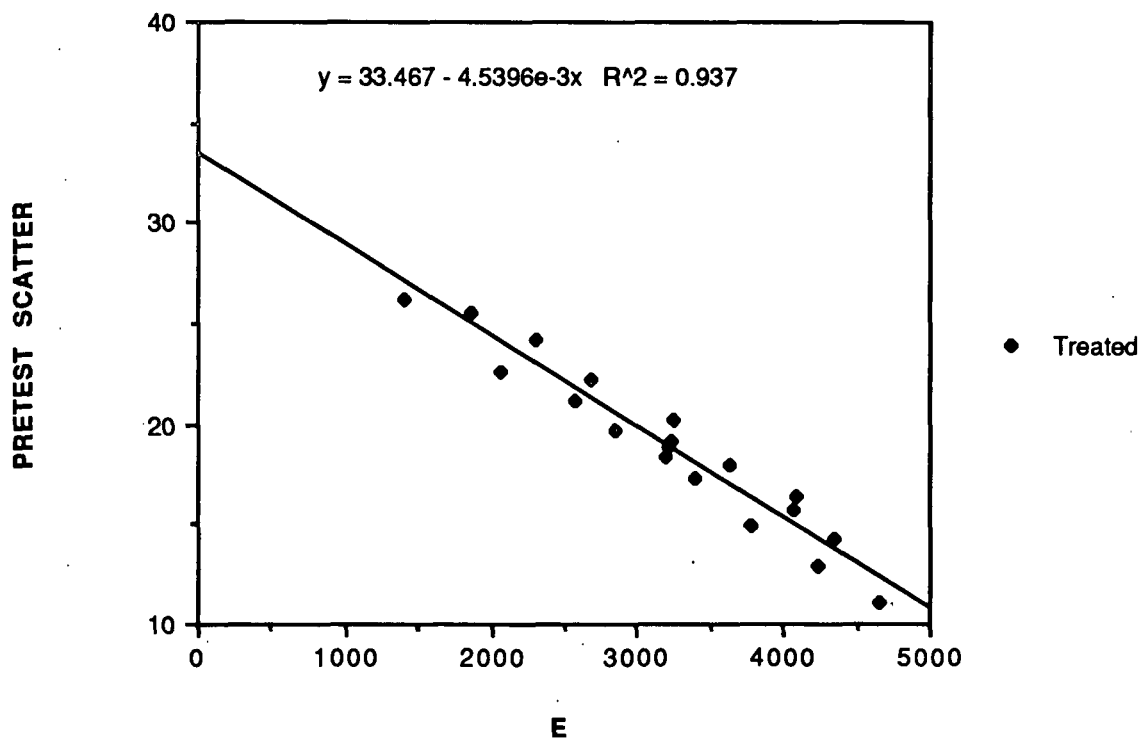
BOND STRENGTH vs TENSILE INDEX
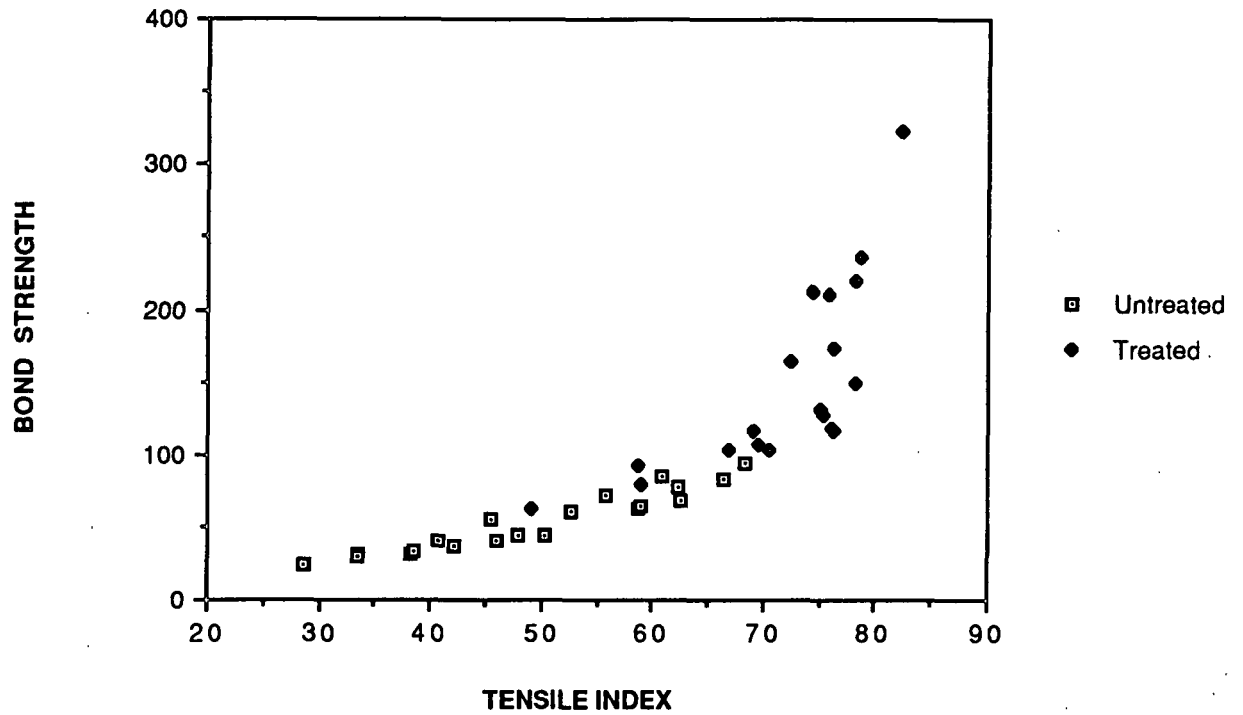
TEA vs BOND STRENGTH
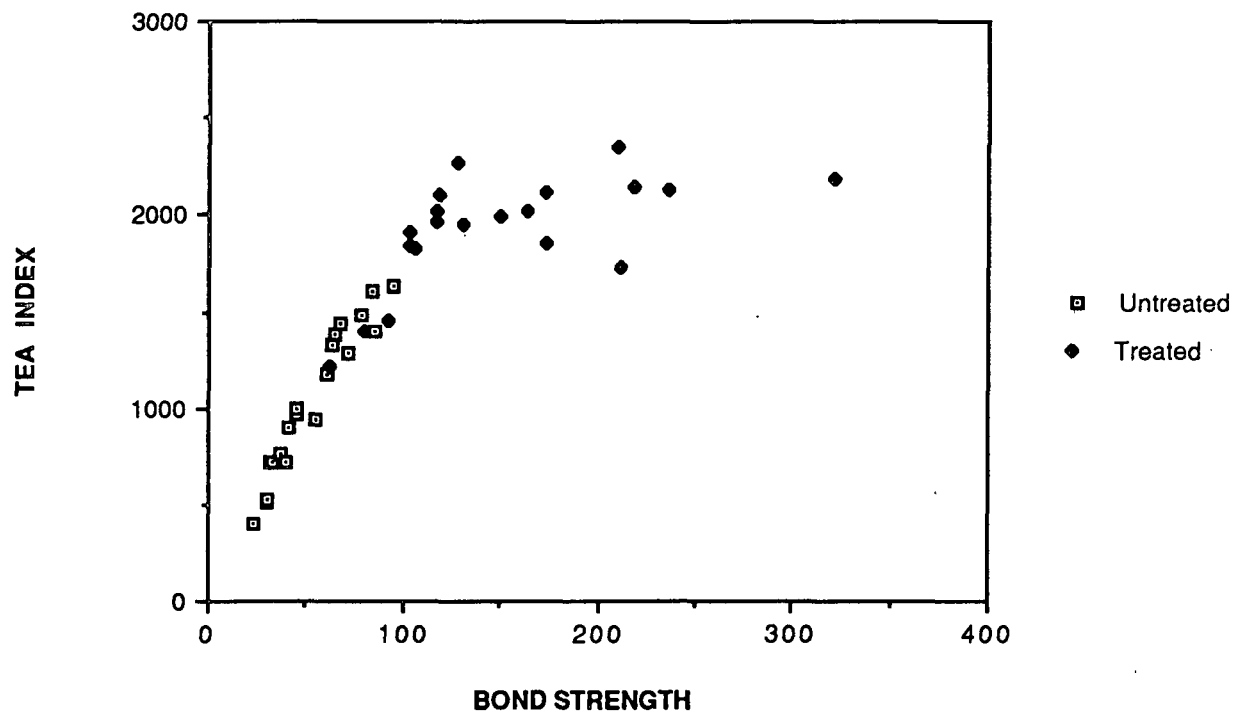
OPTICAL CONTACT AREA CHANGE vs BOND STRENGTH
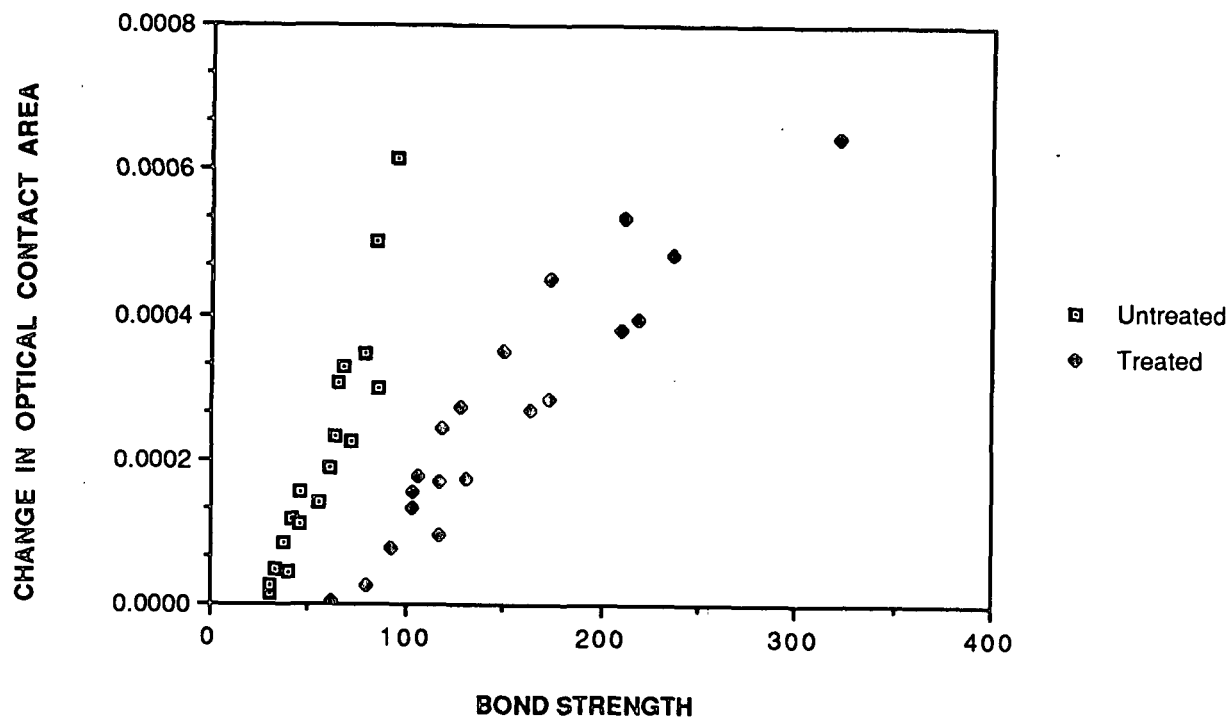
IN PLANE LONGITUDINAL vs TENSILE INDEX
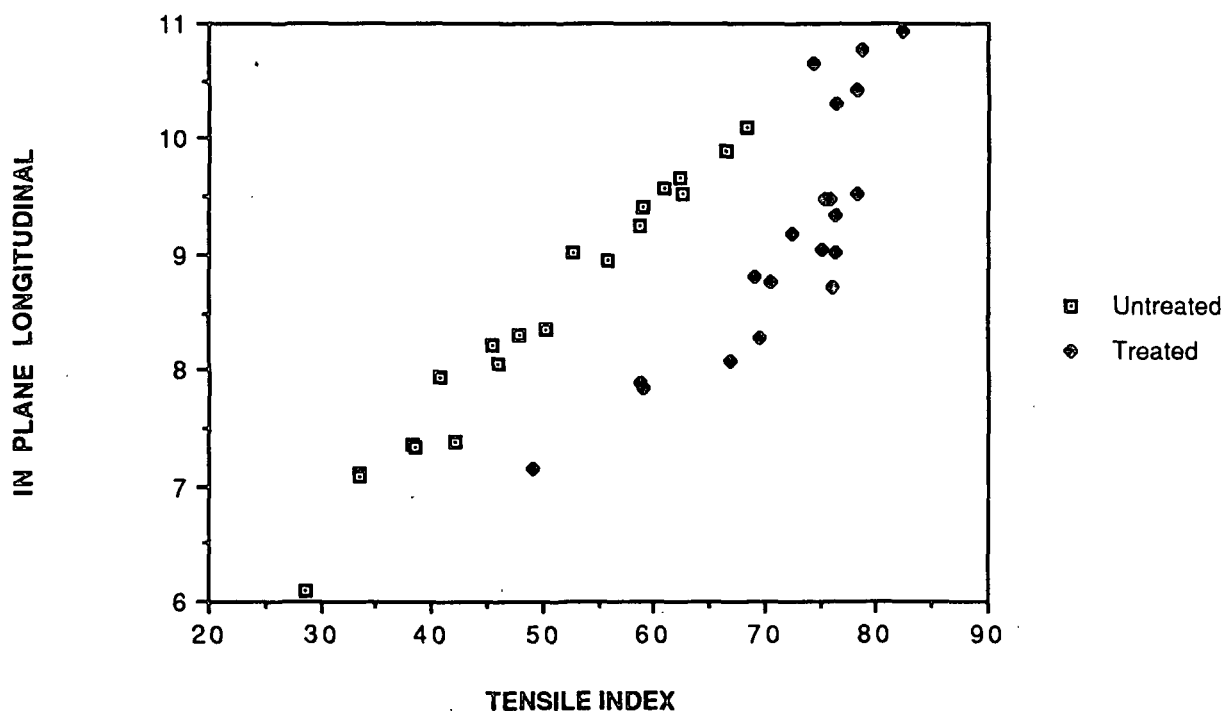
TEA vs TENSILE
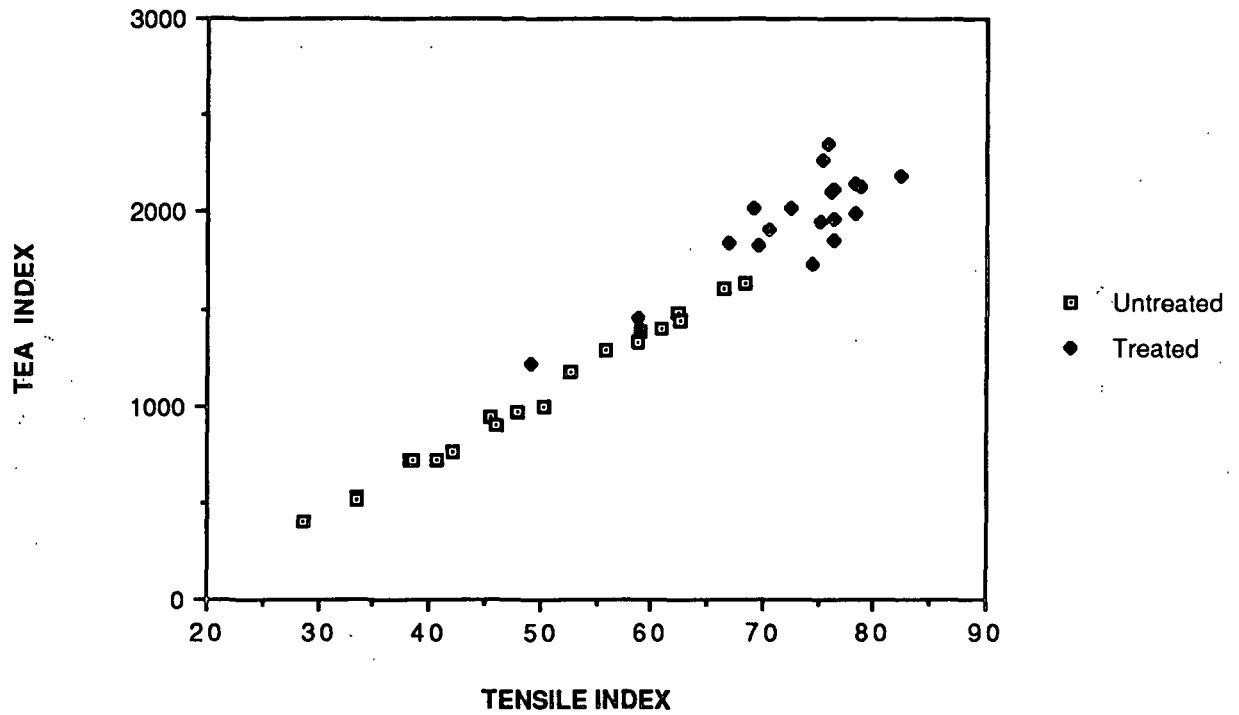
STFI vs TENSILE
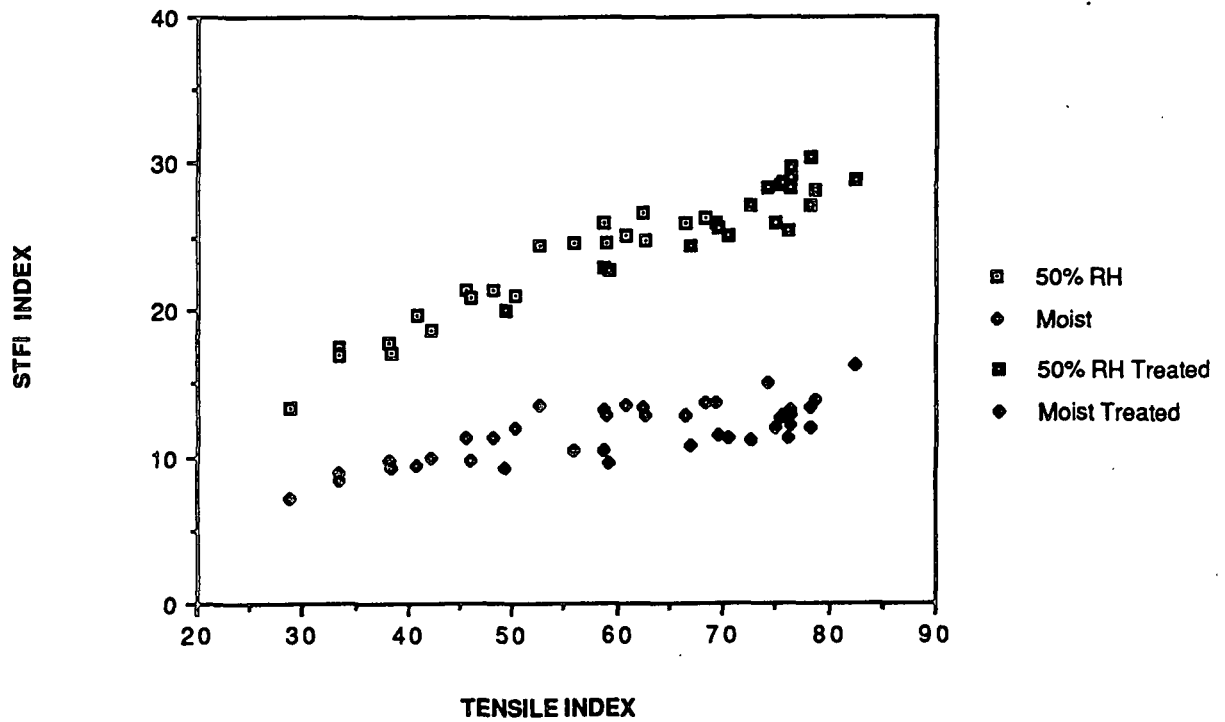
STFI vs BOND STRENGTH
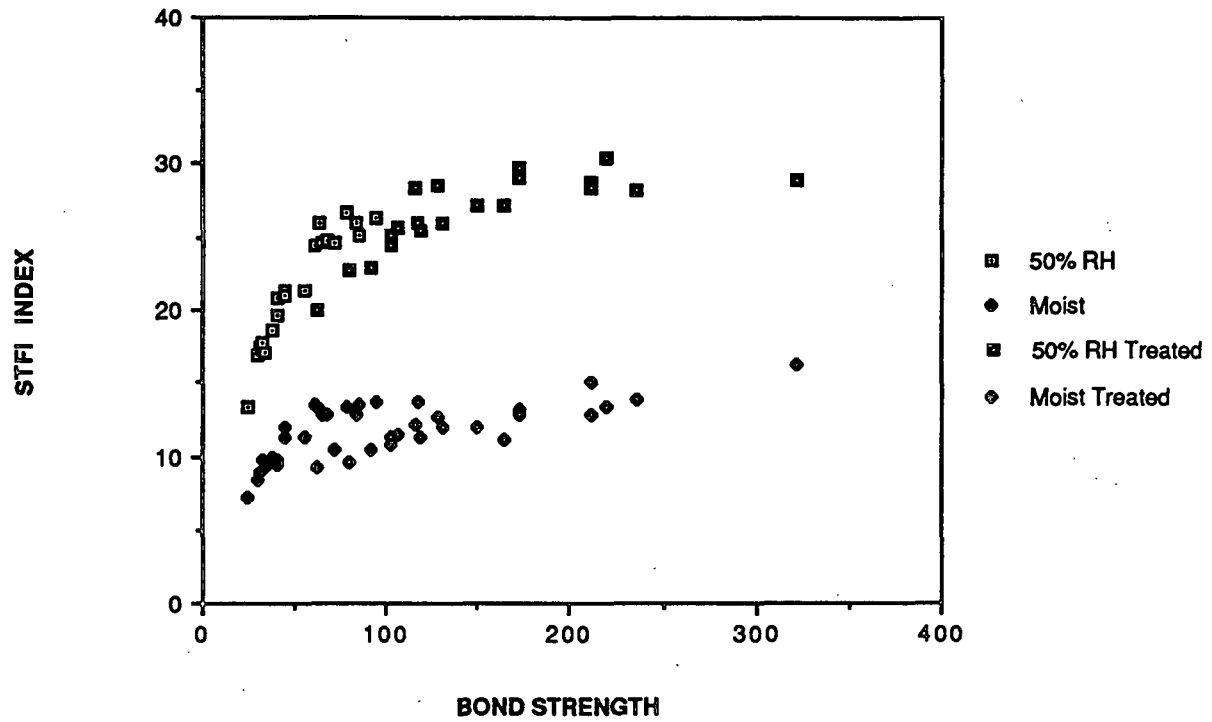
THE EFFECT OF PULPING, BLEACHING, AND REFINING PROCESSES

ON THE ELECTROKINETIC PROPERTIES OF WOOD FIBER FINES

by

Mike T. Goulet

MODEL OF ELECTRIC DOUBLE LAYER
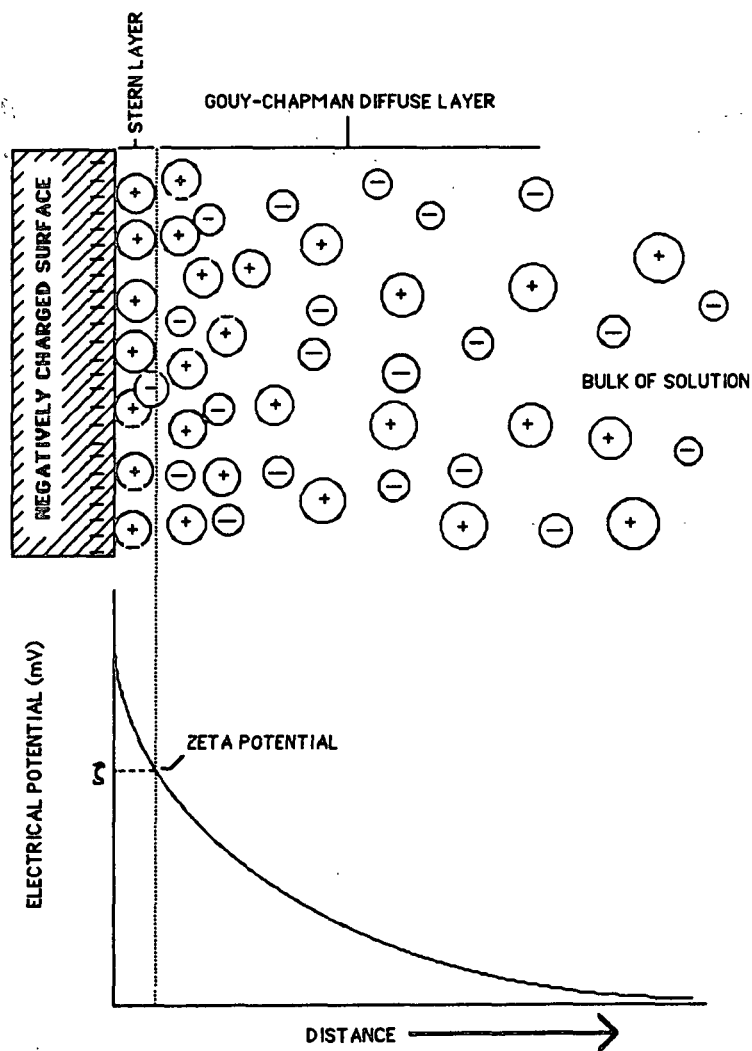
ELECTROPHORETIC MOBILITY
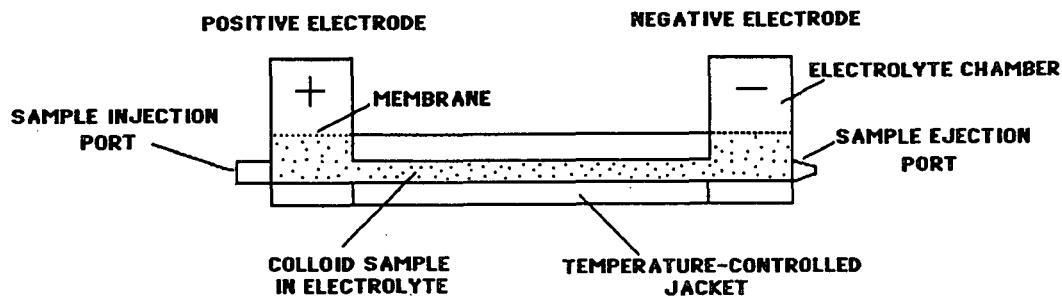
$$\text{ELECTROPHORETIC MOBILITY} = \frac{\text{PARTICLE VELOCITY}}{\text{ELECTRIC FIELD STRENGTH}} = \frac{\text{MICRONS/SEC}}{\text{VOLTS/CM}}$$

Smoluchowski Equation:

$$\mu = \frac{\varepsilon \zeta}{4 \pi \eta}$$

where: μ = electrophoretic mobility

ε = dielectric constant

ζ = zeta potential

η = viscosity of medium surrounding particle

THESIS OBJECTIVES

1. Measure the average electrophoretic mobility (E.M.) and E.M. distribution of wood fiber fines and analyze the changes resulting from pulping, bleaching, and refining operations.

2. Identify the physical and chemical changes occurring in fibers and fiber fines during pulping, bleaching, and refining operations.

3. Ultimately provide a better understanding of the effects of pulping, bleaching, and refining on the electrokinetic properties of fiber fines and the chemical changes responsible for these effects.

EXPERIMENTAL DESIGN
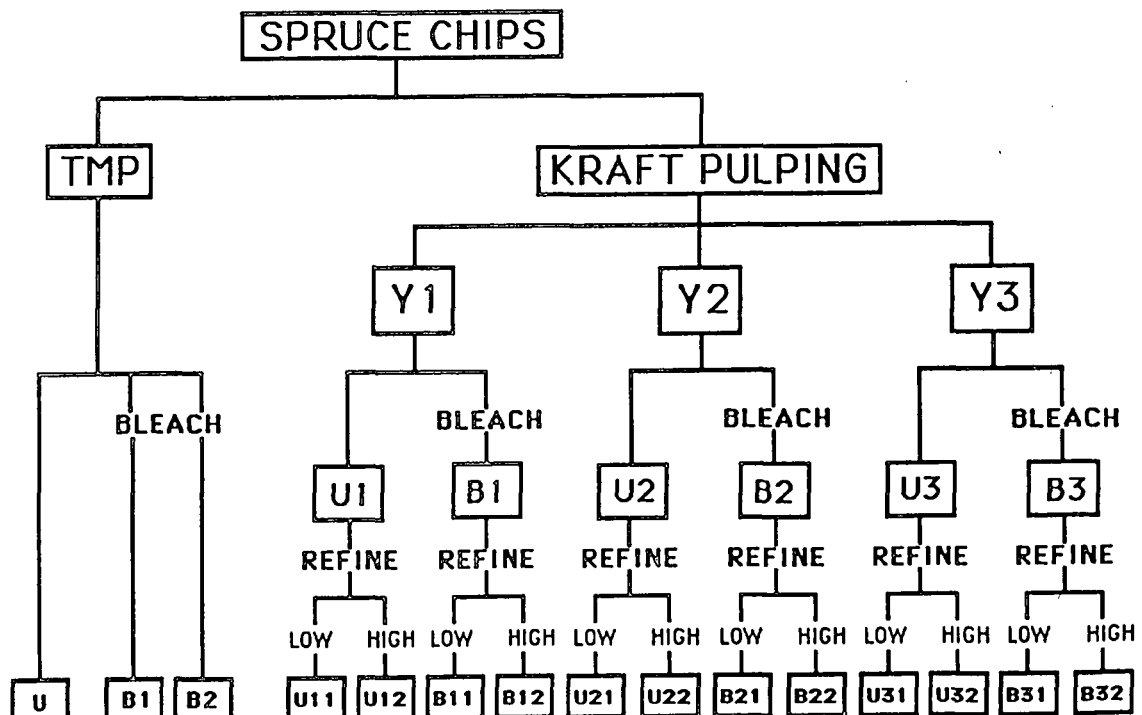
SPRUCE TMP PULP ANALYSIS

Sample	Hypo Number	Weak Acid Content (meq/100g)	TAPPI Brightness
Unbleached	28.01	11.38	60.40
Bleach 1	26.62	25.13	69.86
Bleach 2	27.07	23.81	70.35

UNBLEACHED SPRUCE KRAFT PULP ANALYSIS

H-Factor	Unscr. Yield	%Rejects	Screened Yield	Kappa No.	Hypo No.	W.A.C.
576	54.35	5.61	48.74	72.58	10.50	11.22
927	49.92	1.61	48.31	36.06	5.41	8.08
3300	44.71	0.41	44.30	17.78	2.67	4.67

BLEACHED KRAFT PULP ANALYSIS

H-Factor	Unscreened Yield (%)	TAPPI Brightness	Weak Acid Content (meq/100g.)
576	54.35	89.41	4.15
927	49.92	86.60	3.57
3300	44.71	87.35	3.08

KRAFT PULP REFINING ANALYSIS

Pulp Type*	PFI Revolutions	CSF (ml)
54.35% - U	7,500	598
54.35% - U	15,000	271
49.92% - U	7,500	513
49.92% - U	15,000	217
44.71% - U	7,500	437
44.71% - U	15,000	152
54.35% - B	7,500	498
54.35% - B	15,000	247
49.92% - B	7,500	511
49.92% - B	15,000	262
44.71% - B	7,500	460
44.71% - B	15,000	196

(* %Yield - Unbleached/Bleached)

PC 602c SYSTEM COMPONENTS

```
MALVERN      ZETASIZER    II c
------------------------------------------------------------------
sample  : SPLIT PLOT 576-U-7.5 0.0002

 File data from b:splplot block : 5 Cell type  1
 Refractive Index 1.33 Viscosity  0.8905  Dielectric const. 80.0 Temperature 25.0
------------------------------------------------------------------
      f(Hz)    MOBILITY (Mic/sec / Volt/cm)                  % VALUE
------------------------------------------------------------------
 0   200.0     0.94      *+                              (   0.0)
 1   209.3     0.77      |+                              (   0.0)
 2   218.6     0.59      |+                              (   0.0)
 3   227.8     0.42      |+                              (   0.0)
 4   237.1     0.24      |+                              (   0.0)
 5   246.4   6.816E-02   |+                              (   0.0)
 6   255.7    -0.11      |+                              (   0.0)
 7   264.9    -0.28      |+                              (   0.0)
 8   274.2    -0.46      |+                              (   0.0)
 9   283.5    -0.63      |+                              (   0.0)
10   292.8    -0.80      |+                              (   0.0)
11   302.0    -0.98      |+                              (   0.0)
12   311.3    -1.15      |+                              (   0.0)
13   320.6    -1.33      |+                              (   0.0)
14   329.9    -1.50      -+                              (   0.3)
15   339.1    -1.68      |----+                          (   2.2)
16   348.4    -1.85      |---------+                     (   6.2)
17   357.7    -2.03      |----------------+              (  13.3)
18   367.0    -2.20      |----------------------+        (  20.1)
19   376.2    -2.38      |-----------------------+       (  21.5)
20   385.5    -2.55      |--------------------+          (  16.6)
21   394.8    -2.73      |-------------+                 (  10.1)
22   404.1    -2.90      |------+                        (   5.7)
23   413.3    -3.07      |----+                          (   3.0)
24   422.6    -3.25      |--+                            (   1.0)
25   431.9    -3.42      |+                              (   0.0)
26   441.2    -3.60      |+                              (   0.0)
27   450.4    -3.77      |+                              (   0.0)
28   459.7    -3.95      |+                              (   0.0)
29   469.0    -4.12      |+                              (   0.0)
30   478.3    -4.30      |+                              (   0.0)
31   487.5    -4.47      |+                              (   0.0)
32   496.8    -4.65      |+                              (   0.0)
33   506.1    -4.82      |+                              (   0.0)
34   515.4    -5.00      |+                              (   0.0)
35   524.7    -5.17      |+                              (   0.0)
36   533.9    -5.34      |+                              (   0.0)
37   543.2    -5.52      |+                              (   0.0)
38   552.5    -5.69      |+                              (   0.0)
39   561.8    -5.87      |+                              (   0.0)
40   571.0    -6.04      |+                              (   0.0)
41   580.3    -6.22      |+                              (   0.0)
42   589.6    -6.39      |+                              (   0.0)
43   598.9    -6.57      |+                              (   0.0)
44   608.1    -6.74      |+                              (   0.0)
45   617.4    -6.92      |+                              (   0.0)
46   626.7    -7.09      |+                              (   0.0)
47   636.0    -7.27      |+                              (   0.0)
48   645.2    -7.44      |+                              (   0.0)
49   654.5    -7.61      |+                              (   0.0)
50   663.8    -7.79      |+                              (   0.0)
51   673.1    -7.96      |+                              (   0.0)
52   682.3    -8.14      |+                              (   0.0)
53   691.6    -8.31      |+                              (   0.0)
54   700.9    -8.49      |+                              (   0.0)
55   710.2    -8.66      |+                              (   0.0)
56   719.4    -8.84      |+                              (   0.0)
57   728.7    -9.01      |+                              (   0.0)
58   738.0    -9.19      |+                              (   0.0)
59   747.3    -9.36      |+                              (   0.0)
60   756.5    -9.54      |+                              (   0.0)
61   765.8    -9.71      |+                              (   0.0)
62   775.1    -9.88      |+                              (   0.0)
63   784.4   -10.06      *+                              (   0.0)
------------------------------------------------------------------
 Mean value  -2.36     %width    13.3 Integration Limits  15 to  23

 Cell Voltage  119.0    Field strength (V/cm)   23.8
------------------------------------------------------------------
```

E.M. vs. LOG SP. CONDUCTANCE
(Bleached Kraft Cook #4)

ELECTROPHORETIC MOBILITY VS. pH
(TMP fines in 0.004 M NaCl)

ELECTROPHORETIC MOBILITY OF TMP FINES

y = - 3.7980 + 1.0093x   R^2 = 0.993

y = - 3.7934 + 0.83566x   R^2 = 1.000

y = - 3.7198 + 0.81301x   R^2 = 0.993

UNBLEACHED
BLEACH 1
BLEACH 2
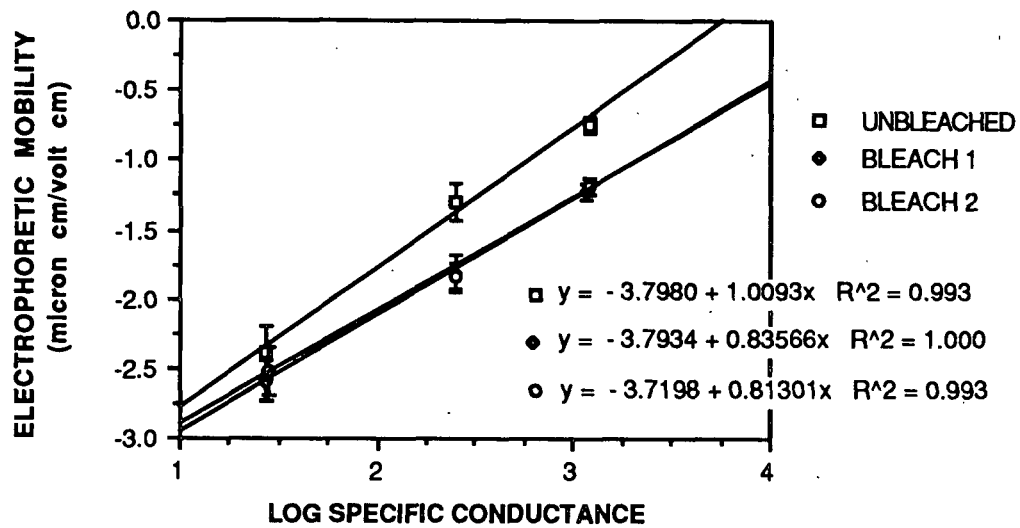
DISTRIBUTION ST. DEVIATION
(TMP Fiber Fines)

UNBLEACHED
BLEACH 1
BLEACH 2
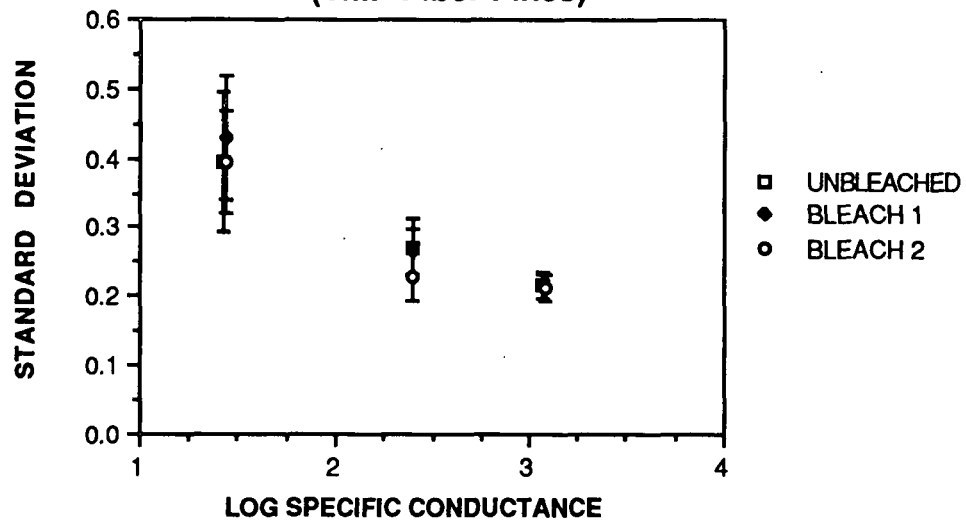
ELECTROPHORETIC MOBILITY OF KRAFT FINES
(Unbleached, 7,500 Revolutions)

- □ 44.71% YIELD
- ◆ 49.92% YIELD
- ○ 54.35% YIELD

□ y = - 3.3602 + 0.83672x   R^2 = 0.999
◆ y = - 3.4479 + 0.80259x   R^2 = 1.000
○ y = - 3.5219 + 0.77285x   R^2 = 1.000
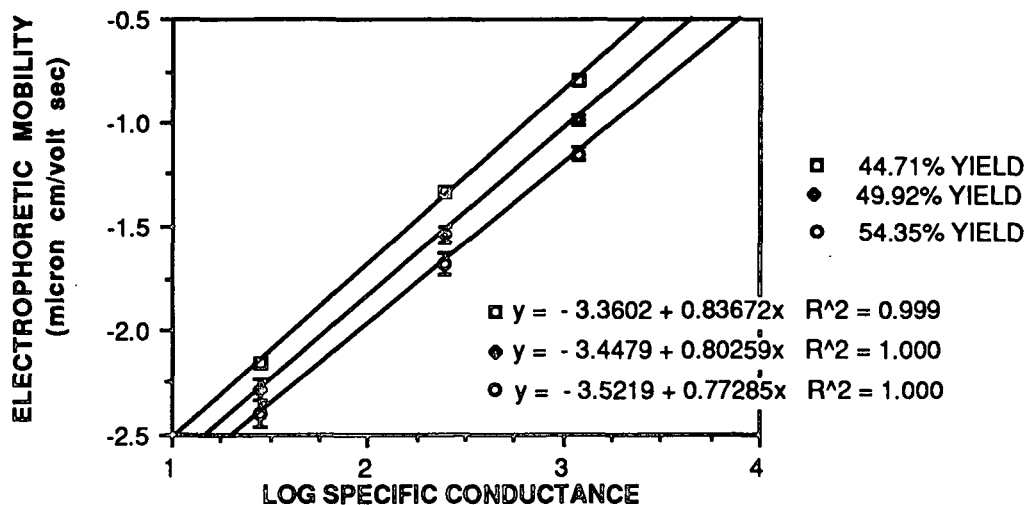
DISTRIBUTION STANDARD DEVIATION
(Unbleached kraft; 7,500 Rev.)

- □ 54.35% YIELD
- ● 49.92% YIELD
- ○ 44.71% YIELD
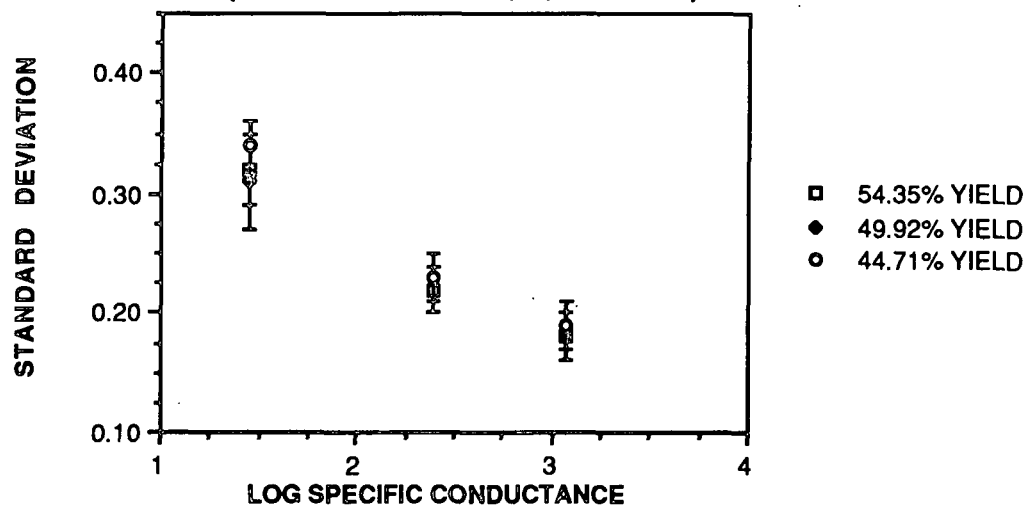
ELECTROPHORETIC MOBILITY OF KRAFT FINES
(Bleached, 15,000 Revolutions)

□   44.71% YIELD
◆   49.92% YIELD
○   54.35% YIELD

□ $y = -3.1801 + 0.81134x$ $R^2 = 1.000$
◉ $y = -3.3685 + 0.85379x$ $R^2 = 0.999$
○ $y = -3.4459 + 0.85053x$ $R^2 = 1.000$
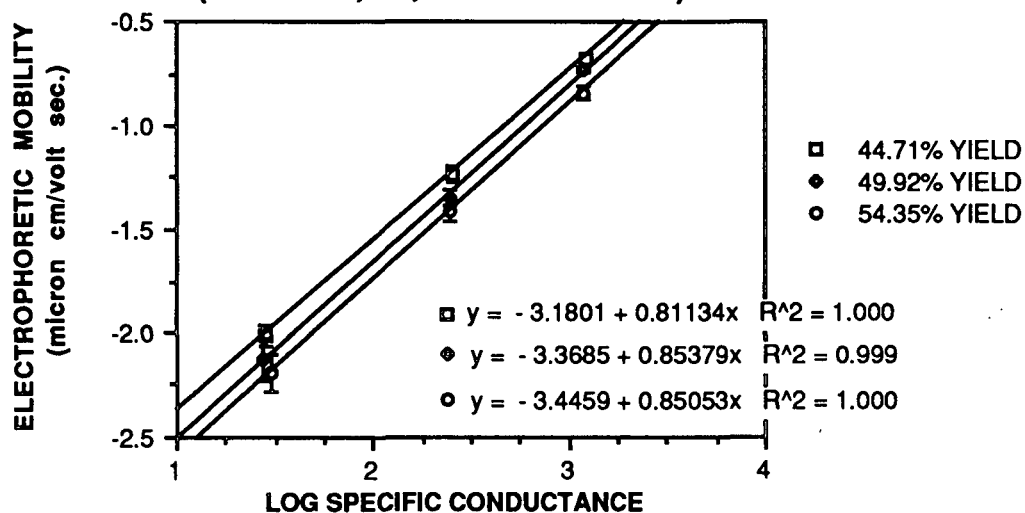
DISTRIBUTION STANDARD DEVIATION
(Bleached kraft; 15,000 Rev.)

□   54.35% YIELD
◆   49.92% YIELD
○   44.71% YIELD
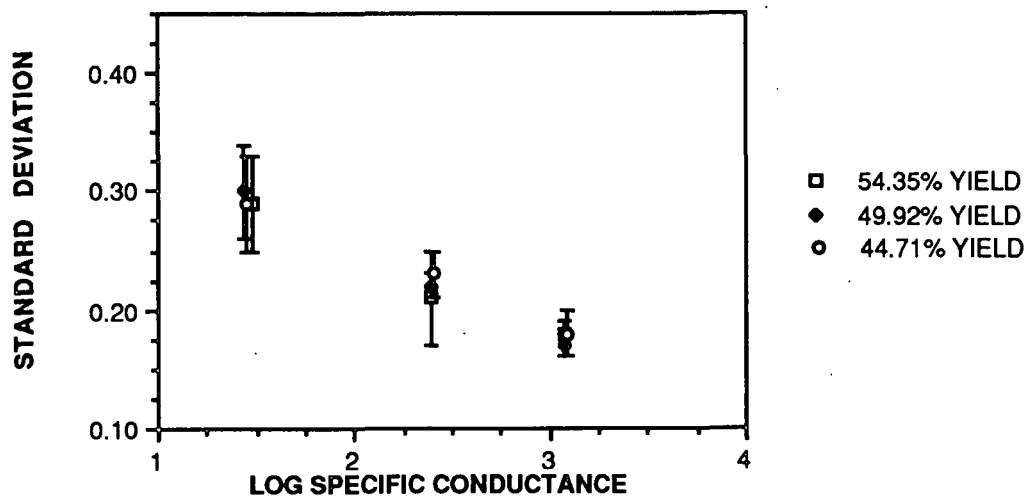
ELECTROPHORETIC MOBILITY OF KRAFT FINES
(Effect of Bleaching:7,500 Revolutions)
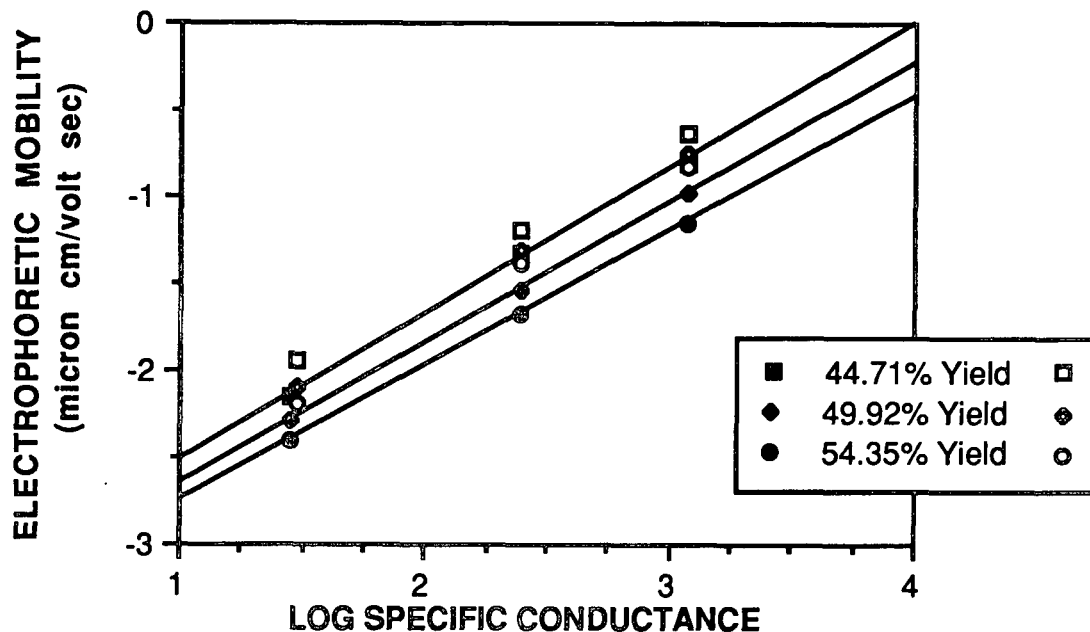
ELECTROPHORETIC MOBILITY OF KRAFT FINES
(7,500 and 15,000 Revolutions)
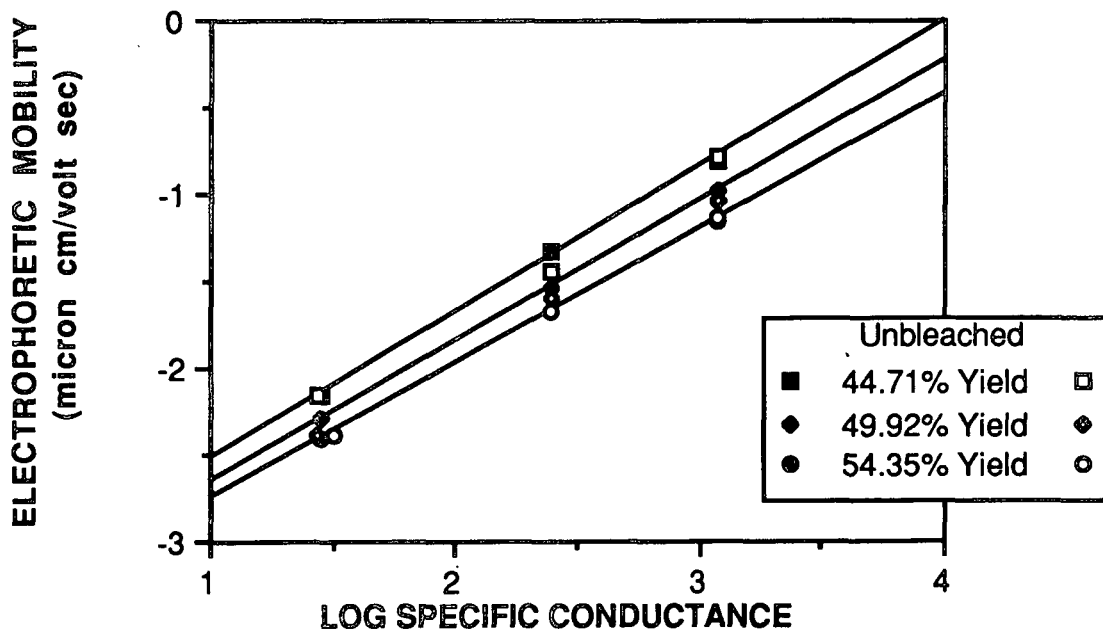
SECTION 5

Project 3571

BOARD PROPERTIES AND PERFORMANCE

BOARD PROPERTIES AND PERFORMANCE

GENERAL OBJECTIVES

- ANALYZE BOX PERFORMANCE NEEDS

- IDENTIFY CRITICAL BOARD PROPERTIES

- IMPROVE MEDIUM AND LINER PERFORMANCE

CURRENT RESEARCH

o COMBINED BOARD WARP (WHITSITT)

o LINER AND MEDIUM IMPROVEMENT (WHITSITT)

o RUNNABILITY MODELING (WHITSITT AND HALCOMB)

o FLAT CRUSH AND FLUTE FORMATION MODELING (DEES)

o COMMERCIAL BOX ABUSE STUDY (DEES)

COMBINED BOARD WARP -- LINER ORIENTATION EFFECTS

- SF AND DF POLAR ANGLES IN OPPOSITE DIRECTIONS
  -- MAJOR TWIST WARP AS MOISTURE CHANGES
  -- WARP INCREASES AS POLAR ANGLE DEVIATION INCREASES

- SF AND DF POLAR ANGLES IN SAME DIRECTION
  -- MINOR TWIST WARP AS MOISTURE CHANGES
  -- ONLY SMALL EFFECTS FOR ANGLES UP TO 15 DEGREES

- REDUCING CD STIFFNESS VARIATION ON PAPER MACHINE SHOULD REDUCE TWIST WARP OCCURRENCE
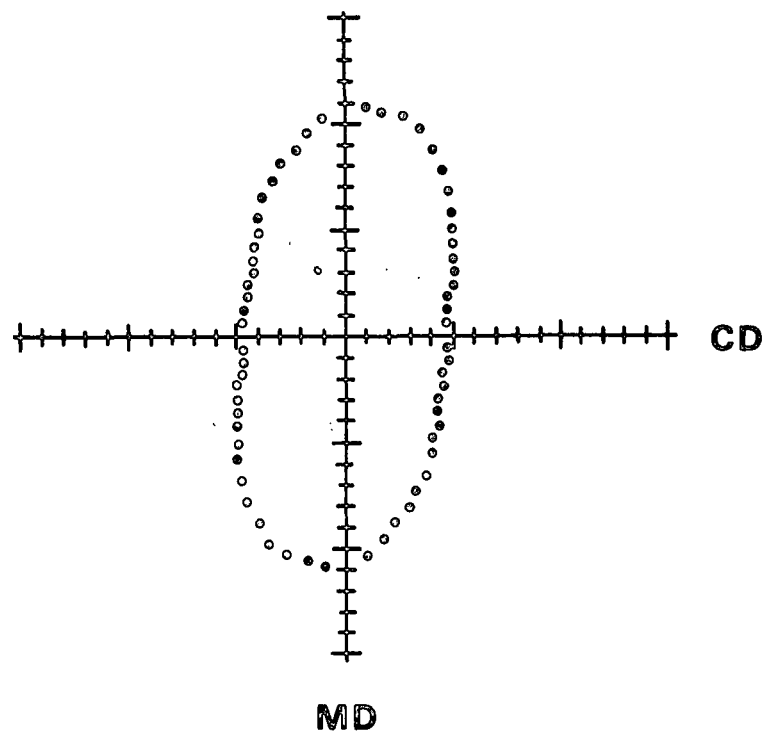
Typical in-plane polar plot.
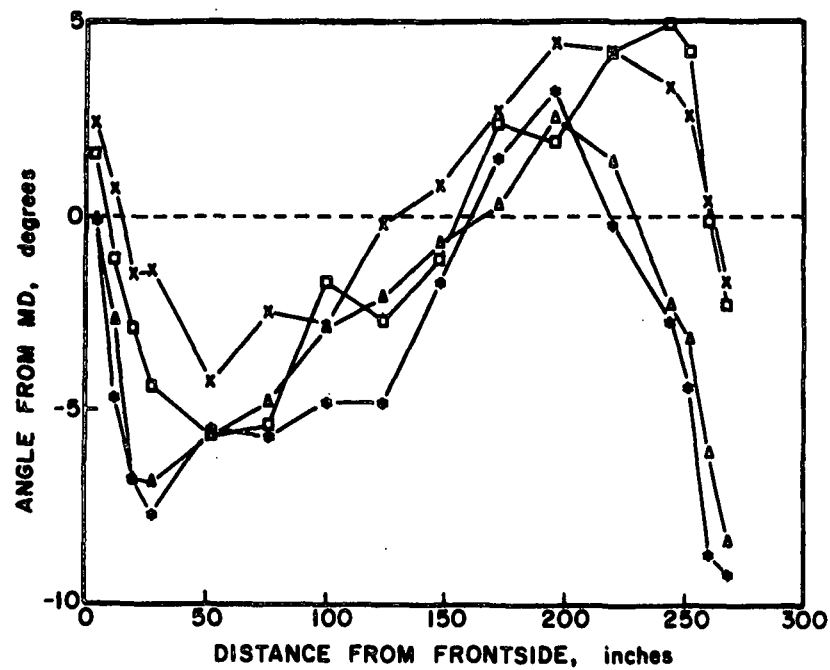
Angle of lean (polar angle) vs. position across the
machine for four separate reel turn-ups.
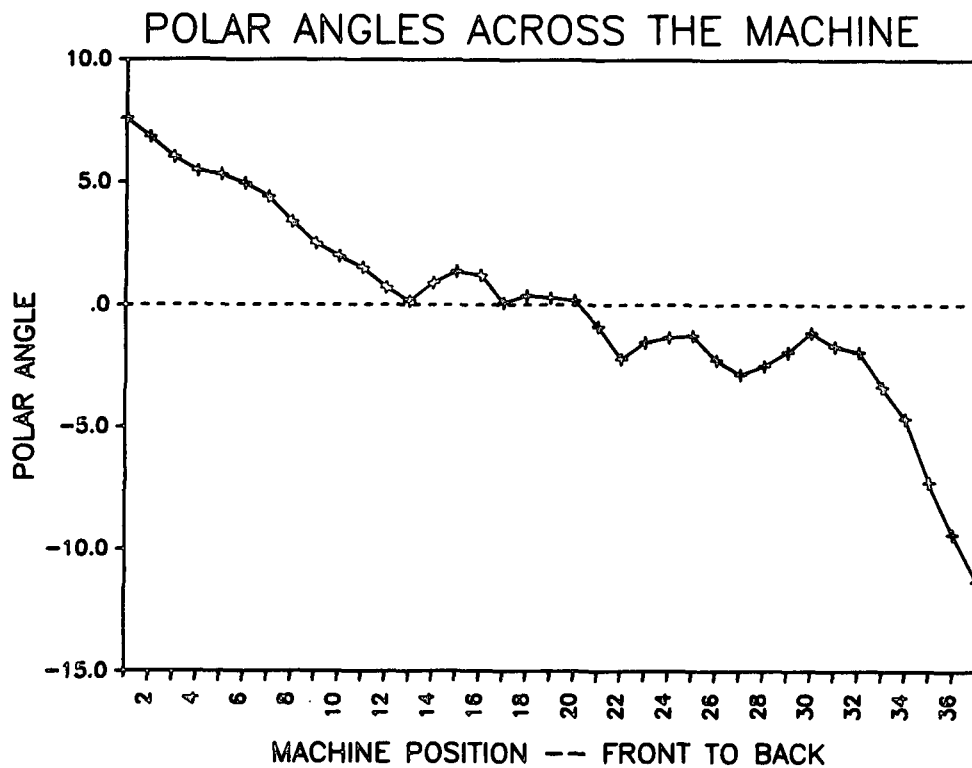
POLAR ANGLES ACROSS THE MACHINE

Large changes in polar angle can occur across a
linerboard machine and, hence affect quality.

a) Liner polar angles in
   same direction

b) Liner polar angles in
   opposite direction
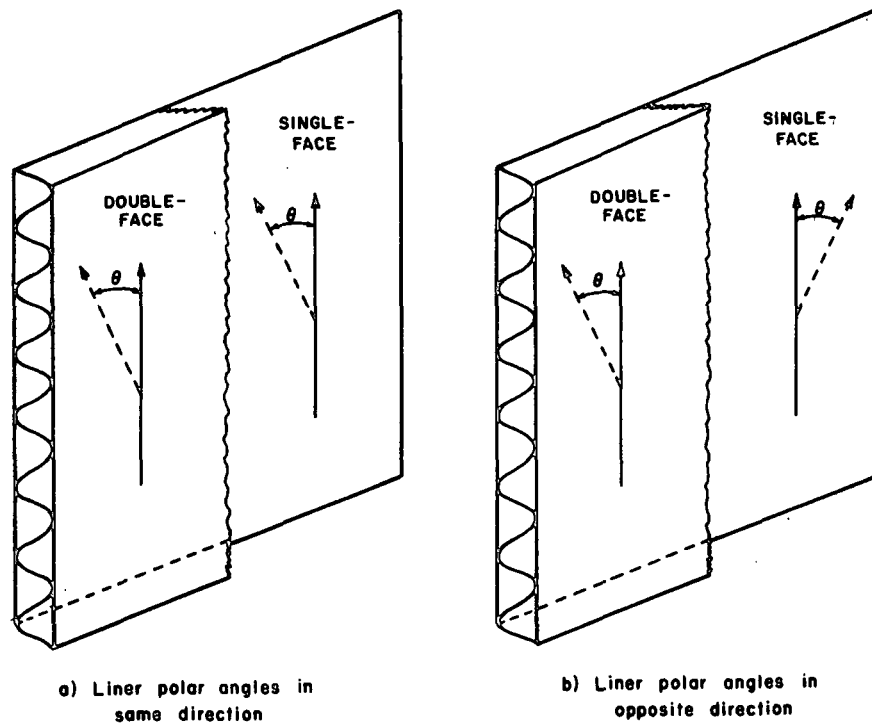
Two opposite cases of liner polar angle misalignment.
Case (b) promotes twist warp.
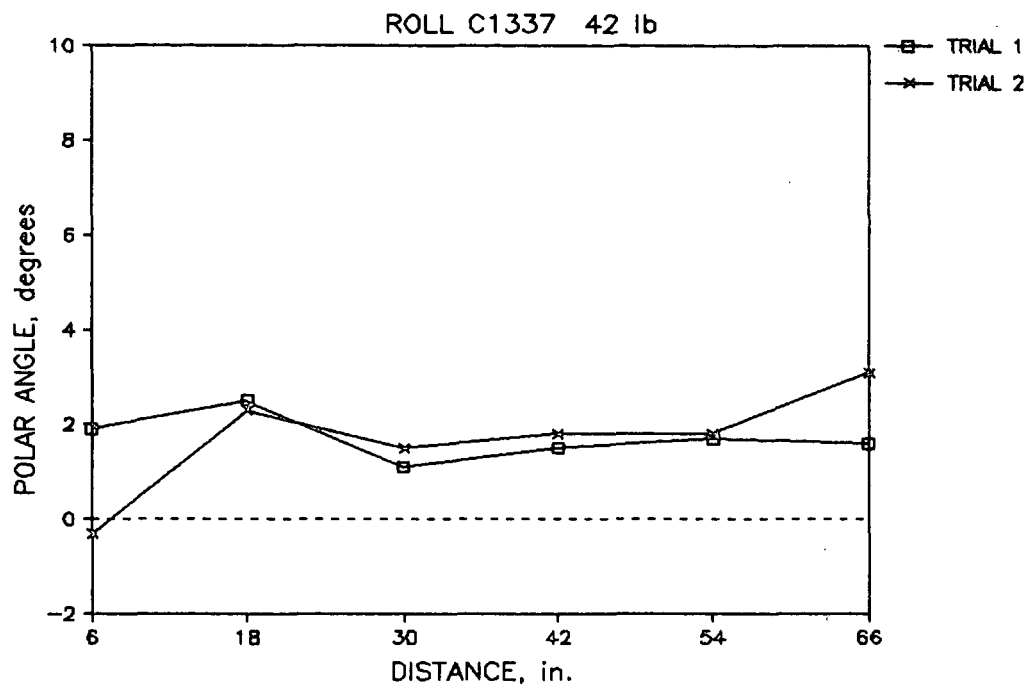
Polar angle deviations from machine direction for the
42-lb liner used in fabricating combined board.

COMBINED BOARD WARP PROFILE
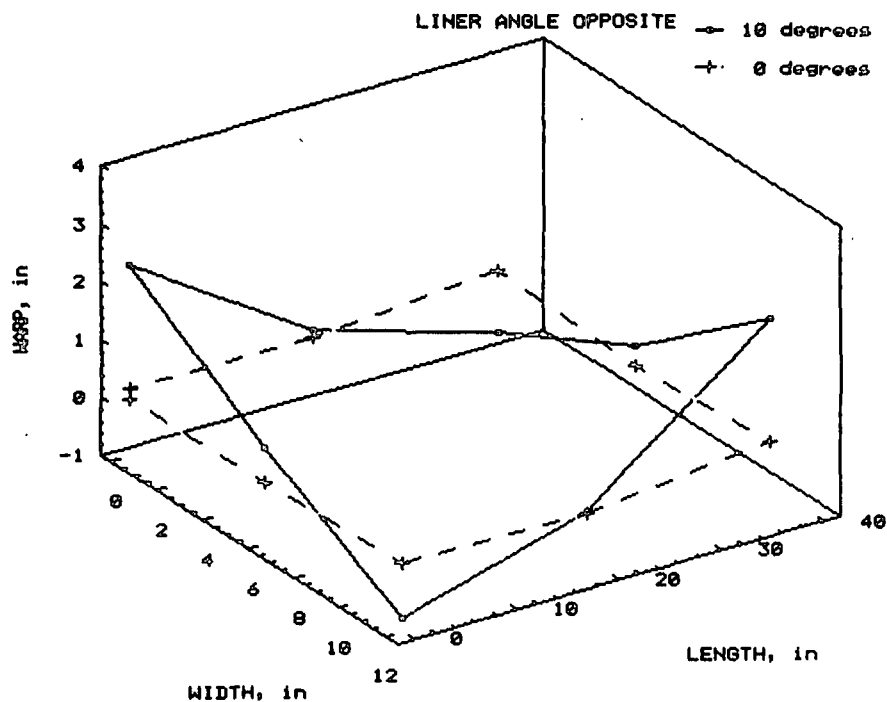
Comparison of warp obtained with 0 and 10 degrees
of liner polar angle deviation in opposite
directions from the MD of the combined board.

COMBINED BOARD WARP PROFILE

The amount of twist warp at 90% RH increased steadily
with increasing polar angle deviation in opposite
directions from MD of combined board.

COMBINED BOARD WARP PROFILE
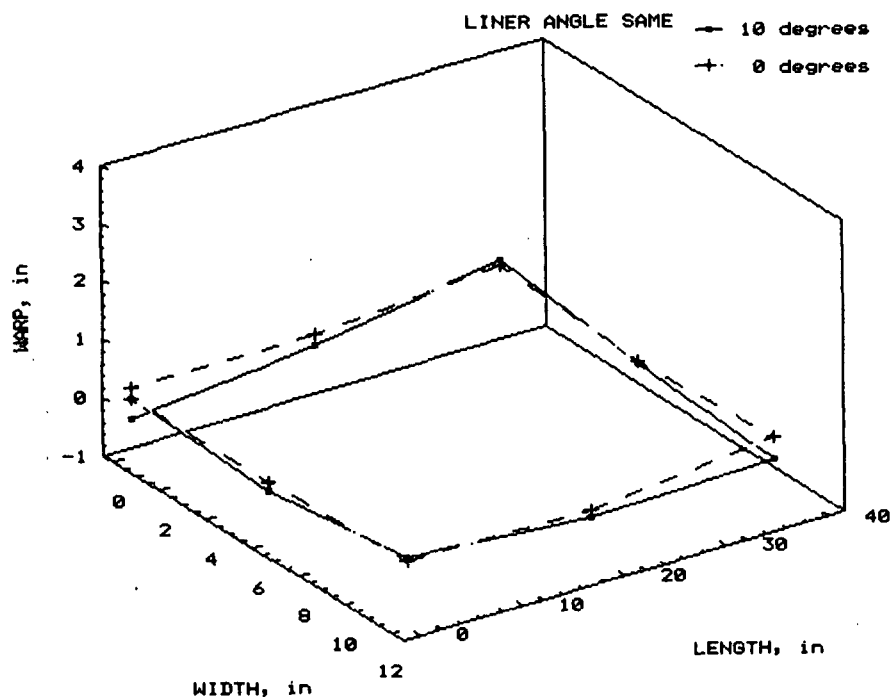
LINER ANGLE SAME •— 10 degrees
+· 0 degrees

Combined board warp profiles for boards made with
SF and DF liner polar angles of 0 and 10°, in same
direction.

COMBINED BOARD WARP PROFILE

LINER ANGLE SAME •— 15 degrees
+· 10 degrees
⁕· 5 degrees
☒· 0 degrees
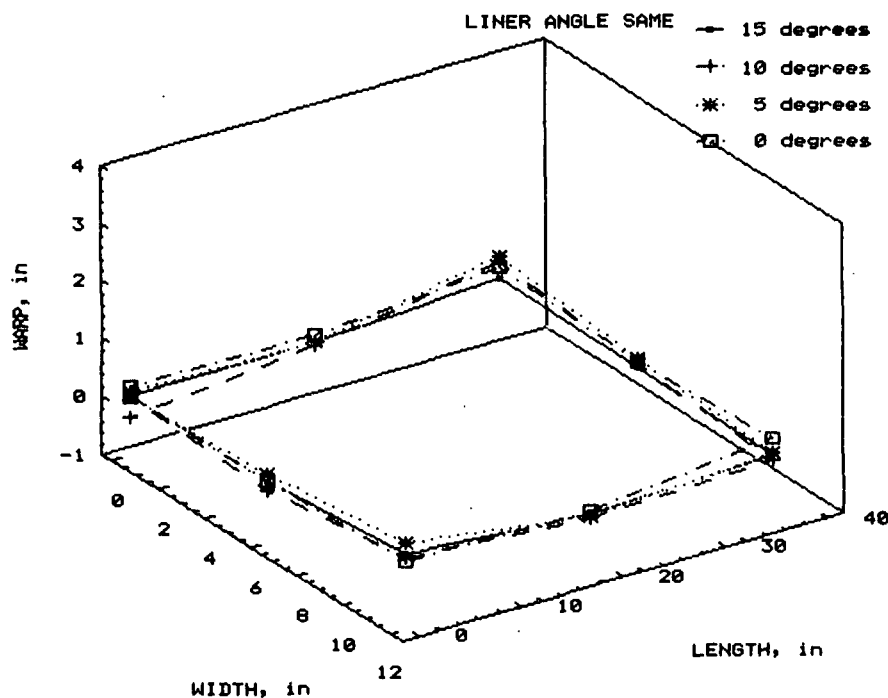
Combined board warp profiles for boards made with SF
and DF liner polar angles in same direction.

-- MEDIUM AND LINER IMPROVEMENT --

- SURFACE TREATMENTS EVALUATED: PAE, STARCH,
    CMPS AND COMBINATIONS

- SIGNIFICANT STRENGTH INCREASES OBTAINED WITH:
    - PAE
    - PAE/STARCH AND PAE/CMPS

- COMPRESSION AND TENSILE IMPROVEMENTS RETAINED
    AT HIGH RH

- TREATMENTS IMPROVED FLAT CRUSH

- MODEST IMPROVEMENTS IN ECT

- NO APPARENT EFFECT ON HIGH-LOWS

- TREATMENTS DECREASED WETTABILITY, MADE CORRUGATING
    BONDING MORE DIFFICULT

MEDIUM AND LINER IMPROVEMENT

- SCREENING ADDITIVES TO:

  -- INCREASE STRENGTH

  -- MAINTAIN WETTABILITY FOR GLUEING AND
      PRINTING

RUNNABILITY MODELING

  - STRENGTH LOSSES

  - HIGH TEMPERATURE FURNISH EFFECTS

  - SPEED AND STRAIN-RATE EFFECTS
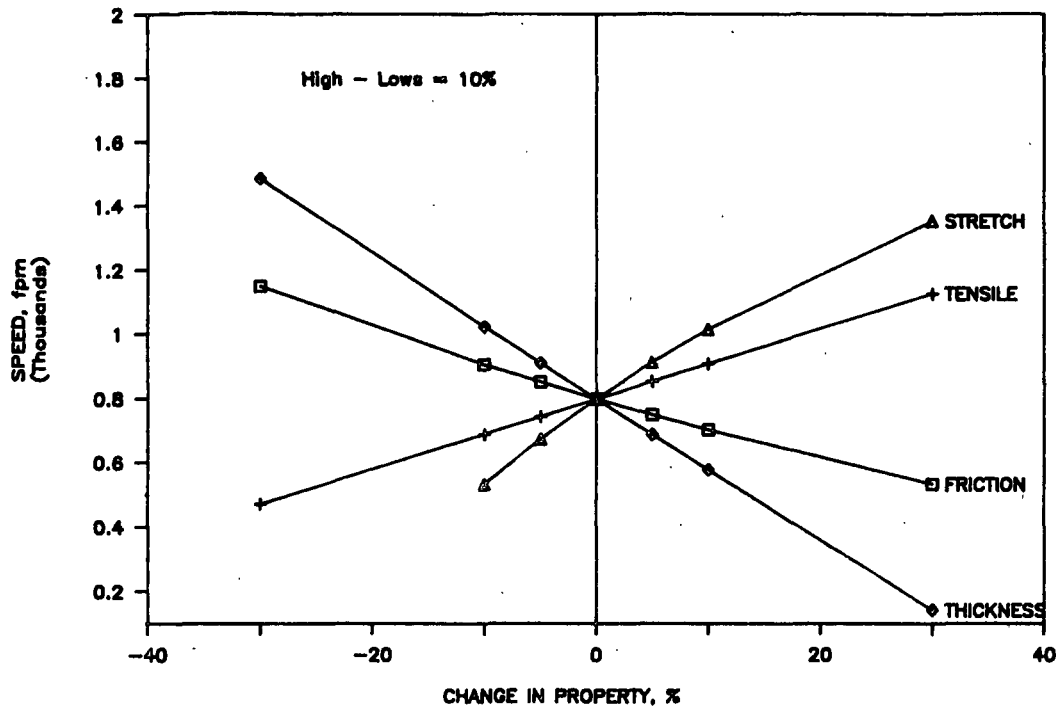
Effects of changes in medium properties on the speed
at which high-lows equal 10%.
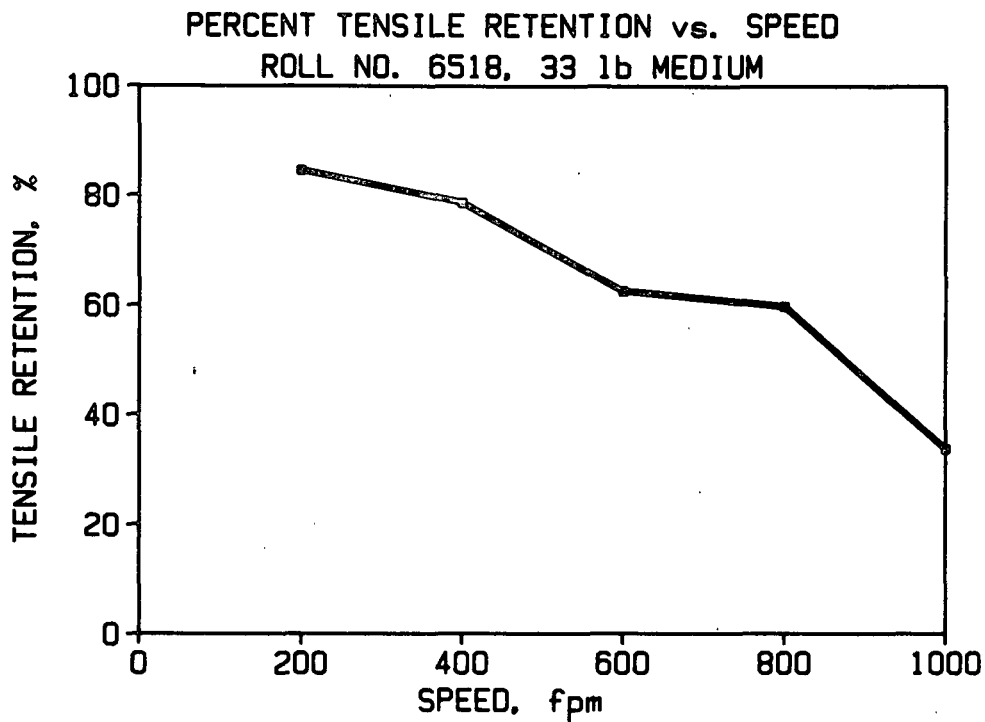
Tensile strengths of the fluted medium decline as
corrugator speed increases and the medium is
more highly stressed.

TENSILE RETENTION VS. STRESS RATIO
33 lb MEDIUMS
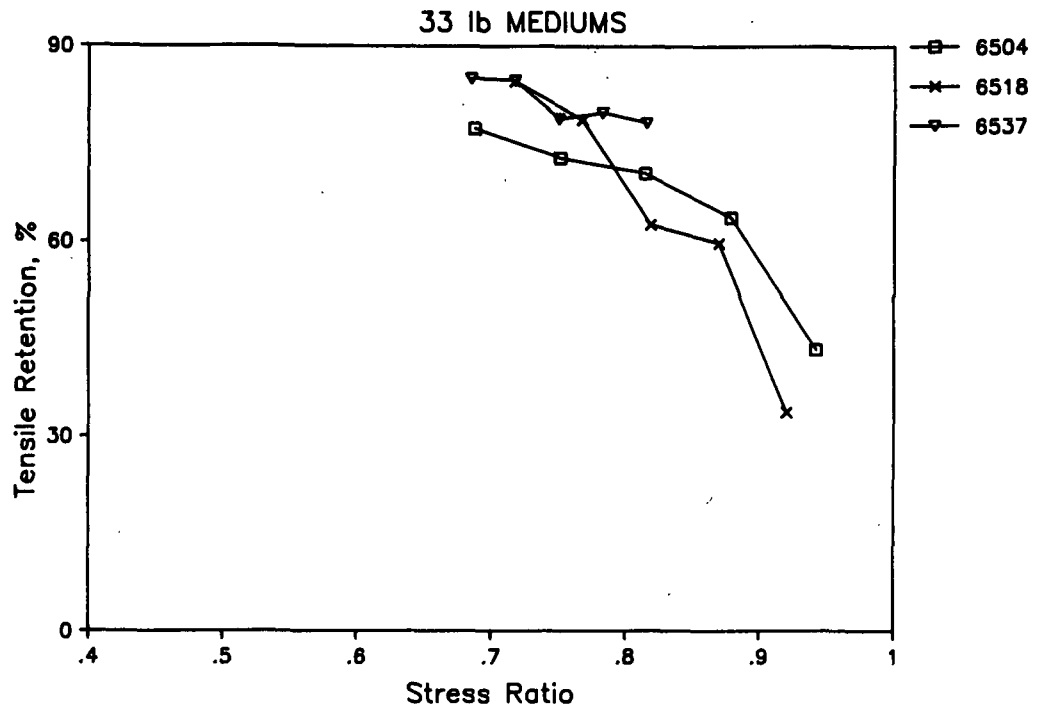
Tensile strengths of fluted 33-lb mediums decrease at high levels of applied stress during fluting.

TENSILE RETENTION VS. STRESS RATIO
40 lb MEDIUMS
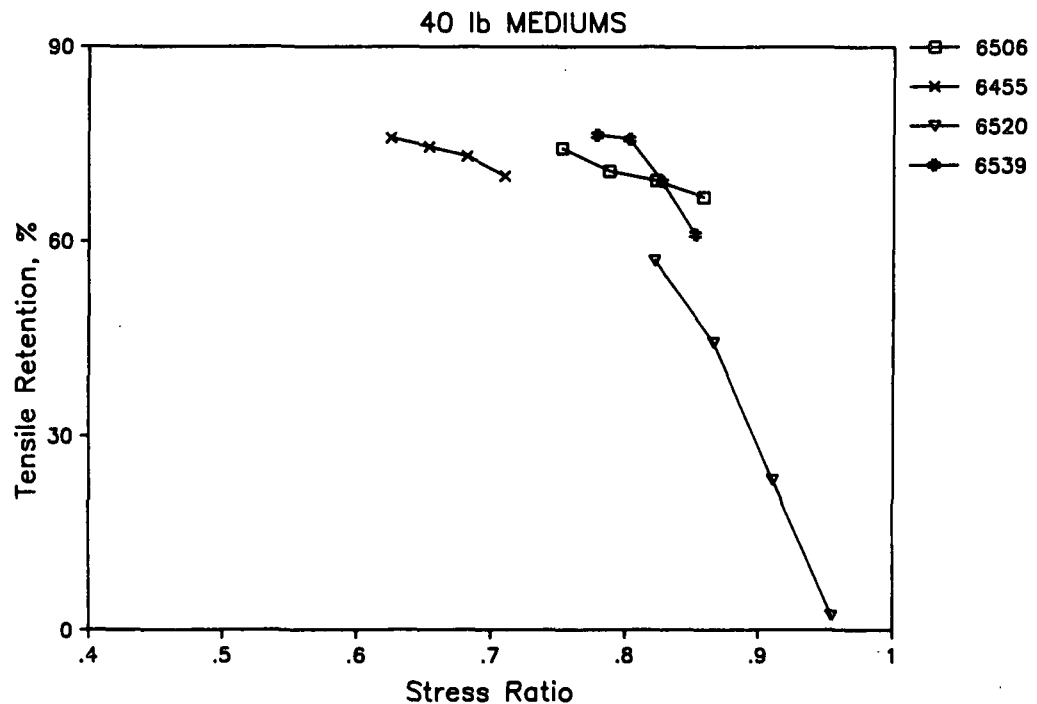
Tensile strengths of 40-lb mediums decrease at high levels of applied stress during fluting.

TENSILE RETENTION VS. STRESS RATIO
Model: $y=(1-x^2)^{.4}$
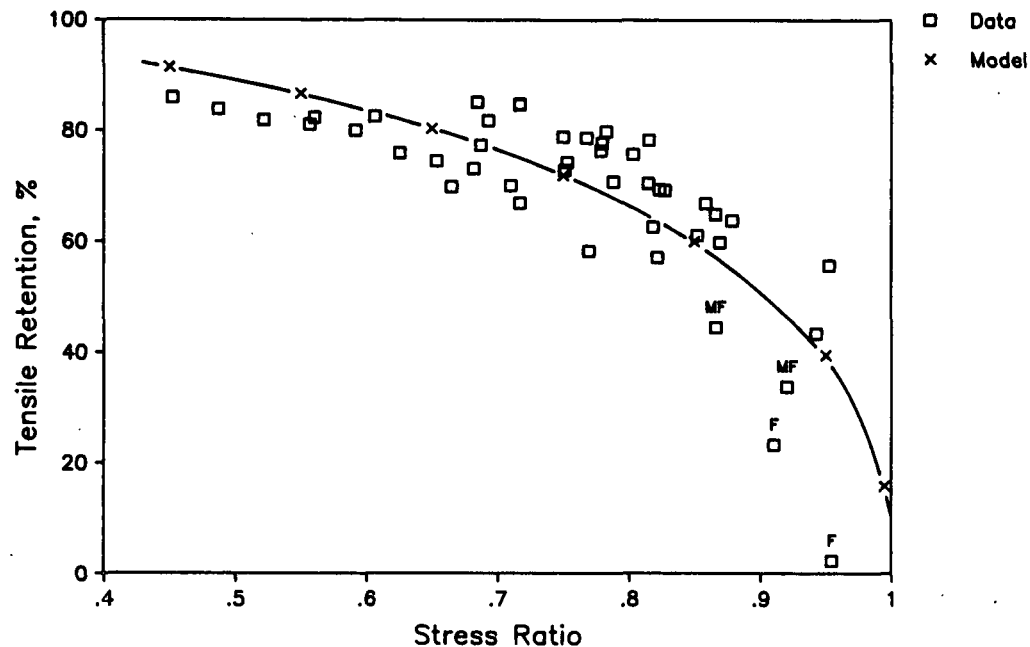
General relationship between tensile strength
losses and the stresses applied to the medium
during fluting.

TENSILE RETENTION VS. DRAW FACTOR
$R^2 = .85$
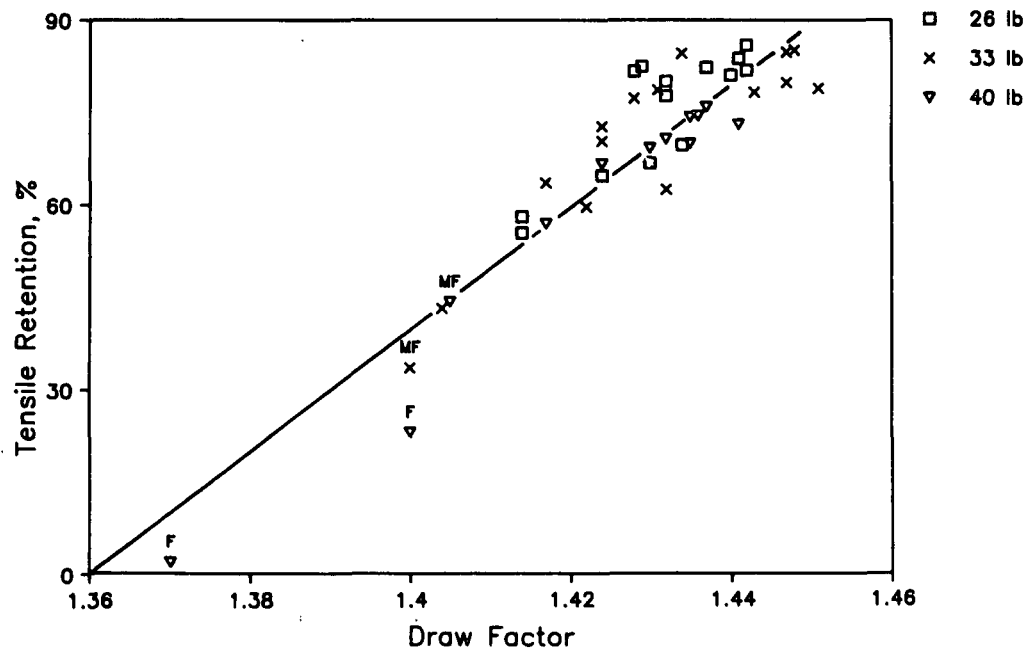
Relationship between medium draw factor and
tensile strength losses. (Note: F denotes
fracture, MF denotes minor sporatic fractures.)
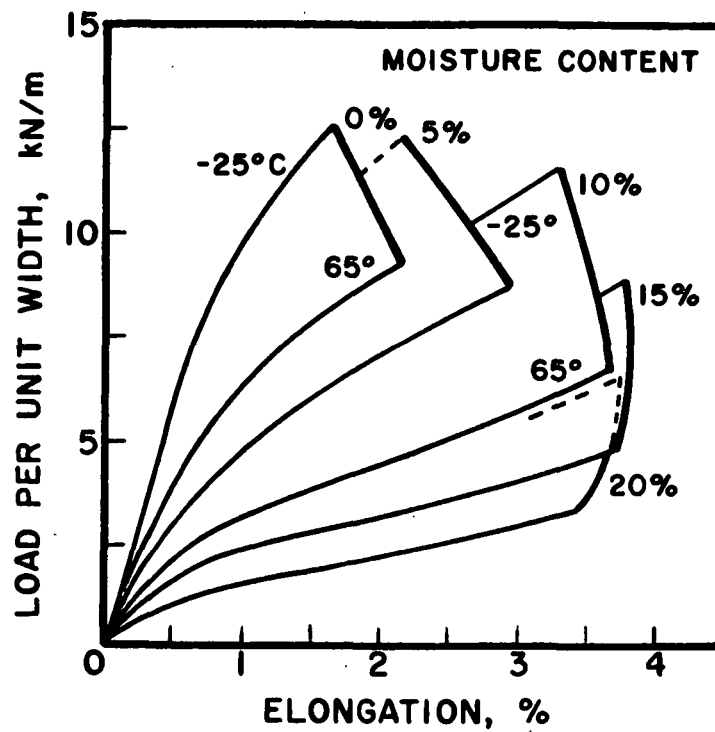
Effect of temperature and moisture on stress-strain properties of a sack paper.
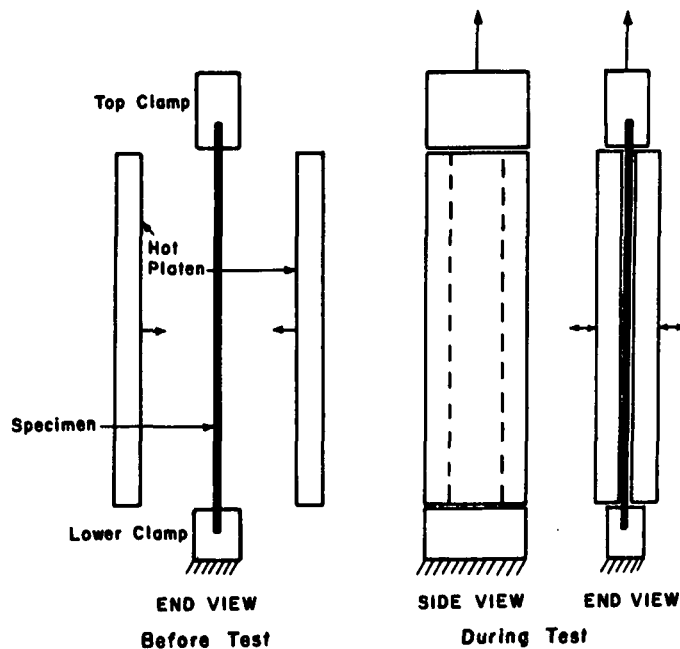
Hot platen schematic for tensile tests.
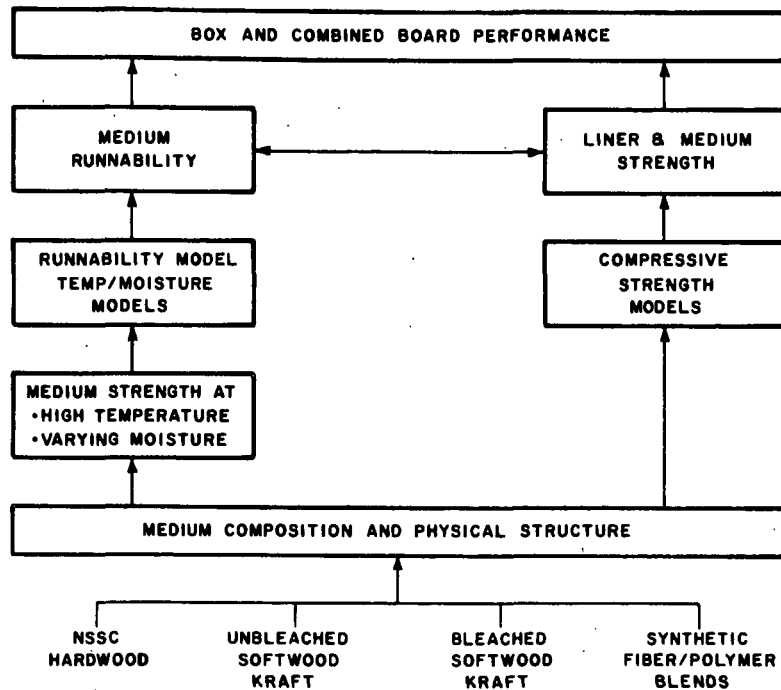
Schematic plan for high temperature medium
furnish study.

RUNNABILITY MODELING

• HIGH FLUTING STRESSES CAUSE LARGE TENSILE
  LOSSES

• MODEL STRESS PREDICTIONS CORRELATE WELL
  WITH TENSILE LOSSES

• STUDYING EFFECTS ON MODEL OF:

  -- HIGH TEMPERATURE BEHAVIOR FOR VARIOUS
     MEDIUM FURNISHES AND CHEMICAL COMPOSITION

  -- MEDIUM STRAIN-RATE AND SPEED EFFECTS

RUNNABILITY MODELING

- SPEED EFFECTS -

FRACTURE SPEED DECREASES

WITH INCREASING BRAKE TENSION

Dashpot
μ_3

Spring
λ_1

Spring
λ_2
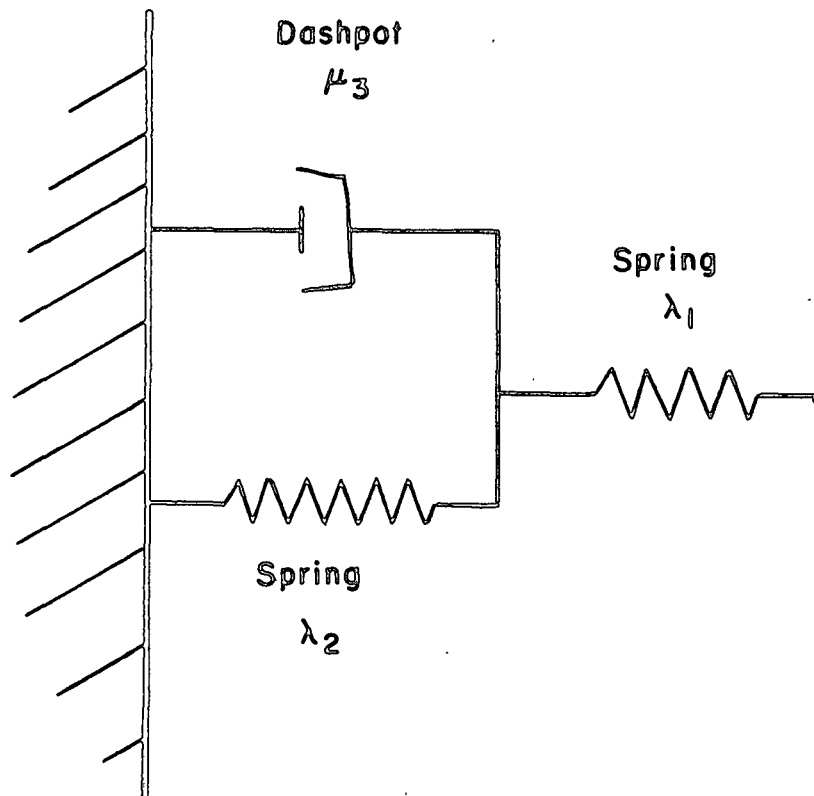
Simple viscoelastic model for describing the
dynamic behavior of medium.

HIGH TEMPERATURE DATA

ET = 1700 lb/in.

TENSILE = 19 lb/in.

STRETCH = 0.02 in./in.

PARAMETER SELECTION

λ_1 = 1700 lb/in.

λ_2 = 2100 lb/in.

μ_3 = 3 lb-sec/in.
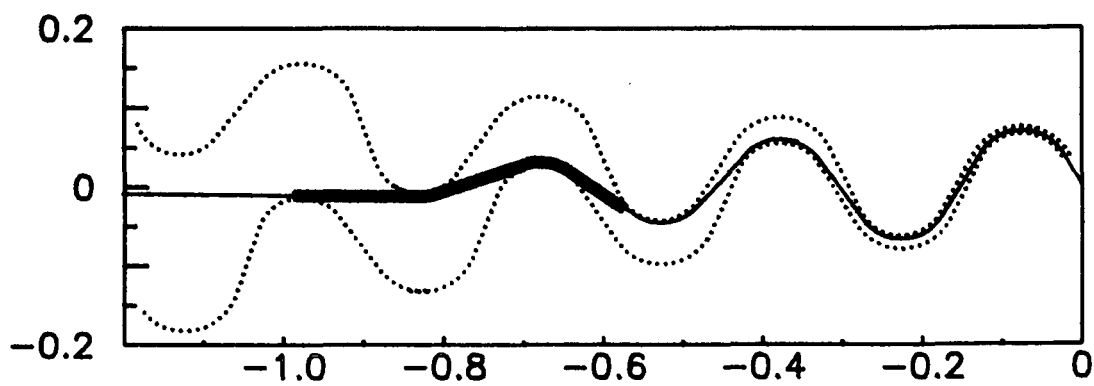
Simulation of web and corrugating rolls.

$$T = T_0 e^{f\theta}$$

T   TENSION IN THE LABYRINTH

T_0 INITIAL BRAKE TENSION

θ WRAP ANGLE (TIME, SPEED, GEOMETRY)

f   COEFFICIENT OF FRICTION

HYPOTHESIS:

FRACTURING OCCURS WHEN THE LOAD

ACROSS THE DASHPOT REACHES A

CRITICAL VALUE.

COMPUTER PROGRAM
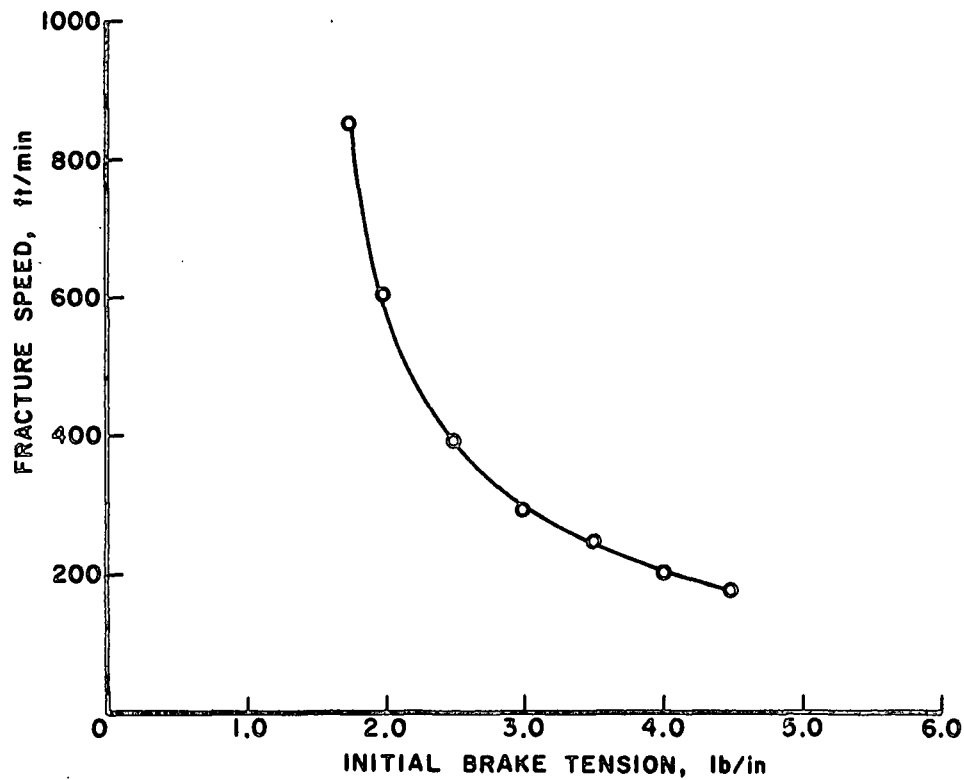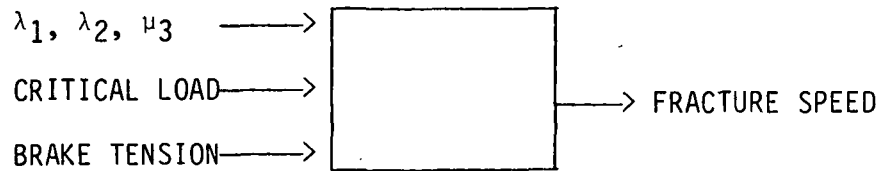
λ_1, λ_2, μ_3 ──────⟶

CRITICAL LOAD──────⟶   ──⟶ FRACTURE SPEED

BRAKE TENSION──────⟶

Linear viscoelastic model relationship between corrugating
speed and brake tension.

THIS HEURISTIC WORK SUGGESTS A MECHANISM FOR
RELATING HOW FURNISH AND PAPERMAKING FACTORS
INFLUENCE FRACTURE SPEED, HIGH-LOWS AND
STRENGTH RETENTION.

FLAT CRUSH

AND

FLUTE FORMATION MODELING

ITERATION
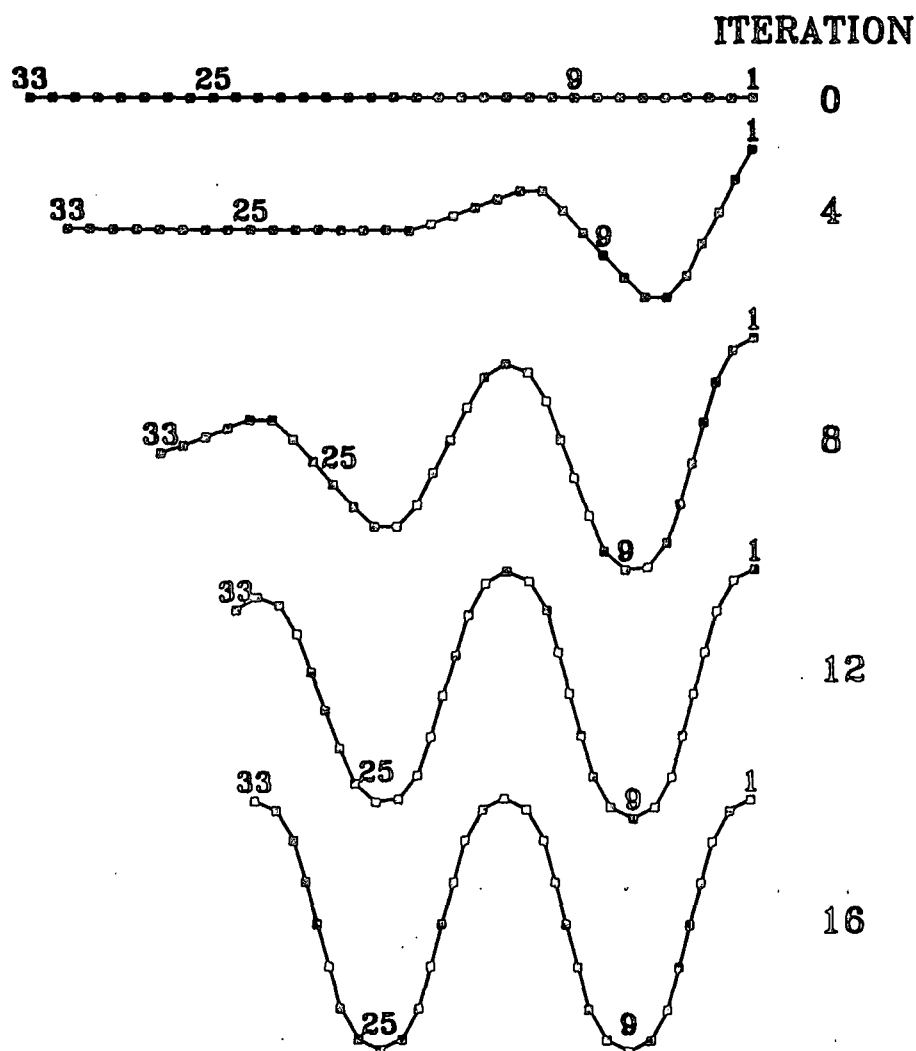
Flute formation model.
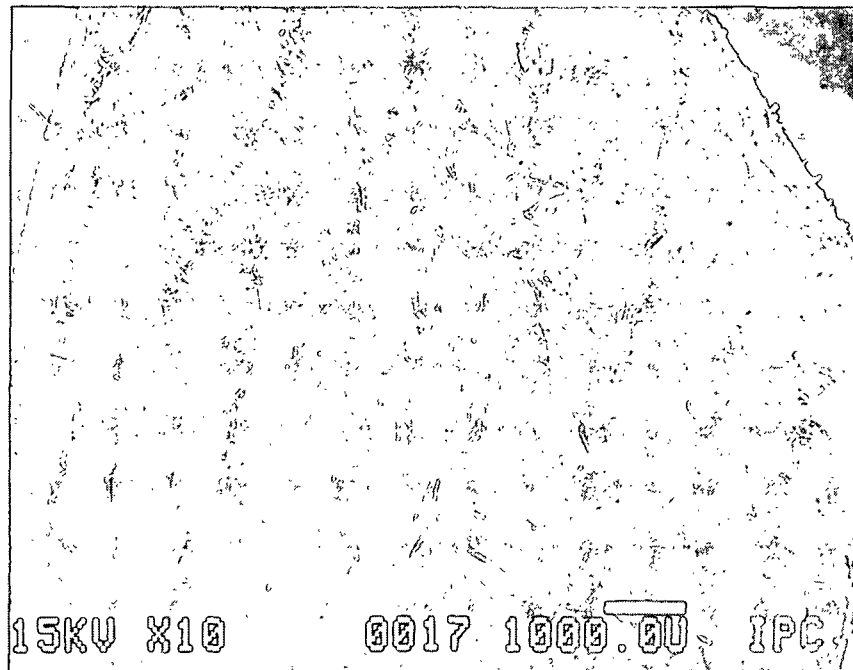
Surface checking was observed on the compression side of the medium after bending (view magnification = 10).
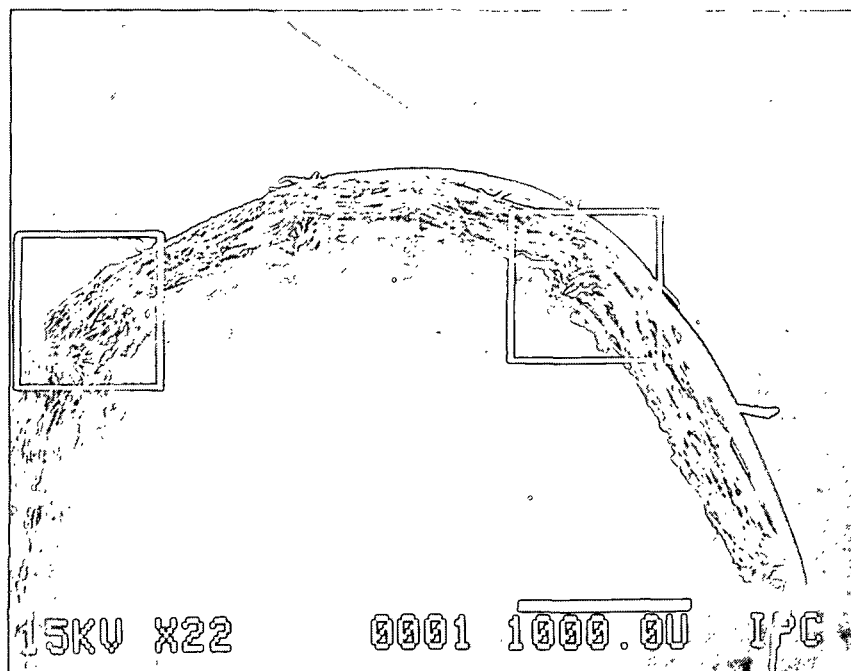
A side view of the specimen after bending shows three damage locations (view magnification = 22). The damaged area in the box at the right has been magnified and is shown on Page 5-19 (top). The damaged area in the box on the right has also been magnified and is shown on Page 5-19 (bottom).
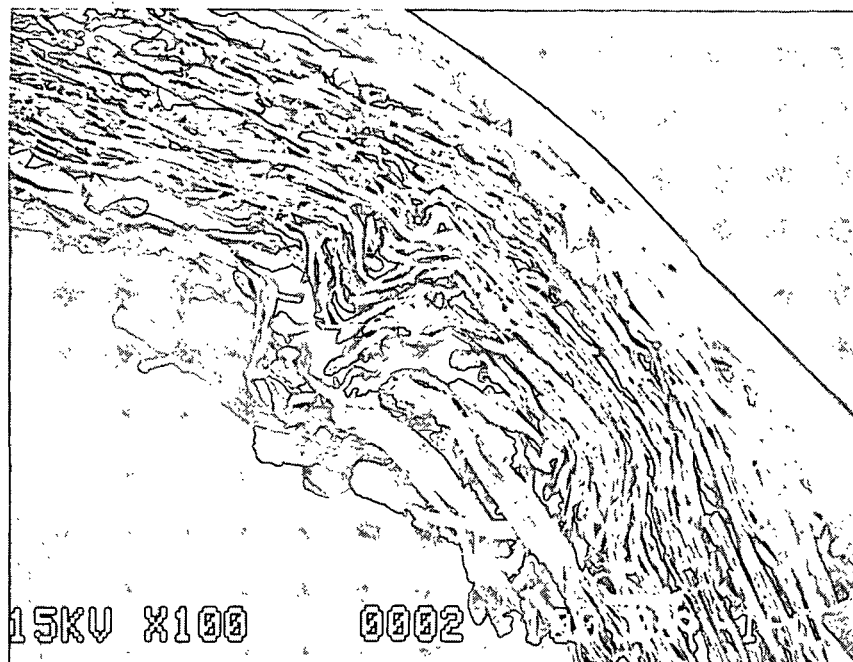
Fiber buckling in the damaged area occurred through about
75% of the thickness (view magnification = 100).
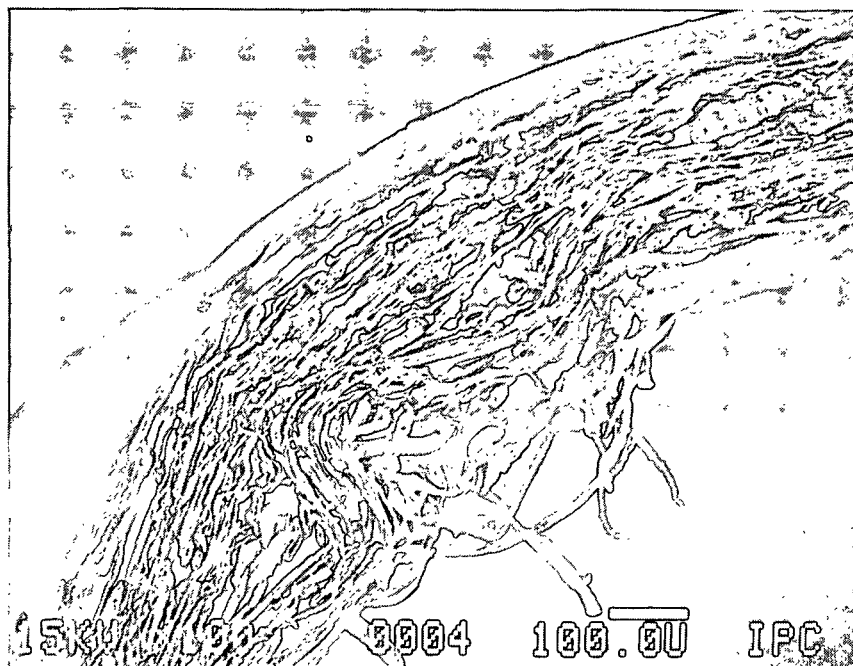
An inward buckling of the fibers appears to have occurred in this
damaged area, through about 50% of the thickness (view magnification
= 100).
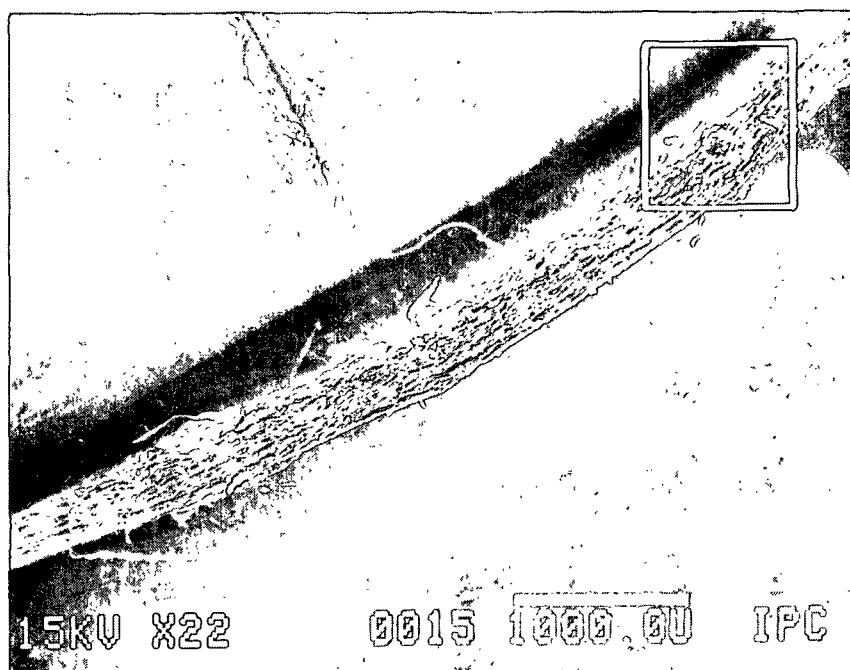
Side view of a specimen after bending and straightening back to a nearly flat configuration (view magnification = 22). The only detectable damage is a surface disturbance shown in the box on the right (this area has been magnified and is shown below).
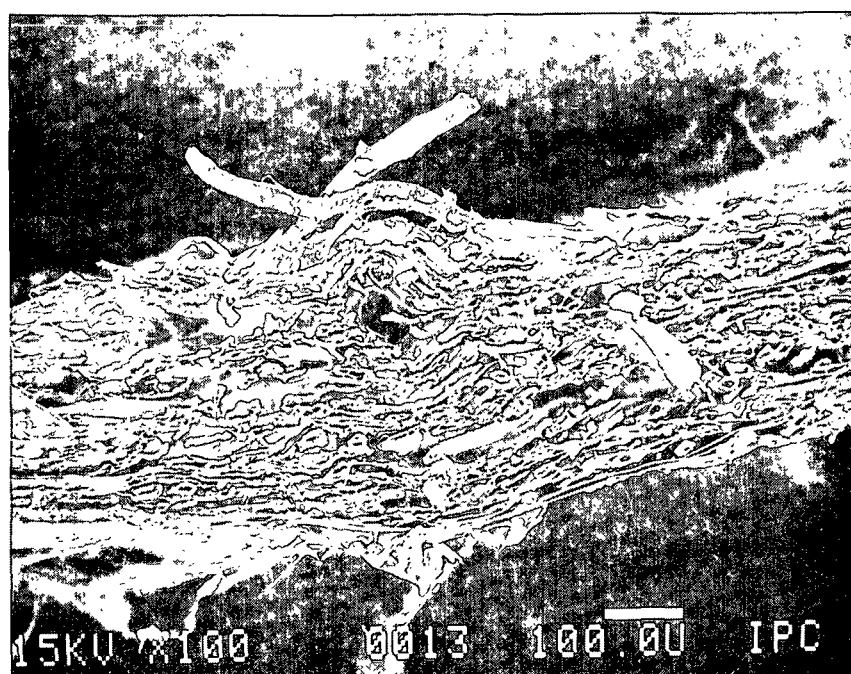
Side view of surface checking (view magnification = 100).
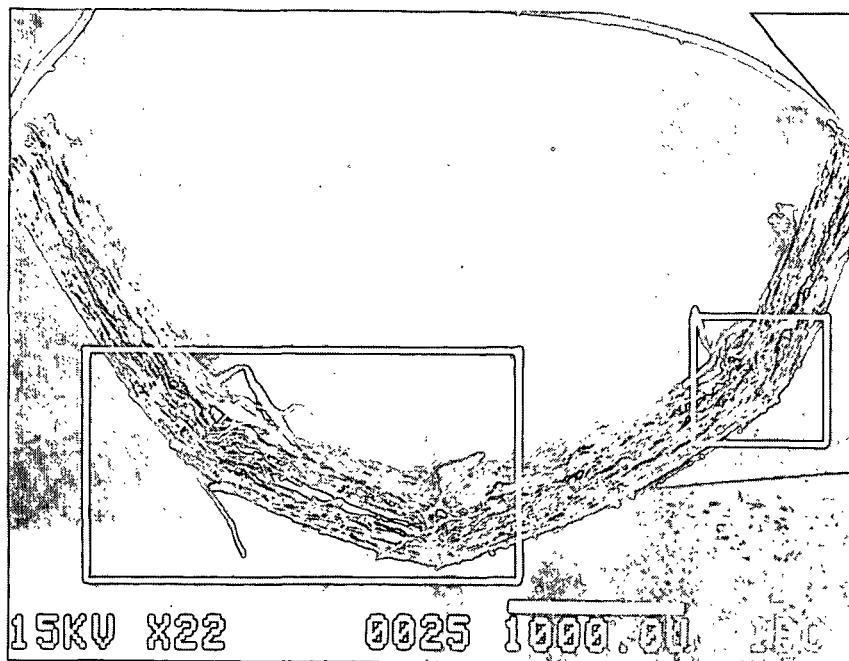
Side view of the specimen in on Page 5-20 (top), after it was re-
formed around a 0.125 in. dia. rod (view magnification = 22). The
boxed area on the right shows the rebuckling of the fibers at what
looked like a surface disturbance on Page 5-20 (top) (this area has
been magnified further and is shown on below. The damaged area out-
lined at the right was undetectable on Page 5-20 (top)(this area has
also been magnified and is shown on Page 5-22 (top).
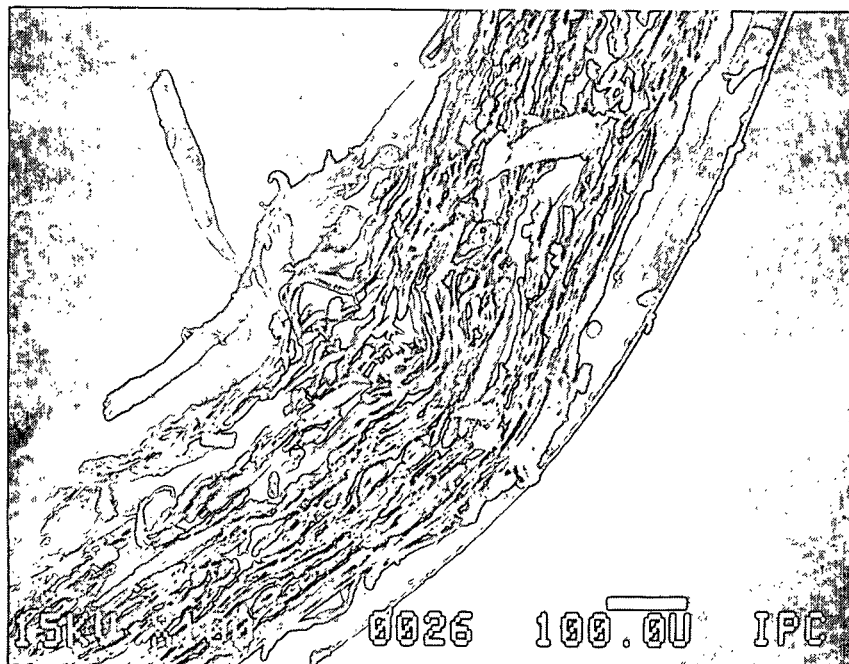
The fibers, in compression, buckle at a surface disturbance of the
fibers when the specimen was reformed around the radius (view
magnification = 100).
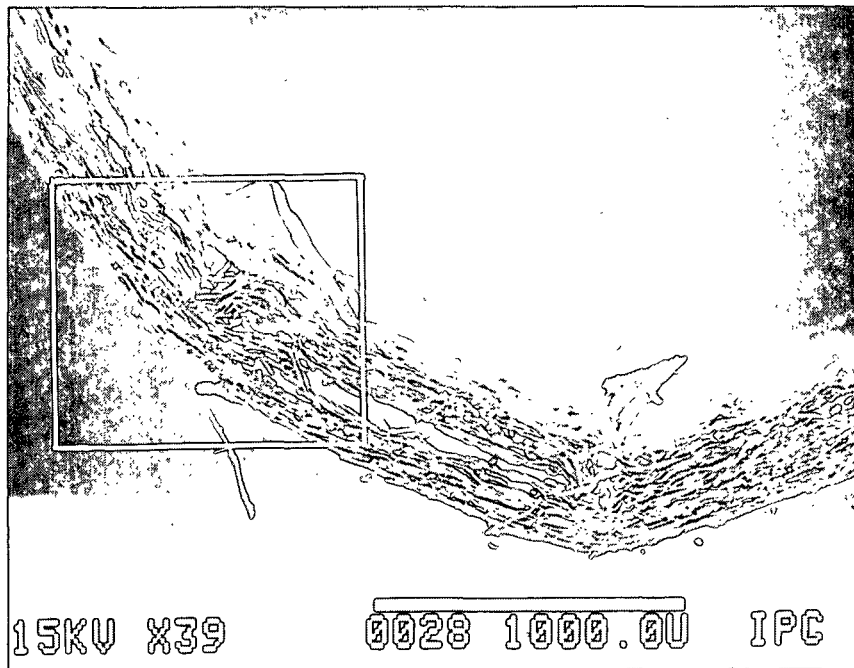
This damaged area appears to be fiber buckling at each end of a
delamination in the sheet (view magnification = 39). The boxed
area on the left side of the delamination has been magnified
further and is shown below.
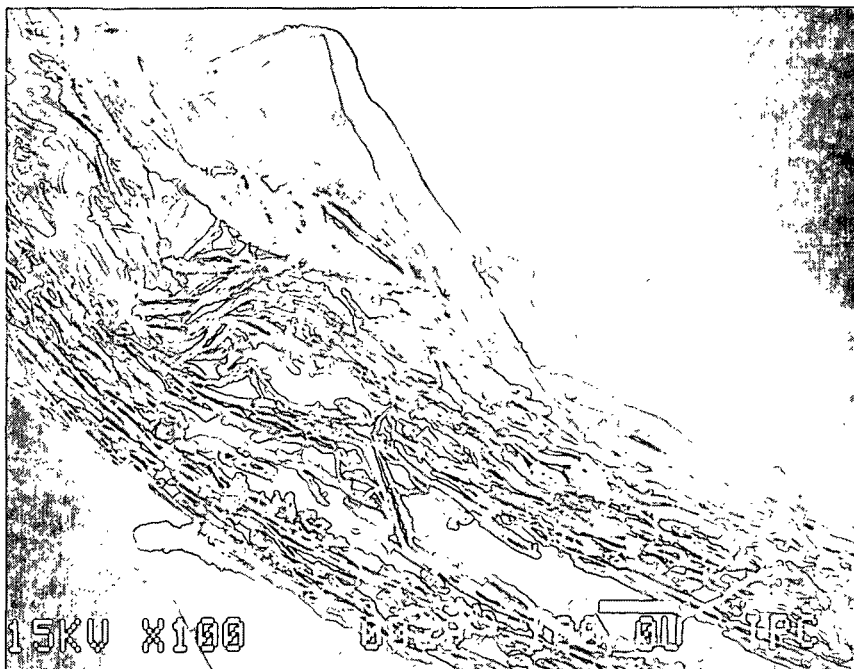
Side view of a damaged zone showing fiber buckling and sheet
delamination (view magnification = 100).

OBSERVATIONS OF MEDIUM BENDING

FIBER DAMAGE:

- AT INTERVALS OF ABOUT 0.030 in.

- AFFECTS 50% - 75% OF THICKNESS

- PRIMARILY BUCKLING

- SOME SHEAR DELAMINATION

FLAT CRUSH MODEL

PERIODIC FIBER
DAMAGE
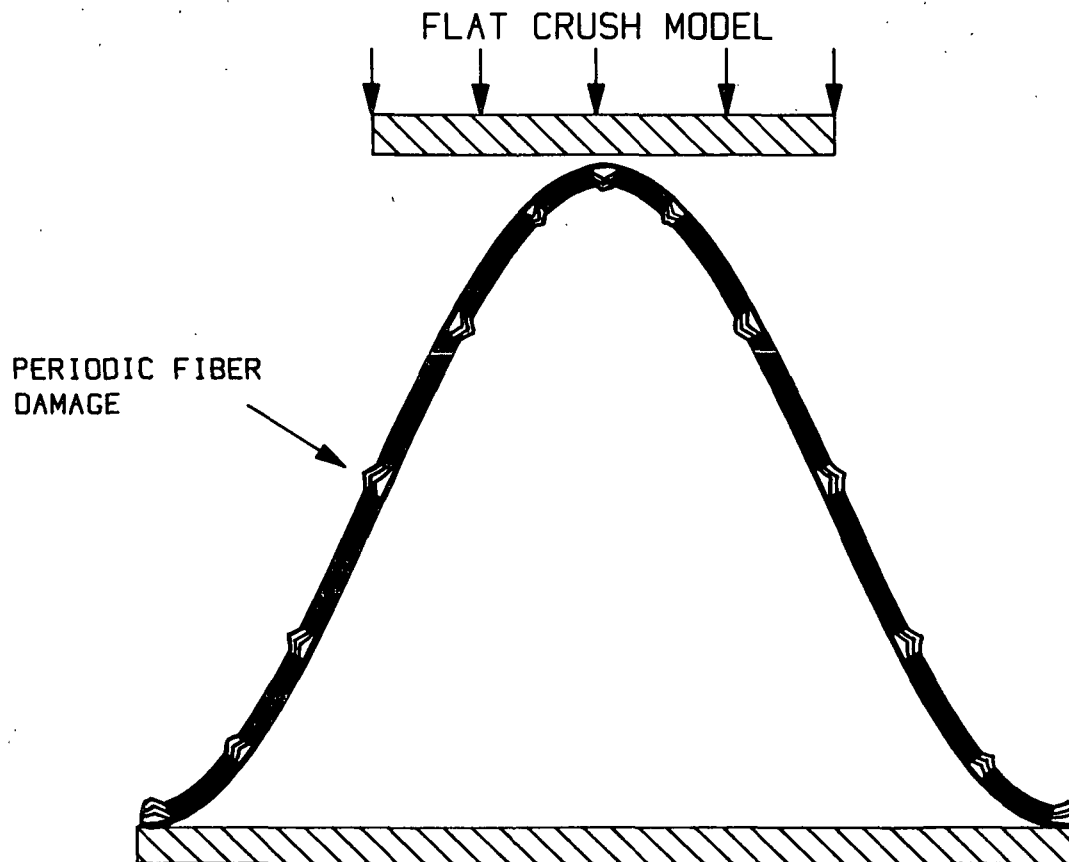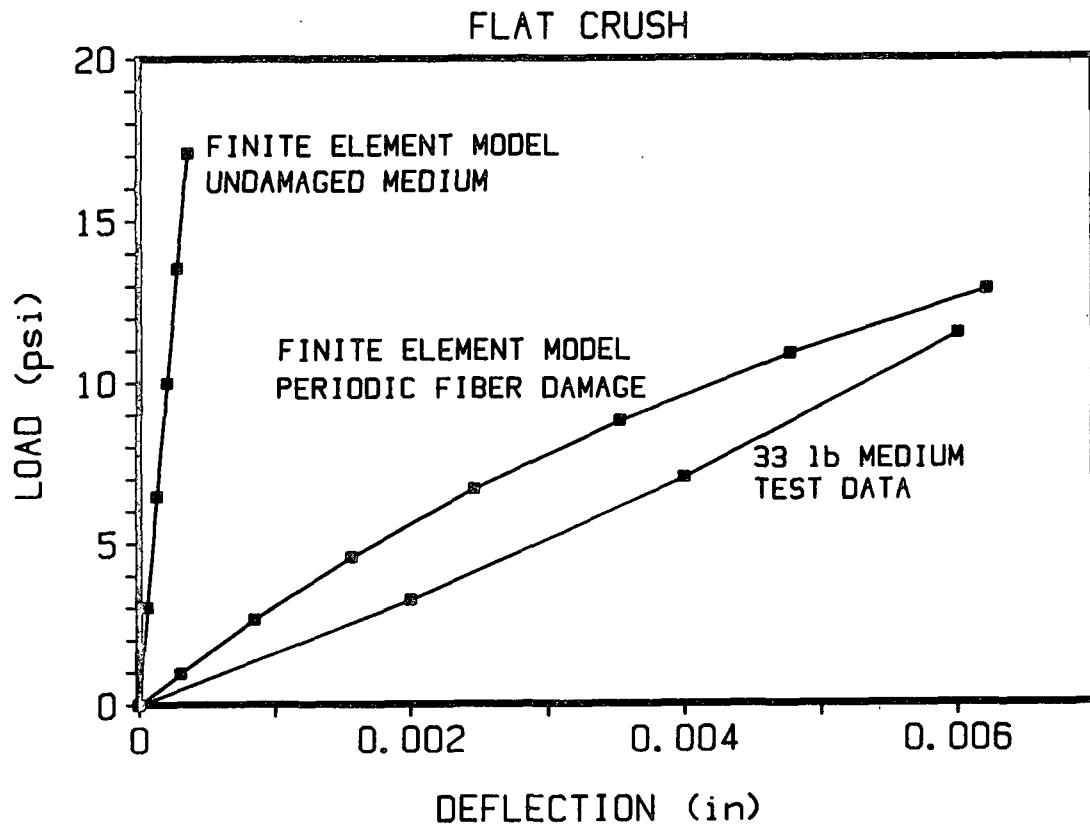
FLAT CRUSH

SUMMARY OF FLAT CRUSH F.E. MODEL

o MODELED INITIAL CURVE

o USED OBSERVED DAMAGE PATTERN

⊕ ASSUMED 75% FIBER DAMAGE AT INTERVALS

⊕ GOOD CORRELATION WITH TEST DATA

FUTURE TESTING

MEDIUM FORMING DAMAGE - DETERMINE:

- FACTORS AFFECTING

- LOCATION

- EXTENT

NEW BENDING APPARATUS WILL VARY:

- RADIUS, TENSION, WRAP ANGLE,
    FRICTION

FUTURE FINITE ELEMENT MODELING

FLAT CRUSH

- INITIAL CURVE

- FIRST PEAK

- FAILURE

BOARD BENDING

ECT

PANEL BULGE

COMMERCIAL BOX ABUSE STUDY

PURPOSE:

ASSESS COMMERCIAL BOARD PERFORMANCE

- BASELINE RESULTS

- SERVICE ABUSE CONDITIONS

SERVICE ABUSE CONDITIONS

- PRECRUSH (3 LEVELS)

- RELATIVE HUMIDITY (2 LEVELS)

- COMBINED PRECRUSH AND RH

COMMERCIAL BOARD

- C-FLUTE

- 60-LB LINERS

- 26-LB AND 33-LB MEDIUMS

TESTING

- FLAT CRUSH

- ECT

- FLEXURAL STIFFNESS

- BOX COMPRESSION

SECTION 6

Project 3467

PROCESS, PROPERTIES AND PRODUCT RELATIONSHIPS

USING POLAR PLOTS TO DETERMINE ELASTIC STIFFNESSES

- IMPROVED POISSON RATIOS

- FIRST MEASUREMENT OF C_{16} AND C_{26}

MEASURED POLAR PLOT VELOCITIES, USING POINT SOURCE TRANSDUCERS, ARE VELOCITIES OF "INFORMATION PROPAGATION"

PLANE WAVE PHASE VELOCITY POLAR PLOTS CAN BE DETERMINED FROM INFORMATION PROPAGATION POLAR PLOTS

PLANE WAVE PHASE VELOCITY POLAR PLOTS CAN BE DETERMINED FROM THE C_{ij}'s

THE OPTIMUM C_{ij}'s GIVE THE BEST REPRODUCTION OF THE EXPERIMENTAL PHASE VELOCITY POLAR PLOTS

GENERAL ELASTIC RELATIONSHIPS

$$\sigma_{11} = C_{11}\epsilon_1 + C_{12}\epsilon_2 + C_{16}\epsilon_6$$

$$\sigma_{22} = C_{12}\epsilon_1 + C_{22}\epsilon_2 + C_{26}\epsilon_6$$

$$\sigma_{12} = C_{16}\epsilon_1 + C_{26}\epsilon_2 + C_{66}\epsilon_6$$

IF THE MATERIAL IS ORTHOTROPIC AND THE COORDINATES ARE ALIGNED ALONG THE PRINCIPAL AXES,

$$\sigma_{11} = C_{11}\epsilon_1 + C_{12}\epsilon_2$$

$$\sigma_{22} = C_{12}\epsilon_1 + C_{22}\epsilon_2$$

$$\sigma_{12} = C_{66}\epsilon_6$$

THE INSTITUTE OF PAPER CHEMISTRY
ROBOTIC IN-PLANE ULTRASONIC VELOCITIES

POLAR PLOT OF LONGITUDINAL INFORMATION PROPAGATION VELOCITY SQUARED

OPERATOR: C. C. Habeger   DATE: SEPTEMBER 12, 1988
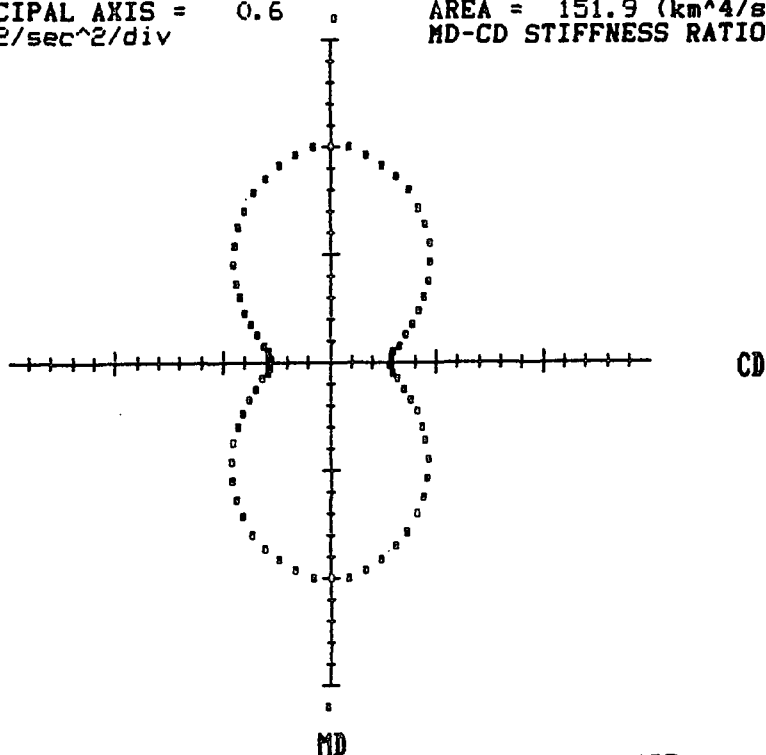PROJECT : 3467   TIME: 17:32:45
SAMPLE : Chipboard top

SIGNALS AVERAGED PER MEASUREMENT =   4
NUMBER OF TESTS PER ANGLE   =   16
SIGNAL DISTANCE   = 50.0 mm
SAMPLE HOLDER NUMBER   =   2

ANGLE DEGREES	VEL SQR KM2/SEC2	COEF OF VARIATION	ANGLE DEGREES	VEL SQR KM2/SEC2	COEF OF VARIATION
0	10.12	0.019	90	2.86	0.016
5	9.86	0.026	95	2.85	0.017
10	9.47	0.031	100	2.86	0.023
15	8.83	0.036	105	2.89	0.018
20	8.02	0.025	110	2.98	0.014
25	7.17	0.042	115	3.13	0.019
30	6.39	0.030	120	3.35	0.018
35	5.67	0.024	125	3.68	0.021
40	5.00	0.023	130	4.00	0.019
45	4.45	0.025	135	4.40	0.017
50	4.01	0.019	140	4.93	0.013
55	3.62	0.021	145	5.55	0.016
60	3.38	0.020	150	6.25	0.016
65	3.17	0.026	155	6.98	0.023
70	3.02	0.029	160	7.76	0.015
75	2.95	0.025	165	8.64	0.020
80	2.90	0.017	170	9.32	0.034
85	2.88	0.013	175	9.79	0.028

ANGLE TO MAJOR PRINCIPAL AXIS =   0.5   AREA =   109.3 (km^4/sec^4)
GRAPH SCALE = 1 km^2/sec^2/div   MD-CD STIFFNESS RATIO = 3.54

PLOT OF VEL SQR VS ANGLE AS SEEN FROM FELT SIDE

Longitudinal polar plot of information propagation
velocity squared for a chipboard sample.

THE INSTITUTE OF PAPER CHEMISTRY
ROBOTIC IN-PLANE ULTRASONIC VELOCITIES

POLAR PLOT OF LONGITUDINAL PHASE VELOCITY SQUARED

OPERATOR: C. C. Habeger   DATE: SEPTEMBER 12, 1988
PROJECT : 3467   TIME: 17:33:56
SAMPLE : Chipboard top

SIGNALS AVERAGED PER MEASUREMENT =   4
NUMBER OF TESTS PER ANGLE   =   16
SIGNAL DISTANCE   = 50.0 mm
SAMPLE HOLDER NUMBER   =   2

ANGLE DEGREES	VEL SQR KM2/SEC2	ANGLE DEGREES	VEL SQR KM2/SEC2
0	10.12	90	2.86
5	10.04	95	2.85
10	9.81	100	3.02
15	9.56	105	3.31
20	9.20	110	3.72
25	8.84	115	4.20
30	8.36	120	4.69
35	7.80	125	5.24
40	7.25	130	5.82
45	6.62	135	6.48
50	6.02	140	7.09
55	5.38	145	7.65
60	4.81	150	8.22
65	4.29	155	8.69
70	3.81	160	9.13
75	3.36	165	9.49
80	3.01	170	9.81
85	2.88	175	10.04

ANGLE TO MAJOR PRINCIPAL AXIS =   0.6   AREA =   151.9 (km^4/sec^4)
GRAPH SCALE = 1 km^2/sec^2/div   MD-CD STIFFNESS RATIO = 3.54

MD
PLOT OF VEL SQR VS ANGLE AS SEEN FROM FELT SIDE

Longitudinal polar plot of phase velocity squared for
a chipboard sample.

THE INSTITUTE OF PAPER CHEMISTRY
ROBOTIC IN-PLANE ULTRASONIC VELOCITIES

OPTIMUM MASS SPECIFIC STIFFNESSES FROM LEAST SQUARED FIT TO LONGITUDINAL PHASE VELOCITY

OPERATOR: C. C. Habeger   DATE: SEPTEMBER 12, 1988
PROJECT : 3467   TIME: 17:34:58
SAMPLE : Chipboard top

ORTHOTROPIC STIFFNESSES   GENERAL STIFFNESSES
C11 / rho =   10.038 KM2/SEC2   C11 / rho =   10.039 KM2/SEC2
C22 / rho =   2.787 KM2/SEC2   C22 / rho =   2.788 KM2/SEC2
C66 / rho =   1.889 KM2/SEC2   C66 / rho =   1.889 KM2/SEC2
C12 / rho =   1.194 KM2/SEC2   C12 / rho =   1.193 KM2/SEC2
                                 C16 / rho =   -0.007 KM2/SEC2
                                 C26 / rho =   0.014 KM2/SEC2

                                 C66 / rho (Campbell) =   1.746 KM2/SEC2

Average relative error = 0.000952   Average relative error = 0.000931
Stiffness ratio = 3.60   Stiffness ratio = 3.60

Poisson's Ratios   Poisson's Ratios
Vxy =   0.119   Vxy =   0.119
Vyx =   0.429   Vyx =   0.428
Geometric Mean =   0.226   Geometric Mean =   0.225

ANGLE TO MAJOR PRINCIPAL AXIS =   0.6   AREA =   135.4 (km^4/sec^4)
GRAPH SCALE = 1 km^2/sec^2/div

POLAR PLOT OF LONGITUDINAL MASS SPECIFIC STIFFNESS

CD

MD

PLOT OF SPECIFIC STIFFNESS AS SEEN FROM FELT SIDE

In-plane elastic stiffnesses from polar plot optimization
for a chipboard sample.

DETERMINE C_{66} DIRECTLY FROM SHEAR VELOCITY
MEASUREMENTS, THEN FIND C_{11}, C_{22}, C_{12}, C_{16},
AND C_{26} BY LEAST SQUARE OPTIMIZATION OF PHASE
VELOCITY POLAR PLOTS.

ON HIGHLY ORIENTED SHEETS, C_{12} DETERMINED FROM
THE POLAR PLOTS IS LOWER THAN C_{12} DETERMINED
FROM SHEAR 45° MEASUREMENTS.

MEASURED VALUES OF C_{16} AND C_{26} ARE NOT
SIGNIFICANTLY DIFFERENT FROM ZERO ON ALL
PAPER SAMPLES TESTED.

MEASURED VALUES OF C_{16} AND C_{26} ARE
SIGNIFICANTLY DIFFERENT FROM ZERO ON
AN EXTRUDED POLYESTER SHEET.

PULSE ECHO TRANSDUCERS

- MEASUREMENT OF ACOUSTIC REFLECTION
    COEFFICIENTS

- RIGOROUS DETERMINATION OF INTERNAL
    LOSSES

THE INSTITUTE OF PAPER CHEMISTRY
ROBOTIC IN-PLANE ULTRASONIC VELOCITIES

OPTIMUM MASS SPECIFIC STIFFNESSES FROM LEAST SQUARED
FIT TO LONGITUDINAL PHASE VELOCITY

OPERATOR: C. C. Habeger   DATE: AUGUST 12, 1988
PROJECT : 3467   TIME: 15:12:58
SAMPLE : Polypropylene 9 72 F

ORTHOTROPIC STIFFNESSES
C11 / rho = 10.010 KM2/SEC2
C22 / rho =   5.028 KM2/SEC2
C66 / rho =   2.195 KM2/SEC2
C12 / rho =   2.026 KM2/SEC2

GENERAL STIFFNESSES
C11 / rho = 10.012 KM2/SEC2
C22 / rho =   5.029 KM2/SEC2
C66 / rho =   2.195 KM2/SEC2
C12 / rho =   2.024 KM2/SEC2
C16 / rho =   0.003 KM2/SEC2
C26 / rho = -0.006 KM2/SEC2

C66 / rho (Campbell) =   2.423 KM2/SEC2

Average relative error = 0.000884
Stiffness ratio = 1.99

Average relative error = 0.000880
Stiffness ratio = 1.99

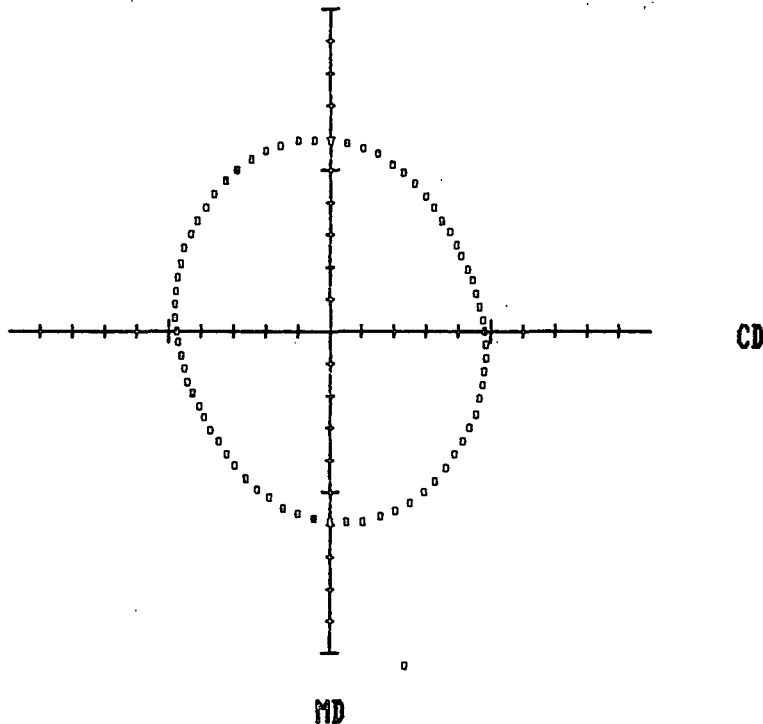Poisson's Ratios
Vxy =   0.202
Vyx =   0.403
Geometric Mean =   0.286

Poisson's Ratios
Vxy =   0.202
Vyx =   0.403
Geometric Mean =   0.285

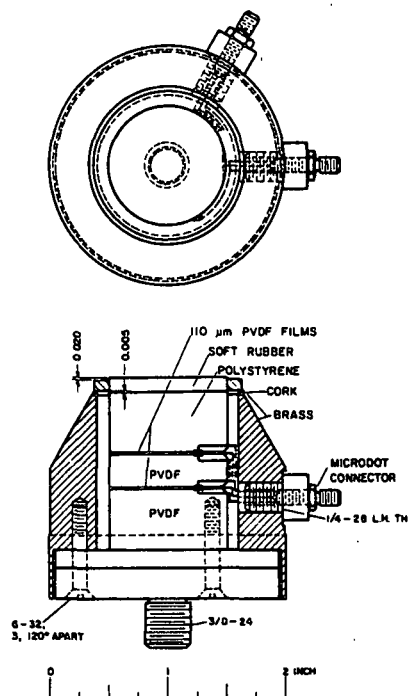ANGLE TO MAJOR PRINCIPAL AXIS = -6.2
GRAPH SCALE = 1 km^2/sec^2/div

AREA =   174.3 (km^4/sec^4)

POLAR PLOT OF LONGITUDINAL MASS SPECIFIC STIFFNESS


PLOT OF SPECIFIC STIFFNESS AS SEEN FROM FELT SIDE

Longitudinal polar plot of information propagation velocity
squared for a polypropylene sheet.

THE INSTITUTE OF PAPER CHEMISTRY
ROBOTIC IN-PLANE ULTRASONIC VELOCITIES

POLAR PLOT OF LONGITUDINAL INFORMATION PROPAGATION VELOCITY SQUARED

OPERATOR: C. C. Habeger   DATE: AUGUST 30, 1988
PROJECT : 3467   TIME: 17:59:28
SAMPLE : Polyester 101 top 72 F

SIGNALS AVERAGED PER MEASUREMENT =   4
NUMBER OF TESTS PER ANGLE   =   8
SIGNAL DISTANCE   = 50.0 mm
SAMPLE HOLDER NUMBER   =   2

ANGLE DEGREES	VEL SQR KM2/SEC2	COEF OF VARIATION	ANGLE DEGREES	VEL SQR KM2/SEC2	COEF OF VARIATION
0	5.93	0.025	90	4.76	0.009
5	5.95	0.011	95	4.84	0.012
10	5.77	0.027	100	4.89	0.010
15	5.63	0.019	105	4.93	0.016
20	5.48	0.024	110	5.03	0.011
25	5.32	0.026	115	5.08	0.014
30	5.17	0.019	120	5.19	0.003
35	5.11	0.021	125	5.23	0.010
40	4.98	0.017	130	5.36	0.010
45	4.90	0.027	135	5.48	0.009
50	4.86	0.027	140	5.58	0.007
55	4.77	0.016	145	5.68	0.011
60	4.71	0.011	150	5.79	0.014
65	4.67	0.011	155	5.84	0.013
70	4.70	0.008	160	5.97	0.009
75	4.70	0.012	165	5.97	0.011
80	4.67	0.019	170	5.98	0.016
85	4.74	0.010	175	5.97	0.012

ANGLE TO MAJOR PRINCIPAL AXIS = -13.4   AREA =   87.7 (km^4/sec^4)
GRAPH SCALE = 1 km^2/sec^2/div   MD-CD STIFFNESS RATIO = 1.25

CD

MD

PLOT OF VEL SQR VS ANGLE AS SEEN FROM FELT SIDE

Longitudinal polar plot of information propagation velocity
squared for a polyester sheet.

THE INSTITUTE OF PAPER CHEMISTRY
ROBOTIC IN-PLANE ULTRASONIC VELOCITIES

OPTIMUM MASS SPECIFIC STIFFNESSES FROM LEAST SQUARED
FIT TO LONGITUDINAL PHASE VELOCITY

OPERATOR: C. C. Habeger   DATE: AUGUST 30, 1988
PROJECT : 3467   TIME: 18:1:36
SAMPLE : Polyester 101 top 72 F

ORTHOTROPIC STIFFNESSES   GENERAL STIFFNESSES
C11 / rho =   6.007 KM2/SEC2   C11 / rho =   6.008 KM2/SEC2
C22 / rho =   4.701 KM2/SEC2   C22 / rho =   4.701 KM2/SEC2
C66 / rho =   1.685 KM2/SEC2   C66 / rho =   1.685 KM2/SEC2
C12 / rho =   1.758 KM2/SEC2   C12 / rho =   1.756 KM2/SEC2
                                C16 / rho =   -0.051 KM2/SEC2
                                C26 / rho =   0.060 KM2/SEC2

                                C66 / rho (Campbell) =   1.769 KM2/SEC2

Average relative error =   0.001481   Average relative error =   0.000811
Stiffness ratio = 1.28   Stiffness ratio = 1.28

Poisson's Ratios   Poisson's Ratios
Vxy =   0.293   Vxy =   0.292
Vyx =   0.374   Vyx =   0.373
Geometric Mean =   0.331   Geometric Mean =   0.330

ANGLE TO MAJOR PRINCIPAL AXIS = -12.6   AREA =   88.7 (km^4/sec^4)
GRAPH SCALE = 1 km^2/sec^2/div

POLAR PLOT OF LONGITUDINAL MASS SPECIFIC STIFFNESS

MD   CD

PLOT OF SPECIFIC STIFFNESS AS SEEN FROM FELT SIDE

In-plane elastic stiffnesses from polar plot optimization
for a polyester sheet.

Schematic diagram of the pulse-echo PVDF transducer.
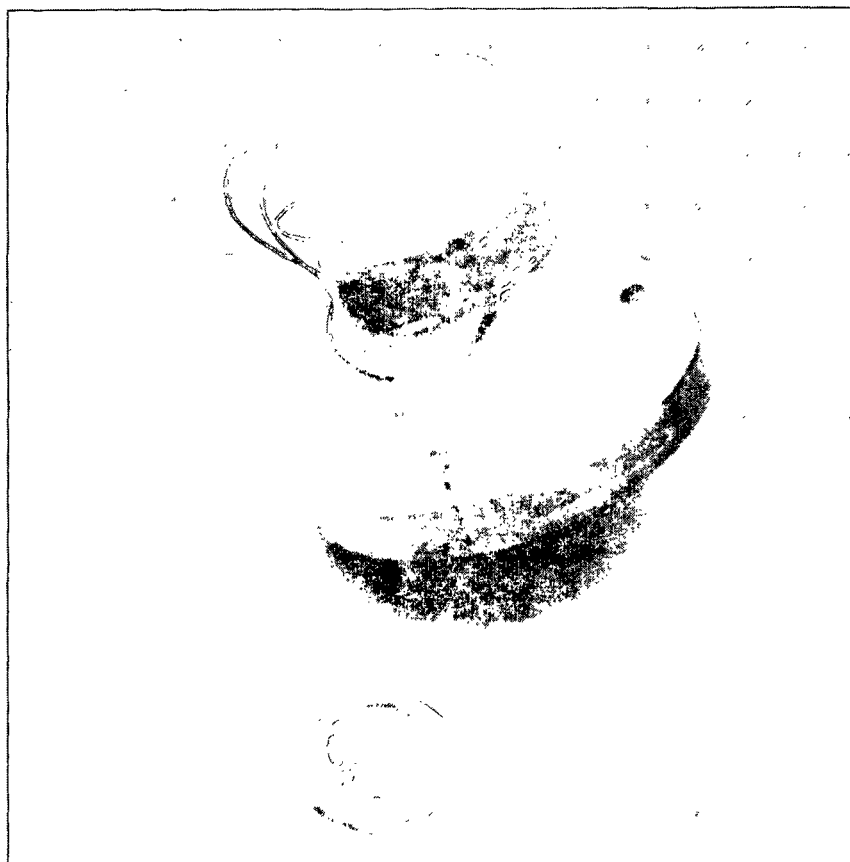
Photograph of the assembled pulse-echo PVDF transducer.
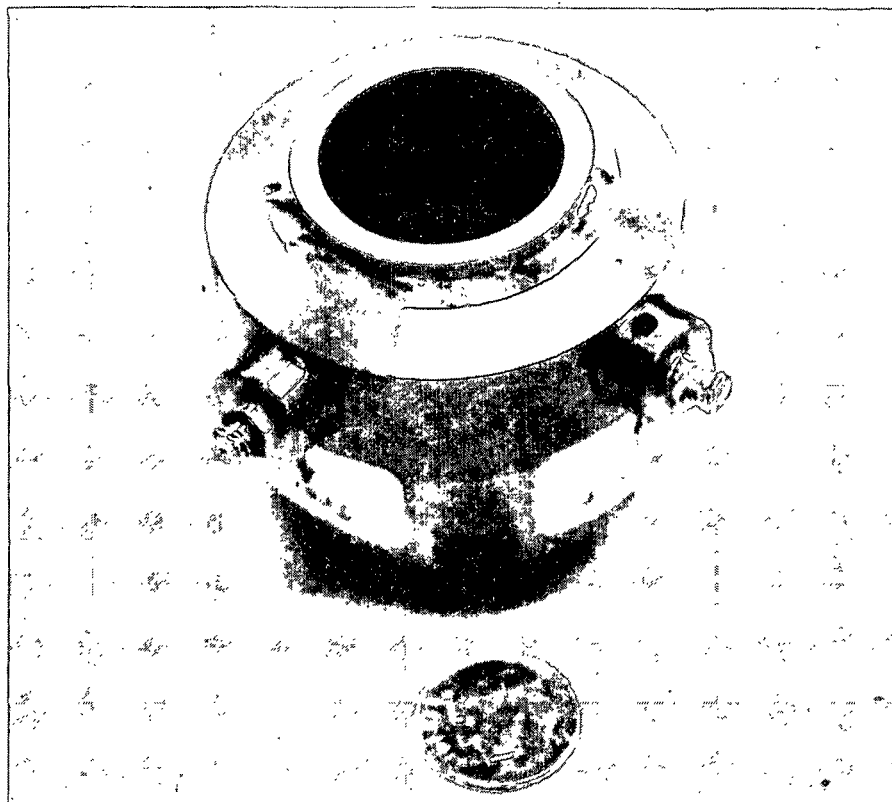
Photograph of the assembled pulse-echo PVDF transducer.
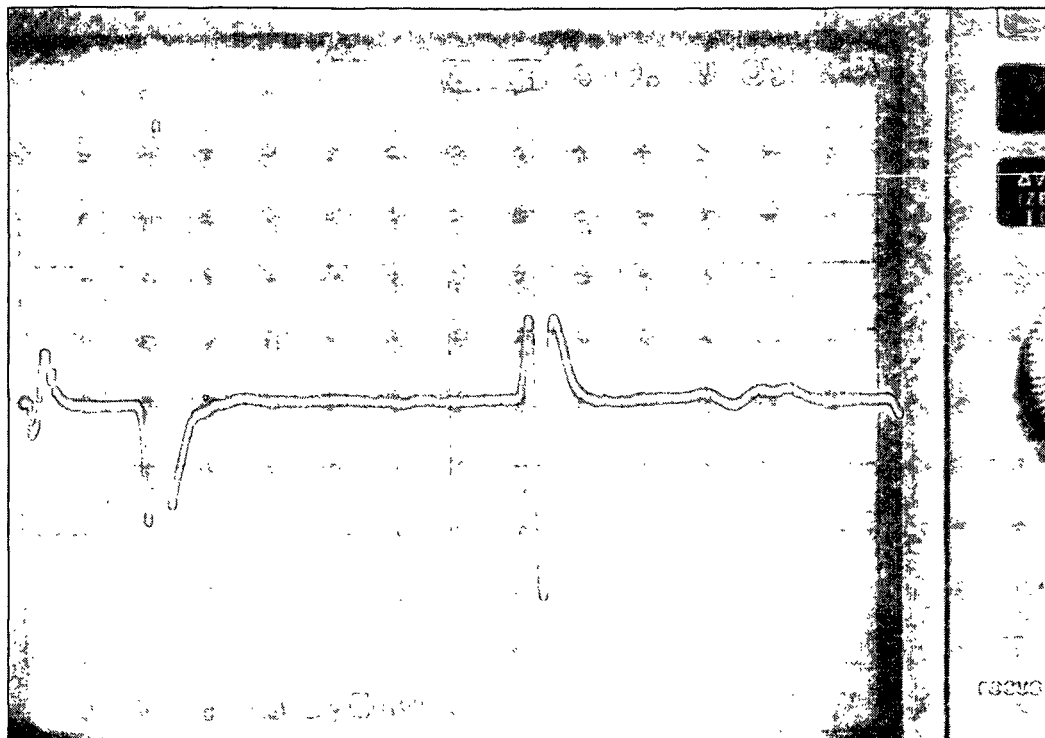
Before application of neoprene front-face, oscilloscope trace of
the receiver signal of the pulse-echo transducer resulting from
a single pulse at the transmitter.
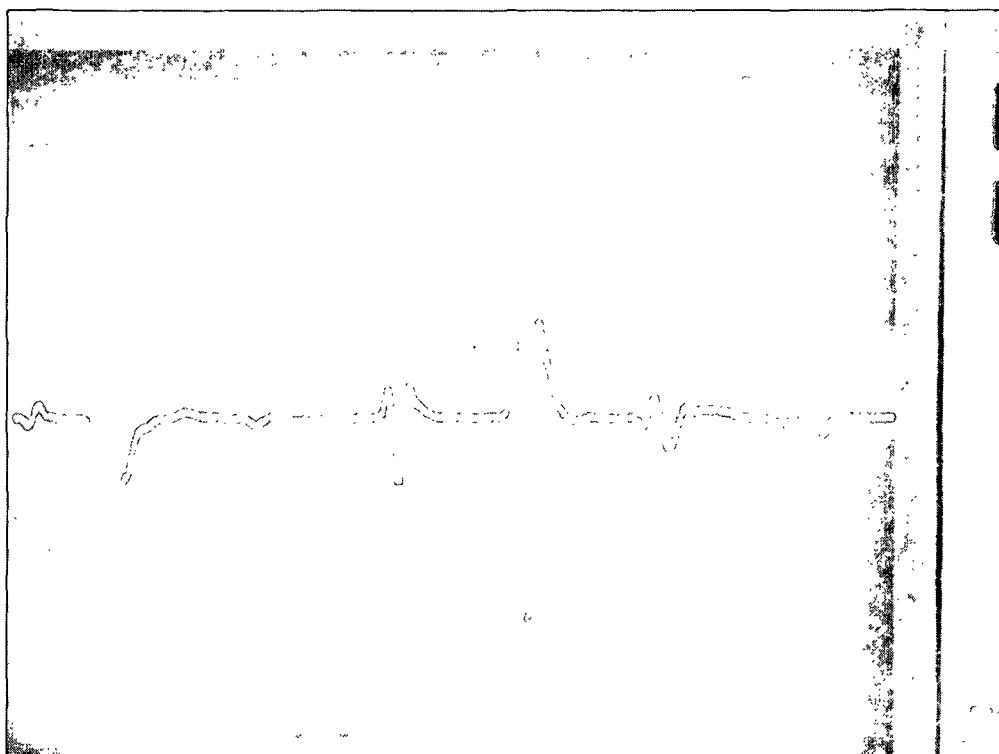
After application of neoprene front-face, oscilloscope trace of
the receiver signal of the pulse-echo transducer resulting from
a single pulse at the transmitter.
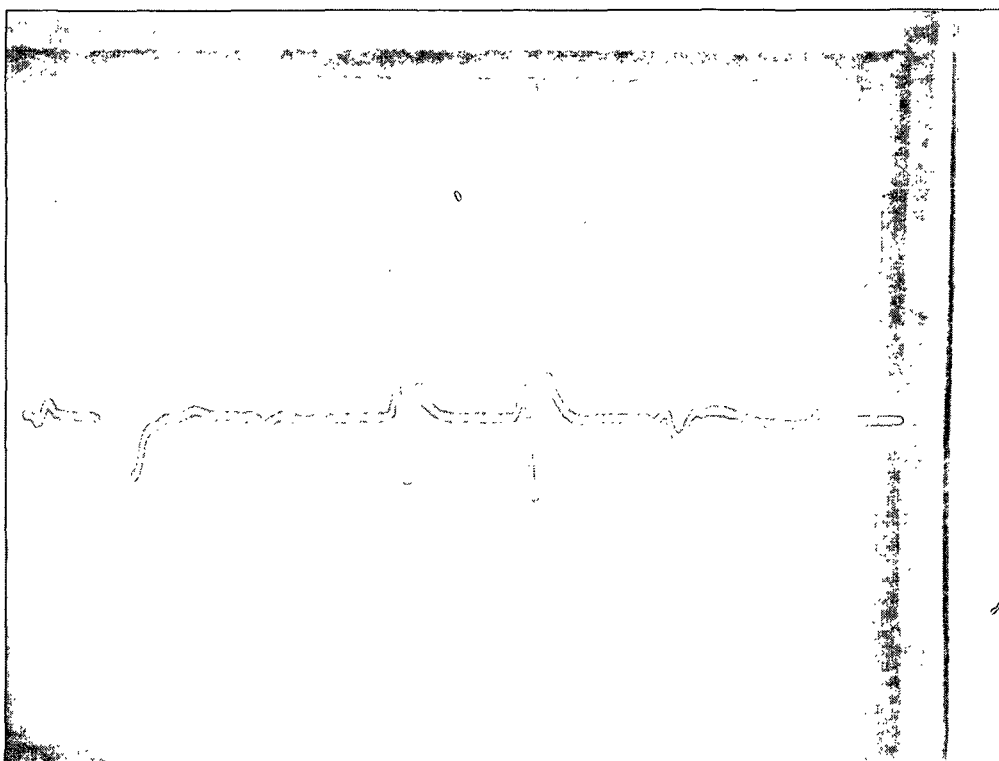
After loading of a linerboard sample to the neoprene front face,
oscilloscope trace of the receiver signal of the pulse-echo
transducer resulting from a single pulse at the transmitter.
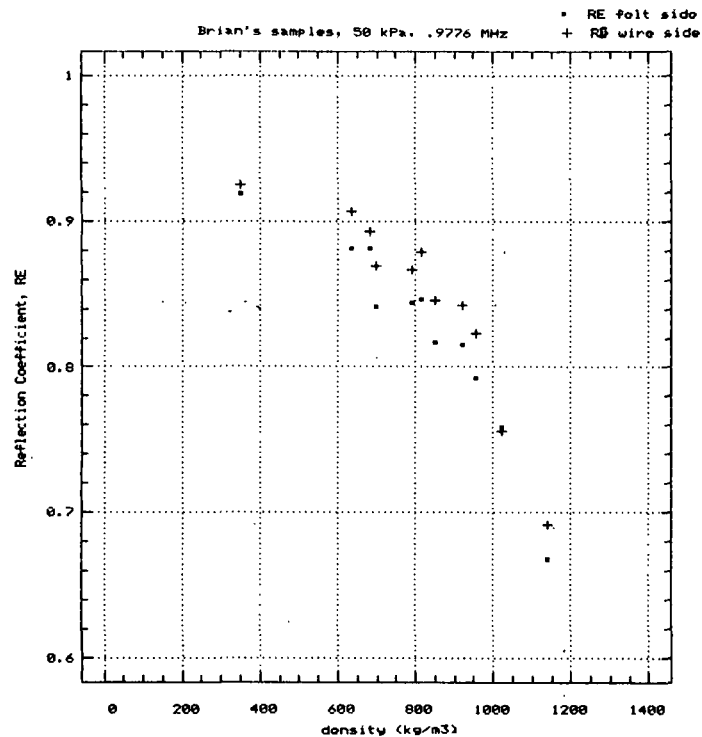
Figure 13. Ultrasonic reflection coefficient as a function of
            density for a series of samples varying in wet
            pressing, refining, and yield.
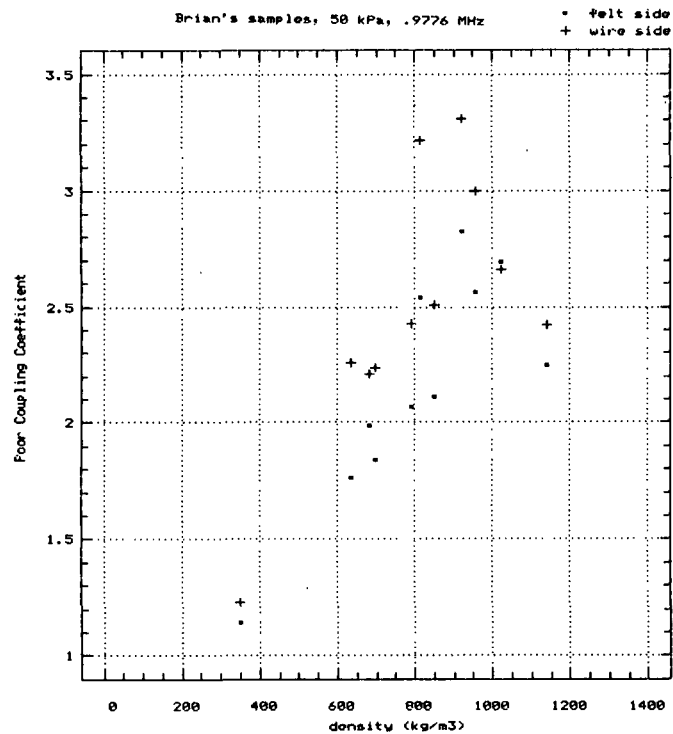
Figure 14. Ultrasonic poor coupling coefficient as a function
            of density for a series of samples varying in wet
            pressing, refining, and yield.
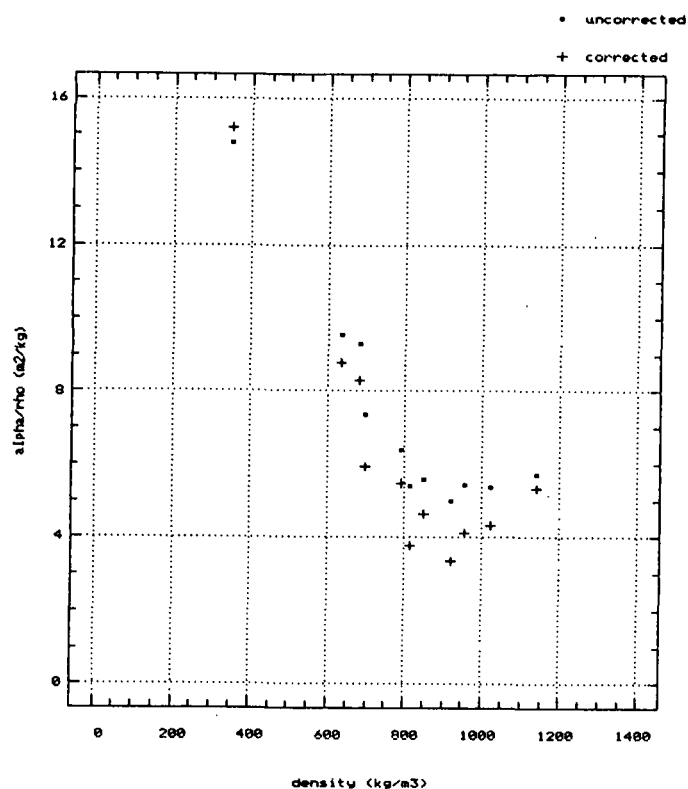
Mass specific ultrasonic attenuation coefficient as a function
of density for a series of samples varying in wet pressing,
refining, and yield.
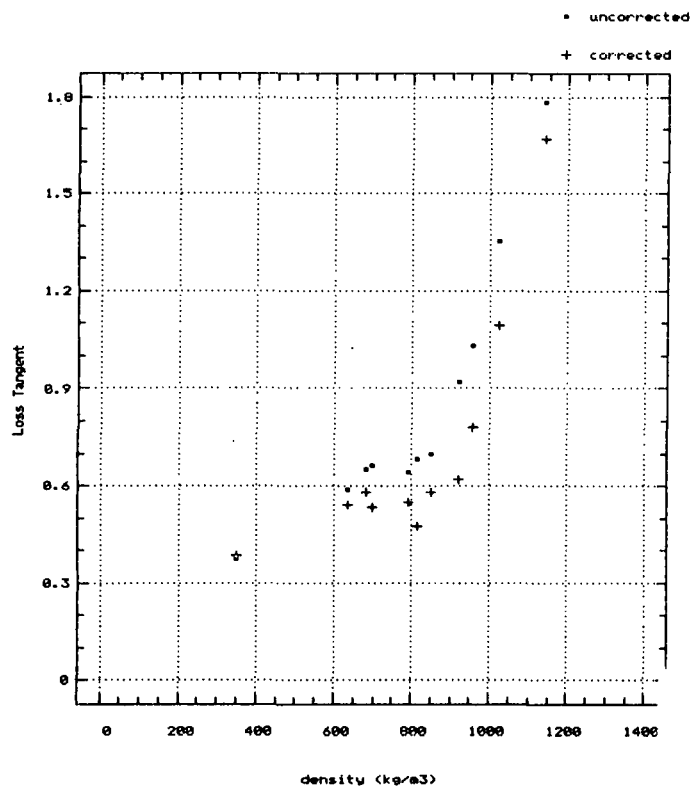
Ultrasonic loss tangent as a function of density for a series
of samples varying in wet pressing, refining, and yield.

EMPIRICAL RELATIONSHIPS BETWEEN TISSUE SOFTNESS AND OUT-OF-PLANE ULTRASONIC MEASUREMENTS

Status report

Project 3467

Paper Physics Group
The Institute of Paper Chemistry

OBJECTIVE

* Understand the impact of paper-making variables on ultrasonic properties of tissue papers.

* Develop relationships between tissue softness and the ultrasonically measured parameters.

ACTIVITIES TO DATE

* Establishment of stable conditions for ultrasonic measurements of tissue.

* Investigating relations between ultrasonically measured parameters and tissue softness.

TISSUE SOFTNESS

* Softness is a subjective property perceived
  by the tactile sensory system of human being.

* Tissue softness can be divided into:

  <u>Bulk softness</u> —— *Crumpling softness*,
  correlated with the flexibility of tissue paper.

  <u>Surface softness</u> —— *Tactile softness*,
  related to the distribution and magnitude
  of the surface irregularities.

SUBJECTIVE SOFTNESS EXPRESSION

Softness ——— ⌐——— Scaling
           ├——— Rating
           └——— *Ranking*
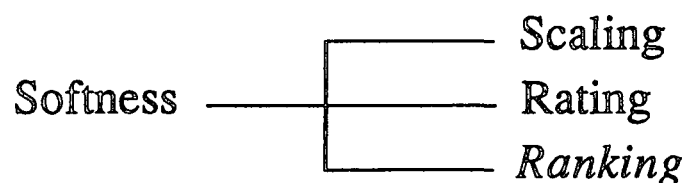
Softness ranking was obtained using
a pair-comparison technique.

PANEL RANKING OF SOFTNESS OF TISSUE SAMPLES

NAME: **DATE:**

EXPERIENCED: YES/NO

SAMPLE   A

	1	2	3	4	5	6	7	8	9	10	11	12	13	14	+	TOTAL −	o
1	■																
2		■															
3			■														
4				■													
5					■												
6						■											
7							■										
8								■									
9									■								
10										■							
11											■						
12												■					
13													■				
14														■			
TOTAL																	

(left margin label: S A M P L E   B)

+ denotes softer than;
− denotes harsher than;
o denotes no difference.

APPARATUS FOR STUDYING TISSUE SOFTNESS

1. Clark Stiffness Tester
2. Handle-O-Meter
3. Brown graduate cylinder test
4. Peirce tester
5. Pure bending stiffness tester
6. Torsion pendulum
7. Surface friction tester
8. Surface smoothness analyzer

FACTORS AFFECTING TISSUE SOFTNESS
(Panel assessment conditions)

* Color
* Smell
* The sound of crumpling

FACTORS AFFECTING TISSUE SOFTNESS
(Physical properties of tissue)

* Flexural rigidity
* Density
* Compressibility or resilience
* Surface smoothness
* Basis weight
* Caliper
* Sample size
* Ply number

FUNDAMENTAL ASPECTS OF TISSUE SOFTNESS

* Fiber length
* Flextural rigidity of individual fibers
* Fiber bonding levels

Description of the tissue samples

Sample No.	Origin (Co.)	Plies No.	Basis weight* g/m^2	Type
1	A	1E	24.78	Toilet tissue
2	B	1P	29.19	Toilet tissue
3	C	2	15.73	Toilet tissue
4	D	2	16.45	Facial tissue
5	E	2	15.50	Facial tissue
6	F	1	41.90	Towel tissue
7	G	2P	16.69	Toilet tissue
8	B	2	14.74	Facial tissue
9	B	2L	19.75	Facial tissue
10	C	2	14.34	Facial tissue
11	C	2	21.80	Toilet tissue
12	F	2	15.50	Toilet tissue
13	A	2	16.86	Facial tissue
14	H	2	14.50	Facial tissue

E — highly embossed; L — lotion treated;
P — pattern printed.
* — Basis weight are all measured by a single piece.

Correlation between softness ranking by an individual panelist and the average of a panelists.

Panelist Code	Correlation coefficients	
	Crumpling	Tactile
A	0.98	0.87
B	0.97	0.96
C	0.98	0.94
D	0.93	0.96
E	0.98	0.98
F	0.97	0.95
Average	0.97	0.94
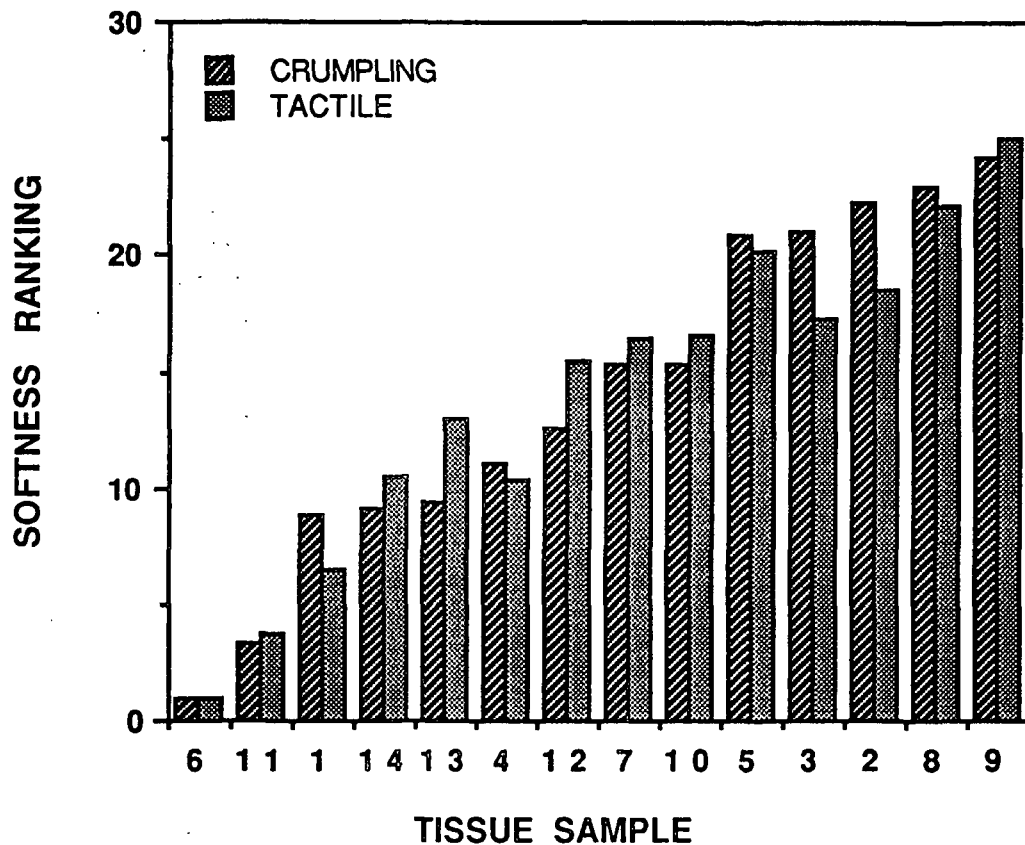
Softness ranking of commercially available tissue samples.

VELOCITY MEASUREMENT

Out-of-plane stiffness: $C_{33} / Density = V_{ZD}^2$

Acoustic impedance: $Z = V_{ZD} * Density$

$= Basis\ weight / Caliper$

$C_{33} = Z * V_{ZD}$
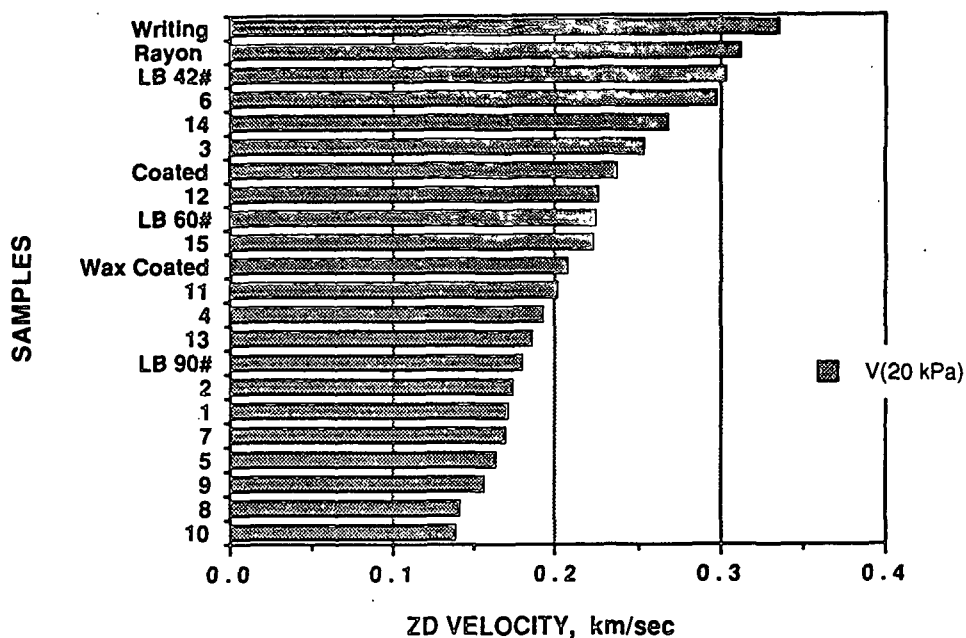
Z-direction ultrasonic velocity of regular papers and tissue samples.
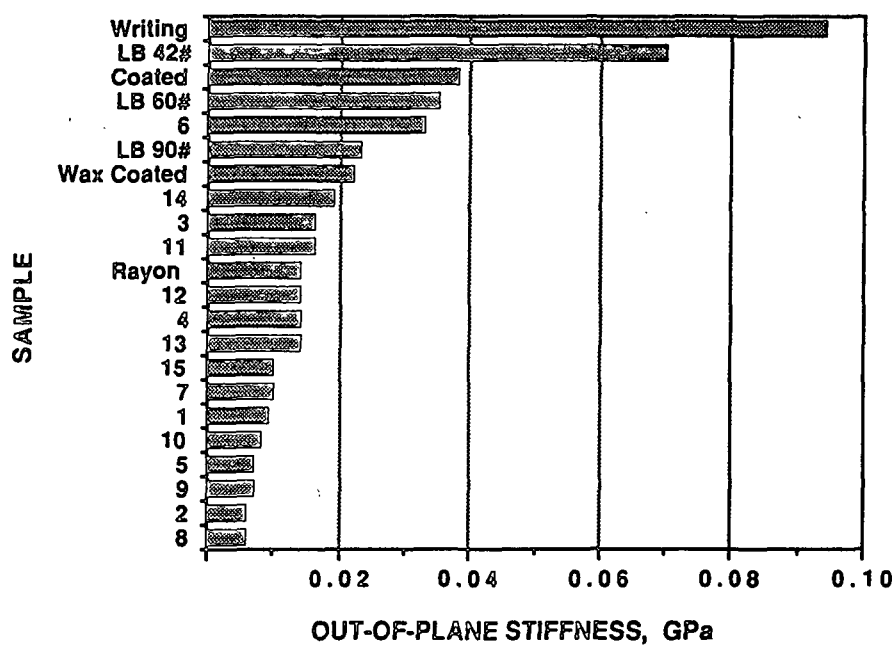
Out-of-plane stiffness of regular papers and tissue samples.
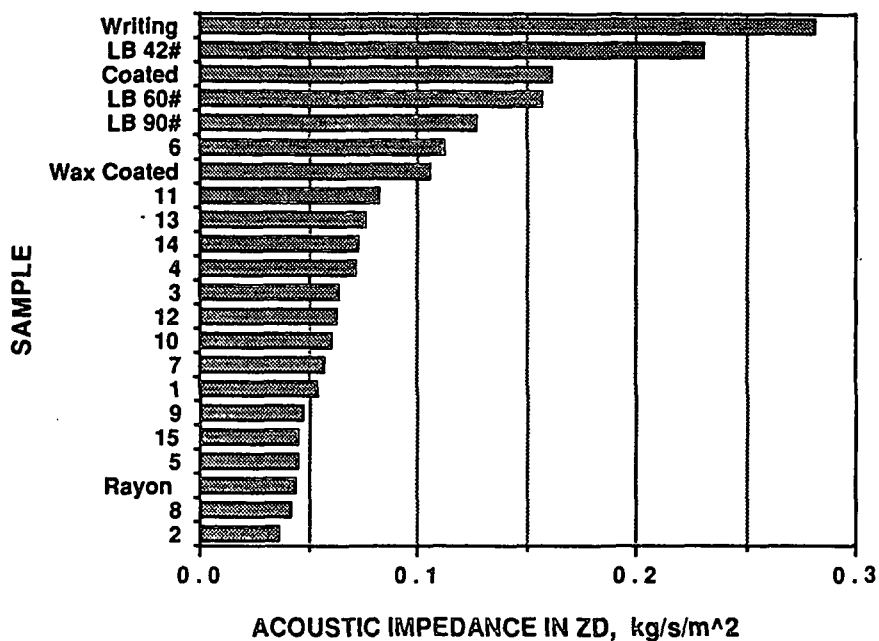
Acoustic impedance of regular papers and tissue samples.

LOSS MEASUREMENT

$$R_{mean} \equiv A_{paper} / A_{foil}$$

Perfect coupling assumption:

$$R_{mean} = t^2 e^{-\alpha x}$$

where, $t^2 \equiv 4Z_{paper}Z_{rubber} / (Z_{paper} + Z_{rubber})$

Imperfect coupling:

$$R_{mean} = (Coupling\ coef.)\ t^2 e^{-\alpha x}$$

Z —— Acoustic impedance
α —— Ultrasonic attenuation coefficient
A —— Amplitude of signal
x —— Caliper
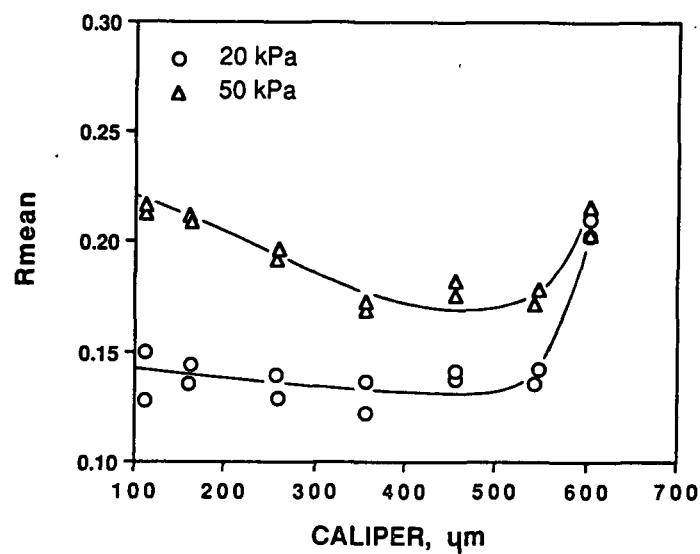
Energy loss measured as a function of caliper and the load pressure.
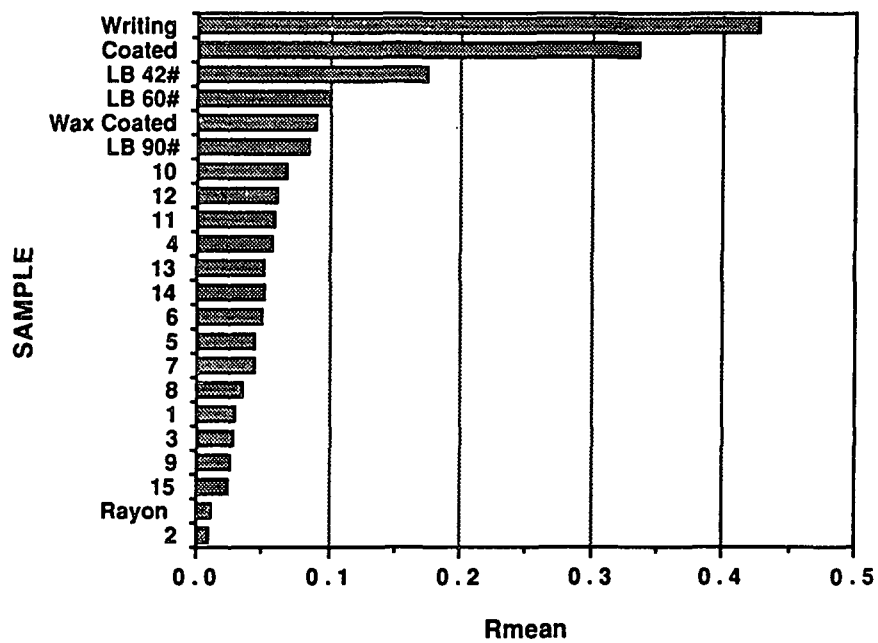
Energy loss measured on regular papers and tissue samples.

**Correlations between measured physical properties
and both bulk and surface softness ranking**

Sample No.	Variables	Variance ratio (F-ratio)		Correlation coefficient	
		Crumpling ranking	Tactile ranking	Crumpling ranking	Tactile ranking
1	Acoustic impedance, Z, $[kg/s/m^2]$	27.83	23.75	-0.836	-0.815
2	Mass specific attenuation, A/BW, $[dBm^2/g]$	16.71	15.95	0.763	0.755
3	Basis weight, BW, $[g/m^2]$	2.94	4.11	-0.444	-0.505
4	Tensile stiffness, Et, $[kN/m]$	5.54	5.92	-0.562	-0.575
5	Young's modulus, E, $[MPa]$	8.41	8.25	-0.635	-0.638
	Emd, $[MPa]$	8.09	7.86	-0.635	-0.629
	Ecd, $[MPa]$	8.78	8.82	-0.650	-0.651
6	Out-of-Plane stiffness, C_{33}, $[GPa]$	13.06	14.45	-0.722	-0.739
7	Attenuation level, A, $[dB]$	4.75	2.52	0.532	0.417
8	Thickness t, $[um]$	0.03	0.26	0.051	-0.144
9	Density, rho, $[kg/m^3]$	2.74	1.38	0.431	-0.322
10	Delay, $[usec]$	11.31	0.64	0.314	0.225
11	ZD compressibility, % $(1-t_{20kPa}/t_{8.95kPa})$	0.21	0.05	0.131	0.066

MULTIPLE REGRESSION ANALYSIS

$$y = a_1 x_1 + a_2 x_2 + \cdots + a_n x_n + c$$

y —— Panel softness ranking
a —— Partial regression coefficient of factor, x
x —— Measured physical properties
c —— A constant

An example of multiple regression analysis
(Stepwise selection of variables into the model)

Selection Formard	Maximum steps: 500	F-to-enter: 4.00
Control: Manual		F-to-remove: 4.00

R-squared: 0.88386   Adjusted: 0.84902   MSE: 8.85884   d.f.: 10

Variables in Model	Coeff.	F-Remove	Variables Not in Model		P.Corr.	F-Enter
1. Z	-187.989	10.0602	4.	meanE	0.4803	2.6990
2. A/BW	22.2496	15.6484	5.	Et	0.4325	2.0713
3. BW	0.6662	9.0702	6.	Emd	0.5344	3.5974
			7.	Ecd	0.3595	1.3362
			8.	thickness	0.3778	1.4985
			9.	compressibility	0.0534	0.0257
			10.	C_{33}	0.3611	1.3492
			11.	delay	0.2438	0.5686

Correlation between ultrasonically predicted softness ranking and crumpling ranking.

Correlation between ultrasonically predicted softness ranking and tactile ranking.

Results of multiple regression analysis

| | | Corresponding coefficient | | | | Correlation coeff. of multiple |
		Z [MPa/s]	A/BW [dBm^2/g]	BW [g/m^2]	Constant	regression (r^2)
Overall	Crumpling	-187.99	22.25	0.67	-21.48	0.884
	Tactile	-188.04	15.95	0.37	-6.13	0.785
Facial	Crumpling	-441.86	1.21	0.59	30.54	0.997
	Tactile	-412.18	-0.05	1.08	22.51	0.971
Toilet	Crumpling	-103.31	26.90	0.77	-36.46	0.970
	Tactile	-95.18	19.71	0.437	-19.83	0.896

CONCLUSION

*   Lotion tends to increase, and embossing tends to reduce subjective softness.

*   Acoustic impedance and mass specific attenuation are main parameters to predict tissue softness.

Calendering and creping reduces Z and increase A/BW, which means increases softness.
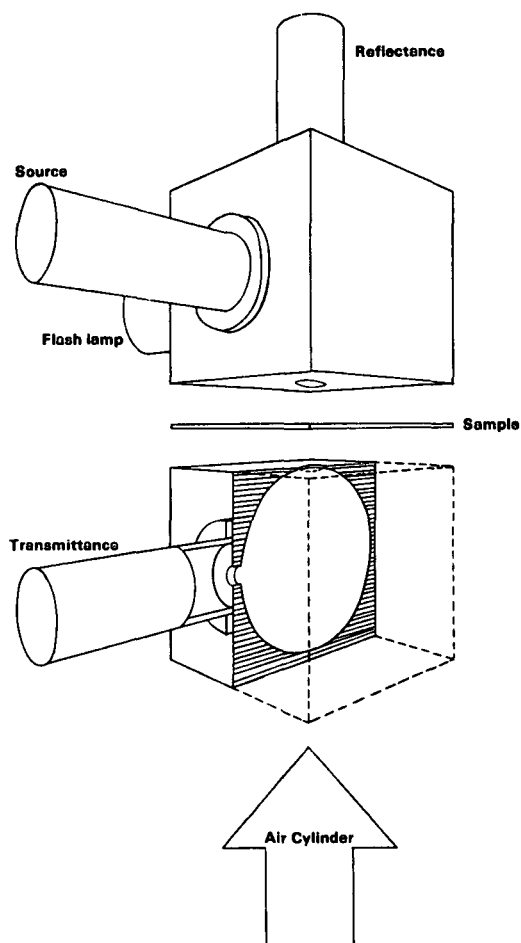
Schematic of the Board Optical Transmission Meter.
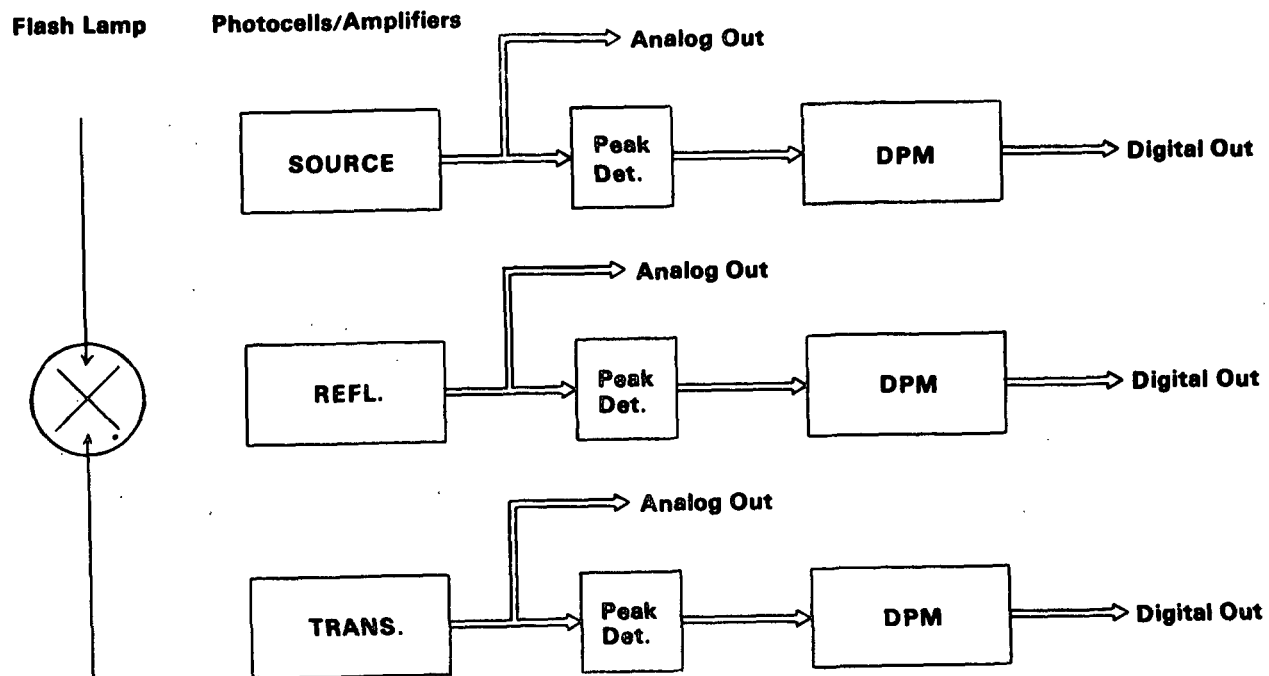
Block diagram of the detector circuits.
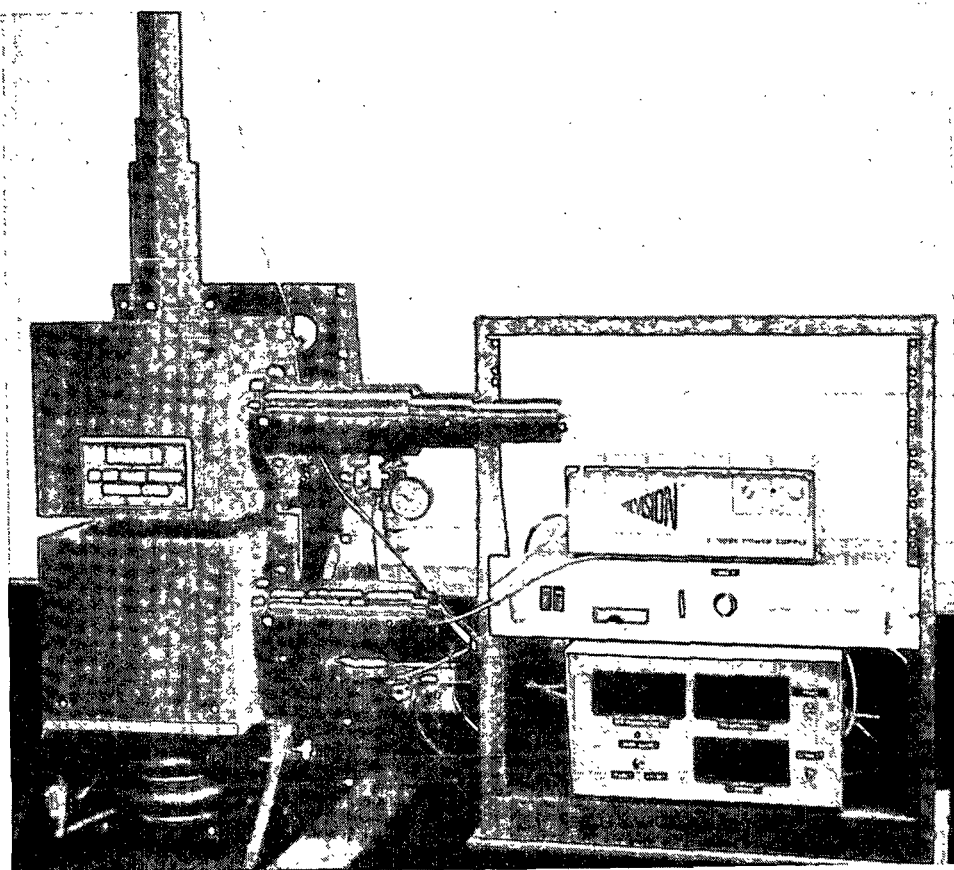
The Board Optical Transmission Meter.

TRANSMITTANCE VALUES OF LIGHT-WEIGHT SHEETS
CALCULATED FROM KUBELKA-MONK THEORY

| Sample | TB-1 (Y-function) | | | BOTM | |
	R_0	R_∞	T, calc	T_A	T, calc
White bond	0.728	0.799	0.192	0.453	0.193
White bond	0.721	0.780	0.205	0.490	0.210
Pink memo	0.584	0.633	0.221	0.308	0.204
Deinked	0.708	0.750	0.162	0.366	0.171
Yellow memo	0.721	0.823	0.225	0.500	0.214
Cream tab card stock	0.767	0.815	0.148	0.378	0.147

Readings are the average of one reading on each of five specimens.

T_A is the apparent transmittance of the specimen sandwiched between the Teflon sheets.

APPARENT TRANSMITTANCE AND SPECIFIC SCATTERING COEFFICIENT
FOR RANGE OF T-PORTS AND TWO PMT VOLTAGES

Specimen	g/m^2	R(s)	PMT Supply	T-Port Dia., in.	T_A	s, cm^2/g
90#	434	.267	1000 V	.81	1.65e-5	145
(Unbl. kraft liner)		.267		.51	5.40e-6	160
		.267		.375	1.52e-5	146
J	339	.273	700 V	.81	9.70e-6	200
(Unbl. kraft liner)		.273		.51	9.42e-6	200
		.273		.375	1.11e-5	197
		.273	1000 V	.81	1.05e-5	198
		.273		.375	1.09e-5	198
		.273		.15	9.70e-6	200
H	131	.178	700 V	.81	3.93e-4	219
(Unbl. kraft medium)		.178		.51	3.21e-4	225
		.178		.375	3.91e-4	219
		.178		.15	3.31e-4	224
		.178		.082	3.71e-4	221
		.178	1000 V	.15	3.02e-4	227
		.178		.082	3.51e-4	222
		.178		.0459	3.70e-4	221
		.178		.028	3.75e-4	220
I	159	.367	700 V	.15	4.84e-3	277
(Semibl. kraft medium)		.367		.082	5.17e-3	273
		.367		.0459	5.72e-3	268
		.367		.028	5.59e-3	269
		.367	1000 V	.028	5.14e-3	273
		.367		.0157	5.54e-3	269
		.367		.0093	6.36e-3	262
L	163	.619	700 V	.082	1.49e-2	459
(Buff cover stock)		.619		.0459	1.50e-2	458
		.619		.028	1.38e-2	468
		.619		.0157	1.55e-2	454
		.619		.0093	1.54e-2	454
		.619	1000 V	.0157	1.39e-2	467
		.619		.0093	1.41e-2	466
A	39.2	.728	700 V	.0157	2.06e-1	834
(White bond)		.728		.0093	1.97e-1	860
None	0	0	700 V	.0093	1.00e0	---

One reading per specimen per condition.

EFFECT OF AIR GAPS

Specimen	g/m^2	s, cm^2/g
UK liner; 0"/side	206	209
		209
		210
UK liner; .011"/side		209
		210
		210
UK liner; .022"/side		209
		210
		209

No-specimen reference; 0"/side.
File folder stock with 2" hole used as spacers.

EFFECT OF SPECIMEN SIZE

Size, inch	Transmission meter readout
9 x 9	238
8 x 8	237
7 x 7	239
6 x 6	238
5 x 5	237
4 x 4	239
3 x 3	239
2 disk	238
1.5 disk	238

----

206 g/m^2 unbl. kraft liner.
1 inch port above specimen.
1-1/8 inch port below specimen.
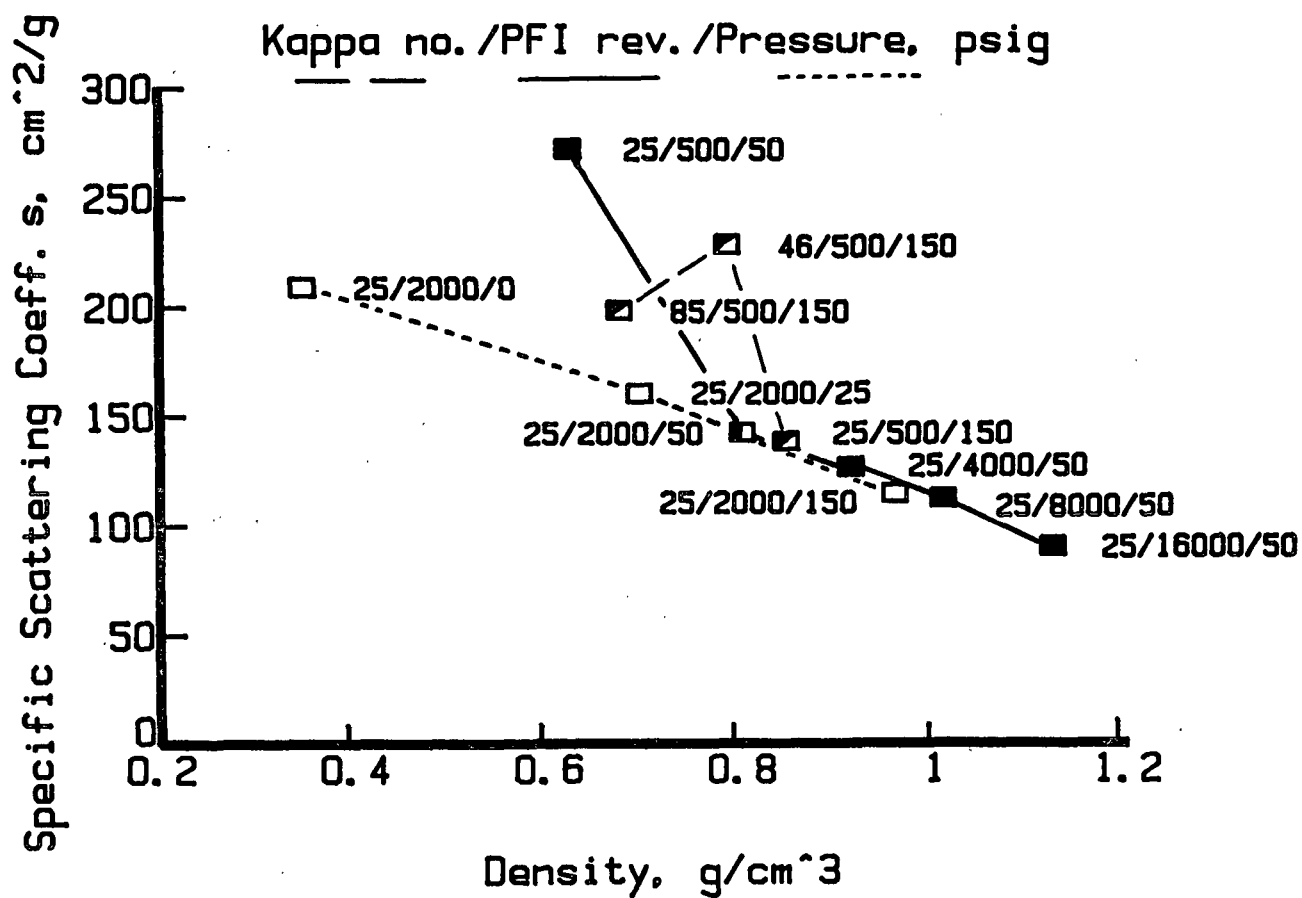
Data for unbleached kraft handsheets.

SECTION 4

Project 3646

FUNDAMENTALS OF PAPER SURFACE WETTABILITY
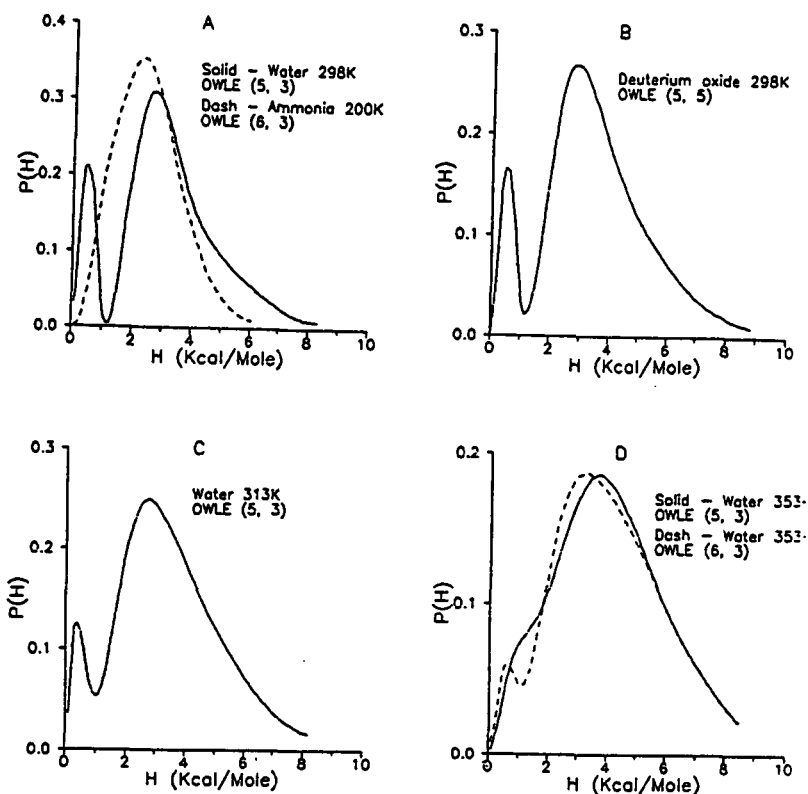
Stey's distribution functions. Probability, P(H), vs. enthalpy, H. (A) Water at 298 K and NH_3 at 200 K. (B) D_2O at 298 K. (C) H_2O at 313 K. (D) H_2O at 353 K.
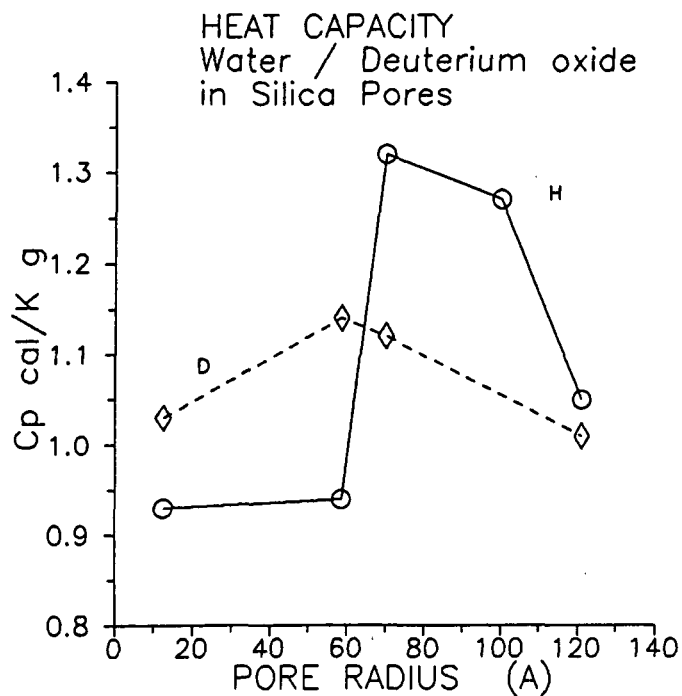
Heat capacities of water in silica pores as a function of pore radius at 298 K: squares H_2O; diamonds, D_2O. Radius in Angstroms (10 Å = 1 nm).
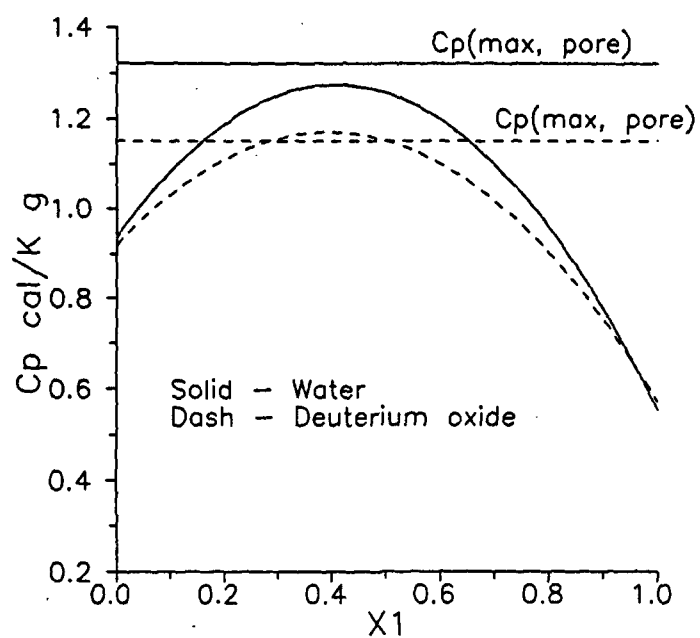
Hypothetical heat capacity of water and deuterium
oxide as a function of x(1) at 298 K.
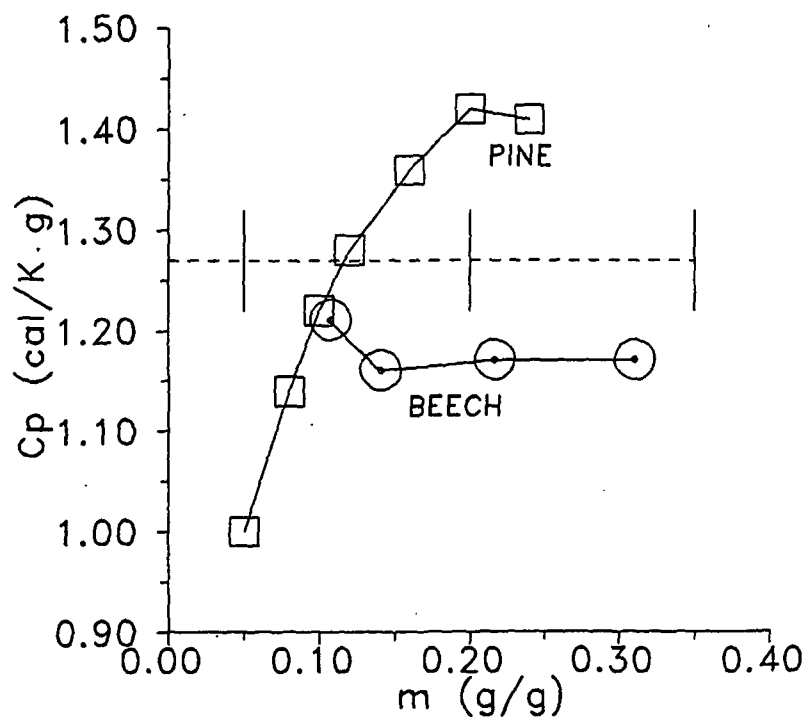
Apparent heat capacity of water in woods. Squares - pine;
circles - beech; dashed line - maximum heat capacity as
calculated from author's model
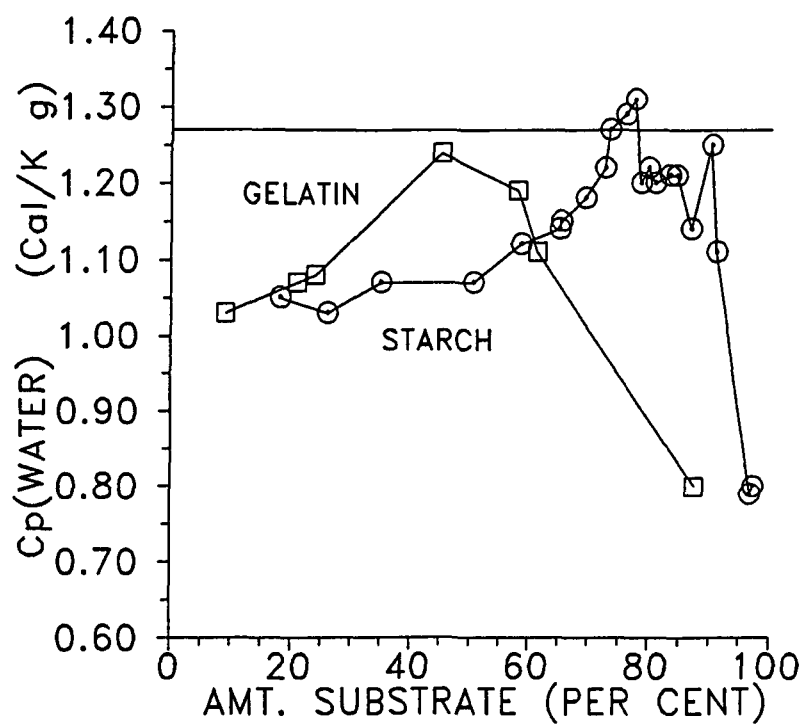
Apparent heat capacity of water versus per cent of
substrate material in mixture. Squares - gelatin;
circles - starch. Horizontal line - maximum heat
capacity calculated from author's model.

SECTION 7

Project 3332

ON-LINE MEASUREMENT OF PAPER MECHANICAL PROPERTIES

ON-LINE MEASUREMENTS

- ZD WITH IPC NEOPRENE-FACED WHEELS

- ZD WITH COMMERCIAL FLUID-FILLED WHEELS

- IN-PLANE WITH BIMORPH TRANSDUCERS

SPEED TRIALS WITH IPC WHEELS

- APPARENT CALIPER INCREASES WITH SPEED

- APPARENT DELAY TIME INCREASES WITH SPEED

- CORRECTION USING NEOPRENE-NEOPRENE HELP

NEW WHEELS UNDER CONSTRUCTION

- IMPROVED PVDF FILMS

- MOLDED NEOPRENE FRONT-FACE

- HARDER NEOPRENE FRONT-FACES
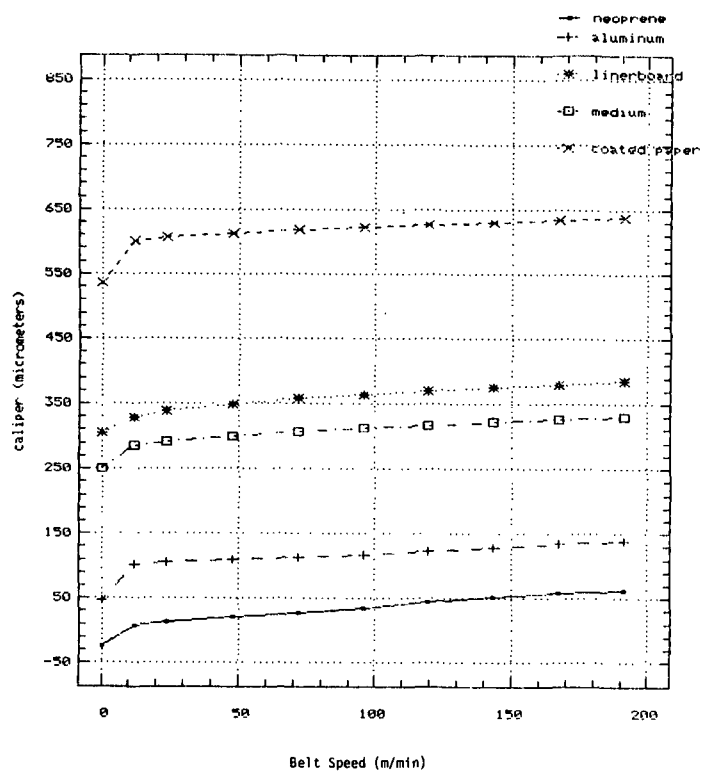
IPC wheel raw caliper readings
versus belt speed.
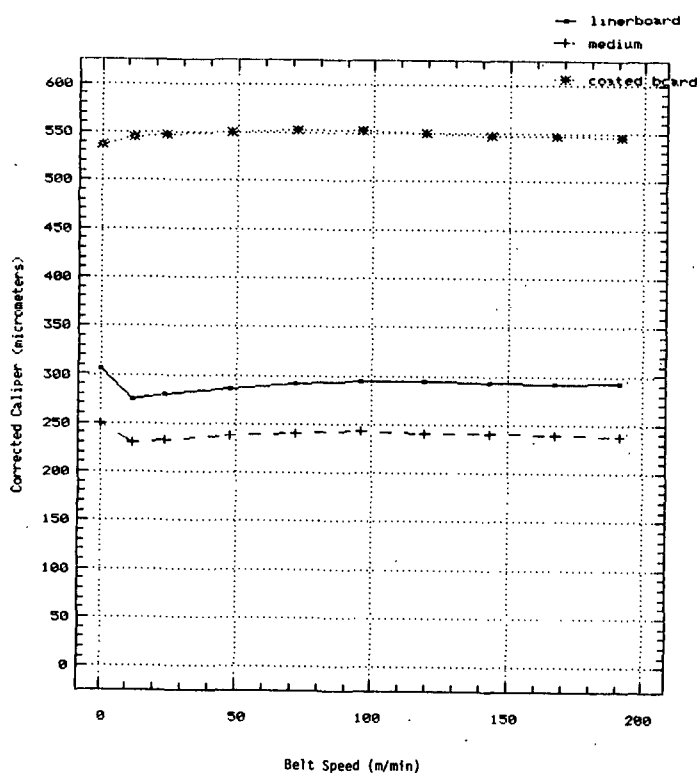
IPC wheel caliper corrected for changes
in foil caliper versus belt speed.
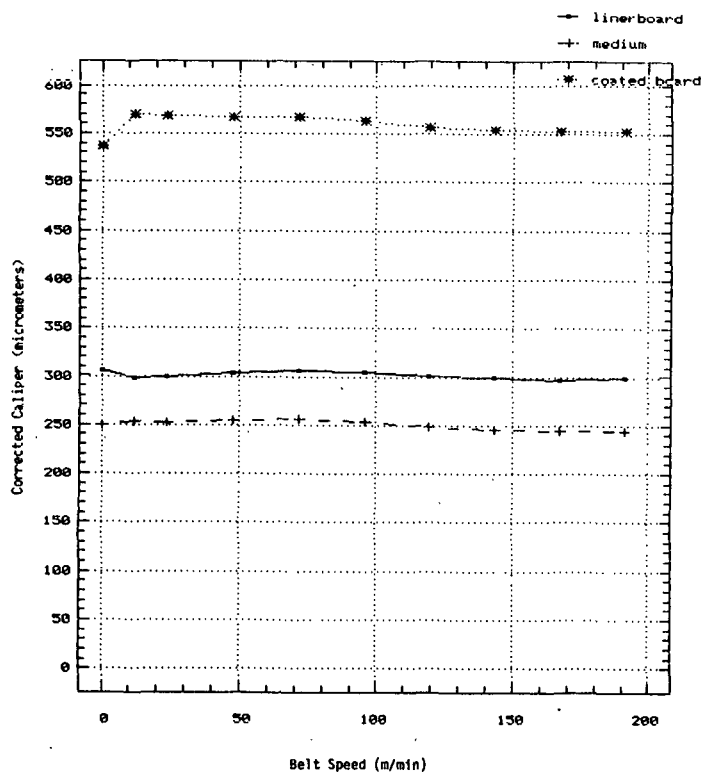
IPC wheel caliper corrected for
changes in neoprene-neoprene
separation versus belt speed.
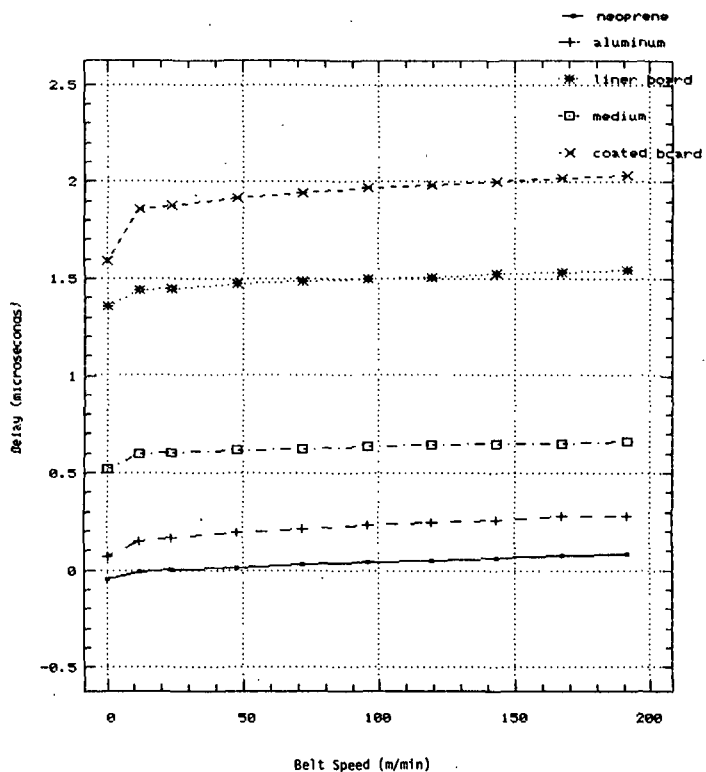
IPC wheel raw time-of-flights versus
belt speed.
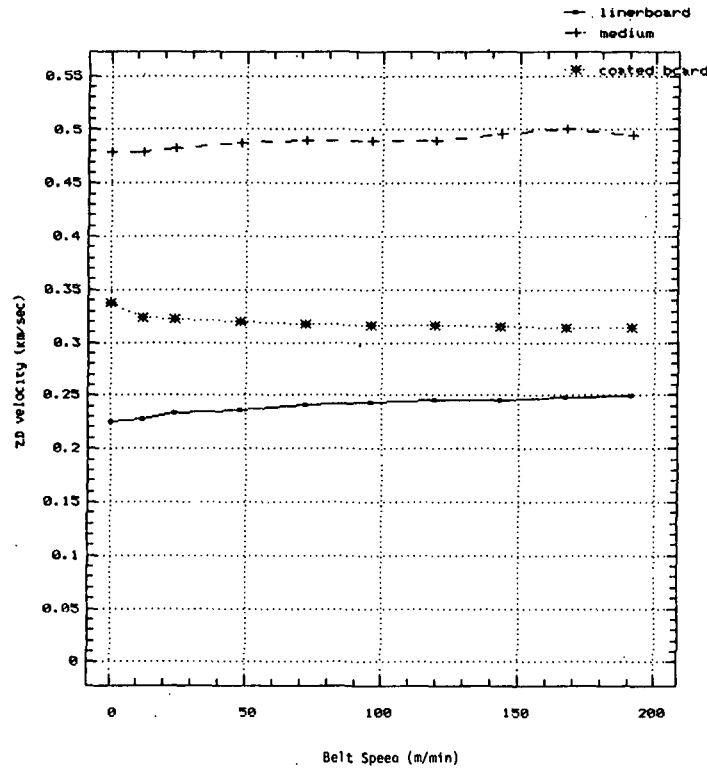
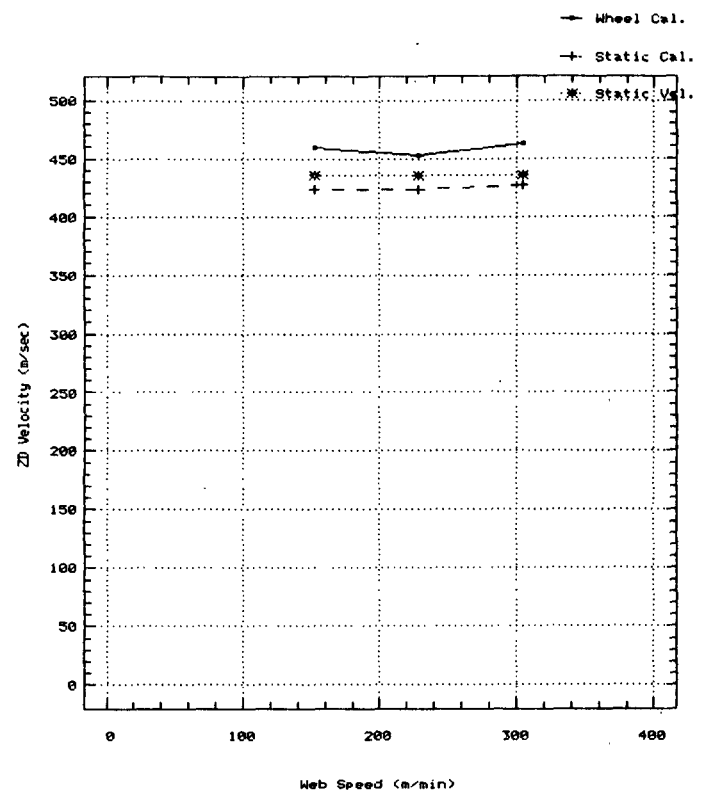IPC wheel raw ZD velocities versus
belt speed.
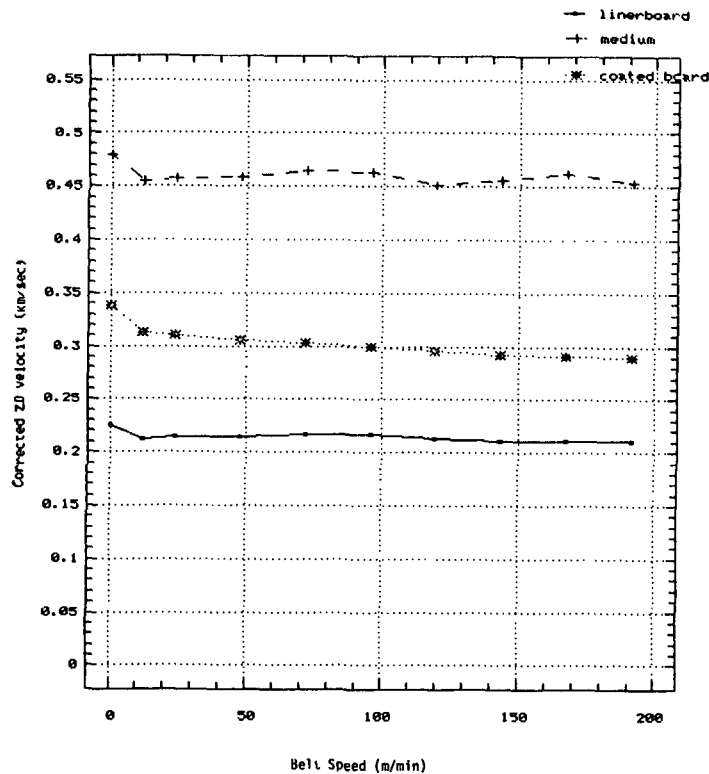
IPC wheel ZD velocities corrected for
neoprene-neoprene separation and time-
of-flight changes versus belt speed.
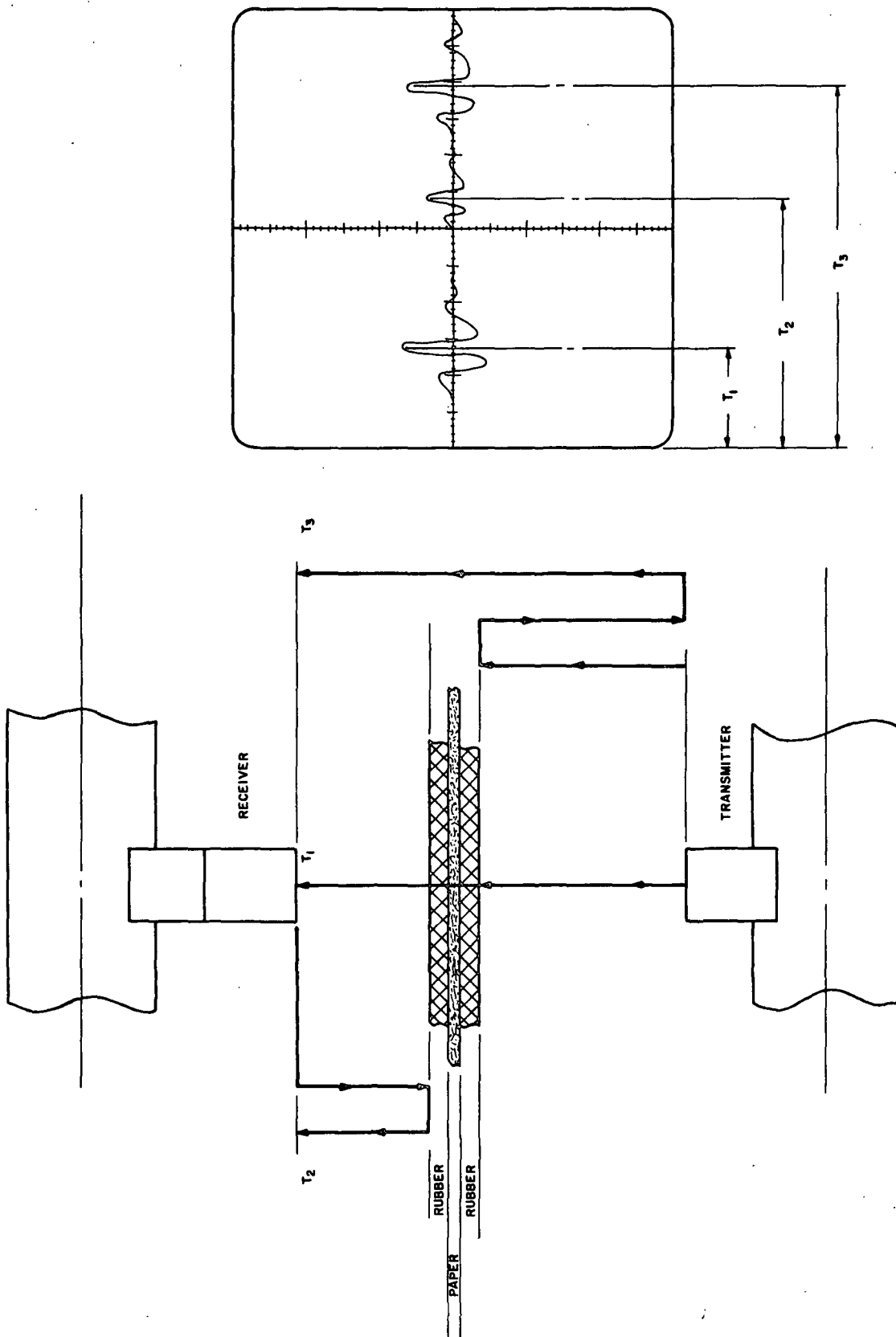
Schematic diagram of the definition of T_1, T_2, and T_3.
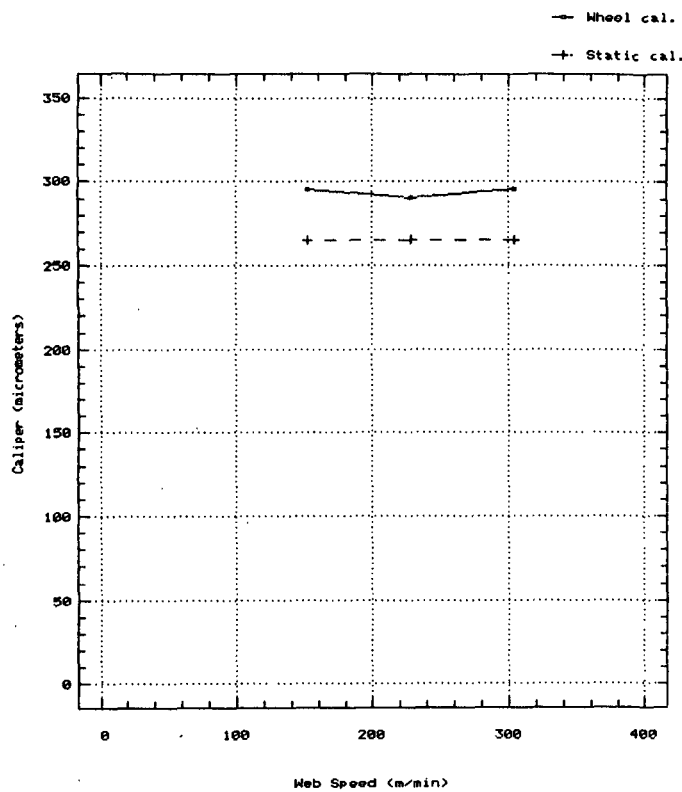
Fluid-filled wheel calipers
versus belt speed.

Fluid-filled wheel ZD velocities
versus belt speed.

SPEED TRIALS WITH FLUID-FILLED WHEELS

- COMPLICATED BY FLUID TEMPERATURE
    CHANGES

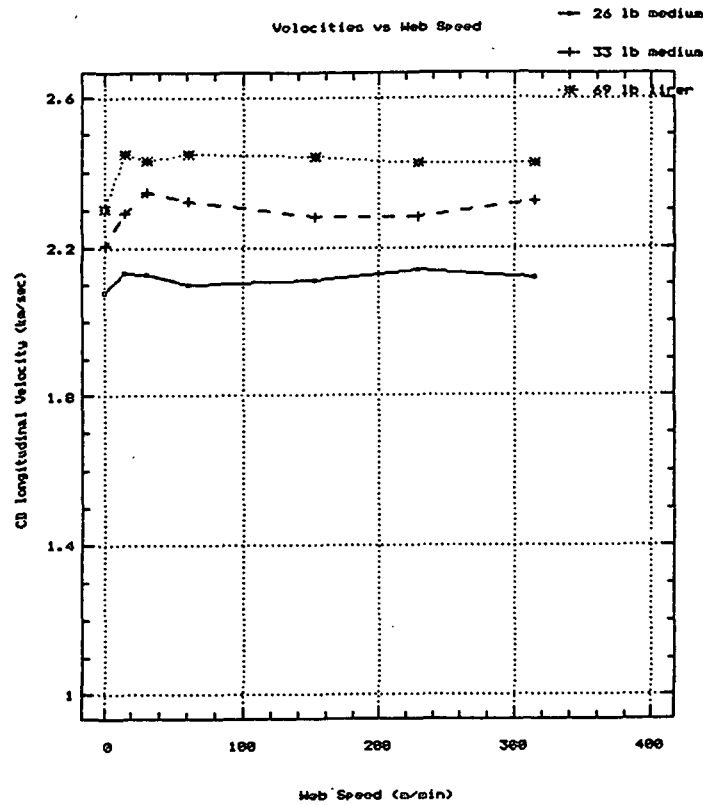- COMPENSATION IS FEASIBLE

FLUID-FILLED WHEEL ACTIVITIES

- REAL TIME TEMPERATURE COMPENSATION

- CONSTRUCTION OF IPC IMMERSION
  TRANSDUCERS

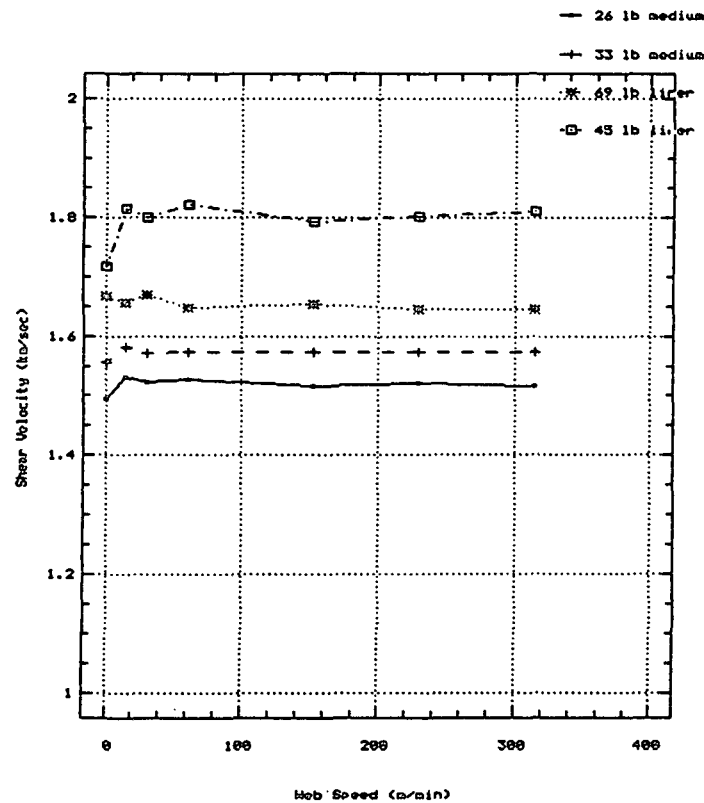## SPEED TRIALS WITH IN-PLANE BIMORPH TRANSDUCERS

- VERY GOOD STABILITY WITH SPEED

- SOME WEAR ON TRANSDUCER SURFACE

- DISPLACEMENT FROM ROBOT RESULTS
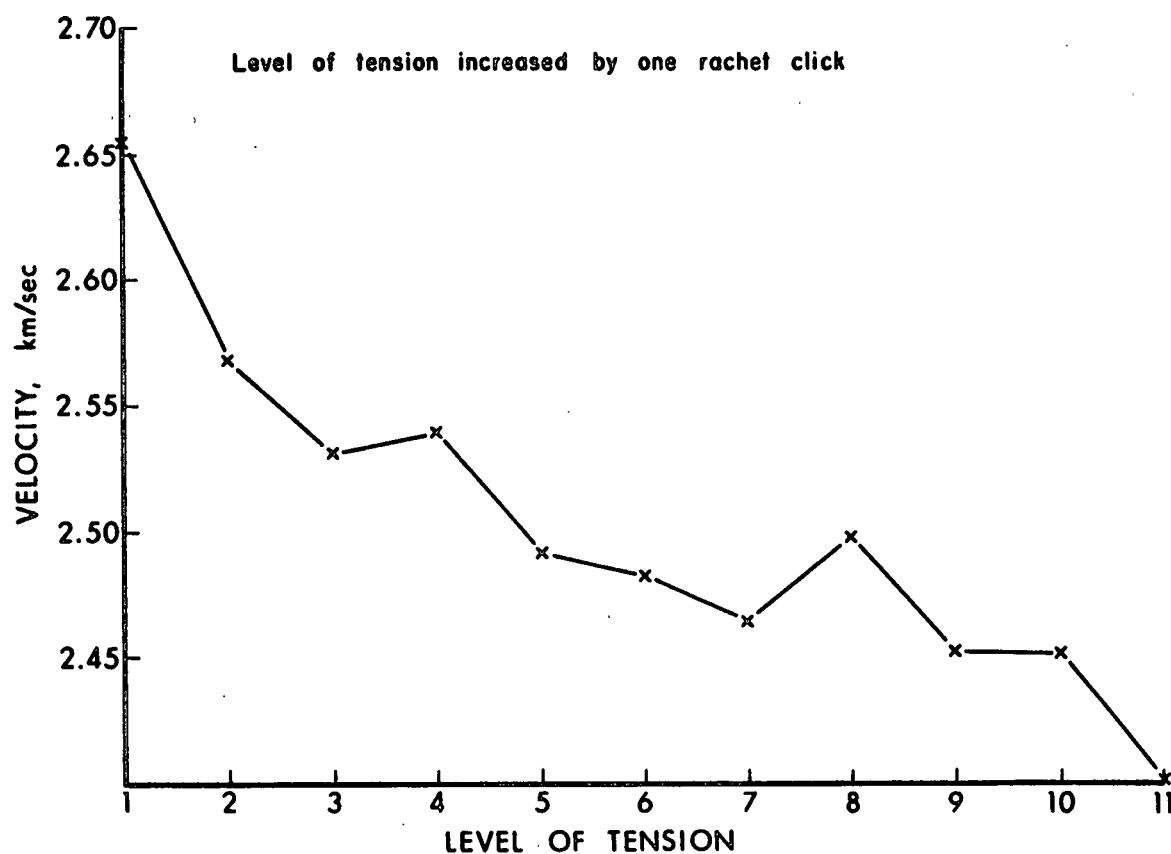
On-line bimorph CD longitudinal velocities versus web tension.

On-line bimorph CD longitudinal velocities versus web speed.

On-line bimorph shear velocities versus web speed.